Final Report

University of Florida
Civil and Coastal Engineering

UF

University of Florida
Civil and Coastal Engineering

Task 7 Deliverable July 2026

Phase III: Implementation of Shallow Foundations on Florida Limestone in FB-MultiPier

Principal Investigator:
Michael Rodgers, Ph.D., P.E. (UF)

Co-Principal Investigator:
Scott Wasman, Ph.D. (FSU)

Senior Contributors:
Michael Faraone, Ph.D., P.E., Anand Patil, P.E., Michael McVay, Ph.D.

Graduate Researchers:
Kunyu Yang, Ph.D. (Princeton University), Mayesha Farzana Islam (FSU), Suchana Podder (FSU)

Department of Civil and Coastal Engineering
University of Florida
P.O. Box 116580
Gainesville, Florida 32611

Sponsor:
Florida Department of Transportation (FDOT)
Rodrigo Herrera, P.E.

Contract:
BED31-977-17
Final Report

DISCLAIMER

The opinions, findings, and conclusions expressed in this publication are those of the authors and not necessarily those of the Florida Department of Transportation.

SI (MODERN METRIC) CONVERSION FACTORS (from FHWA)

APPROXIMATE CONVERSIONS TO SI UNITS

SYMBOL	WHEN YOU KNOW	MULTIPLY BY	TO FIND	SYMBOL
LENGTH				
in	inches	25.4	millimeters	mm
ft	feet	0.305	meters	m
yd	yards	0.914	meters	m
mi	miles	1.61	kilometers	km

SYMBOL	WHEN YOU KNOW	MULTIPLY BY	TO FIND	SYMBOL
AREA				
in^2	square inches	645.2	square millimeters	mm^2
ft^2	square feet	0.093	square meters	m^2
yd^2	square yard	0.836	square meters	m^2
ac	acres	0.405	hectares	ha
mi^2	square miles	2.59	square kilometers	km^2

SYMBOL	WHEN YOU KNOW	MULTIPLY BY	TO FIND	SYMBOL
VOLUME				
fl oz	fluid ounces	29.57	milliliters	mL
gal	gallons	3.785	liters	L
ft^3	cubic feet	0.028	cubic meters	m^3
yd^3	cubic yards	0.765	cubic meters	m^3
NOTE: volumes greater than 1000 L shall be shown in m^3				

SYMBOL	WHEN YOU KNOW	MULTIPLY BY	TO FIND	SYMBOL
MASS				
oz	ounces	28.35	grams	g
lb	pounds	0.454	kilograms	kg
T	short tons (2000 lb)	0.907	megagrams (or "metric ton")	Mg (or "t")

SYMBOL	WHEN YOU KNOW	MULTIPLY BY	TO FIND	SYMBOL
TEMPERATURE (exact degrees)				
°F	Fahrenheit	5 (F-32)/9 or (F-32)/1.8	Celsius	°C

SYMBOL	WHEN YOU KNOW	MULTIPLY BY	TO FIND	SYMBOL
ILLUMINATION				
fc	foot-candles	10.76	lux	lx
fl	foot-Lamberts	3.426	candela/m^2	cd/m^2

SYMBOL	WHEN YOU KNOW	MULTIPLY BY	TO FIND	SYMBOL
FORCE and PRESSURE or STRESS				
Lbf*	poundforce	4.45	newtons	N
kip	kip force	1000	pounds	lbf
lbf/in^2 (psi)	poundforce per square inch	6.89	kilopascals	kPa
ksf	kips per square foot	0.04788	Megapascals	Mpa
tsf	tons per square foot	0.09576	Megapascals	Mpa

APPROXIMATE CONVERSIONS TO ENGLISH UNITS

SYMBOL	WHEN YOU KNOW	MULTIPLY BY	TO FIND	SYMBOL
LENGTH				
mm	millimeters	0.039	inches	in
m	meters	3.28	feet	ft
m	meters	1.09	yards	yd
km	kilometers	0.621	miles	mi

SYMBOL	WHEN YOU KNOW	MULTIPLY BY	TO FIND	SYMBOL
AREA				
mm^2	square millimeters	0.0016	square inches	in^2
m^2	square meters	10.764	square feet	ft^2
m^2	square meters	1.195	square yards	yd^2
ha	hectares	2.47	acres	ac
km^2	square kilometers	0.386	square miles	mi^2

SYMBOL	WHEN YOU KNOW	MULTIPLY BY	TO FIND	SYMBOL
VOLUME				
mL	milliliters	0.034	fluid ounces	fl oz
L	liters	0.264	gallons	gal
m^3	cubic meters	35.314	cubic feet	ft^3
m^3	cubic meters	1.307	cubic yards	yd^3

SYMBOL	WHEN YOU KNOW	MULTIPLY BY	TO FIND	SYMBOL
MASS				
g	grams	0.035	ounces	oz
kg	kilograms	2.202	pounds	lb
Mg (or "t")	megagrams (or "metric ton")	1.103	short tons (2000 lb)	T

SYMBOL	WHEN YOU KNOW	MULTIPLY BY	TO FIND	SYMBOL
TEMPERATURE (exact degrees)				
°C	Celsius	1.8C+32	Fahrenheit	°F

SYMBOL	WHEN YOU KNOW	MULTIPLY BY	TO FIND	SYMBOL
ILLUMINATION				
lx	lux	0.0929	foot-candles	fc
cd/m^2	candela/m^2	0.2919	foot-Lamberts	fl

SYMBOL	WHEN YOU KNOW	MULTIPLY BY	TO FIND	SYMBOL
FORCE and PRESSURE or STRESS				
N	newtons	0.225	poundforce	lbf
kPa	kilopascals	0.145	poundforce per square inch	lbf/in^2

*SI is the symbol for International System of Units. Appropriate rounding should be made to comply with Section 4 of ASTM E380. (Revised March 2003)

TECHNICAL REPORT DOCUMENTATION PAGE

1. Report No.	2. Government Accession No.	3. Recipient's Catalog No.

4. Title and Subtitle
Phase III: Implementation of Shallow Foundations on Florida Limestone in FB-MultiPier

5. Report Date
July 2026

6. Performing Organization Code

7. Author(s)
Michael Rodgers, Scott Wasman, Michael Faraone, Anand Patil, Michael McVay, Kunyu Yang, Suchana Podder, Mayesha Islam

8. Performing Organization Report No.

9. Performing Organization Name and Address
University of Florida – Dept. of Civil and Coastal Engineering
Engineering School of Sustainable Infrastructure and Environment
365 Weil Hall – P.O. Box 116580
Gainesville, FL 32611-6580

10. Work Unit No. (TRAIS)

11. Contract or Grant No.
BED31-977-17

12. Sponsoring Agency Name and Address
Florida Department of Transportation
605 Suwannee Street, MS 30
Tallahassee, FL 32399

13. Type of Report and Period Covered
Final Report
4/2023 – 7/2026

14. Sponsoring Agency Code

15. Supplementary Notes

16. Abstract:
The study highlights the implementation of shallow foundation analysis and design into the finite element software FB-MultiPier. Key details of the report are: i) Bearing capacity, settlement, and passive resistance of shallow foundations in Florida limestone are characterized with a graphical user input/output FEM software; ii) Bearing capacity of rigid rock using the Hoek-Brown method, iii) Strength envelops specific to Florida limestone formations can be selected by the engineer or defined by entry of the intact properties and adjusted recovery or the mass properties; iv) Single limestone layer and limestone over sand cases can be modeled for bearing capacity and settlement; v) Strength envelopes that describe passive resistance (extension q-p space) are discussed and implemented; vi) Lateral resistance on a shallow foundation from base friction or passive soil/rock resistance for normal and oblique loading conditions are considered; vii) Case of inclined loading, i.e. reduced bearing capacity of Florida limestone as a function of the angle of the inclined load (ratio of horizontal to vertical loads) and the limestone friction angle are included; note, using the inclination factor methods for soil in AASHTO LRFD Bridge Design Specifications and may be underpredicted; viii) Bearing capacity of eccentrically loaded shallow foundations on Florida limestone may be estimated using Meyerhof's effective footing width (B' = B – 2e); ix) Implementation outcomes and design example sets covering the full range of shallow foundation design features for bearing capacity, settlement, passive resistance, and base friction are included, as are recommendations for assessing the heterogeneity of limestone with the minimum number of field and lab tests to identify spatial varying unit weight, friction angle, cohesion, modulus in the foundation footprint of the site.

17. Key Words
Shallow Foundation Design, Florida Limestone, Bearing Capacity, Load-settlement response, Passive load-displacement, FB-MultiPier

18. Distribution Statement
No restrictions.

19. Security Classif. (of this report)	20. Security Classif. (of this page)	21. No. of Pages	22. Price
Unclassified	Unclassified	514	

ACKNOWLEDGEMENTS

The researchers would like to thank the Florida Department of Transportation (FDOT) for the financial support to carry out this research; the State Materials Office (SMO) for laboratory testing of all samples; and Districts 4 and 6 materials office for assistance with obtaining additional core samples.

EXECUTIVE SUMMARY

The Florida Department of Transportation (FDOT) has investigated the use of shallow foundations as alternatives to deep foundations (piles, drilled shafts, etc.) for support of bridge piers where limestone is near the ground surface (e.g., south Florida). Florida limestone is very young (average 2 million years) and much of it has been exposed to the weathering process, including frequent past submersions making the formations highly heterogeneous (dry unit weights from 85 pcf to 140 pcf), porous (median porosity 37%), and ductile.

The design of any shallow foundation requires the assessment of bearing capacity (ultimate strength) and its load-settlement response (service limit state). In Phase I (FDOT BDV31-977-51), researchers investigated the strength envelope of several Florida limestone formations as well as existing bearing capacity equations for shallow foundation design. Due to the porous nature of Florida limestone, the research revealed that the strength envelope of the rock is not linear but bilinear, or curved (concave downward). Similarly, both the unconfined compression and triaxial compression results of limestone showed linear stress vs. strain response up to failure and then constant (i.e., bilinear) under further strain (ductile case). In Phase II (FDOT BDV31-977-124) results from full scale load tests validated the bearing capacity equations and developed predictions of load-settlement response for cases of shallow foundations on a single layer and rock over sand. In Phase III, using the stress vs. strain response, and strength envelopes, bearing capacity equations, axial load vs settlement, lateral (passive) load vs displacement, and coulombic bottom friction on shallow foundations were implemented into the existing finite element software, FB-MultiPier. The software includes a user interface for development of a shallow foundation model, soil and rock engineering property input as well as analysis and subsequent graphical view of results (forces, stresses and displacements) within the structure and supporting soil and rock. A user can select from a database of engineering properties and relationships for established strength envelopes for Anastasia, Miami, Fort Thompson, Key Largo, Hawthorn, and Ocala formations, or enter specific user defined properties. Examples of shallow foundation bearing capacity for concentric, eccentric, and inclined load, and passive resistance to oblique loading are included for validation.

Due to the heterogeneous nature of Florida limestone, recommendations are made about the importance of assessing site spatial variability in the design of shallow foundations (e.g., differential settlement due to spatial varying modulus). Significant recommendations are included for property assessment through lab (e.g. triaxial, moisture content, total and dry unit weight), field invasive (e.g., measuring while drilling (MWD), coring) or non-invasive methods (e.g., Seismic full-waveform inversion (FWI) tomography). Also, the user needs to determine the mass properties of limestone for a site based on intact properties and the adjusted core recoveries, as well as accurately measure natural moisture content for bulk dry unit weight. The latter includes immediately (within a week) testing cores in their natural moisture content state or appropriately storing core boxes in a moisture room to retain natural moisture.

TABLE OF CONTENTS

LIST OF FIGURES

LIST OF TABLES

CHAPTER 1
INTRODUCTION

The Florida Department of Transportation (FDOT) has investigated the use of shallow foundations as alternatives to deep foundations (piles, drilled shafts, etc.) for support of bridge piers when limestone is near the ground surface (e.g., south Florida). Two research projects comprise the investigation: 1) FDOT BDV31-977-51 a Phase I investigation of the strength envelopes of several Florida limestone formations that established bi-linear strength envelopes based on dry unit weight (porosity) and formation (e.g., near-surface carbonate rock like Anastasia, Miami, Fort Thompson, Key Largo, Hawthorn, and Ocala formations). From that, bearing capacity equations for surface and embedded square, rectangular, and strip footings were developed that capture the bi-linear nature of the limestone strength. 2) FDOT BDV31-977-124: a Phase II investigation where the bearing capacity equations from Phase I were validated with three full scale load tests, load-settlement response prediction for single layer and rock over sand cases. All field load tests involved collecting core samples and developing the bi-linear stress-strain relationship (initial modulus and secant modulus at 2% strain) of the rock, as well as the importance of assessing site spatial variability (through lab and field invasive and non-invasive methods) around and beneath the shallow foundations. For instance, the latter was needed when assessing the mass properties of limestone as well as determining the CV of rock's modulus. It was also recommended that changes to core sample storage occur in order to correctly measure the bulk dry unit weight of samples.

The objectives of this project (Phase III) were to implement new shallow foundation analysis and design features and user-interface (UI) controls into the FB-MultiPier software package, and to develop corresponding software documentation. The objectives correspond to thrusts in the following areas:

1. Implementation of the Florida limestone bearing capacity equations (Phase I) to facilitate predictions of shallow foundation capacities in design applications for Florida formations.
2. Implementation of nonlinear load-settlement analysis for bearing on Florida limestone (Phase II) so that distributions of internal forces throughout bridge substructures and pressures that develop in the underlying limestone can be predicted.
3. Development and implementation of lateral resistance of shallow foundations under uni-directional and bi-directional loading, which is required for stability of the numerical model.
4. Investigation of the effects of inclined and eccentric loads applied to shallow foundations.
5. Documentation of multiple sets of design examples for the four thrusts areas (above) within the FEA software manual.

To address these objectives, this report is organized as follows:

- Chapter 2: Implementation of Strength Envelope methods developed in the Phase I and Phase II.
- Chapter 3: Implementation of non-linear load settlement analysis for homogeneous and heterogeneous (layered limestone over sand).
- Chapter 4: Development and implementation of passive force deformation for non-oblique and oblique loading.
- Chapter 5: Investigation of inclined and eccentric loads on limestone bearing capacity.
- Chapter 6: Documentation of outcomes and feature sets.
- Chapter 7: Summary, Conclusions and Recommendations.

The study highlights the following key details: i) the analysis and design of shallow foundations on Florida limestone for bearing capacity, settlement, and passive resistance that was implemented into FB-MultiPier; ii) Strength envelops specific to Florida limestone formations can be selected by the engineer or defined by entry of the intact properties and adjusted recovery or the mass properties; iii) Commonly encountered layering at shallow depths of single limestone layer and limestone over sand cases can be modeled for bearing capacity and settlement; iv) Strength envelopes for passive resistance can be defined with parameters characterizing limestone stress behavior at conditions where the horizontal stress is greater than vertical stress (extension q-p space); v) Lateral resistance on a shallow foundation can be analyzed with base friction, side friction and passive resistance springs for oblique loading conditions; vi) Inclined loading on a shallow foundation on Florida limestone results in a reduced bearing capacity as a function of the angle of the inclined load (ratio of horizontal to vertical loads) and the limestone friction angle and may be underpredicted using the inclination factor methods for soil in AASHTO LRFD Bridge Design Specifications; vii) Bearing capacity of eccentrically loaded shallow foundations on Florida limestone may be estimated using Meyerhof's effective footing width ($B' = B - 2e$); viii) Hand solutions for all design cases are compared to software results and are featured in the user manual in FB-MultiPier.

CHAPTER 2
IMPLEMENTATION OF STRENGTH ENVELOPES

2.1 Introduction

A shallow foundation design in Florida limestone typically involves either homogeneous rock or rock-over-sand layer conditions. Since the median porosity of Florida limestone is quite high (>37%), the rock is ductile, and exhibits bilinear stress-strain response (linear up to yield/failure) with a bilinear strength envelope (e.g., Miami Formation, Figure 2-1) having intercept of a, initial slope a, the onset of crushing, p_p, and second slope, w for a specified bulk dry unit weight (g_{dt} = 90, 95, 100, …130 pcf). Users may generally use default strength parameters by formation with specification of the bulk dry unit weight, or user-supplied values from laboratory triaxial testing.

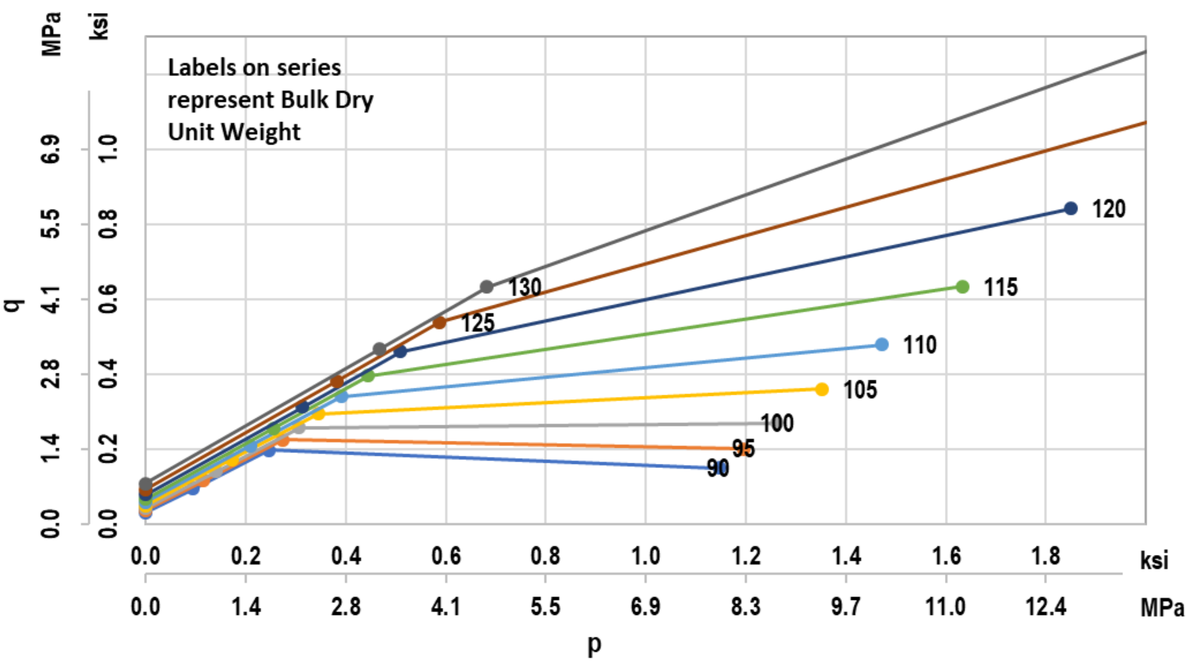

Figure 2-1 Bilinear strength envelope of Florida limestone.

Due to the rock's bilinear stress-strain and strength envelope, the load-settlement of the shallow foundation may be represented as a linear, function of E_i (initial Young's Modulus), up to bearing capacity, Q_u, Figure 2-2. In the case of homogeneous rock, further loading leads to unlimited deformation (Figure 2-2a), whereas rock over sand exhibits punching shear of the rock along with further compression (Figure 2-2b) of the rock as a function of the secant Young's Modulus (E_s) of both the rock and the sand layers. Note, the punching shear failure of the rock is a function of the thickness of the rock beneath the footing and the Young's Modulus Ratio of the rock to the sand layer. A description of bearing capacity equations and required parameters are in the following section.

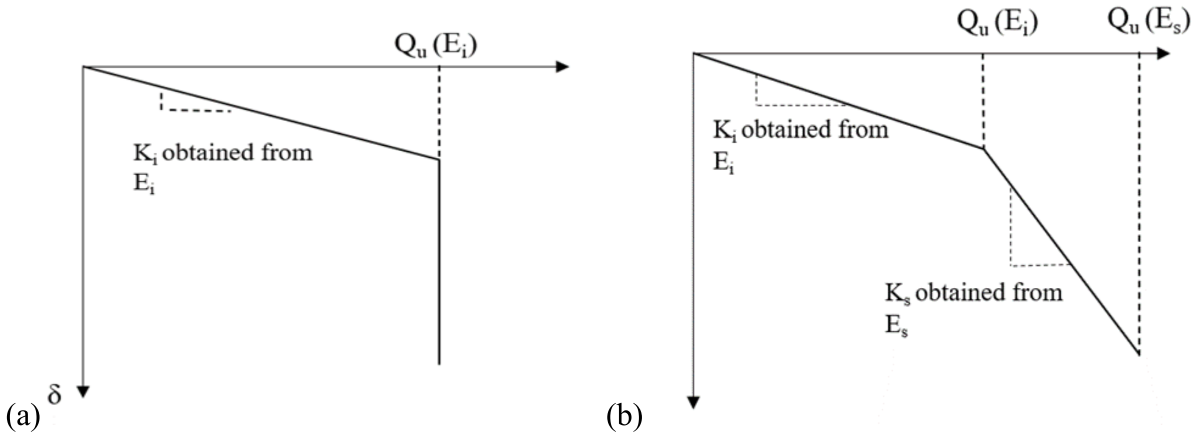

Figure 2-2 Shallow foundation load-settlement: a) homogeneous rock, and b) rock over sand.

2.2 Analysis Approaches

The most general bearing capacity equations developed specifically for Florida Limestone are those given in FDOT Phase I (BDV31-977-51) report: "Strength Envelopes for Florida Rock and Intermediate Geomaterials." It covers multiple shapes (2D and 3D), and embedment for homogeneous (Figure 2-3a) as well as layered (rock over sand) cases (Figure 2-3b). It doesn't cover eccentric loading; consequently, the user must first compute the resultant force on the footing, followed by the eccentricity and the equivalent footing size (B′ & L′) and supply them as new input dimensions to FB-MultiPier.

In the case of abutment footings (2D strip) in homogeneous rock (no layering), the user may also use the Carter and Kulhawy bearing capacity equation (no embedment factor) which employs Hoek and Brown strength criterion with a GSI value. Likewise, for eccentric loading, the user must compute an equivalent footing width (B′) for input to FB-MultiPier. A discussion of each bearing capacity method follows.

2.2.1 FDOT Bearing Capacity Method

The general bearing capacity (Force) is given by Equation 2-1 which accounts for bilinear strength envelope, shape, embedment and homogeneous or layered (rock over sand) conditions. In Equation 2-1, Q_{u1} (Equation 2-2) is the capacity (Force) based on the footing's equivalent stress path intersecting the strength envelope before the onset of microcracking (p_p). Depending on strength parameters and microcracking pressure (p_p), the equivalent stress path may intersect the second slope, and a lower capacity, Q_{u2} (Equation 2-3) may be obtained. Note, cohesion terms in Q_{u1} and Q_{u2} are different, i.e., N_c and N'_c. Whichever force is smaller (Q_{u1} or Q_{u2}) is the footing's bearing capacity (Force). In Equation 2-1 and Equation 2-2, N_q (Equation 2-12) and q (Equation 2-11) are influences of embedment. The terms n (Equation 2-4) and ξ (Equation 2-5) are corrections for the footings' size and shape. Finally, the term N_R is the correction for layering (rock over sand). In the case of homogeneous (Figure 2-3a), thick rock,

N_R is 1, otherwise it's greater than 1 and is a function of rock thickness (T, Figure 2-3b) below the footing to the sand layer, and the modulus ratio of soil to rock layers (E_{soil} / E_{rock}), Equation 2-6 & Equation 2-7.

$Q_u = \min(Q_{u1}, Q_{u2}) \times \xi / N_R$ Equation 2-1

$Q_{u1} = n \times c \times N_c + q \times N_q$ Equation 2-2

$Q_{u2} = n \times [c \times N'_c + p_p \times N_g] + q \times N_q$ Equation 2-3

$n = \left(\frac{4}{\text{B in meter}}\right)^{(-0.055)}$ or $n = \left(\frac{4}{0.3048\text{B in ft}}\right)^{(-0.055)}$ Equation 2-4

ξ= shape factor = $1 + 0.245 \left(\frac{B}{L}\right)^{(0.66)}$ Equation 2-5

N_R = Rock thickness reduction factor Equation 2-6

$N_R = 0.86 * R^{-0.25}$ if $R < 0.3$

$N_R = 1.2 - 0.1 \times R$ if R^3 0.3

$R = T^2 E_{soil} / E_{rock}$, limit R to 2.0 Equation 2-7

T = Rock thickness in meter (if T is in ft, then $R = 0.093\, T^2 E_{soil} / E_{rock}$)

E_{soil} / E_{rock} = Mass modulus ratio of soil and rock layers

$N_c = \frac{1.8 \cos\varphi}{0.8 - \sin j}$ Equation 2-8

$N'_c = \frac{1.8 \cos\varphi}{0.8 - \sin\omega}$ Equation 2-9

$N_g = \frac{1.8\,[\sin\varphi - \sin\omega]}{0.8 - \sin\omega}$ Equation 2-10

$q = \gamma' \times D_f$ Equation 2-11

$N_q = (1.53 \times \frac{p_p}{\sigma_a} - 10) \times (3 \times \sin\varphi - 1)$ Equation 2-12

σ_a = Sea level standard atmospheric pressure

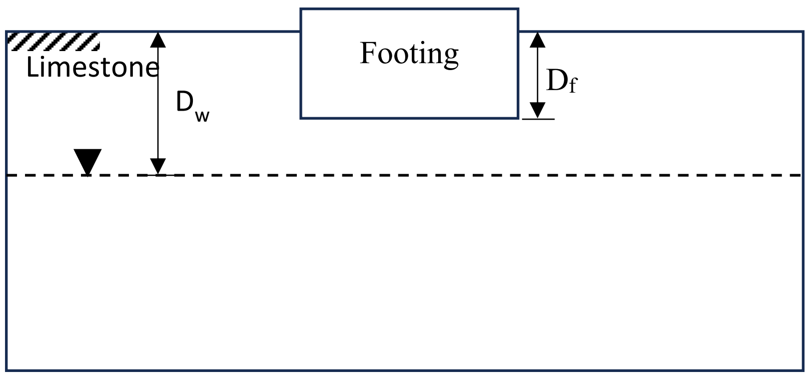

(a)

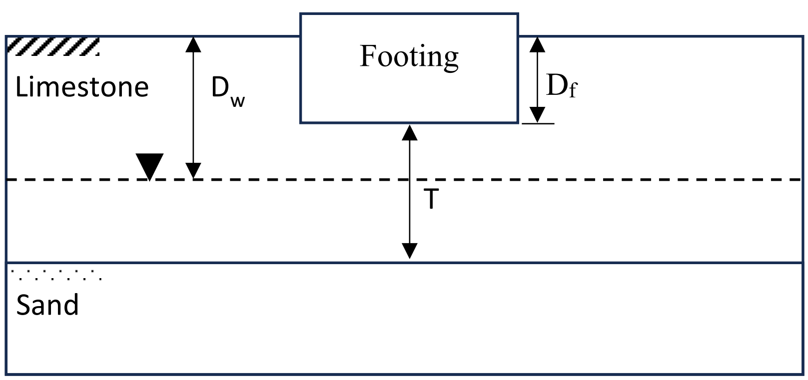

(b)

Figure 2-3 Schematic drawing of subsurface: a) single homogeneous layer and b) rock-over-sand subsurface.

2.2.2 Carter and Kulhawy Method

Carter and Kulhawy (1988) developed a lower bound solution for the bearing capacity of strip footings residing on weightless rock mass by using the nonlinear Hoek-Brown (Hoek and Brown, 1980) strength criteria. The Carter and Kulhawy bearing method is widely used throughout the United States and worldwide, and it is referenced in multiple national and international publications. Hoek-Brown (Hoek and Brown, 1980) strength criteria was originally developed for the jointed rock with brittle (rupture) failure and can be expressed as:

$$\sigma_1 = \sigma_3 + q_u(m\frac{\sigma_3}{q_u} + s)^a$$ Equation 2-13

where,

s_1 and s_3 = major and minor principal stresses.

s = rock mass discontinuity factor.

$$s = e^{(GSI-100)/(9-3D)}$$ Equation 2-14

GSI is the Geological Strength Index, which approaches 80 to 100 for intact or massive rock (blocky, very well interlocked undisturbed rock mass), and reduces to as low as 10 for very weathered, heavily broken rock mass.

$$m = m_i\, e^{(GSI-100)/(28-14D)}$$ Equation 2-15

m_i ranges from approximately 8±3 to 12±3 for different carbonate rocks (Table 2). A typical value of m_i = 10 for Florida carbonate rocks is recommended.

D = disturbance factor caused by the rock removal methodology. For shallow foundation excavation, D is set as 0 in the program.

$a = 0.5 + (e^{-GSI/15} - e^{-20/3})/6$; a is set as 0.5 in the program.

Table 2-1 Recommend values of the constant m_i for carbonate rocks (after Marinos and Hoek, 2000).

Texture	Coarse	Medium	Fine	Very Fine
Rock	Crystalline Limestone	Sparitic Limestone	Micritic Limestone	Dolomite
m_i	12 ± 3	10 ± 5	8 ± 3	9 ± 3

For a strip footing on the ground surface, as shown in Figure 2-4, Carter and Kulhawy divided the rock mass beneath the footing into two zones: passive zone I and active zone II. In zone I, the vertical stress is assumed to be zero (no surcharge), then the horizontal stress (major principal stress) is equal to $q_u s^a$ based on the Equation 2-13. In zone II, the horizontal stress (minor principal stress) equals to $q_u s^a$ because of limit equilibrium, the vertical stress (bearing stress, Q_u) is assessed by using Equation 2-13 and expressed as follows:

$$Q_u = \left[\sqrt{s} + \sqrt{m\sqrt{s} + s}\right] q_u$$ Equation 2-16

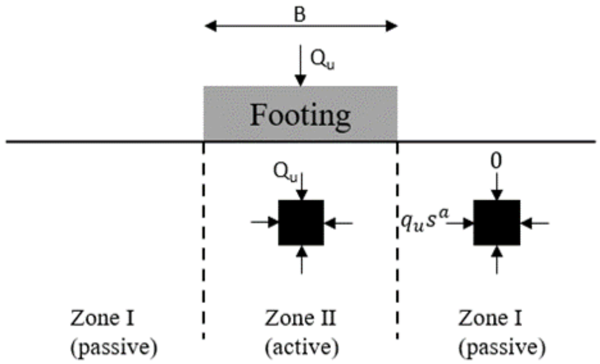

Figure 2-4 Active and passive zones under a footing (adapted from Carter and Kulhawy, 1988).

2.3 Key Parameters

The direct inputs of Florida bearing analysis (Equation 2-1 and Equation 2-2) are mass strength parameters: c_m, φ_m, P_p, ω_m. The mass strength parameters are assessed by using a site-specific adjusted recovery (REC) and the intact strength parameters, as shown in Table 2. The key indexes of Florida limestone are the bulk dry unit weight/porosity and formations (carbonate content and crystalline structure), which are directly correlated to the intact strength and stiffness parameters. Users can use the intact properties shown in Table 2-2 as a first approximation of the bearing capacity analyses or generate a site-specific strength envelope from laboratory tests (Appendix F of Phase I final report (McVay et al., 2019)) and supply the intact strength parameters (c_i, φ_i, P_p, ω_i) for a site-specific bearing capacity. Equation 2-17 and Equation 2-18 are used for the evaluation of mass strength parameters from intact strength parameters in FB-MultiPier. However, users can directly input the customized mass strength parameters for a bearing analysis. For the rock-over-sand condition, additional parameters (mass modulus of rock and sand layer, E_{soil} / E_{rock}, rock layer thickness, T) are needed for the rock-over-sand reduction factor.

$$q_{mass} = q_{intact} \times \text{REC} \qquad \text{Equation 2-17}$$

$$p_{mass} = p_{intact} \qquad \text{Equation 2-18}$$

Due to the weathering and varying degrees of submersion in the past, Florida limestone is naturally high variability and exhibits high coefficient of variation (CV). In the load tests of the Phase II effort (BDV31-977-124), CV of bulk dry unit weight is around 0.1 and CV of modulus in rock layer in larger than 1. The geometric mean bulk dry unit weight is recommended to characterize the homogeneous rock layer and the median bulk dry unit weight is recommended to characterize the rock layer for rock-over-sand subsurface.

For the Florida bearing analyses, users need to specify homogeneous and rock-over-sand conditions. For each specified condition, three options are presented to ensure maximum flexibility. The first option is that users need to select the formation and bulk dry unit weight with a site-specific recovery, the recommended intact strength parameters (Table 2-2) will be used and reduced to mass strength parameters for the bearing analysis. The second option is that users can supply the intact strength parameters (c_i, φ_i, P_p, ω_i) with a site-specific recovery and the third option is that users directly input the mass strength parameters (c_m, φ_m, P_p, ω_m). For the rock-over-sand condition, mass modulus of rock and sand layer are needed additional inputs. In addition, Carter and Kulhawy (1988) method is implemented in FB-MultiPier for the bearing capacity of strip footing on the ground surface. The evaluation of mass strength parameters under each condition will be discussed in the follow sections.

Table 2-2 Intact properties of Florida limestone in tau-sigma space and p-q space.

Formation	γ_{dt}, (pcf)	c_i, (psi)	φ_i, (deg)	$\sigma_{peak\ i}$, (psi)	ω_i, (deg)	a_i, (psi)	α_i, (deg)	Pp, (psi)	β_i, (deg)
Miami Limestone	90	42.0	42.2	444	-3.0	31.1	33.9	247	-3
	95	49.9	43.2	498	-1.4	36.4	34.4	274	-1.4
	100	58.9	44.2	562	0.8	42.2	34.9	306	0.8
	105	70.9	45.3	640	3.7	49.9	35.4	345	3.7
	110	84.1	46.4	730	7.3	58	35.9	390	7.2
	115	99.9	47.3	840	11.6	67.8	36.3	445	11.4
	120	118.8	48.2	969	16.6	79.2	36.7	510	15.9
	125	141.8	49.1	1126	22.2	92.8	37.1	588	20.7
	130	169.0	50.1	1314	28.5	108.4	37.5	682	25.5
	135	202.5	51.1	1541	35.4	127.1	37.9	795	30.1
Anastasia Limestone	90	52.0	37.4	416	-6.7	41.3	31.3	233	-6.7
	95	62.1	38.7	474	-6.7	48.5	32	262	-6.7
	100	74.0	39.8	542	-6.7	56.9	32.6	296	-6.7
	105	88.1	40.9	624	-6.7	66.6	33.2	337	-6.7
	110	104.9	41.8	722	-6.7	78.2	33.7	386	-6.7
	115	124.9	42.8	839	-6.7	91.6	34.2	445	-6.7
	120	149.1	44.0	980	-6.7	107.2	34.8	515	-6.7
	125	178.3	45.1	1151	-4.3	125.9	35.3	600	-4.3
	130	211.8	45.9	1354	1.6	147.3	35.7	702	1.6
	135	253.1	47.0	1603	10.9	172.5	36.2	826	10.7
	140	301.3	48.0	1904	23.7	201.8	36.6	977	21.9
Hawthorn Limestone	85	26.0	41.8	368	1.4	19.4	33.7	209	1.4
	90	31.0	43.0	408	2.4	22.7	34.3	229	2.4
	95	37.0	44.0	452	4.1	26.6	34.8	251	4.1
	100	44.0	45.1	506	6.2	31.1	35.3	278	6.2

Formation	γ_{dt}, (pcf)	c_i, (psi)	φ_i, (deg)	$\sigma_{peak\ i}$, (psi)	ω_i, (deg)	a_i, (psi)	α_i, (deg)	Pp, (psi)	β_i, (deg)
	105	52.9	45.9	568	9.0	36.8	35.7	309	8.9
	110	63.1	47.0	642	12.3	43	36.2	346	12
	115	75.0	48.0	728	16.1	50.2	36.6	389	15.5
	120	88.8	48.9	832	20.5	58.4	37	441	19.3
	125	106.0	49.9	956	25.5	68.3	37.4	503	23.3
	130	126.1	50.9	1104	31.1	79.6	37.8	577	27.3
	135	149.8	51.6	1279	37.1	93	38.1	665	31.1
Key Largo Limestone	65	31.0	38.1	340	-23.2	24.4	31.7	195	-21.5
	70	36.9	39.2	378	-19.7	28.6	32.3	214	-18.6
	75	43.9	40.3	424	-16.3	33.5	32.9	237	-15.7
	80	51.9	41.4	478	-12.8	38.9	33.5	264	-12.5
	85	62.0	42.6	542	-9.4	45.6	34.1	296	-9.3
	90	74.0	43.6	618	-5.9	53.6	34.6	334	-5.9
	95	88.1	44.7	708	-2.5	62.7	35.1	379	-2.5
	100	104.9	45.5	815	1.0	73.5	35.5	433	1
	105	125.0	46.6	946	4.4	85.9	36	498	4.4
	110	148.8	47.5	1099	7.9	100.5	36.4	575	7.8
	115	177.3	48.7	1288	11.4	117.1	36.9	669	11.2
	120	210.4	49.4	1513	14.8	137	37.2	782	14.3
Shallow Fort Thompson Limestone	90	22.9	38.7	314	-23.6	17.9	32	182	-21.8
	95	28.0	39.9	347	-15.8	21.5	32.7	198	-15.2
	100	32.9	40.9	384	-7.9	24.9	33.2	217	-7.8
	105	39.0	42.0	428	-0.1	29	33.8	239	-0.1
	110	46.9	43.0	480	7.8	34.3	34.3	265	7.7
	115	55.9	44.0	542	15.7	40.2	34.8	296	15.1
	120	66.0	45.1	614	23.4	46.6	35.3	332	21.7
Ocala Limestone	85	9.1	30.8	188	13.5	7.8	27.1	119	13.1
	90	17.1	35.4	254	16.6	13.9	30.1	152	15.9
	95	28.2	37.6	320	19.3	22.3	31.4	185	18.3
	100	43.0	38.0	386	21.8	33.9	31.6	218	20.4
	105	62.7	37.1	454	24.0	50	31.1	252	22.1

2.3.1 Florida Limestone (Homogeneous)

2.3.1.1 Formation, Bulk Dry Unit Weight and Adjusted Rock Recovery

Phase I and II conducted more than 250 triaxial tests and more than 3,000 unconfined compression tests and split tensile tests (summarized in Table 2). Users can input data from Table 2 for a first approximation bearing capacity by selecting the formation and bulk dry unit weight with a site-specific REC. In Table 2-3, an example is presented where the data from Table 2-2 and a REC of 80 % is used.

Table 2-3 Intact and mass strength parameters conversion from formation, bulk dry unit weight and REC.

Formation	-	Miami Limestone
REC	%	80
γ_{dt}	pcf	100
Intact Properties (Output)	c_i, psi	58.9 (Interpolated from Table 2.2 based on γ_{dt})
	φ_i, °	44.2 (Interpolated from Table 2.2 based on γ_{dt})
	$\sigma_{peak\ i}$, psi	562 (Interpolated from Table 2.2 based on γ_{dt})
	ω_i, °	0.8 (Interpolated from Table 2.2 based on γ_{dt})
	a_i, psi	42.2 (Interpolated from Table 2.2 based on γ_{dt})
	α_i, °	34.9 (Interpolated from Table 2.2 based on γ_{dt})
	P_p, psi	306 (Interpolated from Table 2.2 based on γ_{dt})
	β_i, °	0.8 (Interpolated from Table 2.2 based on γ_{dt})
Mass Properties (Output)	a_m, psi	$a_m = REC*a_i = 33.8$
	α_m, °	$\alpha_m = \mathrm{atan}(REC*\tan\alpha_i) = 29.2$
	P_p, psi	$P_p = P_p = 306$
	β_m, °	$\beta_m = \mathrm{atan}(REC*\tan\beta_i) = 0.6$
	c_m, psi	$c_m = \frac{a_m}{\cos\varphi_m} = 40.7$
	φ_m, °	$\varphi_m = \mathrm{asin}(\tan\alpha_m) = 33.9$
	$\sigma_{peak\ m}$, psi	$\sigma_{peak\ m} = P_p + \tan\alpha_m * P_p + a_m = 511$
	ω_m, °	$\omega_m = \mathrm{asin}(\tan\beta_m) = 0.6$

2.3.1.2 Intact Strength and Recovery (Rock Core)

For a design project, it is recommended to establish site-specific strength envelopes (Appendix F of Phase I final report (McVay et al., 2019)), a minimum of 10 unconfined compression strength test samples, 10 split tensile test samples, 8 to 16 triaxial test samples to estimate p_p and the second slope, w. With the site-specific intact strength parameters and REC, the mass strength parameters can be obtained by using Table 2-4 and bearing capacity analysis of a footing on Florida homogeneous limestone can be performed in FB-MultiPier.

Table 2-4 Intact and mass strength parameters conversion from intact strength parameters.

REC (Input)	%	80
Intact properties (Input)	c_i, psi	58.9
	φ_i, °	44.2
	P_p, psi	306
	ω_i, °	0.8
Intact properties (Output)	a_i, psi	$a_i = c^*\cos(\varphi_i) = 42.2$
	α_i, °	$\alpha_i = \text{atan}(\sin(\varphi_i)) = 34.9$
	$\sigma_{peak\ i}$, psi	$\sigma_{peak\ i} = a_i + \tan(\alpha_i)^*P_p + P_p = 562$
	β_i, °	$\beta_i = \text{atan}(\sin(\omega_i)) = 0.8$
Mass Properties (Output)	a_m, psi	$a_m = REC^*a_i = 33.8$
	α_m, °	$\alpha_m = \text{atan}(REC^*\tan\alpha_i) = 29.2$
	P_p, psi	$P_p = P_p = 306$
	β_m, °	$\beta_m = \text{atan}(REC^*\tan\beta_i) = 0.6$
	c_m, psi	$c_m = \frac{a_m}{\cos\varphi_m} = 40.7$
	φ_m, °	$\varphi_m = \text{asin}(\tan\alpha_m) = 33.9$
	$\sigma_{peak\ m}$, psi	$\sigma_{peak\ m} = P_p + \tan\alpha_m * P_p + a_m = 511$
	ω_m, °	$\omega_m = \text{asin}(\tan\beta_m) = 0.6$

2.3.1.3 Mass Strength (Rock Mass)

Users can directly input the mass strength parameters (c_m, φ_m, P_p, ω_m), and Equation 2-1 to Equation 2-12 will be used for the bearing analysis of shallow foundation on Florida limestone.

2.3.2 Florida Limestone (Rock Over Sand)

For the rock-over-sand bearing capacity analysis, the rock-over-sand reduction, N_R, is needed. N_R should be calculated using Equation 2-6 and Equation 2-7, which are a function of mass modulus ratio of the sand and rock layer, E_{soil}/E_{rock}, and the rock layer thickness, T (Figure 2-3b). The intact modulus as a function of the bulk dry unit weight for the Miami, Ocala, and Key Largo formations is shown in Figure 2-5. Settlement Plot dialog will be added into FB-MultiPier in Chapter 3 for the load-settlement response. For the mass modulus of the rock layer, the relationship in Figure 2-6 is recommended and it was validated through three full-scale field load tests in Phase II (Rodgers et al., 2022). It is recommended to use the in-situ methods (SPT, PMT, seismic, etc.,) to obtain the mass modulus of the sand layer. In Phase II, Bowles's method (Bowles, 1996) was employed to predict the mass modulus of sand layer, Equation 2-19.

$$E_{sand} = 250\,(N + 15),\ E_{sand} \text{ in kPa} \qquad \text{Equation 2-19}$$

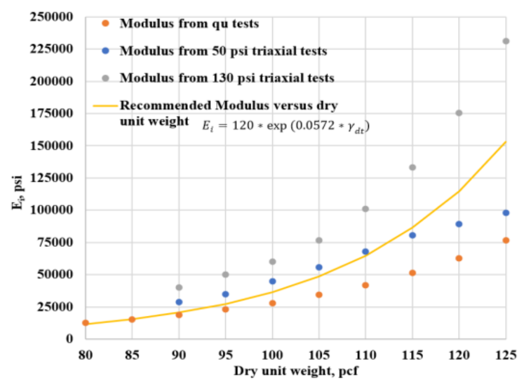

(a)

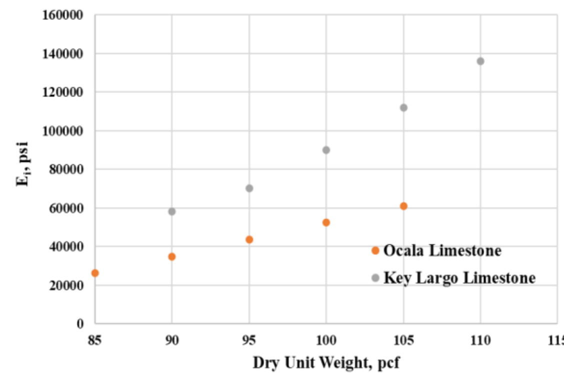

(b)

Figure 2-5 Initial modulus versus dry unit weight: a) Miami limestone, and b) Ocala and Key Largo limestone (limited data).

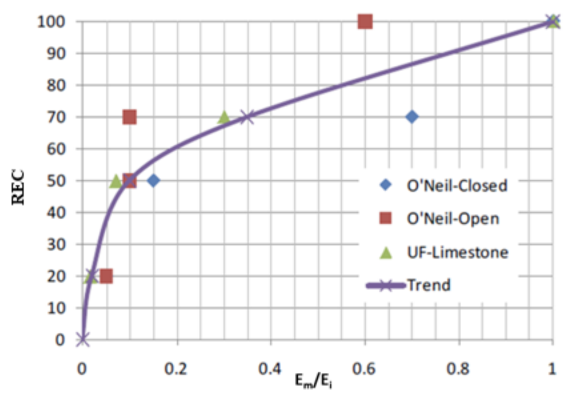

Figure 2-6 REC versus E_m/E_i.

2.3.3 Carter and Kulhawy (Strip Footing)

For Carter and Kulhawy bearing analysis, Equation 2-16 is employed. The strength parameters, s and m can be evaluated using the GSI and m_i, Equation 2-15 and Equation 2-14. For Florida limestone, a typical value $m_i = 10$ is recommended. Please note that this method is only for the case of a plane-strain condition at the ground surface of an infinite rock subsurface.

2.4 FB-MultiPier User-Interface (UI) and Analytical Engine Enhancements

The user-interface and the analytical engine of the FB-MultiPier program is proposed to be updated to implement the shallow foundation analysis feature using the research efforts from the Phase I (BDV31-977-51) and Phase II (BDV31-977-124) projects. The aim is to equip bridge design engineers with the capability to add and analyze a shallow foundation system on a Florida limestone layer beneath a bridge pier. Chapter 2 is focused on the implementation of strength envelopes and the bearing capacity equations for shallow foundation on Florida limestone in homogeneous, & heterogeneous (rock over sand) conditions along with strip foundation on rock using the Hoek and Brown method.

2.4.1 Shallow Foundation Enhancements in FB-MultiPier UI

The FB-MultiPier UI update includes enhancements to the 'Soil' page, including the ability to select axial resistance models for shallow foundation. This feature is only available for pier models with footing embedded in the soil. In other words, access to the shallow foundation features is enabled only when the substructure footing is embedded such that the ground surface elevation for a given substructure is not above the footing base elevation.

Users can modify the footing base elevation by updating either the 'Footing Midplane' elevation or the 'Thickness' input on the 'Footing' page (Figure 2-7). Users can also modify the ground surface elevation using the 'Top of the Layer' input parameter for soil layer 1 on the 'Soil' page (Figure 2-8).

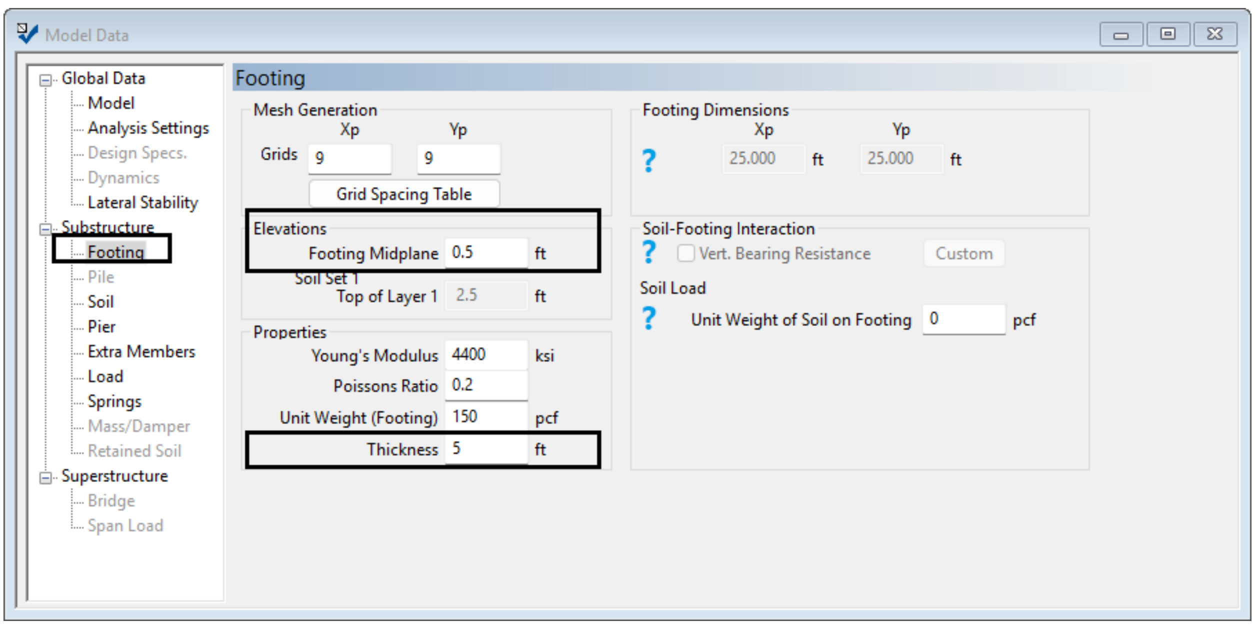

Figure 2-7 'Footing Midplane' and 'Thickness' input on the 'Footing' page.

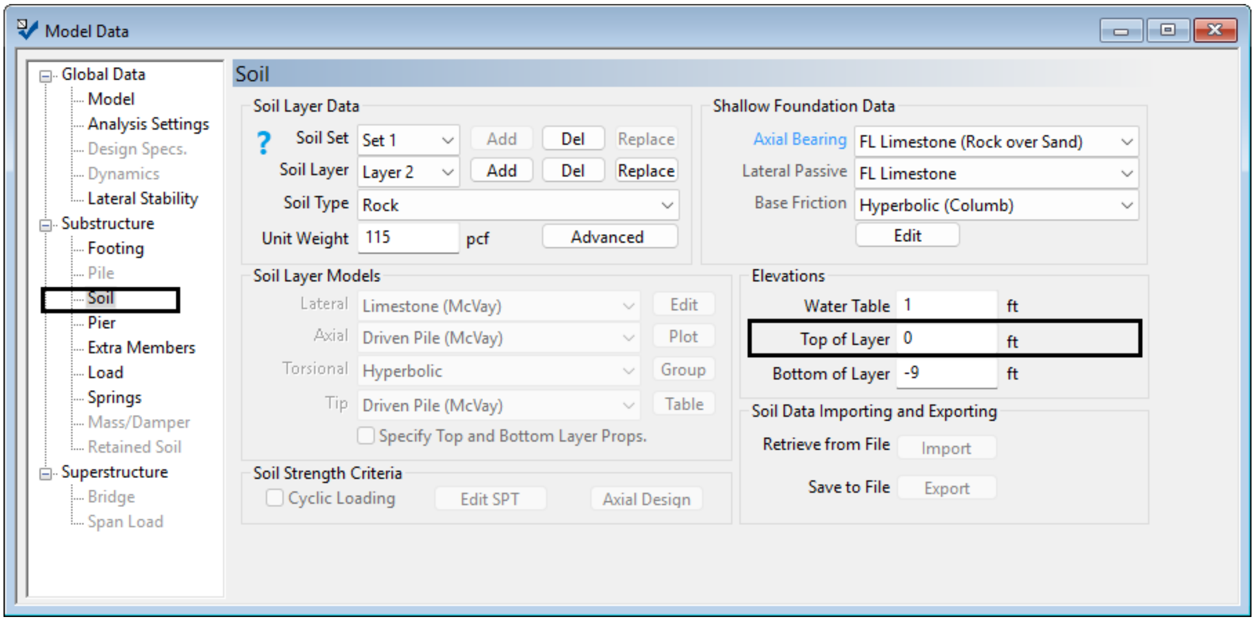

Figure 2-8 ‘Top of Layer’ elevation input on the ‘Soil’ page.

The shallow foundation feature is inactive/disabled if the footing base elevation is above the ground surface elevation (Figure 2-9).

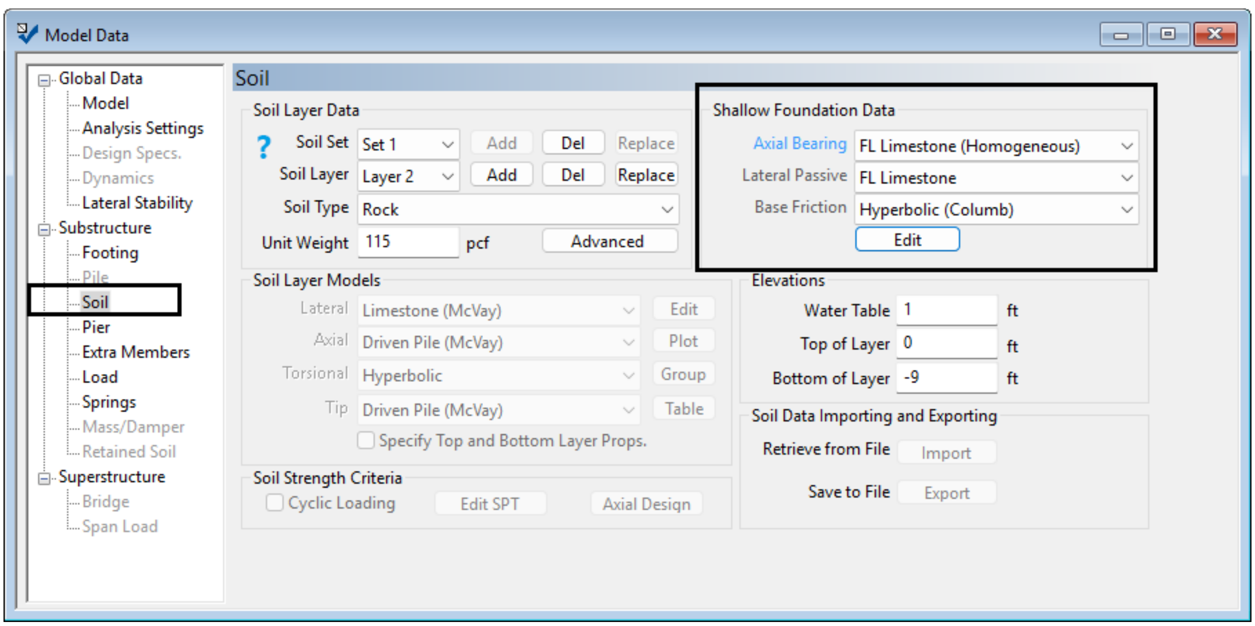

Figure 2-9 Shallow foundation feature is disabled on the ‘Soil’ page.

As discussed before, the shallow foundation feature is only available when the footing is embedded within the soil/rock or resting on the ground surface. The shallow foundation feature is comprised of footing axial bearing, lateral passive, and base friction resistance models (Figure

2-10). Chapter 2 includes the implementation of the strength envelope and bearing capacity equations for axial soil resistance models. Additionally, the implementation of 'Lateral Passive' and 'Base Friction' soil resistance models are part of Chapter 4.

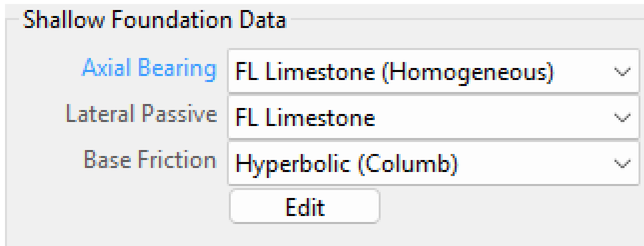

Figure 2-10 'Shallow Foundation Data' frame on the 'Soil' page.

The user can select from available axial bearing soil resistance models using the dropdown control, namely:

1. FL Limestone (Homogeneous)
2. FL Limestone (Rock over Sand)
3. Hoek & Brown (Carter & Kulhawy)
4. Linear (Subgrade)
5. Custom

FL Limestone (Homogeneous) model is available for when the shallow foundation is embedded in the limestone/rock layer. FL Limestone (Rock over Sand) model is available when the shallow foundation is embedded in the limestone/rock layer above a cohesionless layer. After the appropriate axial bearing soil resistance model is selected, click the 'Edit' button (Figure 2-10) on the shallow foundation data frame. This will launch the dialog where additional input data needs to be provided for the selected axial bearing soil resistance model.

2.4.1.1 Axial Bearing Soil Resistance Model: FL Limestone (Homogeneous)

The FL Limestone (Homogeneous) dialog (Figure 2-11) can be accessed when the 'FL Limestone (Homogeneous)' axial bearing soil resistance model is selected from the dropdown (Figure 2-10) on the 'Soil' page. The 'FL Limestone (Homogeneous)' model needs user input parameters to calculate the strength envelope and the bearing capacity, particularly, footing dimensions, and rock properties.

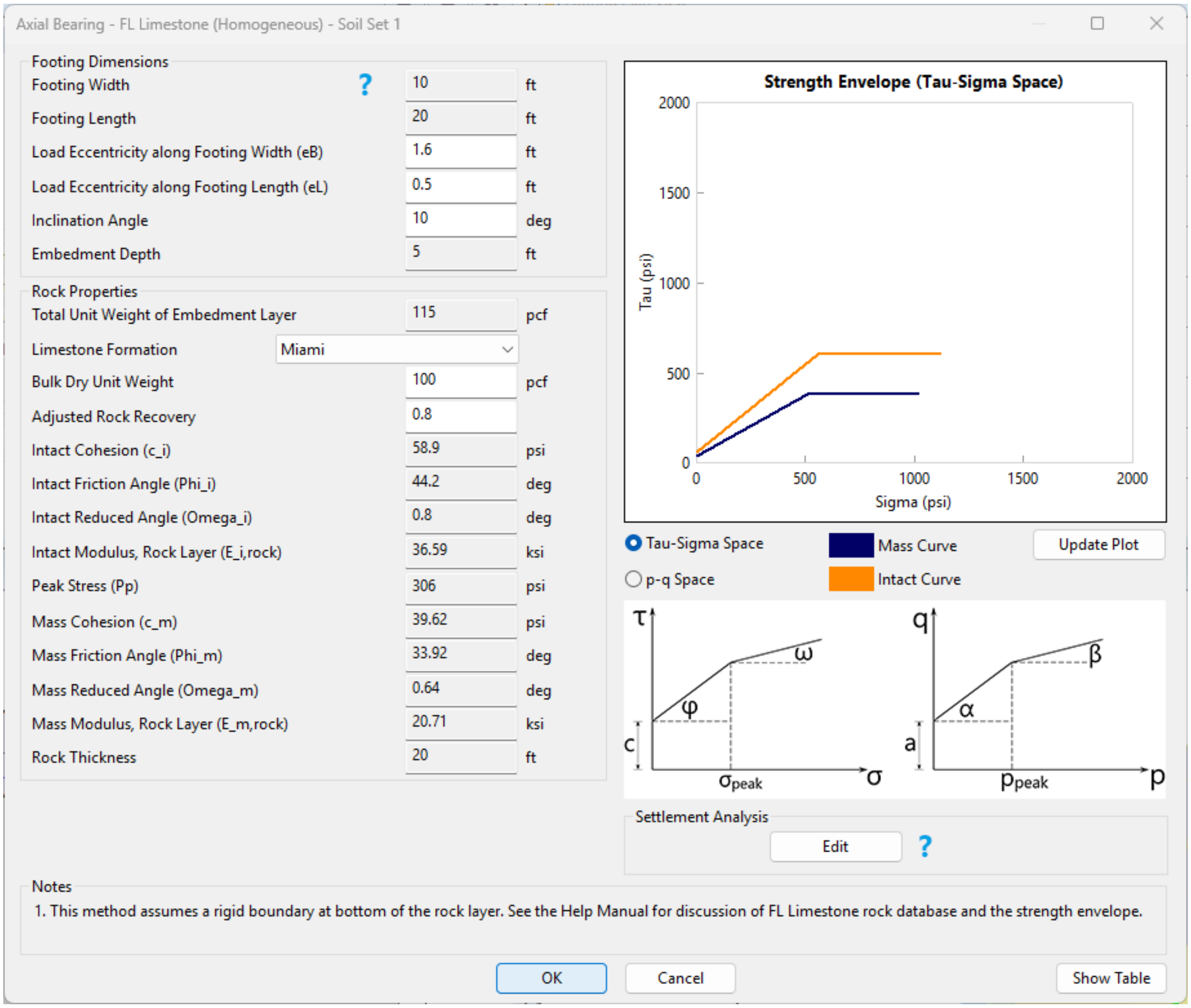

Figure 2-11 FL limestone (homogeneous) dialog with the required key input parameters.

Some footing geometry inputs are read-only on this dialog, and are calculated by the program-based input, namely the following: footing width (B), footing length (L), and embedment depth (D_f). Other input parameters for footing dimensions consist of Load Eccentricity along Footing Width (eB), Load Eccentricity along Footing Length (eL) and Inclination Angle (alpha). The FB-MultiPier UI and analytical engine calculates the effective footing dimensions (B′ and L′) values using the Footing Width (B), Footing Length (L) along with Load Eccentricity (eB, eL), which are subsequently used in the bearing capacity calculation. The user input "Inclination Angle" allows the user to reduce the estimated bearing capacity, based on the "All Formation" factors specified in Chapter 5.

The input parameters for rock properties consist of total unit weight of embedment layer (γ_t), limestone formation, bulk dry unit weight, adjusted rock recovery, intact and mass strength parameters, namely, peak stress (P_p), intact and mass cohesion (c_i and c_m), intact and mass friction angle (φ_i and φ_m), intact and mass reduced angle (ω_i and ω_m), and intact and mass modulus, rock layer (E_i,rock and E_m,rock). These intact and mass strength parameters are used to plot the strength envelopes in tau-sigma space and p-q space.

The Limestone Formation dropdown consists of eight options, namely:

1. Miami
2. Anastasia
3. Hawthorn
4. Key Largo
5. Shallow Fort Thompson
6. Ocala
7. Custom Intact
8. Custom Mass

The user does not have to input all the discussed rock properties. The required input parameters for rock properties depends on one of the options selected within the limestone formation dropdown.

Option 1: When the 'Custom Mass' option is selected from the limestone formation dropdown, only the mass properties, namely, P_p, c_m, φ_m, ω_m and E_m,rock, are enabled (Figure 2-12). whereas the bulk dry unit weight, adjusted rock recovery, and intact strength parameters are not required.

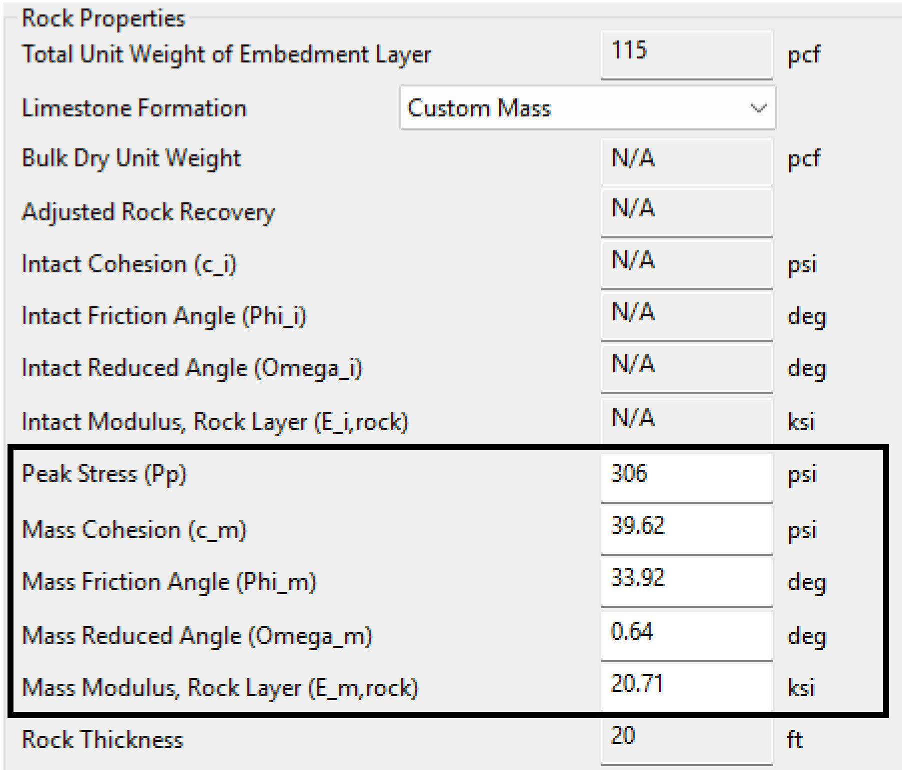

Figure 2-12 ‘Custom Mass’ selection requires input of mass properties.

Option 2: When the ‘Custom Intact’ option is selected from the limestone formation dropdown, only the adjusted rock recovery and intact properties, namely, P_p, c_i, φ_i, ω_i, and E_i,rock, are enabled (Figure 2-13). In this case, adjusted rock recovery and intact strength parameters will be used in Equation 2-17 and Equation 2-18 to calculate the mass strength parameters, which in turn are shown in the respective inactive edit boxes.

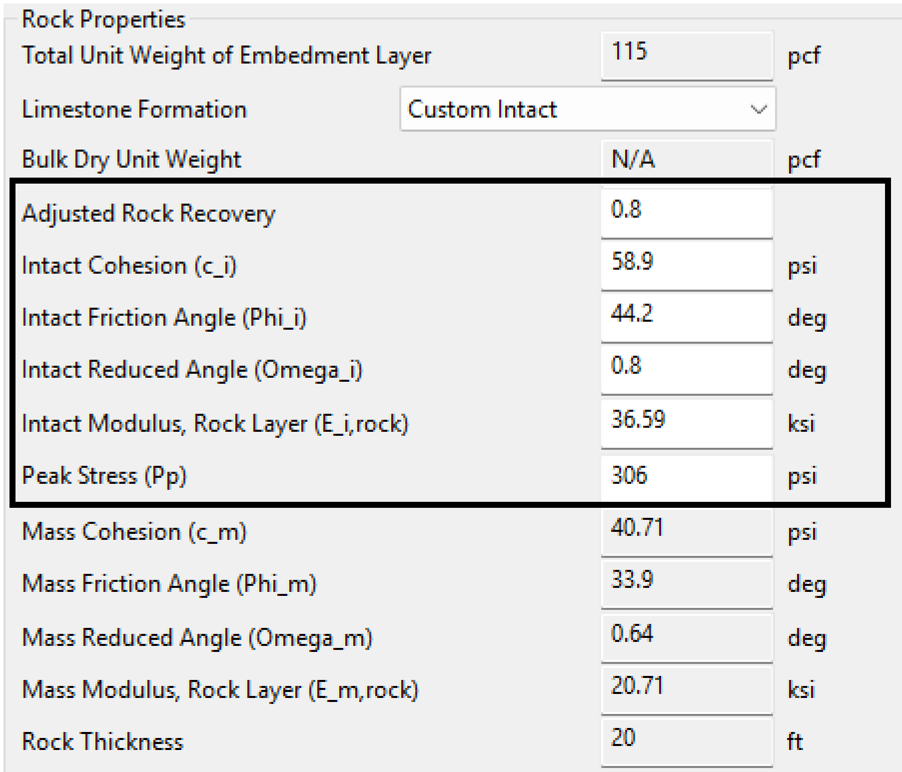

Figure 2-13 ‘Custom Intact’ selection requires adjusted rock recovery and intact properties.

Option 3: Lastly, when any standard limestone formation (i.e. Miami, Anastasia, Hawthorn, Key Largo, Shallow Fort Thompson, or Ocala) is selected from the limestone formation dropdown, only the bulk dry unit weight and adjusted rock recovery are enabled (Figure 2-14). For the given bulk dry unit weight, intact strength parameters in tau-sigma and p-q space are taken from Table 2-2, which is shown in the respective inactive intact properties edit boxes. Additionally adjusted rock recovery along with the intact strength parameters will be used in the Equation 2-17 and Equation 2-18 to calculate the mass strength parameters, which is shown in the respective inactive mass properties edit boxes.

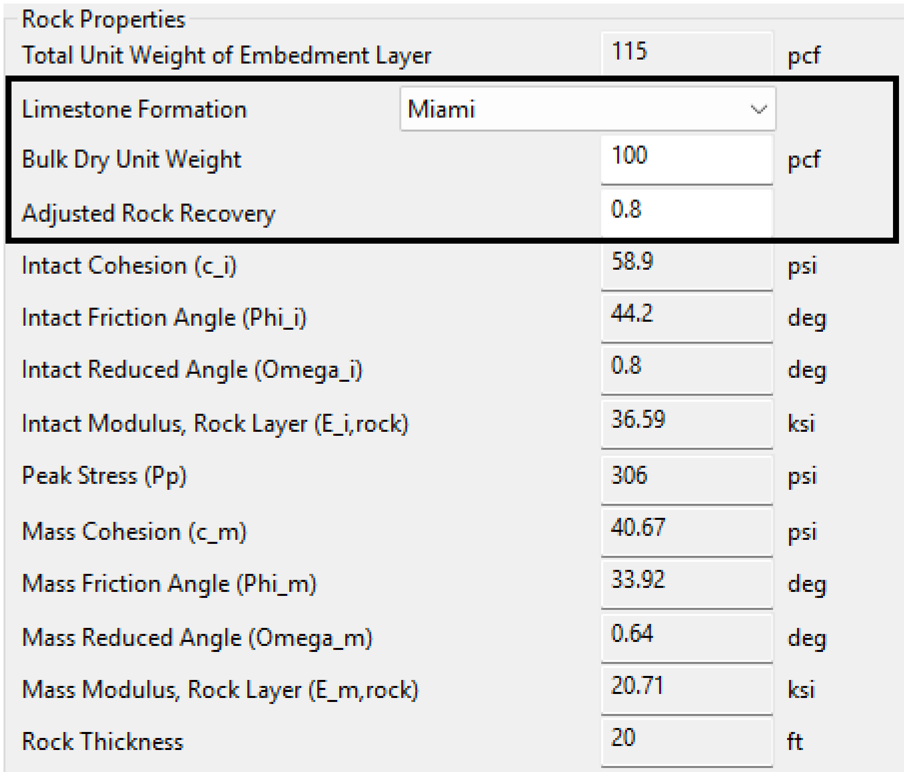

Figure 2-14 Selection of any standard limestone formation (e.g. Miami) requires input of bulk dry unit weight and adjusted rock recovery.

For option 1 above, only the mass strength envelope is calculated, whereas for option 2 and 3 above, the intact and mass strength envelopes are calculated in the tau-sigma and p-q space. The strength envelopes are displayed in graphical representation and can be viewed using the 'Tau-Sigma Space' and 'p-q Space' radio buttons. The plot curve legends are shown underneath the plot, namely, 'Mass Curve' and 'Intact Curve'. Below the legend is an image with the templete graphical representation of the strength envelope in tau-sigma space and p-q space using the (intact and mass) rock properties. The table containing the points on the strength envelopes can be shown or hidden by clicking the "Show Table" or "Hide Table" button, respectively. The curve points are displayed in the "Mass Curve Points" and "Intact Curve Points" tables to the right of the plot.

For example if the "Tau-Sigma Space" radio button is selected, the strength envelope in tau-sigma space is plotted, and the curve points are displayed in the "Mass Curve Points" and "Intact Curve Points" tables (Figure 2-15). Whereas, if the "p-q Space" radio button is selected, the strength envelope in p-q space is plotted, and the curve points are displayed in the "Mass Curve Points" and "Intact Curve Points" tables to the right of the plot (Figure 2-16). Settlement Plot dialog can be accessed by clicking on the "Edit" button in the Settlement Analysis frame. More on that in Chapter 3.

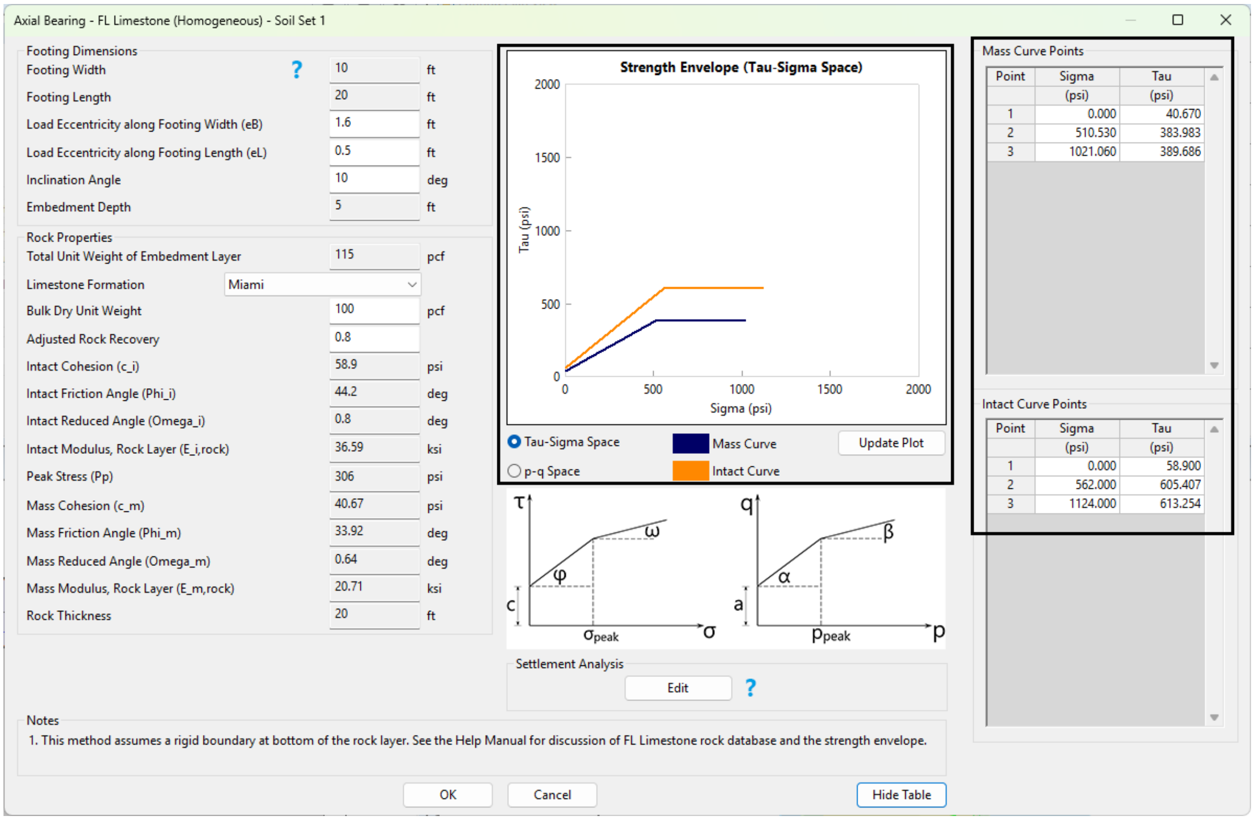

Figure 2-15 'Tau-Sigma Space' radio button is selected on FL limestone (homogeneous) dialog.

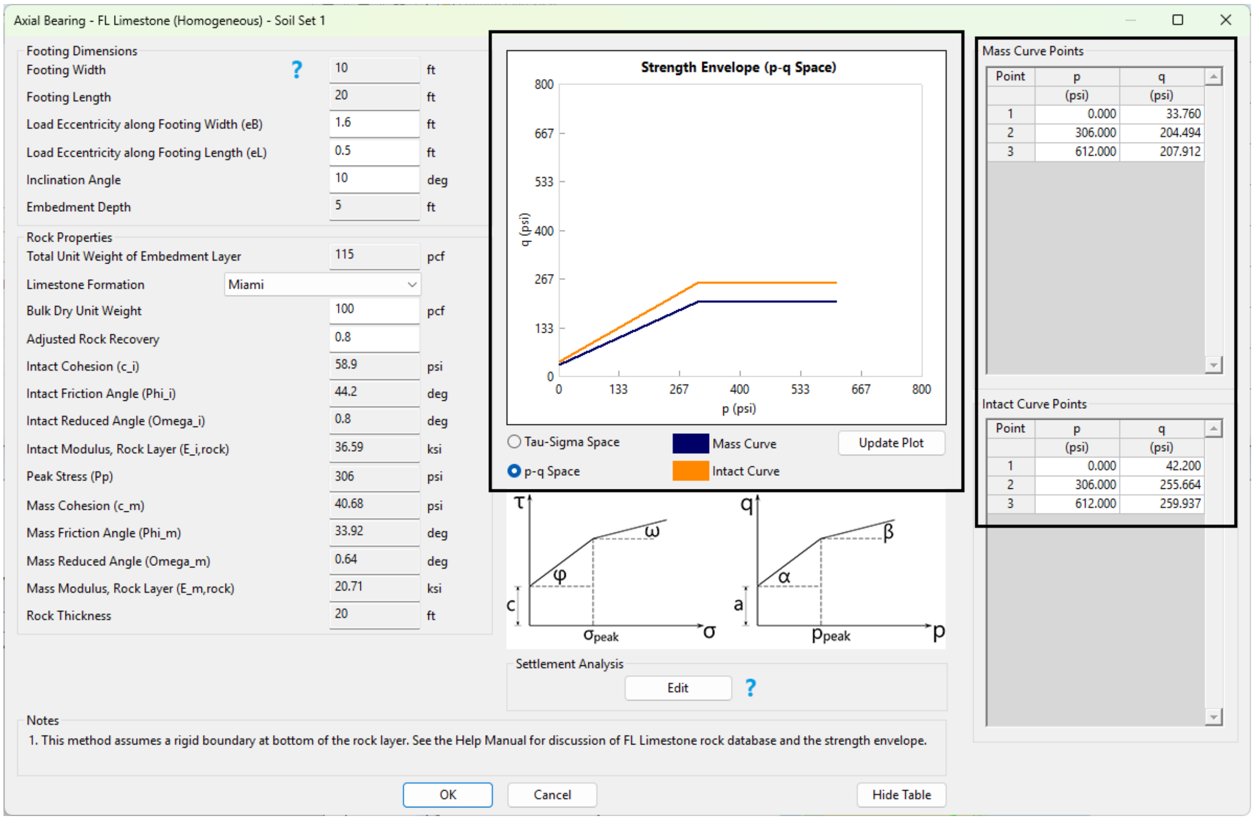

Figure 2-16 p-q space radio button selected is selected on the FL limestone (homogeneous) dialog.

2.4.1.2 Axial Bearing Soil Resistance Model: FL Limestone (Rock Over Sand)

The FL Limestone (Rock over Sand) dialog (Figure 2-17) can be accessed when the ‘FL Limestone (Rock over Sand)’ axial bearing soil/rock resistance model is selected from the dropdown (Figure 2-10) on the ‘Soil’ page. The ‘FL Limestone (Rock over Sand)’ model needs user input parameters to calculate the strength envelope and the bearing capacity, particularly, footing dimensions, rock, and sand properties. The FL Limestone (Rock over Sand) dialog has the same behavior as that of the FL Limestone (Homogeneous) dialog. The plots for the strength envelopes in tau-sigma space and p-q space are displayed by selecting the “Tau-Sigma Space” (Figure 2-17) and “p-q Space” radio buttons, respectively. Settlement Plot dialog can be accessed by clicking on the “Edit” button in the Settlement Analysis frame. More on that in Chapter 3.

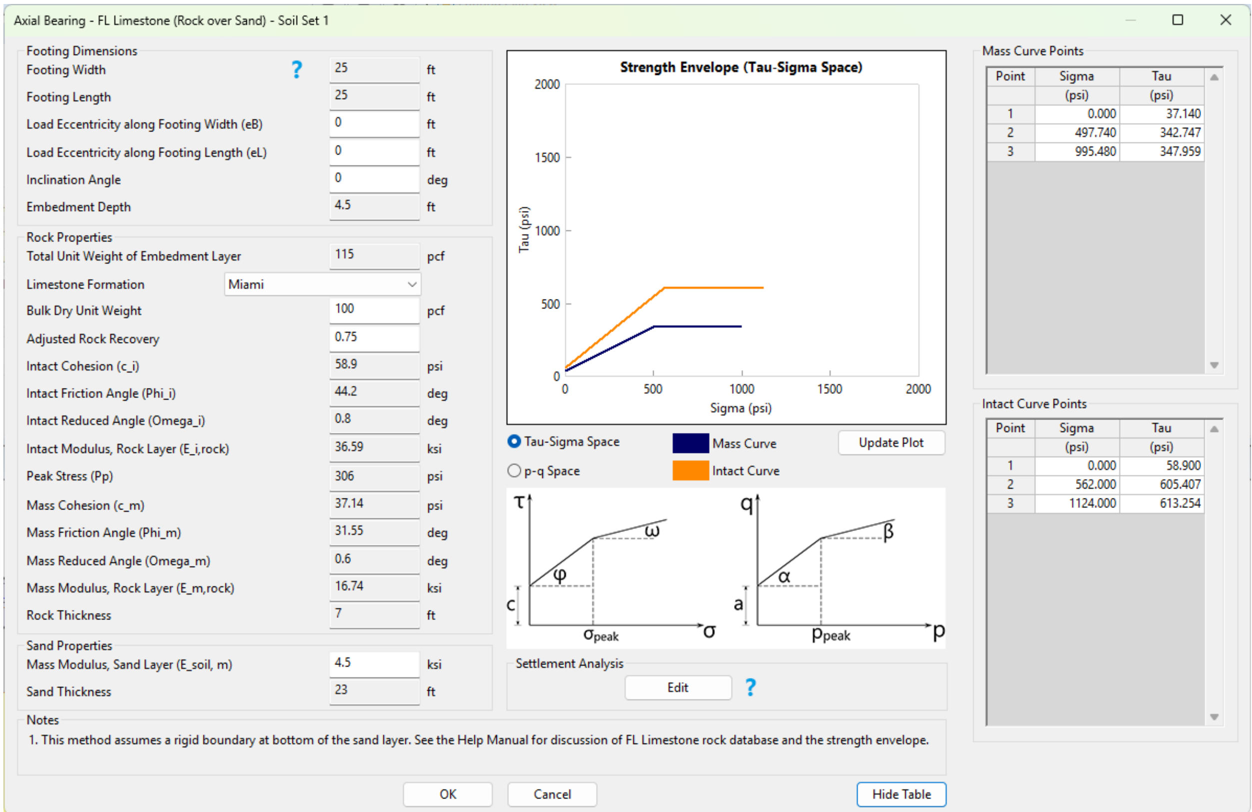

Figure 2-17 FL limestone (rock over sand) dialog with the required key input parameters.

2.4.1.3 Axial Bearing Soil Resistance Model: Hoek & Brown (Carter & Kulhawy)

The Hoek & Brown (Carter & Kulhawy) dialog (Figure 2-18) can be accessed when the 'Hoek & Brown (Carter & Kulhawy)' axial bearing soil/rock resistance model is selected from the dropdown (Figure 2-10) on the 'Soil' page. The 'Hoek & Brown (Carter & Kulhawy)' model needs user input parameters to calculate the strength envelope and the bearing capacity, particularly, the rock properties. Settlement Plot dialog can be accessed by clicking on the "Edit" button in the Settlement Analysis frame. More on that in Chapter 3.

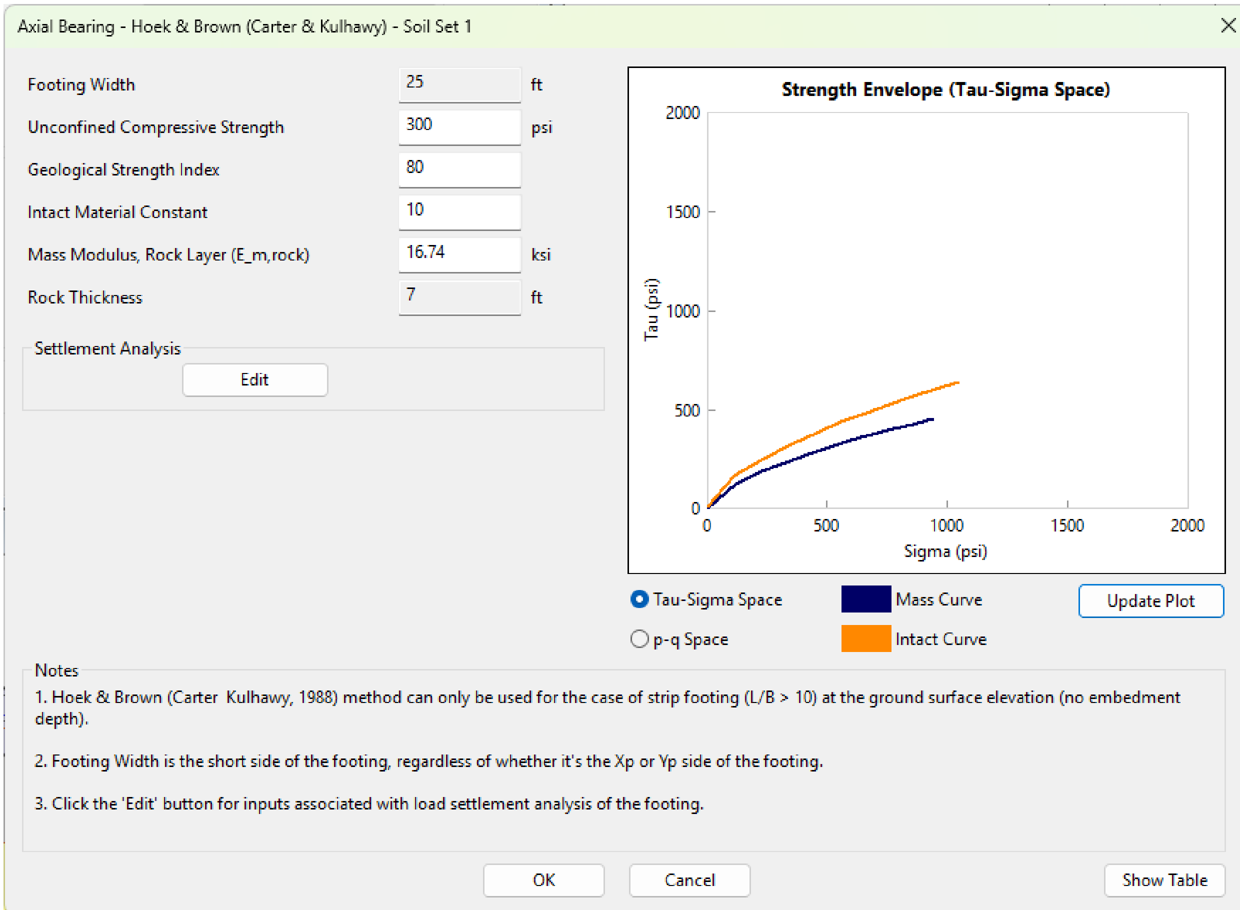

Figure 2-18 Hoek & Brown (Carter & Kulhawy) dialog with the required key input parameters.

The input parameters for rock properties consist of unconfined compressive strength (q_u), Geological Strength Index (GSI), and intact material constant (m_i). These input parameters are used to calculate and plot the strength envelopes in tau-sigma space and p-q space. Similar to the other axial soil resistance models, the table containing the points on the strength envelopes can be shown or hidden by clicking the "Show Table" or "Hide Table" button, respectively. The curve points are displayed in the "Mass Curve Points" and "Intact Curve Points" tables to the right of the plot. It is noted in the UI that this method should be applied for the case of a strip footing (L/B >10) with no embedment.

2.4.2 Shallow Foundation Enhancements in FB-MultiPier Analytical Engine

The input parameters from the FB-MultiPier UI dialogs pertaining to the shallow foundation soil resistance models are saved in the input file under the header 'SHALLOWFOUND' as stated in 2.5 Input-associated updates to model input files. The analytical engine reads this header and calculates the bearing capacity using the Equation 2-1 to Equation 2-16. Bearing capacity is printed in the output (.out) file as shown below:

```
Sum of Total Soil Spring Forces for Foundation Nodes (Load CASE   1)


  Est. of Ultimate Bearing Capacity  =         70.8758  ksf
```

2.5 Input-Associated Updates to Model Input Files

The inputs associated with the axial bearing resistance for the shallow foundation and the input parameters associated with them are entered using the FB-MultiPier UI. These shallow foundation data are then saved in the input (.in) file under header SHALLOWFOUND as mentioned in Appendix F.1 User-Guide for Input File Update.

2.6 Conclusion

Florida limestone has a high bulk porosity and exhibits bi-linear strength envelopes, volumetric compression behavior and ductile stress-strain response. Shallow foundations constructed on Florida Limestone exhibit much smaller bearing capacities than traditional theories (e.g., Vesić). Based on the more than 3,000 unconfined compression strength tests, split tensile strength tests, 223 triaxial tests and thousands of Finite Element Simulations, Florida bearing capacity equations were developed in Phase I, and validated in Phase II with three field load tests in different formations and layering conditions in Florida. In general, the bearing capacity of a footing in Florida limestone is found to be less than 50% of the classical general shear failure of Vesić and 20% smaller than the estimates of Carter and Kulhawy (e.g., GSI = 100%).

In the current Chapter 2, Florida bearing capacity equations and Carter and Kulhawy bearing analyses are implemented into FB-MultiPier for pier design. The bi-linear strength parameters as a function of bulk dry unit weight/porosity and formation are provided. The mass strength envelope is obtained by using the adjusted rock recovery and intact strength. For the rock-over-sand case, the modulus ratio of the rock and sand layer is needed. Intact modulus as a function of bulk dry unit weight/porosity and formation are suggested, along with the mass/intact modulus ratio versus adjusted rock recovery. For shallow foundation design in Florida limestone, FB-MultiPier UI was updated along with the analytical engines.

The selection of axial bearing model for shallow foundation in FB-MultiPier occurs on the Soil Page (Figure 2-8) of the UI. To be active, the footing base must be rested on or below the top of the ground surface (Figure 2-3). The user first needs to select one of the axial bearing model (Figure 2-10): FL Limestone (Homogeneous), layered (rock over sand), Hoek & Brown (Carter-Kulhawy), Linear (Modulus), or Custom. Based on the selection, additional windows will appear for input of rock and soil properties. Note, in case of eccentric and inclined loading, the user needs to provide load eccentricity along footing width and length, and inclination angle.

Finally, extensive bearing capacity comparisons between FB-MultiPier and the developed Florida equations for homogeneous, and rock-over-sand subsurface cases for both English and SI units were undertaken with all errors less than 2.5%, which is considered acceptable. Discussion of bearing capacity equations, user input, and rock properties with be provided in the help manual.

CHAPTER 3
IMPLEMENTATION OF NON-LINEAR LOAD-SETTLEMENT ANALYSIS

3.1 Introduction

Florida Limestone (calcium carbonate & dolomite) occurs in many different formations near the ground surface (e.g. Miami, Fort Thompson, Anastasia, Key Largo, etc.). Existing at many different bulk dry unit weights (85 pcf to 145 pcf), the majority of the rock exhibits ductile stress-strain response: a linear increasing stress vs strain response until yielding/failure (Mohr-Coulomb) and then a constant stress vs increasing strain. In general, Florida Limestone has a constant Young's Modulus that is 5 to 50 times (depending on bulk dry unit weight) the value of sand until yielding/failure; however, due to formation and age, Florida Limestone has median (i.e. 37%) porosity which has a significant impact on volumetric and strength characteristics of the material. Specifically, under increasing hydrostatic or triaxial shear loading, the material will undergo significant compression volumetric straining as well as matrix crushing resulting in ductile response (bilinear stress-strain), as well as bilinear Mohr-Coulomb Strength Envelope (FDOT, Phase I report).

As a result of its stress vs strain and strength characteristics, a spread footing founded on a homogeneous Florida Limestone formation at constant dry unit weight will undergo a bilinear load vs. displacement response, i.e., a linear load vs. displacement up to bearing and then excessive deformations upon further loading (Yang et al., 2023). However, the bearing capacity values will be different (Yang et al. 2023) than the traditional bearing capacity (bilinear load vs. displacement – Vesić, 1973) of a dense sand (Figure 3-1e). In the case of the dense sand shearing, its volume dilates, resulting in the soil being pushed laterally and upward (development of passive stress state) with collapse (large deformation) occurring when the shear surface exits the ground surface. However, as the Florida Limestone shears, the rock undergoes volumetric compression and subsequent matrix crushing (Figure 3-1 b) occurring only in the triangular zone beneath the footing. Moreover, as the strain within the wedge (Figure 3-1 b) approaches 0.5% to 1%, the triangular zone approaches a state of complete failure, i.e. bearing collapse (associated with large vertical deformation and volumetric compression) due to the stress state (yielding/failure) occurring throughout the whole zone. Note, outside this triangular zone. there is no large increase in lateral stress, upward movement of material or development of a shearing rupture surface (Figure 3-1 c). Again, this behavior (matrix crushing/volumetric compression) is associated with the large porosity (median > 37%) of the rock. In addition, the load vs. displacement of the footing is linear up to bearing collapse (characterized with linear elastic theory) due to the ductile stress-strain behavior of the rock (Yang et al., 2023). The initial modulus (E_i) from 50 psi triaxial tests (limited lateral stress developed up to bearing) is selected based on the formations and representative bulk dry unit weights (lower values of geomean and median), probabilistic settlement is characterized by the elastic theory for settlement under uniform loads and Fenton and Griffiths method (Fenton and Griffiths, 2002) due to high coefficients of variation of E_i (up to 3) observed at different sites.

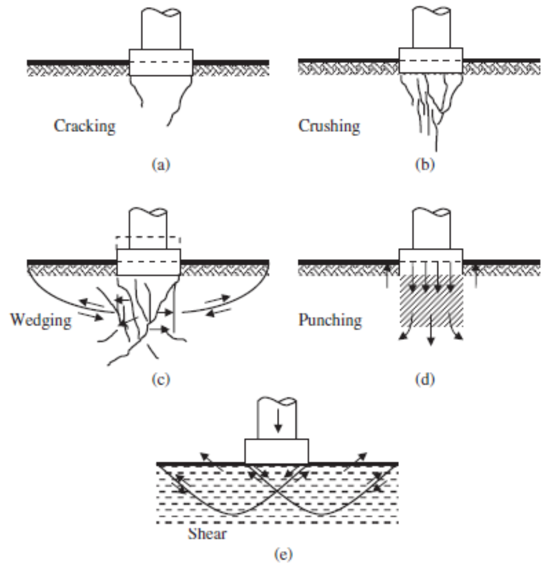

Modes of failure of a footing on rock including development of failure through crack propagation and crushing beneath the footing (a-c), punching through collapse of voids (d), and shear failure (e) (based on Goodman, 1989).

Figure 3-1 Potential failure modes of footing on rock (Goodman, 1989).

In the case of footing on Florida Limestone with sand underneath (e.g., Miami), both its load vs. displacement and bearing capacity will change. As discussed by Burmister (1958) and Fox (1948), both the vertical stresses and strains are influenced by the Young's Modulus of each layer (rock and sand). In addition, both the crushing zone (Figure b) thickness and sand/rock modulus ratio impacts the onset of the footing's bearing capacity (Yang et al., 2023). Moreover, as the stress within the rock zone beneath footing approaches the bearing stress, the rock modulus drops approaching the sand modulus resulting in large deformations with small changes in stress.

To characterize settlement of a footing on a two-layer medium (rock over sand), Burmister elastic solution may be employed or Winkler approach of converting a two layered problem to an equivalent homogeneous problem with a stress-dependent harmonic mean modulus. The stress-dependent harmonic mean modulus is selected to result in the same deformation in the homogeneous layer as the two-layer problem. Important in coming up with the harmonic mean modulus are the stresses in center of the rock layer and the center of zone of influence in the sand layer. Extensive Finite element method (FEM) analysis of two-layer problems to identify the stress zone of influence in the sand layer as a function of modulus ratio of rock/sand, L/B of the footing and rock thickness, T_r/footing width, B were investigated for the harmonic modulus. For settlements up to bearing, the initial modulus (E_i) of rock and sand modulus (E_{sand}, Bowles, 1996) were used. As loads exceed the bearing (up to 1.175×bearing), the secant modulus (E_s) of the rock was used and reduced to half of E_i to show the loss of rock stiffness and ensuing larger deformations. A discussion of worked problems for each case (homogeneous and rock over sand) follows. In addition, all three load tests are included in the worked examples.

3.2 Analysis Approaches

For homogeneous rock subsurface (Figure 3-2a), probability settlement analysis is used up to bearings (Q_u) from either Florida method or Hoek and Brown (Carter and Kulhawy) (1988) method (only for strip footing at the ground surface) with initial modulus (E_i), Figure 3-3a. The correlation length, coefficient of variation (CV) should be evaluated within the rock thickness, T_r (generally, 2B for square footing and 4B for strip footing). The representative porosity-dependent rock properties and adjusted recoveries (REC_{adj}) need to be provided to assess mass strength and stiffness parameters of Florida limestone; representative intact unconfined compression strength (q_u) and Geological Strength Index (GSI) are required for Carter and Kulhawy method. It is recommended to obtain at least 30 rock cores within the influence zone of footing to characterize the load-settlement behavior.

For heterogeneous rock subsurface (Figure 3-2b), deterministic settlement analysis is used for bearing (Q_u) and post-bearing ($Q_{pu} = 1.175Q_u$) based on the stress-dependent harmonic mean modulus ($E_{eq} = \frac{\sum T_i \sigma_i}{\sum \frac{T_i \sigma_i}{E_i}}$) with initial modulus ($E_i$) and secant modulus ($E_{secant}$), Figure 3-3b. A parametric study of FEM analysis was performed to validate the rock-sand interface stress σ_{sand} from Fox (1948) and to provide the influence zone (T_{sz} or T_s, Figure 3-2b) in the sand layer based on the rock thickness, T_r/equivalent footing radius, $a = \sqrt{BL/\pi}$ and modulus ratio of rock (E_i or E_{secant}) and sand (E_s). The shape and rigidity factor C proposed by Mayne and Poulos (1999) is used based on the modulus of footing and rock (E_{eq}) as well as footing thickness. The proposed solution was validated for all cases of $L/B < 3$, $E_m/E_s < 50$, $0.44 \leq T_r/a \leq 3.54$.

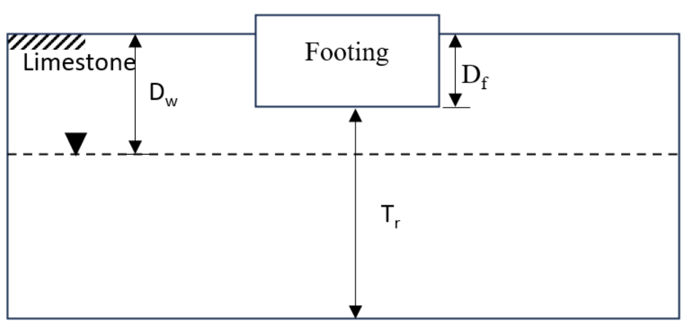

(a)

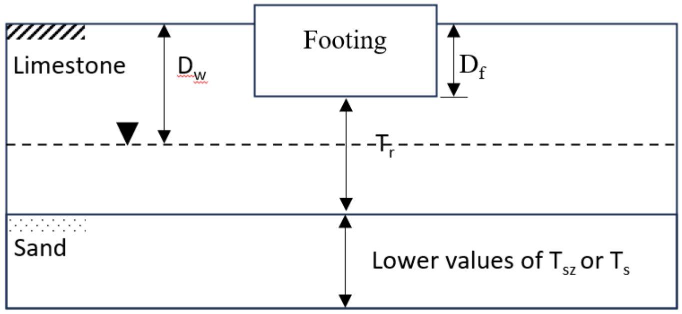

(b)

Figure 3-2 Schematic drawing of homogeneous subsurface (a) and rock-over-sand subsurface (b).

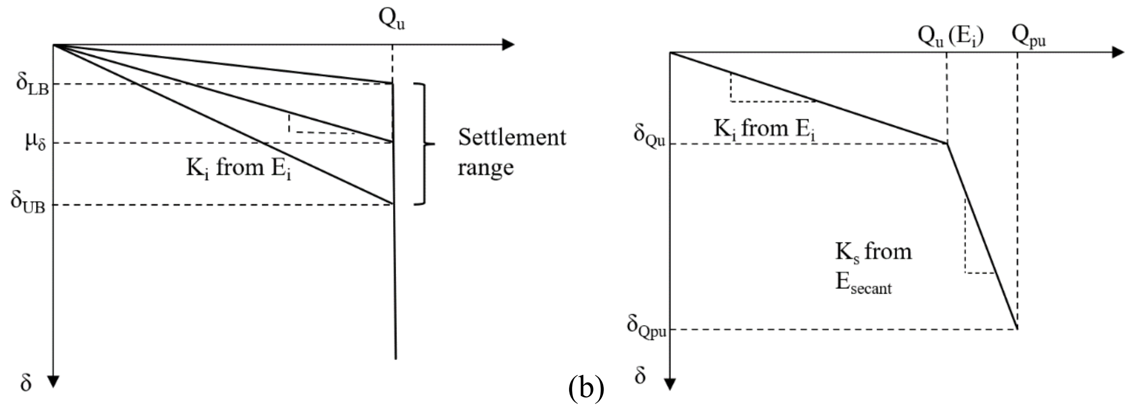

Figure 3-3 Load-settlement response of homogeneous (a) and rock-over-sand (heterogeneous, b) subsurface.

3.2.1 Florida Homogeneous Settlement

In the case of Florida settlement analysis, the bearing capacity is derived from the mass properties of bearing layer using Florida bearing capacity equations implemented in Chapter 2. The effective footing dimensions (B′ and L′) are used in the bearing capacity calculation based on the input parameters: footing dimensions (B and L), the load eccentricity along the footing width (e_B) and the load eccentricity along the footing length (e_L). However, the actual footing dimensions (B and L) are used for the settlement calculation. The mass modulus ($E_m = E_i$ * E_{mass}/E_{intact} ratio, Figure 3-5) is evaluated based on the bi-linear stress-strain response (E_i at 0.5% vertical strain, Figure 3-4) of 50 psi confining stress triaxial tests and the ratio (E_{mass}/E_{intact}) of mass modulus to intact laboratory sample modulus. Mass/intact modulus ratio are assessed as a function of site-specific REC_{adj} based on the experiments from Ko (2010) and numerical simulations from Faraone (2014) as well as the recommendation from O'Neil and Reese (1999), Figure 3-5.

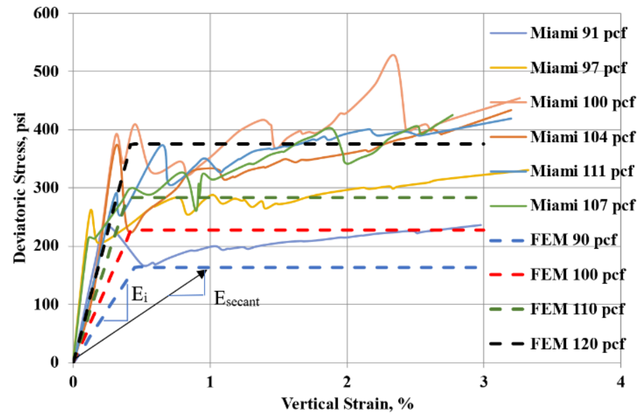

Figure 3-4 Measured and predicted stress-strain response of Miami limestone.

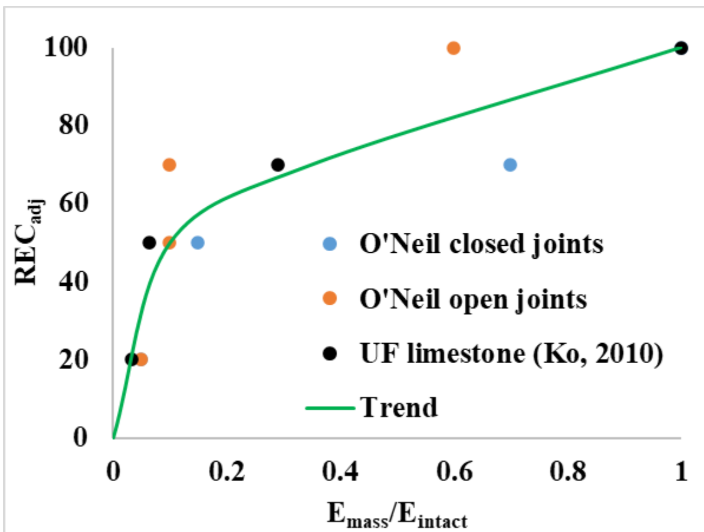

Figure 3-5 Adjusted REC versus E_{mass}/E_{intact}.

The probabilistic load-settlement prediction employs Fenton and Griffiths (Equation 3-1 to Equation 3-10) method and characterizes the lower bound settlement and upper bound settlement based on the CV of mass modulus (Equation 3-1), bearing layer thickness (T_r), vertical correlation length (a_v) and variance function (Equation 3-6). The correlation length describes the distance within which the rock mass shows strong correlation and can be evaluated through normalized variogram analysis via Geostat assuming an exponential theoretical variogram function $\widehat{\gamma(h)} = \sigma^2\left(1 - \exp\left(-\frac{3h}{a_v}\right)\right)$. σ^2 is the variance and should approach unity (equal to sill) since the variogram is normalized, h is the separation (lag) distance between two locations. Equation 3-2 converts the log-normal distribution of mass modulus to a normal distribution; Equation 3-4 calculates the deterministic settlement using elastic solutions with a shape and rigidity factors C; Equation 3-3 and Equation 3-5 give the prediction of settlement in normal distribution and Equation 3-7 and Equation 3-8 converts the normal distributed settlement prediction back to log-normal distribution. The settlement range factor n in Equation 3-9 and Equation 3-10 gives the lower bound (δ_{LB}) and upper bound settlements (δ_{UB}).

$$CV = \frac{\sigma_E}{\mu_E} \qquad \text{Equation 3-1}$$

$$\sigma_{\ln E}^2 = ln(1 + \sigma_E^2/\mu_E^2) \qquad \text{Equation 3-2}$$

$$\mu_{\ln \delta} = \ln(\delta_{det}) + \frac{1}{2}\sigma_{\ln E}^2 \qquad \text{Equation 3-3}$$

$$\delta_{det} = Q_u \frac{B}{\mu_E} C(1 - \nu^2) \qquad \text{Equation 3-4}$$

$$\sigma_{\ln \delta} = \sqrt{\gamma(T)}\sigma_{\ln E} \qquad \text{Equation 3-5}$$

$$\gamma(T) = \frac{2a_v^2}{9{T_r}^2}\left[\frac{3|T_r|}{a_v} + e^{(-\frac{3|T_r|}{a_v})} - 1\right] \qquad \text{Equation 3-6}$$

$$\mu_\delta = exp\left\{\mu_{\ln \delta} + \frac{1}{2}\sigma_{\ln \delta}^2\right\} \qquad \text{Equation 3-7}$$

$$\sigma_\delta = \mu_\delta\sqrt{e^{\sigma_{\ln \delta}^2} - 1} \qquad \text{Equation 3-8}$$

$$\delta_{LB} = \exp(\mu_{\ln\delta} - n\ \sigma_{\ln\delta}) \qquad \text{Equation 3-9}$$

$$\delta_{UB} = \exp(\mu_{\ln\delta} + n\ \sigma_{\ln\delta}) \qquad \text{Equation 3-10}$$

where,

σ_E = standard deviation of mass modulus

μ_E = mean mass modulus (equal to $E_m = E_i * E_{mass}/E_{intact}$)

σ_{lnE} = standard deviation of log-elastic mass modulus

δ_{det} = footing settlement when E = μ_E everywhere

C = shape and rigidity factors based on the Table 3-1 and Equation 3-11 and Equation 3-12

B = footing width

ν = Poisson's ratio (0.1 for Florida limestone)

T_r = rock thickness

$\mu_{\ln\delta}$ = mean of log-settlement

$\sigma_{\ln\delta}$ = standard deviation of log-settlement

μ_δ = mean footing settlement

σ_δ = standard deviation of footing settlement

n = settlement range factor

The shape and rigidity factor C (Equation 3-4) is the product of shape factors C_s (Table 3) and rigidity correction factor I_F (Equation 3-13). Mayne and Poulos (1999) suggested using the Equation 3-11 and Equation 3-12 to account for rigidity, where K_F is the foundation flexible factor, $E_{foundation}$ is the elastic modulus of foundation material, E_m is the mean mass modulus, t is the foundation thickness and a is the equivalent foundation radius (a = $\sqrt{BL/\pi}$). I_F is limited by the analytical solution of perfectly flexible circular footing and perfectly rigid circular footing at 1 and $\pi/4$. Following assumptions are made regarding C values: (1) perfectly rigid with $K_F > 10$, C = C_s*I_F (C_s is based on the L/B, Table 3-1); (2) intermediate flexibility with $0.01 \leq K_F \leq 10$, C = C_s*I_F (C_s is based on the L/B, Table 3-1); and (3) perfectly flexible with $K_F < 0.01$, C = C_s (C_s is based on the L/B, Table 3-1).

$$K_F = \frac{E_{foundation}}{E_m} \left(\frac{t}{a}\right)^3 \qquad \text{Equation 3-11}$$

$$I_F = \frac{\pi}{4} + \frac{1}{(4.6+10K_F)} \qquad \text{Equation 3-12}$$

$$C = C_s \times I_F \qquad \text{Equation 3-13}$$

Table 3-1 Shape factors, C_s for settlement at the center of flexible footing based on the footing length, L/footing width, B (Fang, 2012).

L/B	C_s
Circle	1.00
1	1.12
1.5	1.36
2	1.52
3	1.78
5	2.1

L/B	C_s
10	2.54

3.2.2 Hoek and Brown (Carter and Kulhawy) Homogeneous Settlement

Carter and Kulhawy bearing analysis use the intact qu strength and GSI to characterize the mass strength and bearing capacity values. For the settlement prediction, the same approach of Florida homogeneous settlement is adopted (Equation 3-1 to Equation 3-10) except the shape and rigidity factor term C. Since Carter and Kulhawy bearing analysis was developed for strip footings (L/B ≥ 10) at the ground surface (i.e., no embedment), C value of 2.54 for flexible footing and 2.10 for rigid footing based on the elastic solution of a strip uniform loading on a half-infinite surface (Poulos and Davis, 1974; Craig and Kanppett, 2012; Lommler, 2012; Briaud, 2023 and Fang, 2012) were implemented.

3.2.3 Florida Rock-Over-Sand Settlement

For the case of two-layered system settlement prediction, the approach of equivalent footing radius ($a = \sqrt{BL/\pi}$) with stress-dependent harmonic mean modulus ($Eeq = \frac{\sum T_i \sigma_i}{\sum \frac{T_i \sigma_i}{E_i}}$, Equation 3-16) is used to convert the two-layered subsurface to a homogeneous single layer, Equation 3-13 and Equation 3-14. Extensive FEM analysis was performed to validate the rock-sand interface stress, σsand from Fox (1948) and to provide the influence zone in the sand layer based on the rock thickness, Tr/equivalent footing radius, $a = \sqrt{\mathrm{BL}/\pi}$ and modulus ratio of rock mass and sand (Em/Es) for harmonic modulus assessment. The FEM analysis (Figure 3-6a) of a surface loading on a two-layered system with linear elastic models initiated with the validation of vertical stress distribution, Figure 3-6b, for the case of a square footing with Tr/B = 4 and Em/Es = 100 (Hazzard et al., 2007) and Figure 3-6c is the case of circular footing with Tr/(2a) = 1 and Em/Es = 10 (Burmister, 1958); great agreements were achieved for both cases.

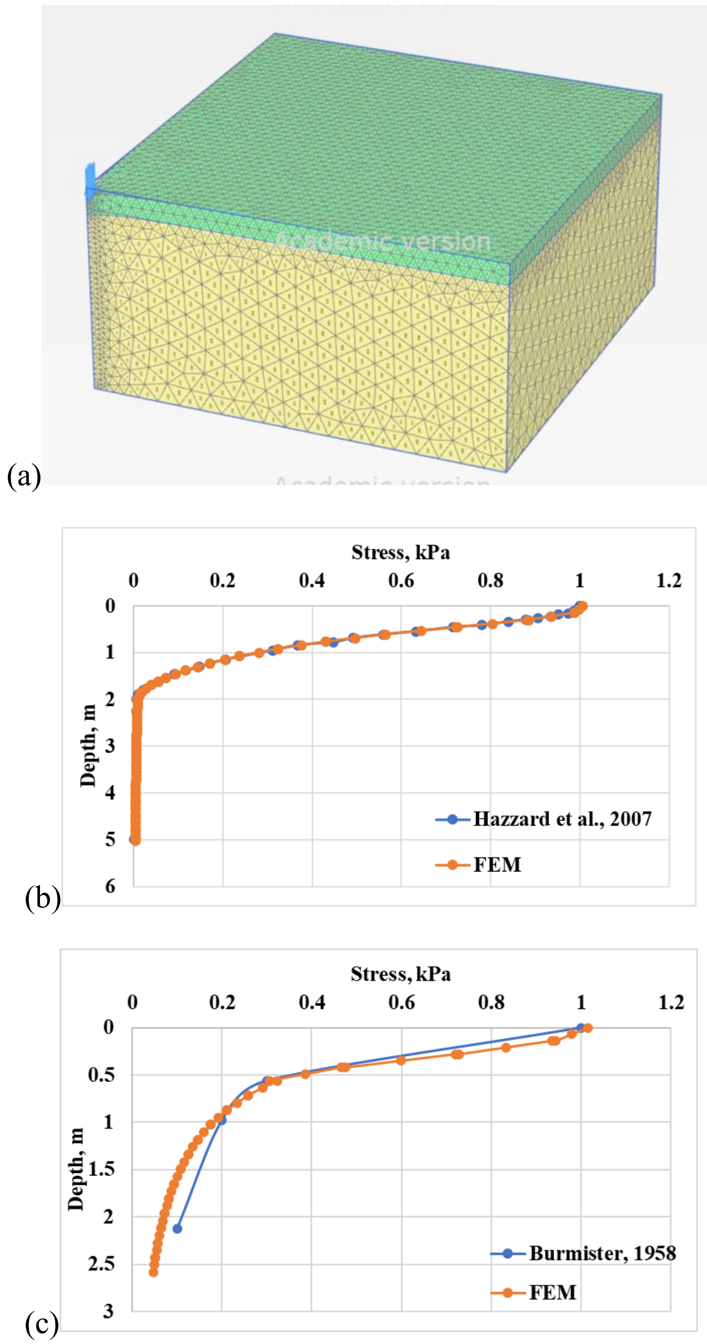

Figure 3-6 (a) FEM mesh of two-layered system (b) validation of vertical stress distribution beneath the footing with Hazzard et al., 2007 and (c) validation of vertical stress distribution beneath the footing with Burmister, 1958.

For the rigidity and shape factor C in Equation 3-14 and Equation 3-15, Equation 3-11 to Equation 3-13 was again used with a shape factor $C_s = 1$ (Table 3-1) for equivalent circular footing (Mayne and Poulos, 1999). For the equivalent modulus, the induced stress due to bearing (σ_i in Equation 3-16) is averaged with the stress the top of the sand layer (Figure 3-7) or (σ_{sand} + Q_u)/2. The sand layer thickness, T_s, is a user input based on the layering scheme being modeled. However, in Equation 3-16, the thickness and average stress in the sand layer needs to be determined based on the influence zone determined from Figure 3-8. Based on the Sand Layer Influence zone, T_{sz}, two conditions listed in Table 3 are checked to determine the average stress and thickness values in the sand layer that will be used in Equation 3-16. The post-bearing stress (Q_{pu}) is assumed to be 1.175 of bearing stress (Q_u) based on the observations from the load tests in Phase II. Compared to the initial modulus (E_i in Figure 4) used for rock layer in Equation 3-14, the secant modulus (E_{secant} = E_i/2, Figure 3-4) at 1% vertical strain is used for rock layer in the post-bearing settlement analysis (Equation 3-15) to characterize the volumetric compression and matrix crushing behaviors after yielding.

$$\delta_{Qu} = Q_u \frac{2a}{E_{eq}} C(1-\nu^2) \qquad \text{Equation 3-14}$$

$$\delta_{QPu} = Q_{Pu} \frac{2a}{E_{eq}} C(1-\nu^2) \qquad \text{Equation 3-15}$$

$$E_{eq} = \frac{\sum T_i \sigma_i}{\sum \frac{T_i \sigma_i}{E_i}} \qquad \text{Equation 3-16}$$

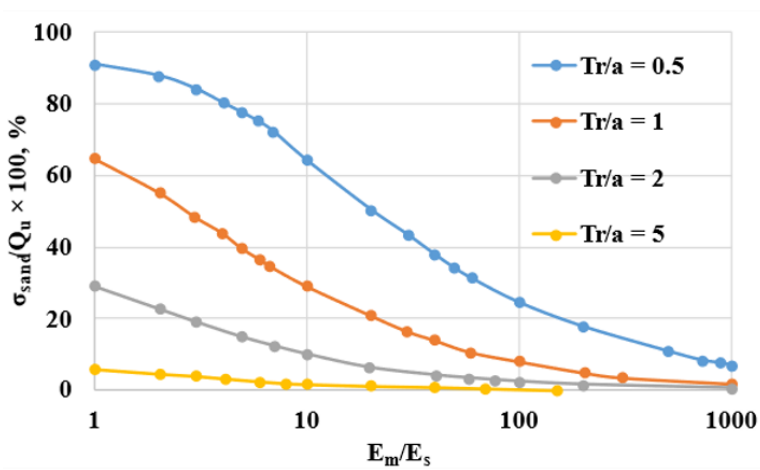

Figure 3-7 Rock-sand interface stress (Fox, 1948), T_r is rock layer thickness and a is radius of footing converted from sqrt(BL/π).

Note, the values of σ_{sand}/Q_u are in percentage and shown below:

- For $T_r/a = 0$:
  - $\sigma_{sand}/Q_u = 100$
- For $T_r/a = 0.5$:
  - $\sigma_{sand}/Q_u = -2.9785\times(E_m/E_s) + 93.277$ for $E_m/E_s \leq 10$,
  - $\sigma_{sand}/Q_u = -17.54\times\ln(E_m/E_s) + 103.88$ for $10 < E_m/E_s \leq 100$,
  - $\sigma_{sand}/Q_u = 310.36\times(E_m/E_s)$^(-0.564) for $100 < E_m/E_s \leq 1000$
- For $T_r/a = 1$:
  - $\sigma_{sand}/Q_u = -15.9\times\ln(E_m/E_s) + 66.352$ for $E_m/E_s \leq 10$,
  - $\sigma_{sand}/Q_u = 111.58\times(E_m/E_s)$^(-0.5854)+0.75 for $10 < E_m/E_s \leq 100$,
  - $\sigma_{sand}/Q_u = 148.2\times(E_m/E_s)$^(-0.647)+0.75 for $100 < E_m/E_s \leq 1000$
- For $T_r/a = 2$:
  - $\sigma_{sand}/Q_u = -8.358\times\ln(E_m/E_s) + 29.51$ for $E_m/E_s \leq 10$,
  - $\sigma_{sand}/Q_u = 41.244\times(E_m/E_s)$^(-0.637)+0.75 for $10 < E_m/E_s \leq 100$,
  - $\sigma_{sand}/Q_u = 52.287\times(E_m/E_s)$^(-0.689)+0.75 for $100 < E_m/E_s \leq 1000$
- For $T_r/a = 5$:
  - $\sigma_{sand}/Q_u = -1.89\times\ln(E_m/E_s) + 6.7198$ for $E_m/E_s \leq 10$,
  - $\sigma_{sand}/Q_u = -0.599\times\ln(E_m/E_s) + 3.7515$ for $10 < E_m/E_s \leq 100$
  - $\sigma_{sand}/Q_u = -0.0198\times(E_m/E_s) + 2.97$ for $100 < E_m/E_s \leq 150$
  - $\sigma_{sand}/Q_u = 0$ for $150 < E_m/E_s \leq 1000$

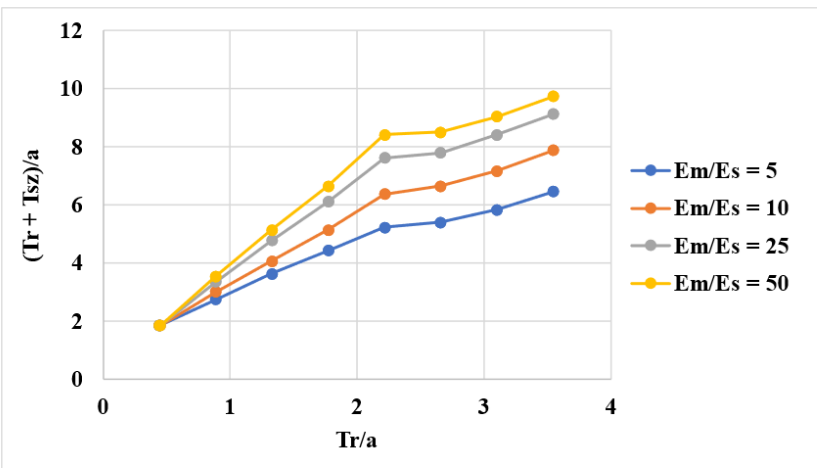

Figure 3-8 Influence zone/a versus rock thickness/a based on the modulus ratio of rock and sand layers.

Curves from Figure 3-8 based on the modulus ratio of rock and sand are shown below:

- For $E_m/E_s = 5$:
  - $(T_r + T_{sz})/a = 1.899\times T_r/a+1.025$ for $0.44 \leq T_r/a \leq 2.215$,
  - $(T_r + T_{sz})/a = 0.405\times T_r/a +4.332$ for $2.215 < T_r/a \leq 2.659$,

    - $(T_r + T_{sz})/a = 1.203 \times T_r/a + 2.211$ for $2.659 < T_r/a \leq 3.54$
- For $E_m/E_s = 10$:
    - $(T_r + T_{sz})/a = 2.546 \times T_r/a + 0.74$ for $0.44 \leq T_r/a \leq 2.215$,
    - $(T_r + T_{sz})/a = 0.158 \times T_r/a + 6.031$ for $2.215 < T_r/a \leq 2.659$,
    - $(T_r + T_{sz})/a = 1.635 \times T_r/a + 2.104$ for $2.659 < T_r/a \leq 3.54$
- For $E_m/E_s = 25$:
    - $(T_r + T_{sz})/a = 3.245 \times T_r/a + 0.432$ for $0.44 \leq T_r/a \leq 2.215$,
    - $(T_r + T_{sz})/a = 0.405 \times T_r/a + 6.722$ for $2.215 < T_r/a \leq 2.659$,
    - $(T_r + T_{sz})/a = 1.510 \times T_r/a + 3.786$ for $2.659 < T_r/a \leq 3.54$
- For $E_m/E_s = 50$:
    - $(T_r + T_{sz})/a = 3.696 \times T_r/a + 0.234$ for $0.44 \leq T_r/a \leq 2.215$,
    - $(T_r + T_{sz})/a = 0.203 \times T_r/a + 7.971$ for $2.215 < T_r/a \leq 2.659$,
    - $(T_r + T_{sz})/a = 1.407 \times T_r/a + 4.767$ for $2.659 < T_r/a \leq 3.54$

Table 3-2 Sand layer thickness for stress-dependent harmonic mean modulus.

Condition	Sand Thickness	Average Stress in sand layer
$T_s > T_{sz}$	T_{sz}	$(\sigma_{sand} + 0)/2$
$T_s \leq T_{sz}$	T_s	$(\sigma_{sand} + (1-T_s/T_{sz})\sigma_{sand})/2$

Identifying the significance of layer stress on Harmonic modulus, a parametric study was conducted, using the boundary condition and mesh validated in Figure 3-6 for the cases of L/B < 3, Em/Es < 50, 0.44 ≤ Tr/a ≤ 3.54 with Florida limestone material model developed in Yang et al. (2023) for rock layer and linear elastic model for sand layer. The interface stresses (σ_{sand}) from Figure 3-7 were compared to FEM results in Figure 3-9, i.e. excellent agreement was observed. Figure 3-10 presents the results of parameter study of flexible footing and Figure 3-11 presents the results of parameter study of rigid footing; again great agreements is achieved. The parameters for the parametric study of flexible footing were summarized in Table 3-3 and the cases of rigid footing were summarized in Table 3-4.

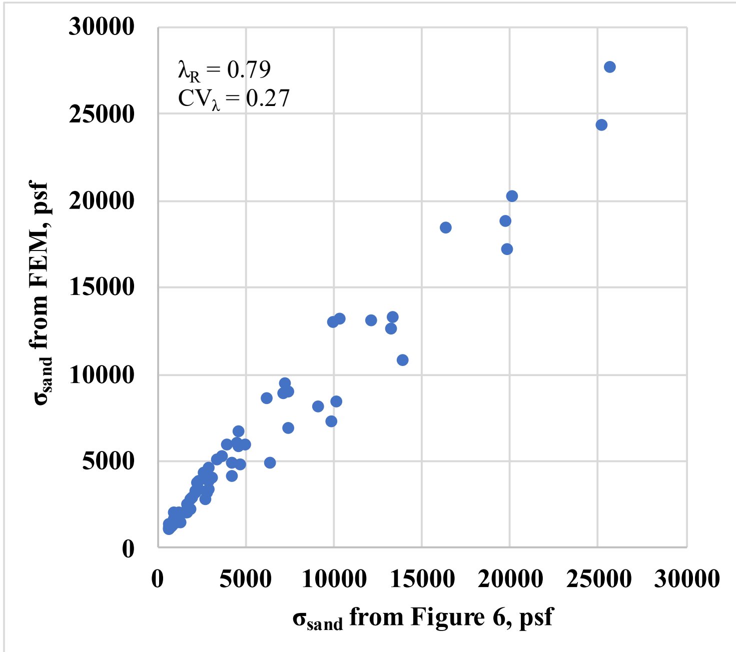

Figure 3-9 Validation of the interface stress (σ_{sand}) with FEM parametric study.

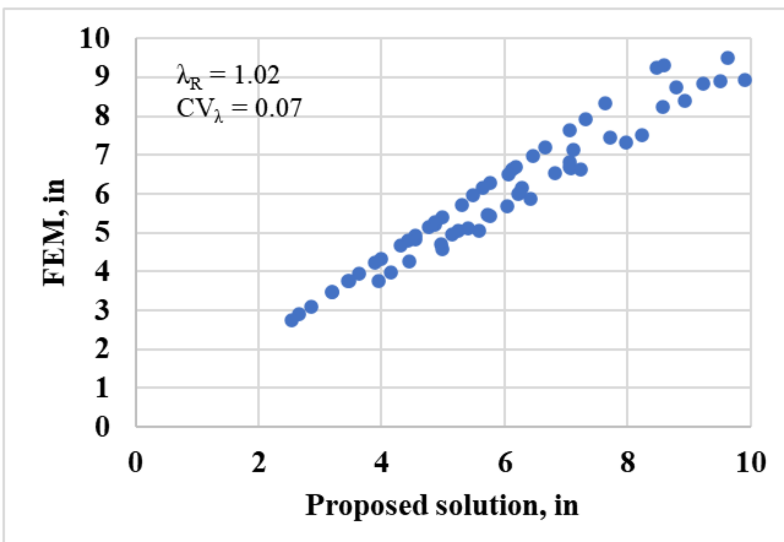

Figure 3-10 Parametric study of flexible footing.

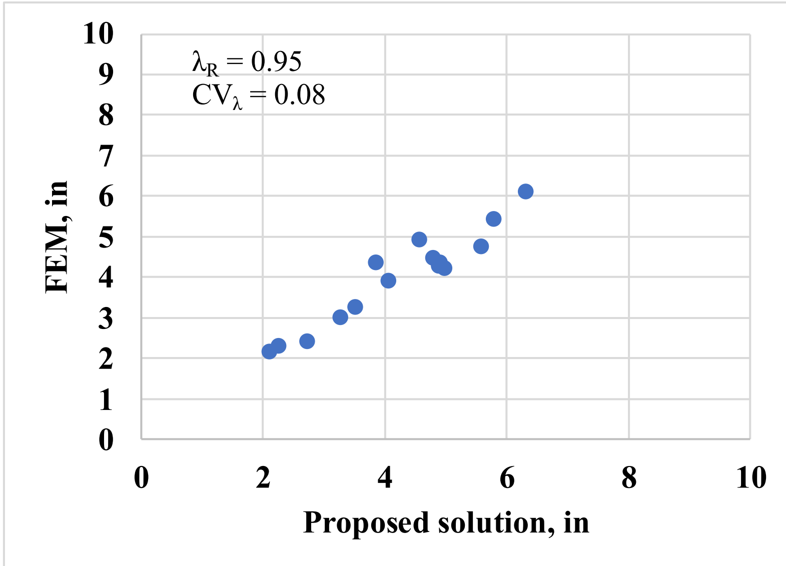

Figure 3-11 Parametric study of rigid footing.

Table 3-3 Parametric study for flexible footing.

CASE	B, ft	L, ft	T, ft	γ_{dt}, pcf	REC_{adj}, %	E_m/E_s	Bearing Stress, psi	Predicted settlement, in	Measured settlement, in
1	10	10	2.50	100	80	5	209.13	4.54	4.82
2	10	30	4.33	100	80	5	237.53	8.93	8.39
3	10	10	5.00	100	80	5	267.02	4.55	4.93
4	10	30	8.66	100	80	5	260.96	7.71	7.45
5	10	10	7.50	100	80	5	281.19	4.00	4.32
6	10	30	12.99	100	80	5	276.75	6.81	6.55
7	10	10	10.00	100	80	5	303.75	3.63	3.95
8	10	30	17.32	100	80	5	276.75	5.72	5.46
9	10	10	12.50	100	80	5	308.01	3.20	3.47
10	10	30	21.65	100	80	5	276.75	4.99	4.58
11	10	10	15.00	100	80	5	308.01	2.86	3.11
12	10	30	25.98	100	80	5	276.75	4.45	4.25
13	10	10	17.50	100	80	5	308.01	2.66	2.90
14	10	30	30.31	100	80	5	276.75	4.14	3.97
15	10	10	20.00	100	80	5	308.01	2.54	2.76
16	10	30	34.64	100	80	5	276.75	3.95	3.76
17	10	10	2.50	100	80	10	87.93	3.46	3.75
18	10	30	4.40	100	80	10	104.81	7.07	6.83
19	10	10	5.00	100	80	10	248.70	7.32	7.93
20	10	30	8.66	100	80	10	122.43	6.24	6.03
21	10	10	7.50	100	80	10	268.37	6.13	6.62
22	10	30	12.99	100	80	10	132.66	5.25	5.04
23	10	10	10.00	100	80	10	278.24	4.98	5.40
24	10	30	17.32	100	80	10	276.75	8.58	8.25
25	10	10	12.50	100	80	10	292.04	4.31	4.66
26	10	30	21.65	100	80	10	276.75	7.08	6.68
27	10	10	15.00	100	80	10	308.01	3.89	4.22
28	10	30	25.98	100	80	10	276.75	6.05	5.68
29	10	10	17.50	100	80	10	308.01	3.48	3.77
30	10	30	30.31	100	80	10	276.75	5.41	5.10
31	10	10	20.00	100	80	10	308.01	3.19	3.48
32	10	30	34.64	100	80	10	276.75	4.97	4.70
33	10	10	2.50	100	80	25	69.93	6.19	6.70
34	10	30	4.40	100	80	25	41.68	6.29	6.15
35	10	10	5.00	100	80	25	98.89	6.07	6.52

CASE	B, ft	L, ft	T, ft	γ_{dt}, pcf	REC_{adj}, %	E_m/E_s	Bearing Stress, psi	Predicted settlement, in	Measured settlement, in
36	10	30	8.66	100	80	25	58.47	6.21	5.99
37	10	10	7.50	100	80	25	121.12	5.31	5.72
38	10	30	12.99	100	80	25	121.68	9.23	8.85
39	10	10	10.00	100	80	25	264.88	8.48	9.25
40	10	30	17.32	100	80	25	127.14	7.05	6.71
41	10	10	12.50	100	80	25	269.74	6.65	7.20
42	10	30	21.65	100	80	25	134.92	5.76	5.43
43	10	10	15.00	100	80	25	275.92	5.48	5.96
44	10	30	25.98	100	80	25	276.75	9.52	8.91
45	10	10	17.50	100	80	25	283.60	4.87	5.23
46	10	30	30.31	100	80	25	276.75	8.23	7.52
47	10	10	20.00	100	80	25	293.00	4.43	4.81
48	10	30	34.64	100	80	25	276.75	7.24	6.65
49	10	10	2.50	100	80	50	29.40	4.76	5.14
50	10	30	4.40	100	80	50	35.05	9.63	9.51
51	10	10	5.00	100	80	50	83.16	8.59	9.32
52	10	30	8.66	100	80	50	49.17	8.80	8.75
53	10	10	7.50	100	80	50	101.85	7.07	7.64
54	10	30	12.99	100	80	50	59.20	7.11	7.14
55	10	10	10.00	100	80	50	117.60	5.77	6.28
56	10	30	17.32	100	80	50	60.47	5.14	4.94
57	10	10	12.50	100	80	50	131.48	4.87	5.28
58	10	30	21.65	100	80	50	124.35	7.98	7.33
59	10	10	15.00	100	80	50	265.95	7.65	8.33
60	10	30	25.98	100	80	50	128.79	6.41	5.89
61	10	10	17.50	100	80	50	269.46	6.47	6.99
62	10	30	30.31	100	80	50	134.46	5.59	5.05
63	10	10	20.00	100	80	50	273.64	5.65	6.16
64	10	30	34.64	100	80	50	276.75	9.90	8.93

Table 3-4 Parametric study for rigid footing.

CASE	B, ft	L, ft	T, ft	γ_{dt}, pcf	REC_{adj}, %	E_m/E_s	Bearing Stress, psi	Predicted settlement, in	Measured settlement, in
1	10	10	15.00	100	80	5	308.01	2.26	2.33
2	10	30	25.98	100	80	5	276.75	3.51	3.27
3	10	10	17.50	100	80	5	308.01	2.10	2.17
4	10	30	30.31	100	80	5	276.75	3.27	3.04
5	10	10	2.50	100	80	10	87.93	2.73	2.44
6	10	30	4.40	100	80	10	104.81	5.58	4.77
7	10	10	5.00	100	80	10	248.70	5.78	5.45
8	10	30	8.66	100	80	10	122.43	4.93	4.29
9	10	10	2.50	100	80	25	69.93	4.89	4.29
10	10	30	4.40	100	80	25	41.68	4.97	4.24
11	10	10	5.00	100	80	25	98.89	4.79	4.50
12	10	30	8.66	100	80	25	58.47	4.91	4.39
13	10	10	10.00	100	80	50	117.60	4.56	4.94
14	10	30	17.32	100	80	50	60.47	4.06	3.92
15	10	10	12.50	100	80	50	131.48	3.85	4.37
16	10	30	21.65	100	80	50	124.35	6.30	6.11

3.3 Key Parameters

Besides geometry, a key parameter for the settlement prediction is the rock mass modulus. The rock mass mean modulus ($E_m = \mu_E$ in probabilistic settlement) is obtained from the intact modulus (E_i) and the ratio of mass modulus to intact modulus (E_{mass}/E_{intact}, Figure 3-5). Green trend line (Ko, 2010) in Figure 3-5 is recommended to obtain the mass modulus based on the REC_{adj}:

a. When $REC_{adj} \leq 50\%$, $E_m/E_i = 0.2 \times REC_{adj}$
b. When $50\% < REC_{adj} \leq 70\%$, $E_m/E_i = 1.25 \times REC_{adj} - 0.525$
c. When $70\% < REC_{adj}$, $E_m/E_i = 2.17 \times REC_{adj} - 1.17$

Due to the high porosity of Florida limestone, limited lateral stress is developed at the bearing stress; consequently, a modulus from the 50 psi confining pressure triaxial tests is recommended (both initial modulus at 0.5% strain and secant modulus at 1% strain). Figure 3-12 provides the intact initial modulus versus bulk dry unit weights for 6 formations from Phase I & II. However, the intact moduli are recommended to be measured for a specific site due to the inherent variability of Florida limestone (CV of modulus around 1~3) and uncertainty of the site investigation (method errors).

(a) 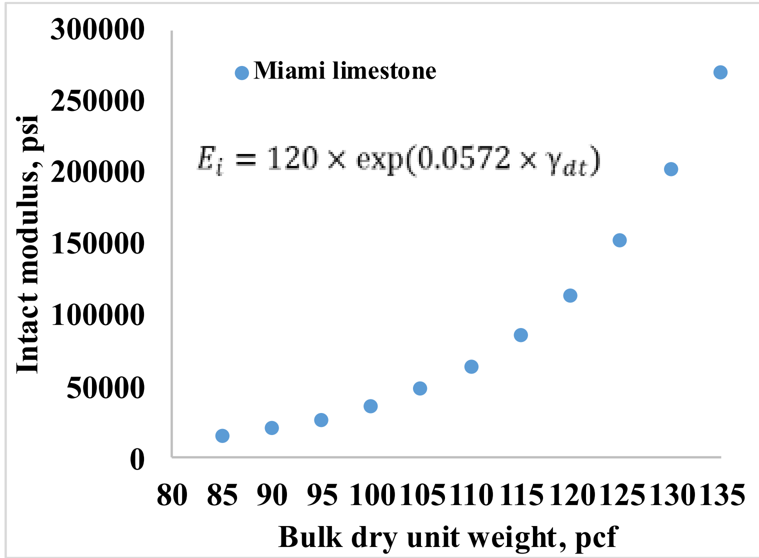
300000
250000
200000
150000
100000
50000
0
Intact modulus, psi
Miami limestone
$E_i = 120 \times \exp(0.0572 \times \gamma_{dt})$
80 85 90 95 100 105 110 115 120 125 130 135
Bulk dry unit weight, pcf

(b) 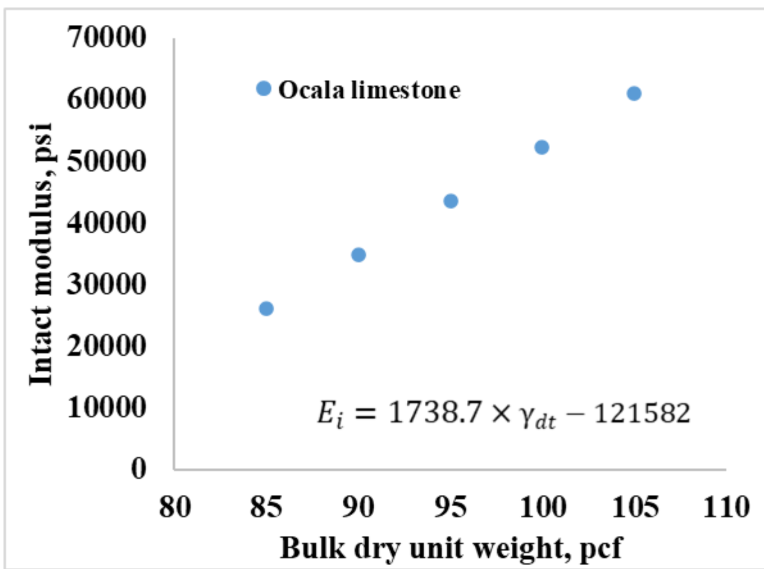
70000
60000
50000
40000
30000
20000
10000
0
Intact modulus, psi
Ocala limestone
$E_i = 1738.7 \times \gamma_{dt} - 121582$
80 85 90 95 100 105 110
Bulk dry unit weight, pcf

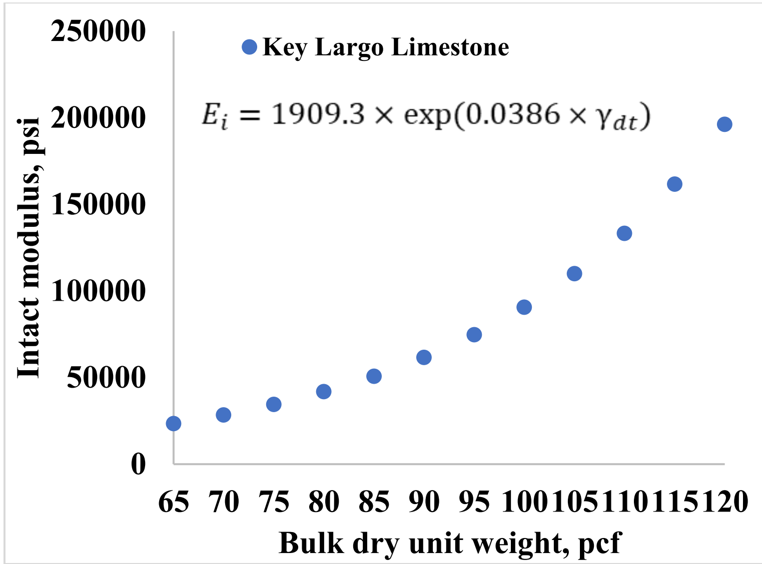
Key Largo Limestone
$E_i = 1909.3 \times \exp(0.0386 \times \gamma_{dt})$
Intact modulus, psi
250000
200000
150000
100000
50000
0
65 70 75 80 85 90 95 100 105 110 115 120
Bulk dry unit weight, pcf

(c)

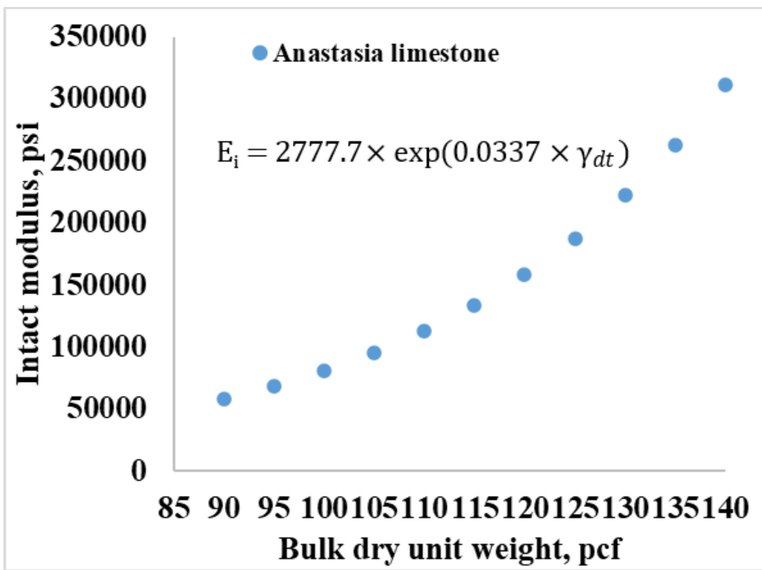
Anastasia limestone
$E_i = 2777.7 \times \exp(0.0337 \times \gamma_{dt})$
Intact modulus, psi
350000
300000
250000
200000
150000
100000
50000
0
85 90 95 100 105 110 115 120 125 130 135 140
Bulk dry unit weight, pcf

(d)

(e) 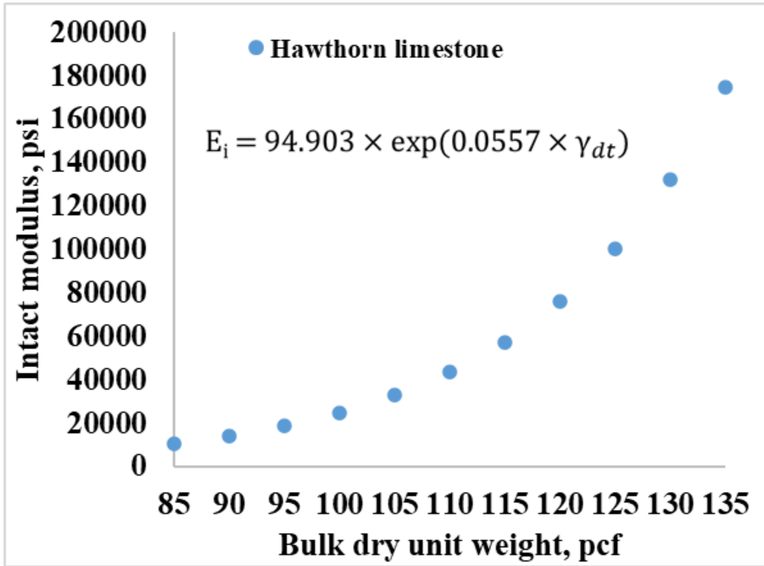

(f) 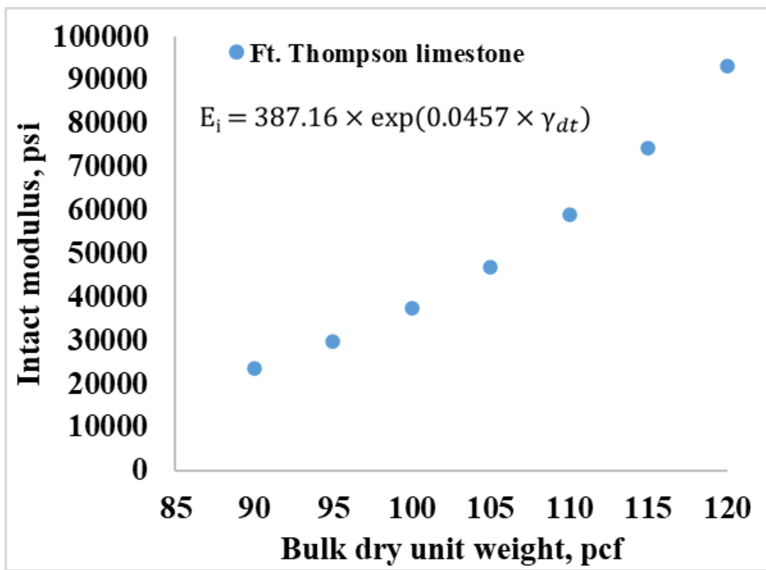

Figure 3-12 Intact initial modulus versus bulk dry unit weight for (a) Miami limestone (b) Ocala limestone (c) Key Largo limestone (d) Anastasia limestone (e) Hawthorn limestone (f) Fort Thompson limestone from phase I & II.

3.4 FB-MultiPier User-Interface (UI) and Analytical Engine Enhancements

The user-interface and the analytical engine of the FB-MultiPier program is proposed to be updated to implement the shallow foundation analysis feature using the research efforts from the Phase I (BDV31-977-51) and Phase II (BDV31-977-124) projects. The aim is to equip bridge design engineers with the capability to add and analyze a shallow foundation system on a Florida limestone layer beneath a bridge pier. Chapter 3 is focused on the implementation of pressure vs settlement springs for shallow foundation on Florida limestone in homogeneous, &

heterogeneous (rock over sand) conditions along with strip foundation on rock using the Hoek and Brown method.

3.4.1 Shallow Foundation Enhancements in FB-MultiPier UI

The update to the FB-MultiPier UI includes the creation of the 'Settlement Plot' dialog and enhancements to the 'FL Limestone (Homogeneous)' dialog, the 'FL Limestone (Rock over Sand)' dialog, and the 'Hoek & Brown (Carter & Kulhawy)' dialog. The access point for these dialogs is the 'Soil' page (Figure 3-13). On the 'Soil' page within the 'Shallow Foundation Data' frame, the 'Axial Bearing' model must be specified and the 'Edit' button clicked. These shallow foundation features are only available when footing is embedded in the soil or rested on the ground surface. The constitute properties of the foundation can be updated using the 'Footing' Page.

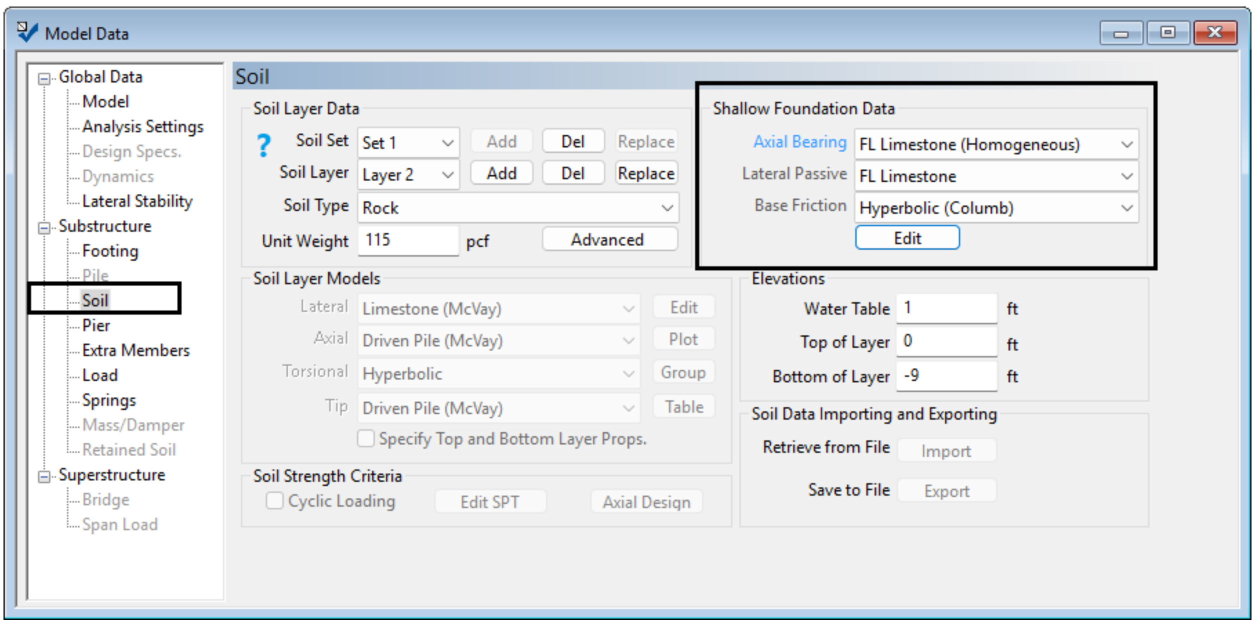

Figure 3-13 'Shallow Foundation Data' controls on 'Soil' page.

The user can select from available axial bearing soil resistance models using the dropdown control, namely:

1. FL Limestone (Homogeneous)
2. FL Limestone (Rock over Sand)
3. Hoek & Brown (Carter & Kulhawy)
4. Linear (Subgrade)
5. Custom

3.4.1.1 Axial Bearing Soil/Rock Resistance Model: FL Limestone (Homogeneous)

The ‘FL Limestone (Homogeneous)’ dialog (Figure 3-14) can be accessed when the ‘FL Limestone (Homogeneous)’ axial bearing soil/rock resistance model is selected from the dropdown (Figure 3-13) on the ‘Soil’ page and the ‘Edit’ button is clicked.

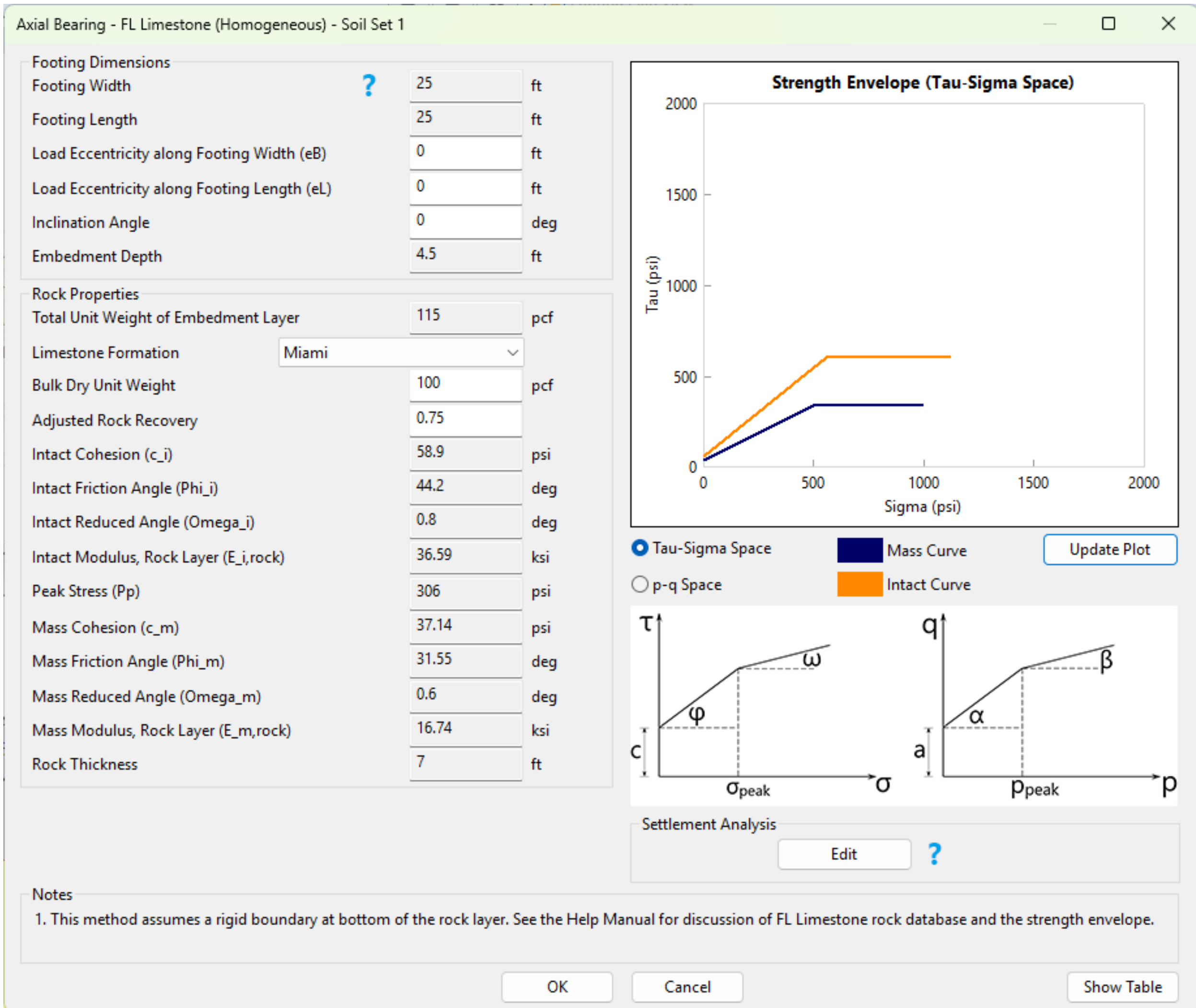

Figure 3-14 ‘FL Limestone (Homogeneous)’ dialog.

This ‘FL Limestone (Homogeneous)’ dialog content is as described in detail in Chapter 2. The ‘FL Limestone (Homogeneous)’ dialog include the Settlement Plot button (Figure 3-14). This button launches the Settlement Plot dialog (Figure 3-15), which plots settlement vs bearing stress relationship. For the ‘FL Limestone (Homogeneous)’, linearly elastic-perfectly plastic settlement curves are calculated by the program using Equation 3-1 to Equation 3-10.

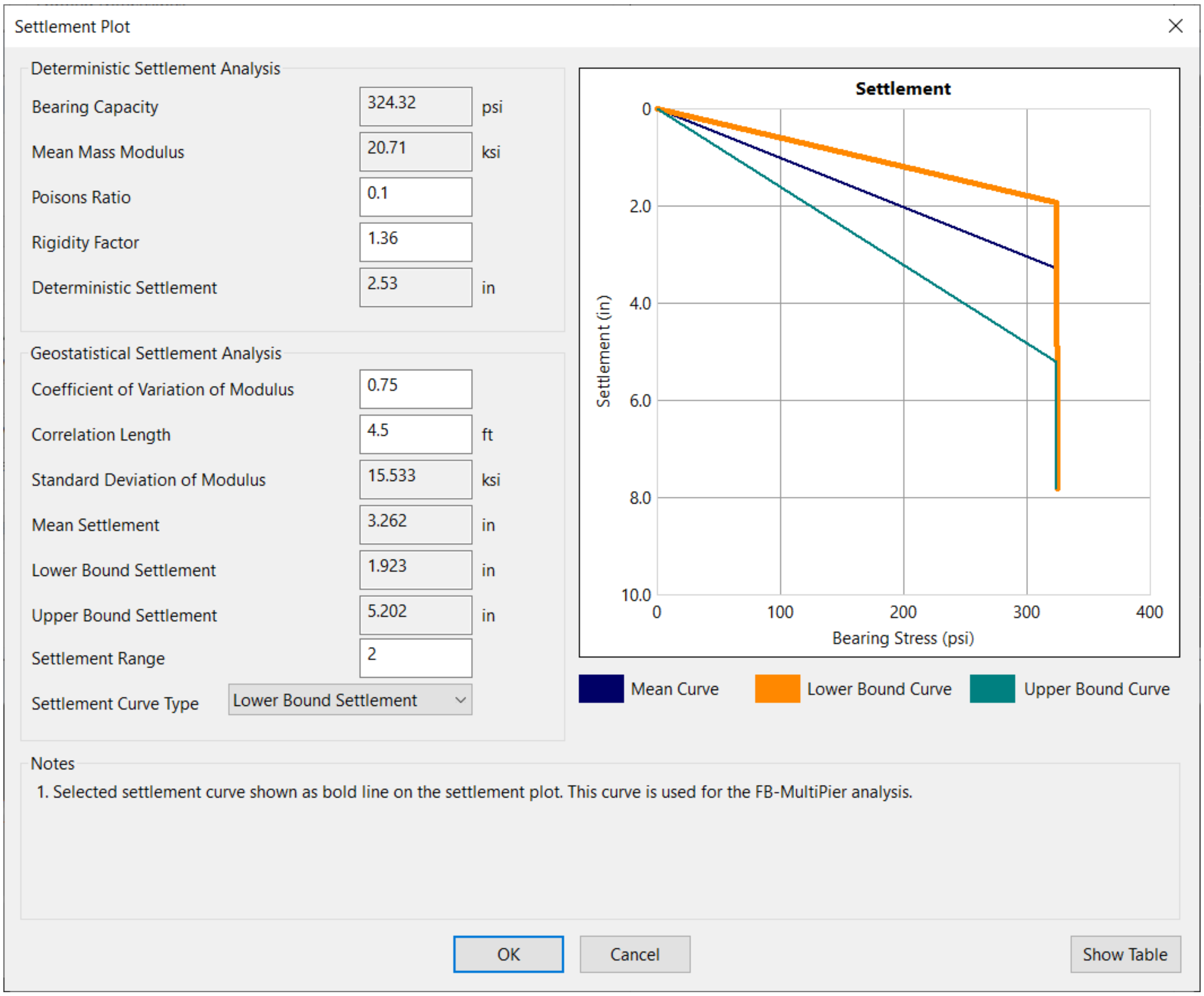

Figure 3-15 'Settlement Plot' dialog for FL limestone (homogeneous).

On the 'Deterministic Settlement Analysis' section (Figure 3-15), the required user input parameters consist of the Poisons Ratio, and Rigidity Factor. 'Bearing Capacity' parameter is calculated by the program in accordance with the analysis approach specified in Chapter 2. 'Mean Mass Modulus' is the 'Mass Modulus, Rock Layer (E_m,rock)' on the 'FL Limestone (Homogeneous)' dialog (Figure 3-14). Deterministic Settlement is calculated as per Equation 3-4, using footing width, Bearing Capacity, Mean Mass Modulus, Rigidity Factor, and Poisons Ratio. 'Bearing Capacity', 'Mean Mass Modulus, and 'Deterministic Settlement' are then displayed as read-only parameters on the 'Settlement Plot' dialog.

On the 'Geostatistical Settlement Analysis' section (Figure 3-15), the required input parameters consist of the 'Coefficient of Variation of Modulus', 'Correlation Length', 'Settlement Range', and 'Settlement Curve Type'. 'Standard Deviation of Modulus', 'Mean Settlement', 'Lower Bound Settlement', 'Upper Bound Settlement' are calculated by the program using Equation 3-1 to Equation 3-10. 'Standard Deviation of Modulus', 'Mean

Settlement', 'Lower Bound Settlement', and 'Upper Bound Settlement' are then displayed as read-only parameters on the 'Settlement Plot' dialog.

The Settlement Curve Type dropdown consists of three options (Figure 3-16), namely, Mean Settlement, Upper Bound Settlement, and Lower Bound Settlement. The selected 'Settlement Curve Type' is used by analytical engine to compute the settlement vs bearing stress relationship to be used in the compression only soil springs, which represents the soil response for the shallow foundation (More detail in 3.4.2 Shallow foundation enhancements in FB-MultiPier analytical engine).

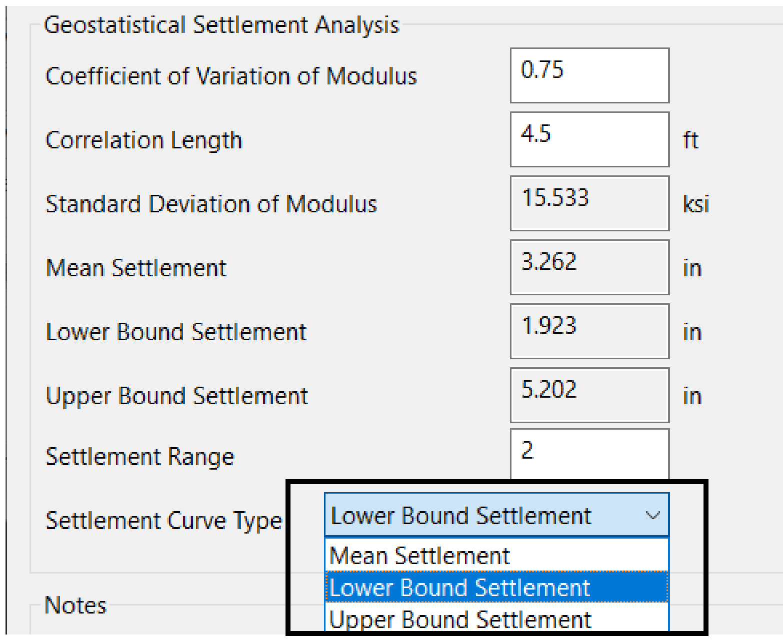

Figure 3-16 'Settlement Curve Type' dropdown on 'Settlement Plot' dialog for FL limestone (homogeneous).

The displayed settlement vs. bearing stress curves can be viewed in a tabular format by clicking the 'Show Table'or hidden by clicking 'Hide Table' button (Figure 3-17). The curve points are displayed in the following tables positioned to the right of plot: Mean Curve Points, Lower Bound Curve Points, and Upper Bound Curve Points.

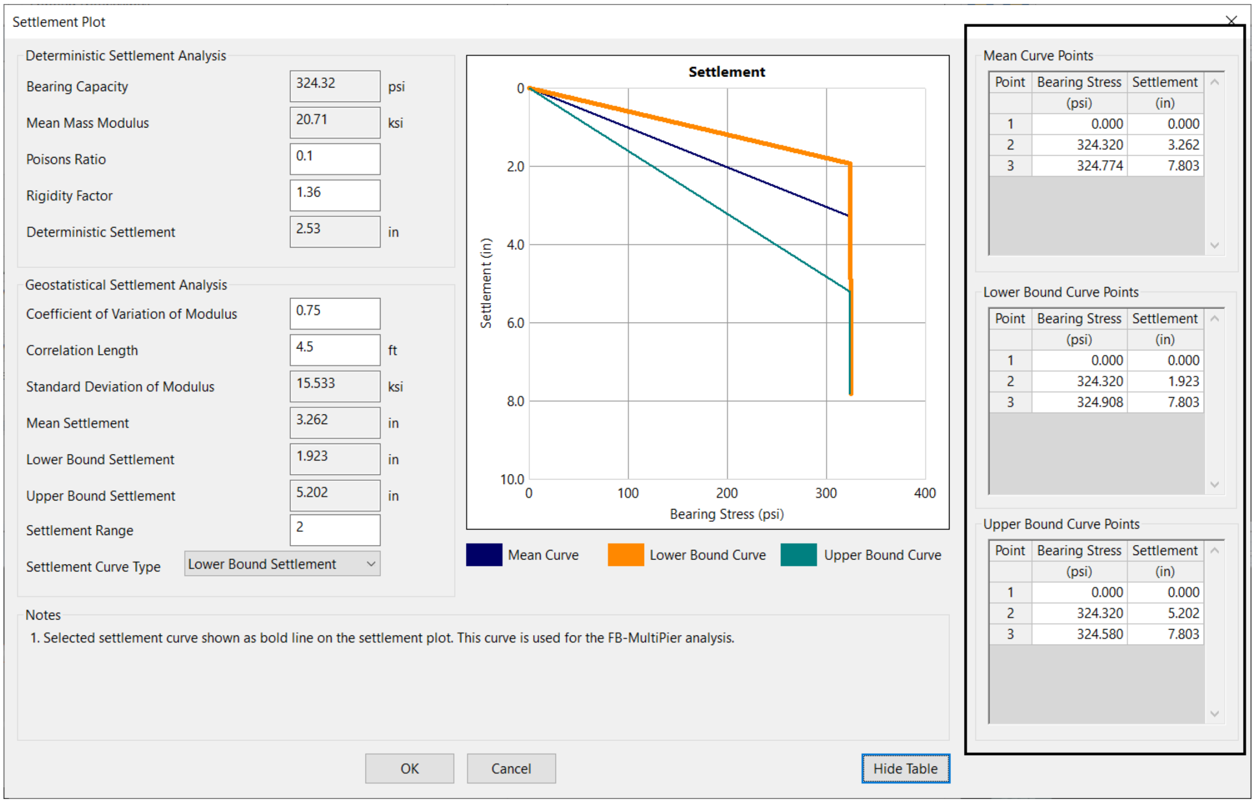

Figure 3-17 Curve points tables on ‘Settlement Plot’ dialog for FL limestone (homogeneous).

3.4.1.2 Axial Bearing Soil Resistance Model: FL Limestone (Rock over Sand)

The ‘FL Limestone (Rock over Sand)’ dialog (Figure 3-18) can be accessed when the ‘FL Limestone (Rock over Sand)’ axial bearing soil/rock resistance model is selected from the dropdown on the ‘Soil’ page and the ‘Edit’ button is clicked.

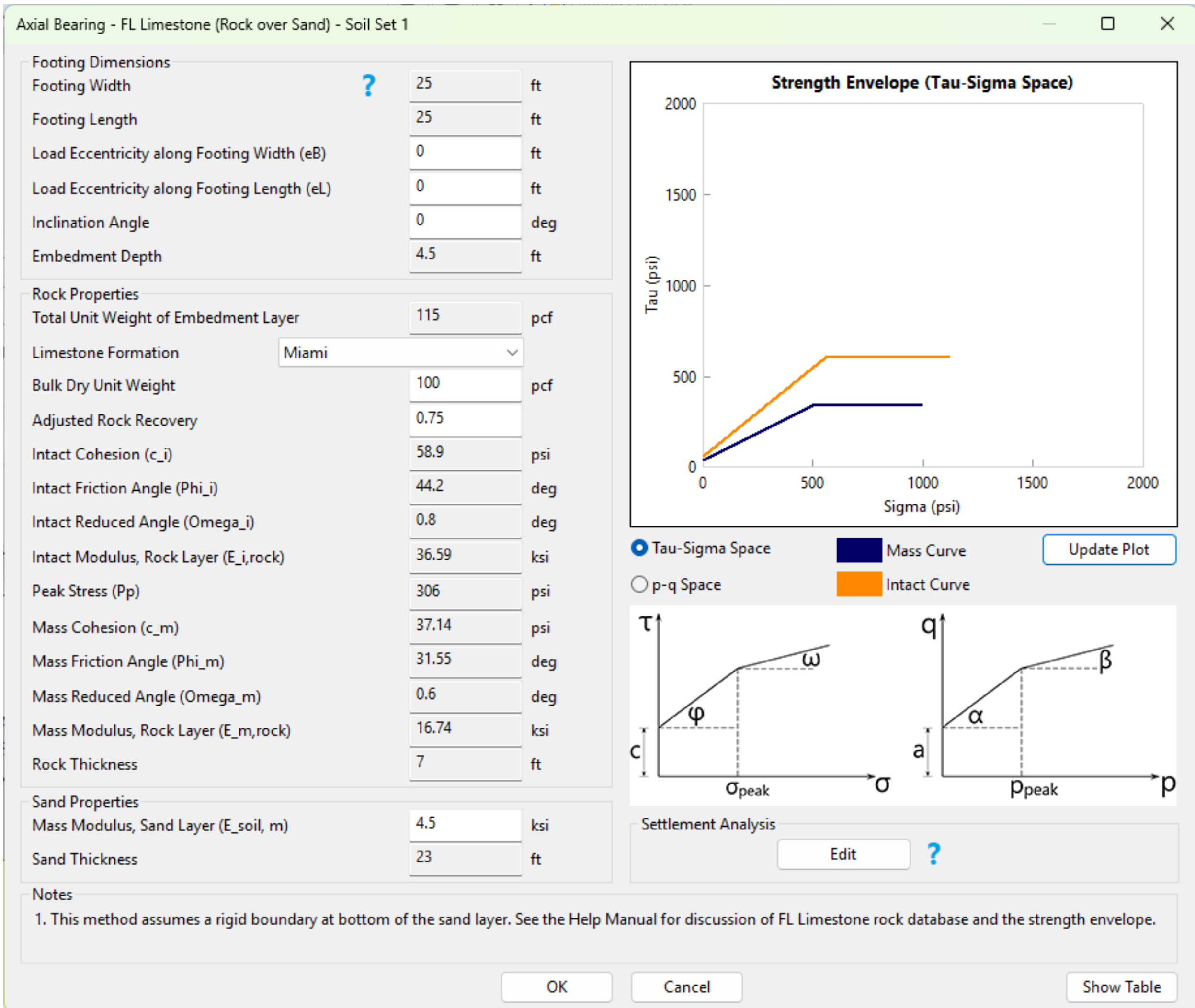

Figure 3-18 ‘FL Limestone (Rock over Sand)’ dialog.

The ‘FL Limestone (Rock over Sand)’ dialog content is described in detail in Chapter 2. The ‘FL Limestone (Rock over Sand)’ dialog (Figure 3-18) includes the “Settlement Plot” button. This button launches the ‘Settlement Plot’ dialog, which displays settlement vs bearing stress curves (Figure 3-19). For the ‘FL Limestone (Rock over Sand)’, bi-linear settlement curves are calculated by the program using analysis approach stated in 3.2.3 Florida rock-over-sand settlement.

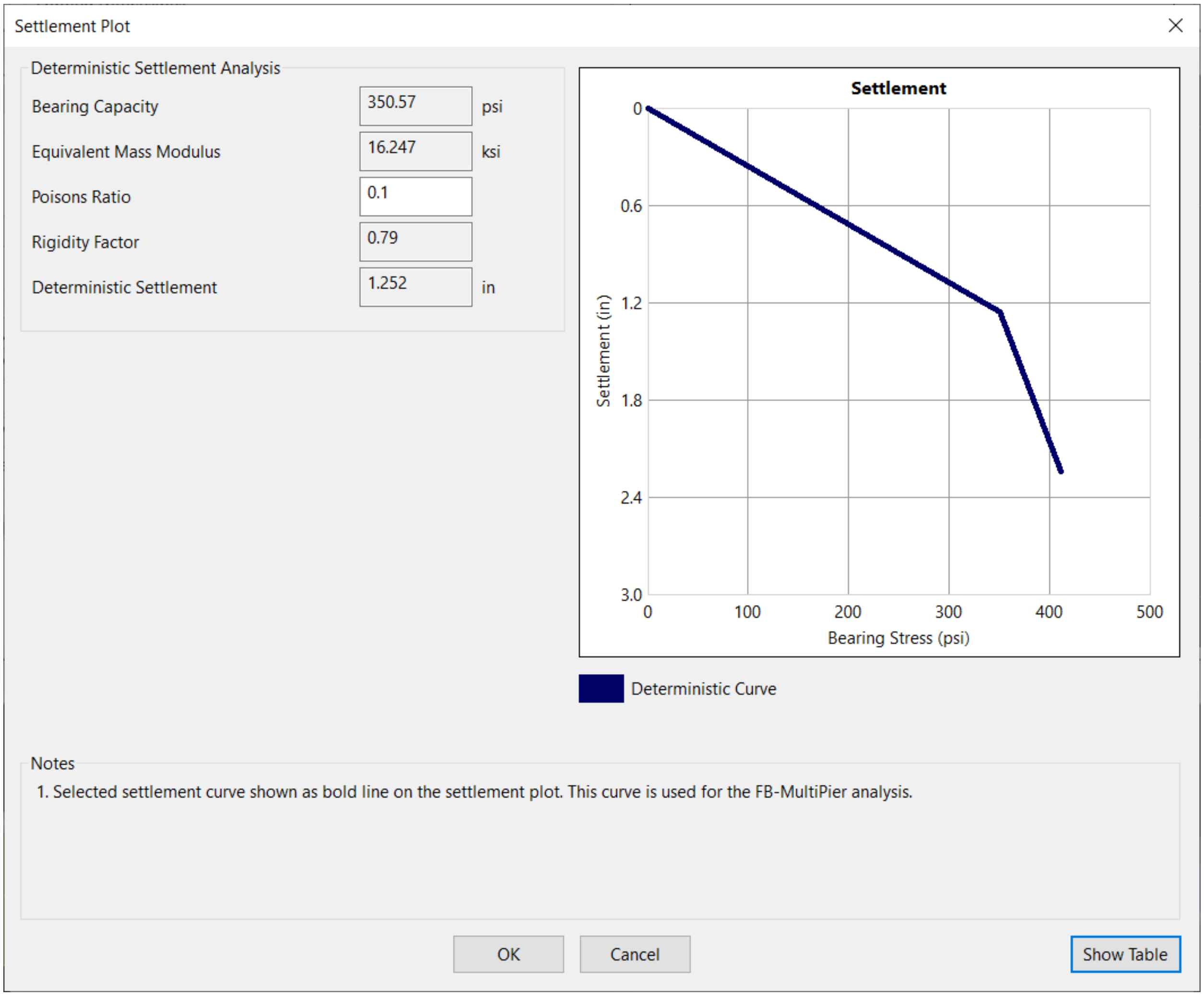

Figure 3-19 ‘Settlement Plot’ dialog for FL limestone (rock over sand)’.

For the Deterministic Settlement Analysis (Figure 3-19), the required user input of Poisons Ratio is needed. ‘Bearing Capacity’ parameter is calculated by the program in accordance with the analysis approach for ‘FL Limestone (Rock over Sand)’ case specified in Chapter 2. ‘Equivalent Mass Modulus’ is calculated by the program in accordance with the analysis approach stated in 3.2.3 Florida rock-over-sand settlement. The Rigidity Factor is calculated by the program as per Equation 3-11, Equation 3-12 and Equation 3-13. Deterministic Settlement is calculated as per Equation 3-4, using Footing Width, Bearing Capacity, Equivalent Mass Modulus, Rigidity Factor and Poisons Ratio. ‘Bearing Capacity’, ‘Equivalent Mass Modulus, Rigidity Factor and ‘Deterministic Settlement’ are then displayed as a read-only parameter on the ‘Settlement Plot’ dialog.

The displayed settlement vs. bearing stress curves can be viewed in a tabular format by clicking the ‘Show Table’or hidden by clicking ‘Hide Table’ button (Figure 3-20). The curve points are displayed in the “Deterministic Curve Points” table to the right of the plot.

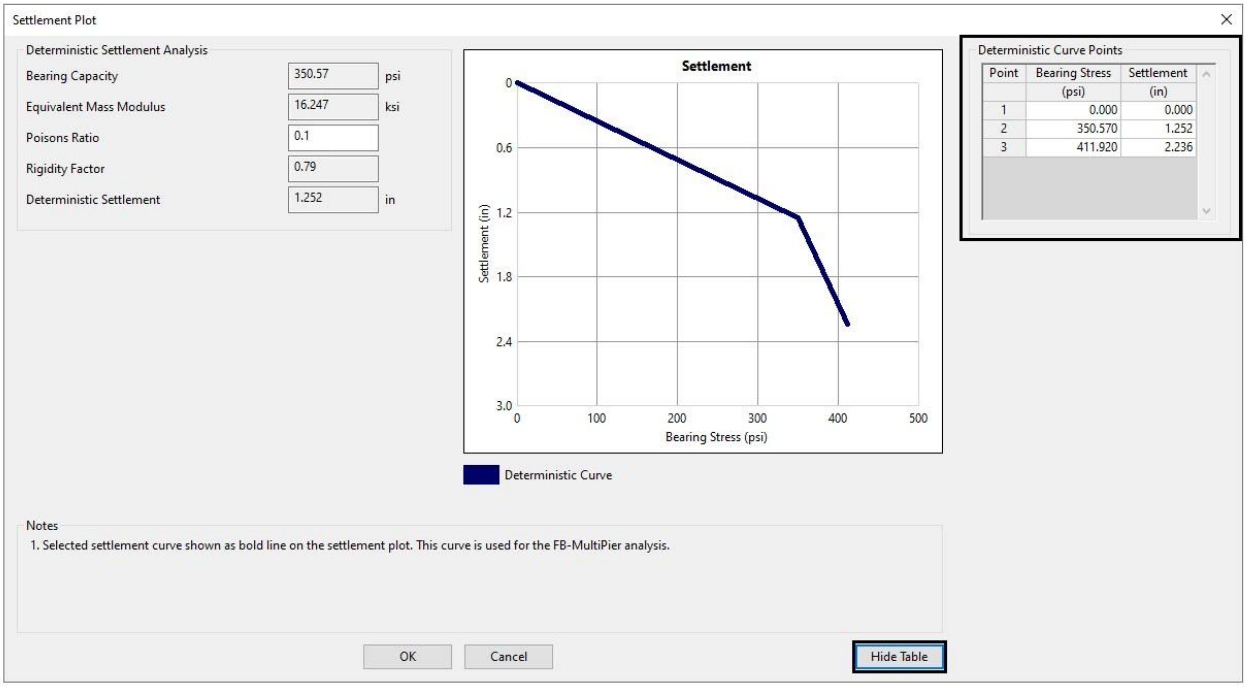

Figure 3-20 ‘Deterministic Curve Points’ table on ‘Settlement Plot’ dialog for FL limestone (rock over sand).

3.4.1.3 Axial Bearing Soil Resistance Model: Hoek & Brown (Carter & Kulhawy)

The ‘Hoek & Brown (Carter & Kulhawy)’ dialog (Figure 3-21) can be accessed when the ‘Hoek & Brown (Carter & Kulhawy)’ axial bearing rock resistance model is selected from the dropdown on the ‘Soil’ page and the ‘Edit’ button is clicked.

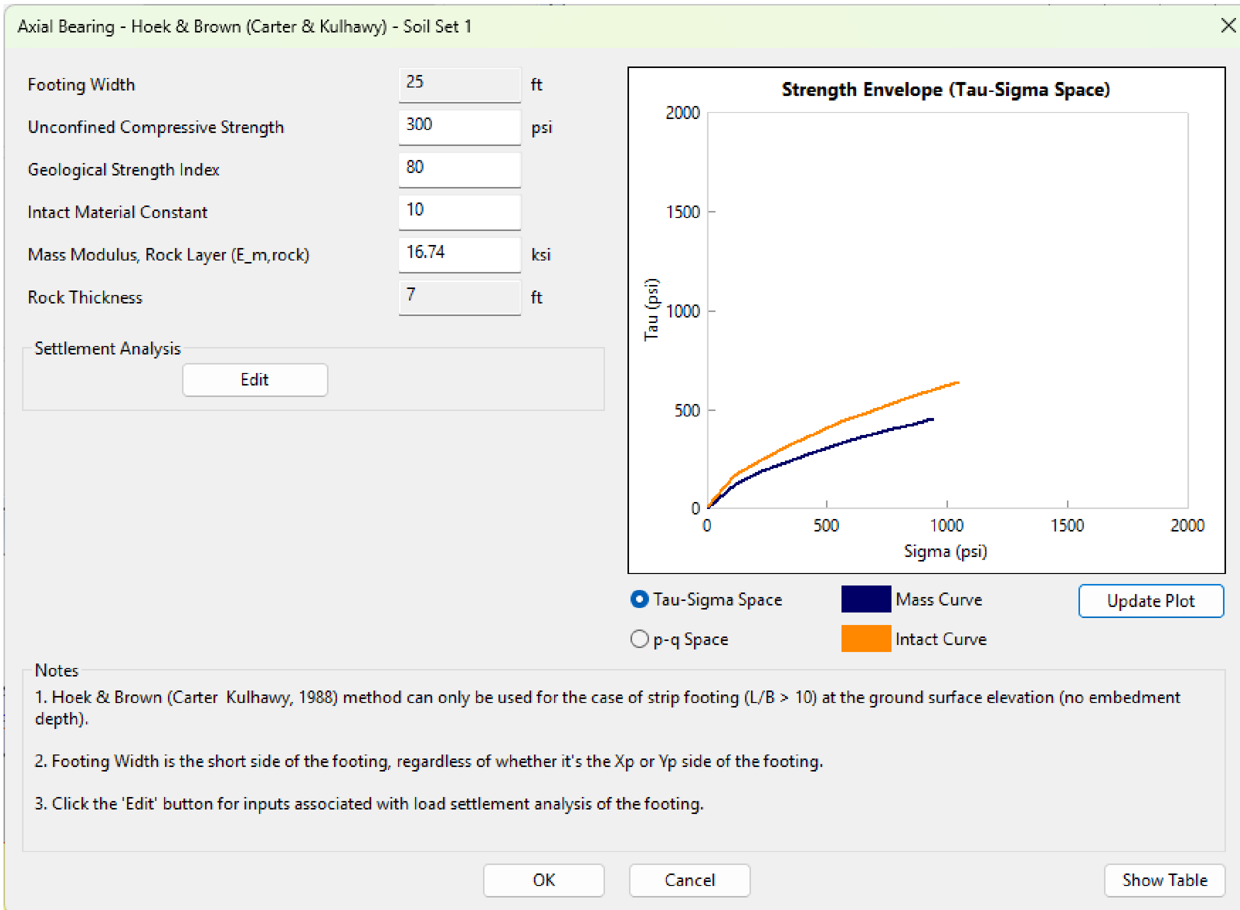

Figure 3-21 'Hoek & Brown (Carter & Kulhawy)' dialog.

The 'Hoek & Brown (Carter & Kulhawy)' dialog content is described in detail in Chapter 2. The 'Hoek & Brown (Carter & Kulhawy)' dialog includes the "Settlement Plot" button (Figure 3-21). This button launches the Settlement Plot dialog (Figure 3-22), which displays settlement vs. bearing stress curves.

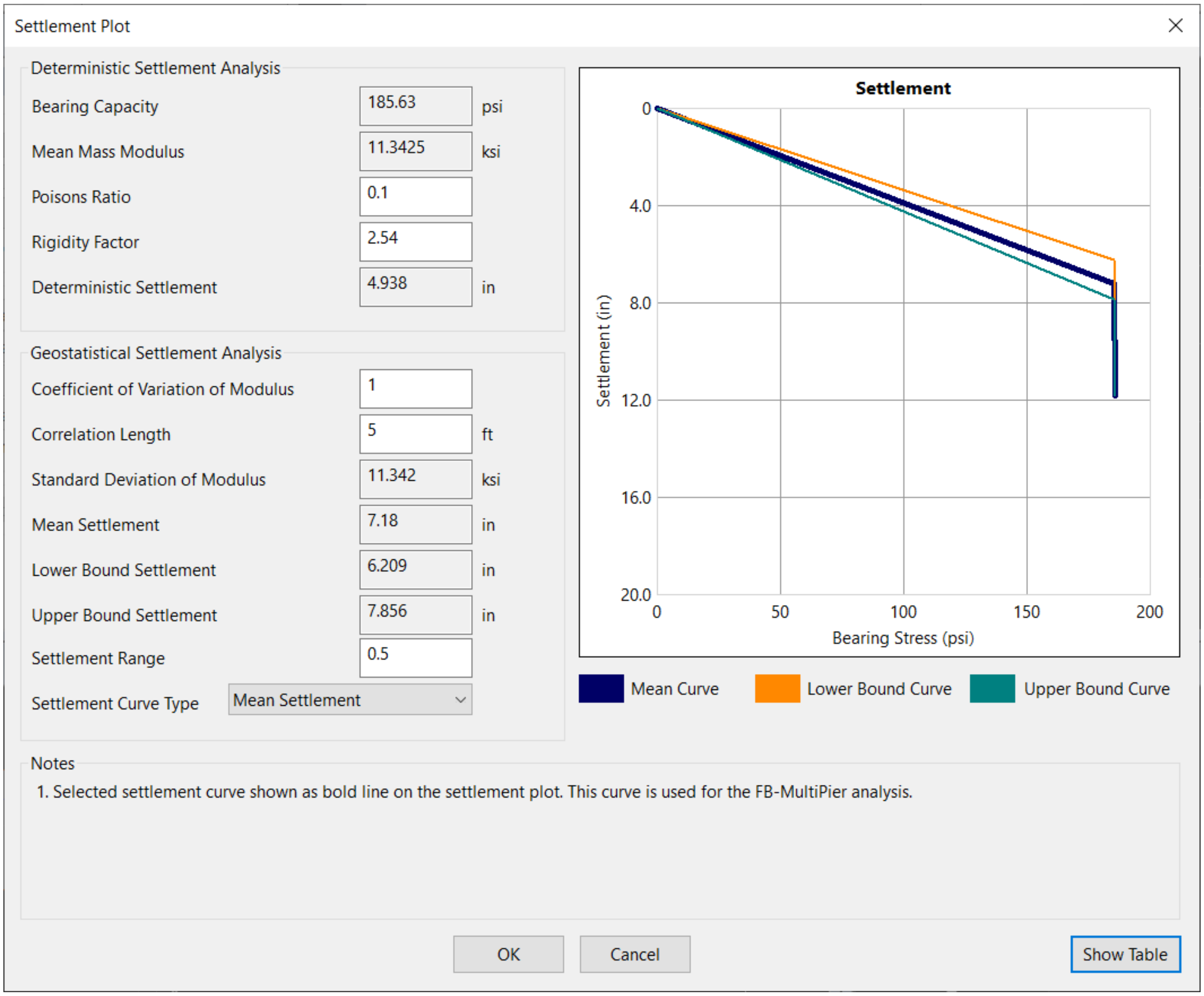

Figure 3-22 'Settlement Plot' dialog for Hoek & Brown (Carter & Kulhawy).

The input parameters and the analysis approach are similar to Settlement plot of 'FL Limestone (Homogeneous)'. Please refer 3.4.1.1 Axial Bearing Soil/Rock Resistance Model: FL Limestone (Homogeneous) for more detail regarding the 'Settlement Plot' dialog.

3.4.1.4 Axial Bearing Soil Resistance Model: Linear (Subgrade)

The 'Axial Bearing Linear (Subgrade)' dialog (Figure 3-24) can be accessed when the 'Linear (Subgrade)' model is selected from the dropdown within the 'Shallow Foundation Data' frame on 'Soil' page, and the 'Edit' button is clicked.

Enhancement to the shallow foundation soil models include the addition of Axial Bearing – 'Linear (Subgrade)'. This linear model type is implemented in the program not only for design but also as a debugging tool. All the shallow foundation soil resistance models in both axial and lateral directions exhibit perfectly plastic failure behavior. This can introduce non-convergence issues when the applied loading approaches the plastic ultimate resistance in either direction. The linear model is a useful tool for verification, as it provides linear resistance with no failure, thereby eliminating convergence issues associated with soil yielding.

Once convergence is achieved using linear model, the results can be evaluated to better understand the source of the problem. For example, excessive displacement may indicate weak soil properties or excessive loading. In such cases, footing dimensions, applied loads, or soil properties, can be individually reviewed and adjusted as necessary. After these modifications, the original soil models can be reactivated and the analysis repeated. This highlights the importance of including a linear model option for debugging purpose.

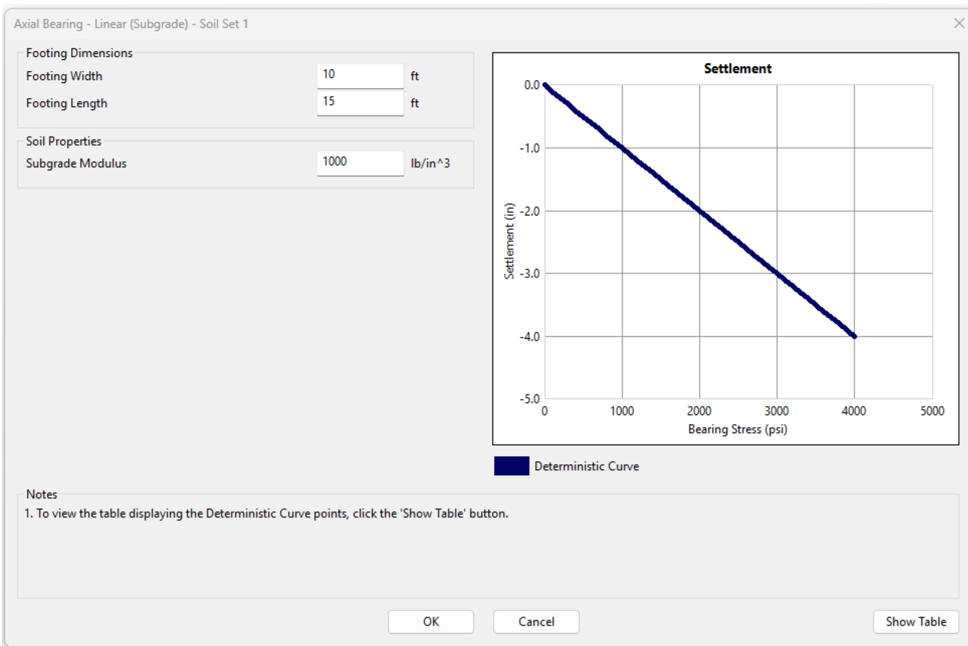

Figure 3-23 Axial bearing – ‘Linear (Subgrade)’ dialog.

Footing geometry inputs are read-only on this dialog (Figure 3-23), and are calculated by the program-based input, namely the following: footing width (B), footing length (L). Additionally, ‘Soil Properties’ input, Subgrade Modulus is required.

After entering the required input, the deterministic curve will plot in the ‘Settlement’ plot window. The displayed deterministic curve can be viewed in a tabular format by clicking the ‘Show Table’ button. The curve points are displayed to the right of the plot (Figure 3-24).

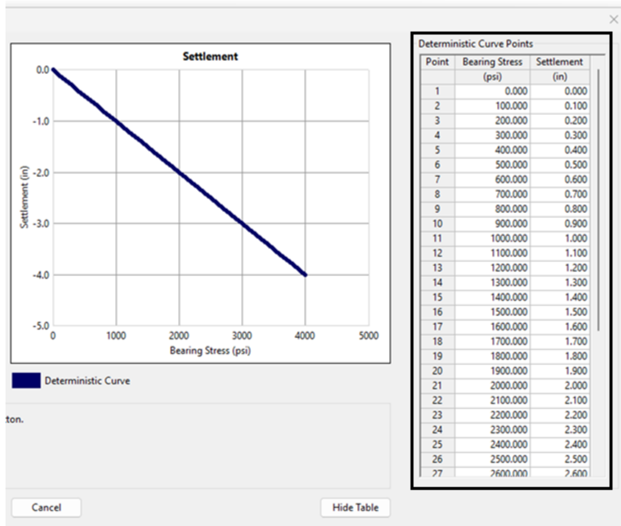

Figure 3-24 ‘Deterministic Curve Points’ table on ‘Axial Bearing Linear (Subgrade)’ dialog.

3.4.1.5 Axial Bearing Soil Resistance Model: Custom

The ‘Custom Curve’ dialog can be accessed when the ‘Custom’ model type is selected for Axial Bearing soil resistance model. The ‘Custom’ model can be selected for the ‘Axial Bearing’ model within the ‘Shallow Foundation Data’ frame on ‘Soil’ page, and the ‘Edit’ button is clicked. After inputting the desired number of curve points in the table and clicking the ‘Update Plot’ button, the custom curve will display (Figure 3-25).

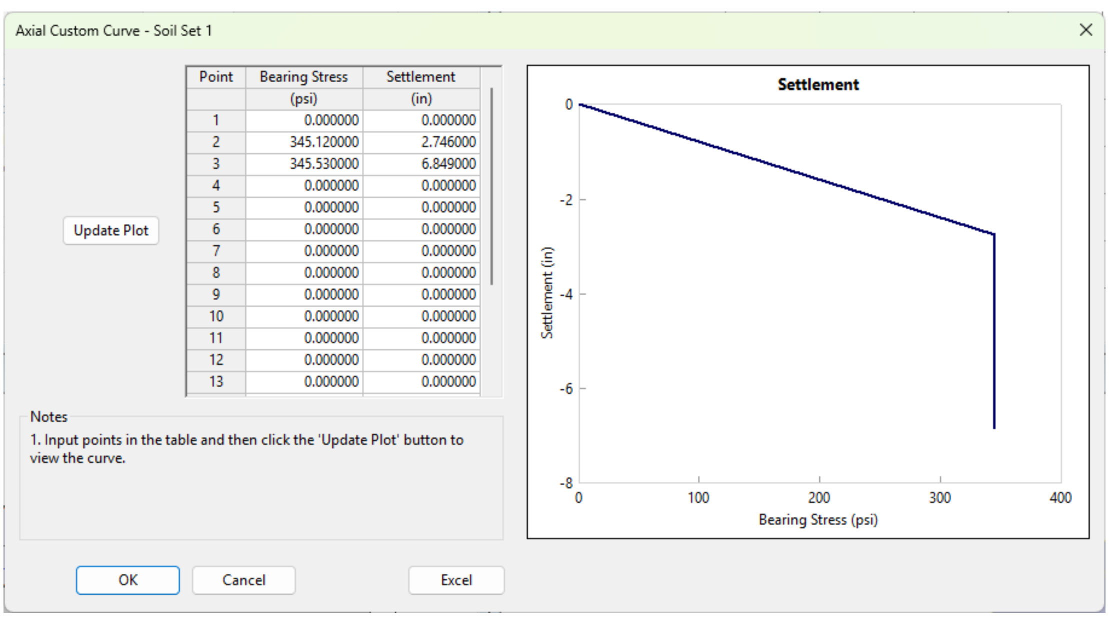

Figure 3-25 ‘Custom Curve’ dialog for axial bearing model.

3.4.2 Shallow Foundation Enhancements in FB-MultiPier Analytical Engine

The input parameters mentioned in Section 3.4.1 Shallow foundation enhancements in FB-MultiPier UI pertaining to the shallow foundation soil resistance models are saved in the input file under the header 'SHALLOWFOUND' as stated in 3.5 Input-associated updates to model input files. The analytical engine reads this header and calculates the bearing capacity for the axial model selected in accordance with Chapter 2.

FB-MultiPier uses finite element model with Beam on Non-linear Winkler Foundation (BNWF) approach to analyze the embedded shallow foundation model (Figure 3-26(b)). A set of distributed 9-node thick shell elements are used to represent shallow foundation (footing in FB-MultiPier UI). The shell element nodes are discretized as per the grid spacing specified on the 'Footing' page and are positioned at the midplane of the foundation. Additionally, a set of non-linear soil springs are used to model the vertical soil resistance on the shallow foundation and are applied at each foundation node. These non-linear soil springs correspond to the bearing stresses developed due to foundation settlement and are calculated as per 3.2 Analysis approaches. These soil springs are compression only and not active in tension. The tributary area for each foundation node is then used to calculate the developed soil spring forces due to the loading.

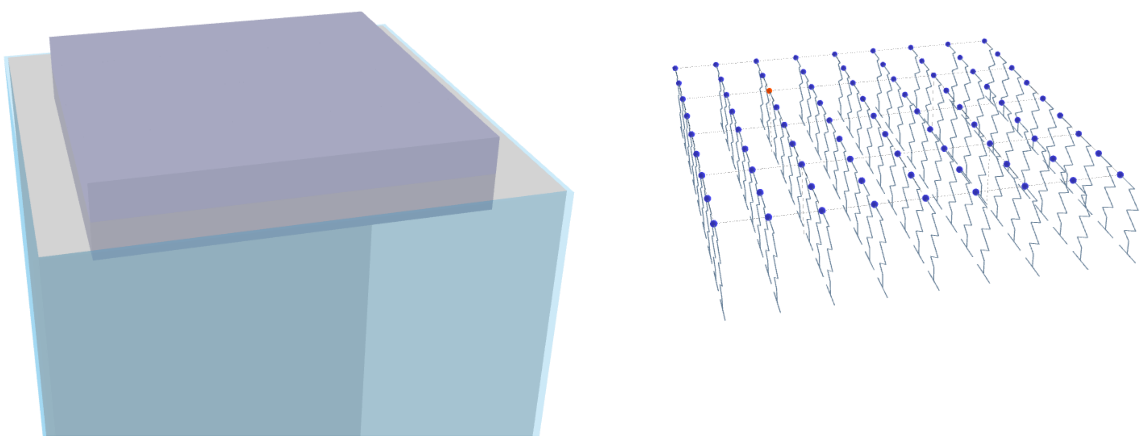

(a) (b)

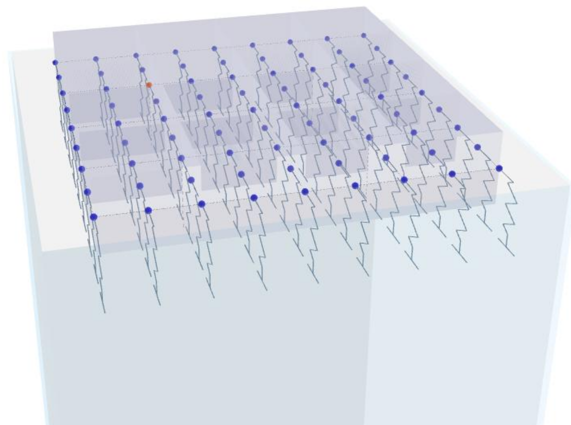

(c)

Figure 3-26 a) Shallow foundation (thick view), b) shallow foundation (thin element view), and c) shallow foundation (overlay view).

Bearing capacity and soil bearing pressure developed per footing node are printed in the output (.out) under the file as shown below:

```
_______________________________________________________________
Sum of Total Soil Spring Forces for Foundation Nodes (Load CASE   1)



 Soil Set   1
 Xp Direction                         =           0.0000  kips
    Base Friction                     =           0.0000  kips
    Lateral Passive                   =           0.0000  kips
 Yp Direction                         =           0.0000  kips
    Base Friction                     =           0.0000  kips
    Lateral Passive                   =           0.0000  kips
 Zp Direction                         =         656.2525  kips
 Est. of Ultimate Bearing Capacity    =         492.1933  psi



 _______________________________________________________________
Soil Bearing Pressures at Foundation Nodes


         Node         Pressure       Trib. Area       Spring Force
                           ksf             ft^2               kips
            1       7.7633E-01       2.2500E+00       1.7467E+00
            2       6.2379E-01       2.2500E+00       1.4035E+00
            3       7.7633E-01       2.2500E+00       1.7467E+00
          ...              ...              ...              ...
          167       2.3342E-01       1.1250E+00       2.6259E-01
          168       2.8563E-01       1.1250E+00       3.2133E-01
          169       3.3253E-01       1.1250E+00       3.7410E-01
```

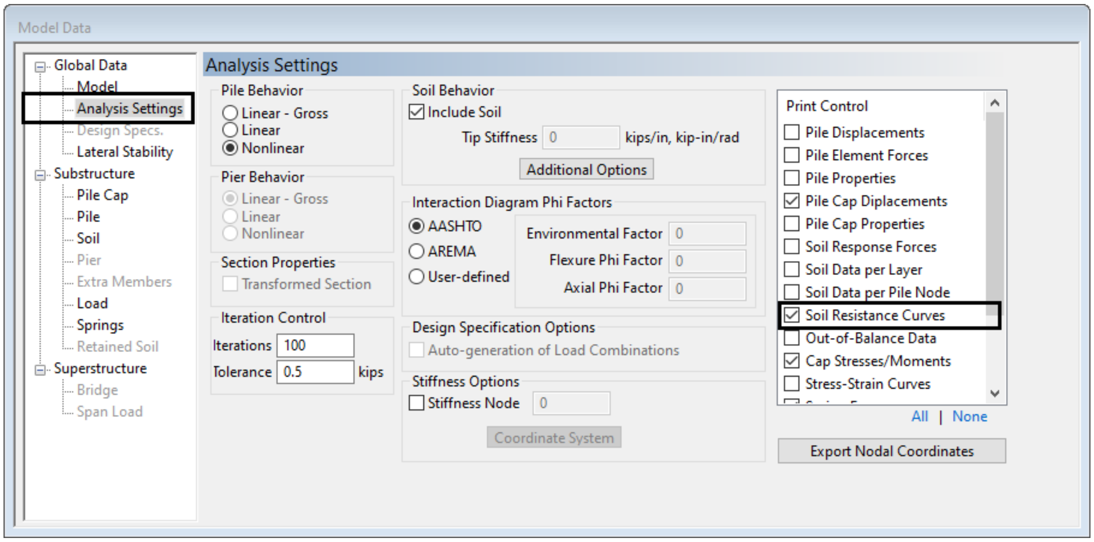

Figure 3-27 Print control option on the ‘Analysis Settings’ page in FB-MultiPier UI.

The analytical engine also prints the bearing pressure vs settlement curve in the output file (.out) if the print control ‘Soil Resistance Curve’ option is checked in the FB-MultiPier UI (Figure 3-27). The Bearing pressure vs settlement curve is printed under the header ‘Soil Resistance Curves for Footing Bearing’ as shown below:

```
**************************************************************
 *      SOIL RESISTANCE CURVES FOR FOOTING AXIAL BEARING       *
 **************************************************************



 ______________________________________________________________
 - Pressure-Z Curves for Footing: Soil Set  1



 Curves are compression only, and are applied per soil set to
 each footing element node.



             z         Pressure
            in              psi
      0.000000         0.000000
      0.102564         2.693447
      0.205128         5.386895
      0.307692         8.080342
      0.410256        10.773790
      0.512821        13.467237
      0.615385        16.160685
      0.717949        18.854132
      0.820513        21.547580
      0.923077        24.241027
      1.025641        26.934474
      1.128205        29.627922
      1.230769        32.321369
      1.333333        35.014817
      1.435897        37.708264
      1.538462        40.401712
      1.641026        43.095159
      1.743590        45.788606
      1.846154        48.482054
      1.948718        51.175501
      2.051282        53.868949
      2.153846        56.562396
      2.256410        59.255844
      2.358974        61.949291
      2.461538        64.642739
      2.564103        67.336186
      2.666667        70.029633
      2.769231        72.723081
      2.871795        75.416528
      2.974359        78.109976
      3.076923        80.803423
      3.179487        83.496871
      3.282051        86.190318
      3.384615        88.883765
      3.487179        91.577213
      3.589744        94.270660
```

3.5 Input-Associated Updates to Model Input Files

The inputs associated with the axial soil resistance models for the shallow foundation and the input parameters associated with them are entered using the FB-MultiPier UI. These shallow foundation data are then saved in the input (.in) file under header SHALLOWFOUND as mentioned in F.1 User-Guide for Input File Update.

3.6 Validation and Stress Comparisons in the Analysis Output

To ensure the accuracy of the coding implemented in the FB-MultiPier UI and engine, a comprehensive validation process was conducted using several distinct sources. The validation sets were selected to include detailed worked solutions, multiple examples with varying ranges of variable inputs, and a comparison between standard English and SI units. Three specific sources were employed to validate the implementation: a worked example set, an Excel spreadsheet utilized for in-depth sensitivity analysis, and selected problems from previous FDOT reports. Together, these methods form a robust assessment of the validations of the FB-MultiPier UI and engine.

3.6.1 Florida Limestone Homogeneous Validation

For this project the first validation problems were a set of problems for single rock layer, using the Florida Limestone homogeneous model. The validation consisted of confirming bearing capacity and settlement calculations from FB-MultiPier UI dialogs and engine output (i.e., .out file). Additionally, the load settlement response determine by FB-MultiPier was compared with the settlement calculations. The following cases were analyzed.

- Case 1 - Florida Limestone Homogeneous based on formation (Worked Example)
- Case 2 - Florida Limestone Homogeneous based on formation (Sensitivity Study)
- Case 3 - Florida Limestone Homogeneous based on formation (Sensitivity Study)
- Case 4 - Florida Limestone Homogeneous based on formation (Sensitivity Study)
- Case 5 - Florida Limestone Homogeneous based on formation (Sensitivity Study)
- Case 6 - Florida Limestone Homogeneous based on formation (Sensitivity Study)
- Case 7 - CMEX Load Test

In total 7 cases were analyzed, the first being based on the worked example which walks through the design method in detail, Appendix B.1.1 . The case examples 2 through 6 are a sensitivity study, where input parameters for the settlement calculation are perturbated, to ensure FB-MultiPier is using each one appropriately. The last case study is based on the CMEX Load Test from the phase 2 project BDV31-977-124 (details are shown in Appendix B.1.2). Results from this validation set are shown in Table 3-5 through Table 3-7. Table 3-5 presents results of the bearing capacity comparison. Table 3-6 shows results of the settlement calculation for each case. Table 3-7 presents a comparison of the settlement results from the excel spreadsheet calculations and FB-MultiPier. In all tables it can be seen the observed percent error is below 0.12%, thus showing excellent agreement between the excel calculation and FB-MultiPier.

Table 3-5 Florida limestone homogeneous bearing capacity comparison.

CASE	-	1	2	3	4	5	6	CMEX
Mass Properties	c, psi	40.68	40.68	40.68	40.68	40.68	40.68	31.9
	φ, ˚	33.92	33.92	33.92	33.92	33.92	33.92	32.4
	ω, ˚	0.64	0.64	0.64	0.64	0.64	0.64	4.35
	P_p, psi	306	306	306	306	306	306	341.8
	E_m, ksi	20.71	20.71	20.71	20.71	20.71	20.71	13.32
Footing Geometry	B, ft	10	10	10	10	10	10	3.5
	L, ft	15	15	15	15	15	15	3.5
	e_b	0	1	0	0	0	0	0
	e_l	0	1.5	0	0	0	0	0
	D_f, ft	3	3	3	3	3	3	5
Depth of Water Table	D_w	1.5	1.5	1.5	1.5	1.5	1.5	0
Total Unit Weight	g_{total}, pcf	115	115	115	115	115	115	115
REC	%	80	80	80	80	80	80	72
Rock Thickness	T_r, ft	20	20	20	20	20	20	5.3
E_{rock} (mass modulus)	psi	20710	20710	20710	20710	20710	20710	13320
Qu Excel	psi	324.31	320.73	324.31	324.31	324.31	324.31	247.79
Qu FBMP UI	psi	324.32	320.74	324.32	324.32	324.32	324.32	247.81
% ERROR	%	0.00%	0.00%	0.00%	0.00%	0.00%	0.00%	-0.01%
Qu FBMP ENGINE	psi	324.32	320.74	324.32	324.32	324.32	324.32	247.81
% ERROR	%	0.00%	0.00%	0.00%	0.00%	0.00%	0.00%	-0.01%

Table 3-6 Florida limestone homogeneous settlement calculation.

CASE	-	1	2	3	4	5	6	CMEX
Mass properties	μ_E, psi	20710	20710	20710	20710	20710	20710	13320
	CV_E	0.75	0.75	1	0.75	0.75	0.75	1.37
	σ_E, psi	15532.5	15532.5	20710	15532.5	15532.5	15532.5	18248.4
	ν	0.1	0.1	0.1	0.1	0.2	0.1	0.1
	a_v, ft	4.5	4.5	4.5	10	4.5	4.5	4.5
	n	2	2	2	2	2	1	0.75
Geometry	t, ft	6	6	6	6	6	6	0.166667
Foundation Rigidity	$E_{foundation}$, psi	4400000	4400000	4400000	4400000	4400000	4400000	29000000
	L/B	1.5	1.5	1.5	1.5	1.5	1.5	1
	a	6.91	6.91	6.91	6.91	6.91	6.91	1.97
	K_F	139.096	139.096	139.096	139.096	139.096	139.096	1.31
	I_F	0.786	0.786	0.786	0.786	0.786	0.786	0.842
	C_s	1.36	1.36	1.36	1.36	1.36	1.36	1.12
	C	1.069	1.069	1.069	1.069	1.069	1.069	0.943
Bearing value	Q_u, psi	324.31	320.73	324.31	324.31	324.31	324.31	247.79
Fenton and Griffiths' method	δ_{det}, in	1.989	1.967	1.989	1.989	1.929	1.989	0.729
	$\sigma_{\ln E}$	0.668	0.668	0.833	0.668	0.668	0.668	1.028
	$\gamma(T_r)$	0.139	0.139	0.139	0.278	0.139	0.139	0.411
	$\sigma_{\ln\delta}$	0.249	0.249	0.310	0.352	0.249	0.249	0.659
	$\mu_{\ln\delta}$	0.911	0.900	1.034	0.911	0.880	0.911	0.213
	μ_δ, in	2.564	2.536	2.951	2.645	2.487	2.564	1.537
	σ_δ, in	0.648	0.641	0.938	0.961	0.628	0.648	1.133
	δ_{LB}, in	1.511	1.495	1.513	1.229	1.466	1.938	0.76
	δ_{UB}, in	4.090	4.044	5.230	5.028	3.966	3.189	2.03

Table 3-7 Florida limestone homogeneous settlement comparison (FBMP = FB-MultiPier).

CASE	-	1	2	3	4	5	6	CMEX
FBMP UI	μ_δ, in	2.564	2.536	2.951	2.645	2.486	2.564	1.537
% ERROR	%	0.01%	0.00%	0.01%	0.01%	0.03%	0.01%	-0.01%
FBMP UI	δ_{LB}, in	1.511	1.495	1.513	1.229	1.466	1.938	0.331
% ERROR	%	0.03%	-0.02%	-0.02%	0.02%	-0.02%	0.02%	0.12%
FBMP UI	δ_{UB}, in	4.089	4.044	5.230	5.028	3.965	3.188	4.619
% ERROR	%	0.01%	0.01%	0.00%	0.01%	0.02%	0.02%	-0.01%

The final validation of implementation of the load settlement curve, was comparing the nodal displacement from FB-MultiPier finite element analysis to calculate the load settlement curve. For each case a shallow foundation model was created that matches the prescribed geometry (i.e., length, width, etc.) and modulus. A column was located at the center of the footing. The column is connected to the foundation using rigid connector elements which spans column center to edge of column footprint, to prevent unrealistic stress concentration. A load of 1000 kips was then applied to the model. An example of this configuration for case 1 is shown in Figure 3-28. To generate results for load settlement, FB-MultiPier pushover analysis is used in conjunction of a vertical load increment of 250 kips, to generate multiple load cases.

After the model is analyzed with FB-MultiPier engine, the vertical nodal displacement (settlement) per load increment is then extracted from the center of the footing. These settlement values are then plotted against bearing stresses which are calculated at the respective applied load divided by the total footing area. The FB-MultiPier bearing stress vs settlement is then compared to the calculated bearing settlement curve. An example of this is shown in Figure 3-29 for case 1 for the mean settlement curve. Resulting bearing settlement from FB-MultiPier is in good agreement with the specified bearing settlement curve replicating the linearly elastic-perfectly plastic model. Results from the other cases, not shown, are also in good agreement with their corresponding bearing settlement curve.

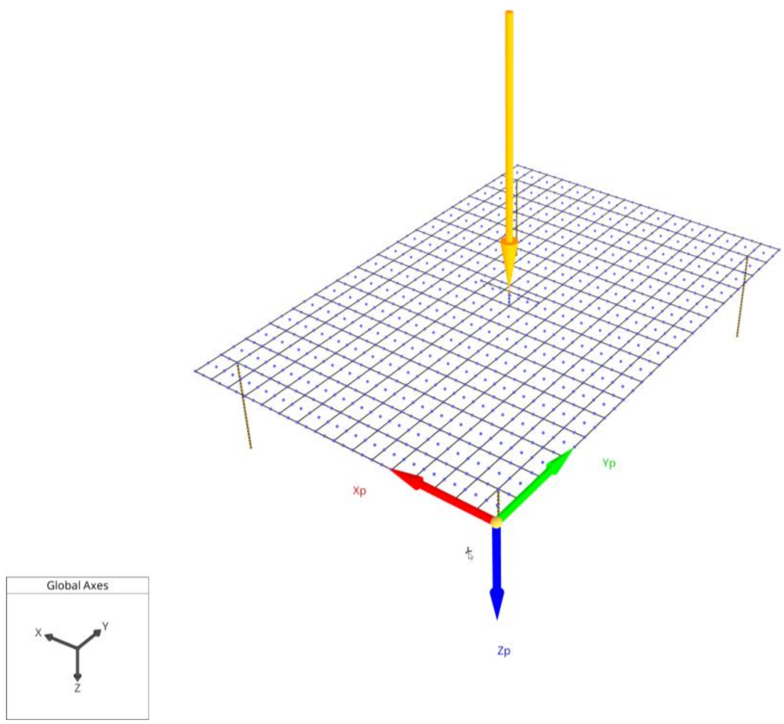

Figure 3-28 FB-MultiPier shallow foundation model.

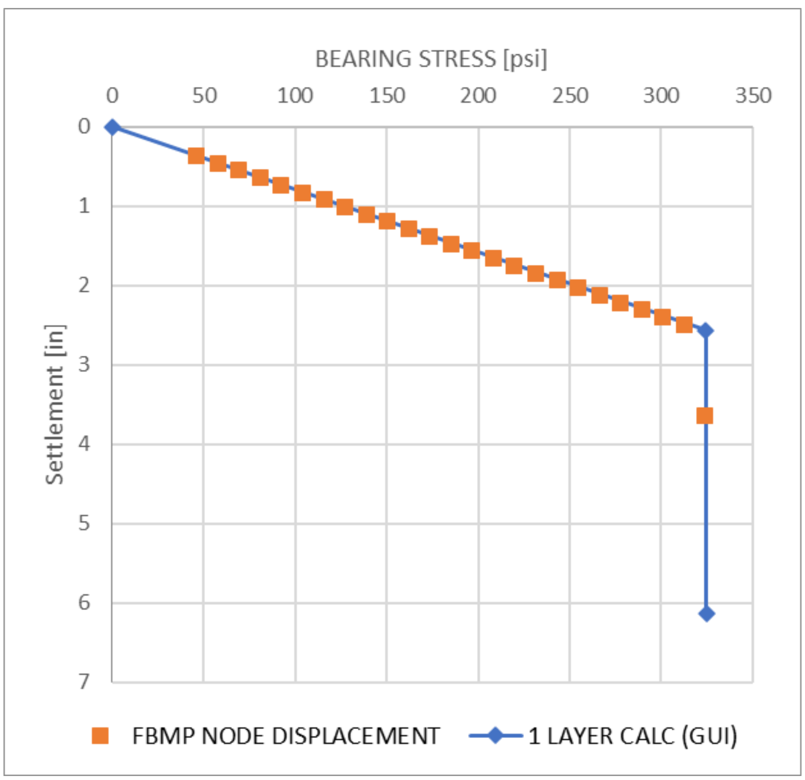

Figure 3-29 Load settlement comparison case 1, mean settlement curve.

3.6.2 Florida Limestone Heterogeneous Validation

To validate implementation of the Florida Limestone Heterogeneous model, the same validation process used for the Homogeneous model was conducted. The following cases were analyzed.

- Case 1 - SR 84 Load Test (Worked Example)
- Case 2 - Bell Site Load Test (Worked Example)
- Case 3 - Florida Limestone Heterogeneous based on formation (Sensitivity Study)
- Case 4 - Florida Limestone Heterogeneous based on formation (Sensitivity Study)
- Case 5 - Florida Limestone Heterogeneous based on formation (Sensitivity Study)
- Case 6 - Florida Limestone Heterogeneous based on formation (Sensitivity Study)
- Case 7 - Florida Limestone Heterogeneous based on formation (Sensitivity Study)
- Case 8 - Florida Limestone Heterogeneous based on formation (Sensitivity Study)
- Case 9 - Florida Limestone Heterogeneous based on formation (Sensitivity Study)

In total 9 cases were analyzed, the first two being based on the worked example which walks through FB-MultiPier.

Table 3-8 Florida limestone heterogeneous bearing capacity comparison (FBMP = FB-MultiPier).

CASE	-	SR84	BELL	3	4	5	6	7	8	9
Mass Properties	c, psi	44.08	44.20	23.38	23.38	23.38	23.38	23.38	23.38	23.38
	φ, ˚	35.40	28.07	31.57	31.57	31.57	31.57	31.57	31.57	31.57
	ω, ˚	6.01	18.48	-6.29	-6.29	-6.29	-6.29	-6.29	-6.29	-6.29
	P_p, psi	392.00	251.50	217.00	217.00	217.00	217.00	217.00	217.00	217.00
	E_m, ksi	33.71		14.60	14.60	14.60	14.60	14.60	14.60	14.60
Footing Geometry	B, ft	5	5	5	5	5	5	5	5	10
	L, ft	6	5	15	15	15	15	15	15	15
	e_b	0	0	0	0	0	0	0	0	0
	e_l	0	0	0	0	0	0	0	0	0
	D_f, ft	3	5	2	2	2	2	2	2	2
Depth of Water Table	D_w	3	12	1.5	1.5	1.5	1.5	1.5	1.5	1.5
Total Unit Weight	$g_{total,}$ pcf	110	80	115	115	115	115	115	115	115
REC	%	0.8	1	1	1	1	1	1	1	1
Rock Thickness	T_r, ft	10	5	5	5	5	10	5	5	5
Sand Thickness	T_s, ft	20	2	39	39	39	39	2	39	39
E_{rock} (mass modulus)	psi	33711	31710	14600	11000	14600	14600	14600	14600	14600
E_{soil} (mass modulus)	psi	2031	2067	2000	2000	500	2000	2000	2000	2000
Qu Excel	psi	351.08	199.23	127.27	128.42	91.83	138.61	127.27	127.27	139.96
Qu FBMP UI	psi	351.1	199.26	127.28	128.42	91.84	138.62	127.28	127.28	139.97
% ERROR	%	0.00%	-0.01%	0.00%	0.00%	-0.01%	-0.01%	0.00%	0.00%	0.00%

CASE	-	SR84	BELL	3	4	5	6	7	8	9
Qu FBMP ENGINE	psi	351.10	199.26	127.28	128.42	91.84	138.62	127.28	127.28	139.97
% ERROR	%	0.00%	0.00%	0.00%	0.00%	0.00%	0.00%	0.00%	0.00%	0.00%

Table 3-9 Florida limestone heterogeneous settlement calculation.

CASE	-	SR84	BELL	3	4	5	6	7	8	9
Problem Geometry	B, ft	5	5	5	5	5	5	5	5	10
	L, ft	6	5	15	15	15	15	15	15	15
	t,ft	0.667	0.558	4	4	4	4	4	4	4
	T_r, ft	10	5	5	5	5	10	5	5	5
	T_s, ft	20	2	39	39	39	39	2	39	39
Settlement Parameters	v	0.1	0.1	0.1	0.1	0.1	0.1	0.1	0.2	0.1
	√(BL), ft	5.48	5.00	8.66	8.66	8.66	8.66	8.66	8.66	12.25
	a, ft	3.09	2.82	4.89	4.89	4.89	4.89	4.89	4.89	6.91
	T_r/a	3.24	1.77	1.02	1.02	1.02	2.05	1.02	1.02	0.72
	E_m/E_s	16.60	15.34	7.30	5.50	29.20	7.30	7.30	7.30	7.30
	$E_{foundation}$, psi	29000000	29000000	4400000	4400000	4400000	4400000	4400000	4400000	4400000
	Q_u, psi	351.08	199.23	127.27	128.42	91.83	138.61	127.27	127.27	139.96
	σ_{sand}, psi	18.76	22.87	43.57	49.68	14.68	17.66	43.57	43.57	77.09
Settlement @ rock bearing stress	Stress in rock: σ_i, psi	184.92	111.05	85.42	89.05	53.25	78.14	85.42	85.42	108.53
	Rock thickness T_i, ft	10	5	5	5	5	10	5	5	5

CASE	-	SR84	BELL	3	4	5	6	7	8	9
	Stress in sand: σ_i, psi	9.38	20.74	21.79	24.84	7.34	8.83	39.36	21.79	38.55
	Sand thickness T_i, ft	14.59	2.00	10.35	9.69	13.55	16.33	2.00	10.35	12.16
	E_{eq}, psi	16247.37	15878.62	4595.72	4265.54	1684.39	7367.41	7371.92	4595.72	3724.70
	K_f	17.92	14.16	525.31	565.97	1433.25	327.68	327.48	525.31	229.16
	C	0.79	0.79	0.79	0.79	0.79	0.79	0.79	0.79	0.79
	δ_{Qu}, in	1.25	0.66	2.53	2.75	4.97	1.72	1.57	2.45	4.85

Table 3-10 Continued Florida limestone heterogeneous settlement calculation.

CASE	-	SR84	BELL	3	4	5	6	7	8	9
Post settlement parameters	Qp_u, psi	412.52	234.10	149.55	150.89	107.90	162.87	149.55	149.55	164.46
	Post E_m, psi	16855.26	15855.20	7300.00	5500.00	7300.00	7300.00	7300.00	7300.00	7300.00
	Post E_m/E_s	8.30	7.67	3.65	2.75	14.60	3.65	3.65	3.65	3.65
	Post σ_{sand}, psi	33.30	40.66	67.50	74.82	25.47	30.07	67.50	67.50	108.57
Post settlement	Stress in rock: σ_i, psi	222.91	137.38	108.52	112.86	66.69	96.47	108.52	108.52	136.52
	Rock thickness T_i, ft	10	5	5	5	5	10	5	5	5
	Stress in sand: σ_i, psi	16.65	35.98	33.75	37.41	12.74	15.04	60.39	33.75	54.29
	Sand thickness T_i, ft	11.49	2.00	9.50	9.50	11.96	14.00	2.00	9.50	11.58
	E_{eq}, psi	10687.17	9712.14	3678.60	3280.83	1386.81	4950.40	4924.11	3678.60	3215.34
	K_f	27.25	23.15	656.27	735.84	1740.79	487.67	490.27	656.27	265.46
	C	0.79	0.79	0.79	0.79	0.79	0.79	0.79	0.79	0.79
	δ_{QPu}, in	2.23	1.27	3.71	4.19	7.09	3.00	2.77	3.59	6.60

Table 3-11 Florida limestone heterogeneous settlement comparison (FBMP = FB-MultiPier).

CASE	-	SR84	BELL	3	4	5	6	7	8	9
FBMP UI	δ_{Qu}, in	1.253	0.664	2.54	2.761	5.001	1.726	1.583	2.463	4.874
% ERROR	%	-0.40%	-0.33%	-0.58%	-0.58%	-0.60%	-0.61%	-0.55%	-0.58%	-0.58%
FBMP UI	δ_{QPu}, in	2.239	1.276	3.729	4.218	7.136	3.018	2.785	3.616	6.634
% ERROR	%	-0.49%	-0.44%	-0.60%	-0.58%	-0.59%	-0.60%	-0.57%	-0.60%	-0.58%

To validate the load settlement response for the Florida Limestone heterogeneous model, the same process of creating a FB-MultiPier model with incremental loading were created for each case. An example bearing settlement results are shown in Figure 3-30, where it can be seen the results matched the specified load settlement curve and recreate the bilinear behavior of the model.

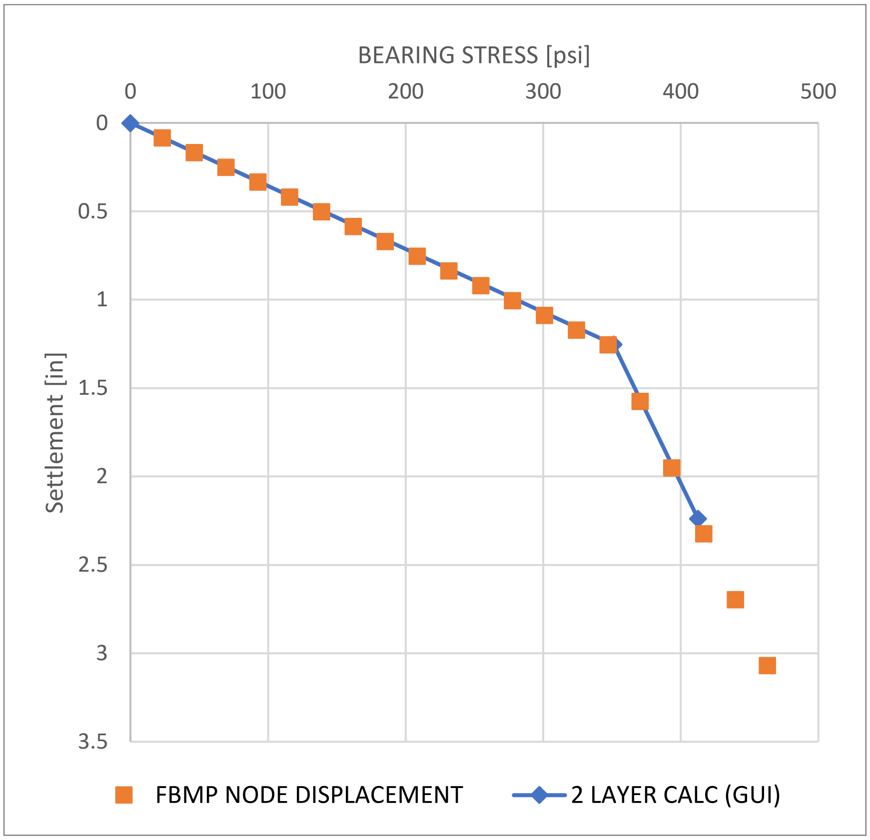

Figure 3-30 SR 84 load settlement curve (Florida limestone heterogeneous model).

3.6.3 Hoek and Brown (Carter and Kulhawy) Homogeneous Validation

To validate implementation of the Hoek and Brown (Carter and Kulhawy) Homogeneous model, the same validation process that was used for the Homogeneous model was conducted. The following cases were analyzed.

1. Worked Example 1 (WE1)
2. Worked Example 2 (WE2)

In total 2 cases were analyzed, based on the worked examples which are detailed in Appendix B.3.1 & B.3.2. Results from this validation set are shown in Table 3-12 through Table 3-14. Table 3-12 presents results of the bearing capacity comparison. Table 3-13 shows results of the settlement calculation for each case.

Table 3-14 presents a comparison of the settlement results from the excel spreadsheet calculations and FB-MultiPier. In all tables it can be seen the observed percent error is below 0.14%, thus showing excellent agreement between the excel calculation and FB-MultiPier (FBMP).

Table 3-12 Hoek and Brown (Carter and Kulhawy) homogeneous bearing capacity comparison.

CASE	-	WE1	WE2
Footing Geometry	B, ft	10	10
	L, ft	100	100
	T_r	40	40
m_i	-	10	10
GSI	-	61	61
q_u, psi	psi	281.2	281.2
s	-	0.01	0.01
m	-	2.48	2.48
E_m	ksi	11.34246	11.34246
Q_u, Excel	psi	185.63	185.63
Q_u FBMP UI	psi	185.63	185.63
% ERROR	%	0.00%	0.00%
Q_u FBMP ENGINE	psi	185.63	185.63
% ERROR	%	0.00%	0.00%

Table 3-13 Hoek and Brown (Carter and Kulhawy) homogeneous settlement calculation.

CASE	-	WE1	WE2
Mass properties	μ_E, psi	11342.46	11342.46
	CV_E	1	1
	σ_E, psi	11342.46	11342.46
	ν	0.1	0.1
	a_v, ft	5	5
	n	0.5	0.5
Geometry	B, ft	10	10
	T, ft	40	40
	t, ft	2	6
	$E_{foundation}$, psi	4400000	4400000
	C	2.54	2.1
Bearing value	Q_u, psi	185.63	185.63
Fenton and Griffiths' method	δ_{det}, in	4.938	4.083
	σ_{lnE}	0.833	0.833
	$\gamma(T_r)$	0.080	0.080
	$\sigma_{ln\delta}$	0.235	0.235
	$\mu_{ln\delta}$	1.944	1.753
	μ_δ, in	7.180	5.936
	σ_δ, in	1.713	1.416
	δ_{LB}, in	6.209	5.133
	δ_{UB}, in	7.856	6.495

Table 3-14 Hoek and Brown (Carter and Kulhawy) Homogeneous Settlement Comparison.

CASE	-	WE1	WE2
FBMP UI	μ_δ, in	7.180	5.940
% ERROR	%	0.00%	-0.06%
FBMP UI	δ_{LB}, in	6.209	5.126
% ERROR	%	0.00%	0.14%
FBMP UI	δ_{UB}, in	7.856	6.504
% ERROR	%	0.00%	-0.14%

To validate the load settlement response for the Hoek and Brown (Carter and Kulhawy) Homogeneous model, the same process of creating a FB-MultiPier model with incremental loading were created for each case. However due to the Hoek and Brown (Carter and Kulhawy) model only being applicable to a strip footing (L/B > 10), the model required multiple columns to distribute the loading. An example of this configuration is shown in Figure 3-31, where five columns are evenly spaced over the footing. The load applied to each column corresponds to their tributary area of the footing.

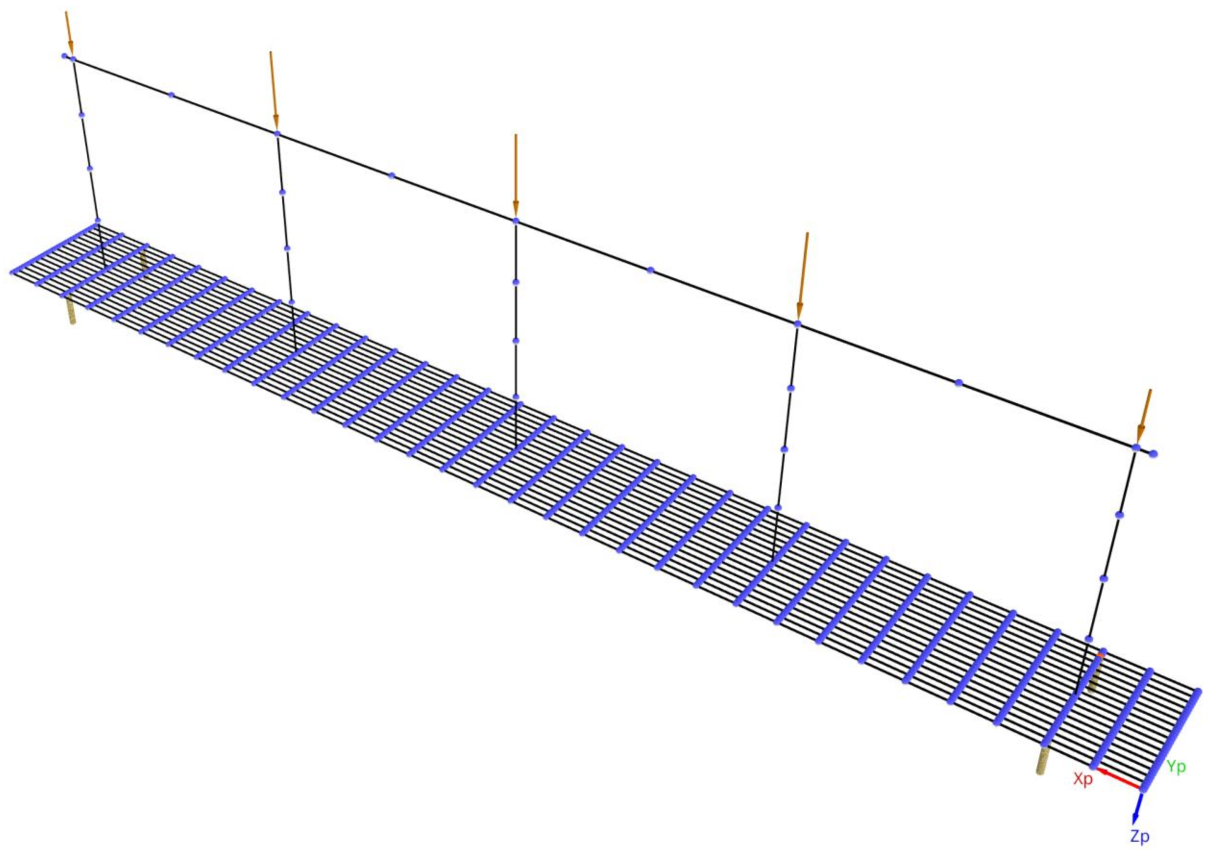

Figure 3-31 Strip footing model FB-MultiPier.

After the model is analyzed with the FB-MultiPier engine, the vertical nodal displacement (settlement) per load increment is then extracted from the center of the footing. These settlement values are then plotted against bearing stresses which are calculated at the respective applied load divided by the total footing area. The FB-MultiPier bearing stress vs settlement is then compared to the calculated bearing settlement curve. Examples of this are shown in Figure 3-32 and Figure 3-33 for the mean settlement curve. Resulting bearing settlement from FB-MultiPier is in good agreement with the specified bearing settlement curve replicating the linearly elastic-perfectly plastic model. The results for the for worked example 1 show a slightly softer response than the specify curve, this is due the higher flexibility of footing, resulting in more localized displacement.

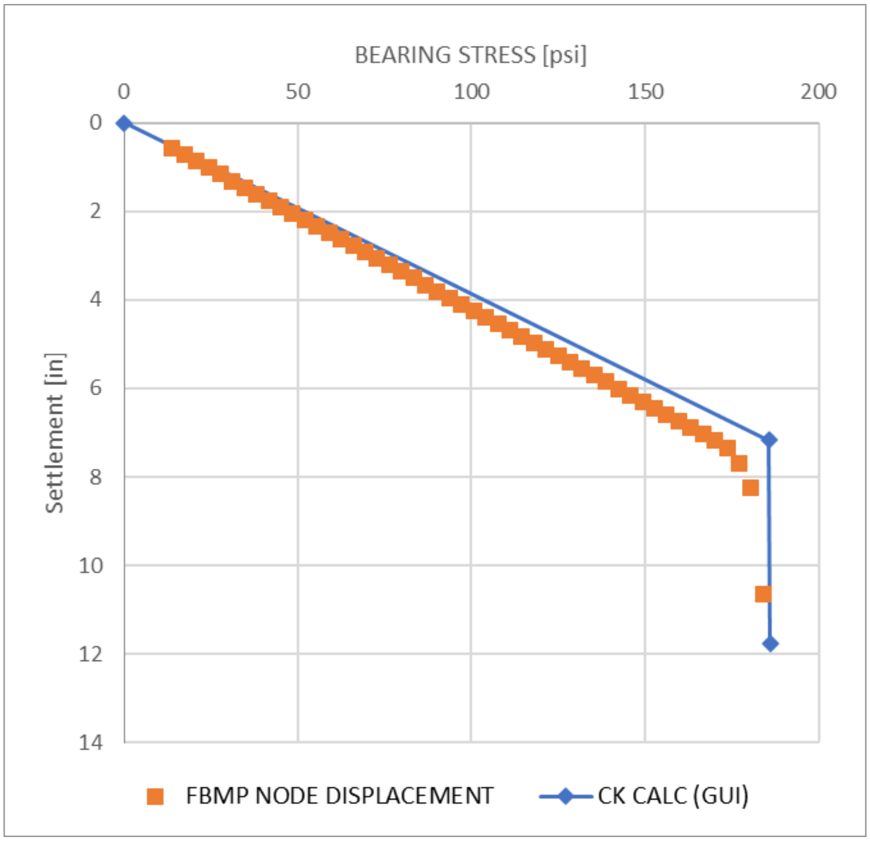

Figure 3-32 Worked example 1 mean settlement curve Hoek and Brown (Carter and Kulhawy) homogeneous.

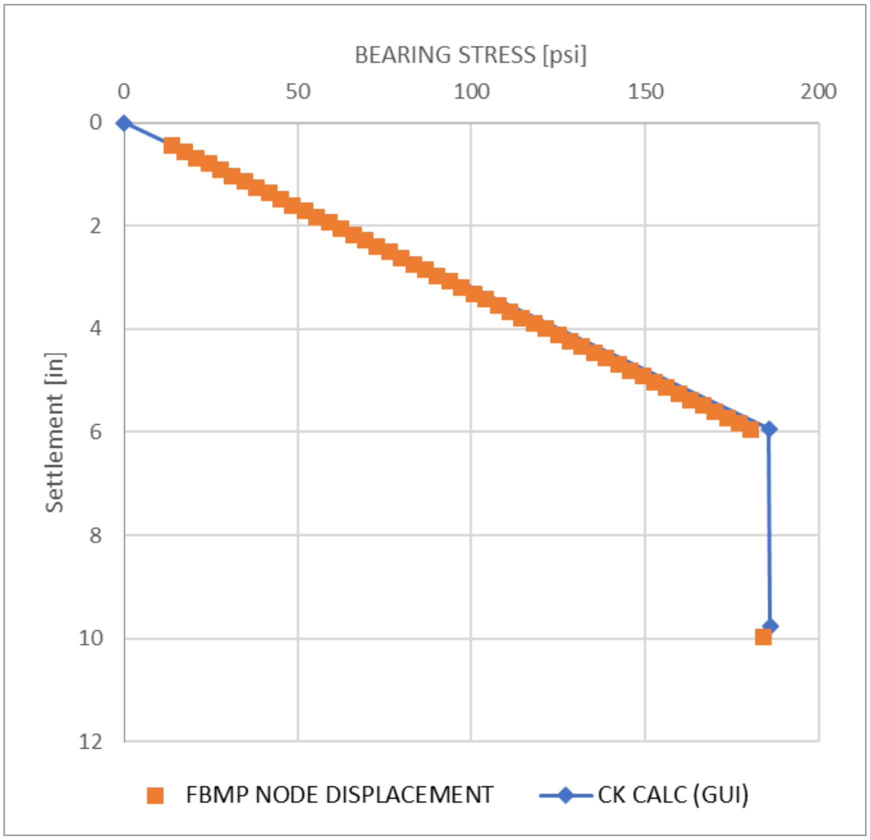

Figure 3-33 Worked example 2 mean settlement curve Hoek and Brown (Carter and Kulhawy) homogeneous.

3.7 Conclusion

Due to its age, Florida limestone has a high bulk porosity (median > 37%) which results in it having bi-linear strength envelopes, large volumetric compression behavior, ductile bilinear stress-strain response, and an initial Young's Modulus only an order of magnitude greater than sand. Consequently, the service limit state, i.e. settlement may control the design of a shallow foundation on Florida limestone. Like the strength parameters (c, phi, etc.) Florida Limestone's Young Modulus is controlled by formation and its mass bulk dry unit weight. However, as a typical site may have a high CV of its Young's Modulus (1 <CV<3), a probabilistic settlement (Fenton and Griffith) approach is proposed, since the zone of influence (2B) is large, and both differential and mean settlement of a footing is affected by high CV of the Young's Modulus. In addition, because of the bilinear nature of the rock's stress-strain response (linear – constant E up to failure/crushing), the load–settlement response of the footing will be linear up to the footing's bearing failure associated very large settlements. Note, the bearing failure is not the typical behavior of a dense sand (Figure 3-1 e), but excessive rock crushing (Figure 3-1 b) associated with the rock's high porosity.

Besides a footing on a homogeneous layer, the case of 2 layers [e.g. footing on 8 ft thick rock layer underlain by sand] was implemented. Since there are limited analytical solutions (e.g., Burmister, Mayne and Poulos) for circular footings, FEM analyses were undertaken to evaluate rectangular footings (1 < L/B <3) as a function of layer thickness, modulus ratio (rock/sand) and footing geometry to develop a Winkler spring model for the case. It was found that an equivalent homogeneous single layer modulus – Harmonic Mean Modulus, Equation 3-16 could replicate the FEM results if stresses and zone of influences (Eq. 16) were characterized appropriately, Figure 3-7 and Figure 3-8.

The proposed homogeneous rock and rock over sand solutions were validated with the three field loads field load tests in different formations and layering conditions in Florida as well as numerical simulations in Phase III for different shapes and rigidities of footing.

In the current Chapter 3, Homogeneous and rock-over-sand settlement predictions are implemented into FB-MultiPier for pier design. For the single-layer case, the CV of rock mass modulus and the correlation length need to be provided to characterize the spatial variability and continuity. Excessive settlement occurs after the yielding. For the rock-over-sand case, assessment of the bearing capacities and load-settlement response depends on the modulus ratio of rock and sand, the thickness of the rock layer using stress-dependent harmonic mean modulus. After yielding, the secant modulus is used up to the post-bearing values.

CHAPTER 4
IMPLEMENTATION OF PASSIVE FORCE-DEFORMATION

4.1. Introduction

Florida Limestone (calcium carbonate & dolomite) occurs in many different formations near the ground surface (e.g. Miami, Fort Thompson, Anastasia, Key Largo, etc.). Existing at many different bulk dry unit weights (85 pcf to 145 pcf), the majority of the rock exhibits ductile stress-strain response: a linear increasing stress vs strain response until yielding/failure (Mohr-Coulomb) and then a constant stress vs increasing strain. In general, Florida Limestone has a constant Young's Modulus that is 5 to 50 times (depending on bulk dry unit weight) the value of sand until yielding/failure; however, due to formation and age, Florida Limestone has a high median porosity (37%) which has a significant impact on volumetric and strength characteristics of the material. Specifically, under increasing hydrostatic or triaxial shear loading, the material will undergo significant compression volumetric straining as well as matrix crushing resulting in ductile response (bilinear stress-strain), as well as bilinear Mohr-Coulomb Strength Envelope (FDOT, Phase I report).

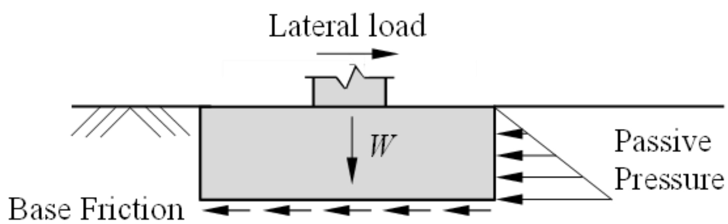

Figure 4-1 Passive pressure and base friction associated with lateral loading.

4.2 Lateral Resistance of Embedded Footing

A Footing, Figure 4-1, subjected to lateral loading will mobilize friction on the base and friction and passive resistance on the face, if embedded. The friction resistance will mobilize with small lateral movements (i.e., 0.1 inch in granular soil) with the primary contribution coming from the base of the footing and a lesser from the sides. The normal resistance on the footing (thickness = H) includes the active resistance and the passive resistance, where the active resistance mobilizes with lateral movements on the order of 0.1%H for loose sand to 4%H for soft clay and the passive resistance mobilizes around 1%H for loose sand to 5%H for soft clay. For typical footings designed to support superstructure loads and embedded in soil and limestone, e.g. 5 – 8 ft thick and widths of 10 – 15 ft significant passive resistance will develop compared to base skin friction resistance.

In Phase I and II the work focused on the bearing capacity and Young's modulus for vertical concentric loading. For that case, the axial stress was the major principal stress (i.e. +q in q-p space), and the strength envelopes for limestone were developed through unconfined compression, split tensile, and triaxial compression testing.

For a footing embedded in Florida limestone under lateral loading, the resistance will develop in a similar manner to soil however controlled by the strength properties specific to formation type, unit weight, porosity, etc. Limestone is a sedimentary rock formed in layers through overburden compression and cementation generally parallel to the ground surface and porous through ground water fluctuations and flows dissolving minerals, creating a non-homogeneous anisotropic condition. It stands to reason that shear stress and horizontal strain may not develop the same when limestone is under applied pressure on the horizontal plane (vertical pressure – bearing capacity) or the vertical plane (horizontal pressure – passive resistance). Therefore, the +q strength envelopes (compression space strength envelopes, Figure 4-2) may not be assumed to capture the passive resistance, Figure 4-2 and that -q strength envelopes (extension space strength envelopes) should be identified. A limited series of triaxial extension tests were conducted at the SMO on samples from the Miami, Fort Thompson, and Ocala formations. Additional triaxial compression, unconfined compression, and split tension tests were also performed for comparison to the existing data sets from Phase I and II.

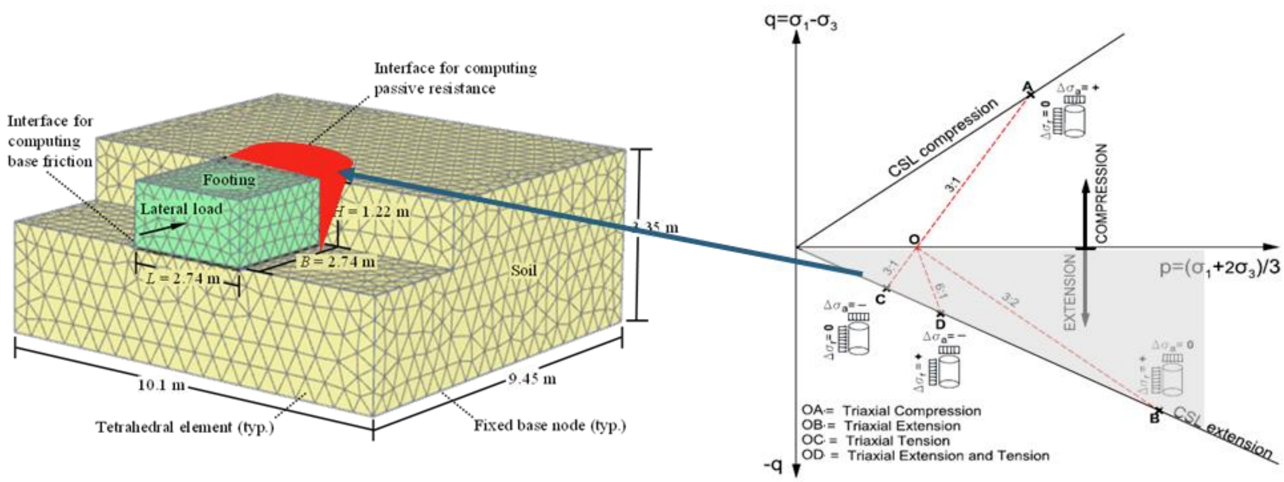

Figure 4-2 Finite element model of footing embedded in soil showing zone of passive resistance (red) and the q-p strength envelopes in compression and extension space.

4.2.1 Laboratory Tests and Strength Envelopes

Samples from the Miami, Fort Thompson, and Ocala formations were collected from existing core runs obtained with the help of FDOT district geotechnical engineers. A minimum number of competent samples with similar dry unit weights was identified for testing at confining pressures of 15 psi, 50 psi and 300 psi under increasing horizontal stress and constant axial stress (triaxial extension (OB in Figure 4-2), the same scenario as the limestone in the footing case (Figure 4-1). These confining stresses represent the range of overburden stresses for typical shallow depths of embedded footings along with the occurrence of higher low porosity, dense limestone. Figure 4-3 shows the Hoeck cell triaxial test and a sample of the Miami limestone formation before and after triaxial extension testing under 15 psi confining pressure. The post test sample clearly shows the failure plane under increasing confinement under constant axial pressure under sample extension.

a) b)

Figure 4-3 a) Hoeck cell triaxial test and b) Miami limestone sample before and after testing.

From the triaxial test results, the deviator stress at failure was identified and the relationship between it and the dry unit weight was established for each confining stress, as needed for the development of the strength envelopes (Figure 4-4). The relationship between qu, qt and dry unit which was also established, as needed for the initial portion of the strength envelopes. For Fort Thompson limestone, the few qu and qt tests for this task agree well with the total dataset collected in Phase I (Figure 4-5 and Figure 4-6). The normalized maximum deviator stress for the extension tests at initial confining stresses of 15 psi, 50 psi, and 300 psi show the strength under increasing lateral stress with increasing dry unit weights, with the exception of a clear trend in the three tests at 15 psi (Figure 4-7, Figure 4-8, and Figure 4-9). For this the average of the deviator stress was taken for development of the strength envelopes. The compression and extension strength envelopes for the Fort Thompson limestone are shown in Figure 4-10 which show reduced strength under increasing lateral pressure (extension space Figure 4-2).

Table 4-1 are the extension/compression strength envelope parameters from Figure 4-10 recommended for use with compression strength measured parameters. The qu and qt versus the dry unit weights for the Ocala limestone formation are shown in Figure 4-11 and Figure 4-12. The normalized maximum deviator stress for the extension tests at initial confining stresses of 15 psi, 50 psi, and 300 psi show the strength under increasing lateral stress with increasing dry unit weights (Figure 4-13, Figure 4-14, and Figure 4-15). The compression and extension strength envelopes for the Ocala limestone are shown in Figure 4-16 which also show reduced strength under increasing lateral pressure (extension space Figure 4-2). Table 4-2 are the extension/compression strength envelope parameters from Figure 4-16 recommended for use with compression strength measured parameters.

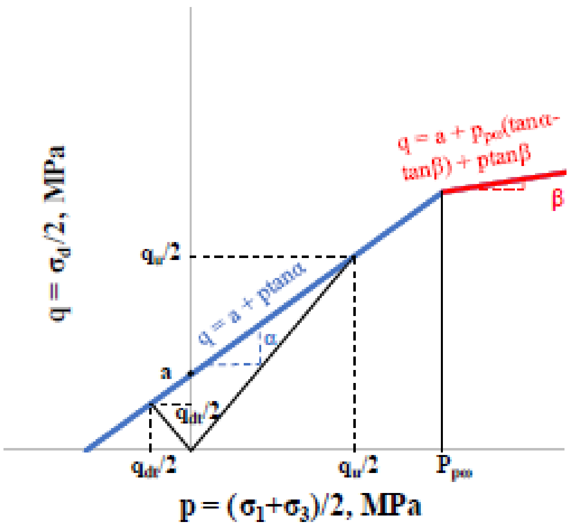

Figure 4-4 Strength envelope model for Florida limestone.

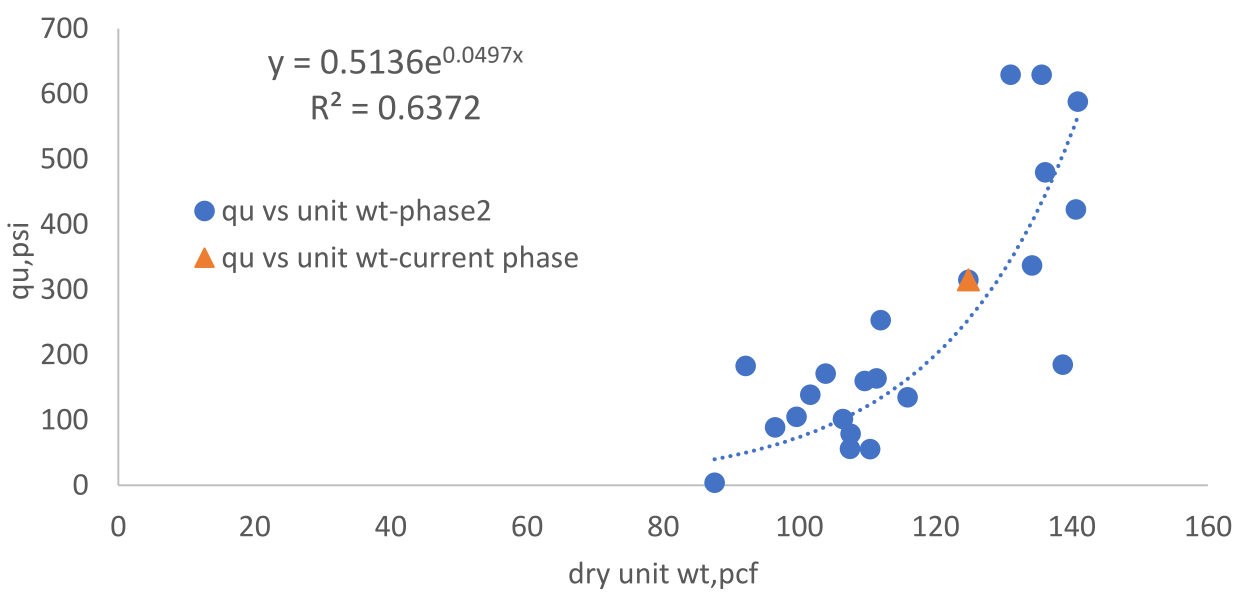

Figure 4-5 Qu versus dry unit weight for Fort Thompson limestone formation.

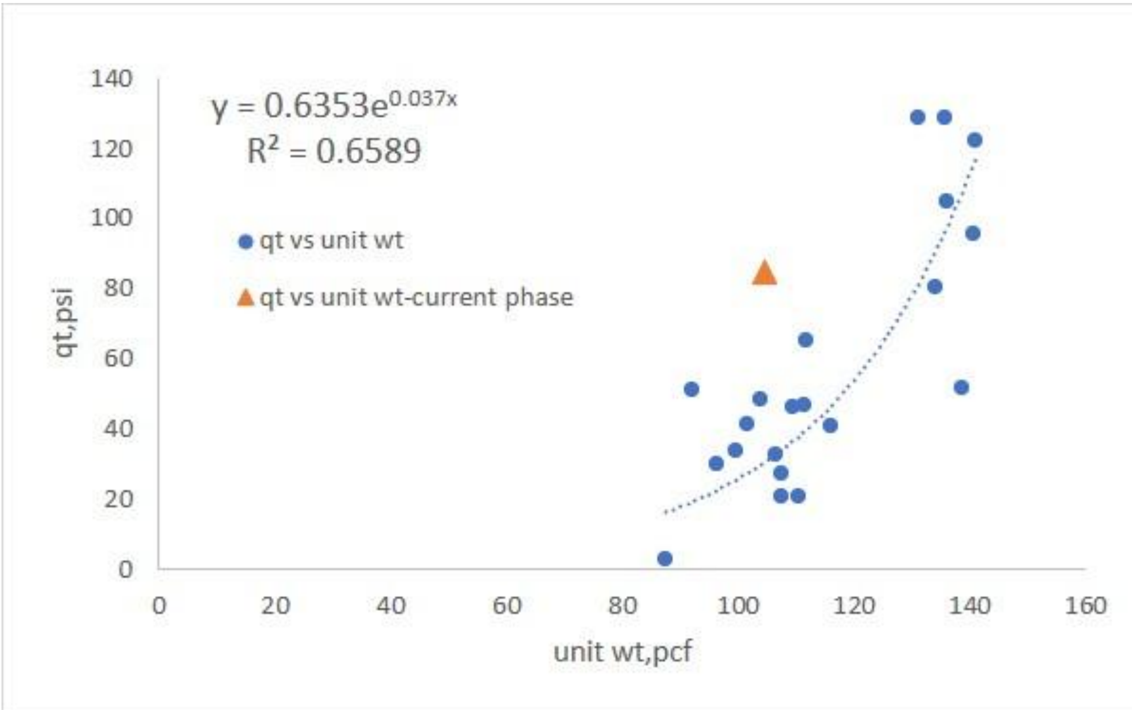

Figure 4-6 Qt versus dry unit weight for Fort Thompson limestone formation.

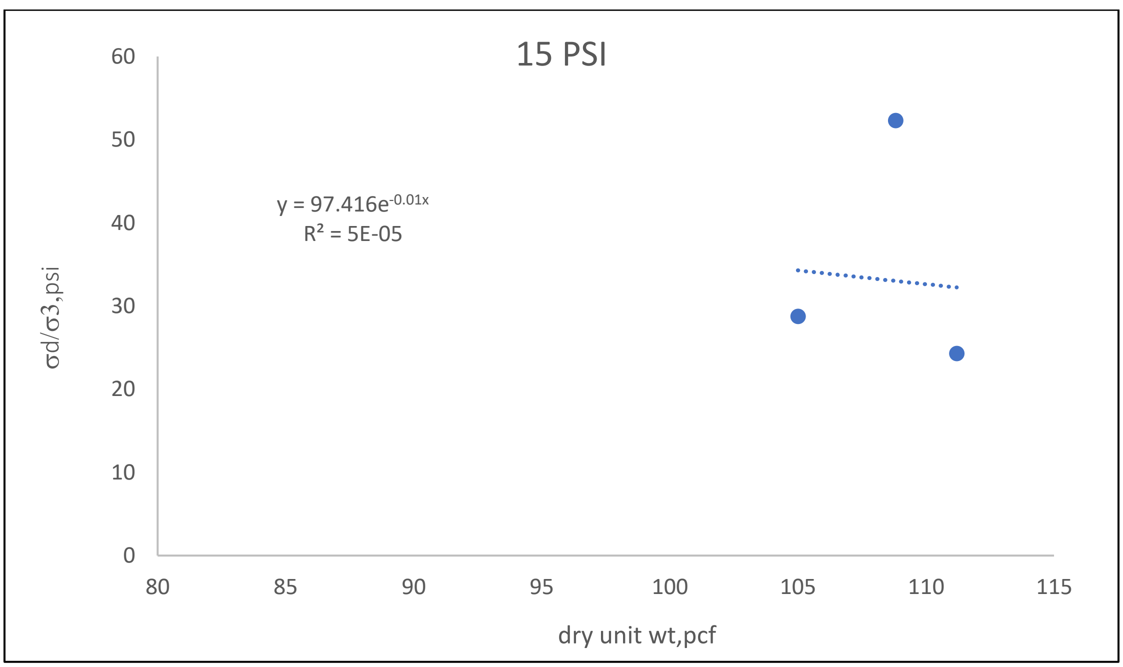

Figure 4-7 Normalized deviator stress at 15 psi confining stress versus dry unit weight for Fort Thompson limestone formation.

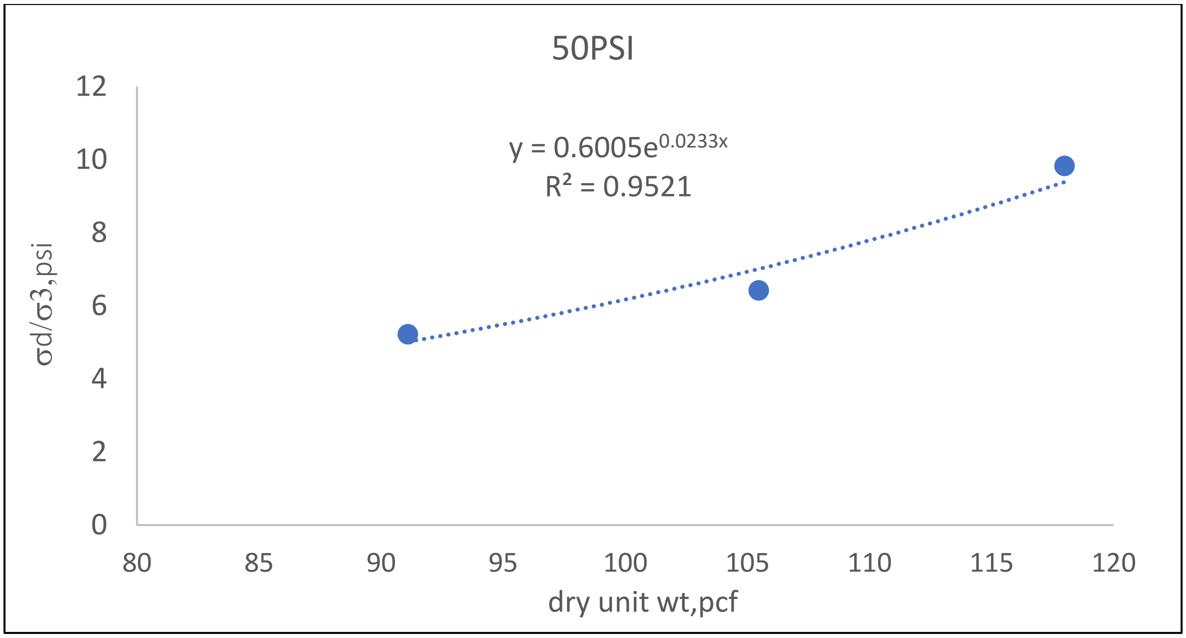

Figure 4-8 Normalized deviator stress at 50 psi confining stress versus dry unit weight for Fort Thompson limestone formation.

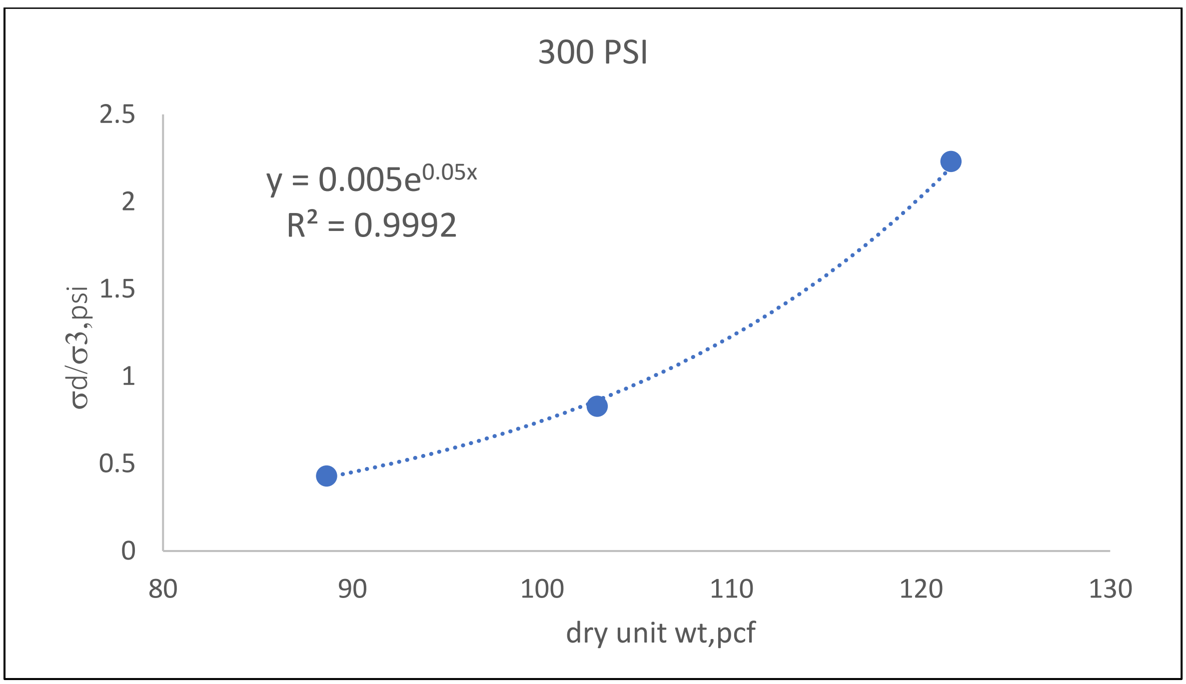

Figure 4-9 Normalized deviator stress at 300 psi confining stress versus dry unit weight for Fort Thompson limestone formation.

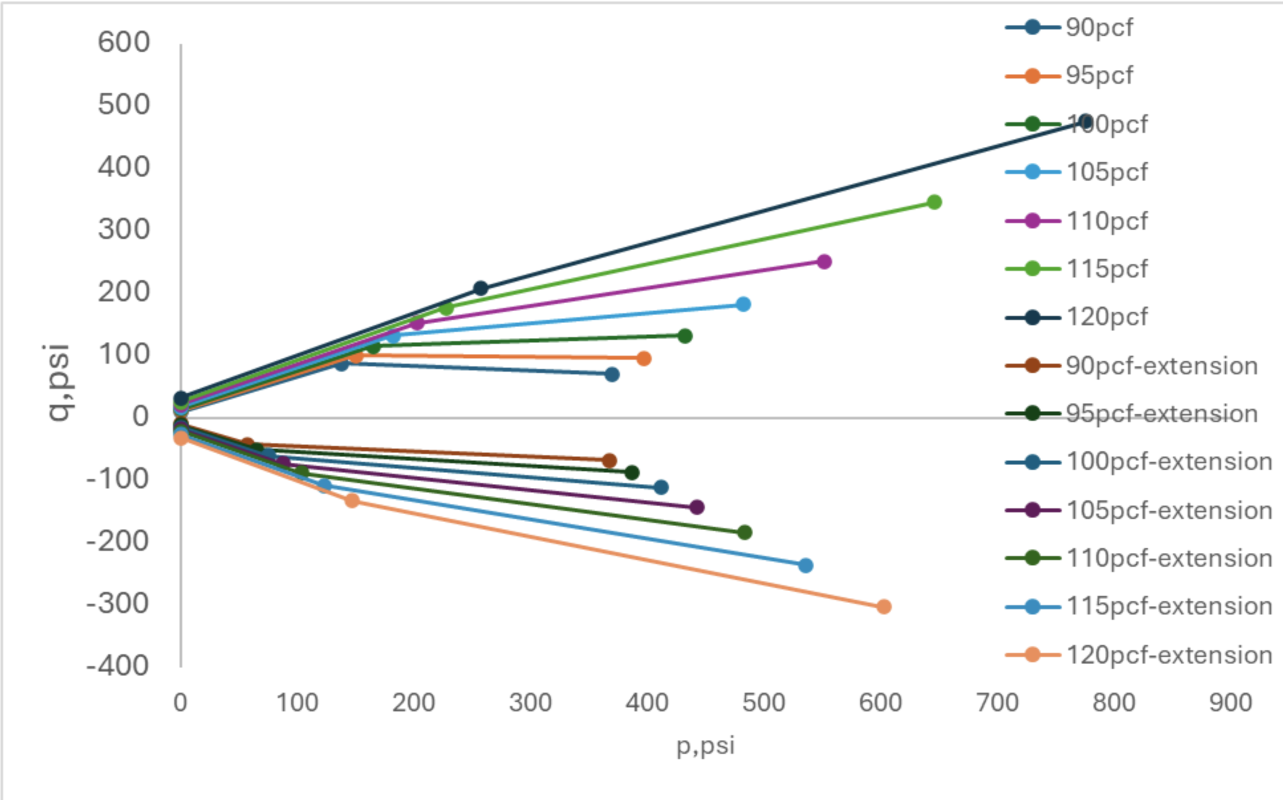

Figure 4-10 Compression and extension strength envelopes for Fort Thompson limestone.

Table 4-1 Extension/compression ratios of Fort Thompson strength envelope parameters.

unit wt (pcf)	c-ext/ c-comp	ϕ-ext/ ϕ-comp	ω-ext/ ω-comp	Pp-ext/ Pp-comp	β-ext/ β-comp	a-ext/ a-comp
90	1	1	-1.23	0.41	-1.23	1
95	1	1	-8.17	0.43	-8.10	1
100	1	1	2.50	0.46	2.47	1
105	1	1	1.26	0.48	1.25	1
110	1	1	0.93	0.51	0.94	1
115	1	1	0.79	0.54	0.82	1
120	1	1	0.73	0.57	0.77	1

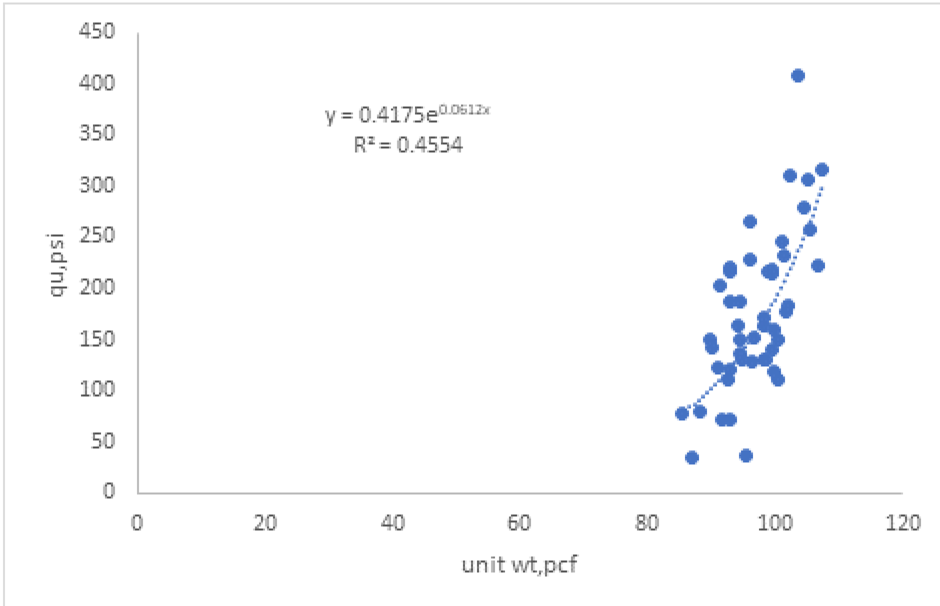

Figure 4-11 Qu versus dry unit weight for Ocala limestone formation.

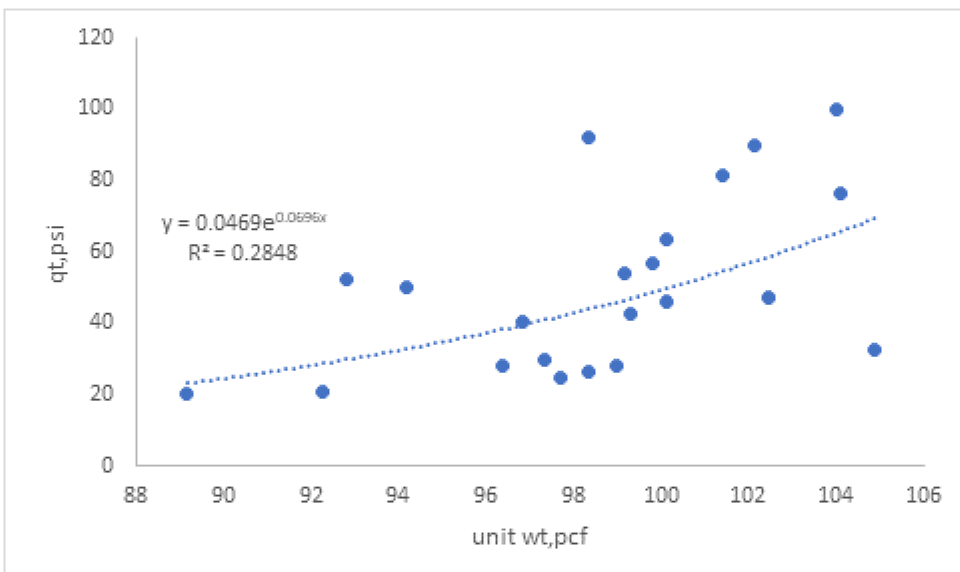

Figure 4-12 Qt versus dry unit weight for Ocala limestone formation.

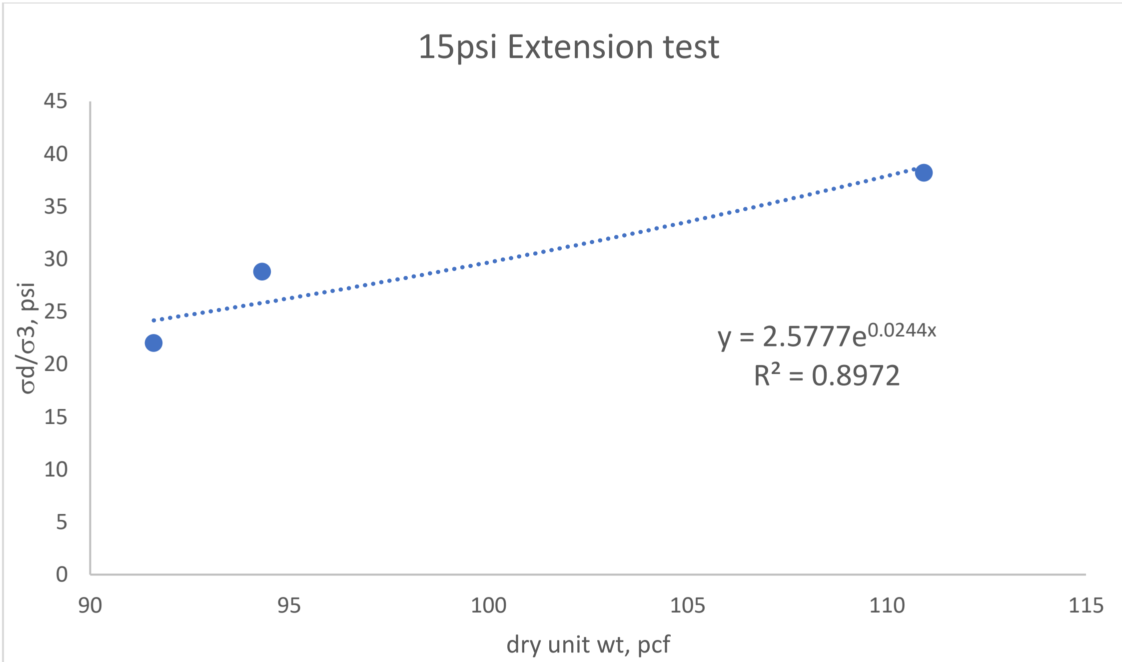

Figure 4-13 Normalized deviator stress at 15 psi confining stress versus dry unit weight for Ocala limestone formation.

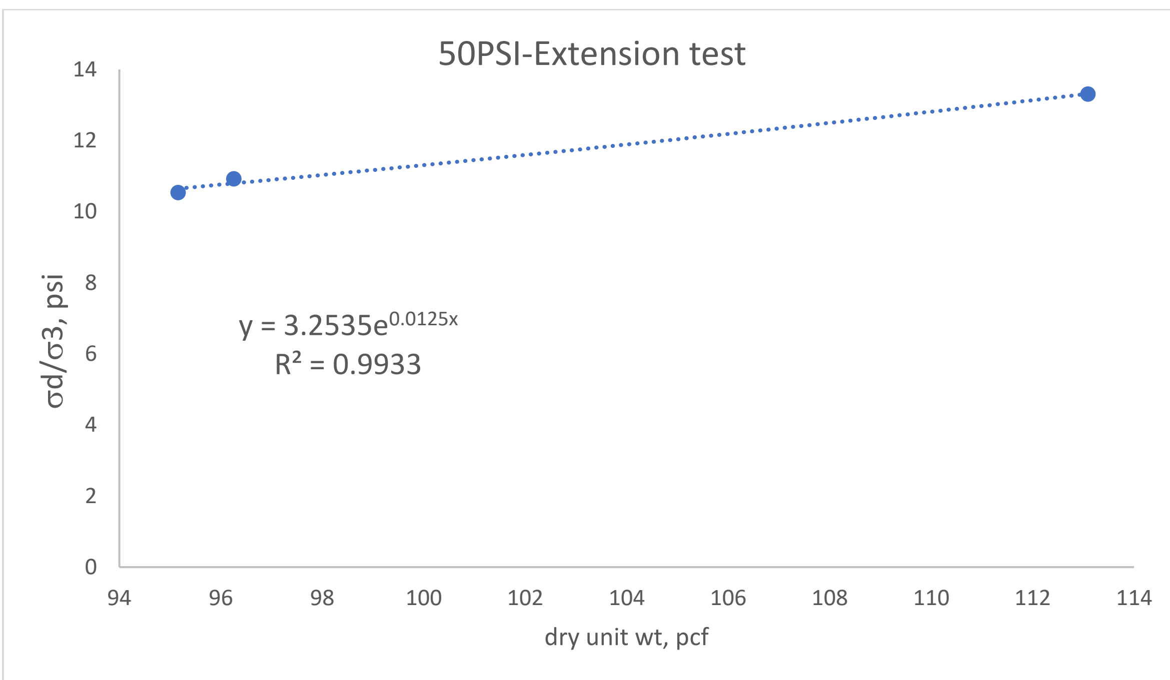

Figure 4-14 Normalized deviator stress at 50 psi confining stress versus dry unit weight for Ocala limestone formation.

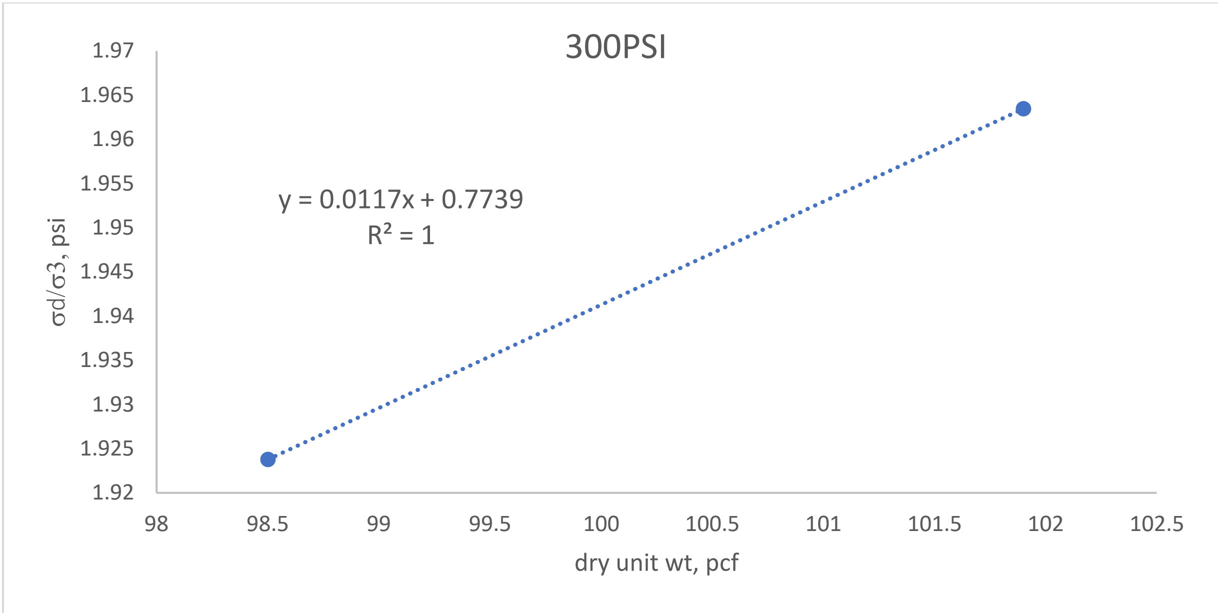

Figure 4-15 Normalized deviator stress at 300 psi confining stress versus dry unit weight for Ocala limestone formation.

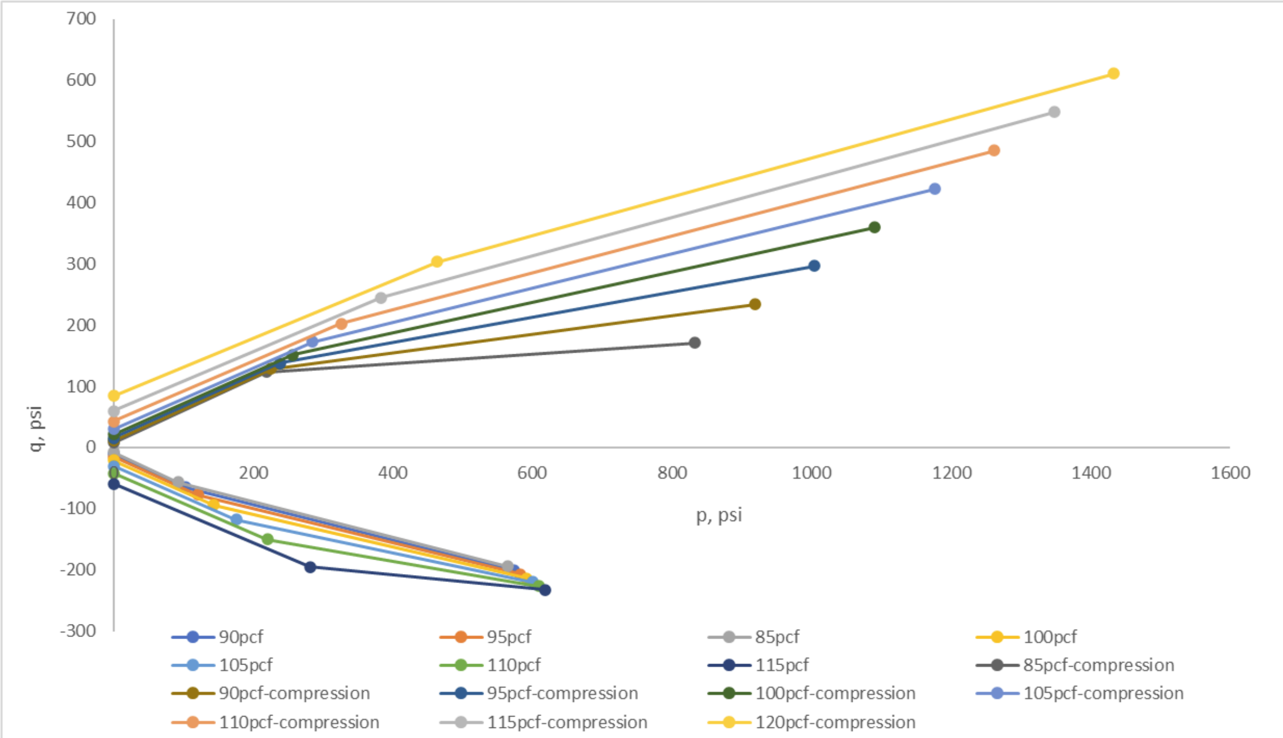

Figure 4-16 Compression and extension strength envelopes for Ocala limestone.

Table 4-2 Extension/compression ratios of Ocala limestone strength envelope parameters.

unit wt (pcf)	c-ext/ c-comp	ϕ-ext/ ϕ-comp	ω-ext/ ω-comp	Pp-ext/ Pp-comp	β-ext/ β-comp	a-ext/ a-comp
85	1	1	3.90	0.42	3.63	1
90	1	1	1.95	0.46	1.84	1
95	1	1	1.38	0.51	1.33	1
100	1	1	1.07	0.56	1.06	1
105	1	1	0.85	0.62	0.87	1
110	1	1	0.64	0.68	0.67	1
115	1	1	0.35	0.73	0.37	1

4.2.2 Finite Element Models of Footing Under Lateral Load

Investigation of and development of the lateral resistance (i.e. Force vs. displacement) of footings embedded in Florida limestone required finite element (FE) model simulations with PLAXIS 3D from the lack of physical experimental results. Fortunately, the FE models built in Phase 2 and from Chapter 2 can be used to model the lateral behavior. Initially though, models of footings in soil were needed to calibrate both the footing-soil interface and the load-deformation analysis. For the soil work, full scale and model experiments in the literature were collected and modeled. A summary of these experiments are shown in Table 4-3 that includes the model geometries and soil properties; the experiments included silty sand to gravel backfill cases that cover the range of observed typical backfills. For example, Figure 4-17 is the FE model of Case 7, a footing with gravel backfill. Figure 4-18 shows the FE results for the passive and base resistance versus lateral displacement compared favorably to the experimental results. The good agreement suggests that an appropriate FE modeling approach (e.g., soil model and soil-footing interface model) was used.

For the FE modeling, a displacement-controlled swipe friction analysis was performed, i.e. applying a specified displacements to the nodes of the footing in such a way that increasing passive resistance (total force acting against plate in Figure 4-2) occurs with increasing displacement. It was standard practice to prescribe movements up to 1 ft for mobilization of the full strength of the soil and limestone. For all cases of the Florida limestone models, two sizes representing the face of the footing were used in the models: 5 ft x 5 ft and 8 ft x 16 ft (height x width) (Figure 4-19 and Figure 4-20). The use of unstructured meshes composed of triangular elements provides flexibility in element arrangement and element size. Model mesh discretization for the study followed non-associated flow with the mesh composed of 6-noded triangular elements with three Gauss quadrature points. Optimized mesh is used for all the model cases in this study. Interface at the contact of soil and footing is used having properties same as that of the soil (limestone). Model boundary conditions consisted of bottom surface fixed in all directions, and a vertical roller was used on each side in the x-direction, and in the y-direction. A point displacement is applied at the center of the plate for prescribed movement.

Table 4-3 Cases of lateral load-deformation experiments.

Cases	Source	Soil Type	Foundation Member Geometry			Backfill Properties			
			L (ft)	B (ft)	H (ft)	c (psf)	ϕ (°)	γ (pcf)	δ (°)
1	(Rollins and Cole, 2006)	Silty Sand	17.0	10.0	3.7	570	27	121	20
2	(Rollins and Cole, 2006)	Clean Sand	17.0	10.0	3.7	0	39	117	30
3	(Rollins and Cole, 2006)	Fine Gravel	17.0	10.0	3.7	79	34	132	26
4	(Rollins and Cole, 2006)	Coarse Gravel	17.0	10.0	3.7	150	40	148	30
5	(Duncan and Mokwa, 2001)	Gravel Backfill	6.3	3.0	3.5	0	52	135	6
6	(Gadre and Dobry 1998)	Clean Sand	3.7	3.7	2.8	0	39	103	39
7	(Rollins and Sparks, 2002)	Gravel Backfill	9.0	9.0	4.0	0	42	148	31.5
8	(Stewart et al., 2007)	Silty Sand	16.0	3.0	5.5	501	40	126	14

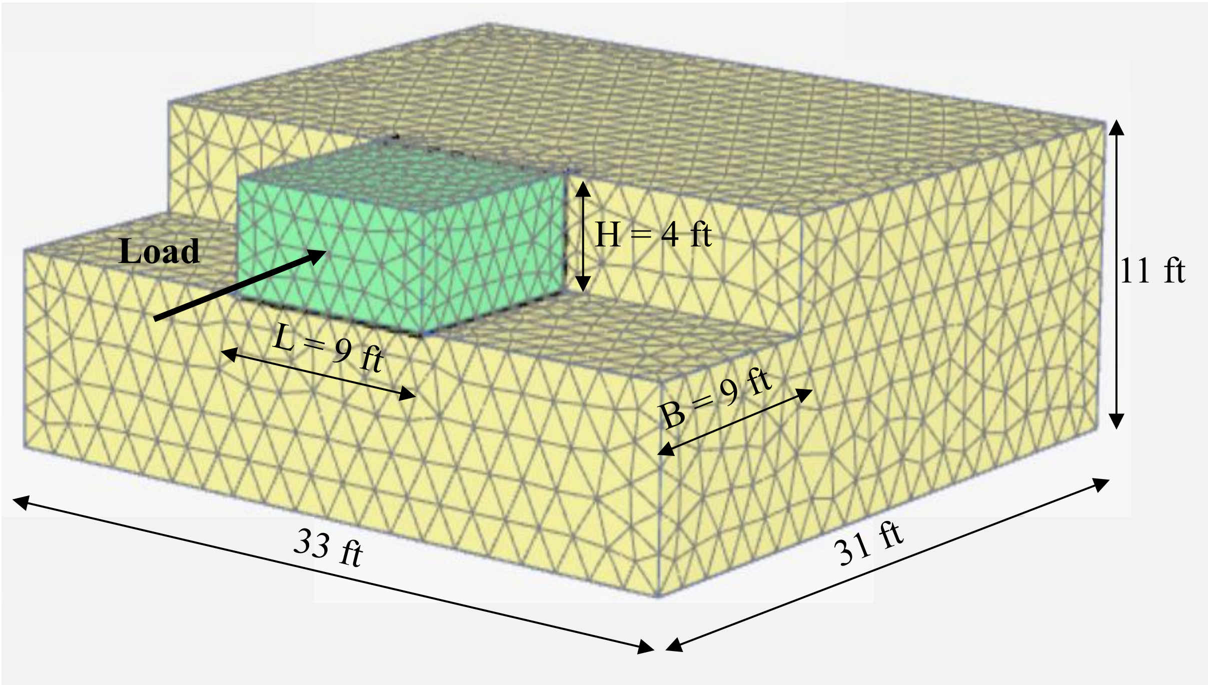

Figure 4-17 3-Dimensional FE model of case 7 in Table 4-3.

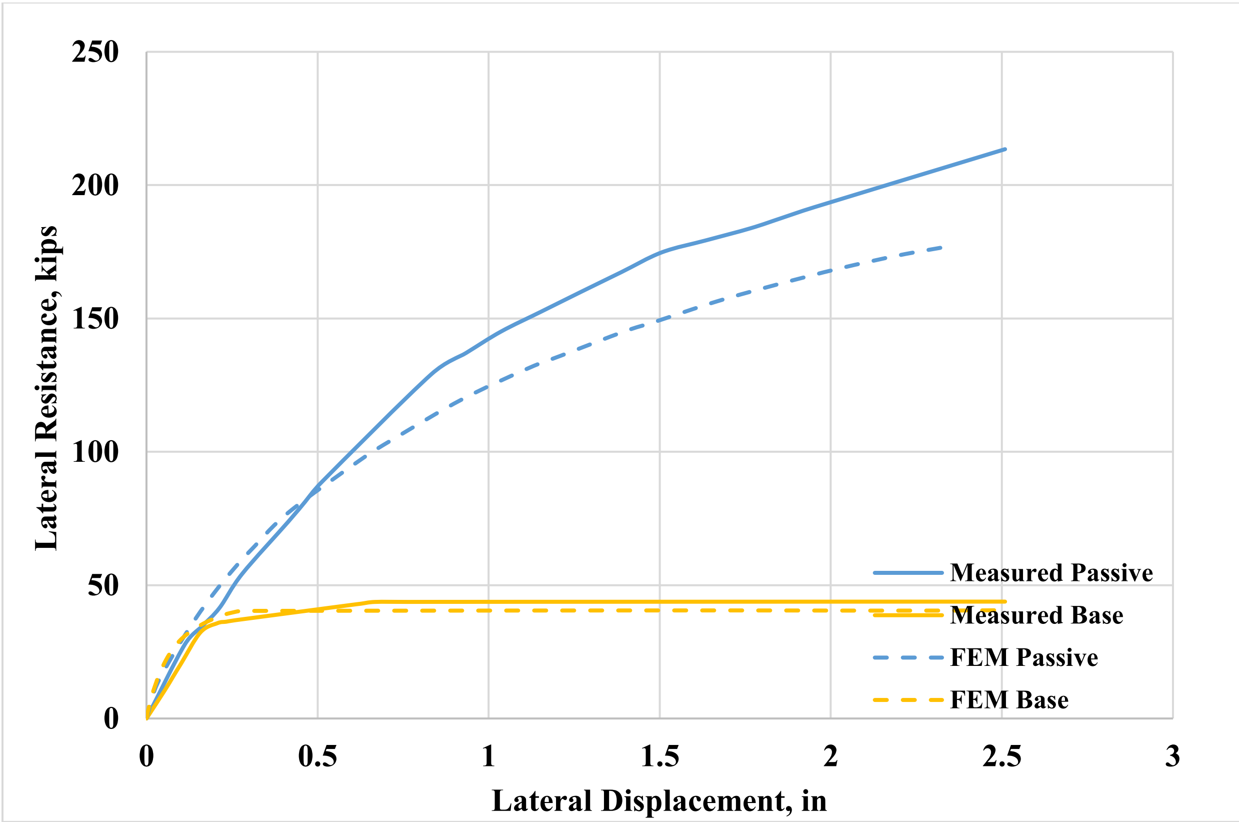

Figure 4-18 FE and experimental results of passive and base resistance versus displacement for case 7 in Table 4-3.

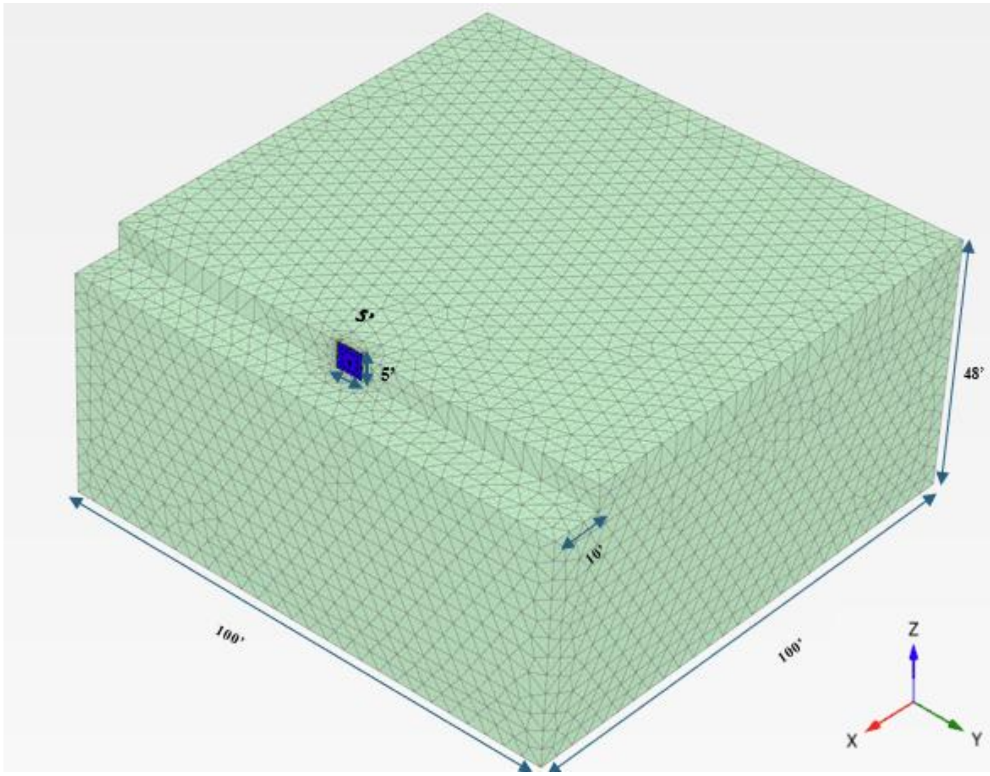

Figure 4-19 5 ft x 5 ft finite element model for passive resistance.

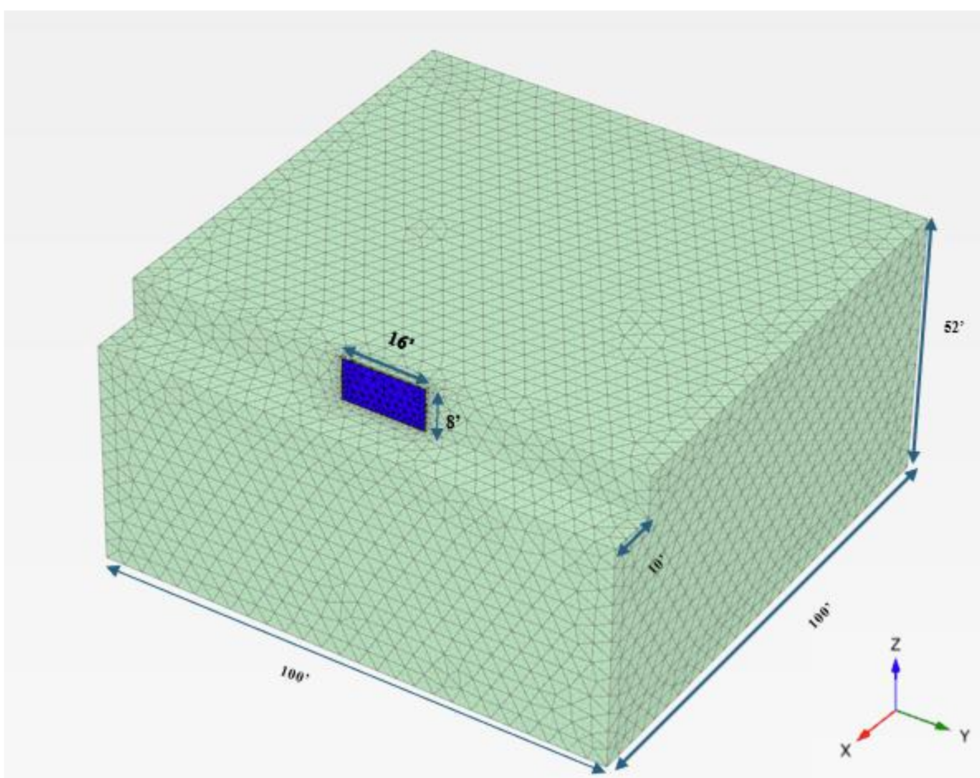

Figure 4-20 8 ft x 16 ft finite element model for passive resistance.

The material model used for the Florida limestone formations tested here (Fort Thompson and Ocala) was developed in Phase II for the bilinear strength envelope and ductile stress–strain response of the Florida limestone (a perfectly elastic–plastic material model (modified MC) with four parameters (a, α, β and $p_{p\omega}$) as input). Table 4-4 and Table 4-5 summarize the mass properties of Fort Thompson Limestone and Ocala Limestone that were modeled for the footing sizes in Figure 4-19 and Figure 4-20. Of importance for the extension space (passive loading) of the Florida limestone was if the horizontal stresses or the stress paths exceeded the Pp, for the lowest dry unit weight cases (lowest Pp values). Stress points in the mesh were selected that covered the area of significant shear strain leading to the passive state. Figure 4-21 shows the points identified on the meshed limestone in the FE model which were taken at the centerline of the footing. Figure 4-22 shows the stress paths of the points in Figure 4-21 which show that up to the 1 ft displacement (well past the passive state) the Pp on the strength envelope is not exceeded. Figure 4-23 shows the same stress paths corresponding to displacements of approx. 0.1 to 0.15 ft, when the material first reached the strength envelope indicating a passive state in the limestone near the footing face. This suggests that the second slope of the strength envelope (b) for the extension models is not necessary, however, this is input variable exists in the GUI and engine to show the complete compression and extension strength envelope for comparison.

Table 4-4 Fort Thompson Limestone Mass Extension Properties.

unit wt (pcf)	a-psi	Pp-psi	β (°)	α (°)
90	9.74	57.17	5.42	29.68
95	11.87	65.29	7.27	30.54
100	14.47	75.33	9.46	31.38
105	17.62	87.79	11.99	32.21
110	21.45	103.32	14.82	33.02
115	26.09	122.76	17.88	33.82
120	31.72	147.20	21.06	34.22
125	38.54	178.00	24.23	34.99

Table 4-5 Ocala limestone mass extension properties.

unit wt (pcf)	a-psi	Pp-psi	β (°)	α (°)
85	7.68	92.12	16.23	27.90
90	10.81	103.77	16.09	27.56
95	15.22	120.36	15.69	27.22
100	21.42	143.63	14.91	26.86
105	30.14	175.93	13.52	26.49
110	42.39	220.46	11.05	26.10
115	59.61	281.59	6.37	25.70

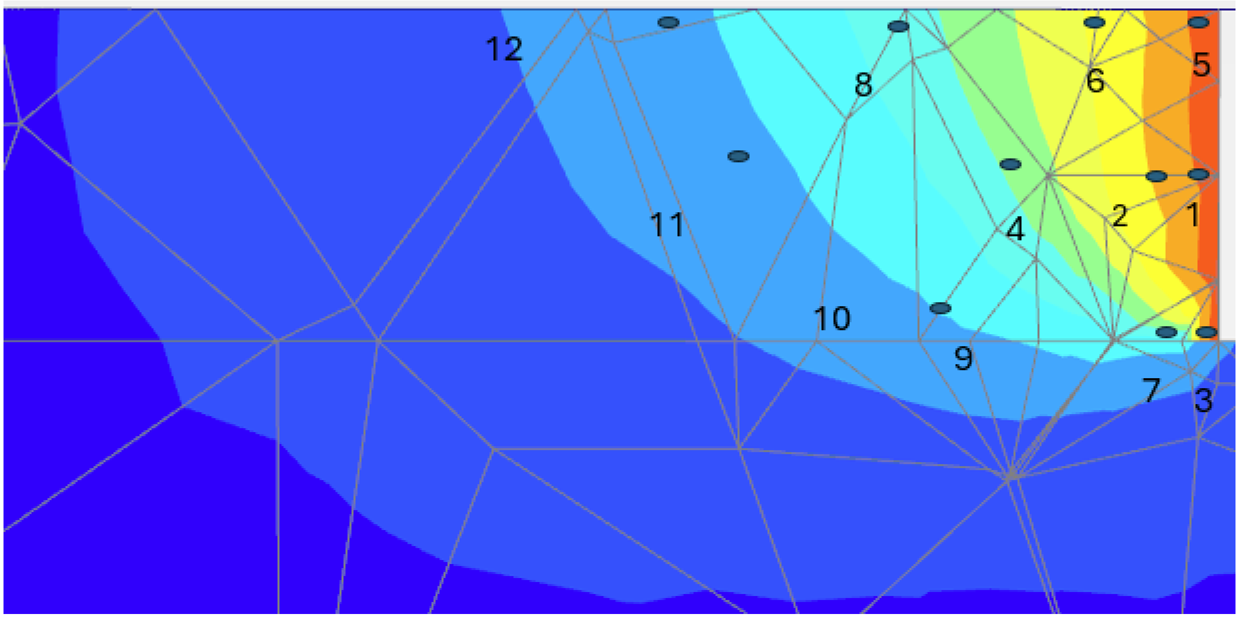

Figure 4-21 Stress contour color plot with mesh elements and stress points 1 – 12 in limestone.

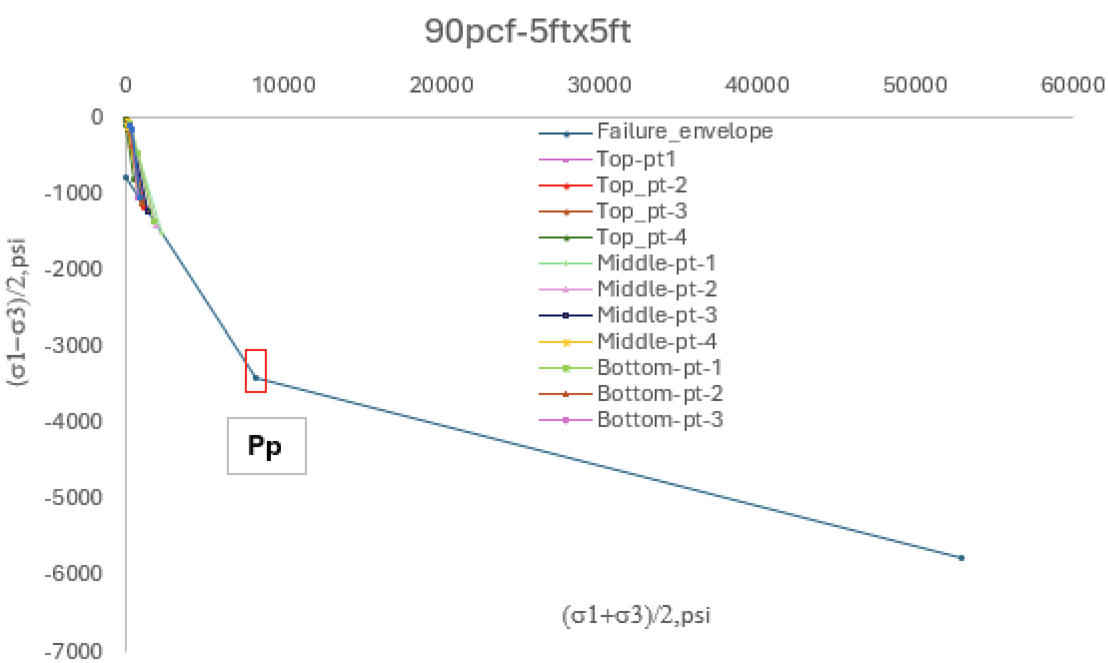

Figure 4-22 Stress paths for stress points in figure 21 and the strength envelope for the 90 pcf Fort Thompson limestone.

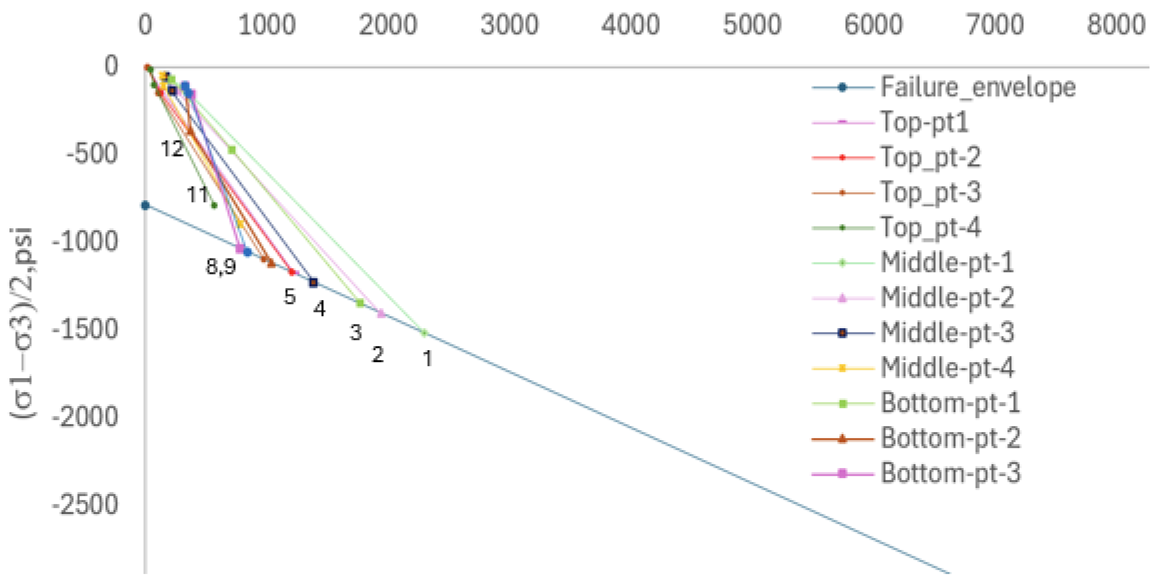

Figure 4-23 Stress paths landing on first segment of strength envelope of the 90 pcf Fort Thompson limestone.

4.2.3 Passive Resistance Design Models

Several previous studies (e.g., Duncan and Mokwa, 2001; Cole and Rollins, 2006; Shamsabadi et al., 2007) have demonstrated that the log-spiral-hyperbolic model (Duncan and Mokwa, 2001; Shamsabadi et al., 2007) is more suitable for predicting the passive resistance of embedded foundation elements, such as bulkheads and pile caps subjected to lateral loads in granular materials, compared to the conventional bi-linear model (CALTRANS, 2013; AASHTO, 2015). As discussed earlier, passive earth pressure coefficients (K_p) can be determined using various methods, including the moment method (Duncan and Mokwa, 2001), the method of slices (Shamsabadi et al., 2007), or the graphical solution (Caquot and Kerisel, 1948), all of which are based on composite log-spiral failure surfaces (Terzaghi, 1943). However, the Coulomb theory tends to overestimate the magnitude of K_p, whereas the Rankine theory underestimates it. The composite log-spiral failure surfaces include the Prandtl zone bounded by the logarithmic spiral segment (BC) followed by a straight-line section that represents the Rankine zone (CD), as illustrated in Figure 4-2. In that case, the ultimate passive force per length, E_P, is expressed as (from Lui et al., 2018):

$$E_P = 0.5\gamma' H^2 K_{p\phi} + c' H K_{pc} + q_{FBMP} H K_{pq} + q_{user} H K_{pq} \quad \text{Equation 4-1}$$

where γ is the unit weight of soil; and H denotes the footing thickness, c is the cohesion, and q corresponds to the surcharge loading. The coefficients $K_{p\varphi}$, K_{pc}, and K_{pq} represent the passive earth pressure coefficients associated with friction angle, cohesion, and surcharge, respectively (Lui et al., 2018). However, the shear zones behind the footing, extends beyond the effective footing length (L_e) as shown in Figure 4-2, increasing the passive resistance. Consequently, a three-dimensional geometric effects (Brinch, 1966) must be accounted for, and the ultimate resultant force, P_{ult}, is given in Equation 4-2. The horizontal component of the ultimate resultant force (needed for spring model in FB-MultiPier) is given in Equation 4-3.

$$P_{ult} = R_{3D} \cdot E_p \cdot B \qquad \text{Equation 4-2}$$

$$P_{ult} = R\left(0.5\gamma' H^2 K_{p\phi} + c'HK_{pc} + q_{FBMP}HK_{pq} + q_{user}HK_{pq}\right)B\cos(\delta) \qquad \text{Equation 4-3}$$

where R_{3D} is a Ovesen's 3-D modifying factor (dimensionless); correction factor to account for 3D effects given underlying use of log-spiral theory (Brinch 1966); B is the footing width or wall length (length units/ft). Please note that the R_{3D} should be obtained from the Rankine active earth pressure coefficient (K_a) and passive earth pressure coefficients of friction angle ($K_{p\varphi}$) with ϕ selected as first slope of strength envelope (i.e. less than Pp).

The formula of R_{3D} is expressed as:

$$R = 1 + \left(K_{p\phi} - K_a\right)^{\frac{2}{3}}\left[1.1S^4 + \frac{1.6x}{1 + 5\frac{B}{H}} + \frac{0.4\left(K_{p\phi} - K_a\right)S^3x^2}{1 + 0.05\frac{B}{H}}\right] \leq 2 \qquad \text{Equation 4-4}$$

where $K_{p\phi}$ and K_a are the passive and active earth pressure coefficients, B is the width of the footing measured horizontally in a direction normal to the applied load; t is the height of the footing; x is based on the spacing of multiple anchor blocks (x=1 for a single footing); and S is based on the depth of embedment of the footing defined as:

$$S = 1 - \frac{H}{D_t + H} \qquad \text{Equation 4-5}$$

Where D_t is the depth of embedment measured from the ground surface to the top of the footing.

The net soil resistance accounts for the active and passive resistance, normal to the faces of the footing in the direction of motion. (side friction on base will be accounted for and side friction on sides may be negligible, investigating in oblique loading models). Active resistance on trailing face of footing is a function of Rankine's active earth pressure coefficient.

$$\begin{aligned} P_{net} = P_{ult} - P_{active} \\ &= R\left(0.5\gamma' H^2 K_{p\phi} + c'HK_{pc} + q_{FBMP}HK_{pq} \right. \\ &\left. + q_{user}HK_{pq}\right)B\cos(\delta) \\ &- \left(0.5\gamma' H^2 K_a - 2c'H\sqrt{K_a} + q_{FBMP}HK_a \right. \\ &\left. + q_{user}HK_a\right)B\cos(\delta) \end{aligned} \qquad \text{Equation 4-6}$$

For the case of $\phi = 0$ (undrained behavior), the P_{net} from Equation 4-3 becomes

$$P_{ult} = (0.5\gamma' H^2 + 2s_u H + q_{FBMP} H + q_{user} H)B \qquad \text{Equation 4-7}$$

If $q_{FBMP} + q_{user} \geq 2s_u$

$$\begin{aligned} P_{net} &= P_{ult} - P_{active} \\ &= (0.5\gamma' H^2 + 2s_u H + q_{FBMP} H + q_{user} H)B \\ &\quad - (0.5\gamma' H^2 - 2s_u H + q_{FBMP} H + q_{user} H)B \end{aligned} \qquad \text{Equation 4-8}$$

Otherwise if $0 \leq q_{FBMP} + q_{user} < 2s_u$

$$\begin{aligned} P_{net} &= P_{ult} - P_{active} \\ &= (0.5\gamma' H^2 + 2s_u H)B - \left(0.5\gamma' H^2 - 2s_u H + 2\frac{s_u^2}{\gamma'}\right)B \end{aligned} \qquad \text{Equation 4-9}$$

Passive earth pressure based on Coulombs (1776) theory accounts for the wall-soil interface friction angle, δ, and assumes a planar failure surface. This has been shown to significantly over estimate the earth pressure coefficient, K_p, as the $\delta > 0.4\phi$ (δ is typically assumed to be up to $2/3\phi$ in soil and could be $\delta = \phi$ for concrete formed against excavation in limestone). Terzaghi (1943) showed that the failure surface is curved where backfill and wall interface friction exists and proposed the logarithmic spiral method. Caquot and Kérisel (1949) developed graphs for K_p that accounted for δ and horizontal backfill. The logarithmic spiral as a failure mechanism in the backfill was evaluated using the limit equilibrium method (Patki et al., 2015) and the kinematical method (Soubra and Macuh, 2002). Duncan and Mokwa (2001) developed K_p for contributions from ϕ, c, and q ($K_{p\phi}$, K_{pc}, K_{pq}) based on method of slices using the log spiral failure surface. Lui et al. (2018) applied a modified log spiral method to develop $K_{p\phi}$, K_{pc}, K_{pq} and validated against finite element models. In Table 4-6 the $K_{p\phi}$ from these different methods, for $\phi = 40°$ and $\delta/\phi = 0$ to 1, shows the Coulomb K_p significant deviation from the other methods for $\delta/\phi > ½$. The most rigorously evaluated and generally conservative K_p values from Lui et al. (2018) were used in this work for the earth pressure coefficients Equation 4-1 ($K_{p\phi}$, K_{pc}, K_{pq}). For implementation into FB-MultiPier, equations were fit to the Lui et al. (2018) data ($\phi = 20°$ and $40°$) and extrapolated to $\phi = 10°$ and $55°$ to account for the range of ϕ observed in triaxial tests of Florida limestone. The $K_{p\phi}$, K_{pc}, K_{pq} are plotted in Figure 4-24, Figure 4-25, and Figure 4-26 based on the equations. The $K_{p\phi}$, K_{pc}, and K_{pq} values from Lui et al. (2018), the equations for $K_{p\phi}$, K_{pc}, and K_{pq} and their values, including error percentages, are provided in the appendix.

Table 4-6 Kp values for multiple methods at $\phi = 40°$.

d/f	Coulomb (1776)	Log spiral		
		Soubra and Macuh (2002)	Duncan and Mokwa (2001)	Lui et al. (2018)
0	4.6	4.6	4.6	4.6
1/3	8.15	7.2	8.17	7.58
1/2	11.77	9.81	10.5	9.67
2/3	18.72	12.6	13.08	12.24
1	92.72	20.01	17.5	18.86

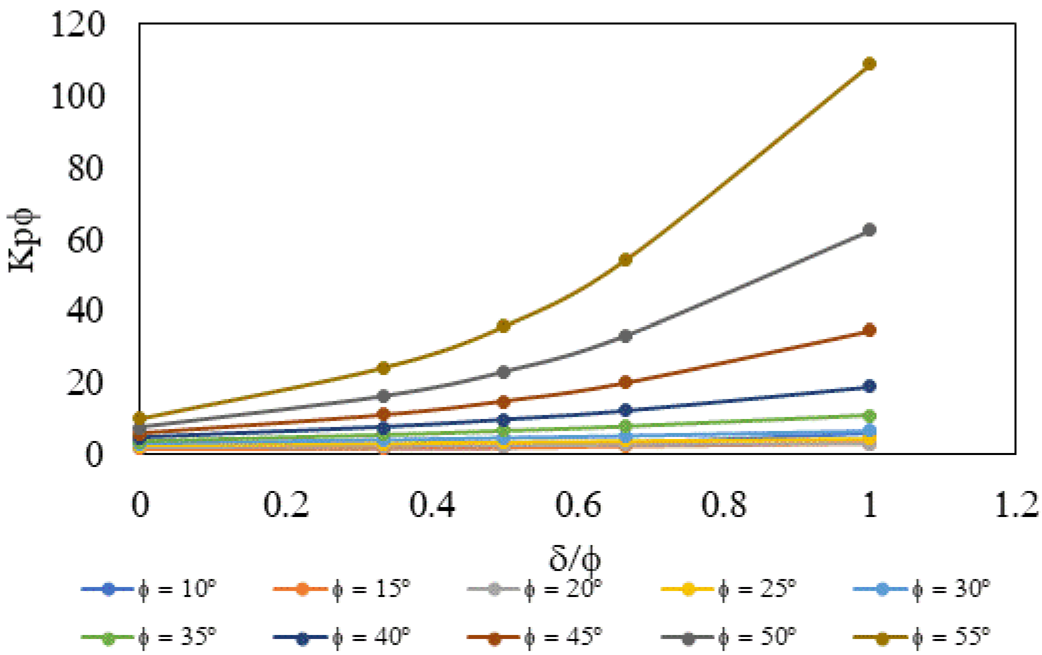

Figure 4-24 $K_{p\phi}$ values based on Lui et al. (2018).

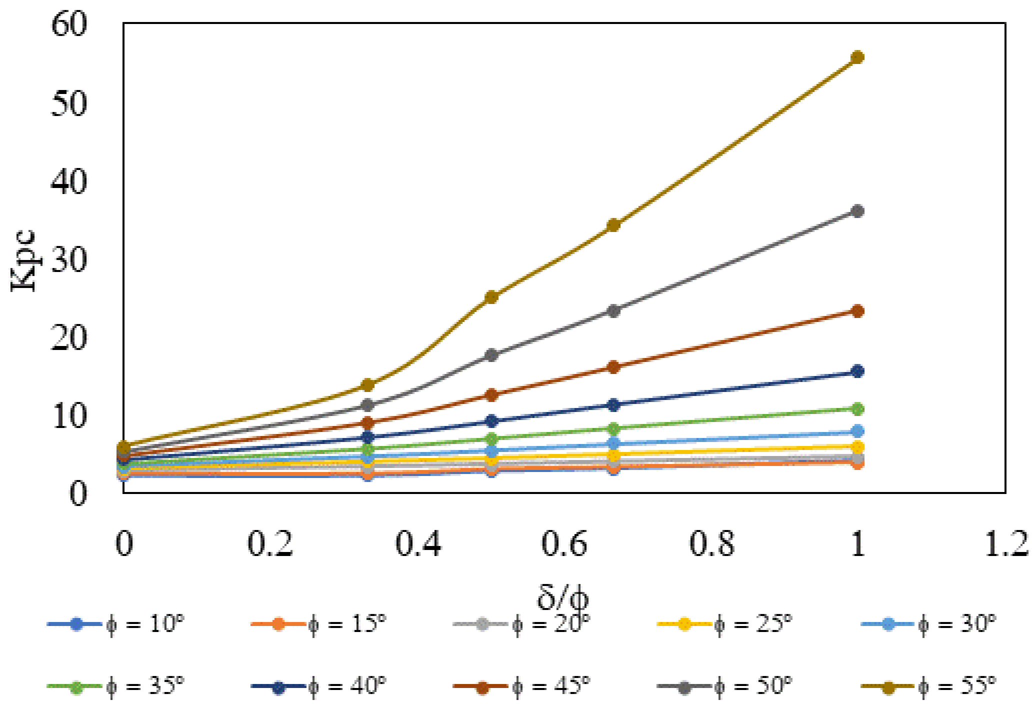

Figure 4-25 K_{pc} values based on Lui et al. (2018).

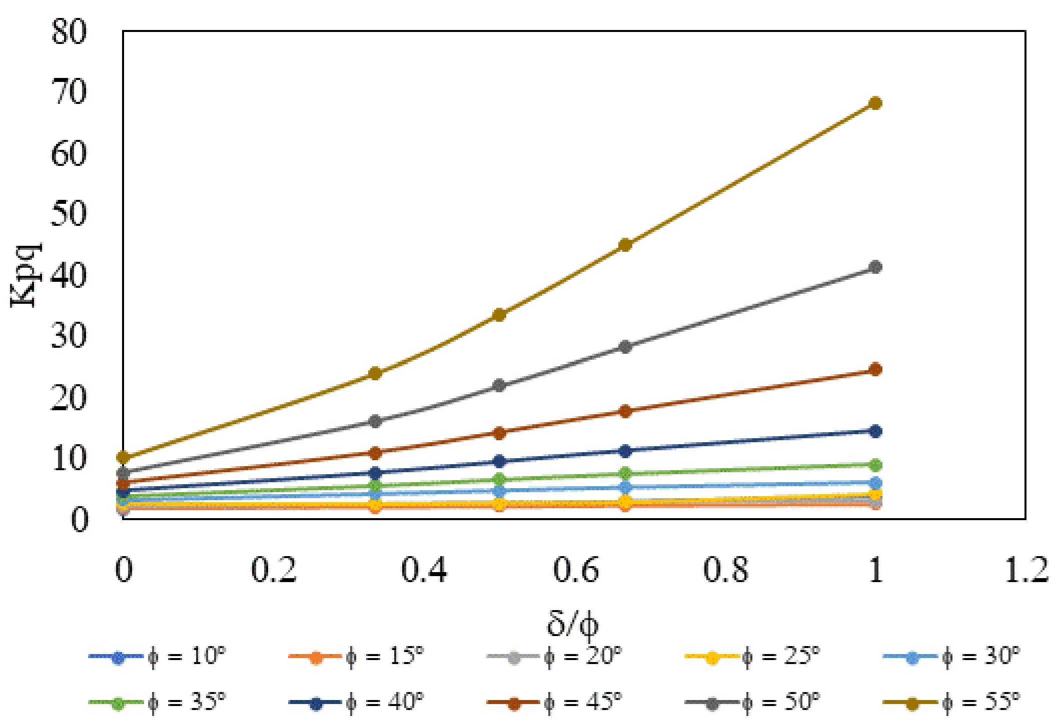

Figure 4-26 K_{pq} values based on Lui et al. (2018).

In this study, the hyperbolic formulation proposed by Duncan and Mokwa (2001) is utilized to model the passive load-displacement behavior up to the peak resistance (Figure 4-2). The fundamental form of this formulation is:

$$P = \frac{y}{\frac{1}{k_{max}} + \frac{R_f}{P_{ult}} y} \leq P_{ult} \qquad \text{Equation 4-10}$$

Where the P is the lateral force on footing and y is the corresponding displacement at the force P, the k_{max} is the initial stiffness and R_f is the failure ratio defined as the ratio between the actual failure force and the hyperbolic ultimate force, which is an asymptotic value that is approached as y approaches infinity. The value of k_{max} is estimated using the elastic solution with initial modulus (E_i) for horizontal displacements of a uniformly loaded vertical rectangular area in an elastic half-space developed by Douglas and Davis (1964). Unless otherwise noted, the value of R_f is smaller than unity, and varies from 0.5 to 0.9 for most soils (Duncan et al. 1980).

4.2.4 Base Friction Design Model

Characterizations of load-displacement behaviors pertaining to base friction models are not as broadly available in the literature as compared to those of passive resistance, given that full mobilization can occur at relatively small displacement levels. However, as stated in, it is reasonable to consider that base friction forces will mobilize at rates similar to those of the initial, steep portions of passive pressure mobilization curves. Further, recall that the initial load-displacement behavior of base friction was found to mimic that of passive resistance. Given the above, a novel two-segment base friction model is proposed for the design model. Here, base friction is assumed to match the load-displacement curve of passive resistance up to a fully mobilized (maximum) friction force, F_b, and then remain constant thereafter.

Values of peak base friction can be determined based on the Coulomb friction law, as dictated by adhesion and friction at the soil-footing interface, and the plan-view area of the footing:

$$F_b = \alpha \cdot c \cdot L \cdot B + W \cdot tan\delta \qquad \text{Equation 4-11}$$

where α is the adhesion factor; and, δ is the interface friction, which depends on the roughness of the interface and the construction technique. The adhesion factor, α, varies from approximately 0.5 for stiff soils to 0.9 for soft soils.

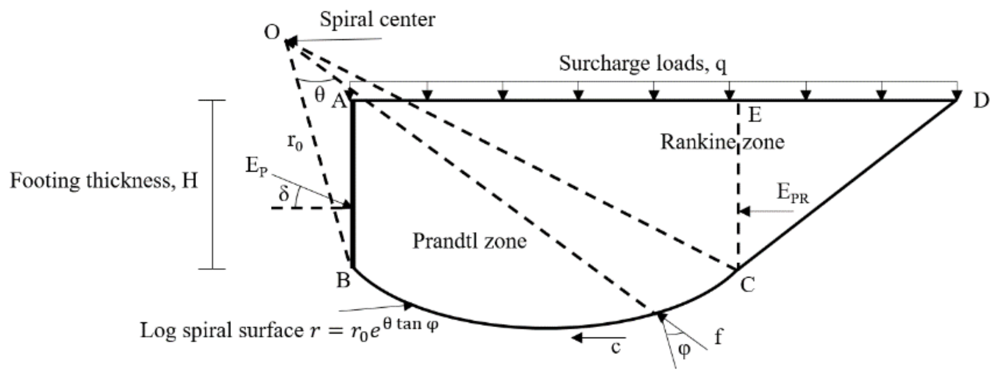

a)

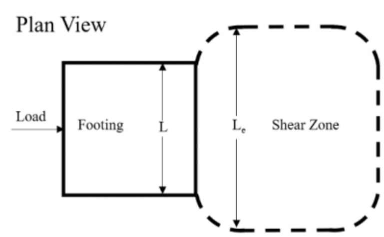

b)

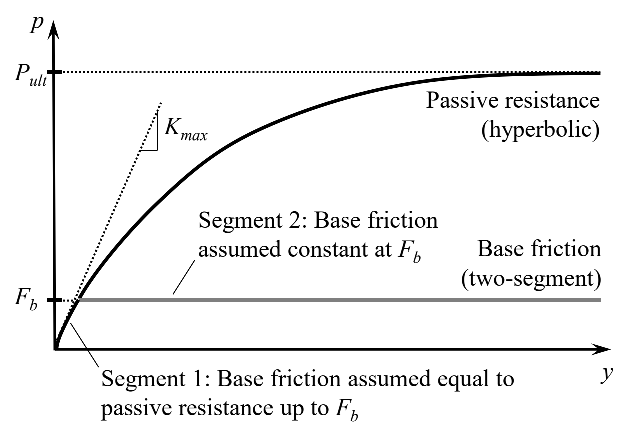

c)

Figure 4-27 Empirical relationships for modeling passive resistance and base friction of laterally loaded shallow foundations: a) log-spiral failure surface; b) illustration of 3d geometry effect; c) hyperbolic (Duncan and Mokwa 2001) and two-segment model for passive resistance and base friction, respectively.

The value of K_{max} is estimated using the elastic solution with initial modulus (E_i) for horizontal displacements of a uniformly loaded vertical rectangular area (Figure 4-28) in a semi-infinite, isotropic, homogeneous, elastic half-space developed by Douglas and Davis (1964).

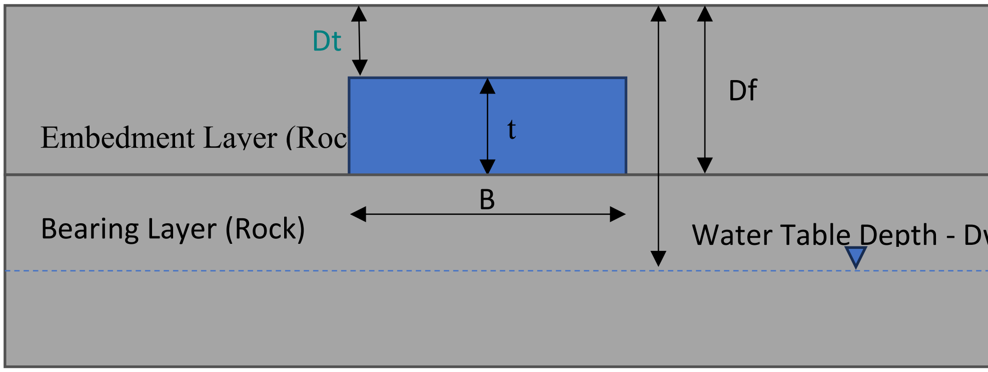

Figure 4-28 Rectangular area in semi-infinite, isotropic, homogeneous, elastic half-space.

The horizontal displacements, y, at the upper (y_1 at A and B) and lower corners (y_2 at C and D) of the rectangular area are calculated as:

$$y_1 = \frac{pB(1+\nu)}{16\pi E_i(1-\nu)}\{(3-4\nu)F_1 + F_4 + 4(1-2\nu)(1-\nu)F_5\} \quad \text{Equation 4-12}$$

$$y_2 = \frac{pB(1+\nu)}{16\pi E_i(1-\nu)}\{(3-4\nu)F_1 + F_2 + 4(1-2\nu)(1-\nu)F_3\} \quad \text{Equation 4-13}$$

Where p = uniform horizontal pressure applied to rectangular area ABCD

v = Poisson's ratio

E_i = initial soil tangent modulus

b = footing width

$F_1 - F_5$ = influence factors defined below

$$F_1 = -(K_1-K_2)\ln\left(\frac{K_1-K_2}{2+\sqrt{4+(K_1-K_2)^2}}\right) - 2\ln\left(\frac{2}{(K_1-K_2)+\sqrt{4+(K_1-K_2)^2}}\right) \quad \text{Equation 4-14}$$

$$F_2 = 2\ln\left(\frac{2\left(K_1+\sqrt{1+K_1^2}\right)}{(K_1+K_2)+\sqrt{4+(K_1+K_2)^2}}\right) + (K_1-K_2)\ln\left(2+\frac{\sqrt{4+(K_1+K_2)^2}}{(K_1+K_2)}\right) - K_1^2\left(\frac{\sqrt{4+(K_1+K_2)^2}}{(K_1+K_2)} - \frac{\sqrt{1+K_1^2}}{K_1}\right)$$ Equation 4-15

$$F_3 = -2K_1\ln\left(\frac{K_1}{1+\sqrt{1+K_1^2}}\right) + (K_1+K_2)\ln\left(\frac{(K_1+K_2)}{2+\sqrt{4+(K_1+K_2)^2}}\right) - \ln\left(\frac{(K_1+K_2)+\sqrt{4+(K_1+K_2)^2}}{2\left(K_1+\sqrt{1+K_1^2}\right)}\right) + \frac{(K_1+K_2)}{4}\left[\sqrt{4+(K_1+K_2)^2}-(K_1+K_2)\right] - K_1\left(\sqrt{1+K_1^2}-K_1\right)$$ Equation 4-16

$$F_4 = -2\ln\left(\frac{2\left(K_2+\sqrt{1+K_2^2}\right)}{(K_1+K_2)+\sqrt{4+(K_1+K_2)^2}}\right) + (K_1-K_2)\ln\left(\frac{2+\sqrt{4+(K_1+K_2)^2}}{(K_1+K_2)}\right) + K_2^2\left(\frac{\sqrt{4+(K_1+K_2)^2}}{(K_1+K_2)} - \frac{\sqrt{1+K_2^2}}{K_2}\right)$$ Equation 4-17

$$F_5 = 2K_2 \ln\left(\frac{K_2}{1+\sqrt{1+K_2^2}}\right) - (K_1+K_2)\ln\left(\frac{(K_1+K_2)}{2+\sqrt{4+(K_1+K_2)^2}}\right) + \ln\left(\frac{(K_1+K_2)+\sqrt{4+(K_1+K_2)^2}}{2\left(K_2+\sqrt{1+K_2^2}\right)}\right) - \frac{(K_1+K_2)}{4}\left[\sqrt{4+(K_1+K_2)^2}-(K_1+K_2)\right] - K_2\left(K_2-\sqrt{1+K_2^2}\right)$$ Equation 4-18

$$K_1 = \frac{2D_f}{B}$$ Equation 4-19

$$K_2 = \frac{2D_t}{B}$$ Equation 4-20

D_t – depth to top of footing (if top of footing is above embedment layer than Dt = 0)

The average deflection at the top corner and the bottom corner of the footing, y_c, is:

$$y_c = \frac{y_1+y_2}{2}$$ Equation 4-21

The initial elastic stiffness, k_{max}, is the slope of the load-deflection curve and calculated as:

$$k_{max} = \frac{P}{y_c}$$ Equation 4-22

where P is the horizontal force on the footing calculated as:

$$P = pBH$$ Equation 4-23

where p is the applied horizontal pressure, B is the footing width, t is the footing thickness, and H is the embedded portion of the footing.

$$H = D_f - D_t \qquad \text{Equation 4-24}$$

The units of k_{max} are force per length, [F/L]. Since calculation of k_{max} max is for the elastic portion of the hyperbolic term, an arbitrary value of p can be specified.

R_f is the failure ratio between P_{ult} and hyperbolic asymptote value of passive resistance. Duncan and Mokwa (2001) adopted $R_f = 0.85$ for passive resistance of footings in natural ground and in prepared granular soil. It typically ranges from 0.75 to 0.95 (Duncan and Mokwa 2001). Shamsabadi et al. (2007) found R_f to be 0.94 – 0.97 sand.

R_f can be estimated by substituting P_{ult} for P, and by substituting the movement required to fully mobilize passive resistance, Δ_{max}, for y, where Δ_{max} = % of the footing thickness. Re-arranging the terms in lateral force on footing equation results in the following expression for R_f:

$$R_f = 1 - \frac{P_{ult}}{\Delta_{max}\, k_{max}} \qquad \text{Equation 4-25}$$

Unless otherwise noted, a value of R_f equal to 0.85 is adopted in the present study, where 0.85 is consistent with Duncan and Mokwa (2001). Without experimental data, Δ_{max} can be estimated based on experiments which showed a range of 3% to 11% for tests on fine gravel to silty sand.

4.2.5 Plaxis Comparison Results to the Proposed Design Model

Figure 4-29 and Figure 4-30 show the Plaxis model results (measured) plotted against the predicted passive force-deformation (Equation 4) for 8 ft x 16 ft footings fully embedded in Fort Thompson and Ocala limestone, respectively. The FE results (measured) and the prediction model P_{Rult} and P_{ult} compare well for both limestone formations. Across all Fort Thompson limestone models (Table 4-4) and footing sizes (5 ft x 5 ft and 8 ft x 16 ft) the mean bias (measured/predicted) is 1.05 and the coefficient of variation, CV, is 5.8%. Across all Ocala limestone models (Table 4-5) and footing sizes (5 ft x 5 ft and 8 ft x 16 ft) the mean bias (measured/predicted) is 1.11 and the coefficient of variation, CV, is 16%.

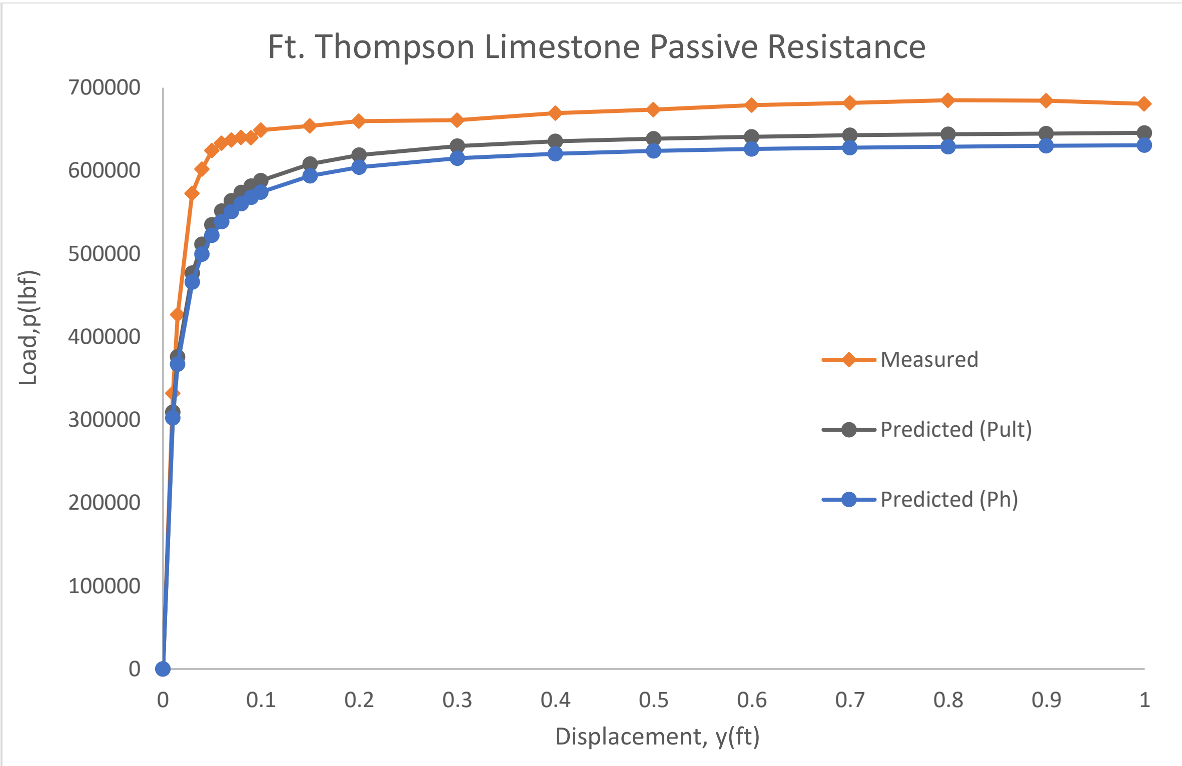

Figure 4-29 Measured and predicted passive force-deformation for 8 ft x 16 ft footing in 90 pcf Fort Thompson limestone.

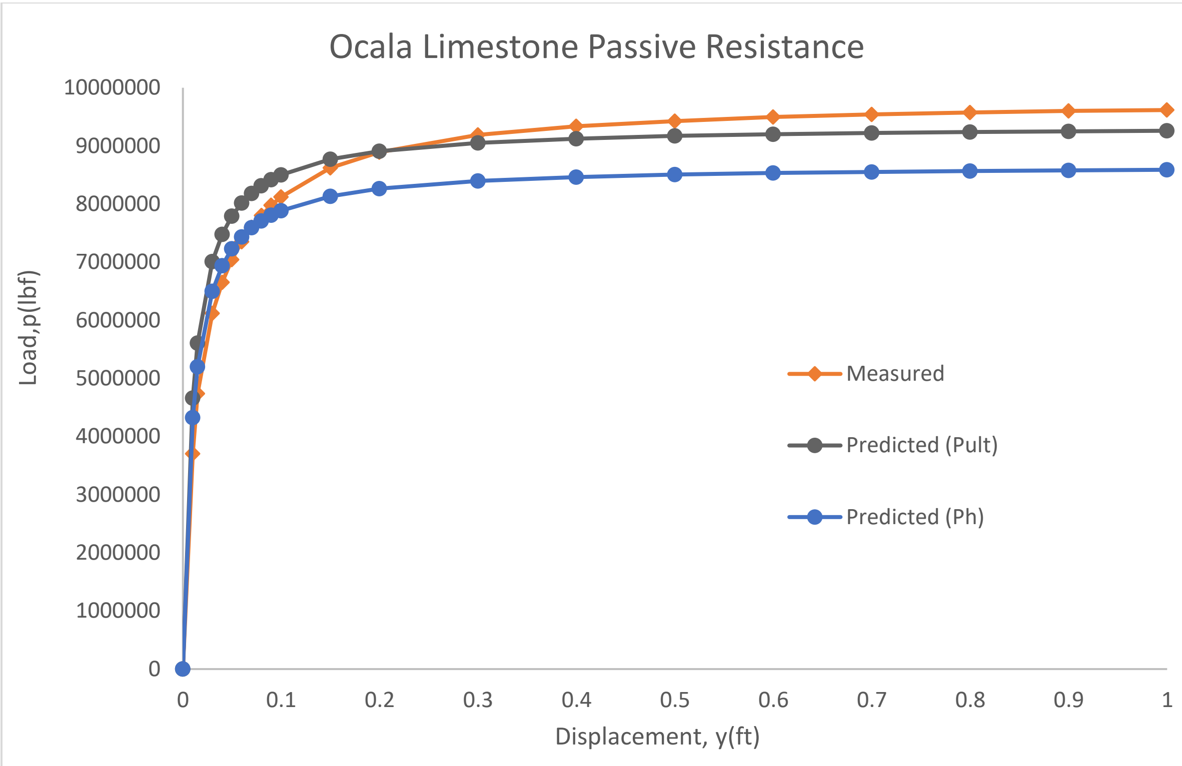

Figure 4-30 Measured and predicted passive force-deformation for 8 ft x 16 ft footing in 90 pcf Ocala limestone.

4.3 Oblique Loading

For footings embedded in Florida Limestone, the stress and strain behavior characteristic of their different formations influence the passive force-deformation in lateral loading scenarios. Recent State Road 84 construction included multiple spread footings in South Florida shallow Limestone formations with some skewed resultant pier design loads (Figure 4-31). The passive response of footings for non-skewed loading resulted in a validated method for use with Florida limestone. Next, the focus is on the passive force-deformation behavior for skewed loading as shown in Figure 4-31.

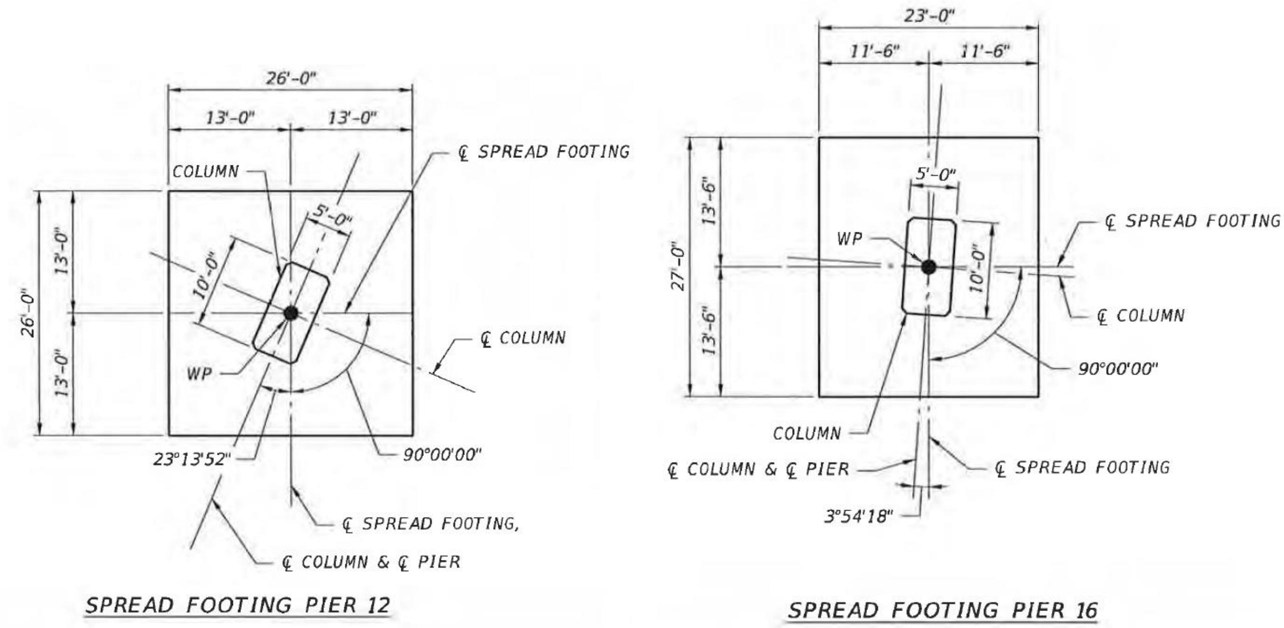

Figure 4-31 SR84 footings with rotated pier illustrating oblique loading.

Passive force-deflection behavior of skewed bridge abutments investigated by Rollins and Jessee (2013) showed the influence of skew angle on the mobilized passive resistance. Their work included laboratory tests on a reinforced concrete wall (representing abutment with compacted dense sand to represent the bridge approach fill. The abutment was placed at 0, 15, 30, and 45° and the applied force and displacement response was measured to mobilized passive states. Figure 4-32 are the force-displacement results for multiple tests at the skewed angles which shows that the passive resistance (ultimate passive force) decreases proportionally to the skew angle of the abutment. Further, the passive state is reached at about 0.025-0.035H (2.5-3.5% of the abutment height). Rollins and Jessee (2013) proposed a reduction factor as the ratio of the ultimate passive force at any skew angle to the ultimate passive force at 0° skew. This and the results of numerical modeling of their tests are shown in Figure 4-33.

Rollins and Jessee (2013) findings indicate a 25% reduction in the passive resistance at a skewed loading of 15° (Pier 12 in Figure 4-31 had an oblique loading of 23° suggesting the need to account for the less passive resistance on the footing face in similar cases. To investigate this for footings in Florida Limestone, 3-D Plaxis models of L/B =1 and L/B = 2 footings in Florida Limestone and soil under 0, 15, 39, 45, 60, and 90 were simulated and the force-deformation response was extracted for each face of the footing models. Subsequent validation for implementation into FB-MultiPier was performed, including revisions to the FB-MultiPier engine and UI. The following sections describe the work in more detail.

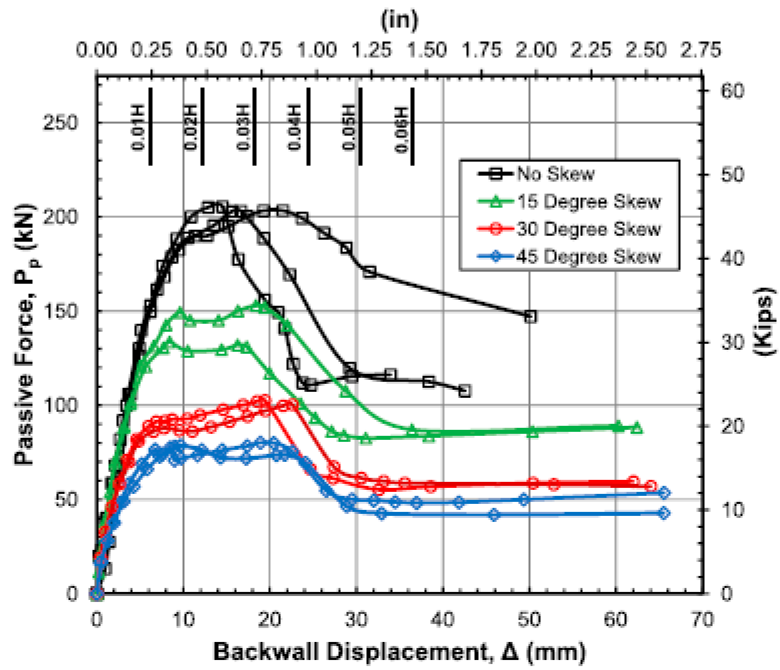

Figure 4-32 Passive force deflection results from loading on skewed abutments (Rollins and Jessee, 2013).

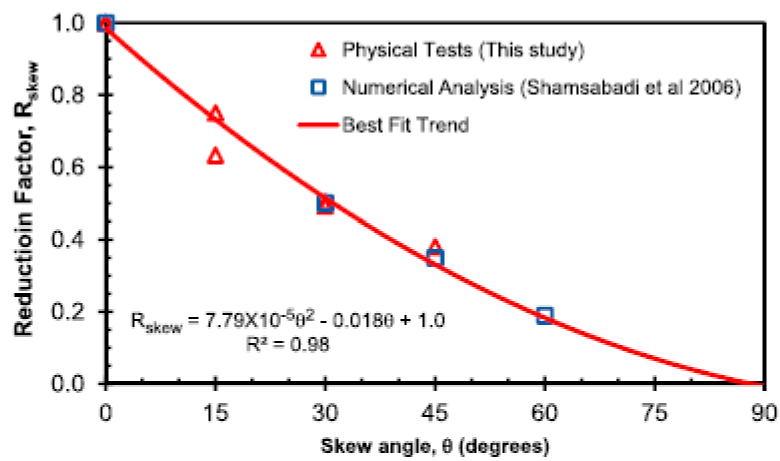

Figure 4-33 Reduction factor versus skew angle for abutments with dense sand (Rollins and Jessee, 2013).

4.3.1 Lateral Resistance of Embedded Footing Under Oblique Loading

For validation of the footing model, a plate model of the abutment in Rollins and Jessee (2013) experiments was constructed in a dense sand with the same properties and dimensions. Skew angles of 0, 15, 39, and 45 were modeled and simulated for comparison to the experimental results. Shown in Figure 4-34 is the reduction factor for the model results and the

Rollins and Jessee (2013) experimental results which indicates good agreement and a valid model approach.

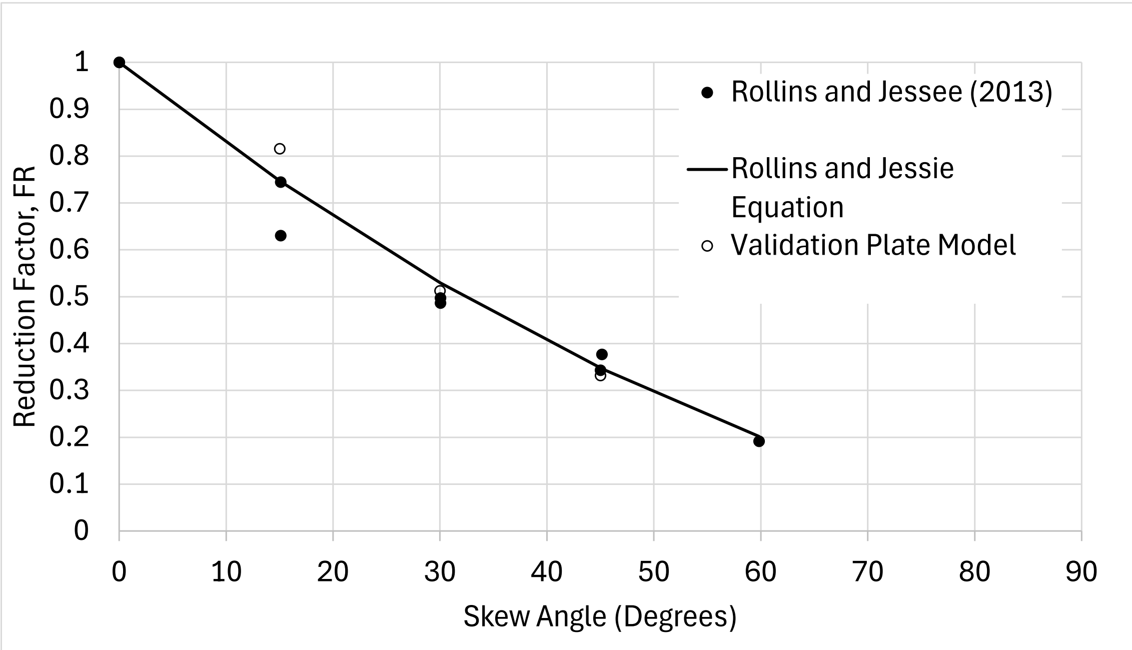

Figure 4-34 Reduction factors versus skew angle for Rollins and Jessee (2013) and current validation model.

A Footing, Figure 4-31, subjected to a lateral displacement (or load) in the L and B direction will mobilize friction on the base and friction and passive resistance on both faces that is dependent on the angle of the lateral load. As with the footings under lateral loading in one direction (Chapter 4) the friction resistance will mobilize with small lateral movements (i.e., 0.1 inch in granular soil) with the primary contribution coming from the base of the footing and the secondary from the sides. Oblique loads induce movements in both the L and B directions with equal movements resulting in equal resistances on the faces of the footing (45° case in Figure 4-35). The normal resistance on the footing (thickness = H) includes the active resistance and the passive resistance, where the active resistance mobilizes with lateral movements on the order of 0.1%H for loose sand to 4%H for soft clay and the passive resistance mobilizes around 1%H for loose sand to 5%H for soft clay. For typical footings designed to support superstructure loads and embedded in soil and limestone, e.g. 5 – 8 ft thick and widths of 10 – 15 ft, significant passive resistance will develop compared to base skin friction resistance.

Investigation of and development of the lateral resistance (i.e. force vs. displacement) of footings embedded in Florida limestone required finite element model simulations with PLAXIS 3D because of the lack of physical experimental results. Fortunately, the FE models built in Phase 2 and for Task 1 of the current phase can be used to model the lateral behavior. Validation of the FE model's footing boundary conditions and prescribed motion for oblique loading was required. The experimental results by Rollins and Jessee (2013) consisted of and embedded concrete wall with compacted soil. Table 4-7 includes the case of soil (with cohesion, c, and friction angle, f) that was used for validation. A soil with lower c and f was also modeled to test the development of the spring models in FB-MultiPier. Included in Table 4-7 are the properties of the Florida limestone cases modeled based on the Fort Thompson formation 90 pcf and 120 pcf, lowest and highest strength cases from the above sections in this Chapter.

For the FE modeling, a displacement-controlled swipe friction analysis was performed, i.e. applying a specified displacements to the nodes of the footing in such a way that increasing passive resistance (total force acting against footing in Figure 4-36) occurs with increasing displacement. It was standard practice to prescribe movements up to mobilization of the full strength of the soil and limestone. For the soil and Florida limestone material models, two footing sizes representing L/B =1 and 2 were modeled: 5 ft x 5 ft x 5 ft and 16 ft x 8 ft x 8 ft (length x width x height) (Figure 4-37). The use of unstructured meshes composed of triangular elements provides flexibility in element arrangement and element size. Model mesh discretization for the study followed non-associated flow with the mesh composed of 6-noded triangular elements with three Gauss quadrature points. Optimized mesh is used for all the model cases in this study. Interface at the contact of soil and footing is used having properties same as that of the soil (limestone). Model boundary conditions consisted of bottom surface fixed in all directions, and a vertical roller was used on each side in the x-direction, and in the y-direction. A point displacement is applied at the center of the footing for prescribed movement.

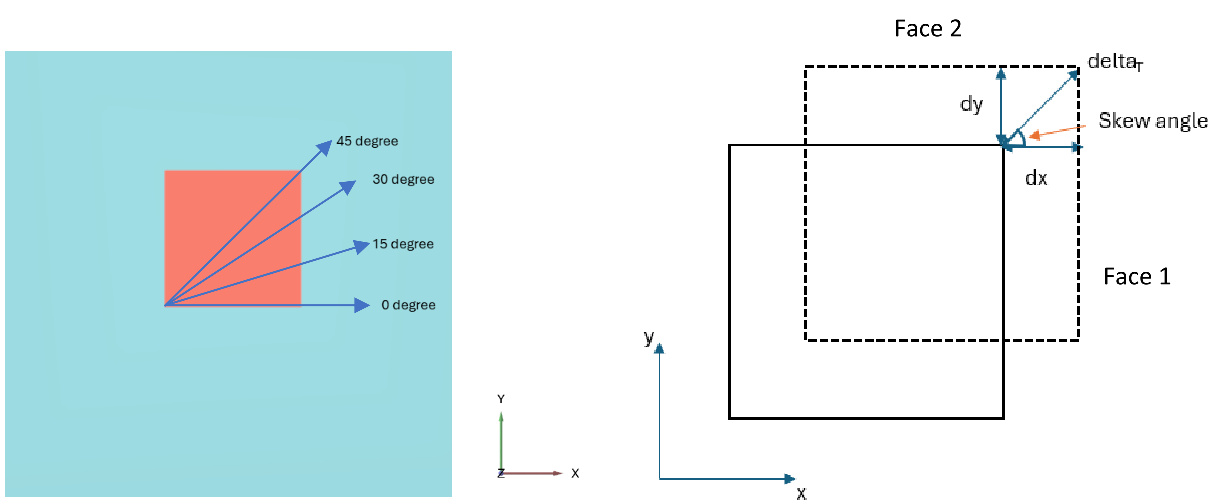

Figure 4-35 Plan view of embedded footing model (L/B =1) with (a) the angles of the direction of motion and (b) the translated footing in the direction of motion with x and y components.

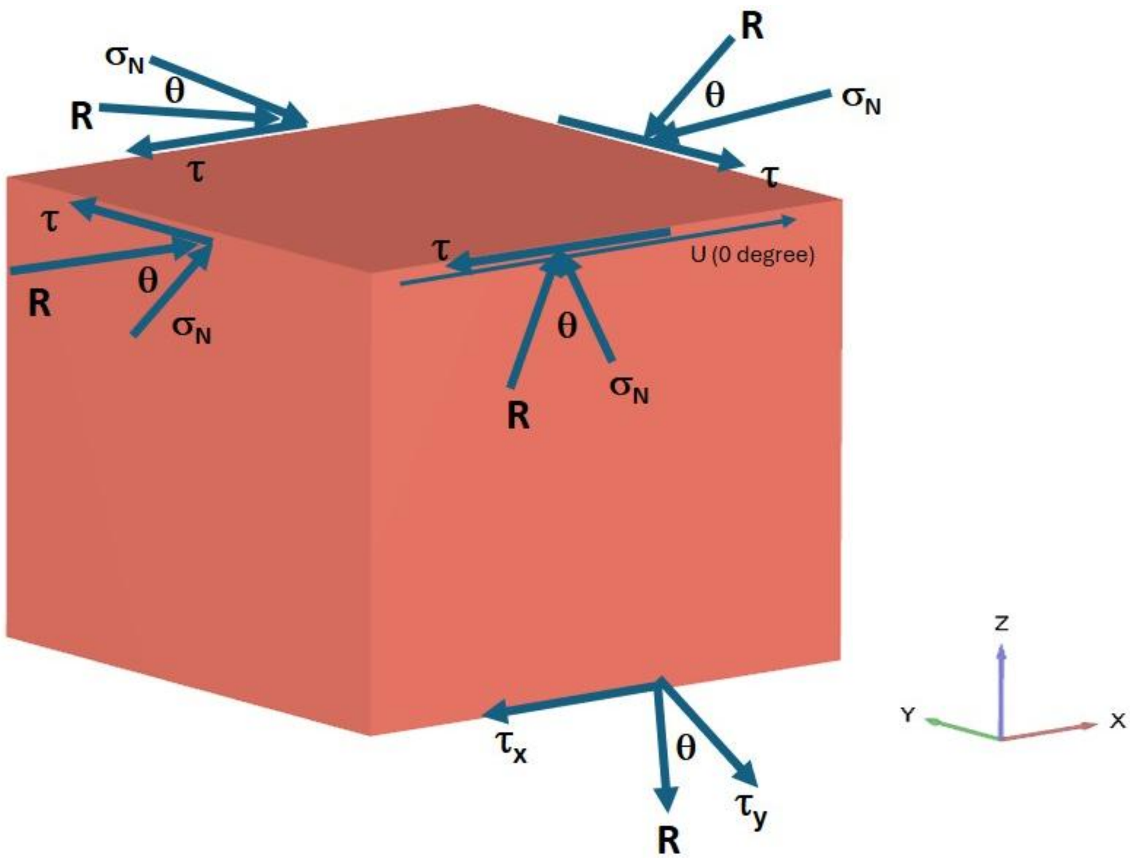

Figure 4-36 Embedded footing model with shear (τ) and normal (σ) forces acting on faces.

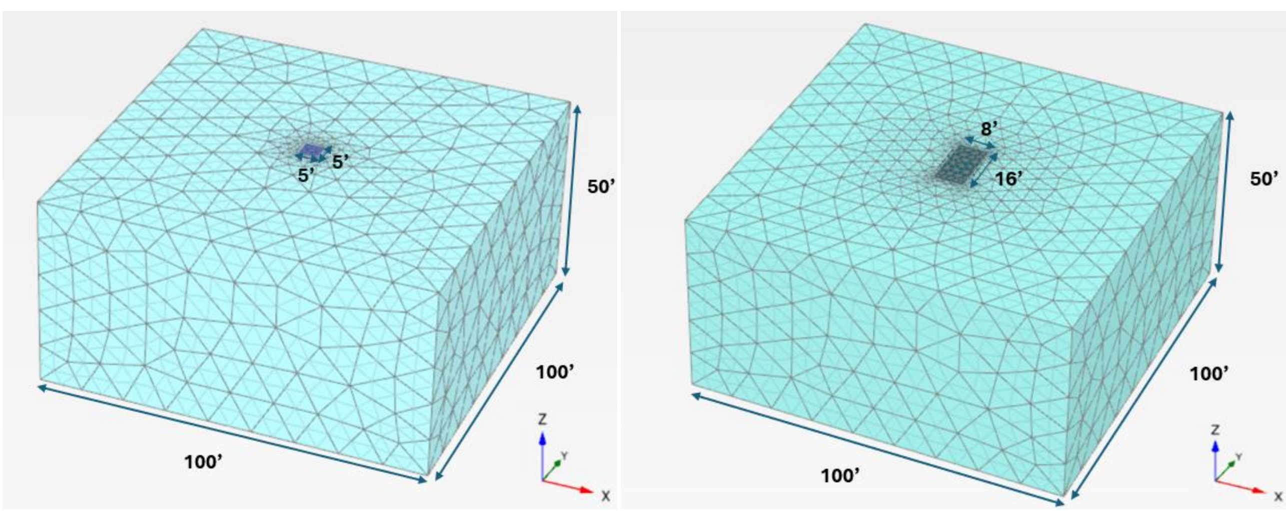

Figure 4-37 3-Dimensional FE model of 5' x 5' and 8' x 16' footings (face 1 perpendicular to x-axis and face 2 perpendicular to y-axis).

Table 4-7 Cases of lateral load-deformation experiments.

Soil Type	Foundation Geometry			Backfill Properties			
	L(ft)	B(ft)	H(ft)	c(psf)	ϕ(°)	γ(pcf)	δ(°)
Sand	5	5	5	208	39	121	26
Sand	16	8	8	208	39	121	26
Weak Sand	5	5	5	69	27	102	18
Fort Thompson Limestone	5	5	5	828	19	90	12
Fort Thompson Limestone	16	8	8	828	19	90	12
Fort Thompson Limestone	5	5	5	2768	22	120	15
Fort Thompson Limestone	16	8	8	2768	22	120	15

The results of the prescribed displacement models for all cases (Table 4-7) were analyzed for the normal and shear forces on each face (Figure 4-36) which were calculated for each displacement step from the Gaussian stress points on the interface elements (about 200 model simulations). For each skew angle, the displacements in the normal and transverse directions were extracted for each face to investigate the force-deformation for the different model soil/limestone and footing dimensions. With this, the passive forces for each skew angle were normalized by the passive force at 0° (Equation 4-26). This process follows Rollins and Jessee (2013) (Figure 4-33) for dense poorly graded sand. Figure 4-38 shows the passive resistance reduction factors for Face 1 (Figure 4-36) of the soil cases and 5 ft x 5 ft and 16 ft x 8 ft footings (Table 4-7). The 16 ft x 8 ft footings were modeled with prescribed displacements for skew angles up to 90° for passive behavior on the L (16 ft) and B (8 ft) sides. For comparison, the Rollins and Jessee (2013) results are included. The differences between the reduction factors are about 20% for footing size and sand and weak sand (Table 4-7). Guo (2015) showed model passive result differences of 15% for the same abutment by Rollins and Jessie (2013) with sand backfill ϕ = 40°-44°.

$$P_{skew} = FR * P_{Ult} \qquad \text{Equation 4-26}$$

Figure 4-39 are the passive force gain factors from face 2 of the soil cases (Table 4-7) where at 0° the factor represents the lowest force and at 90° the factor represents the highest force. As the skew angle increases the passive force on face 2 increases and relative to the maximum passive force (90° – all movement in the y direction), the factor increases. To account for the increase or decrease in the passive resistance on either face the reduction or gain factor for a skew angle is multiplied by the maximum passive resistance (0°) for the face (Equation 4-27). Note, for a L/B =1 footing the maximum passive resistance is the same and for L/B > 1 the maximum passive resistance on the L face will be different than on the B face, requiring the Pult to be calculated for each.

$$P_{skew} = FG * P_{Ult} \qquad \text{Equation 4-27}$$

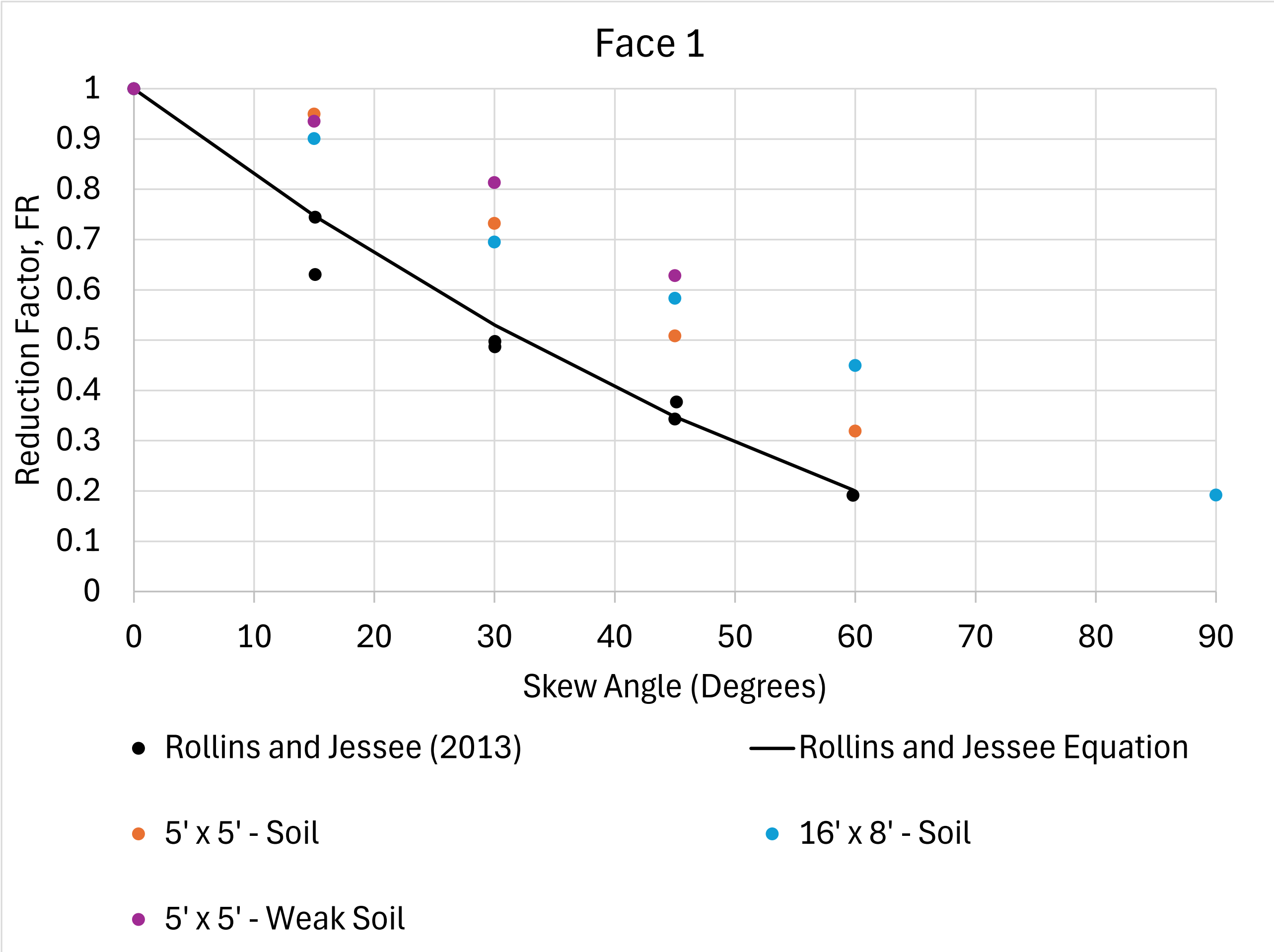

Figure 4-38 FE results of passive reduction factor on face 1 for soil models.

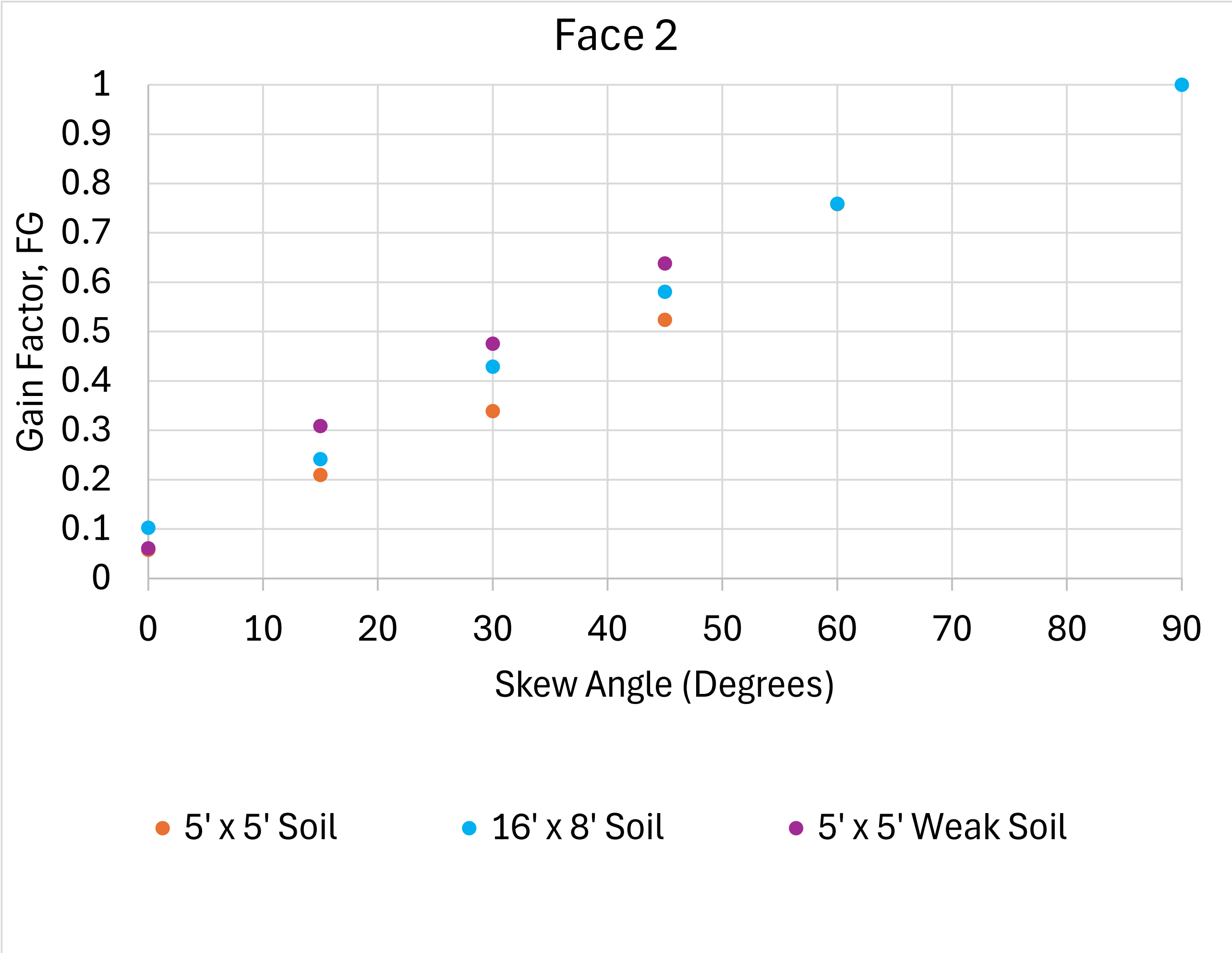

Figure 4-39 FE results of passive gain factor on face 2 for soil models.

The reduction and gain in passive resistance in limestone was investigated for increasing skew angles with prescribed displacement on 5 ft x 5 ft and 16 ft x 8 ft footings embedded in 90 pcf and 120 pcf limestone. Figure 4-40 are the reduction factors for face 1 (Figure 4-35) for skew angles up to 90°. The 16 ft x 8 ft footings were modeled with prescribed displacements for skew angles up to 90° for passive behavior on the L (16 ft) and B (8 ft) sides. In comparison to the results from Rollins and Jessee (2013) and the soil (Figure 4-40), reduction in passive resistance due to oblique loading is less and indicates about a 7% influence from the footing size, slightly more than from the limestone unit weight. The passive resistance of the 120 pcf limestone is more controlling than the footing size than for the 90 pcf, based on the models tested. Figure 4-41 are the gain factors for the limestone models based on the passive forces developed at face 2. Based on the model results, there is generally less reduction in the passive resistance on face 1 for increasing skew angle compared to the soil cases. On face 2, there is generally a significant gain in passive resistance beyond 10° (Figure 4-41). Results indicate the mobilization of significant passive resistance for footings embedded in limestone when small skew angles > 10°.

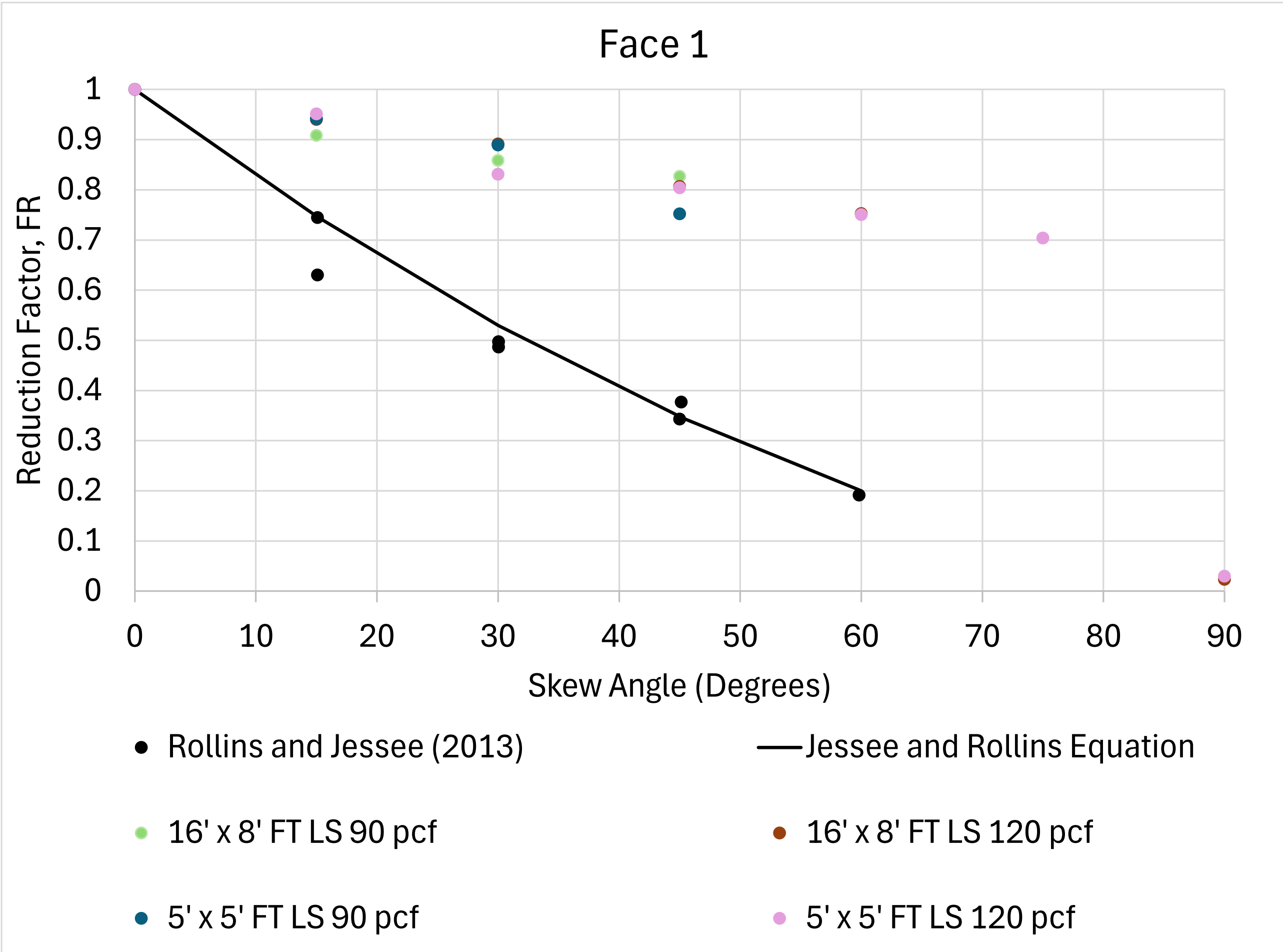

Figure 4-40 FE results of passive reduction factor on face 1 for limestone models.

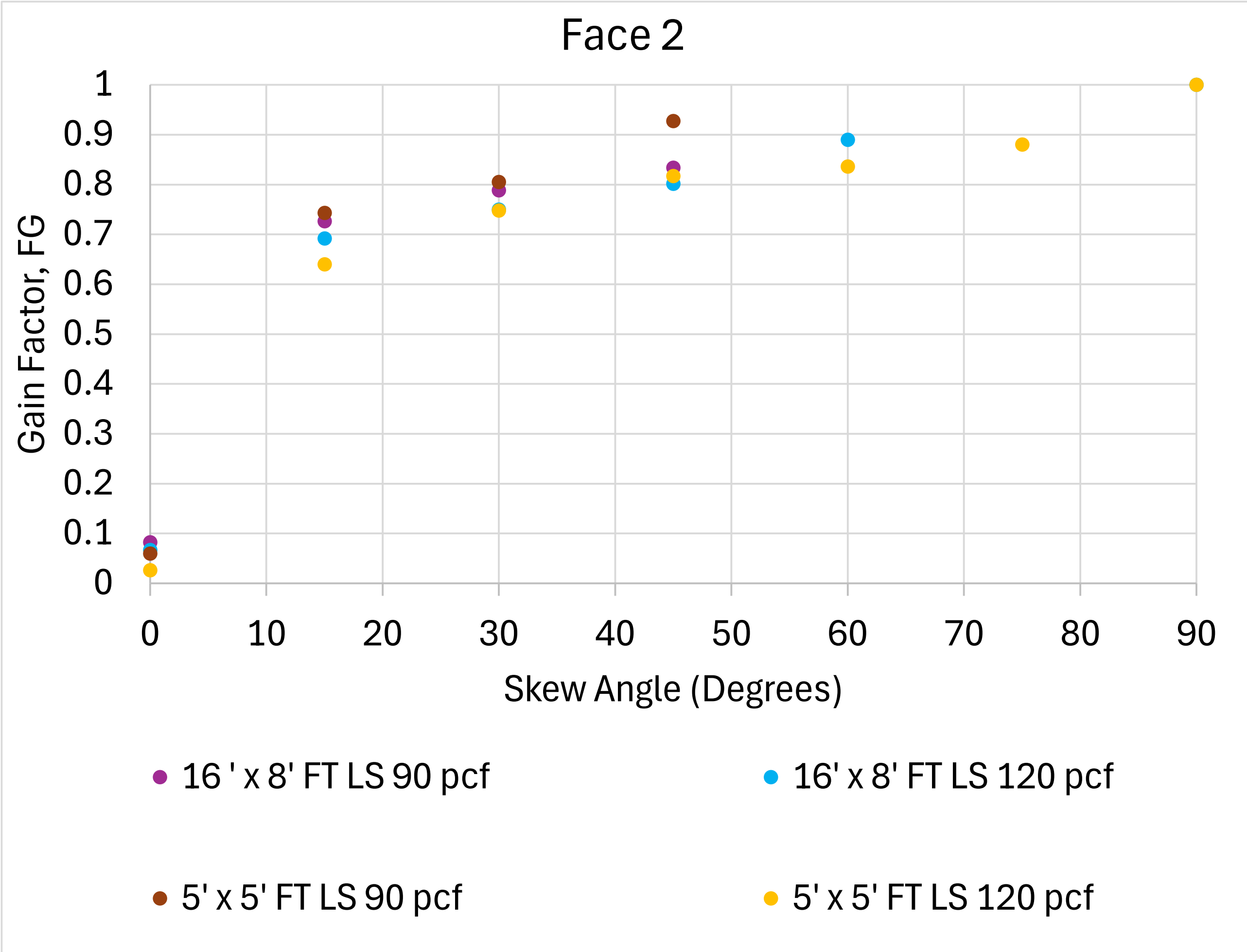

Figure 4-41 FE results of passive gain factor on face 2 for limestone models.

Shear force on the interface between the footing surface and the soil or limestone was calculated for each prescribed displacement and skew angle model. Due to the rotation of the failure planes in the soil or limestone, the shear force on the faces under passive resistance (Figure 4-36) did not reach the Coulombic shear resistance (function of strengths properties c and ϕ) but a less maximum. The maximum shear force reached in each case generally increased with increasing skew angle for face 1 and decreased for face 2 (Figure 4-35), following a similar reduction or gain relative to the maximum. Table 4 are shear force gain factors for face 1 with increasing footing displacement in the x-direction for 5 ft x 5 ft and 16 ft x 8 ft soil models and the 5 ft x 5 ft limestone model. The factors generally increase with displacement, however, are variable and don't reach the Coulombic shear resistance (the normalizing value). For incorporating shear force-deformation into discrete springs on nodes in the FB-MultiPier representation of the embedded footing and converging on a solution for equilibrium of the represented footing, stable force-deformation model is required. The ratios indicate numerical instability and non-convergence. At this time, the Coulombic model representation of the maximum shear force on each face is not appropriate due to the rotation of the shear failure plane. More testing of other soil types and investigation of the stress paths at the stress points in the FE model would be needed to identify the appropriate model of shear resistance. While shear resistance is mobilized before the passive resistance, passive resistance provides the significant portion of total resistance and is predominantly material strength dependent while shear is significantly influenced by the footing-soil interface behavior. Further, footings in limestone require excavation for casting formwork resulting in an annular space between the limestone and sides of footing. FDOT specifications require it to be backfilled with aggregate, however there are not specifications for minimum strength properties. Designing for shear resistance in this case would not be possible, however mobilization of passive resistance will occur with footing movement. Without further testing of the shear resistance, the focus of the analysis is on the passive resistance for different skew angles.

Table 4-8 Model shear force-resistance ratios for increasing x-displacement of skew angle = 30°.

	5x5 soil	16x8 Soil	5x5 120 LS
Ux	FFr	FFr	FFr
Increasi ng	0.00	0.00	0.00
	0.47	0.49	0.71
	0.51	0.61	0.69
	0.51	0.65	0.75
	0.53	0.66	0.75
	0.53	0.66	0.70
	0.54	0.66	0.72

As a check on the equilibrium of the FE models at the prescribed displacements, the direction of the resultant force on the footing (degrees form x-axis – Figure 4-35) was compared to the prescribed direction of motion for the skew angles tested (Figure 4-35). Figure 4-42 shows the resultant force direction of motion and the prescribed direction of motion for the soil models is in good agreement for the displacements considered, indicating force equilibrium. Figure 4-43 is the comparison between the resultant direction of motion and the prescribed for the limestone cases (Table 4-7) at small displacements and maximum displacement. The comparisons indicate an out of balance forcing on the footings at the skew angle approaches 45° form 0° and 90°. This is thought to be due to the shear behavior on the faces of the footing influencing motion more in the x or y direction (Figure 4-35).

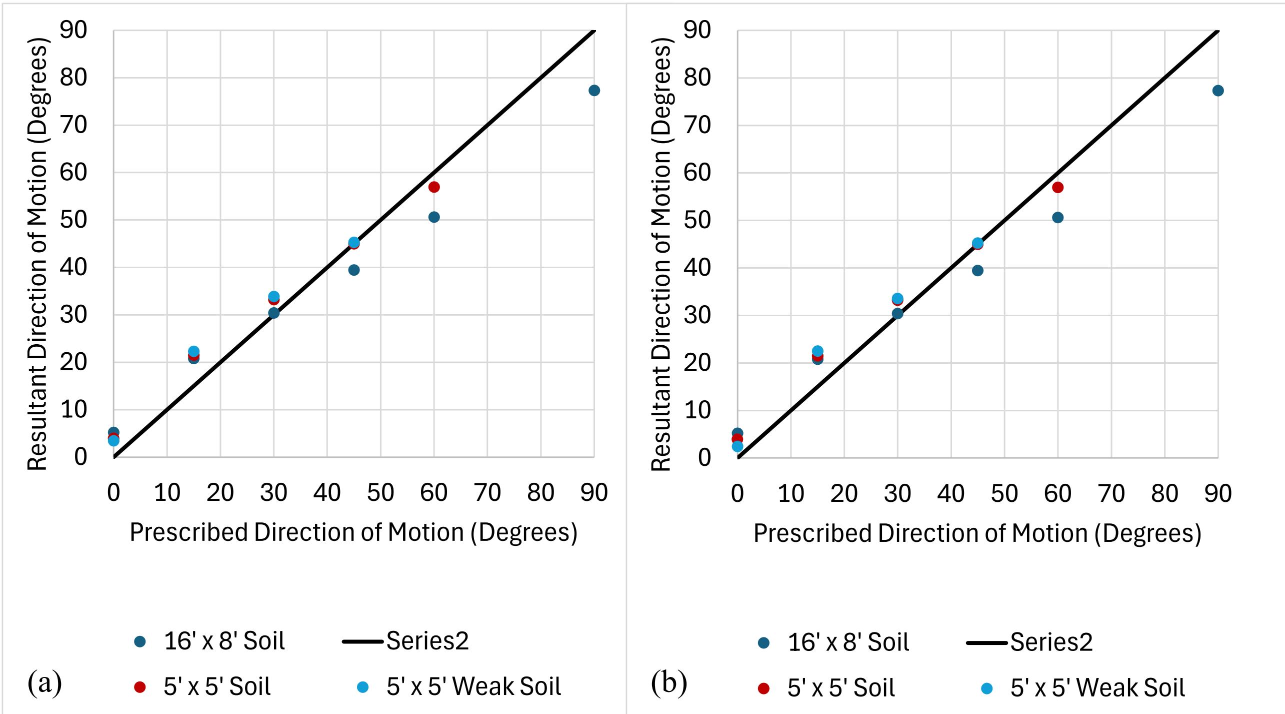

Figure 4-42 Measured and prescribed direction of motion for soil models (a) at initial movement (b) at mobilization movement.

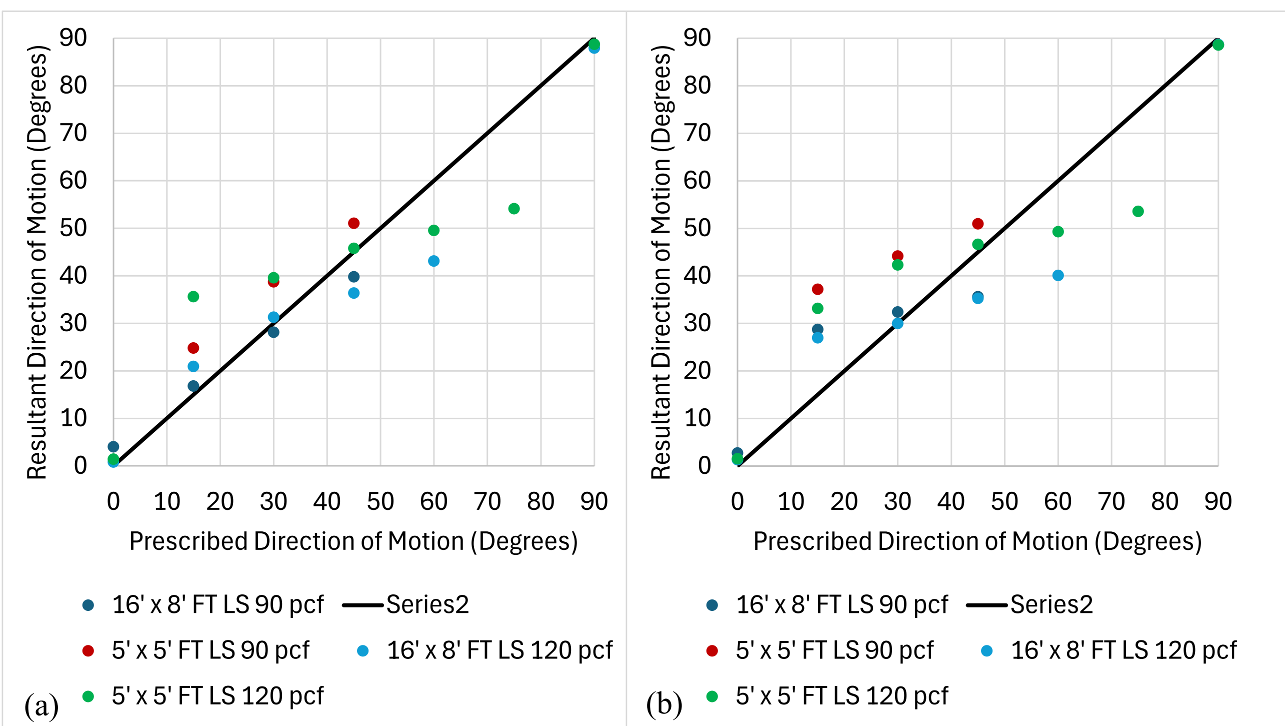

Figure 4-43 Measured and prescribed direction of motion for limestone models (a) at initial movement (b) at mobilization movement.

4.3.2 Passive Resistance Design Models

As identified in 4.2.3, the log-spiral-hyperbolic model (Duncan and Mokwa, 2001; Cole and Rollins, 2006; Shamsabadi et al., 2007) is most suitable for predicting the passive resistance of embedded foundation elements. For oblique loading where passive resistance is developed on adjacent faces (Face 1 and Face 2 Figure 4-36) of the footing and where the resultant direction of motion of the footing is as shown in Figure 4-35, the resultant passive force that accounts for the force reduction on each face due to the skewness is represented in Equation 4-28. The reduction factors (R_x and R_y) are taken as a function of the skew angle for a particular material type and foundation dimension (e.g., for L/B > 1 $P_x \neq P_y$ and for L/B = 1 $P_x = P_y$).

$$P_{SKEW} = \sqrt{(R_x P_x)^2 + \left(R_y P_y\right)^2} \qquad \text{Equation 4-28}$$

4.3.3 Passive Resistance Oblique Model

In Figure 4-44 and Figure 4-45, compares Plaxis results for Case 1, with estimate passive resistance from FB-MultiPier (FBMP) for oblique loading under a resultant displacement of 0.6 inches. Figure 4-44 presents the resultant resistance per oblique angle. The Plaxis resultant is comprised of both passive resistance and shear resistance on the face. The presented FB-MultiPier resultant is from only the passive resistance springs mentioned in Chapter 4. The FB-MultiPier significantly over predicts the resultant resistance as the oblique angel approaches 45 degrees. In Figure 4-45, presents the passive resistance pattern from each component of X and Y lateral resistance. The issue of FB-MultiPier over predicting Plaxis results for each component of X and Y lateral resistance.

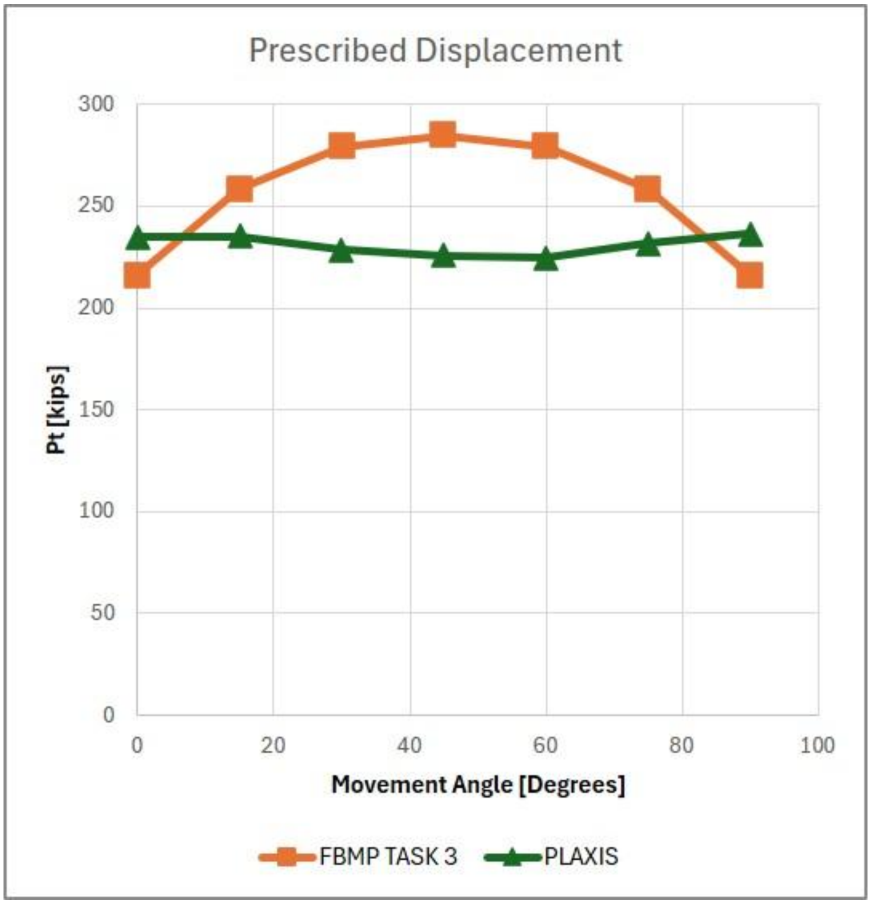

Figure 4-44 FBMP and Plaxis oblique loading comparison – passive resistance.

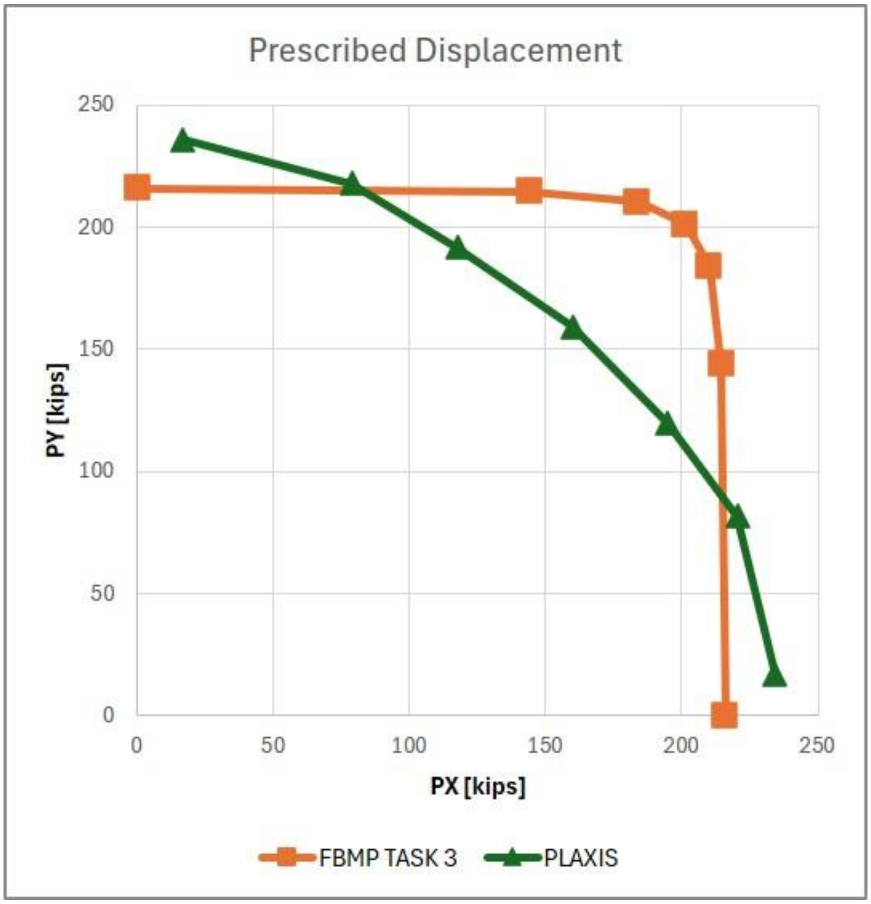

Figure 4-45 Passive resistance pattern under oblique loading.

This over prediction from FB-MultiPier comes from; 1) passive resistance springs are only oriented in the X and Y direction, Figure 4-46, (Xp or Yp axis per FB-MultiPier local axis for the footing) and 2) No reduction is accounted for based on the oblique angle of motion. It's important to note that there are no shear springs on the passive faces (i.e., no friction on vertical face).

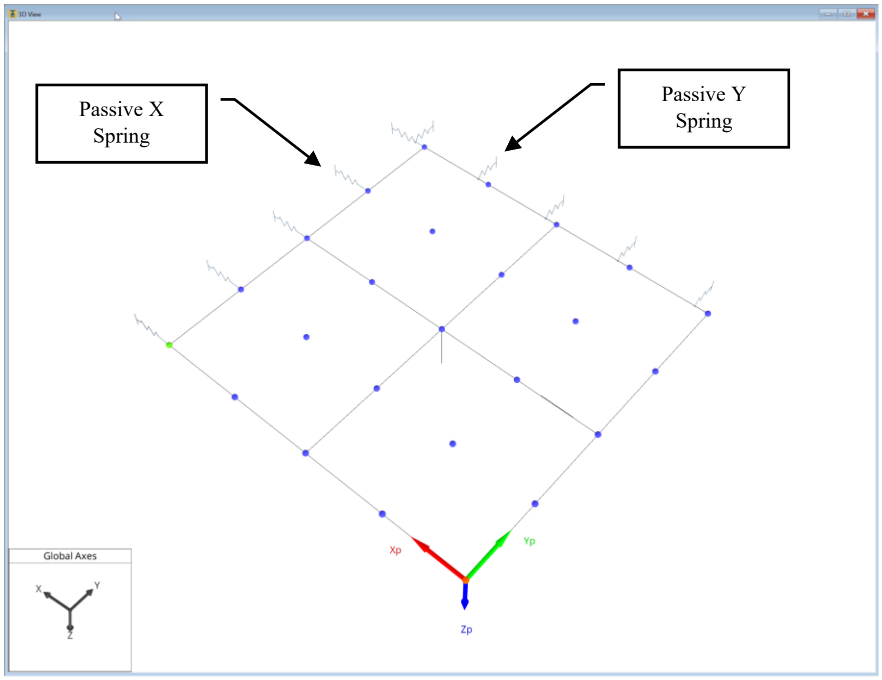

Figure 4-46 FB-MultiPier passive spring orientation.

Issue 1 has been a concern for FB-MultiPier for pile/shaft p-y springs, where lateral resistance springs are oriented in the Xp and Yp directions, Figure 4-47. This concern has been addressed in FB-MultiPier for pile/shaft p-y springs by first determining the direction of motion, orientating the p-y spring in the direction of motion, Figure 4-48, calculating the total resultant displacement and subsequent total resistance then resolving those components into their Xp and Yp force components. Comparison of this implementation is shown in Figure 4-49, where the p-y spring oriented in the displacement direction develops more displacement vs Xp and Yp spring solved independently.

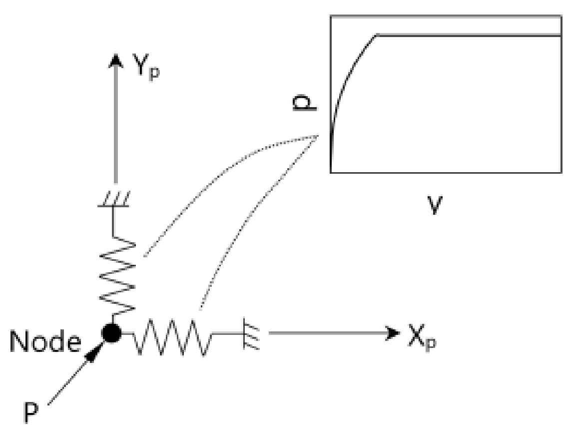

Figure 4-47 Base spring orientation in Xp and Yp directions in task 3.1.

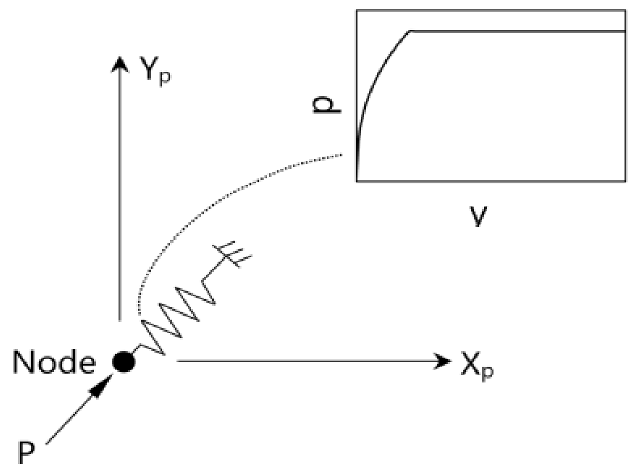

Figure 4-48 FB-MultiPier p-y spring orientation.

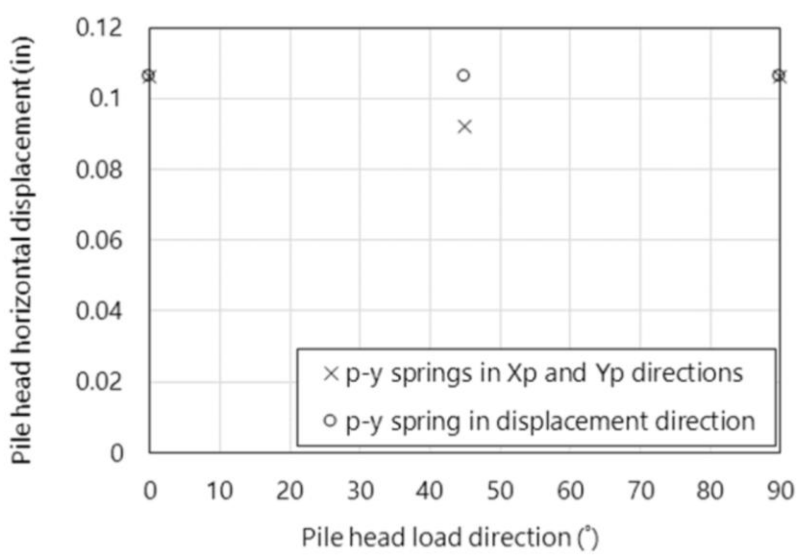

Figure 4-49 FB-MultiPier p-y displacement comparison.

This solution is effective for a pile/shaft, since the nodes are distributed along a line (e.g., vertical axis), each node has a tributary area, along with a corresponding Xp and Yp spring. Unfortunately, this solution is not appropriate for the passive resistance springs since the implemented springs only act perpendicular, Figure 4-46, to each node on their respective faces. Thus, this passive spring will need to have its resistance reduced. This p-y solution is more appropriate for the frictional resistance, to be discussed later.

It is observed in the Plaxis results, Figure 4-44,the resultant resistance is equivalent regardless of direction of motion. Additionally, it was observed that the angle of the resultant resistance is equivalent to the displacement direction (oblique angle), Figure 4-42 and Figure

4-43. These observations necessitate that any reduction of the passive resistance for X or Y face must account for the angle of the displacement direction, while maintaining an equal resultant resistance, regardless of oblique angel. This can be accomplished by first defining the resultant passive force, $\mathrm{P}t$, as Equation 4-29, and its corresponding oblique angle, θ, as Equation 4-30. To maintain that the resultant angle is equal to oblique angle from displacement Equation 4-31 through Equation 4-32 are specified for the individual resistance components. To maintain that $\mathrm{P}t$ is equal for all angles θ, reduction values Rx and Ry are specified in Equation 4-34 and Equation 4-35 respectively. These reduction values are used to reduce the ultimate passive resistance that is used in the hyperbolic equation. Derivation of Equation 4-34 and Equation 4-35 are shown in Appendix Appendix C.

$$\mathrm{P}t = \sqrt{P_x^2 + P_y^2}$$ Equation 4-29

$$\frac{\Delta y}{\Delta x} = \tan\theta$$ Equation 4-30

$$\frac{\mathrm{P}y}{\mathrm{P}x} = \tan\theta$$ Equation 4-31

$$\frac{\mathrm{P}y}{\mathrm{P}t} = \sin\theta$$ Equation 4-32

$$\frac{\mathrm{P}x}{\mathrm{P}t} = \cos\theta$$ Equation 4-33

$$Px = \frac{dx}{\frac{1}{k_{max}} + \frac{R_f}{P_{ult}Rx}dx}$$ Equation 4-34

$$Py = \frac{dy}{\frac{1}{k_{max}} + \frac{R_f}{P_{ult}Ry}dy}$$ Equation 4-35

$$Rx = \cos\theta$$ Equation 4-36

$$Ry = \sin\theta$$ Equation 4-37

Implementation of Equation 4-34 and Equation 4-35 within FB-MultiPier is shown in Figure 4-50. This implementation, blue dotted line, shows that resultant resistance is the same regardless of direction of displacement. It also shows much better agreement with the PLAXIS results. Validation of this methodology with remaining Plaxis cases is discussed in section 1.5.

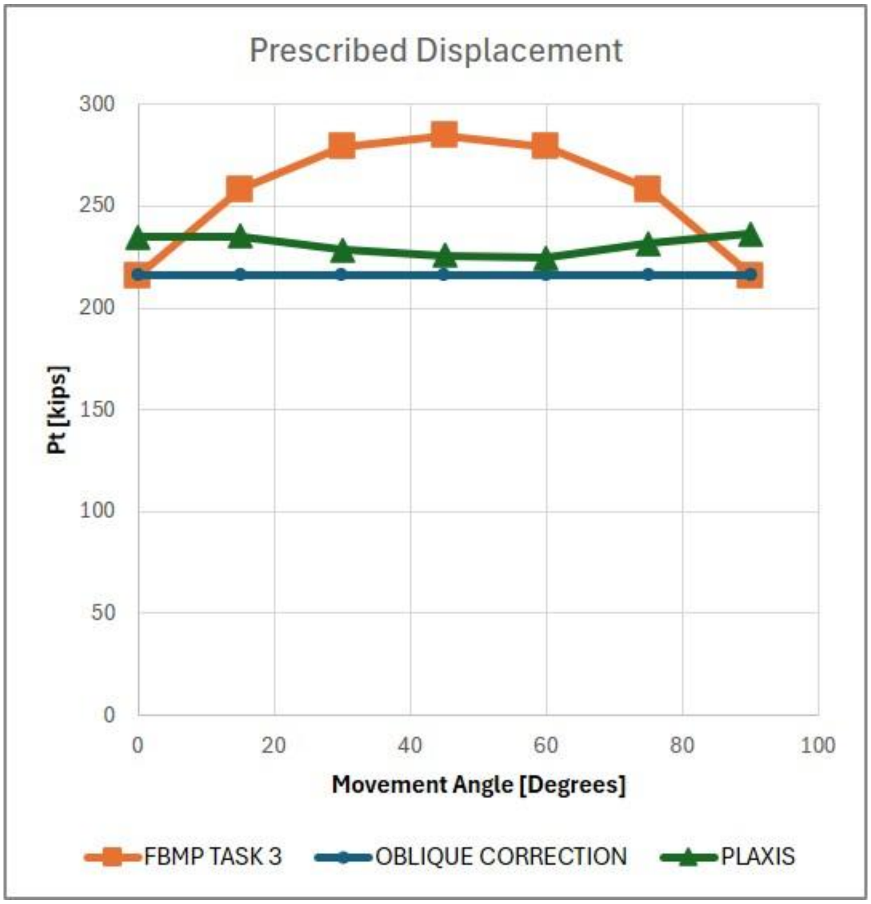

Figure 4-50 Comparison of resultant resistance.

It should be noted that this implementation does not account for shear on face of the footing. Based on the PLAXIS results, the shear was a function of oblique displacement and footing geometry. The complexity of this friction, which is also a function of normal force (passive resistance) raises concerns for FB-MultiPier to reliably converge during lateral loading. Some preliminary investigation found the program to be unstable or provide odd results resulting in the footing rotating to maintain force and moment equilibrium for given loading condition. It is recommended that any future implementation of shear springs in FB-MultiPier should also revise these equations.

For base friction resistance, initial implementation results in frictional resistance in the Xp and Yp direction based on their respective displacements. This results in the same over estimation of resistance, Figure 4-51 and Figure 4-52. In FB-MultiPier each node representing base friction has a Xp and Yp friction resistance spring, along with all nodes being aligned in one plane of the shell element. This allows implementation of FB-MultiPier p-y approach, Figure 4-48, to first determine the direction of motion, orientate a frictional resistance spring in the same direction, calculating the total resultant displacement and subsequent total resistance then resolving those components into their Xp and Yp friction components. Comparison of this implementation is shown in Figure 4-51 and Figure 4-52, where the frictional resistance is now equal in all oblique angles.

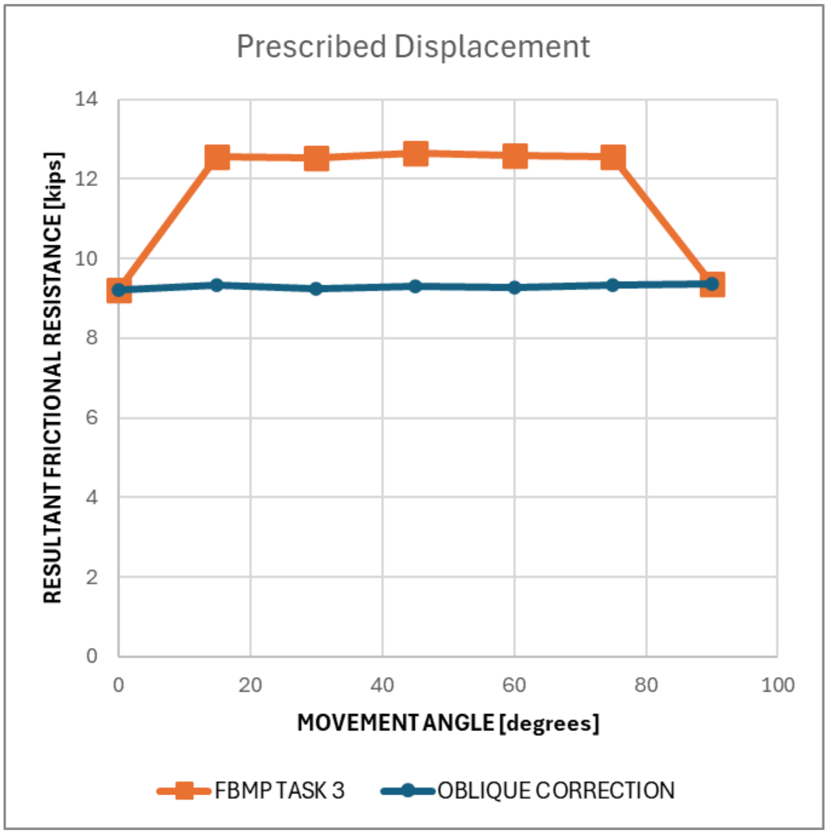

Figure 4-51 FB-MultiPier and Plaxis oblique loading comparison – friction resistance.

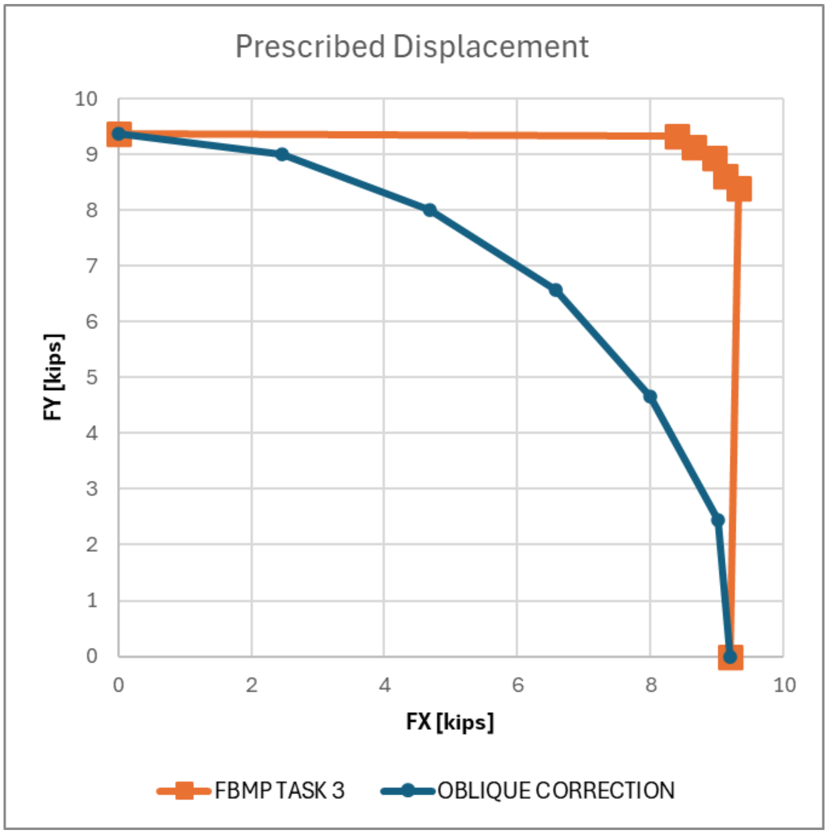

Figure 4-52 Friction resistance pattern under oblique loading.

4.4 FB-MultiPier User-Interface (UI) and Analytical Engine Enhancements

The user-interface and the analytical engine of the FB-MultiPier program is proposed to be updated to implement the shallow foundation analysis feature using the research efforts from the Phase I (BDV31-977-51) and Phase II (BDV31-977-124) projects. The aim is to equip bridge design engineers with the capability to add and analyze a shallow foundation system on a Florida limestone layer beneath a bridge pier. Chapter 4 is focused on the implementation of lateral soil resistance for shallow foundation representing the soil-footing interface. This lateral soil resistance on the shallow foundation will include passive resistance and the base friction. Empirical models are being adopted to represent passive resistance and base friction in the form of distributed non-linear soil resistance springs.

On the Soil page, the Lateral Passive resistance model includes the following options:

1. FL Limestone
2. C-Phi Material
3. Hyperbolic
4. Linear (Subgrade)
5. Custom

6. None

On the Soil page, the Base Friction resistance model includes the following options:

1. Hyperbolic (Coulomb)
2. Linear
3. Custom
4. None

The linear model types where implemented in the program not only for design but also as a debugging tool. All the shallow foundation soil resistance models in both axial and lateral directions exhibit perfectly plastic failure behavior. This can introduce non-convergence issues when the applied loading approaches the plastic ultimate resistance in either direction. The linear model is a useful tool for verification, as it provides linear resistance with no failure, thereby eliminating convergence issues associated with soil yielding.

Once convergence is achieved using linear model, the results can be evaluated to better understand the source of the problem. For example, excessive displacement may indicate weak soil properties or excessive loading. In such cases, footing dimensions, applied loads, or soil properties, can be individually reviewed and adjusted as necessary. After these modifications, the original soil models can be reactivated and the analysis repeated. This highlights the importance of including a linear model option for debugging purpose.

Additionally, recent research has identified the need to reduce the passive resistance of the footing under skew loading, which was not accounted for in the initial implementation of the passive resistance curves in FB-MultiPier. The lateral passive resistance reduces when skewed loading is applied as mentioned in 4.3.3 Passive Resistance Oblique Model. In addition, the implementation includes defining and orienting the base friction resistance spring along the direction of footing movement. These implementations were validated against the hand solutions and PLAXIS models for footing on C-Phi material and Florida Limestone.

4.4.1 Shallow Foundation Lateral Enhancements in FB-MultiPier UI

The update to the FB-MultiPier UI includes enhancements to the 'Soil' page including the ability to select 'Lateral Passive' models for a shallow foundation, the ability to select a 'Base Friction' model for a shallow foundation, and modifications to some of the labeling on the 'Soil' page within the Shallow Foundation Data frame. Each of the model dialogs will include the plot for the soil resistance curve. The results side of the FB-MultiPier UI has also been enhanced to include graphical representation of the lateral passive resistance plots, and a new accompanying dialog to facilitate the viewing of said plots, namely the Passive Resistance Plot dialog. Additionally, the results side of the FB-MultiPier UI also includes graphical representation of the axial bearing resistance, and lateral base friction resistance plots in the contour dialog. Existing dialogs utilized for the 'Axial Bearing' models have also been enhanced.

The shallow foundation is represented by 'Footing' in the program, it's the constitute properties can be updated using the 'Footing' Page. It should be noted that these shallow foundations features are only available when the foundation is rested on or is embedded in the soil. The user will need to modify foundation base elevation or ground surface elevation to achieve the above condition and access the shallow foundation features. You can update the ground surface elevation using the 'Top of the Layer' input parameter for soil layer 1 on the 'Soil' page (Figure 4-54). The user can modify the footing base elevation by updating the 'Footing Midplane' elevation along with 'Thickness' input on the 'Footing' page (Figure 4-53). The '3D View' (Figure 4-55) will show the shallow foundation modeled.

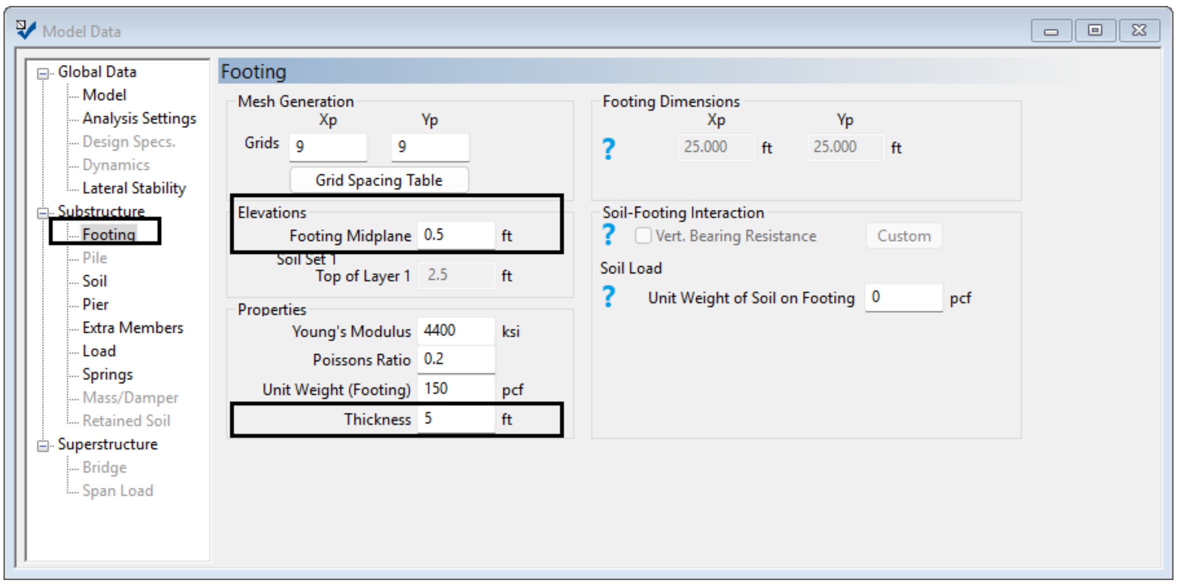

Figure 4-53 'Footing Midplane' and 'Thickness' input on the 'Footing' page.

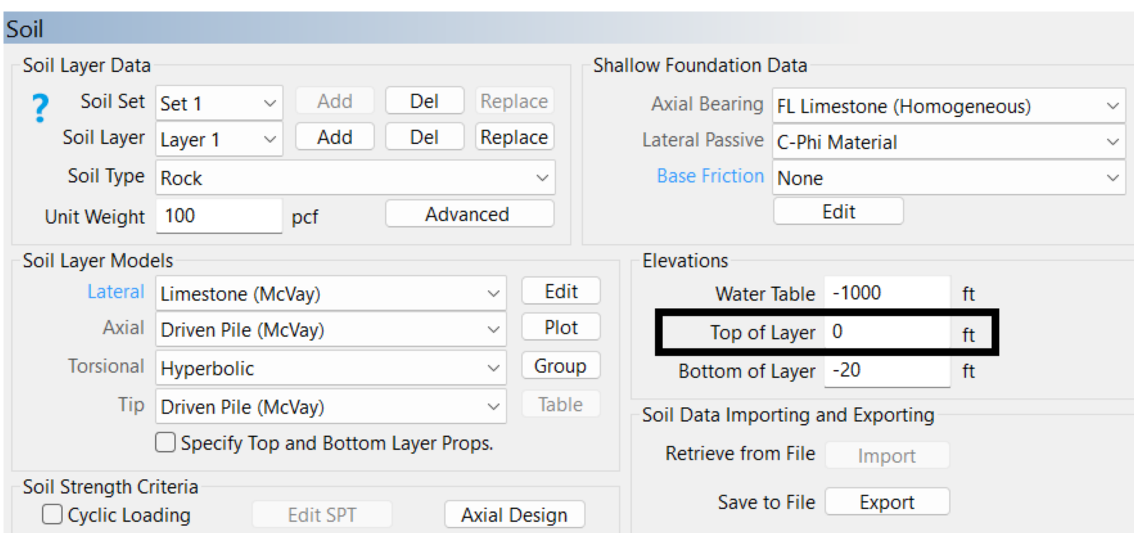

Figure 4-54 'Top of Layer' elevation input on the 'Soil' page.

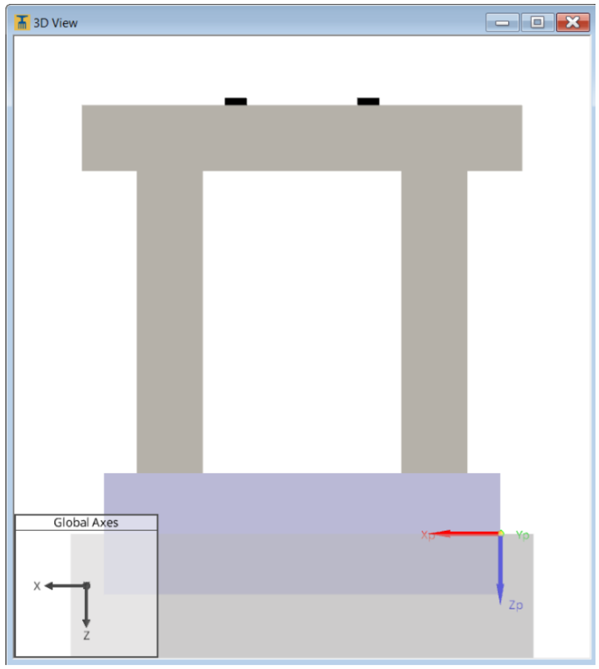

Figure 4-55 3D view of the shallow foundation.

The access point for these shallow foundation models is the ‘Soil’ page (Figure 4-56).

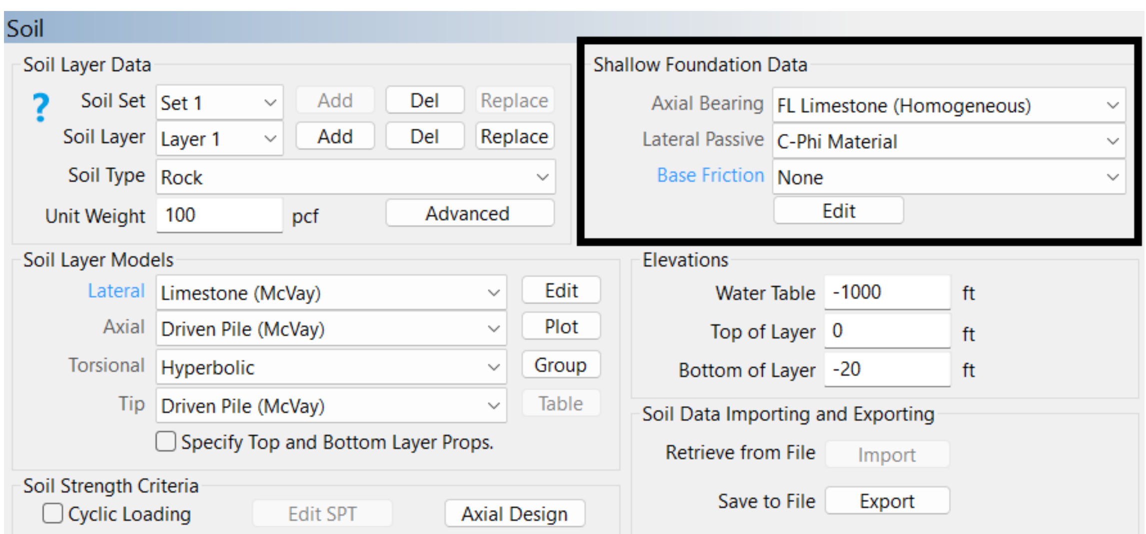

Figure 4-56 ‘Shallow Foundation Data’ controls on ‘Soil’ page.

The shallow foundation feature is inactive/disabled if the footing base elevation is at or above the ground surface elevation (Figure 4-57).

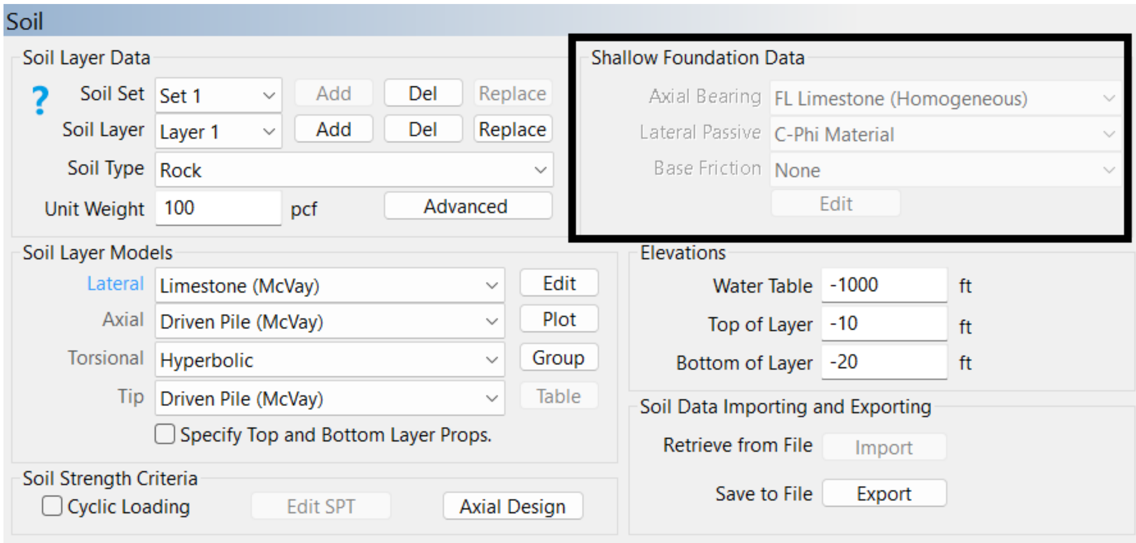

Figure 4-57 'Shallow Foundation Data' controls on soil page disabled due to pile cap elevation above ground surface elevation.

Refer to Appendix E for the various footing in FL Limestone scenarios and the corresponding rock/soil resistance models that can be selected for each case. Use your engineering judgement to select the most appropriate soil/rock resistance model. Once the desired lateral passive and base friction soil/rock resistance model is selected, click the 'Edit' button (Figure 4-62). This will open the dialog box where additional input data must be entered for the chosen soil/rock resistance model. Each of these soil/rock resistance models is discussed in detail in the following section.

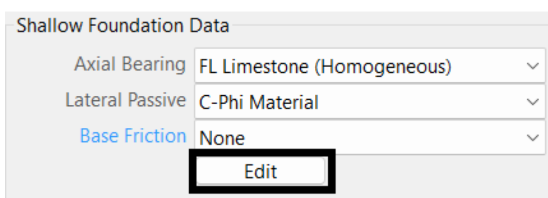

Figure 4-58 'Edit' button in the 'Shallow Foundation Data' frame on the 'Soil' page.

4.4.1.1 New Shallow Foundation Model Types in FB-MultiPier UI

The update to the FB-MultiPier UI includes enhancements to include two new Model Types, namely 'Pier with Shallow Foundation' and 'Shallow Foundation', along with update to results side graphics to showcase the total soil springs results on the shallow foundation. To view the new model type, open the FB-MultiPier UI. Then access the new Model icon from the toolbar (Figure 4-59), or access the 'File Menu', select New (Figure 4-60).

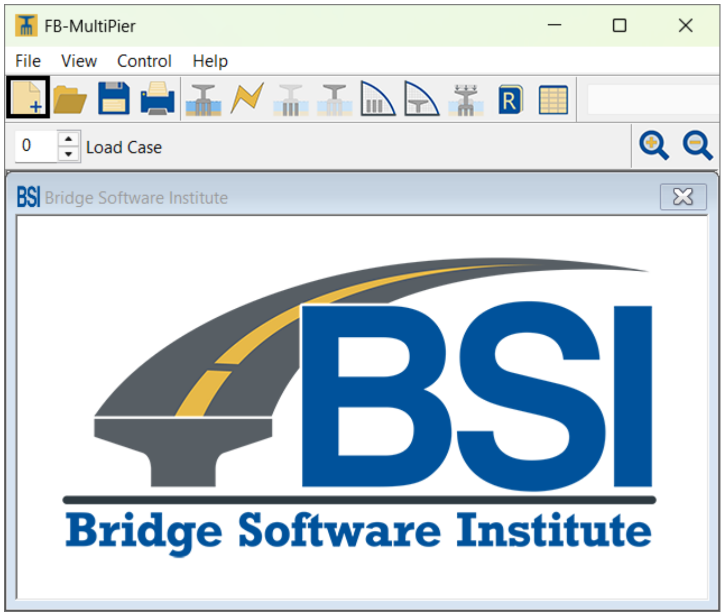

Figure 4-59 New file open toolbar option.

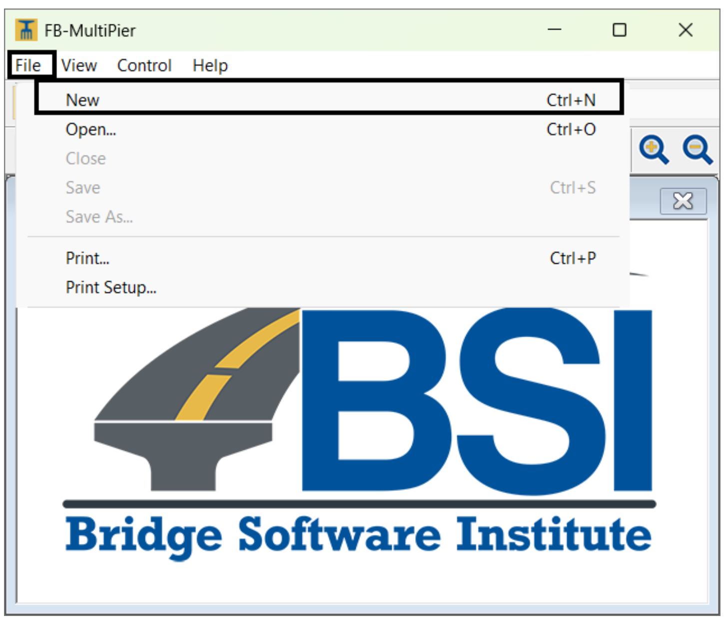

Figure 4-60 New file open from 'File' menu.

When you open new file, the 'Select New Model Type' dialog is opened. The new model types, namely, 'Pier with Shallow Foundation', and 'Shallow Foundation' are highlighted below in (Figure 4-61).

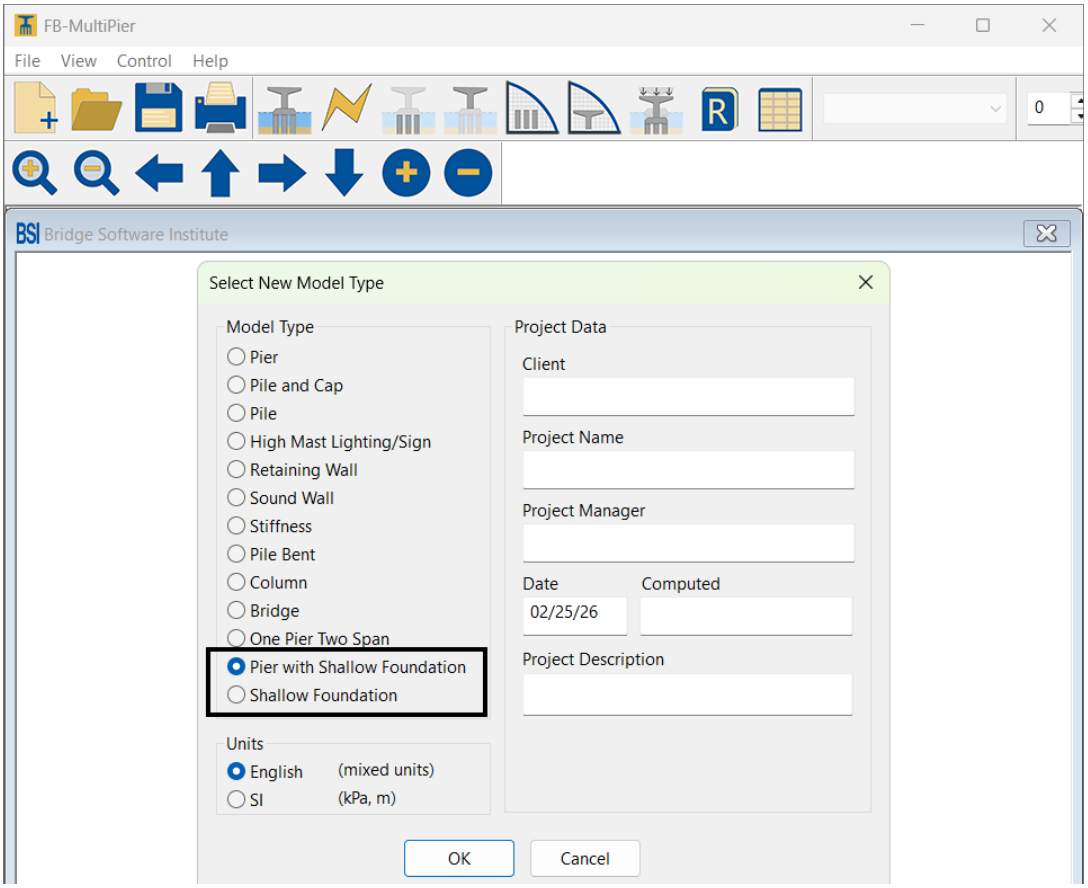

Figure 4-61 New model types (pier with shallow foundation, and shallow foundation).

Figure 4-62 shows the default Pier with Shallow Foundation model type in FB-MultiPier UI. This model has shallow foundation along with the columns and pier cap. Bearing can be included on the pier cap. This will be model type which will eventually be part of a Bridge Model.

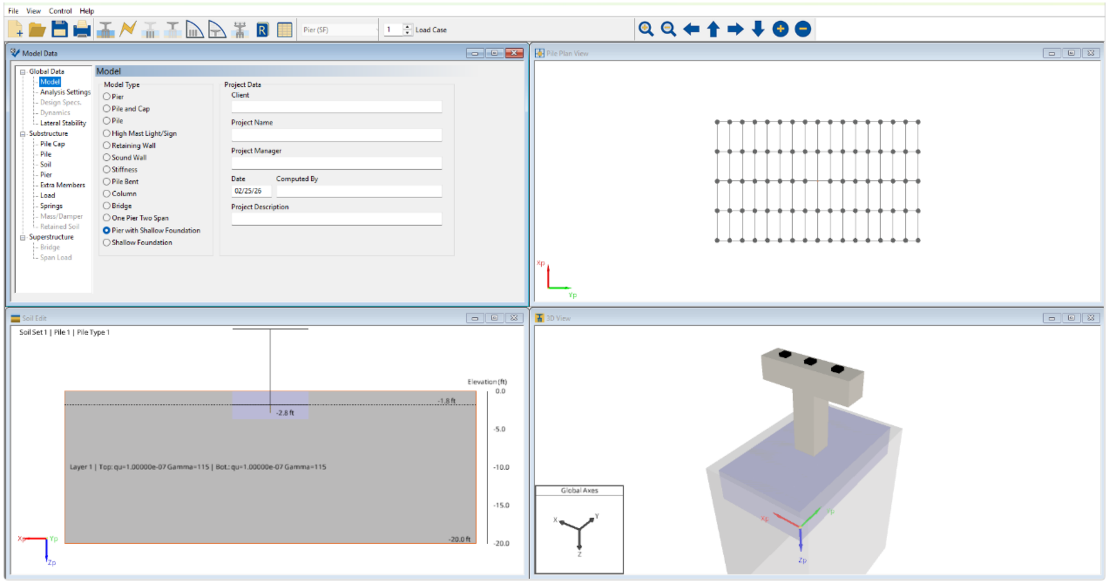

Figure 4-62 ‘Pier with Shallow Foundation’ model type in FB-MultiPier.

Figure 4-63 shows the default ‘Shallow Foundation model type in FB-MultiPier UI. This model has shallow foundation and soil resistance on the footing. This does not have columns, pier cap and bearings. This model type will only be available for single pier analysis, and not in Bridge Model.

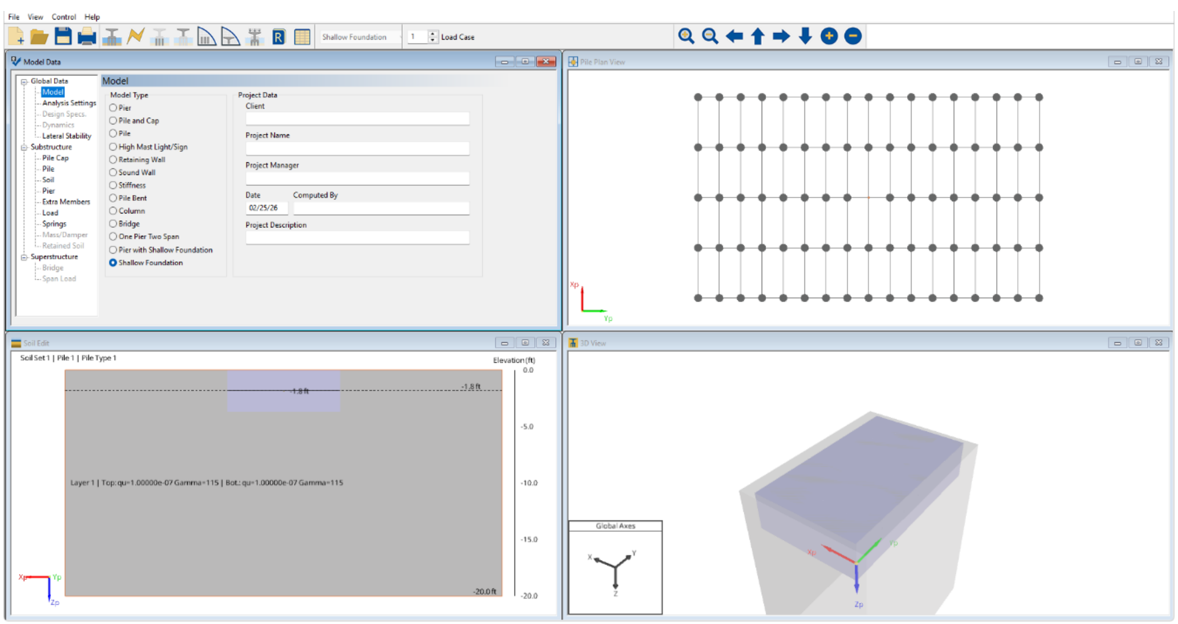

Figure 4-63 ‘Shallow Foundation’ model type in FB-MultiPier.

4.4.1.2 Lateral Passive Soil Resistance Model: FL Limestone

The FL Limestone dialog (Figure 4-64) can be accessed when the ‘FL Limestone’ lateral passive soil/rock resistance model is selected from the dropdown on the ‘Soil’ page.

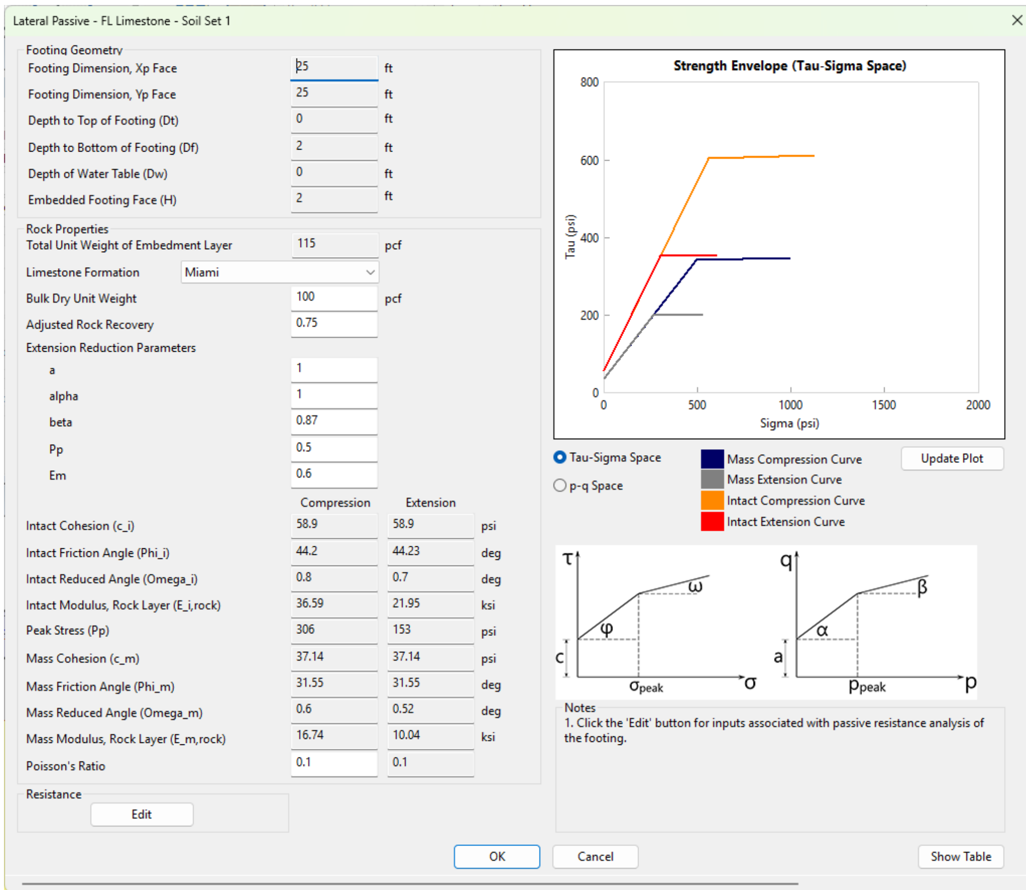

Figure 4-64 Lateral passive - FL limestone dialog with the required key input parameters.

The ‘FL Limestone’ model needs user input parameters to calculate the strength envelope, particularly, footing dimensions, and rock properties. The input parameters for footing geometry are read-only on this dialog, and are calculated by the program-based input, namely the following (Figure 4-64): Footing Dimension Xp Face, Footing Dimention Yp Face, Depth to Top of Footing (D_t), Depth to Bottom of Footing (D_f), Depth of Water Table (D_w), and Embedded Footing Face (H).

The input parameters for rock properties (Figure 4-64) consist of total unit weight of embedment layer (γ_t), limestone formation, bulk dry unit weight, adjusted rock recovery, and the extension reduction parameters (R_a, R_{alpha}, R_{beta}, R_{Pp}, R_{Em}). There are also several intact and mass strength parameters, namely, peak stress in compression and extension space (P_{pc}, P_{pe}), intact and mass cohesion in compression and extension space (c_{ic}, c_{mc}, c_{ie}, and c_{me}), intact and mass friction angle (φ_{ic}, φ_{mc}, φ_{ie}, and φ_{me}), intact and mass reduced angle in compression and extension space

(ω_{ic}, ω_{mc}, ω_{ie}, and ω_{me}), intact and mass elastic modulus in compression and extension space (E_{ic}, E_{mc}, E_{ie} and E_{me}), and poisson's ratio in compression and extension space (ν_c, and ν_e). These intact and mass strength parameters are used to plot the strength envelopes in tau-sigma space and p-q space in compression and extension space.

The user does not have to input all the discussed rock properties. The required input parameters for rock properties depends on one of the options selected within the limestone formation dropdown. The Limestone Formation dropdown consists of ten options, namely:

1. Miami
2. Anastasia
3. Hawthorn
4. Key Largo
5. Shallow Fort Thompson
6. Ocala
7. Custom Intact (Compression)
8. Custom Mass (Compression)
9. Custom Intact (Extension)
10. Custom Mass (Extension)

Option 1-6: When any standard limestone formation (i.e. Miami, Anastasia, Hawthorn, Key Largo, Shallow Fort Thompson, or Ocala) is selected from the limestone formation dropdown (Figure 4-65), the following properties must be input: Bulk Dry Unit Weight, Adjusted Rock Recovery, Extension Reduction Parameters (R_a, R_{alpha}, R_{beta}, R_{Pp}, R_{Em}), and Poisson's Ratio in compression zone (ν_c). For these given input parameters, intact (compression) strength parameters in tau-sigma and p-q space are taken from in-built database data from formation type (Appendix. F), which is shown in the respective 'read-only' intact parameters edit boxes under compression (P_{pc}, c_{ic}, φ_{ic}, ω_{ic}, E_{ic}, and ν_c). Additionally adjusted rock recovery along with the intact compression strength parameters will be used to automatically calculate (refer Appendix F) the mass compression strength parameters (P_{pc}, c_{mc}, φ_{mc}, ω_{mc}, and E_{mc}), which are shown in the respective 'read-only' mass compression parameters edit boxes. Subsequently, the intact and mass compression strength parameters are used along with the extension reduction parameters to automatically calculate the intact and mass extension strength parameters (P_{pe}, c_{ie}, φ_{ie}, ω_{ie}, E_{ie}, c_{me}, φ_{me}, ω_{me}, E_{me}, and ν_e), which are shown in the respective 'read-only' intact and mass extension strength parameters edit boxes.

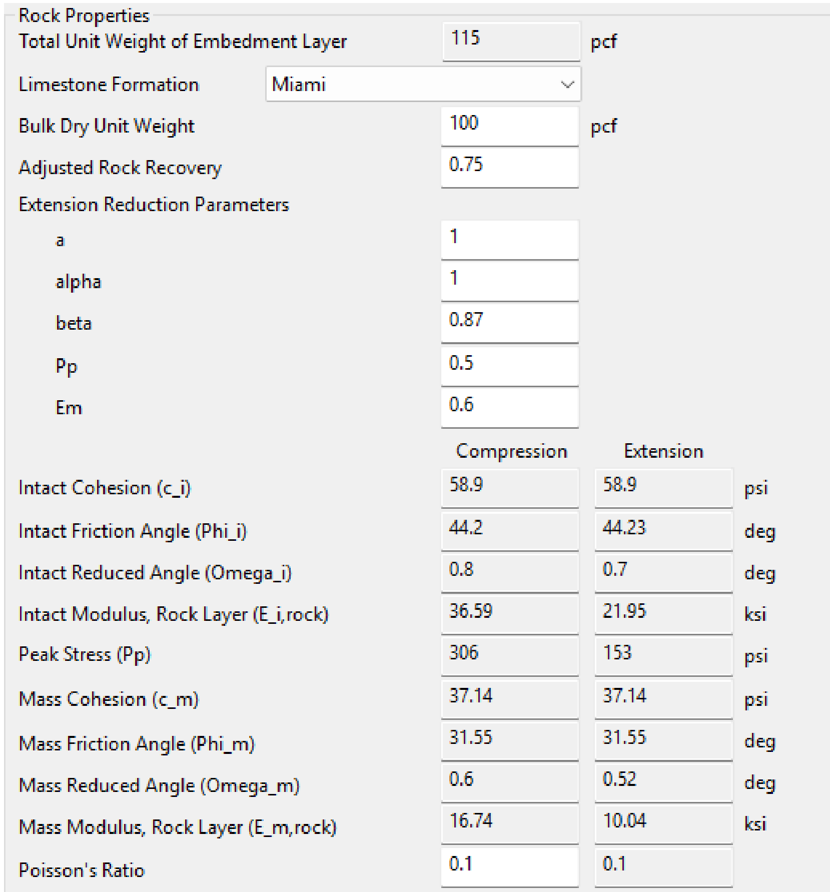

Figure 4-65 Limestone formation 'Miami' selected and corresponding inputs enabled.

Option 7: When the 'Custom Intact (Compression)' option is selected from the limestone formation dropdown (Figure 4-66), the following properties must be input: Adjusted Rock Recovery, Extension Reduction Parameters (R_a, R_{alpha}, R_{beta}, R_{Pp}, R_{Em}), Custom Intact Compression strength parameters (P_{pc}, c_{ic}, φ_{ic}, ω_{ic} and E_{ic}), and Poisson's Ratio (ν_c). Adjusted Rock recovery along with the custom intact compression strength parameters will be used to automatically calculate (refer Appendix F) the mass compression strength parameters (P_{pc}, c_{mc}, φ_{mc}, ω_{mc} and E_{mc}), which are shown in the respective 'read-only' mass compression parameters edit boxes. Subsequently, the intact and mass compression strength parameters are used along with the extension reduction parameters to automatically calculate the intact and mass extension strength parameters (P_{pe}, c_{ie}, φ_{ie}, ω_{ie}, E_{ie}, c_{me}, φ_{me}, ω_{me}, E_{me}, and ν_e), which are shown in the respective 'read-only' intact and mass extension parameters edit boxes.

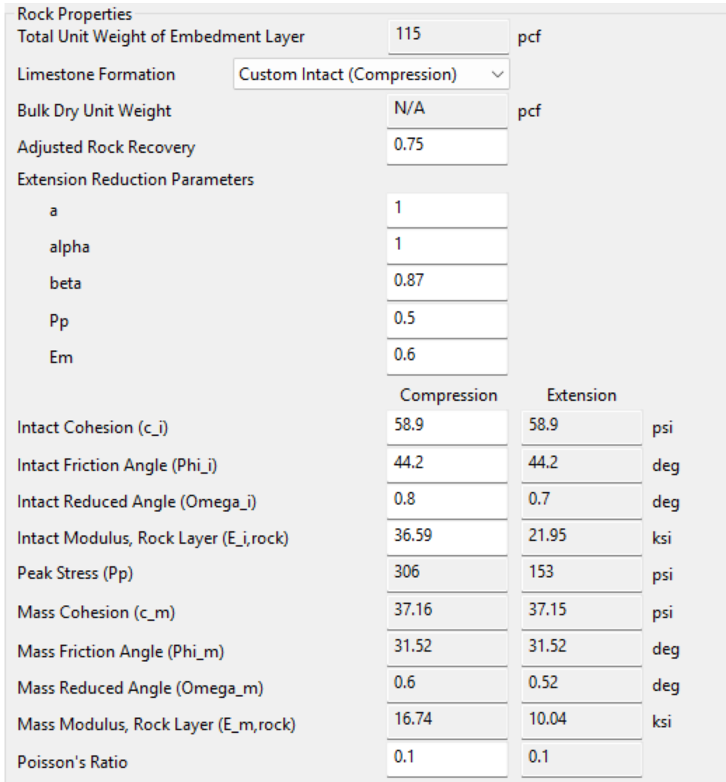

Figure 4-66 Limestone formation 'Custom Intact (Compression)' selected and corresponding inputs enabled.

Option 8: When the 'Custom Mass (Compression)' option is selected from the limestone formation dropdown (Figure 4-67), the following properties must be input: Extension Reduction Parameters (R_a, R_{alpha}, R_{beta}, R_{Pp}, R_{Em}), Custom Mass Compression strength parameters (P_{pc}, c_{mc}, φ_{mc}, ω_{mc} and E_{mc}), and Poisson's Ratio (ν_c). The Custom Mass compression strength parameters are used along with the extension reduction parameters to automatically calculate the mass extension strength parameters (P_{pe}, c_{me}, φ_{me}, ω_{me}, E_{me}, and ν_e), which are shown in the respective 'read-only' mass extension parameters edit boxes.

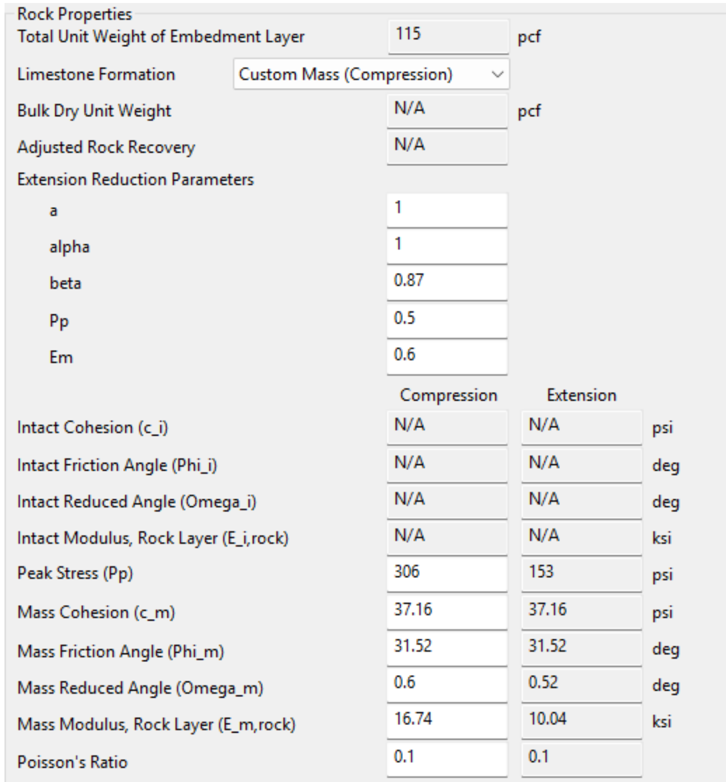

Figure 4-67 Limestone formation 'Custom Mass (Compression)' selected and corresponding inputs enabled.

Option 9: When the 'Custom Intact (Extension)' option is selected from the limestone formation dropdown (Figure 4-68), the following properties must be input: Adjusted Rock Recovery, Custom Intact Extension strength parameters (P_{pe}, c_{ie}, φ_{ie}, ω_{ie} and E_{ie}), and Poisson's Ratio (ν_e). Adjusted rock recovery along with the custom intact extension strength parameters will be used to automatically calculate the mass extension strength parameters (P_{pe}, c_{me}, φ_{me}, ω_{me}, E_{me}, and ν_e), which are shown in the respective 'read-only' mass extension parameters edit boxes.

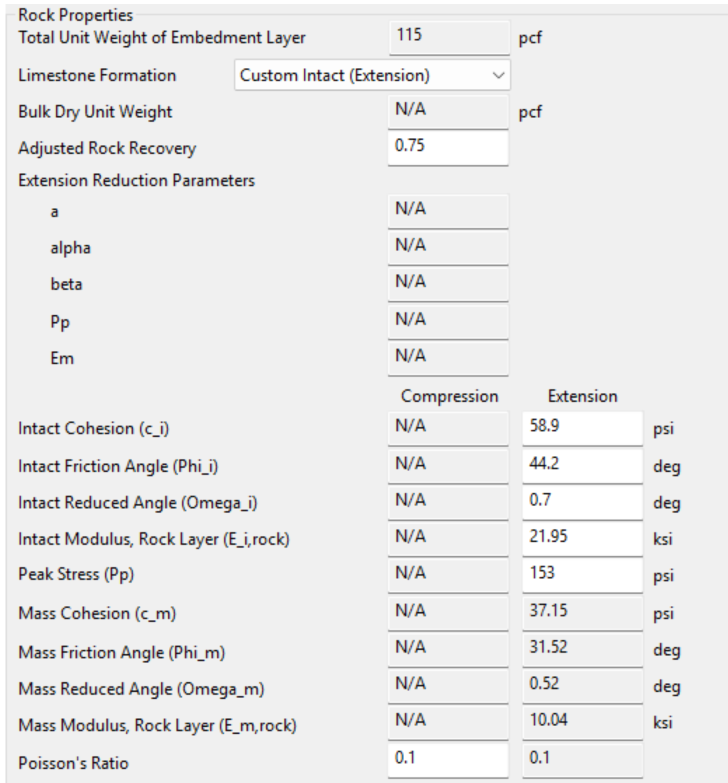

Figure 4-68 Limestone formation 'Custom Intact (Extension)' selected and corresponding inputs enabled.

Option 10: When the 'Custom Mass (Extension)' option is selected from the limestone formation dropdown (Figure 4-69), the following properties must be input: Custom Mass Compression strength parameters (P_{pe}, c_{me}, φ_{me}, ω_{me} and E_{me}), and Poisson's Ratio (ν_e).

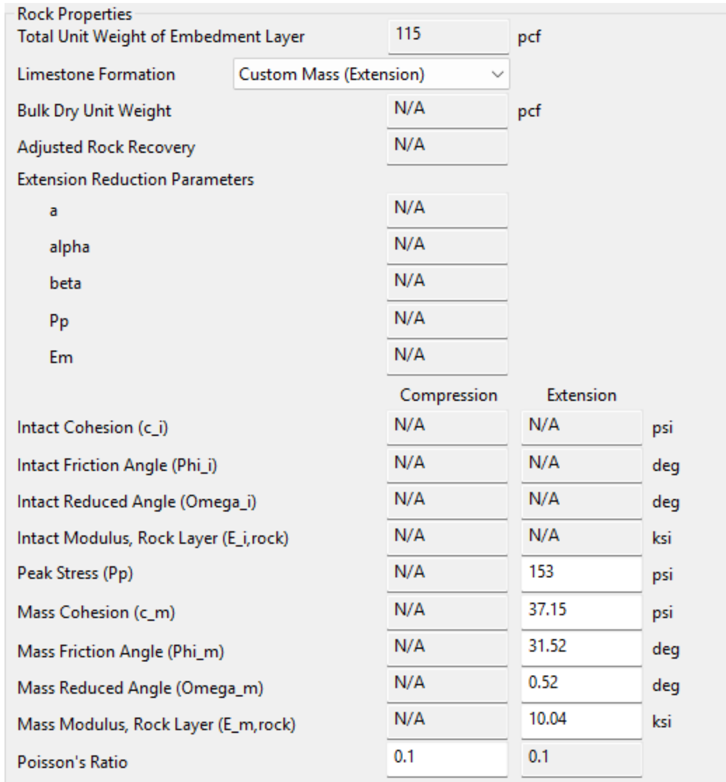

Figure 4-69 Limestone formation ‘Custom Mass (Extension)’ selected and corresponding inputs enabled.

The plot type radio buttons are located below the plot window, namely Tau-Sigma Space and p-q Space (Figure 4-70). These options dictate the displayed plot type. On the Lateral Passive – FL Limestone dialog, clicking the ‘Show Table’ button expands the right side of the dialog to display the curve points in the curve point tables, for example the ‘Intact and Mass Compression Curves Points’ and “Intact and Mass Extension Curve Points’ tables (Figure 4-70).

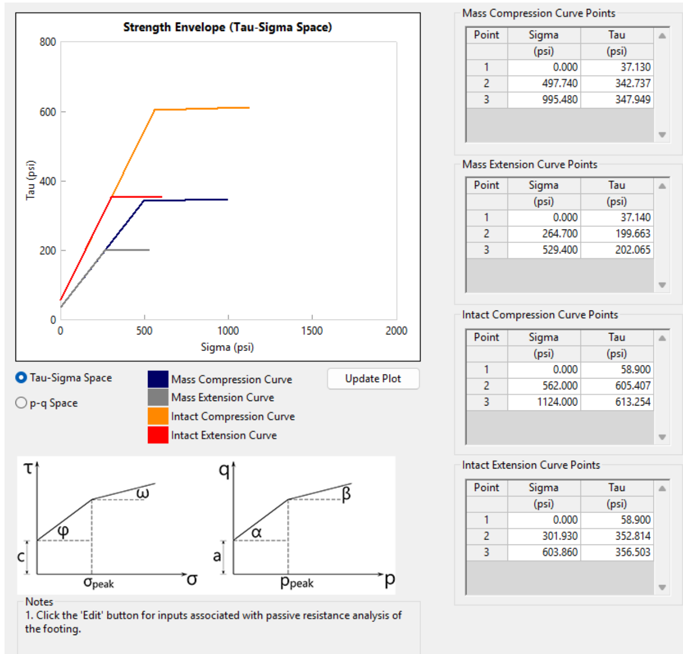

Figure 4-70 Plot type options and curve points tables displayed on lateral passive – FL limestone dialog.

On the Lateral Passive – FL Limestone dialog, clicking the 'Resistance Plot' button launches the 'Resistance Plot' dialog (Figure 4-71).

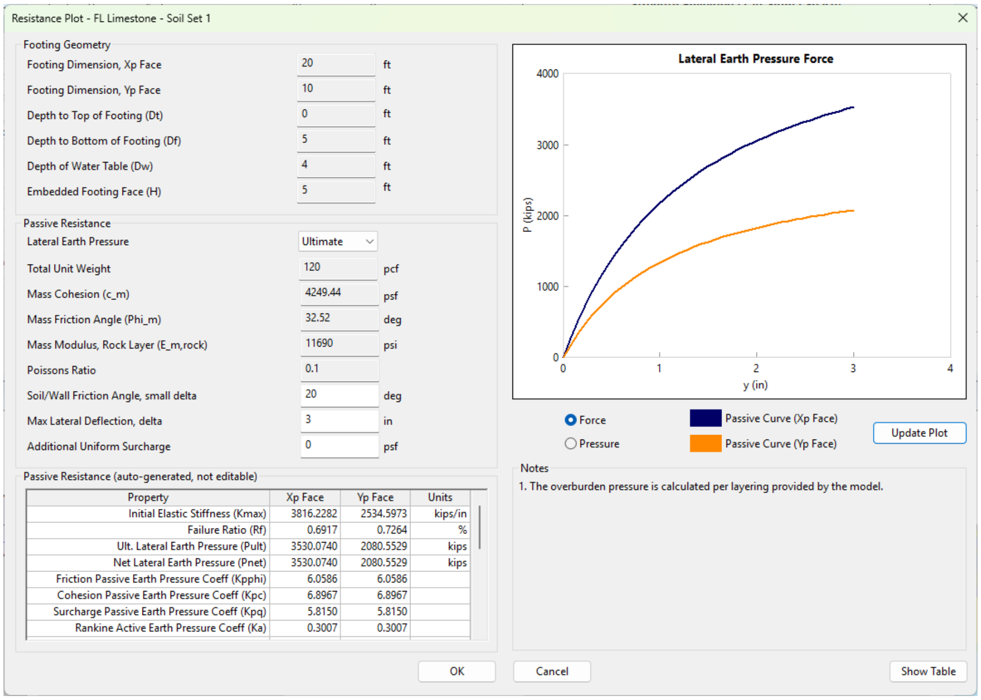

Figure 4-71 Resistance plot dialog for lateral passive - FL limestone model with the required key input parameters.

The input parameters for footing geometry are 'read-only', and are calculated by the program-based input, namely the following (Figure 4-71): Footing Dimension Xp Face, Footing Dimensin Yp Face, Depth to Top of Footing (D_t), Depth to Bottom of Footing (D_f), Depth of Water Table (D_w), and Embedded Footing Face (H).

The input parameters for passive resistance (Figure 4-71) consist of Lateral Earth Pressure (Ultimate or Net), Soil/Wall Friction Angle (small delta), Max Lateral Deflection (delta), and Additional Uniform Surcharge. Several other passive resistance inputs are read-only on this dialog, namely the following: Cohesion, Friction Angle, Mass Modulus (Rock Layer), and Poisson's ratio.

Using the above-mentioned input, passive resistance parameters are calculated, namely, Initial Elastic Stiffness (K_{max}), Failure Ratio (Rf), Ult. Lateral Earth Pressure ($P_{ultimate}$), Net Lateral Earth Pressure (P_{net}), Friction Passive Earth Pressure Coefficient (K_{pphi}), Cohesion Passive Earth Pressure Coefficient (K_{pc}), Surcharge Passive Earth Pressure Coefficient (K_{pq}), and Rankine Active Earth Pressure Coefficient (K_a). These passive resistance parameters displayed (read-only) in tabular form (Figure 4-71), which is subsequently used to calculate the passive resistance plots in load and pressure values. The resistance curve is calculated for Xp and Yp face of the foundation.

The plot type radio buttons are located below the plot window, namely Load and Pressure (Figure 4-71). These options dictate the displayed plot type. The displayed load/pressure vs deflection curves can be viewed in a tabular format by clicking the ‘Show Table’or hidden by clicking ‘Hide Table’ button (Figure 4-72). The curve points are displayed in the following tables positioned to the right of plot: Xp Face Curve Points’ and ‘Yp Face Curve Points’ tables.

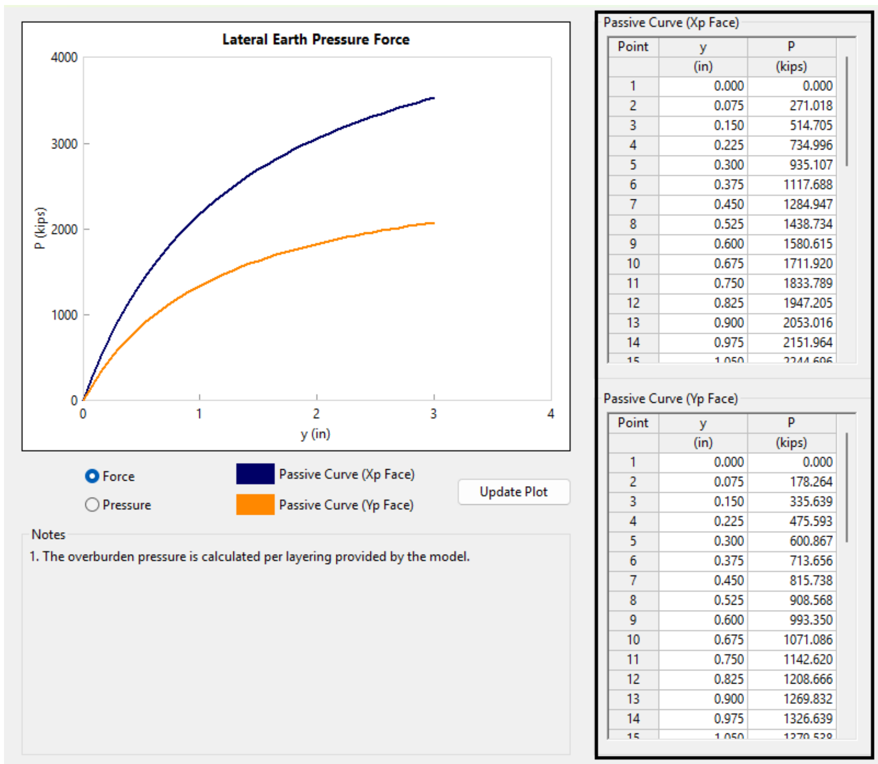

Figure 4-72 Curve points tables displayed on the resistance plot dialog for the lateral passive – FL limestone model.

4.4.1.3 Lateral Passive Soil/Rock Resistance Model: C-Phi Material

The C-Phi Material dialog (Figure 4-73) can be accessed when the ‘C-Phi Material’ lateral passive soil/rock resistance model is selected from the Lateral Passive dropdown on the ‘Soil’ page. The ‘C-Phi Material’ model needs user input parameters to calculate the strength envelope, particularly, footing geometry, and soil properties.

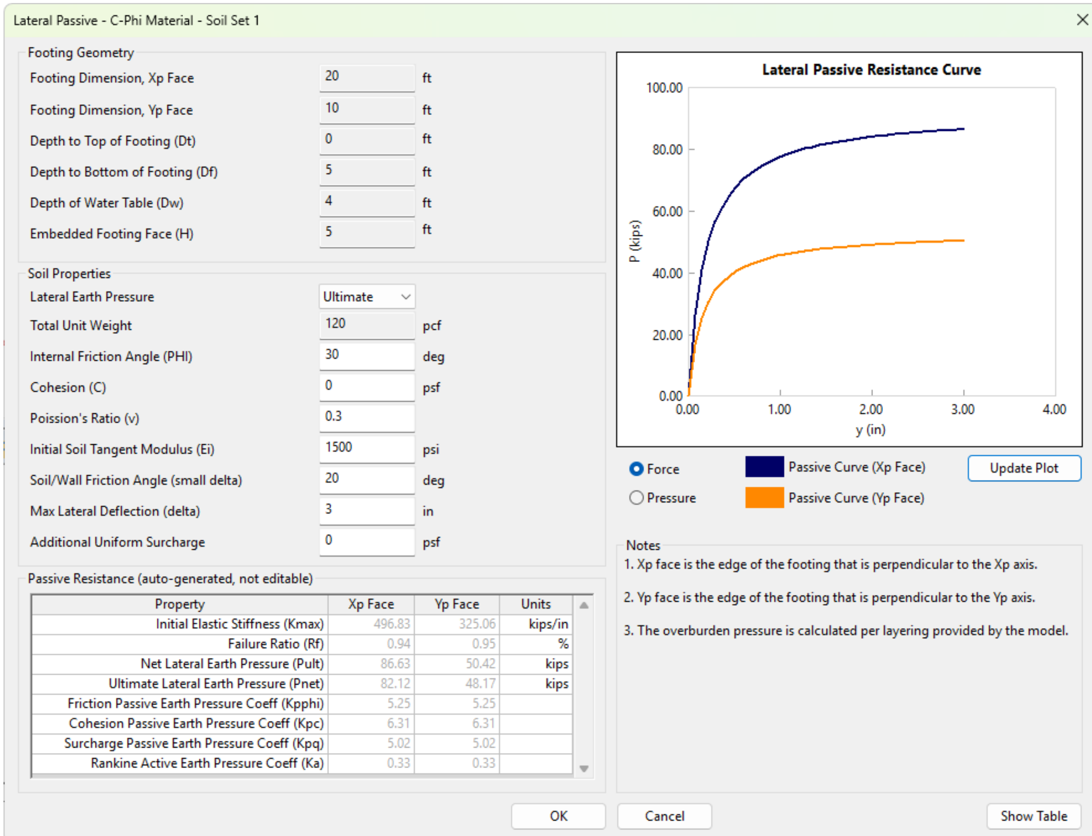

Figure 4-73 Lateral passive – c-phi material dialog with required key input parameters.

The input parameters for footing geometry are ‘read-only’, and calculated by the program-based input, namely the following (Figure 4-73): Footing Dimension Xp Face, Footing Dimension Yp Face, Depth to Top of Footing (D_t), Depth to Bottom of Footing (D_f), Depth of Water Table (D_w), and Embedded Footing Face (H).

The input parameters for Soil Properties (Figure 4-73) consist of Lateral Earth Pressure (Ultimate or Net), Internal Friction Angle (f), Cohesion (c), Poisons Ratio (v), Initial Soil Tangent Modulus (Ei), Soil/Wall Friction Angle (small delta), Max Lateral Deflection (delta), and Additional Uniform Surcharge. Total Unit Weight is displayed as a read-only property, as is it input on a Soil Page.

Using the above-mentioned input, passive resistance parameters are calculated, namely, Initial Elastic Stiffness (K_{max}), Failure Ratio (Rf), Ult. Lateral Earth Pressure ($P_{ultimate}$), Net Lateral Earth Pressure (P_{net}), Friction Passive Earth Pressure Coefficient (K_{pphi}), Cohesion Passive Earth Pressure Coefficient (K_{pc}), Surcharge Passive Earth Pressure Coefficient (K_{pq}), and Rankine Active Earth Pressure Coefficient (K_a). There are several passive resistance parameters which are auto-generated (not editable) are displayed in tabular form (Figure 4-73), which is subsequently used to calculate the passive resistance plots in load and pressure values. The resistance curve is calculated for Xp and Yp face of the foundation.

The plot type radio buttons are located below the plot window, namely Load and Pressure (Figure 4-73). These options dictate the displayed plot type. On the Lateral Passive - C-Phi Material dialog, clicking the 'Show Table' button expands the right side of the dialog to display the curve points in the 'Passive Curve Points (Xp Face)' and 'Passive Curve Points (Yp Face)' tables (Figure 4-73).

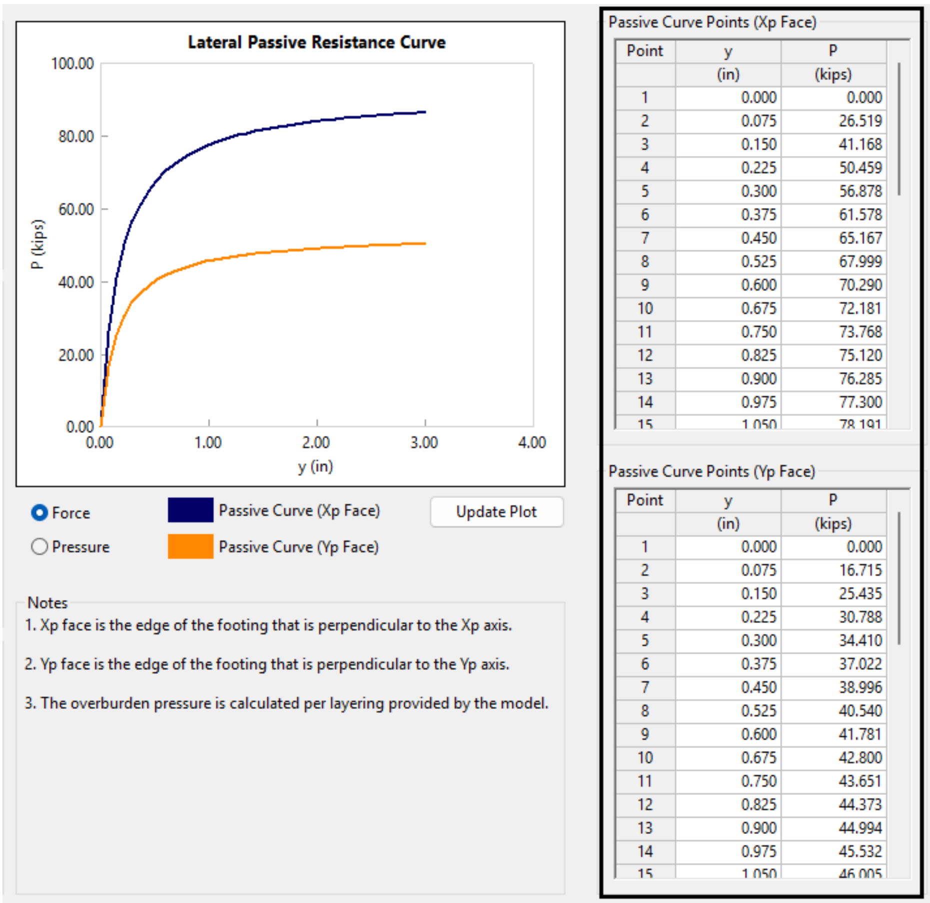

Passive Curve Points (Xp Face)

Point	y (in)	P (kips)
1	0.000	0.000
2	0.075	26.519
3	0.150	41.168
4	0.225	50.459
5	0.300	56.878
6	0.375	61.578
7	0.450	65.167
8	0.525	67.999
9	0.600	70.290
10	0.675	72.181
11	0.750	73.768
12	0.825	75.120
13	0.900	76.285
14	0.975	77.300
15	1.050	78.191

Passive Curve Points (Yp Face)

Point	y (in)	P (kips)
1	0.000	0.000
2	0.075	16.715
3	0.150	25.435
4	0.225	30.788
5	0.300	34.410
6	0.375	37.022
7	0.450	38.996
8	0.525	40.540
9	0.600	41.781
10	0.675	42.800
11	0.750	43.651
12	0.825	44.373
13	0.900	44.994
14	0.975	45.532
15	1.050	46.005

Figure 4-74 Curve points tables displayed on the lateral passive – c-phi material dialog.

4.4.1.4 Lateral Passive Soil Resistance Model: Hyperbolic

The Hyperbolic dialog (Figure 4-75) can be accessed when the 'Hyperbolic' lateral passive soil/rock resistance model is selected from the Lateral Passive dropdown on the 'Soil' page.

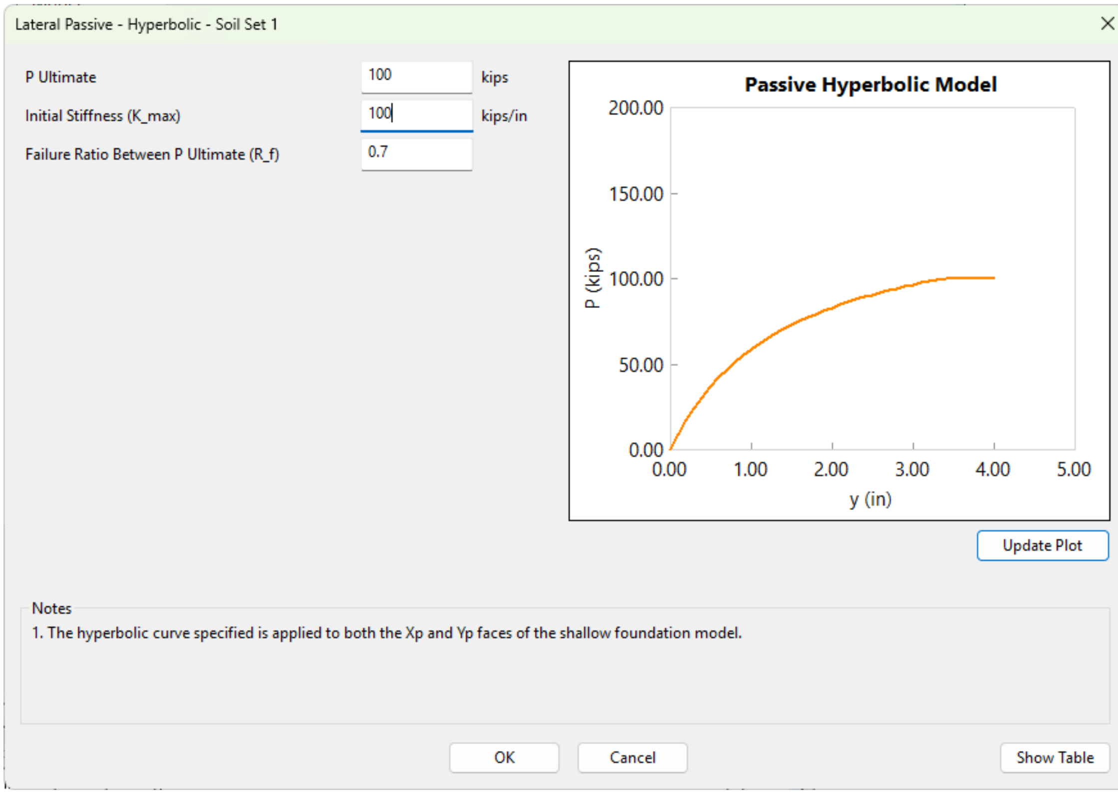

Figure 4-75 Lateral passive – hyperbolic dialog.

The ‘Hyperbolic’ model needs user input parameters to calculate the hyperbolic curve parameter (Figure 4-75), namely P Ultimate, Initial Stiffness (Kmax), and Failure Ratio Between P Ultimate (Rf). These input parameters are subsequently used to calculate the hyperbolic passive resistance plots in load values. The resistance curve similar for length and width face of the foundation

On the Lateral Passive - Hyperbolic dialog, clicking the ‘Show Table’ button expands the right side of the dialog to display the curve points in the ‘Lateral Passive Curve Points’ tables (Figure 4-76).

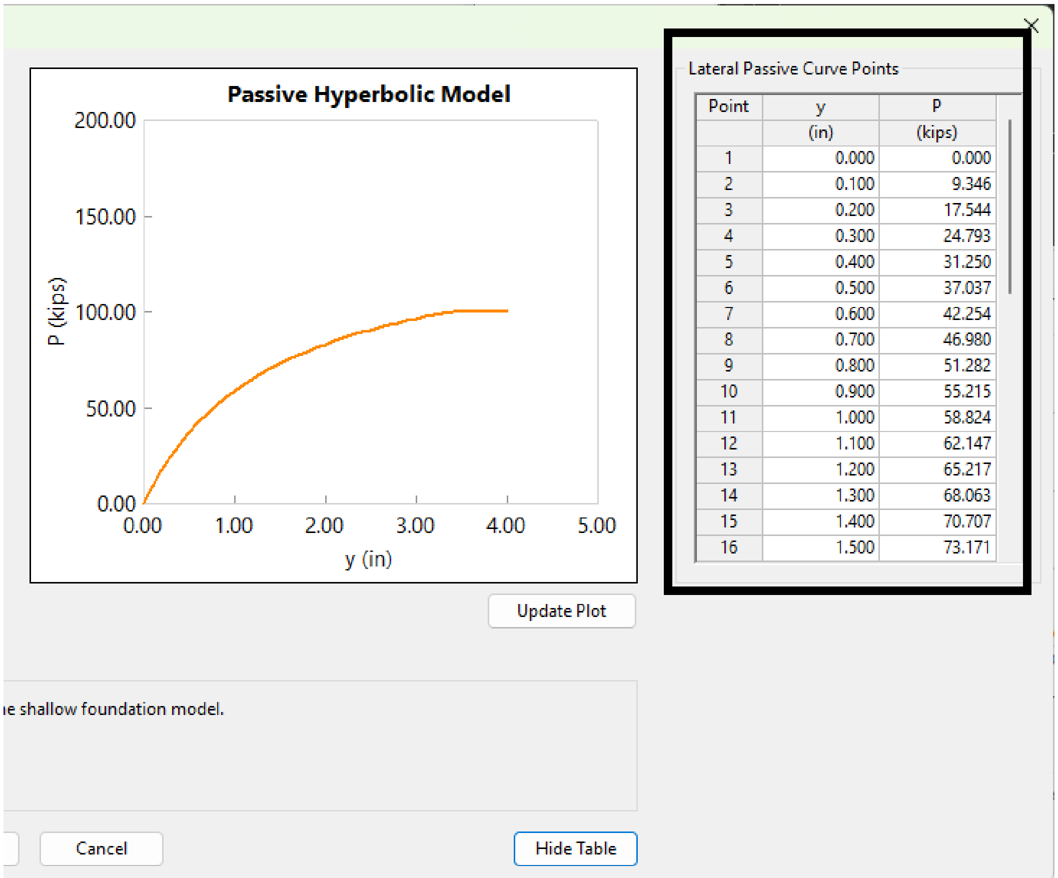

Point	y (in)	P (kips)
1	0.000	0.000
2	0.100	9.346
3	0.200	17.544
4	0.300	24.793
5	0.400	31.250
6	0.500	37.037
7	0.600	42.254
8	0.700	46.980
9	0.800	51.282
10	0.900	55.215
11	1.000	58.824
12	1.100	62.147
13	1.200	65.217
14	1.300	68.063
15	1.400	70.707
16	1.500	73.171

Figure 4-76 Curve points tables displayed on the lateral passive – hyperbolic dialog.

4.4.1.5 Lateral Passive Resistance Model: Linear (Subgrade)

The ‘Lateral Passive - Linear (Subgrade)’ dialog (Figure 4-77) can be accessed when the ‘Linear (Subgrade)’ model is selected from the dropdown within the ‘Shallow Foundation Data’ frame on ‘Soil’ page, and the ‘Edit’ button is clicked.

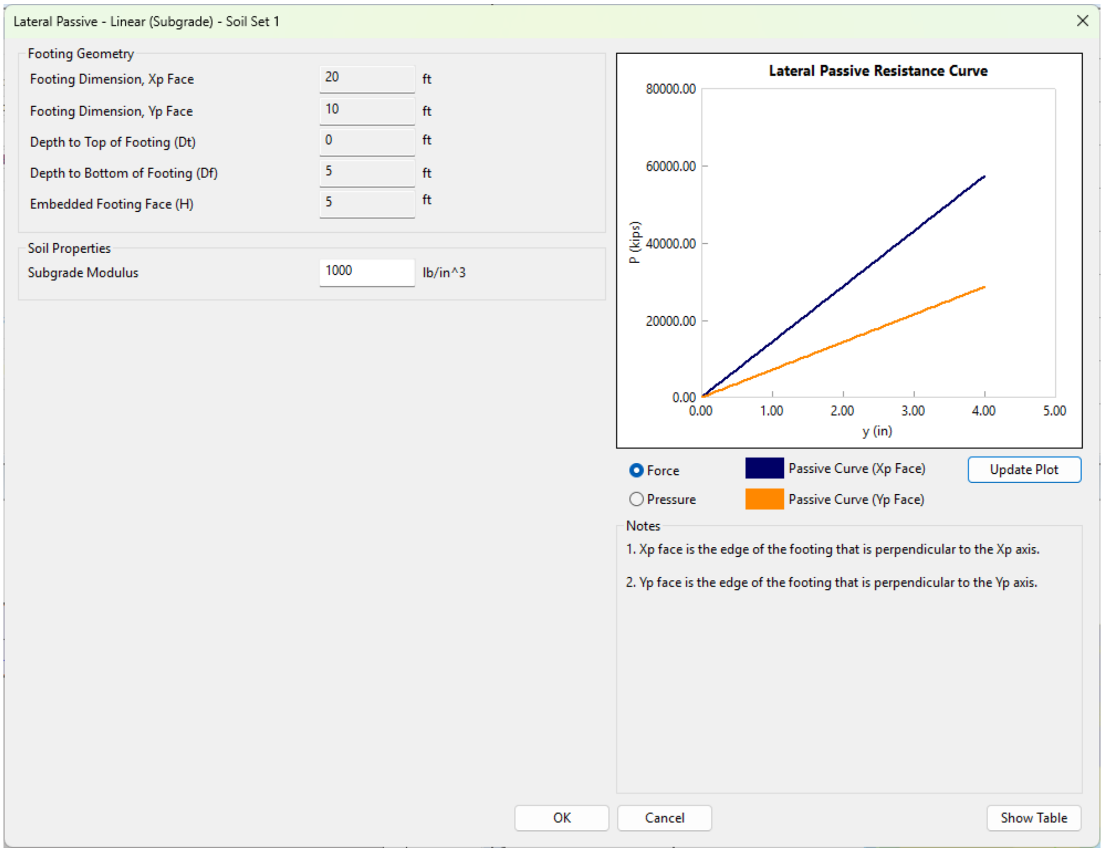

Figure 4-77 ‘Lateral Passive Linear (Subgrade)’ dialog.

The following ‘Footing Geometry’ values are read-only on this dialog. They are calculated based on model input. They are as follows:

- Footing Dimention, Xp Face
- Footing Dimension, Yp Face
- Depth to Top of Footing (Dt)
- Depth to Bottom of Footing (Df)
- Embedded Footing Face (H)

Additionally, ‘Soil Properties’ input, Subgrade Modulus is required. After entering the required input, the passive curve will plot. The curve points are displayed to the right of the plot, based on the selected plot type radio buttons (Load or Pressure). The displayed passive curve can be viewed in tabular format by clicking the ‘Show Table’ button (Figure 4-78).

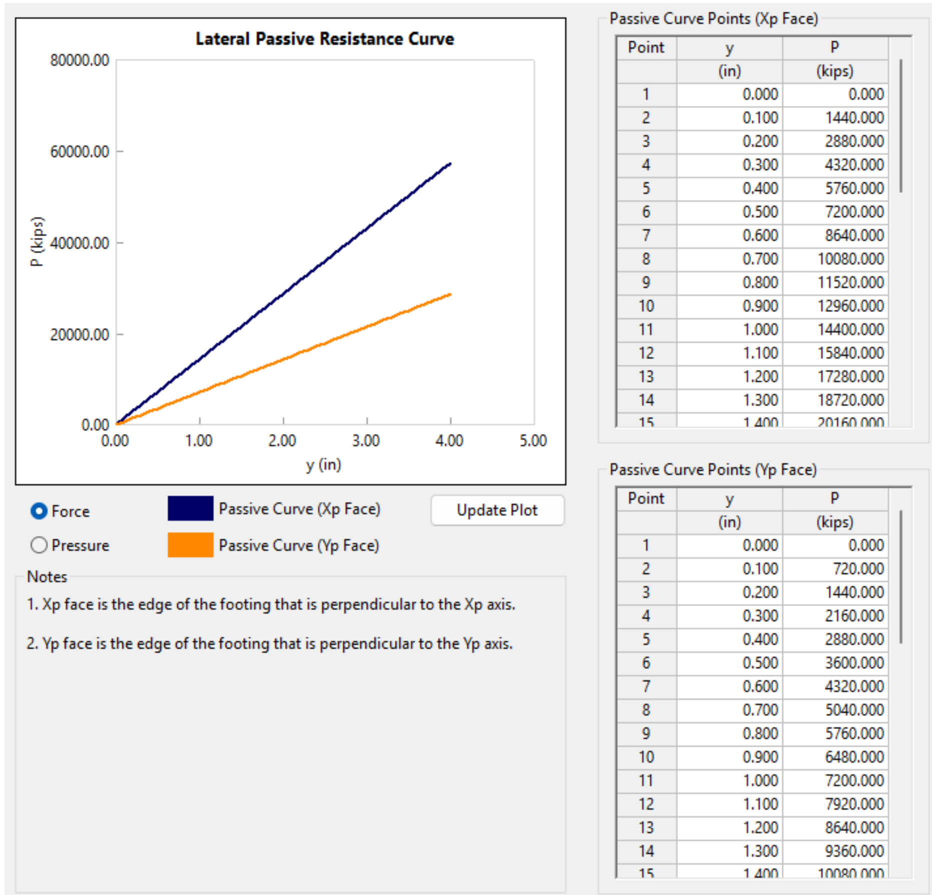

Figure 4-78 Passive curve (pressure) points tables on ‘Lateral Passive Linear (Subgrade)’ dialog.

4.4.1.6 Lateral Passive Resistance Model: Custom

The program includes ‘Custom’ soil models that enables users to implement their own soil resistance curves for foundation design.

The ‘Custom Curve’ dialog can be accessed when the ‘Custom’ model type is selected for Lateral Passive. The ‘Custom’ model can be selected for the ‘Lateral Passive’ model within the ‘Shallow Foundation Data’ frame on ‘Soil’ page, and the ‘Edit’ button is clicked. After inputting the desired number of curve points in the table and clicking the ‘Update Plot’ button, the custom curve will display (Figure 4-79).

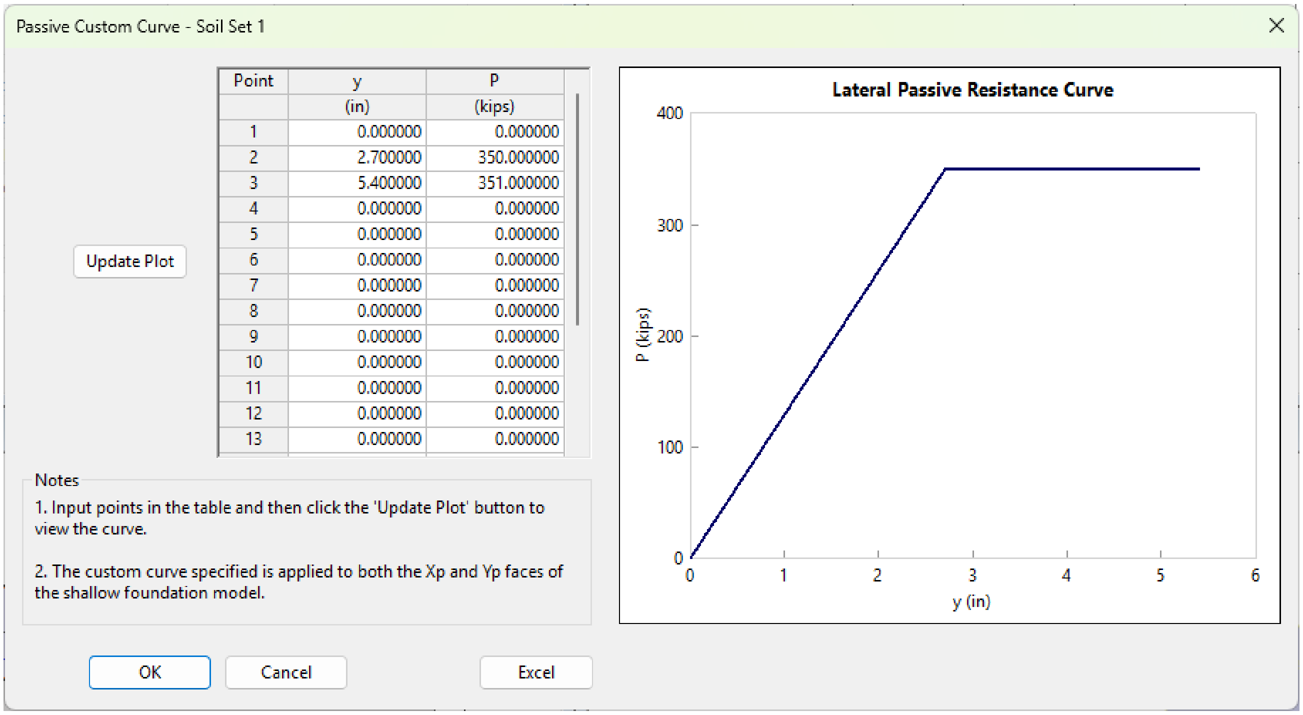

Figure 4-79 ‘Custom Curve’ dialog for lateral passive model.

4.4.1.7 Base Friction Resistance Model: Hyperbolic (Coulomb)

The Hyperbolic (Coulomb) dialog (Figure 4-80) can be accessed when the ‘Hyperbolic (Coulomb)’ base friction soil/rock resistance model is selected from the Base Friction dropdown on the ‘Soil’ page. The ‘Hyperbolic (Coulomb)’ model needs various user input parameters to calculate the friction force curve.

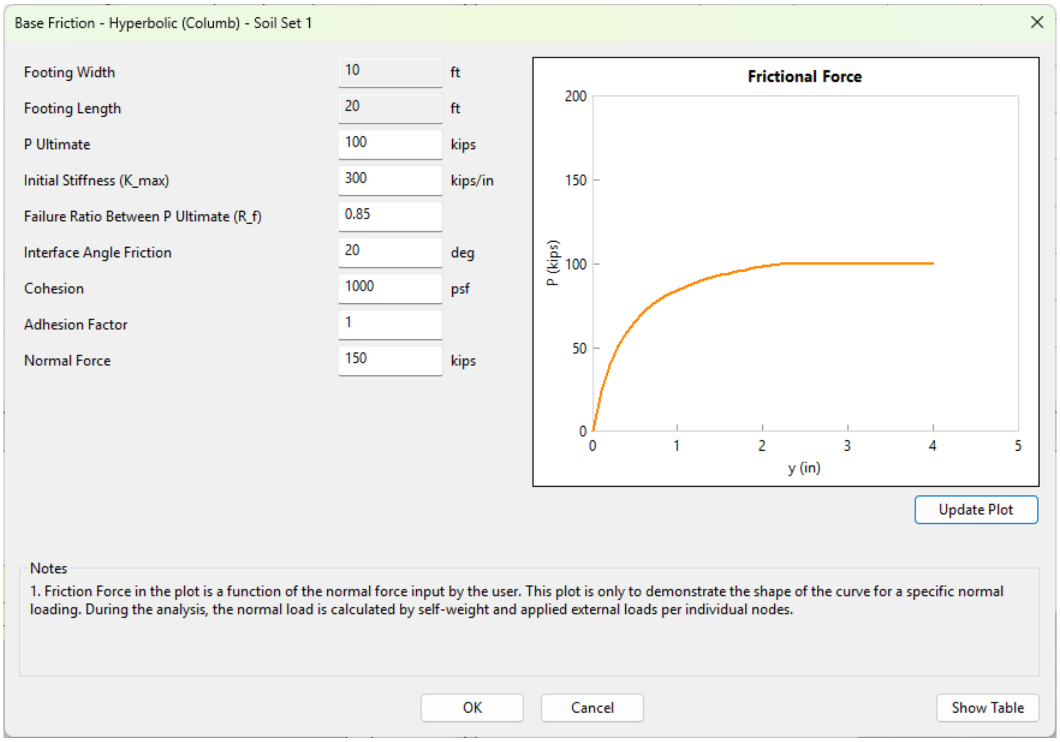

Figure 4-80 Base friction – hyperbolic (Coulomb) dialog with required key input parameters.

The ‘Footing Width (B)’, and ‘Footing Length (L)’ values are read-only in this dialog. They are calculated based on model input. The other input parameters (Figure 4-80) are as follows: P Ultimate, Initial Stiffness (Kmax), Failure Ratio Between P Ultimate (Rf), Adhesion Factor, Cohesion (c), Normal Force, and Interface Friction. These input parameters are subsequently used to calculate the base friction resistance plots in load values. The resistance curve are applied to each foundation node in Xp and Yp direction.

After the input parameters have been entered, the Friction Force curve will display in the plot window (Figure 4-80). The friction force in the plot is a function of the normal force input by the user on this dialog. This plot is only for demonstration purpose for the entered specific normal force. During the analysis, the analytical engine will compute the normal load generated on each foundation nodes under the self-weight and the applied external loads per load combination.

On the Base Friction – Hyperbolic (Coulomb) dialog, clicking the ‘Show Table’ button expands the right side of the dialog to display the curve points in the ‘Length Curve Points’ and ‘Width Curve Points’ tables (Figure 4-81).

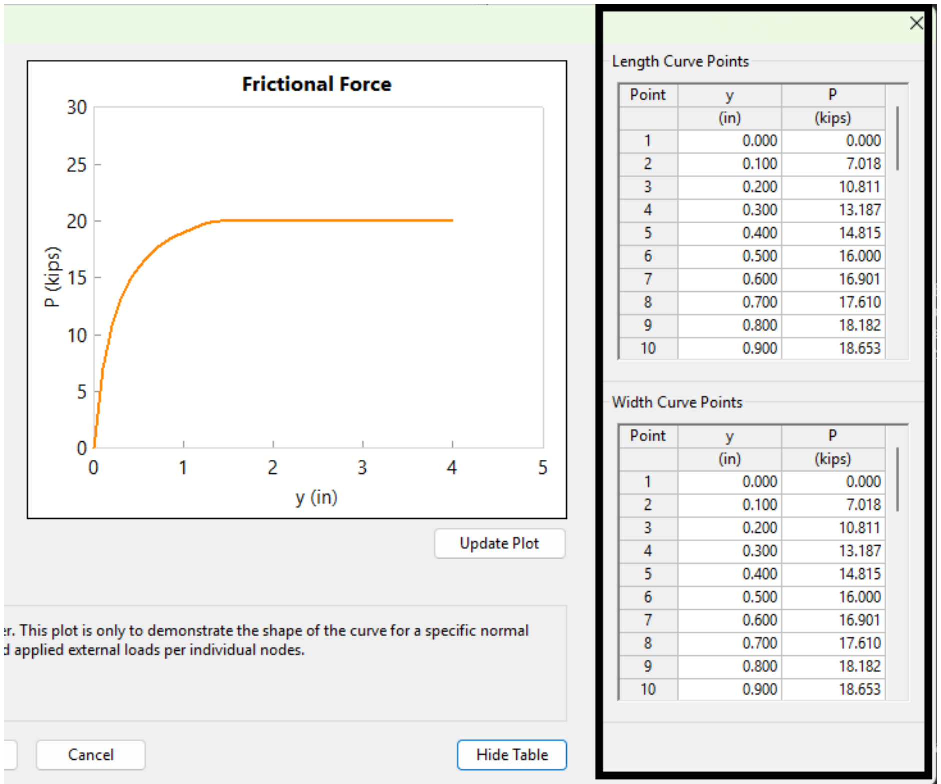

Figure 4-81 Curve points tables displayed on the base friction -- hyperbolic (Coulomb) dialog.

4.4.1.8 Base Friction Resistance Model: Linear

The ‘Base Friction Linear’ dialog (Figure 4-82) can be accessed when the ‘Linear’ model is selected from the dropdown within the ‘Shallow Foundation Data’ frame on ‘Soil’ page, and the ‘Edit’ button is clicked.

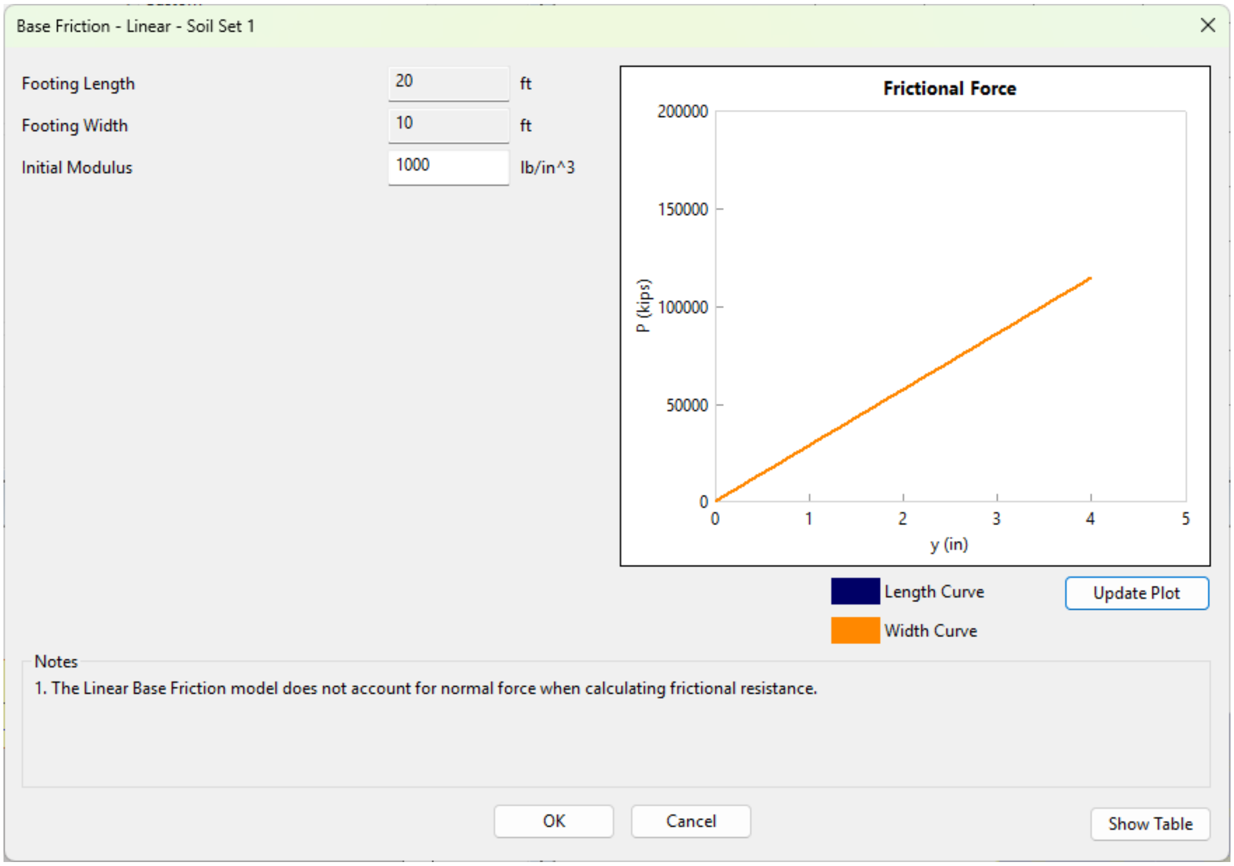

Figure 4-82 'Base Friction Linear' dialog.

The 'Footing Width', and 'Footing Length' values are read-only in this dialog. They are calculated based on model input. Additionally, Initial Modulus' value is required. After entering the required input, the friction force curve will plot. The displayed curve can be viewed in tabular format by clicking the 'Show Table' button.

4.4.1.9 Base Friction Resistance Model: Custom

The program includes 'Custom' soil models that enables users to implement their own soil resistance curves for foundation design.

The 'Custom Curve' dialog can be accessed when the 'Custom' model type is selected for Base Friction. The 'Custom' model can be selected for the 'Base Friction' model within the 'Shallow Foundation Data' frame on 'Soil' page, and the 'Edit' button is clicked. After inputting the desired number of curve points in the table and clicking the 'Update Plot' button, the custom curve will display (Figure 4-83).

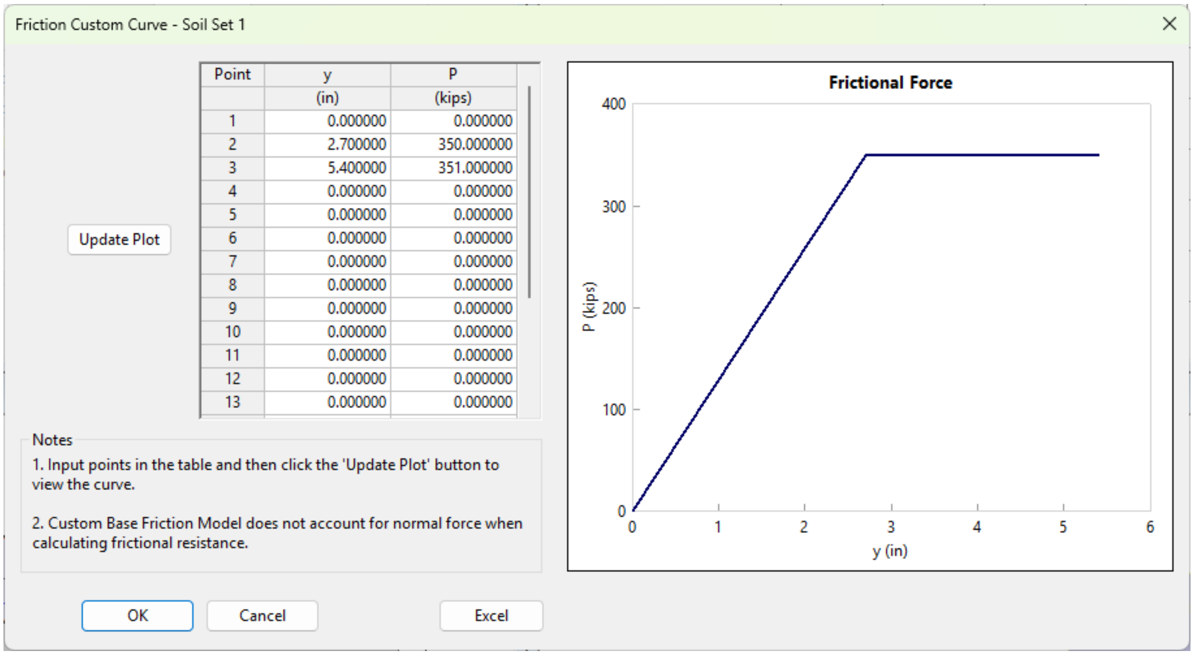

Figure 4-83 ‘Custom Curve’ dialog for base friction model.

4.4.1.10 3D Results View Enhancements

The 3D Results View has been updated to now include the Passive Resistance Plot feature and visibility of the Total Soil Spring Forces data display.

To access the 3D Results View, the ‘3D Results’ toolbar must be clicked (Figure 4-84).

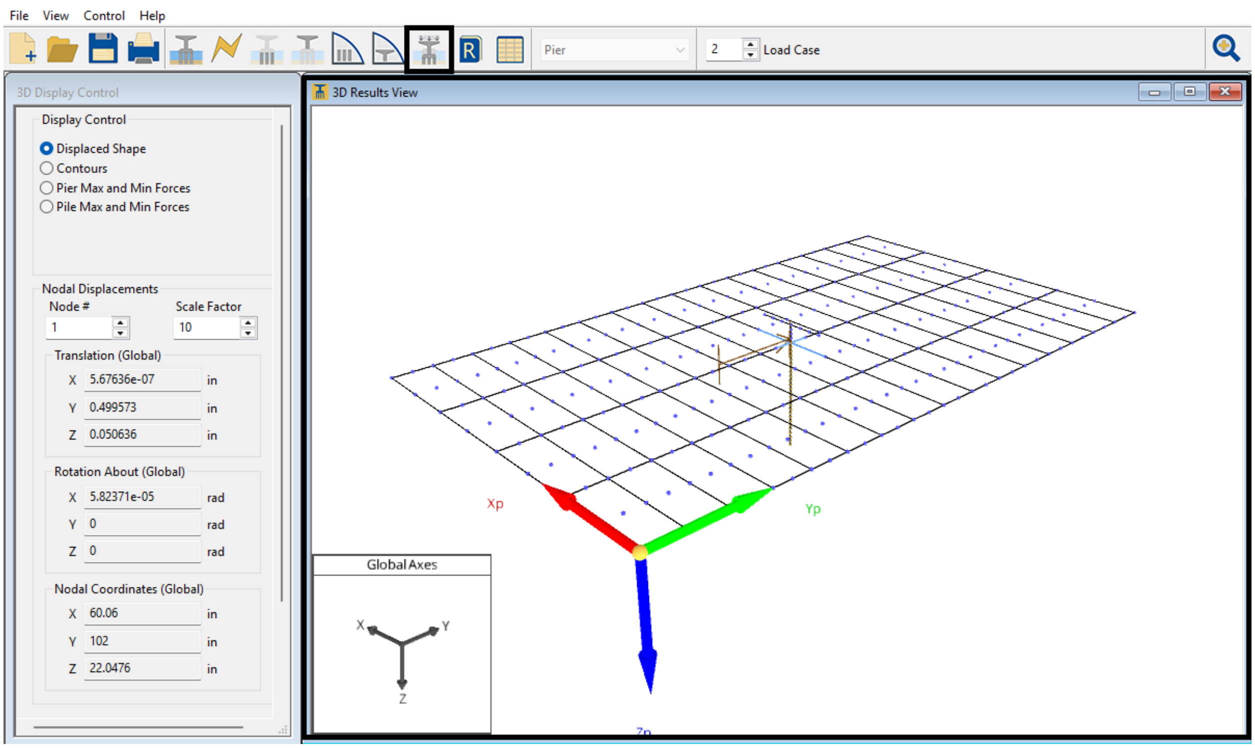

Figure 4-84 3D results toolbar button launches 3d results view.

With the 3D Result View open, right-clicking within said view launches the context menu (Figure 4-85).

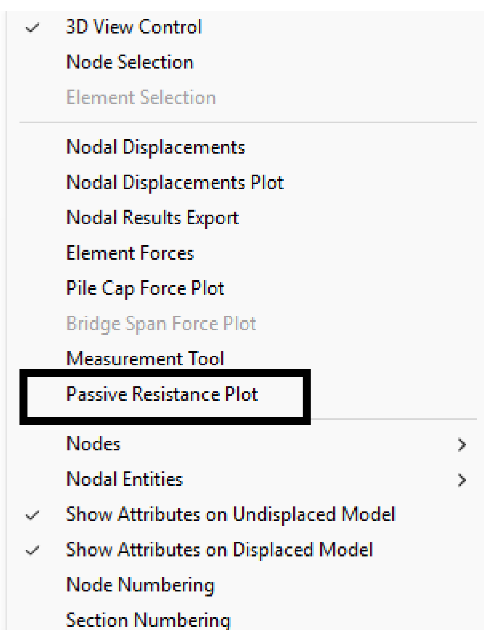

Figure 4-85 Context menu in 3d results view with passive resistance plot menu option.

From the context menu, select the ‘Passive Resistance Plot’ menu item (Figure 4-85). This action will launch the Passive Resistance Plot dialog (Figure 4-86).

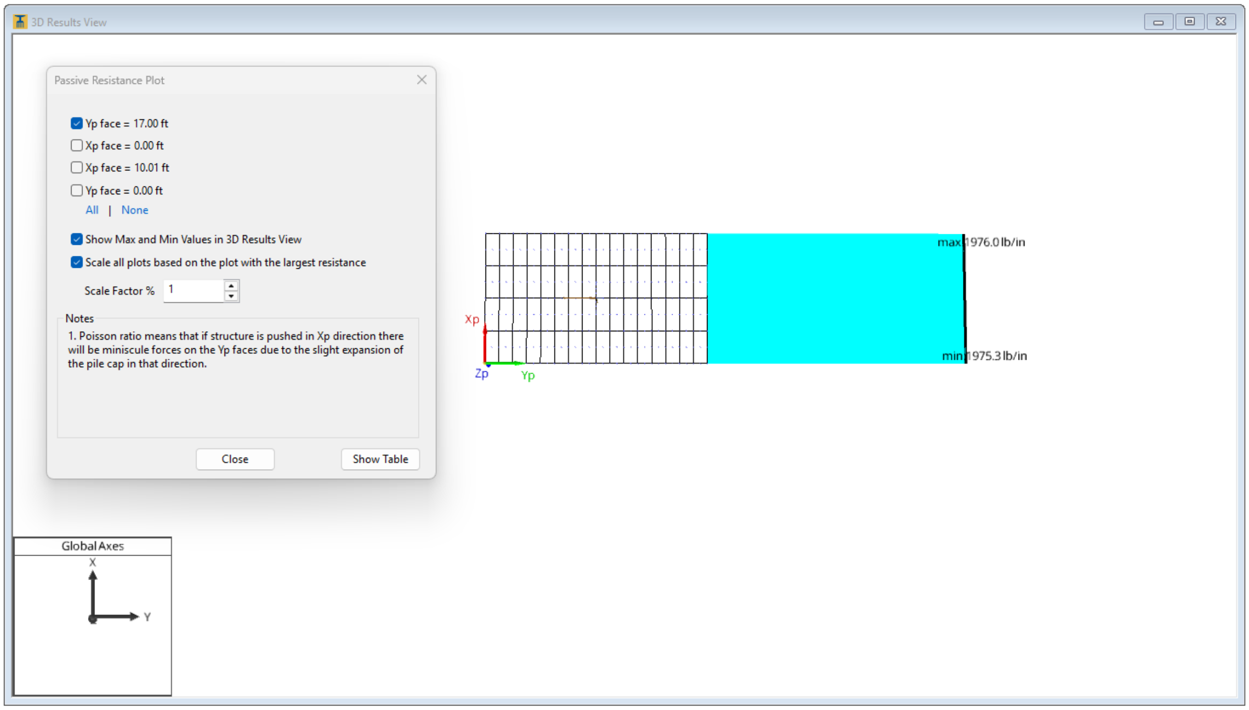

Figure 4-86 Passive resistance plot dialog in 3d results view with plot on Yp face.

The Passive Resistance Plot dialog has options to select the passive resistance plot for the desired pile cap face(s). There are four (4) faces, each utilizing a checkbox for face selection, as follows (Figure 4-87):

- Yp face = 17.00ft (Face that is perpendicular to Yp axis located 17 ft from the origin)
- Xp face = 0.00ft (Face that is perpendicular to Xp axis located at the origin)
- Xp face = 10.00ft (Face that is perpendicular to Xp axis located 10 ft from the origin)
- Yp face = 0.00ft (Face that is perpendicular to Yp axis located at the origin)

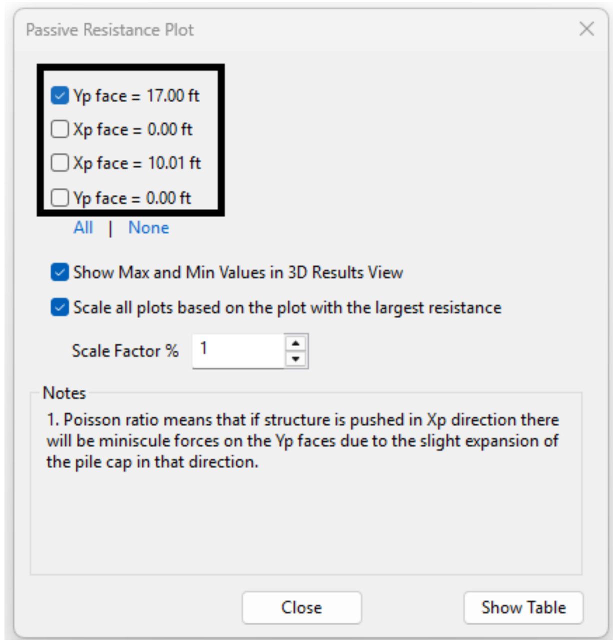

Figure 4-87 Passive resistance plot dialog with face checkboxes to select plots.

On the Passive Resistance Plot dialog, clicking the 'Show Table' button expands the right side of the dialog to display the curve points in the curve point table, for example the 'Yp Face' curve (Figure 4-88).

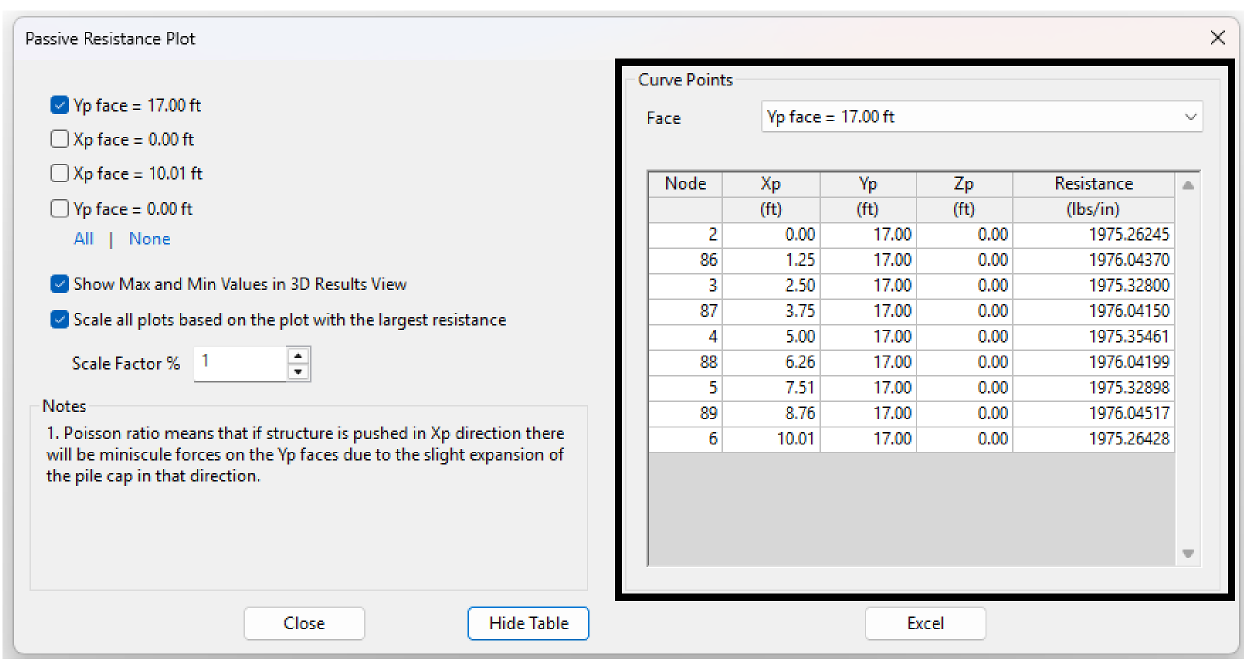

Node	Xp (ft)	Yp (ft)	Zp (ft)	Resistance (lbs/in)
2	0.00	17.00	0.00	1975.26245
86	1.25	17.00	0.00	1976.04370
3	2.50	17.00	0.00	1975.32800
87	3.75	17.00	0.00	1976.04150
4	5.00	17.00	0.00	1975.35461
88	6.26	17.00	0.00	1976.04199
5	7.51	17.00	0.00	1975.32898
89	8.76	17.00	0.00	1976.04517
6	10.01	17.00	0.00	1975.26428

Figure 4-88 Curve points table displayed on the passive resistance plot dialog.

The visibility of the Total Soil Spring Forces data display is controlled by the "Total Soil Spring Forces" context menu item in the 3D Results View. The Total Soil Spring Forces data display is visible by default for models that utilize a shallow foundation (i.e., the "Pier with Shallow Foundation" and "Shallow Foundation" model types). To access the context menu, right-click the mouse within the view (Figure 4-89). In the 3D Results View, the 'Total Soil Spring Forces' data box has been added to the top right of the View (Figure 4-90).

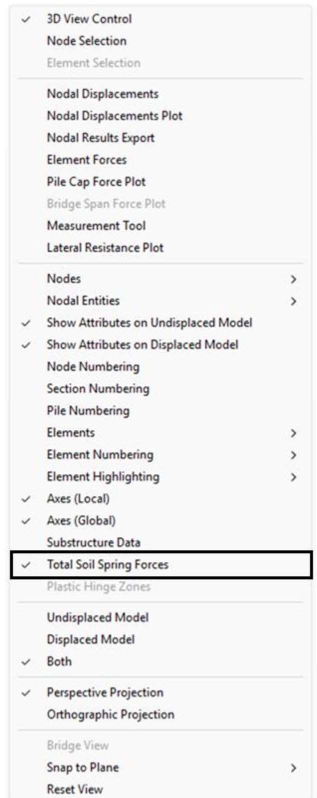

Figure 4-89 'Total Soil Spring Forces' context menu item to show/hide data box in 3d results view.

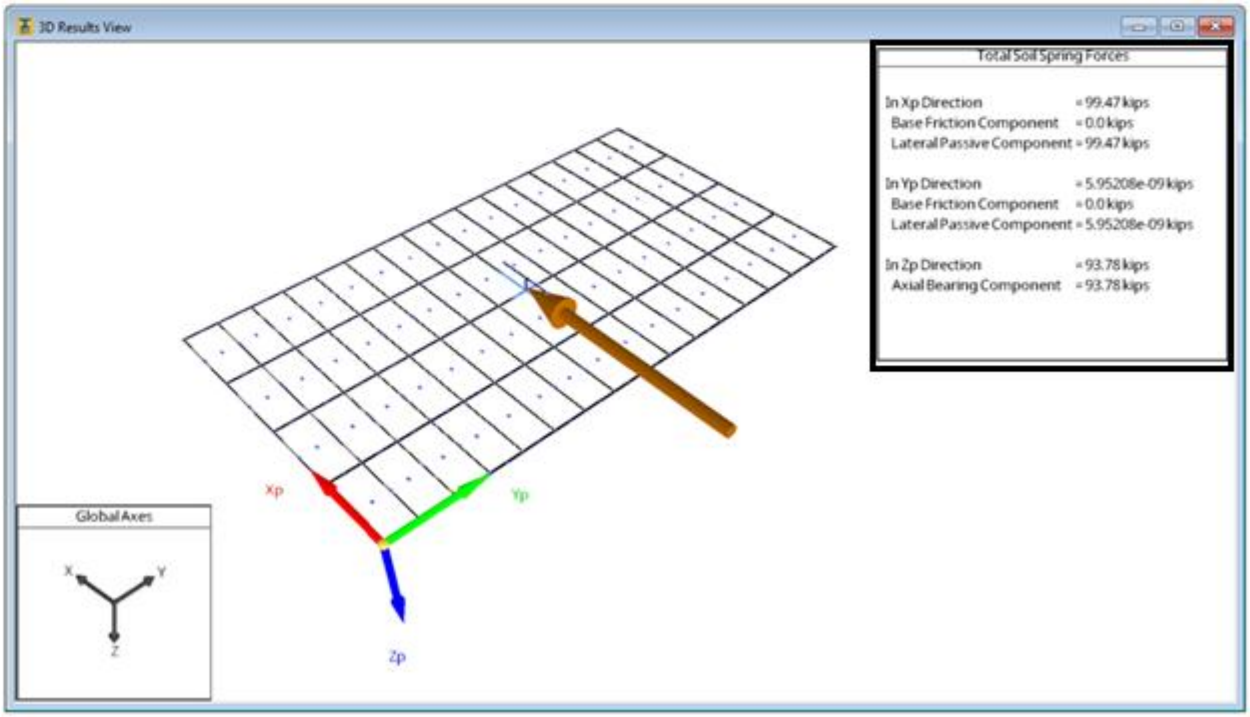

Figure 4-90 ‘Total Soil Spring Forces’ data box in 3d results view.

4.4.2 Shallow Foundation Enhancements in FB-MultiPier Analytical Engine

The input parameters entered through the FB-MultiPier UI dialogs for the shallow foundation soil resistance models are saved in the input file under the header ‘SHALLOWFOUND’, as described in Section 1.4. The analytical engine reads this header and generates the corresponding soil resistance curves for the shallow foundation.

The FB-MultiPier UI utilizes finite element model bases on the Beam on Non-linear Winkler Foundation (BNWF) approach to analyze the embedded shallow foundation model (Figure 3-26(b)). A mesh of distributed 9-node thick shell elements is used to represent shallow foundation. The shell element nodes are discretized as per the grid spacing specified in the program and are positioned at the midplane of the foundation. For this project, in Task #2, non-linear soil springs are used to model the axial bearing resistance on the shallow foundation (Figure 3-26(b)). These springs are applied at each foundation node. The passive resistance and base friction curves are developed and calculated as described in the Task #3.1. Using the soil resistance springs along with the tributary area for each foundation node, the soil spring forces are calculated at particular loading. Users may apply either a prescribed force or a prescribed displacement as the loading condition.

The lateral soil resistance is represented by lateral passive and base friction on the foundation. The base friction resistance is represented by set of non-linear soil springs and are applied at each foundation node. There are two sets of these springs, one applied in the Xp and the other in the Yp directions. Additionally, these springs are active in positive and negative Xp, Yp directions. Subsequently, the lateral passive resistance is represented by set of additionally non-linear soil springs and are applied along the edge of footing. These passive resistance soil springs are compression only (not active in tension). This means that its activation on the edge of the footing depends on the motion of the footing. The program will activate on the edges in the direction of motion. The passive resistance and base friction curves are developed and calculated as described as 4.2 Lateral Resistance of embedded footing. Using the soil resistance springs along with the tributary area for each foundation node, the soil spring forces are calculated for particular loading.

Chapter 4 focuses on implementing updates to the lateral soil resistance for shallow foundations, specifically representing the soil-footing interface. The lateral soil resistance includes both passive resistance and base friction. Recent research has identified the need to reduce the lateral resistance of the footing under skew loading, which was not accounted for in the initial implementation of the passive resistance curves in FB-MultiPier. The lateral passive and base friction resistance reduces when skewed loading is applied as mentioned previously.

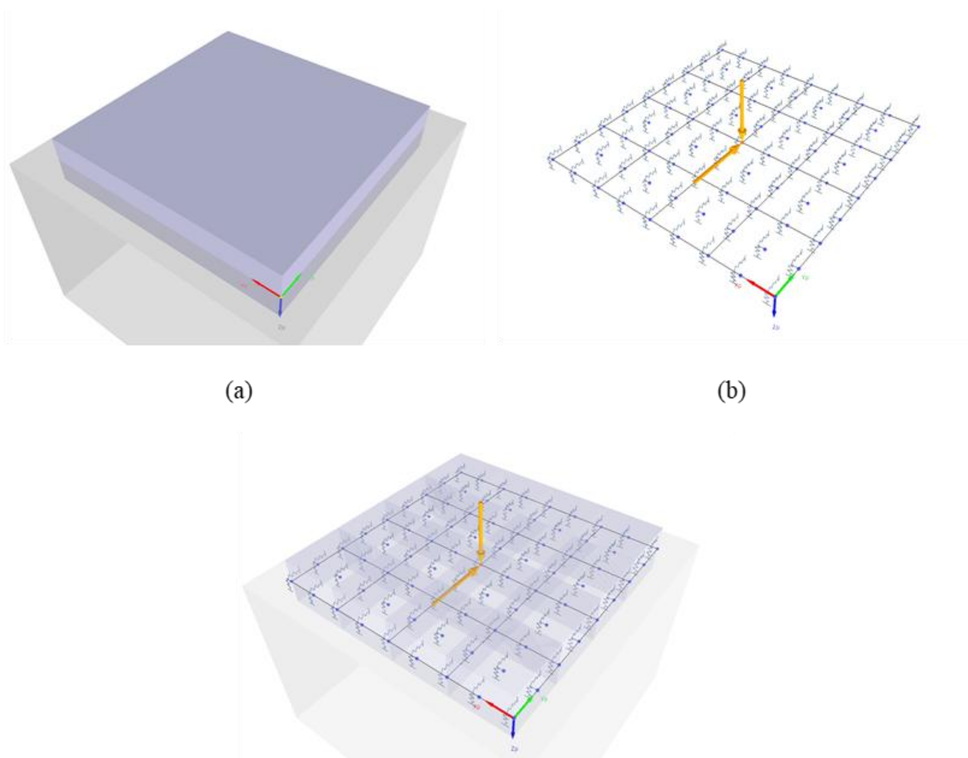

(c)

Figure 4-91 a) Shallow foundation (thick view), b) shallow foundation (thin element view), and c) shallow foundation (overlay view).

4.4.2.1 Enhancement to the Base Friction Resistance Calculation

As a part of this task, the base friction resistance is represented by a set of non-linear soil springs applied at each foundation node. Two sets of springs are assigned per foundation node, one in the Xp and one in the Yp directions. These springs are active in both the positive and negative Xp and Yp directions (Figure 4-48). When skew loading is applied, the resultant stiffness of the two orthogonal springs acts in the direction of the skewed motion. This results in a stiffer base friction response due to the combined contribution of both springs.

Furthermore, updates are being introduced on the base friction curves under skew loading. The enhancement involves defining and orienting a single base friction spring along the actual direction of footing movement. One base friction spring is now applied at each foundation node and is oriented in the direction of motion of that specific node. The program then calculates the corresponding Xp and Yp component from resultant response of this spring.

4.4.2.2 Enhancement to the Lateral Passive Resistance Calculation

As a part of this task, the lateral soil resistance is represented, in addition to the base friction spring, by the lateral passive resistance along the edges of the foundation. These springs are modeled using additional non-linear soil springs. These passive resistance soil springs are compression only (i.e. inactive in tension), meaning their activation depends on the motion of the footing. The program activates the orthogonal springs along the edges engaged in the direction of motion.

As mentioned earlier, recent research has identified the need to reduce the lateral response of the footing under skew loading. This effect was not accounted for in the initial implementation of the passive resistance curves in FB-MultiPier, resulting in over-prediction of the resistance. Furthermore, several approaches were evaluated to introduce a reduction in passive resistance under skew loading. The options explored are summarized below.

- OPTION #1 – Apply Reduction and Gain Factors on the Passive Resistance.
    - The skew angle of the footing underloading is determined.
    - The program identifies the active footing faces. Under skew loading conditions, one Xp face and one Yp face resist the applied load (Figure 4-35).
    - If the skew angle is up to 45 degrees with respect to the Xp axis, the Xp Face is defined as Face 1 and the Yp Face as Face 2. Conversely, if the skew angle is up to 45 degrees with respect to the Yp axis, the Yp Face is defined as Face 1 and the Xp Face as Face 2.
    - A reduction factor, Fr (Figure 4-38 and Figure 4-40), is applied to the passive resistance at nodes on Face 1. A gain factor, Fg (Figure 4-39 and Figure 4-41), is

applied to the passive resistance at nodes on Face 2. These factors can be provided on the FB-MultiPier UI as shown in Figure 4-92.

    - Conclusion: The resultant force was not aligned with the resultant displacement which was observed in the PLAXIS soil-foundation models. Additionally, convergence issues were encountered.

- OPTION #2 – Introduce Shear Spring at Footing Edge with Reduction and Gain Factors.

  - Passive resistance is modified as described in OPTION #1, applying the reduction factor Fr to nodes on Face 1 and the gain factor Fg to nodes on Face 2.

  - Shear springs are applied along Face 1 and Face 2. These springs are formulated similarly to the base friction model.

  - The orthogonal passive resistance on the footing face is used as the nominal force to calculate peak value for shear springs.

  - A reduction factor, FFr (Table 4-8), is applied to the shear resistance at nodes on Face 1. A gain factor, FFg (Table 4-8), is applied to the shear resistance at nodes on Face 2. These factors can be provided on the FB-MultiPier UI as shown in Figure 4-92.

    - Conclusion: Introduction of shear springs resulted in either convergence issues for the model or result in odd displacements or rotations. The convergence issues were associated by difficulty maintaining force and moment equilibrium, while trying to maintain shear spring resistance that is a function of the passive resistance being estimated. A small number of loading cases could converge, but results were unrealistic. Figure 4-93 is an example of this where FB-MultiPier converged on a solution with partial rotation, non-linear passive resistance on Yp face, with large Xp translation. This option was deemed not robust enough to be used.

- OPTION #3 – Modify P-ultimate using Reduction factors

  - The skew angle of the footing underloading is determined.

  - The program identifies the active footing faces, as described in OPTION #1.

  - If the skew angle is up to 45 degrees with respect to the Xp axis, the Xp Face is defined as Face 1 and the Yp Face as Face 2. Conversely, if the skew angle is up to 45 degrees with respect to the Yp axis, the Yp Face is defined as Face 1 and the Xp Face as Face 2.

- A reduction factor of cos(θ), where θ is skew angle, is applied to the calculated ultimate passive resistance, Equation 4-34, for nodes on Face 1. A reduction factor of sin(θ) is applied to the calculated ultimate passive resistance, Equation 4-35, for nodes on Face 2. This factor is automatically calculated by engine and do not require direct input from user.
    - Conclusion: This option was found to be robust to converge for multiple cases and loading orientations. It was also found to be agreeable with Plaxis results discussed in the validation section.

- OPTION #3 is proposed for implementation to reduce the passive resistance response in the FB-MultiPier program. Since OPTION #3 includes automated reduction factor calculation, the reduction and gain factor input options used in OPTION #1 and OPTION #2 have been removed from the FB-MultiPier UI, as shown in Figure 4-92.

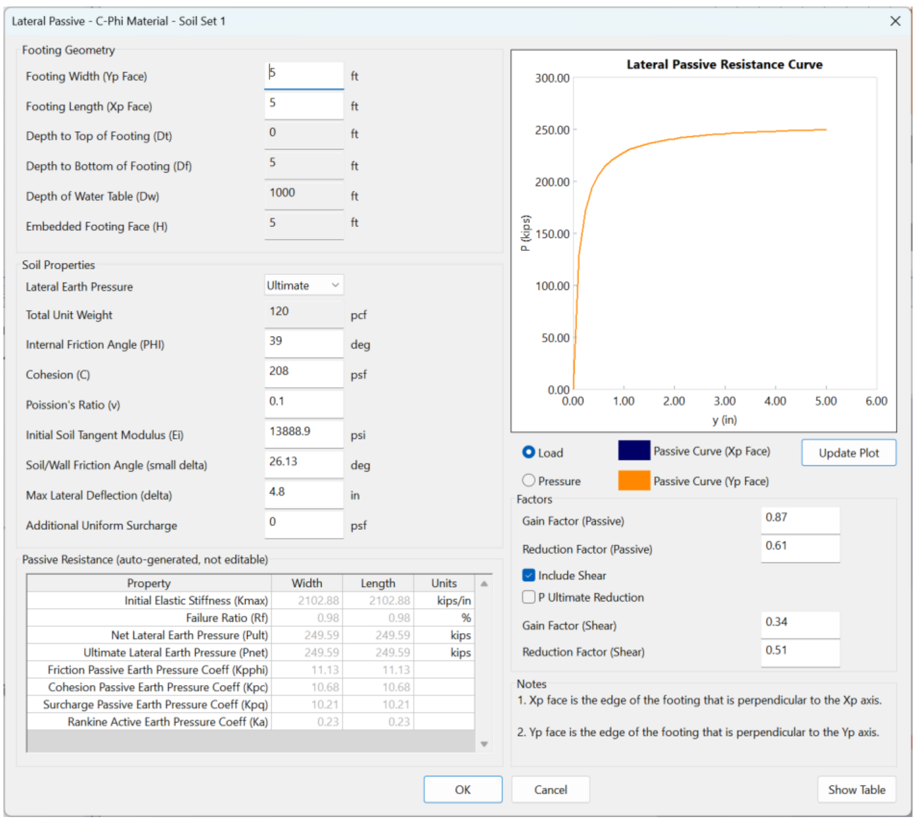

Figure 4-92 FB-MultiPier option 1 and 2 input parameters.

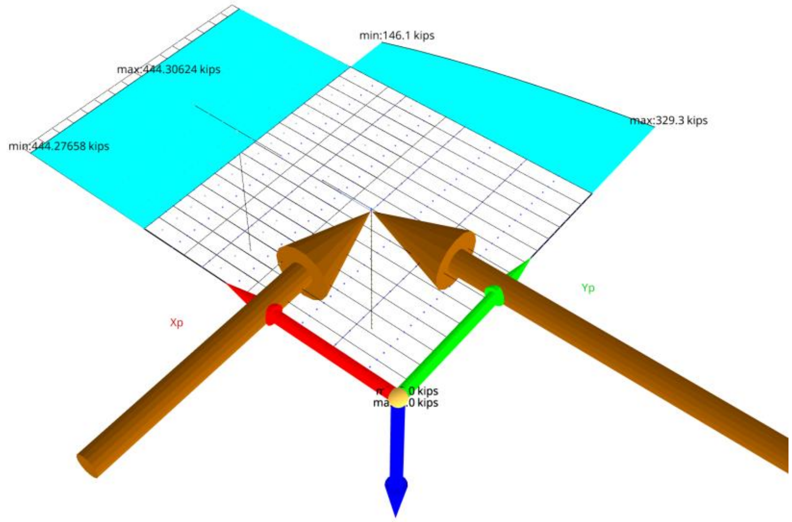

Figure 4-93 FB-MultiPier result with shear resistance spring.

4.4.2.3 Enhancements to the Output (*.out) File Prints

Select the 'Soil Resistance Curve' print flag, to print the Vertical and lateral soil resistance curves developed on per the shallow foundation node in the output (.out) The analytical engine also prints the passive resistance vs displacement curve in the output file (.out) if the print control 'Soil Resistance Curve' option is checked in the FB-MultiPier UI (Figure 4-94).

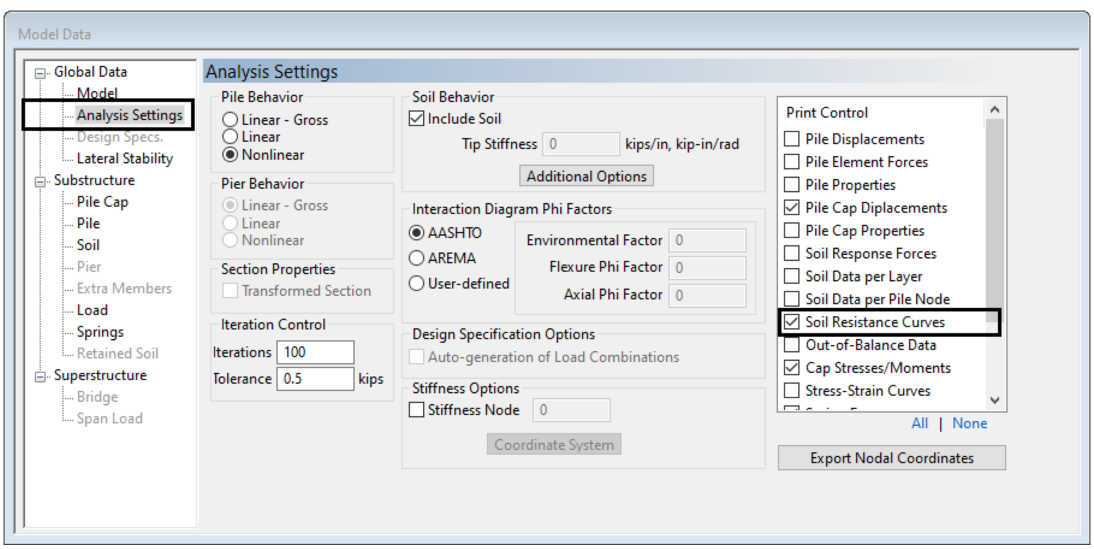

Figure 4-94 Print control option on the 'Analysis Settings' page in FB-MultiPier UI.

The Passive Resistance vs displacement curve is printed under the header 'Passive Resistance Curves for Shallow Foundation' as shown below. The base friction curves are not printed as during the analysis; the engine will compute the normal load generated on each foundation nodes under the self-weight and the applied external loads per load combination. This means each foundation node will have unique base friction resistance curve under each load combination.

```
***************************************************************
 *      PASSIVE RESISTANCE CURVES FOR SHALLOW FOUNDATION       *
 **************************************************************



 ______________________________________________________________
 - Passive (P-y) Curves for Shallow Foundation: Soil Set  1


 Along Footing Yp Face


 Curves are applied per soil set to each edge node of the
 foundation elements.


           y                P
          in           kips
     0.000000        0.000000
     0.102564     1653.239915
     0.205128     2498.225938
     0.307692     3011.252088
     …            …
     2.051282     4626.329096
     2.153846     4647.274923
     2.256410     4657.001762
     2.358974     4657.001762
     4.000000     4657.001762


______________________________________________________________
- Passive (P-y) Curves for Shallow Foundation: Soil Set  1


 Along Footing Xp Face


 Curves are applied per soil set to each edge node of the
 foundation elements.


           y                P
          in           kips
     0.000000        0.000000
     0.102564     2386.276663
     0.205128     3677.337417
     0.307692     4486.446608
     …            …
     2.051282     7167.350233
     2.153846     7203.522577
     2.256410     7220.333036
     2.358974     7220.333036
     4.000000     7220.333036
```

The program will also print the soil total soil response and its component for each foundation node in the output file (.out) with the header and sub-headers shown below:

1. Sum of Total Soil Spring Forces for Foundation Nodes (Load CASE #)
2. Soil Bearing Pressures at Foundation Nodes
3. Lateral Friction Resistance Xp, Yp Force at Foundation Nodes
4. Components for Oblique effect
    a. Xp Face
    b. Yp Face
5. Lateral Passive Resistance Xp, Yp Force at Foundation Nodes
6. Lateral Shear Resistance Xp, Yp Force at Foundation Nodes
7. Lateral Soil Resistance Xp Force at Foundation Nodes
8. Lateral Soil Resistance Yp Force at Foundation Nodes

The header from the .out file is shown below, with abbreviated results to illustrate how the results are presented in the output file.

```
_______________________________________________________________
 Sum of Total Soil Spring Forces at Foundation Nodes (Load CASE  1)


 Soil Set   1
 Xp Direction                        =         141.1049  kips
    Base Friction                    =          25.1299  kips
    Lateral Passive                  =         115.9749  kips
 Yp Direction                        =           0.0000  kips
    Base Friction                    =          -0.0007  kips
    Lateral Passive                  =           0.0008  kips
 Zp Direction                        =          93.7878  kips
 Est. of Ultimate Bearing Capacity   =         492.1933  psi
```

Soil Bearing Pressures at Foundation Nodes

Node	Pressure	Trib. Area	Spring Force
	ksf	ft^2	kips
1	5.5112E-01	6.6473E-01	3.6635E-01
2	4.8662E-01	1.6618E-01	8.0867E-02
...	...	...	...
296	5.6729E-01	3.3236E-01	1.8854E-01
297	5.9949E-01	3.3236E-01	1.9925E-01

Node	Yp Pressure	Trib. Area	Yp Force
	ksf	ft^2	kips
1	-4.3187E-06	6.6473E-01	-2.8708E-06
2	-5.1806E-04	1.6618E-01	-8.6091E-05
...	...	...	...
296	-1.7603E-04	3.3236E-01	-5.8507E-05
297	-4.4903E-04	3.3236E-01	-1.4924E-04

Lateral Friction Resistance Xp, Yp Force at Foundation Nodes

Node	Xp Pressure	Trib. Area	Xp Force
	ksf	ft^2	kips
1	1.4767E-01	6.6473E-01	9.8160E-02
2	1.3039E-01	1.6618E-01	2.1668E-02
...	...	...	...
296	1.5200E-01	3.3236E-01	5.0520E-02
297	1.6063E-01	3.3236E-01	5.3388E-02

Node	Yp Pressure	Trib. Area	Yp Force
	ksf	ft^2	kips
1	-4.3187E-06	6.6473E-01	-2.8708E-06
2	-5.1806E-04	1.6618E-01	-8.6091E-05
...	...	...	...
296	-1.7603E-04	3.3236E-01	-5.8507E-05
297	-4.4903E-04	3.3236E-01	-1.4924E-04

Components for Oblique effect

Xp Face

Node	Face ID	Oblique Angle	P-Ultimate Reduction Factor
		deg	
2	2	1.50E+01	2.59E-01
7	2	1.50E+01	2.59E-01
…	…	…	…
272	2	1.50E+01	2.59E-01
285	2	1.50E+01	2.59E-01

Yp Face

Node	Face ID	Oblique Angle	P-Ultimate Reduction Factor
		deg	
2	1	1.50E+01	9.66E-01
3	1	1.50E+01	9.66E-01
…	…	…	…
88	1	1.50E+01	9.66E-01
89	1	1.50E+01	9.66E-01

Lateral Passive Resistance Xp, Yp Force at Foundation Nodes

Node	Xp Pressure	Trib. Length	Xp Force
	k/ft	ft	kips
1	0.0000E+00	0.0000E+00	0.0000E+00
2	0.0000E+00	2.6563E-01	0.0000E+00
...	...	...	...
296	0.0000E+00	0.0000E+00	0.0000E+00
297	0.0000E+00	0.0000E+00	0.0000E+00

Node	Yp Pressure	Trib. Length	Yp Force
	k/ft	ft	kips
1	0.0000E+00	0.0000E+00	0.0000E+00
2	0.0000E+00	6.2563E-01	0.0000E+00
...	...	...	...
296	-9.6568E-03	1.2513E+00	-1.2083E-02
297	-2.4621E-02	1.2513E+00	-3.0807E-02

Lateral Soil Resistance Xp Force at Foundation Nodes

Node	Xp Friction	Xp Passive	Xp Total
	kips	kips	kips
1	9.8160E-02	0.0000E+00	9.8160E-02
2	2.1668E-02	0.0000E+00	2.1668E-02
...	...	...	...
296	5.0520E-02	0.0000E+00	5.0520E-02
297	5.3388E-02	0.0000E+00	5.3388E-02

Lateral Soil Resistance Yp Force at Foundation Nodes

Node	Yp Friction	Yp Passive	Yp Total
	kips	kips	kips
1	-2.8708E-06	0.0000E+00	-2.8708E-06
2	-8.6091E-05	0.0000E+00	-8.6091E-05
...	...	...	...
296	-5.8507E-05	-1.2083E-02	-1.2142E-02
297	-1.4924E-04	-3.0807E-02	-3.0956E-02

4.5 Input-Associated Updates to Model Input Files

The inputs associated with the lateral passive and base friction soil resistance models for the shallow foundation and the input parameters associated with them are entered using the FB-MultiPier UI. These shallow foundation data are then saved in the input (.in) file under header SHALLOWFOUND as mentioned in F.1 User-Guide for Input File Update.

4.6 Validation and Stress Comparisons in the Analysis Output Normal Loading

To ensure the accuracy of the coding implemented in the FB-MultiPier UI and engine, a comprehensive validation process was conducted using several distinct sources. The validation sets were selected to include detailed worked solutions, multiple examples with varying ranges of variable inputs, and a comparison between standard English and SI units. Four specific sources were employed to validate the implementation: a worked example set, a Matlab code utilized for in-depth sensitivity analysis, Plaxis analysis, and selected problems from previous research papers. Together, these methods form a robust assessment of the validations of the FB-

MultiPier UI and engine. First set of validation is for loading only in X or Y axis which is normal to vertical face of the footing. The second set of validation is for oblique loading.

4.6.1 Passive Hyperbolic Model Validation

For this project, the first validation problems were a set of problems for the passive hyperbolic model. The validation consisted of confirming passive resistance from FB-MultiPier UI dialogs and engine output (i.e., .out file). Additionally, the load settlement response determined by FB-MultiPier was compared with the hyperbolic hand calculations of the models. The following cases were analyzed.

- Result of worked example Appendix A.
- Result of worked example Appendix A converted to SI Units

In total, two cases were analyzed, the first being based on the worked example which walks through the design method in detail, Appendix B.1.1 . The second case analyzes the worked example with the inputs converted to SI units.

The first validation effort was to confirm that the UI and Engine calculate the correct passive resistance curve, Equation 4-10. The passive resistance curve, based on the inputs from worked example in Appendix A, data is collected from the UI and engine and compared with the independent calculated curve, from the Matlab Code, for both English and SI units. The results of this comparison are shown in Figure 4-95 and Figure 4-96, which show excellent agreement in the form of overlapping of the 3 separate passive curves.

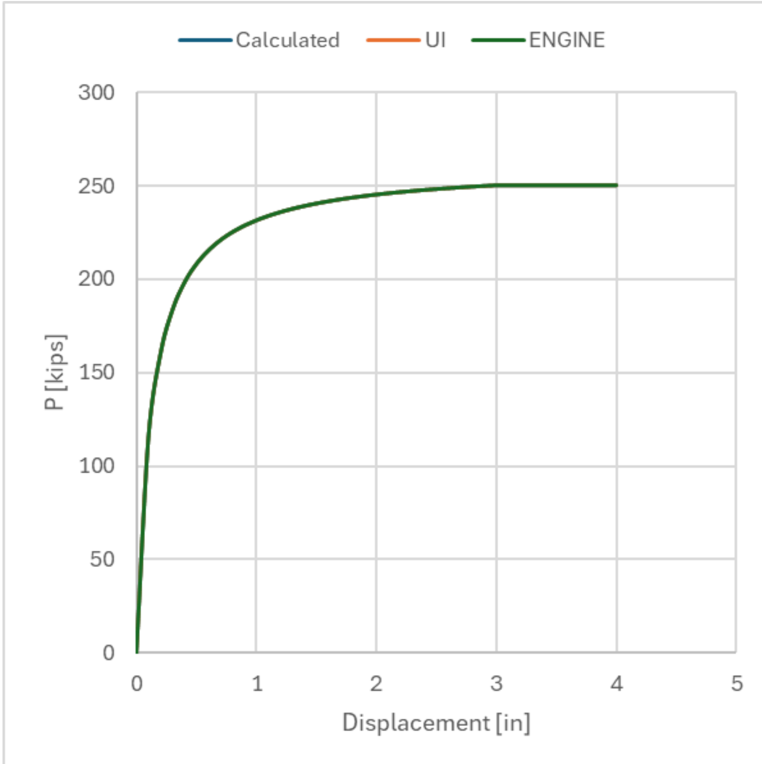

Figure 4-95 Passive resistance curve comparison (english units).

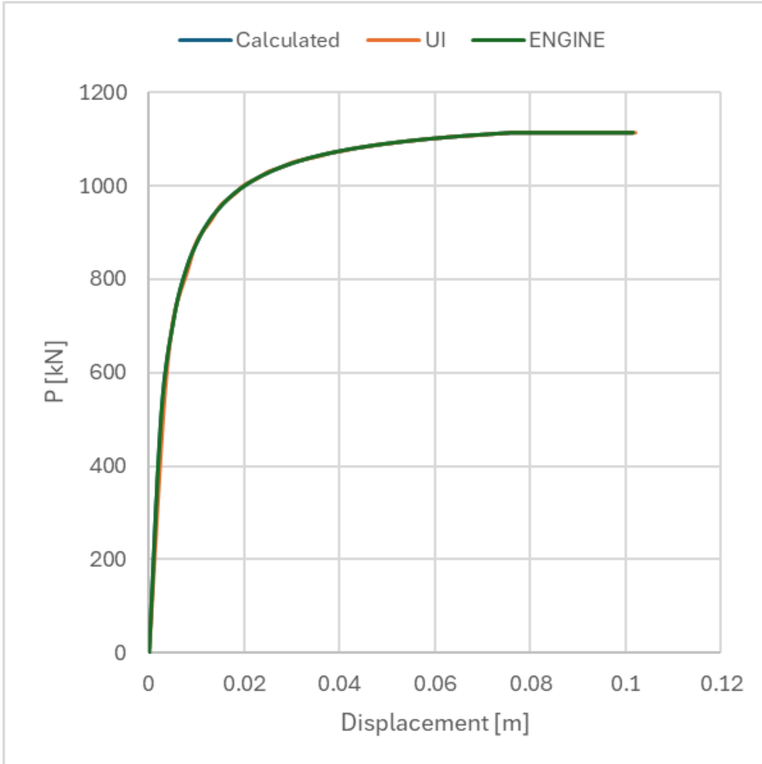

Figure 4-96 Passive resistance curve comparison (SI units).

The final validation of implementation of the passive resistance curve, was comparing the nodal displacement and spring forces from FB-MultiPier finite element analysis to calculated passive resistance curve. For each case a shallow foundation model was created that matches the prescribed geometry (i.e., length, width, etc.) and modulus. A column was located at the center of the footing. The column is connected to the foundation using rigid connector elements which spans column center to edge of column footprint, to prevent unrealistic stress concentration. Two loading validations where conducted, first using the previously described model used with a loading of a prescribed horizontal displacement, Figure 4-97, with increments shown in Table 4-9 . The advantage of using prescribed displacement aids in the FB-MultiPier ability to converge on a solution for loading conditions that reach near ultimate resistance portion of the hyperbolic curve. The model is then run and results from the model corresponding to displacement of the center of the footing in X direction and Passive reactions in the X direction. These FB-MultiPier results are then plot along with calculated hyperbolic curve, Figure 4-98, which shows excellent agreement.

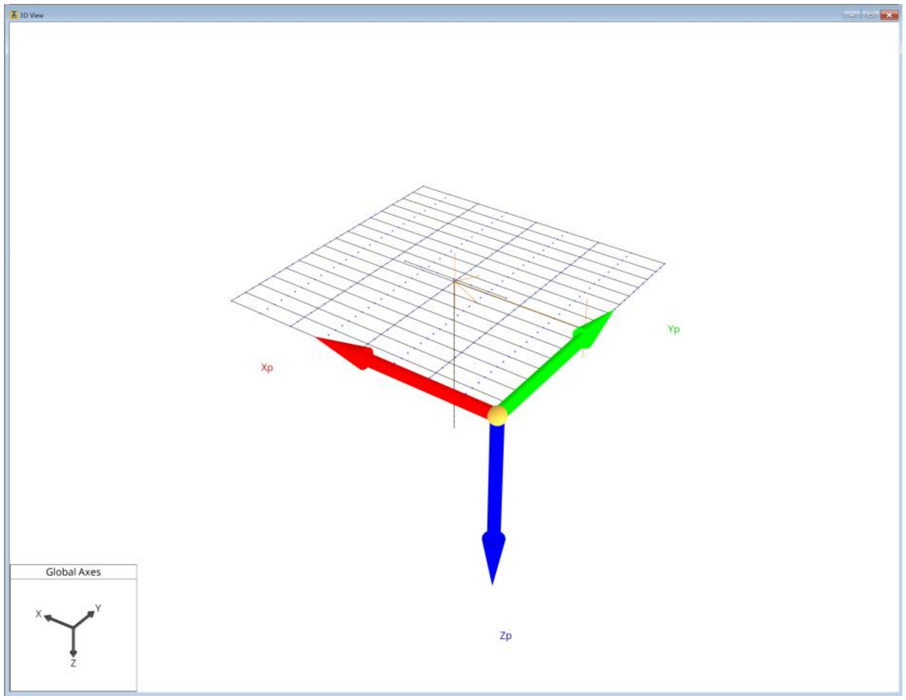

Figure 4-97 FB-MultiPier shallow foundation model prescribed displacement.

Table 4-9 Prescribed displacement.

Load Case	Prescribed Displacement [in]
1	0.01
2	0.05
3	0.10
4	0.25
5	0.50
6	1.00
7	2.50
8	5.00

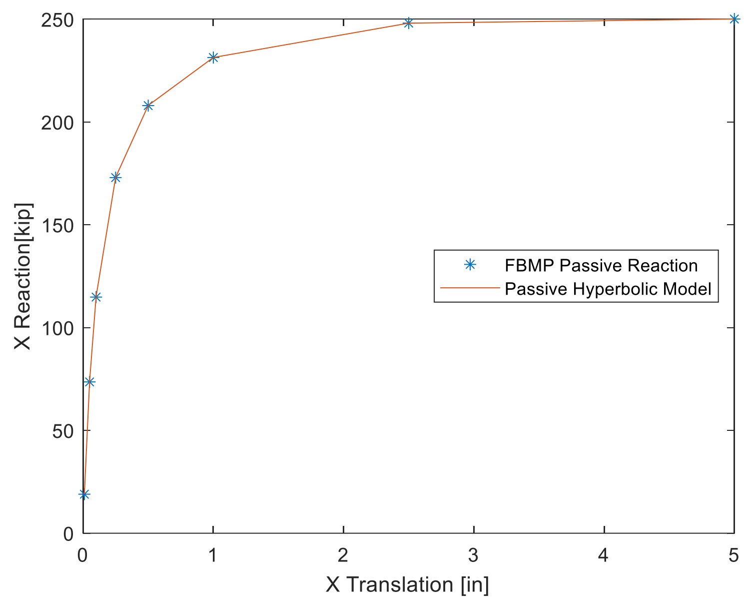

Figure 4-98 Passive resistance hyperbolic model – prescribed displacement.

The second validation method also uses the same model but is horizontally loaded, Figure 4-99, of increments shown in Table 4-10 . The model is then run and results from the model corresponding to displacement of the center of the footing in X direction and Passive Forces in the X direction. These FB-MultiPier results are then plot along with calculated hyperbolic curve, Figure 4-100, which shows excellent agreement.

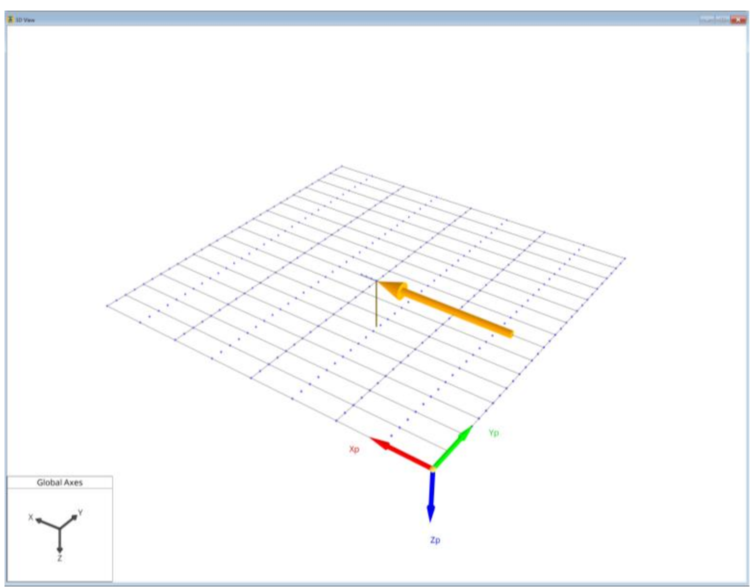

Figure 4-99 FB-MultiPier shallow foundation model prescribed force.

Table 4-10 Loading increments.

Load Case	Load Percentage of P_{ult} [%]
1	1
2	5
3	10
4	25
5	50
6	75
7	95
8	99

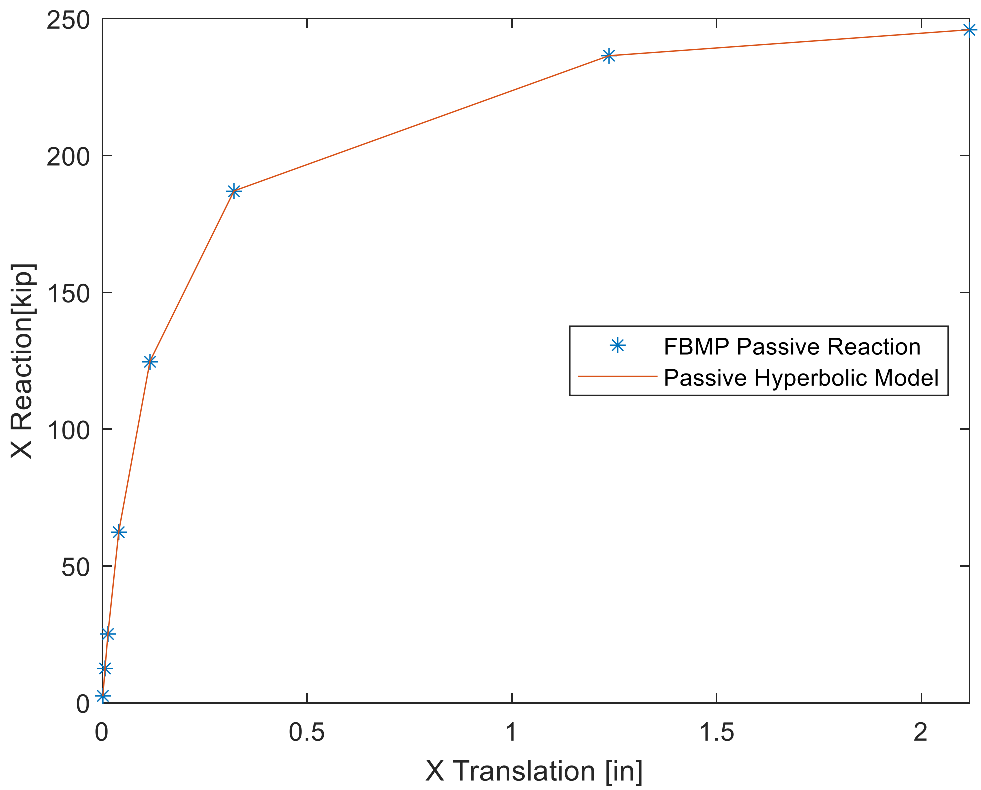

Figure 4-100 Passive resistance hyperbolic model – prescribed load.

The hyperbolic model was also validated for SI units. This validation was conducted in the same manner as discussed previously; however, it used inputs from the worked example that were converted to SI units. Results of this validation process are shown in Figure 4-101 and Figure 4-102, both which show excellent agreement.

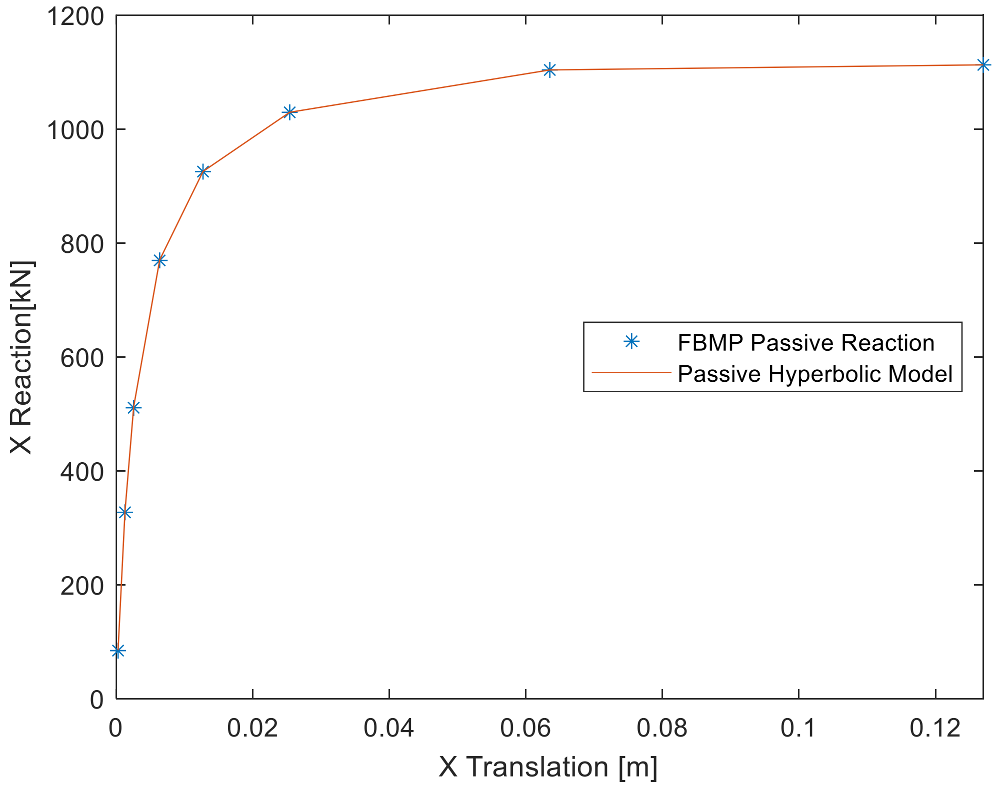

Figure 4-101 Passive resistance hyperbolic model – prescribed displacement SI.

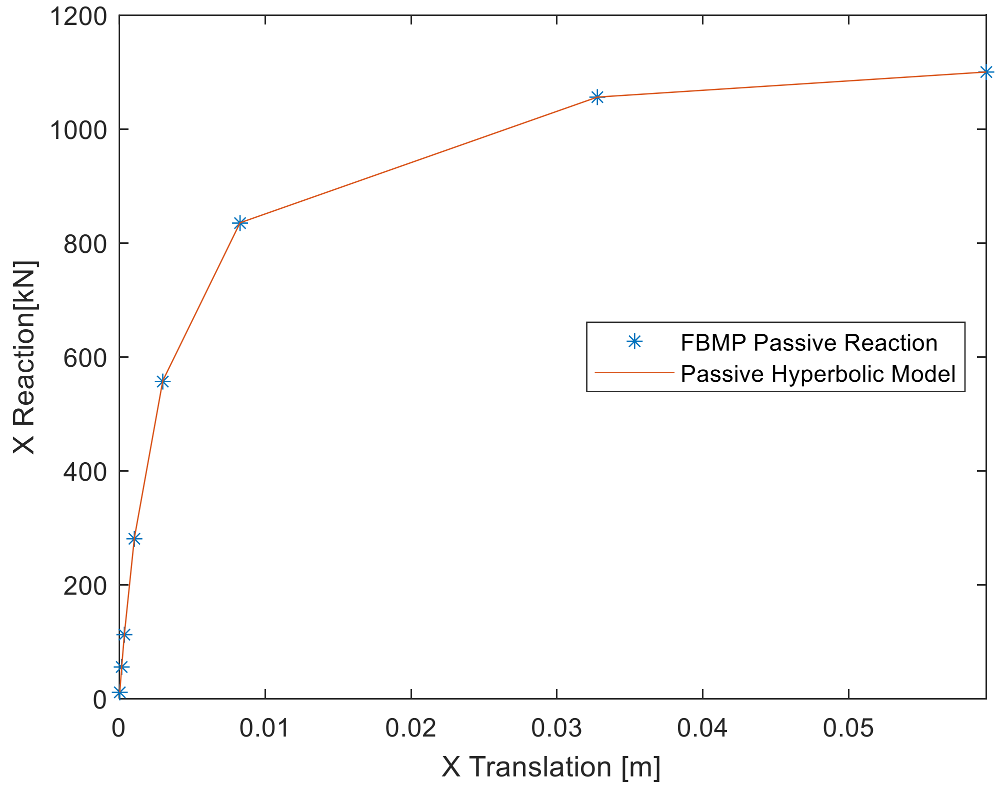

Figure 4-102 Passive resistance hyperbolic model – prescribed load SI.

4.6.2 Passive C-PHI Model Validation

To validate implementation of the C-Phi model. The validation consisted of confirming passive resistance from FB-MultiPier UI dialogs and engine output (i.e., .out file). Additionally, the load settlement response determined by FB-MultiPier was compared with the hyperbolic model calculations. The following cases were analyzed.

- Worked Example Appendix A
- Sensitivity Study – English Units
- Sensitivity Study – SI Units
- Load Tests in granular material

The first validation effort was conducted in same manner as previously discussed for the hyperbolic model. This consists of confirming the UI and Engine are calculating the correct passive resistance curve but now is based on inputs required for Equation 4-3, Equation 4-22, and Equation 4-25. For the C-PHI model first validation effort is based on the worked example in Appendix A, confirming that the UI and Engine calculate the correct P_{ult}, P_{net}, k_{max} and R_f values, along with its corresponding passive resistance curve. Presented in Table 4-11 and Table 4-12 is a comparison of the calculated hyperbolic parameters The results of this comparison are shown in Figure 4-103 and Figure 4-104, which shows excellent agreement in form of overlapping of the 3 separate passive curves.

Table 4-11 C-PHI model work example values.

Value	Worked Example	FBMP UI
Kmax [kips/in]	2062	2062
Rf [-]	0.96	0.96
Pult [kips]	250	250
Pnet [kips]	250	250

Table 4-12 C-PHI model work example values-SI.

Value	Worked Example	FBMP UI
Kmax [kN/m]	361111	361148
Rf [-]	0.96	0.96
Pult [kN]	1112	1112
Pnet [kN]	1112	1112

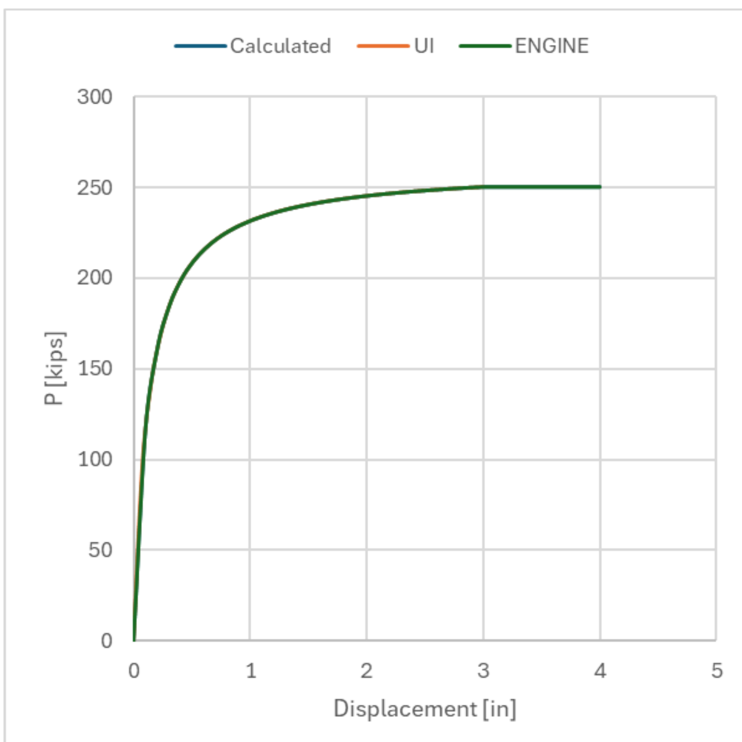

Figure 4-103 Passive c-PHI resistance curve comparison.

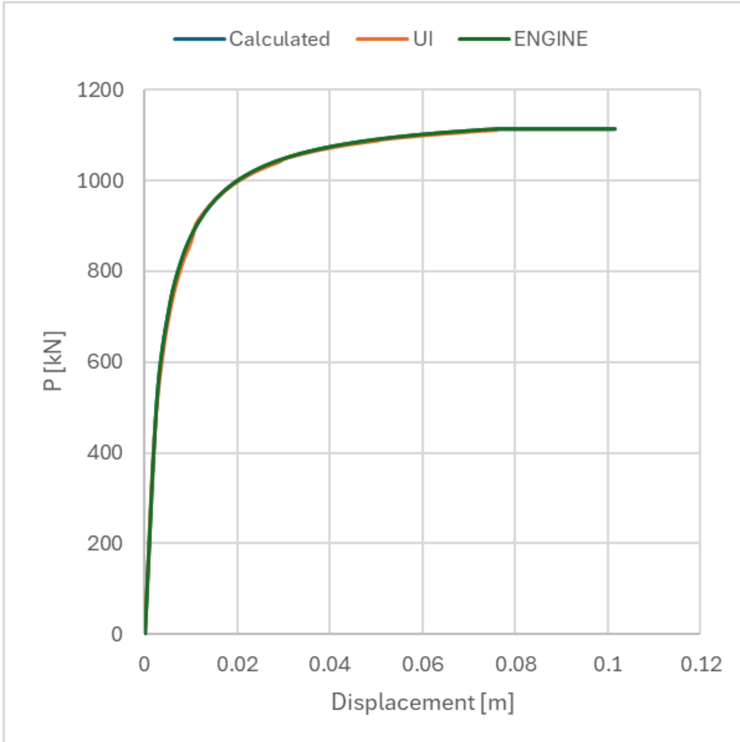

Figure 4-104 Passive c-PHI resistance curve comparison SI units.

Continuing in the validation process in the same manner, prescribed displacements and loads, Table 4-9 and Table 4-10 , were used in FB-MultiPier model using parameters from the worked example in appendix A for both English and SI units. Results from this analysis are shown in Figure 4-105 through Figure 4-108, which show excellent agreement.

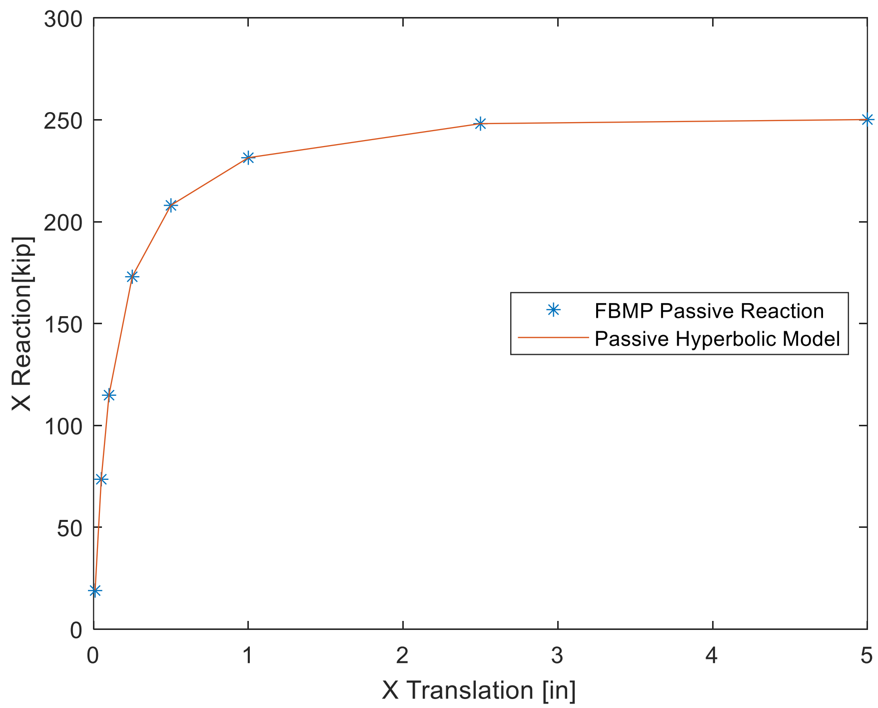

Figure 4-105 Passive resistance c-PHI model – prescribed displacement.

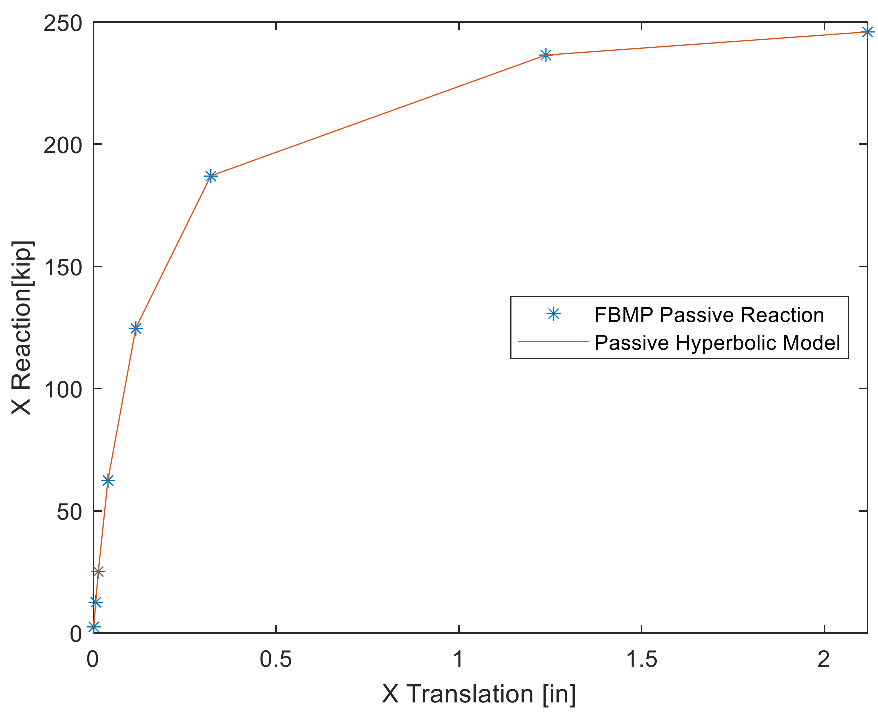

Figure 4-106 Passive resistance c-PHI model – prescribed load.

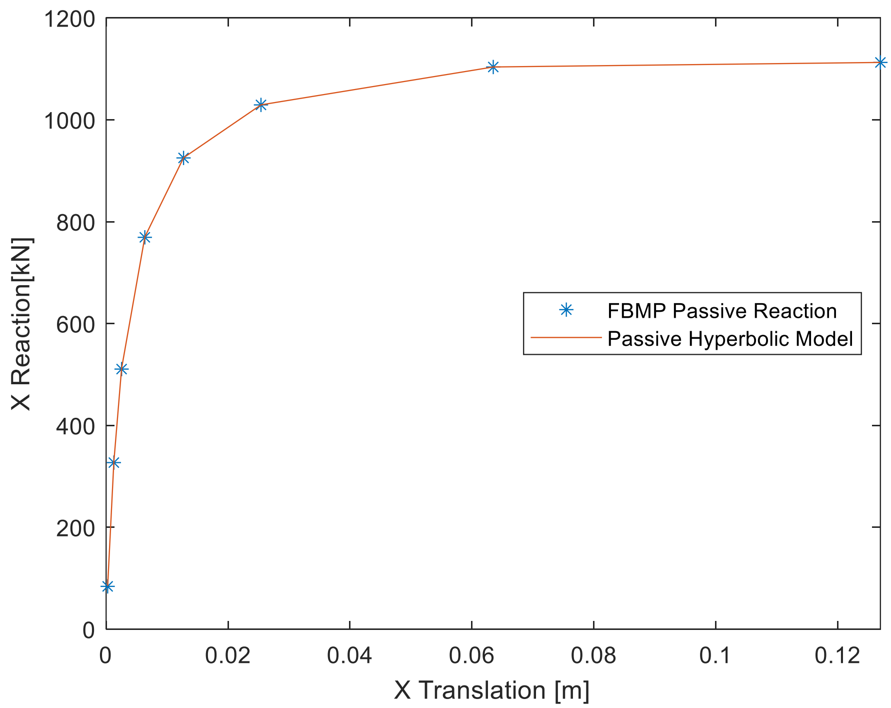

Figure 4-107 Passive resistance c-PHI model – prescribed displacement SI.

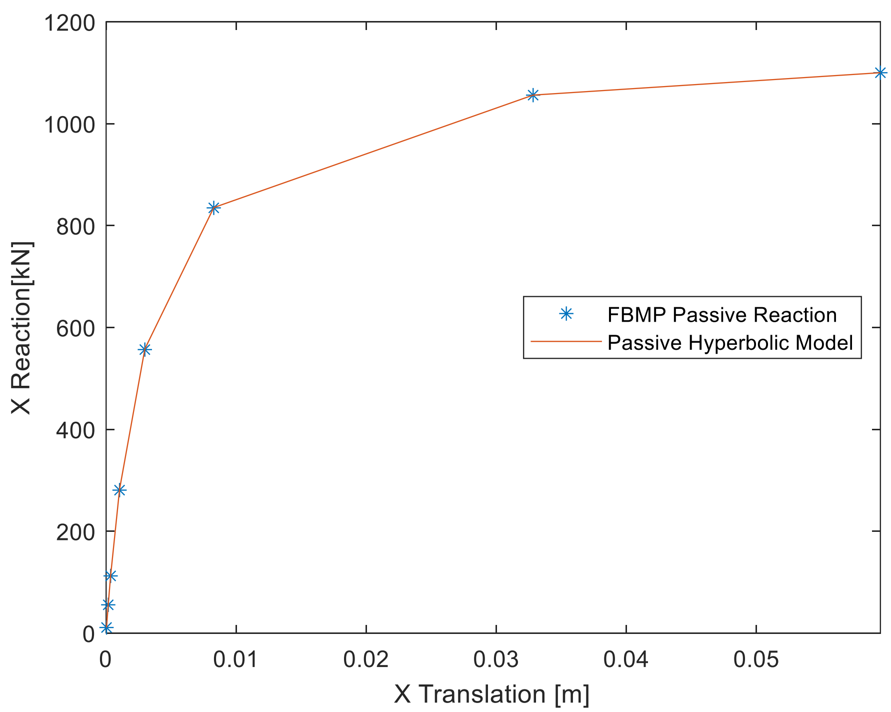

Figure 4-108 Passive resistance c-PHI model – prescribed load SI.

The next validation effort was to conduct a sensitivity study where input parameters for the C-PHI model are perturbated, to ensure FB-MultiPier is using each one appropriately. Input parameters for sensitivity study are shown in Table 4-13 .

Table 4-13 C-PHI Model Sensitivity Study.

Cases	L [ft]	B [ft]	t [ft]	Dw [ft]	Df [ft]	C [psf]	ϕ [°]	γ [pcf]	v	δ [°]	Ei [psi]	Dmax [ft]	q [psf]
1	20	20	5	1000	5	0	30	100	0.25	20	10000	0.30	0
2	20	20	5	1000	5	0	25	100	0.25	16.67	10000	0.30	0
3	20	20	5	1000	5	500	30	100	0.25	20	10000	0.30	0
4	20	20	8	1000	8	0	30	100	0.25	20	10000	0.30	0
5	15	20	5	1000	5	0	30	100	0.25	20	10000	0.30	0
6	20	15	5	1000	5	0	30	100	0.25	20	10000	0.30	0
7	20	20	5	1000	5	0	30	115	0.25	20	10000	0.30	0
8	20	20	5	1000	5	0	30	100	0.15	20	10000	0.30	0
9	20	20	5	1000	5	0	30	100	0.25	10	10000	0.30	0
10	20	20	5	1000	5	0	30	100	0.25	20	10000	0.60	0
11	20	20	5	1000	5	0	30	115	0.25	20	5000	0.30	0
12	20	20	5	0	5	0	30	100	0.25	20	10000	0.30	0
13	20	20	5	3	5	0	30	100	0.25	20	10000	0.30	0
14	20	20	5	1000	3	0	30	100	0.25	20	10000	0.30	0
15	20	20	5	1000	10	0	30	100	0.25	20	10000	0.30	0
16	20	20	5	1000	5	0	30	100	0.25	20	10000	0.30	500
17	20	20	5	1000	10	0	30	100	0.25	20	10000	0.30	500
18	20	20	5	1000	5	250	0	100	0.25	0	10000	0.30	0
19	20	20	5	1000	11.25	250	0	100	0.25	0	10000	0.30	0
20	20	20	5	1000	5	250	0	100	0.25	0	10000	0.30	625

A prescribed displacement and force comparison was conducted for each case in both standard and SI units. Results of this analysis are shown in Figure 4-109 through Figure 4-112, where calculated resistance values are plotted vs their corresponding resultant passive resistance from a FB-MultiPier engine analysis. The points fall closely along a slope of 1. This confirmed with a bias analysis, Equation 4-38 and Equation 4-39, where the ratio of the passive calculated resistance, mi, to FB-MultiPier passive reaction, pi. For this sensitivity study, a $\lambda_R$value (FB-MultiPier/model) of approximately 1 (no significant over or under estimation) from the FB-MultiPier analysis. Additionally, the very low CV_λ confirm no scatter or inherent error in the FB-MultiPier analysis. Results of this analysis were shown in Table 4-14 , where for all loading conditions and unit types resulted in a $\lambda_R$value of approximately 1 (no significant over or under estimation) from the FB-MultiPier analysis. Additionally, the very low CV_λ confirm no scatter or inherent error in the FB-MultiPier analysis.

$$\lambda_R = \frac{1}{n}\sum_{i=1}^{n} \lambda_i = \frac{1}{n}\sum_{i=1}^{n} \frac{m_i}{p_i} \qquad \text{Equation 4-38}$$

$$CV_\lambda = \frac{\sqrt{\frac{1}{n}\sum_{i=1}^{n}(\lambda_i - \lambda_R)^2}}{\lambda_R} \qquad \text{Equation 4-39}$$

Table 4-14 Passive c-PHI sensitivity study results.

Analysis Type	λ_R	CV_λ
Prescribed Displacement	1.0016	0.0027568
Prescribed Load	1.0049	0.0043935
Prescribed Displacement-SI	1.0052	0.0043639
Prescribed Load - SI	1.0018	0.002753

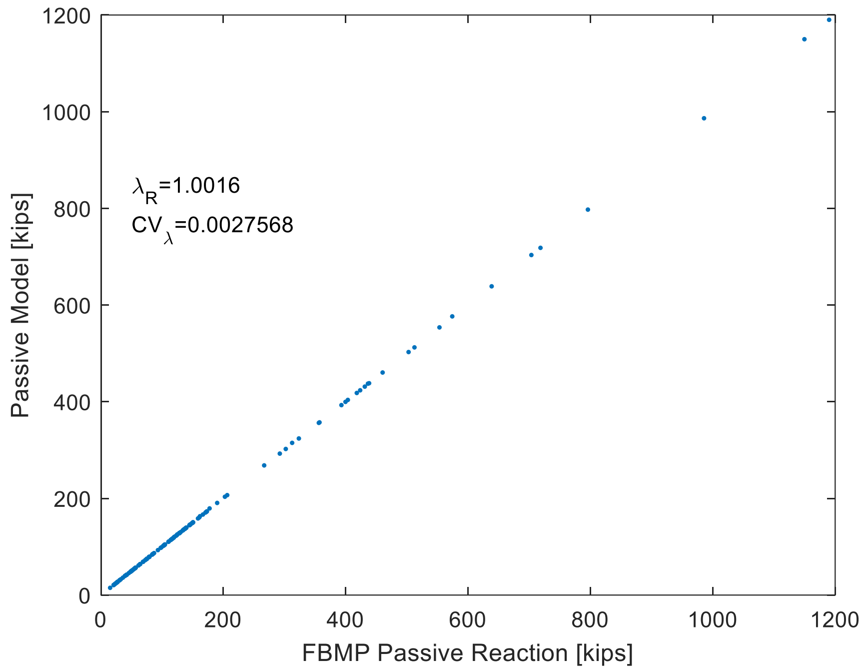

Figure 4-109 Sensitivity study FB-MultiPier (FBMP) passive reaction vs calculated passive reaction – prescribed displacement.

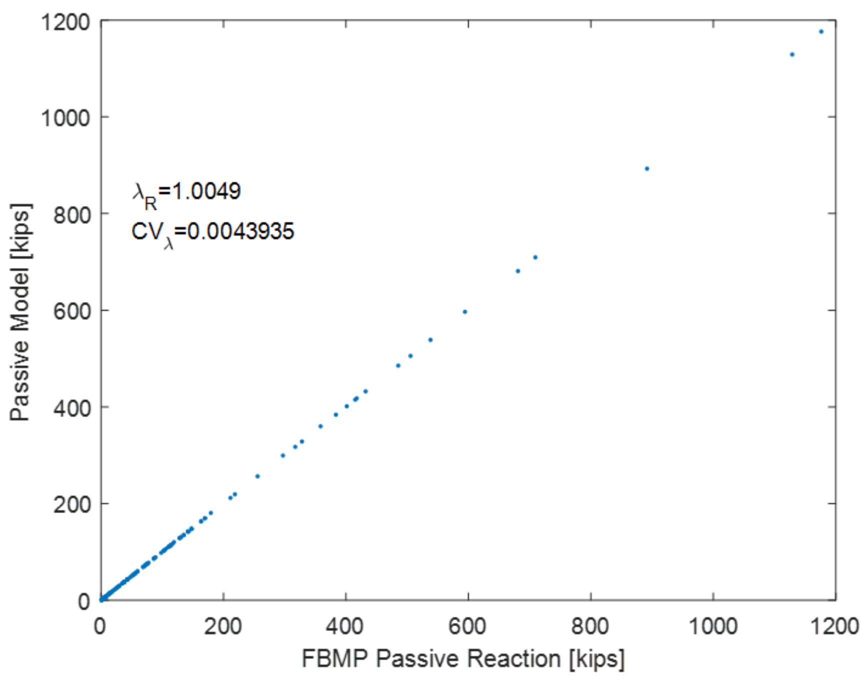

Figure 4-110 Sensitivity study FB-MultiPier (FBMP) passive reaction vs calculated passive reaction – prescribed load.

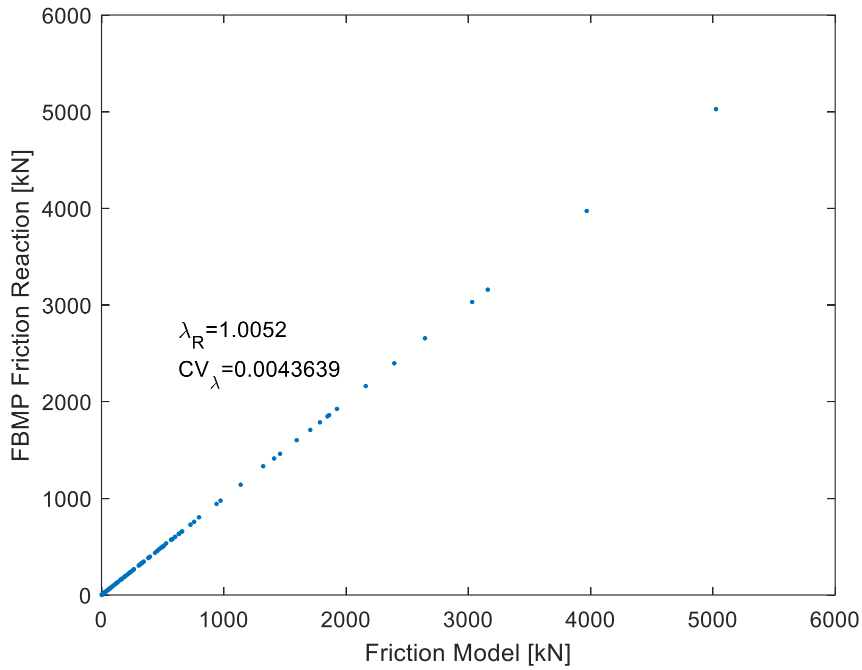

Figure 4-111 Sensitivity study FB-MultiPier (FBMP) passive reaction vs calculated passive reaction – prescribed displacement-SI.

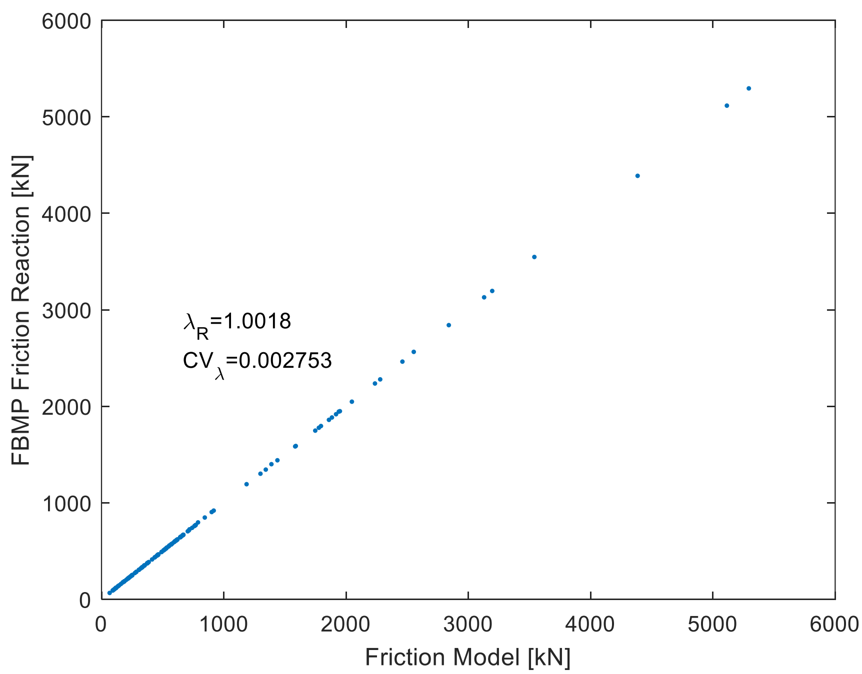

Figure 4-112 Sensitivity study FB-MultiPier (FBMP) passive reaction vs calculated passive reaction – prescribed load-SI.

Literature review found multiple sources of load test of footings in granular material. Summary of these test results and corresponding sources are shown in Table 4-3 . These C-PHI material properties and footing geometries were used to create FB-MultiPier models. These models then were specified with prescribed displacement per the displacement results recorded from each load test result. An example of the result of this analysis for Case 1, Table 4-3 , is shown in Figure 4-113, shows good agreement between FB-MultiPier passive reaction, calculated hyperbolic curve and the measured load test passive resistance. This analysis was conducted for each case and is summarized in Figure 4-114, where the λ_R is less than 1, FB-MultiPier is on average overpredicting. The analysis also resulted in a CV_λ of 0.17, which is due to incorporation of error associated with load testing, lab testing and passive hyperbolic model. For context, CV_λ has been quantified for measured load test vs FB-DEEP predictions for SPT, CPT and McVay method with values ranging from 0.24 to 0.30 (Davidson et al. 2023; Faraone 2014).

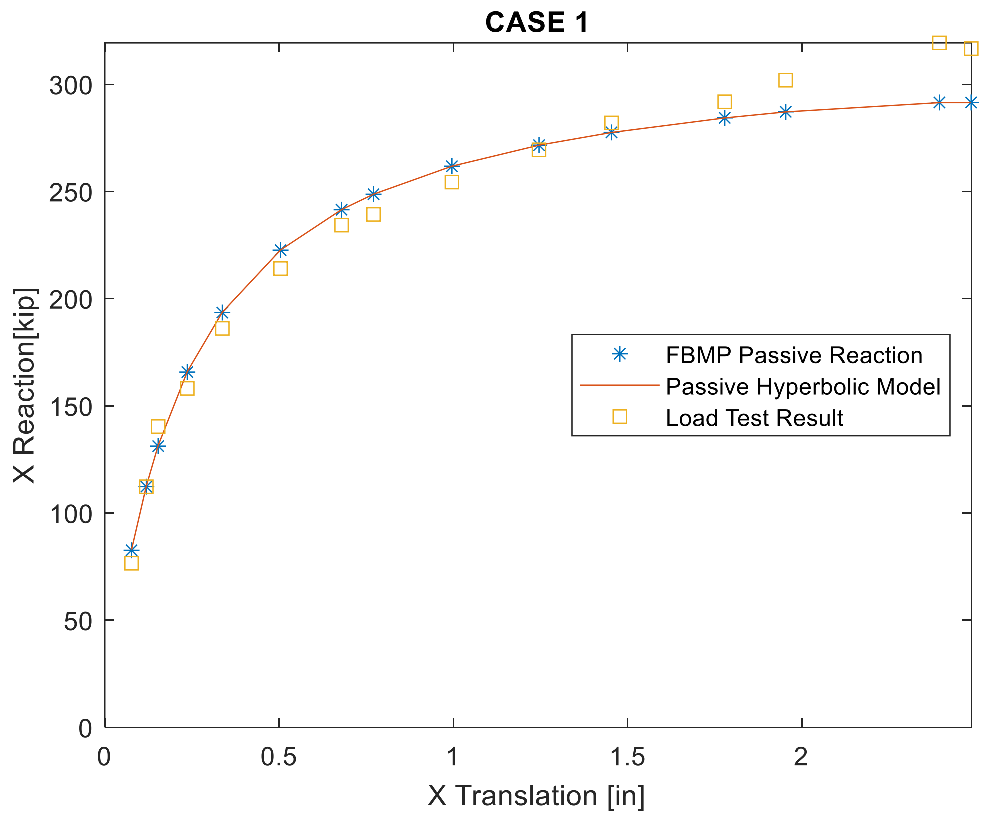

Figure 4-113 Load test and FB-MultiPier (FBMP) passive resistance curves.

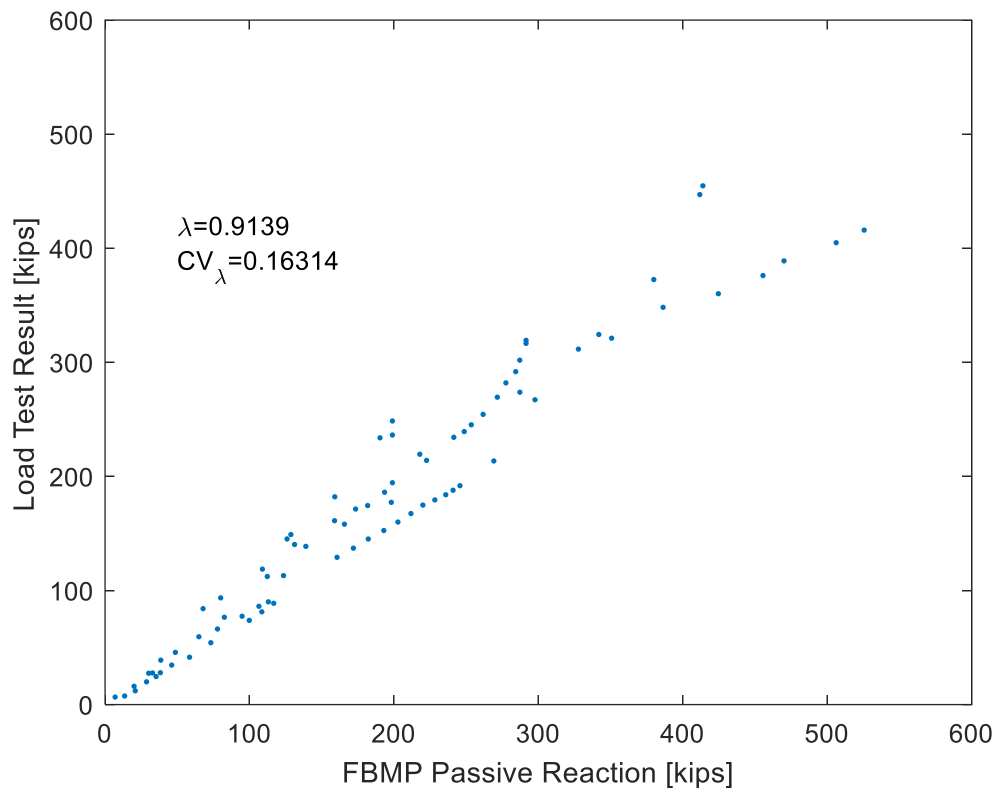

Figure 4-114 Load test vs FB-MultiPier (FBMP) passive reaction.

4.6.3 Passive FL Limestone Validation

To validate implementation of the FL Limestone model. The validation consisted of confirming passive resistance from FB-MultiPier UI dialogs and engine output (i.e., .out file). Additionally, the load settlement response determined by FB-MultiPier was compared with the hyperbolic calculations. The following cases were analyzed.

- Worked Example Appendix B
- Sensitivity Study – English Units
- Sensitivity Study – SI Units
- Plaxis Test Result

The first validation effort was conducted in same manner as previously discussed for the hyperbolic model. This consists of confirming the UI and Engine are calculating the correct passive resistance curve but now is based on inputs required for Equation 4-22, Equation 4-23, and Equation 4-25. For the FL Limestone model first validation effort is based on the worked example in Appendix B, confirming that the UI and Engine calculate the correct Pult, Pnet, Kmax and Rf values, along with its corresponding passive resistance curve. Presented in Table 4-15 and Table 4-16 is a comparison of the calculated hyperbolic parameters. The results of this comparison are shown in Figure 4-115. Passive FL Limestone Resistance Curve Comparison. Figure 4-115 and Figure 4-116, which shows excellent agreement in form of overlapping of the 3 separate passive curves.

Table 4-15 FL limestone model work example values (FBMP = FB-MultiPier).

Value	Worked Example	FBMP UI
k_{max} [kips/in]	2768.4	2767.8293
R_f [-]	0.89301	0.8931
P_{ult} [kips]	888.545	887.2950
P_{net} [kips]	888.545	887.2950

Table 4-16 FL Limestone Model Work Example Values-SI (FBMP = FB-MultiPier).

Value	Worked Example	FBMP UI
k_{max} [kN/m]	484825.3947	484905.1438
R_f [-]	0.8929	0.8931
P_{ult} [kN]	3955.7229	3948.0911
P_{net} [kN]	3955.7229	3948.0911

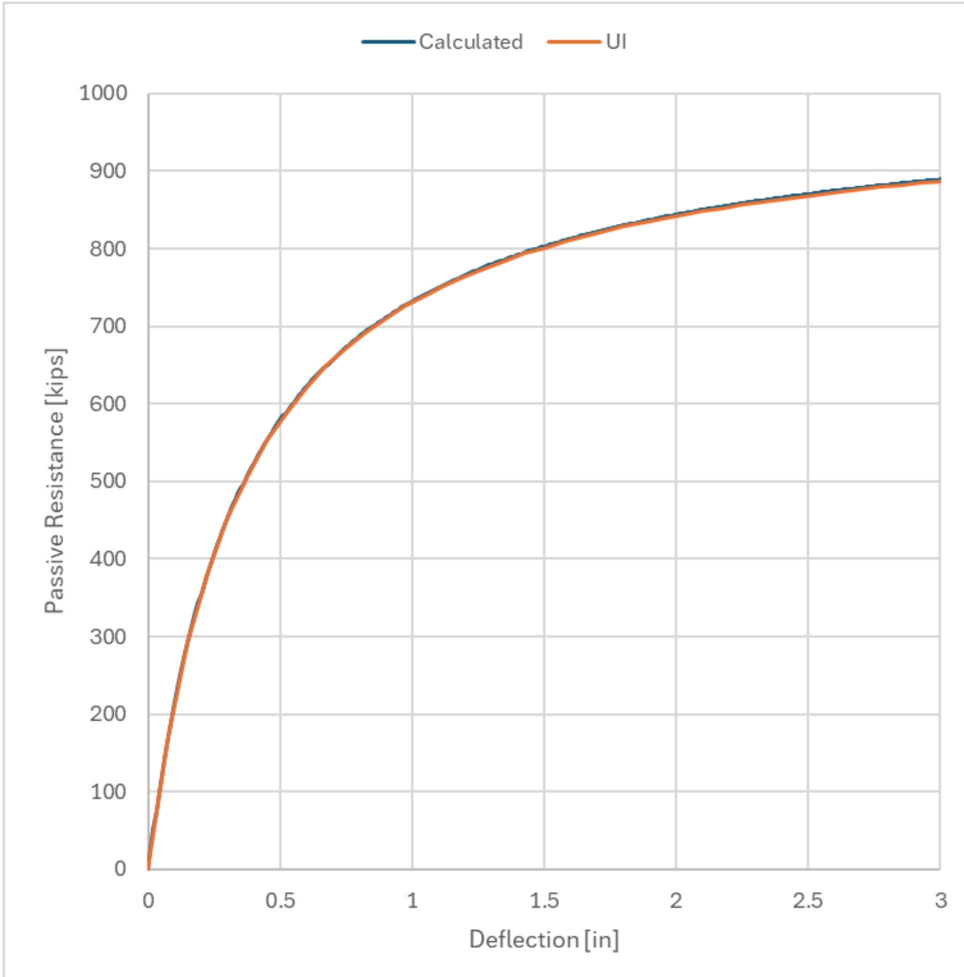

Figure 4-115 Passive FL limestone resistance curve comparison.

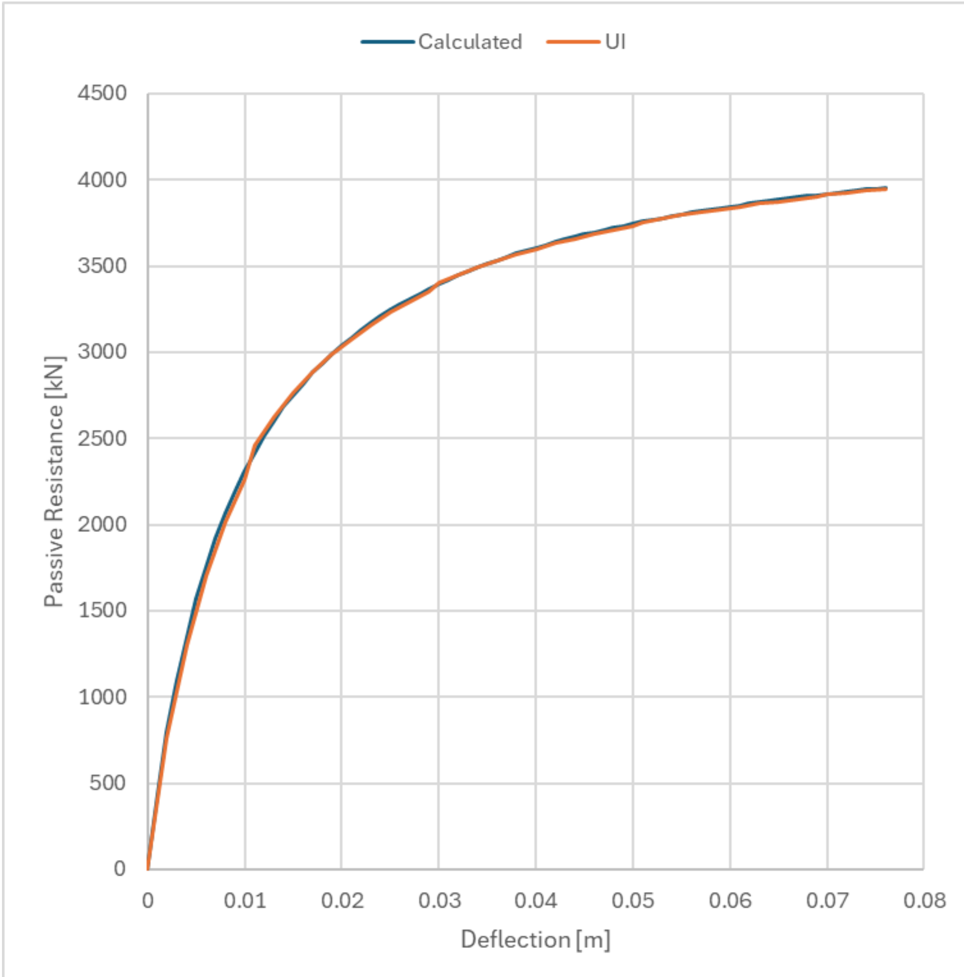

Figure 4-116 Passive FL limestone curve comparison SI units.

Continuing in the validation process in the same manner, prescribed displacements and loads, Table 4-9 and Table 4-10 , were used in FB-MultiPier model using parameters from the worked example in appendix B for both English and SI units. Results from this analysis are shown in Figure 4-105 through Figure 4-108, which show excellent agreement.

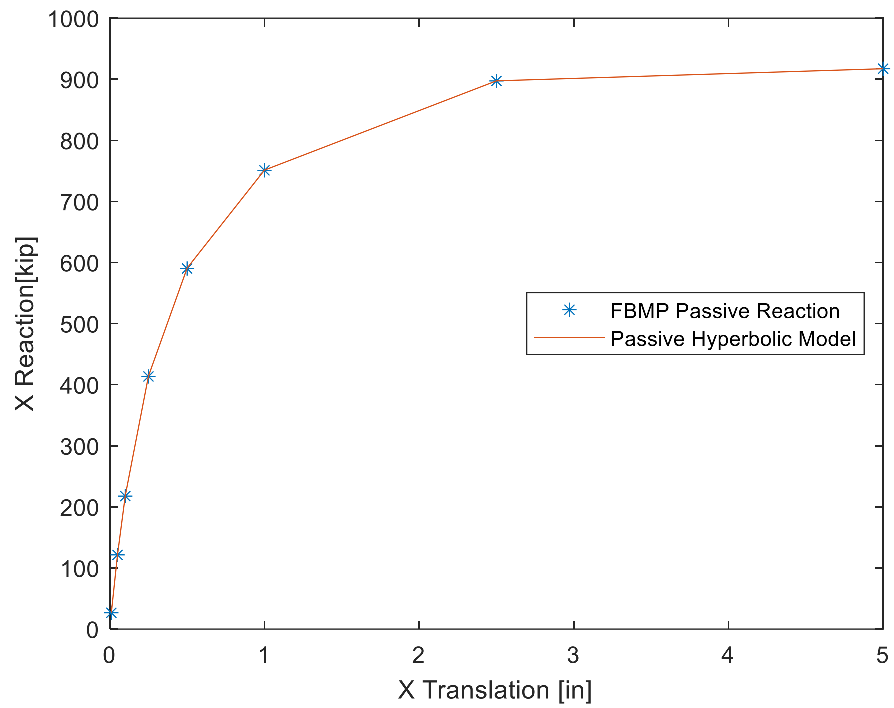

Figure 4-117 Passive resistance FL limestone model – prescribed displacement.

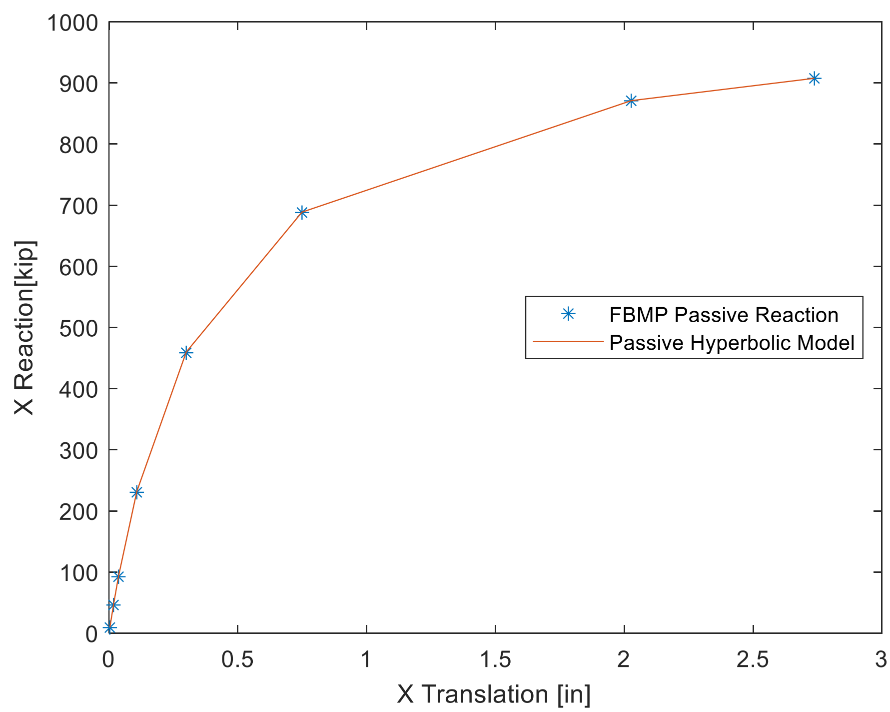

Figure 4-118 Passive resistance FL limestone model – prescribed load.

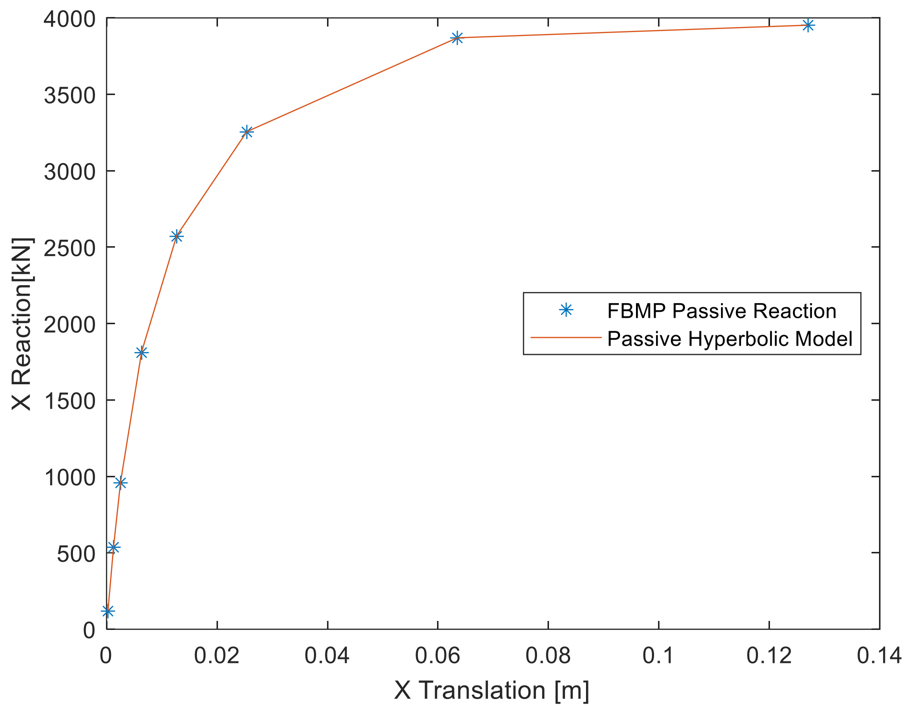

Figure 4-119 Passive resistance FL limestone model – prescribed displacement SI.

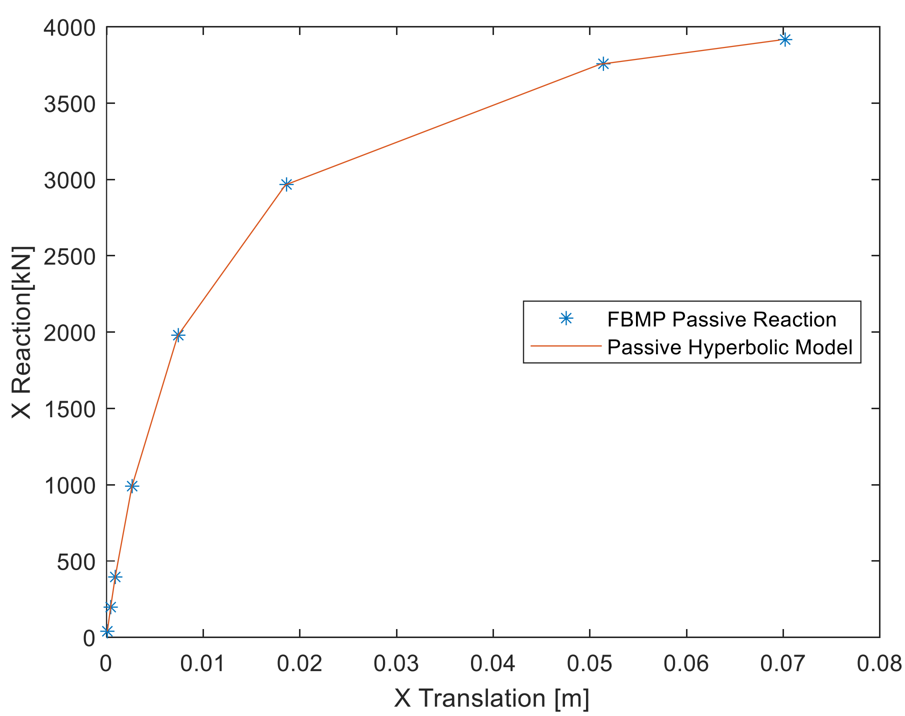

Figure 4-120 Passive resistance FL limestone model – prescribed load SI.

Also added to the Passive FL Limestone model is the feature to calculate the mass extension strength envelope. In the worked example, Appendix B, example calculations for Miami Limestone formation are provided, which calculate the strength envelope parameters for both intact and mass compression and extension spaces. Table 4-17 provides a comparison between the worked example's results to FB-MultiPier (FBMP) UI calculations for the Miami formation. As it can be seen in the table, FB-MultiPier agrees with the work examples calculation.

Table 4-17 Worked example appendix b rock strength envelope.

Parameter	Symbol	Worked Example	FBMP UI
Extension Reduction Parameters	R_a	0.95	0.95
	R_α	0.75	0.75
	R_β	0.75	0.75
	R_{Pp}	0.8	0.8
	R_E	0.9	0.9
Compression Intact Properties	c_{ic}, psi	58.9	58.9
	φ_{ic}, °	44.2	44.2
	ω_{ic}, °	0.8	0.8
	E_{ic}, ksi	36.6	36.59
Compression Mass Properties	c_{mc}, psi	40.7	40.68
	φ_{mc}, °	33.9	33.92
	ω_{mc}, °	0.6	0.64
	E_{mc}, ksi	20.7	20.71
Extension Intact Properties	φ_{ie}, °	29.4	29.44
	c_{ie}, psi	46.0	46.03
	ω_{ie}, °	0.6	0.6
	E_{ie}, ksi	32.9	32.93
Extension Mass Properties	c_{me}, psi	34.9	34.88
	φ_{me}, °	23.2	23.15
	ω_{me}, °	0.5	0.48
	E_{me}, ksi	18.6	18.64

The next validation effort was to conduct a sensitivity study where input parameters for the FL Limestone model are perturbated, to ensure FB-MultiPier is using each one appropriately. Input parameters for sensitivity study are shown in Table 4-13.

Table 4-18 FL limestone model sensitivity study.

Cases	L [ft]	B [ft]	t [ft]	Dw [ft]	DF [ft]	C [psf]	Phi	Gamma [pcf]	v	δ (°)	Ei [psi]	Dmax [ft]	q [psf]
1	20	20	5	1000.0	5.0	3972.96	23.42	100	0.25	5.00	13390.00	0.30	0
2	20	20	5	1000.0	5.0	3972.96	25.00	100	0.25	5.00	13390.00	0.30	0
3	20	20	5	1000.0	5.0	1000.00	30.00	100	0.25	5.00	13390.00	0.30	0
4	20	20	8	1000.0	8.0	3972.96	30.00	100	0.25	5.00	13390.00	0.30	0
5	15	20	5	1000.0	5.0	3972.96	30.00	100	0.25	5.00	13390.00	0.30	0
6	20	15	5	1000.0	5.0	3972.96	30.00	100	0.25	5.00	13390.00	0.30	0
7	20	20	5	1000.0	5.0	3972.96	30.00	115	0.25	5.00	13390.00	0.30	0
8	20	20	5	1000.0	5.0	3972.96	30.00	100	0.15	5.00	13390.00	0.30	0
9	20	20	5	1000.0	5.0	3972.96	30.00	100	0.25	10.00	13390.00	0.30	0
10	20	20	5	1000.0	5.0	3972.96	30.00	100	0.25	5.00	13390.00	0.60	0
11	20	20	5	1000.0	5.0	3972.96	30.00	115	0.25	5.00	5000.00	0.30	0
12	20	20	5	0.0	5.0	3972.96	30.00	100	0.25	5.00	13390.00	0.30	0
13	20	20	5	2.5	5.0	3972.96	30.00	100	0.25	5.00	13390.00	0.30	0
14	20	20	5	1000.0	2.5	3972.96	30.00	100	0.25	5.00	13390.00	0.30	0
15	20	20	5	1000.0	10.0	3972.96	30.00	100	0.25	5.00	13390.00	0.30	0
16	20	20	5	1000.0	5.0	3972.96	30.00	100	0.25	5.00	13390.00	0.30	500
17	20	20	5	1000.0	10.0	3972.96	30.00	100	0.25	5.00	13390.00	0.30	500
18	20	20	5	1000.0	5.0	3972.96	23.42	100	0.25	5.00	13390.00	0.30	0
19	20	20	5	1000.0	5.0	5284.8	21.54	100	0.25	5.00	12660	0.30	0
20	20	20	5	1000.0	5.0	2936.16	23.75	100	0.25	5.00	5850	0.30	0
21	20	20	5	1000.0	5.0	6946.56	23.92	100	0.25	5.00	33170	0.30	0
22	20	20	5	1000.0	5.0	2321.28	22.02	100	0.25	5.00	9440	0.30	0
23	20	20	5	1000.0	5.0	3132	20.74	100	0.25	5.00	19140	0.30	0

Table 4-19 Passive FL limestone sensitivity study results.

Analysis Type	λ_R	CV_λ
Prescribed Displacement	1.0059	0.0057502
Prescribed Load	1.0074	0.0064704
Prescribed Displacement-SI	1.0058	0.0057172
Prescribed Load - SI	1.0075	0.0066023

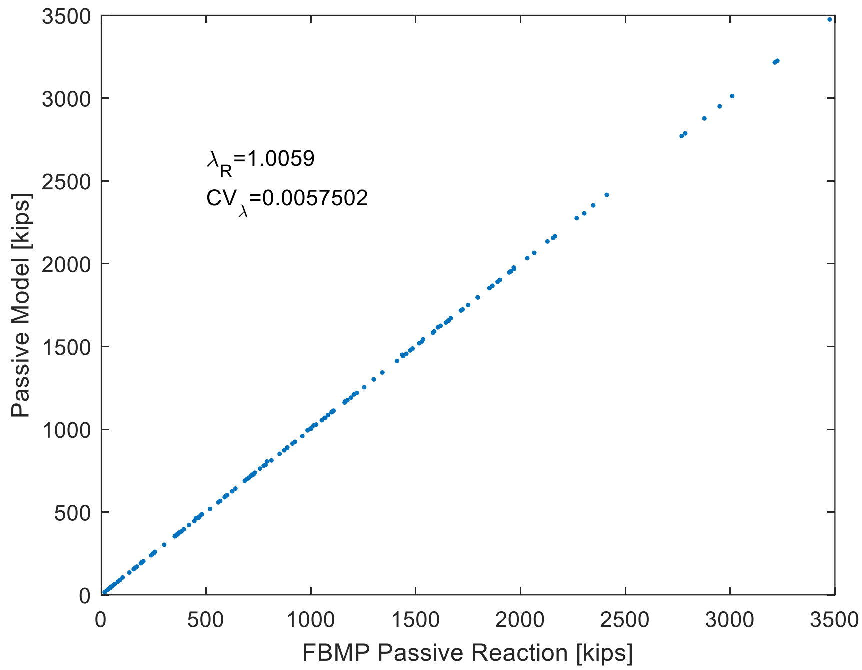

Figure 4-121 FL limestone sensitivity study FB-MultiPier passive reaction vs calculated passive reaction prescribed displacement.

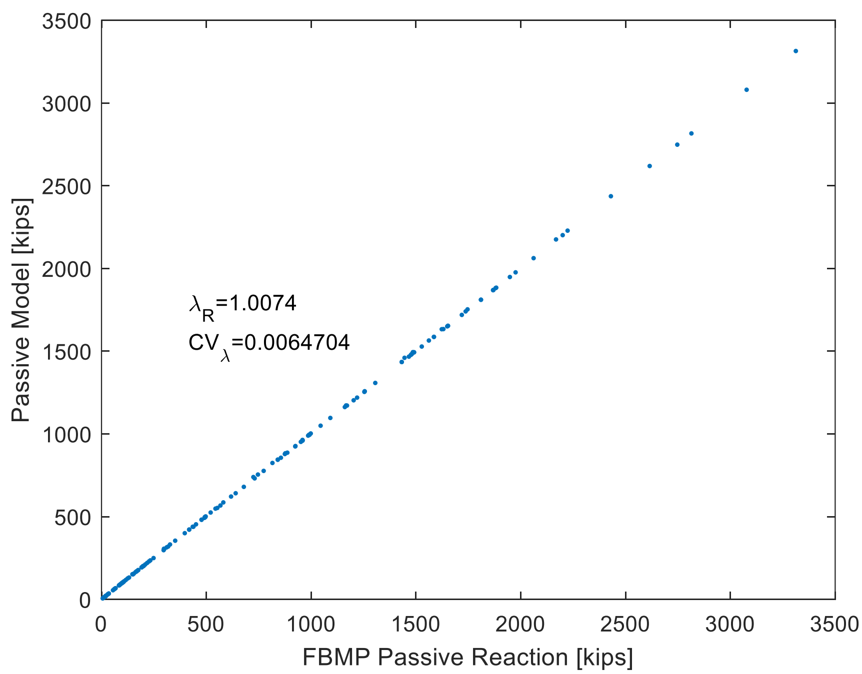

Figure 4-122 FL limestone sensitivity study FB-MultiPier passive reaction vs calculated passive reaction prescribed load.

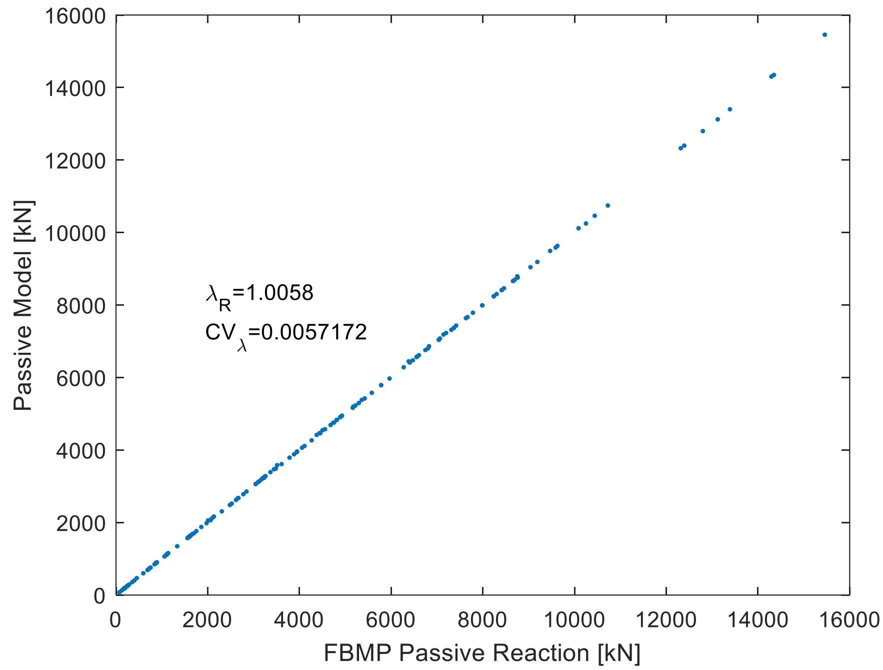

Figure 4-123 FL limestone sensitivity study FB-MultiPier passive reaction vs calculated passive reaction prescribed displacement-SI.

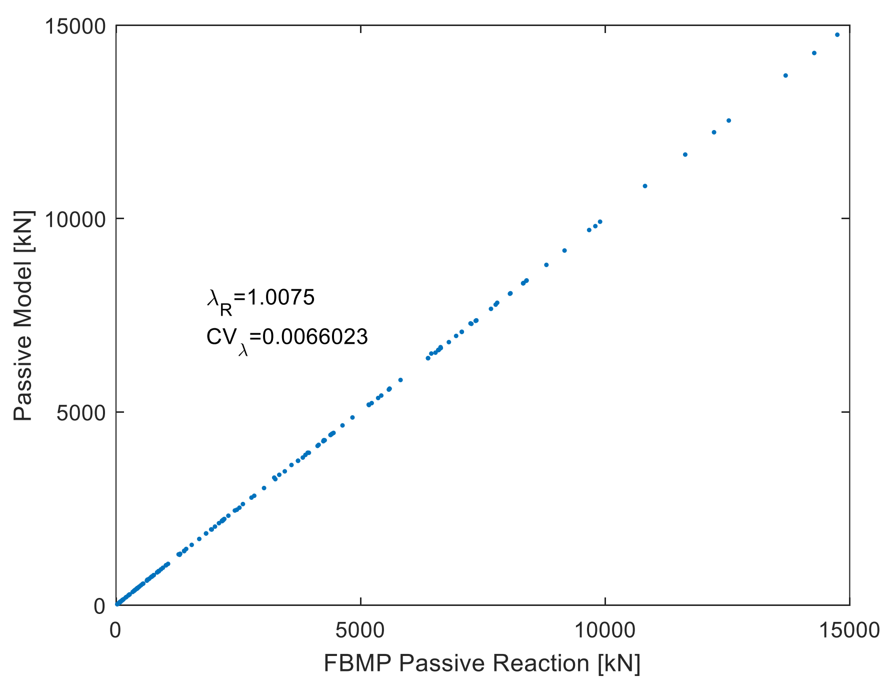

Figure 4-124 FL limestone sensitivity study FB-MultiPier passive reaction vs calculated passive reaction prescribed load-SI.

To confirm accuracy of FB-MultiPier FL Limestone model, results from the Fort Thompson Plaxis analysis were used for comparison. Table 4-20 summarized 204 material properties and footing geometries were used to create FB-MultiPier models, which used a prescribed displacement per the Plaxis models. An example of the result of this analysis for Case 1, Table 4-20 , is shown in Figure 4-125, where good agreement can be seen between the FB-MultiPier Passive reaction, the calculated hyperbolic model and the Plaxis result. This analysis was conducted for each case and is summarized in Figure 4-126, where the λ_R is approximately 1, FB-MultiPier is on average slightly overpredicting. The analysis also resulted in a CV_λ of 0.07, which is more accurate when compared to granular load test prediction.

Table 4-20 Plaxis Fort Thompson test cases.

Cases	L [ft]	B [ft]	t [ft]	Dw [ft]	DF [ft]	C [psf]	Phi	Gamma [pcf]	v	δ (°)	Ei [psi]	Dmax [ft]	q [psf]
1	5	5	5	1000	5	828	18.52	90	0.10	12.35	14280	0.62	0
2	5	5	5	1000	5	1014	19.24	95	0.10	12.83	44240	0.91	0
3	5	5	5	1000	5	1241	19.93	100	0.10	13.29	74200	0.93	0
4	5	5	5	1000	5	1518	20.60	105	0.10	13.73	104160	0.80	0
5	5	5	5	1000	5	1856	21.25	110	0.10	14.17	134120	0.99	0
6	5	5	5	1000	5	2267	21.87	115	0.10	14.58	164080	0.69	0
7	5	5	5	1000	5	2768	22.47	120	0.10	14.98	194040	0.70	0

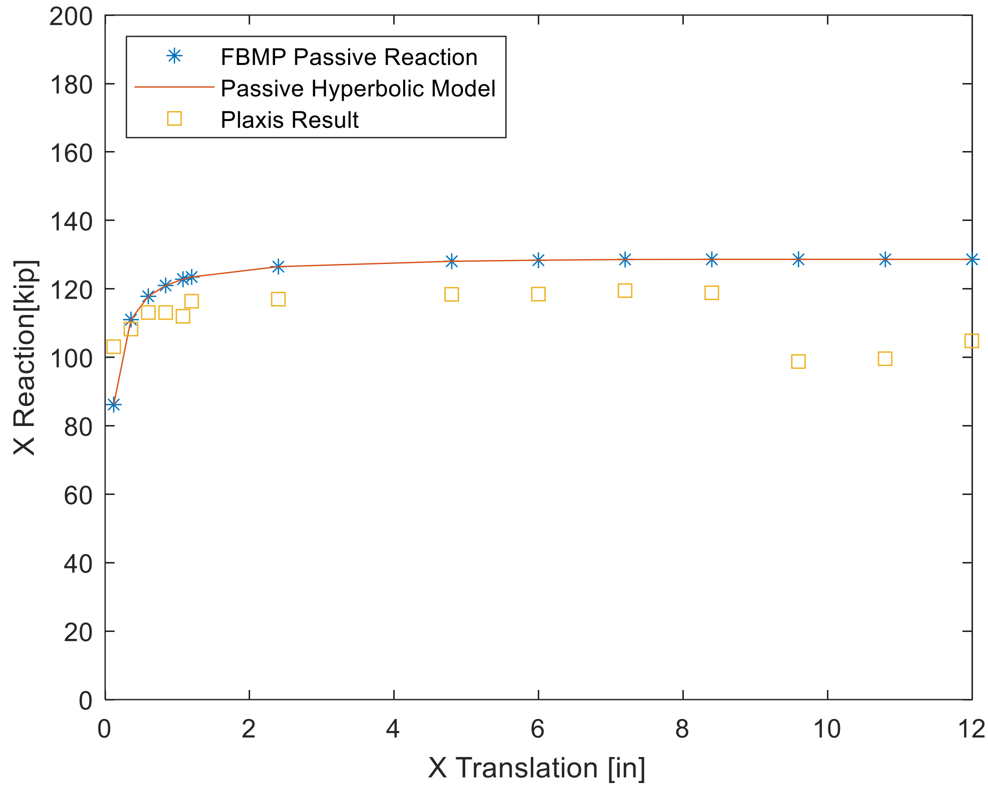

Figure 4-125 Plaxis Fort Thompson and FB-MultiPier (FBMP) passive resistance curves.

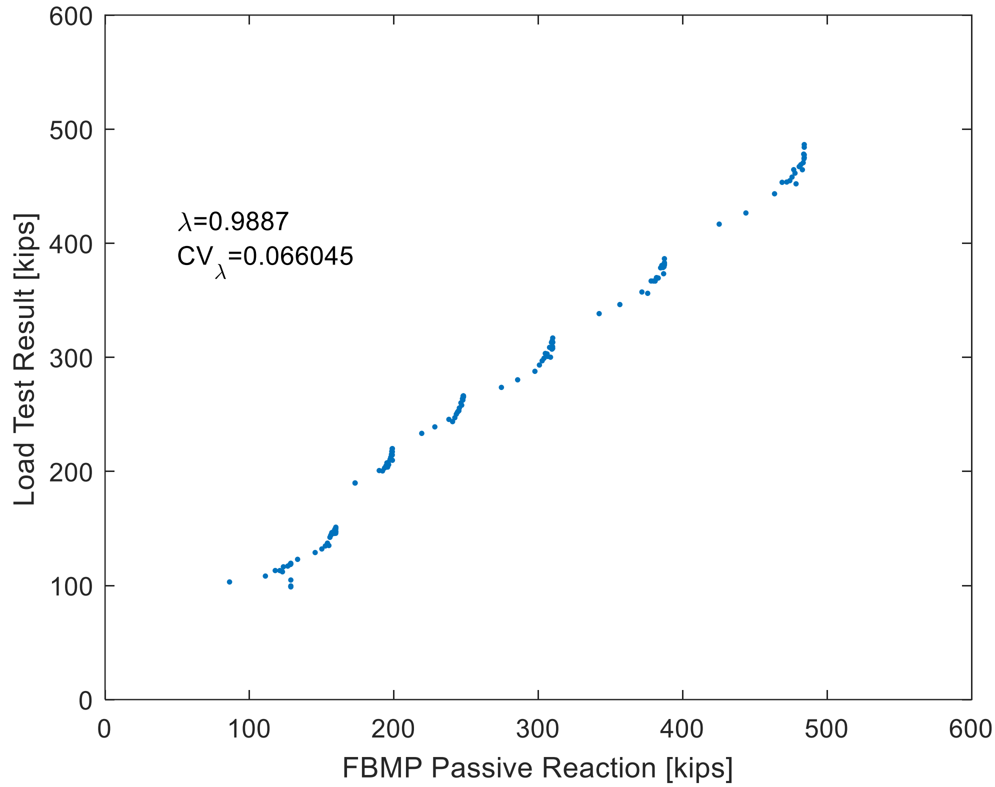

Figure 4-126 Plaxis Fort Thompson vs Fb-MultiPier (FBMP) passive reaction.

4.6.4 Friction Hyperbolic (Coulomb) Model Validation

To validate implementation of the Hyperbolic (Coulomb) model. The validation consisted of confirming passive resistance from FB-MultiPier UI dialogs and engine output (i.e., .out file). Additionally, the load settlement response determined by FB-MultiPier was compared with the hyperbolic calculations. The following cases were analyzed.

- Worked Example Appendix C
- Sensitivity Study – English Units
- Sensitivity Study – SI Units

The first validation effort was conducted in same manner as previously discussed for the hyperbolic model. This consists of confirming the UI and Engine calculation the correct frictional resistance curve but now is based on inputs required for Equation 4-11. For the Hyperbolic (Coulomb) model first validation effort is based on the worked example in Appendix C and was conducted in the same manner as described in the previous Hyperbolic Model validation. First it was confirmed that the UI and Engine calculate the correct passive resistance curve. The results of this comparison are shown in Figure 4-127 and Figure 4-128, which shows excellent agreement in form of overlapping of the 2 separate friction curves. The curves presented in these figures are based on a normal loading from the footing self-weight only. It should be noted that no frictional resistance curve is shown from the engine output file, since the frictional resistance is a function of loading conditions in conjunction with self-weight of the structure.

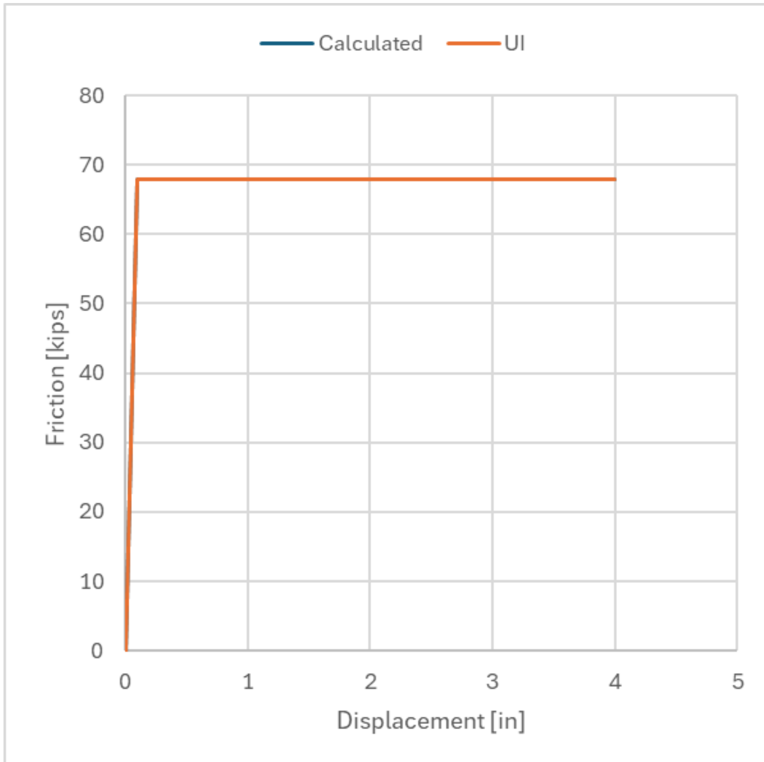

Figure 4-127 Friction hyperbolic (Coulomb) resistance curve comparison.

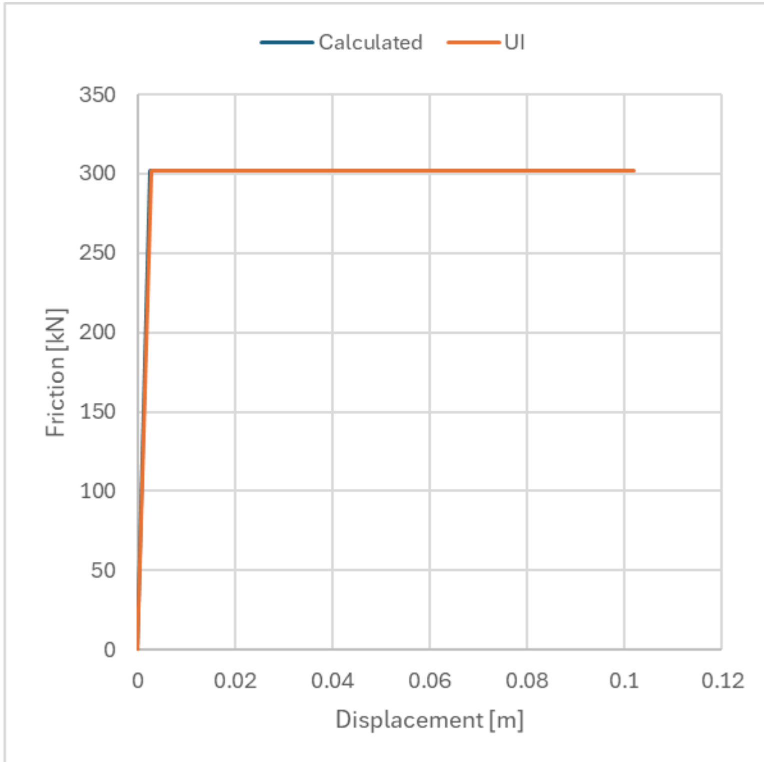

Figure 4-128 Friction hyperbolic (Coulomb) resistance curve comparison SI units.

Continuing in the validation process in the same manner, prescribed displacements and loads, Table 4-9 and Table 4-21 , were used in FB-MultiPier model using parameters from the worked example in appendix C for both English and SI units. Note, loading for friction validation is based on a percentage of ultimate frictional resistance based Coulombic friction properties and footing weight specified in the worked example, Appendix C. Results from this analysis are shown in Figure 4-129 through Figure 4-132, which show excellent agreement. It should be noted that for the prescribed force cases, Figure 4-130 and Figure 4-132, the displacement is relatively small, which is due to the prescribed loading being less the ultimate frictional resistance (i.e., 99% of F_{ult}).

Table 4-21 Friction loading increments.

Load Case	Load Percentage of F_{ult} [%]
1	1
2	5
3	10
4	25
5	50
6	75
7	95
8	99

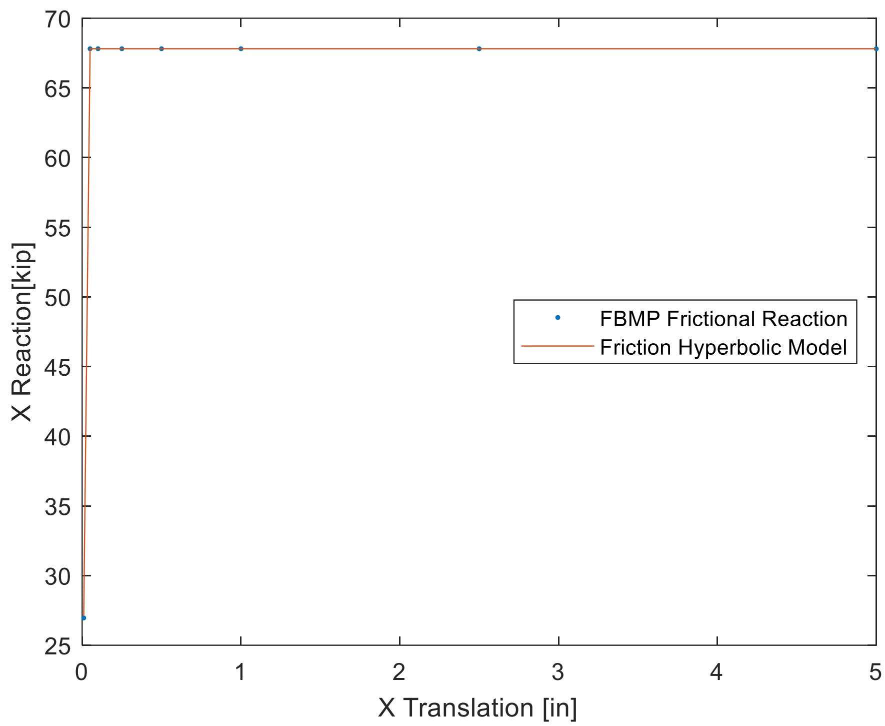

Figure 4-129 Friction hyperbolic (Coulomb) resistance – prescribed displacement worked example appendix c.

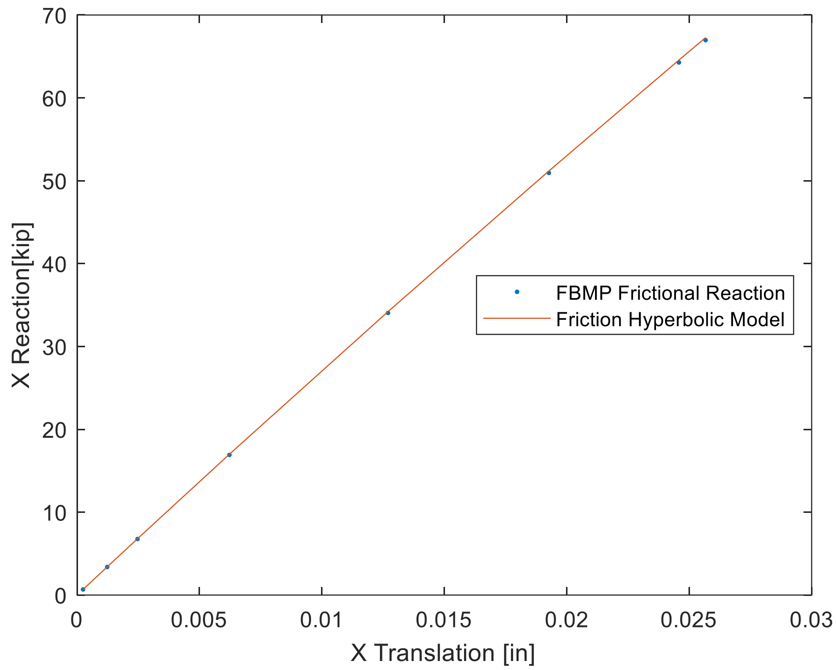

Figure 4-130 Friction hyperbolic (Coulomb) resistance – prescribed load worked example appendix c.

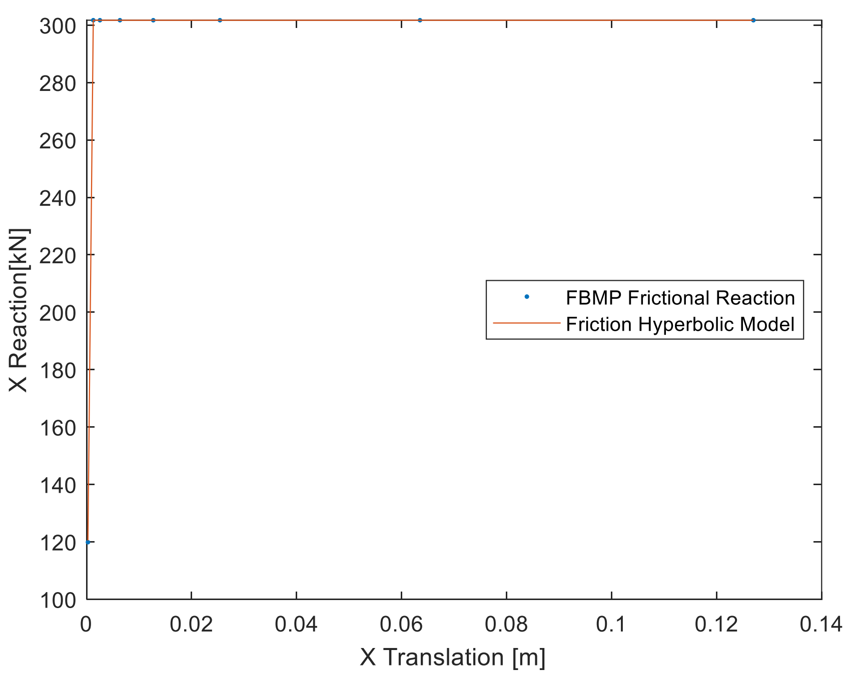

Figure 4-131 Friction hyperbolic (Coulomb) resistance – prescribed displacement SI worked example appendix c.

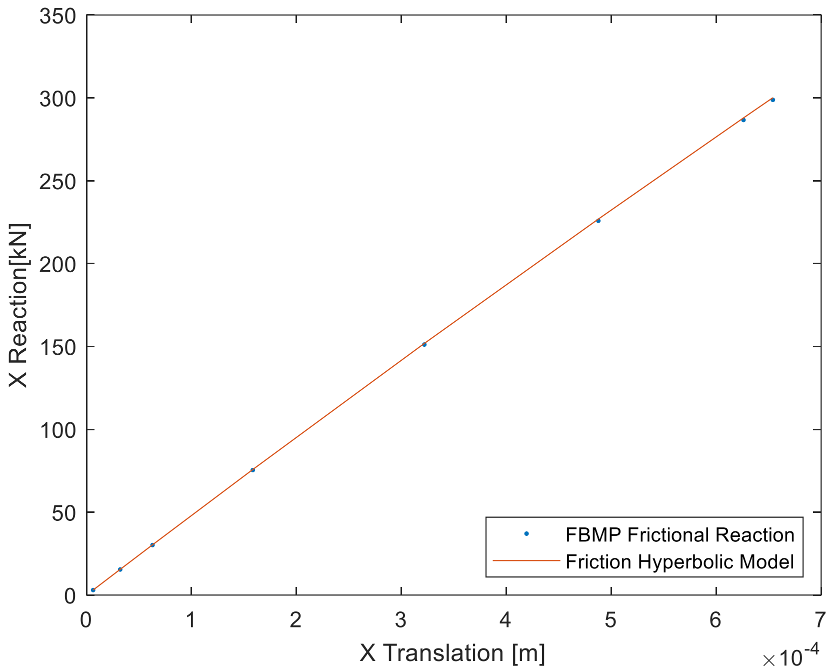

Figure 4-132 Friction hyperbolic (Coulomb) resistance – prescribed load SI worked example appendix c.

The next validation effort was to conduct a sensitivity study where input parameters for the Hyperbolic (Coulomb) model are perturbated, to ensure FB-MultiPier is using each one appropriately. Input parameters for sensitivity study are shown in Table 4-22 . The result of this analysis was shown in Table 4-23 , where for all loading conditions and unit types a $\lambda_R$value of approximately 1 (no significant over or under estimation) from the FB-MultiPier analysis. Additionally, the very low CV_λ confirm no scatter or inherent error in the FB-MultiPier analysis.

Table 4-22 Friction hyperbolic (Coulomb) sensitivity study.

Cases	L [ft]	B [ft]	t [ft]	k_{max}	R_f	P_{ult}	δ (°)	C [psf]	Adhesion	D_w [ft]
1	20	20	5	3000	0.95	500	5	0	0.00	1000
2	20	20	5	3000	0.95	500	10	0	0.00	1000
3	20	20	5	3000	0.95	500	15	0	0.00	1000
4	20	20	5	3000	0.95	500	20	0	0.00	1000
5	20	20	5	3000	0.95	500	0	100	0.10	1000
6	20	20	5	3000	0.95	500	0	500	0.10	1000
7	20	20	5	3000	0.95	500	0	1000	0.10	1000
8	20	20	5	3000	0.95	500	0	2000	0.10	1000
9	20	20	5	3000	0.95	500	0	500	0.25	1000
10	20	20	5	3000	0.95	500	0	500	0.50	1000
11	20	20	5	3000	0.95	500	0	500	0.75	1000
12	20	20	5	3000	0.95	500	0	500	1.00	1000
13	20	20	5	3000	0.95	500	5	100	0.25	1000
14	20	20	5	3000	0.95	500	10	500	0.50	1000
15	20	20	5	3000	0.95	500	15	1000	0.75	1000
16	20	20	5	3000	0.95	500	20	2000	1.00	1000
17	20	20	5	1500	0.95	500	15	1000	0.75	1000
18	20	20	5	3000	0.85	500	15	1000	0.75	1000
19	20	20	5	3000	0.95	2000	15	1000	0.75	1000
20	20	15	5	3000	0.95	500	15	1000	0.75	1000
21	20	20	8	3000	0.95	500	15	1000	0.75	1000
22	20	20	5	3000	0.95	500	15	1000	0.75	0.0

Table 4-23 Friction Hyperbolic (Coulomb) Sensitivity Study Results.

Analysis Type	λ_R	CV_λ
Prescribed Displacement	1.0009	0.0019202
Prescribed Load	1.0037	0.0014754
Prescribed Displacement-SI	1.0009	0.0019639
Prescribed Load - SI	1.0041	0.0009921

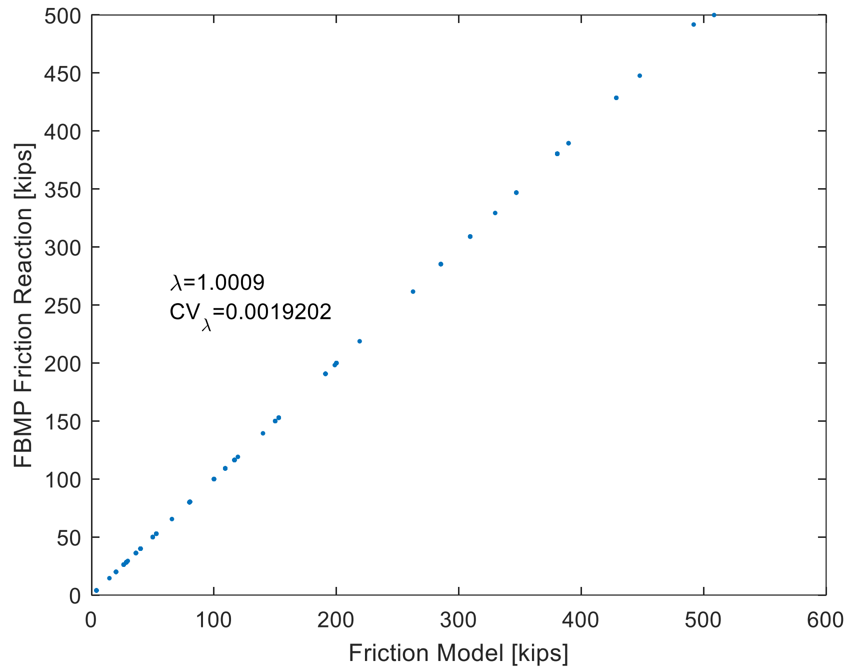

Figure 4-133 Sensitivity study FB-MultiPier (FBMP) friction reaction vs calculated friction reaction – prescribed displacement.

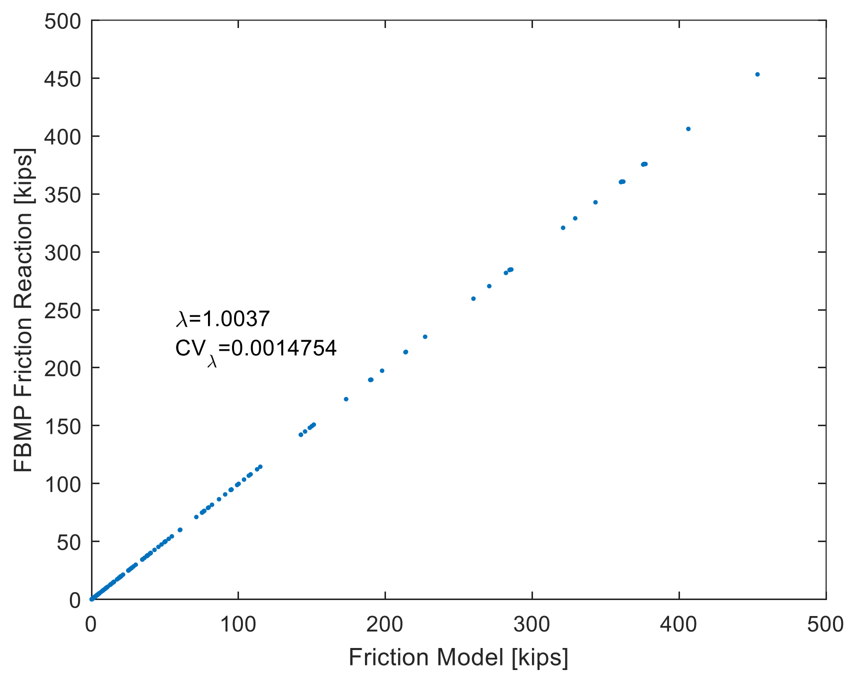

Figure 4-134 Sensitivity study FB-MultiPier (FBMP) friction reaction vs calculated friction reaction – prescribed load.

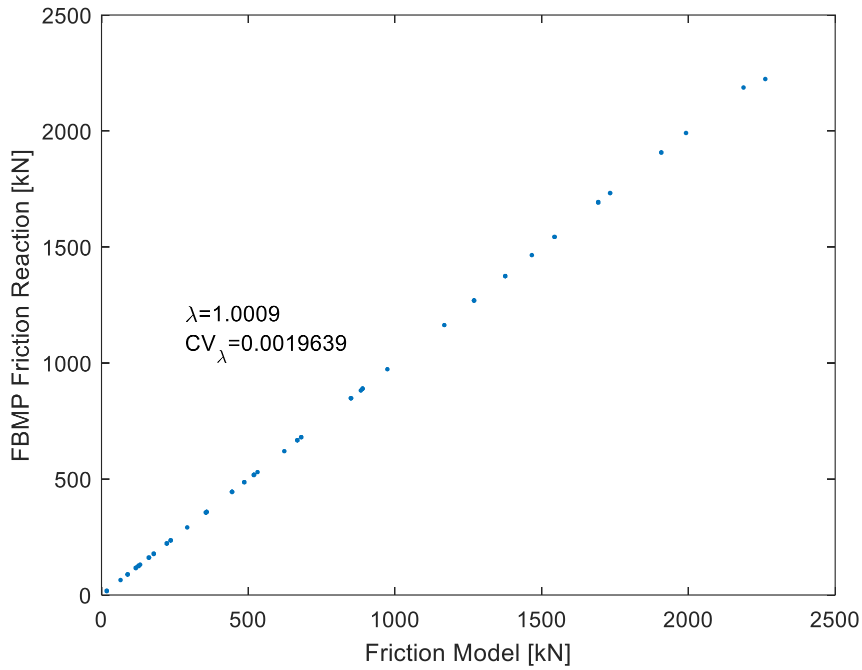

Figure 4-135 Sensitivity study FB-MultiPier (FBMP) friction reaction vs calculated friction reaction – prescribed displacement - SI.

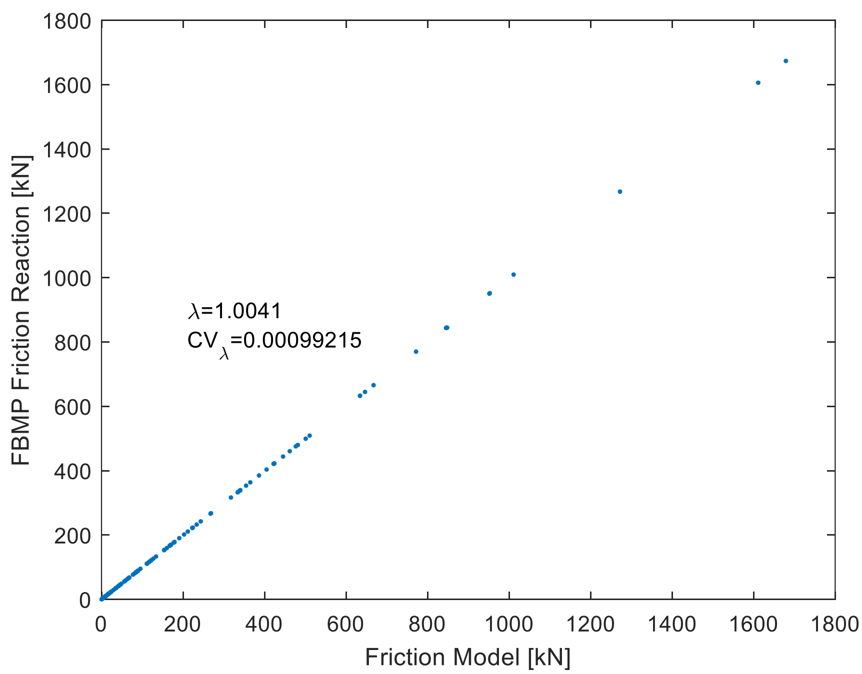

Figure 4-136 Sensitivity study FB-MultiPier (FBMP) friction reaction vs calculated friction reaction – prescribed load - SI.

4.7 Validation and Stress Comparisons in the Analysis Output Oblique Loading

To ensure the accuracy of the coding implemented in the FB-MultiPier UI and engine, a comprehensive validation process was conducted using several distinct sources. The validation sets were selected to include, multiple examples with varying ranges of variable inputs, and FEA results. Two specific sources were employed to validate the implementation: a MATLAB code utilized for in-depth sensitivity analysis and PLAXIS analysis. Together, these methods form a robust assessment of the validations of the FB-MultiPier UI and engine.

4.7.1 Passive Hyperbolic Model Validation

For this project, the first validation problems were a set of problems for the passive hyperbolic model. The validation consisted of confirming passive resistance from engine output (i.e., .out file). Additionally, the load settlement response determined by FB-MultiPier was compared with the hyperbolic hand calculations of the models using MATLAB. The following cases were analyzed.

- 30 Degree Orientation
- 360 Degree Prescribed Displacement
- 360 Degree Prescribed Displacement
- Sensitivity Analysis

The first validation effort was to confirm that the Engine calculates the correct passive resistance reduction, Equation 4-34 and Equation 4-35. Compare the nodal displacement and spring forces from FB-MultiPier finite element analysis to calculated passive resistance curve, Matlab Code. For each case a shallow foundation model was created that matches the prescribed geometry (i.e., length, width, etc.) and modulus. A column was located at the center of the footing. The column is connected to the foundation using rigid connector elements which spans column center to edge of column footprint, to prevent unrealistic stress concentration. Material properties and geometry for this analysis are specified in Table 4-13 , Case 1.

Two loading validations where conducted, first using the previously described model used with a loading of a prescribed resultant horizontal displacement, Figure 4-97, with increments shown in Table 4-9 . These resultant prescribed displacements were then oriented in 15 degree increments shown in Table 4-25, and specified in their corresponding X and Y displacement components. The advantage of using prescribed displacement aids in the FB-MultiPier ability to converge on a solution for loading conditions that reach near ultimate resistance portion of the hyperbolic curve. The model is then run and results from the model corresponding to displacement of the center of the footing in both the X and Y directions along with their corresponding X and Y passive reactions. These FB-MultiPier results are then plot along with calculated hyperbolic curve, Figure 4-98, which shows excellent agreement. It is noted that reactions for the X and Y directions are of different magnitudes, due to oblique angle being oriented in the 30 degree direction. This results in more passive reaction in the X direction as compared to the Y direction.

Results from the other oblique angles, Table 4-25, are shown in Figure 4-139 for X and Y displacements and Figure 4-140 for passive reactions in the X and Y directions. As expected Figure 4-139 shows a radial pattern of displacements, the resultant resistance pattern, Figure 4-140, is also circular, which is expected based on the derivation of Equation 4-34 and Equation 4-35.

To confirm the 360 degree pattern presented above is correct, results of this analysis are shown in Figure 4-141 and Figure 4-142 where calculated resistance values, X and Y direction respectively, are plotted vs their corresponding resultant passive resistance from a FB-MultiPier engine analysis. The points fall closely along a slope of 1. This confirmed with a bias analysis, Equation 4-40 and Equation 4-41, where the ratio of the passive calculated resistance, mi, to FB-MultiPier passive reaction, pi. For this 360 degree study, a $\lambda_R$value (FB-MultiPier /model) of approximately 1 (no significant over or under estimation) from the FB-MultiPier analysis. Additionally, the very low CV_λ confirm no scatter or inherent error in the FB-MultiPier analysis.

$$\lambda_R = \frac{1}{n}\sum_{i=1}^{n} \lambda_i = \frac{1}{n}\sum_{i=1}^{n} \frac{m_i}{p_i} \qquad \text{Equation 4-40}$$

$$CV_\lambda = \frac{\sqrt{\frac{1}{n}\sum_{i=1}^{n}(\lambda_i - \lambda_R)^2}}{\lambda_R} \qquad \text{Equation 4-41}$$

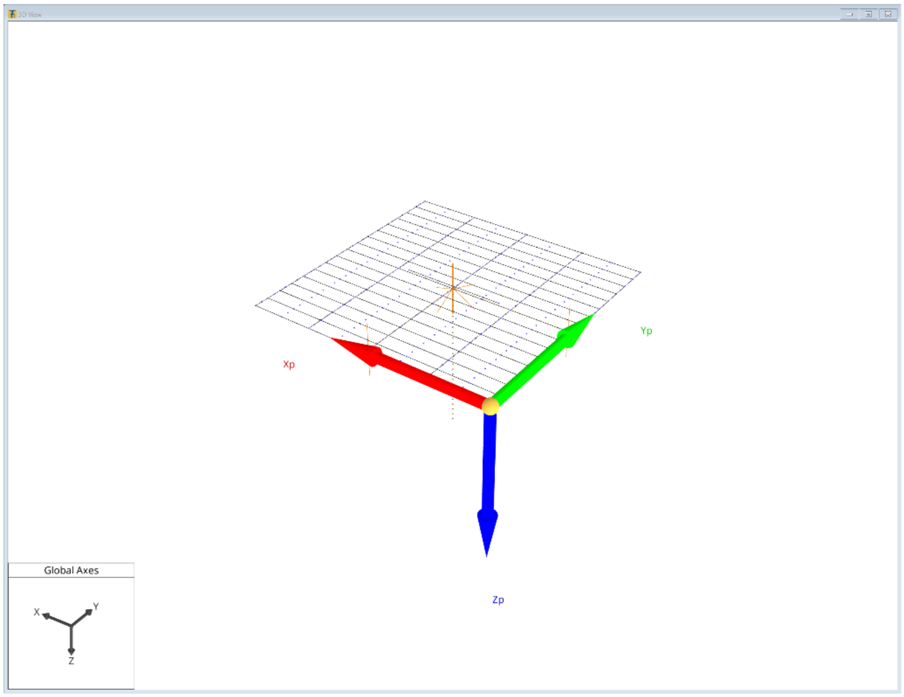

Figure 4-137 FB-MultiPier shallow foundation model prescribed displacement.

Table 4-24 Prescribed resultant displacement.

Load Case	Prescribed Displacement [in]
1	0.01
2	0.05
3	0.10
4	0.25
5	0.50
6	1.00
7	2.50
8	5.00

Table 4-25 Prescribed resultant direction.

Load Case	Direction [Degrees]
1	0
2	15
3	30
4	45
5	60
6	75
7	90
8	105
9	120
10	135
11	150
12	165
13	180
14	195
15	210
16	225
17	240
18	255
19	270
20	285
21	300
22	315
23	330
24	345

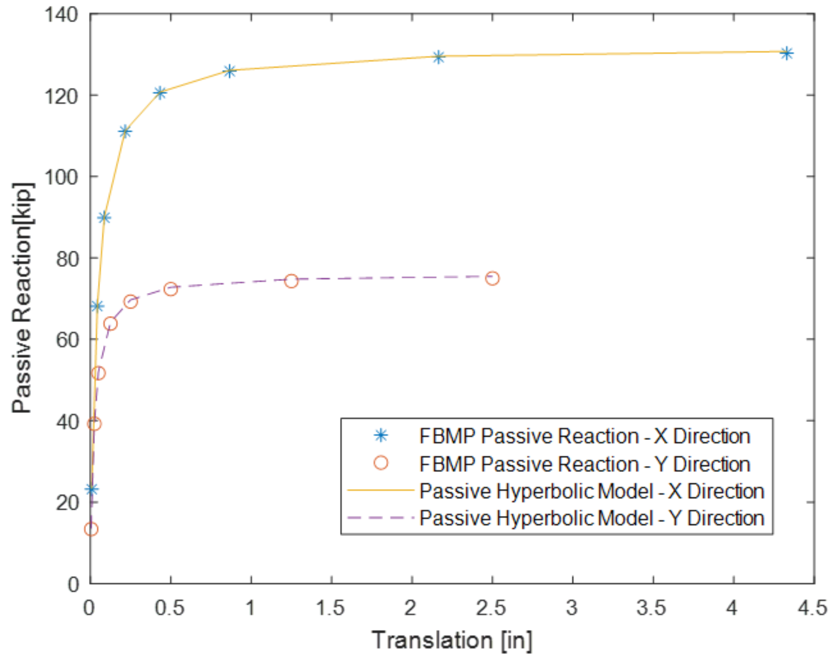

Figure 4-138 Passive resistance: FB-MultiPier (FBMP) and hyperbolic model – prescribed displacement – 30 degrees.

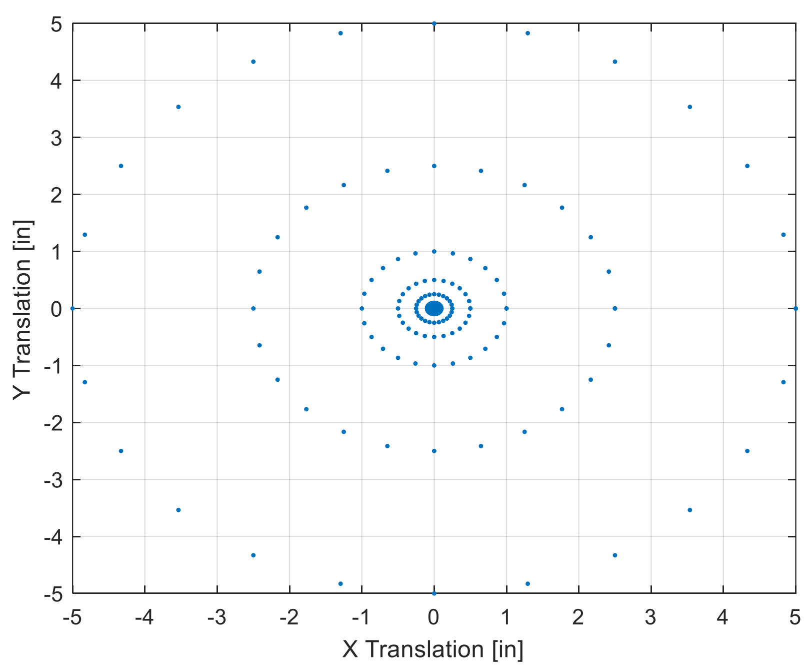

Figure 4-139 Displacement pattern per all prescribed displacements and orientations.

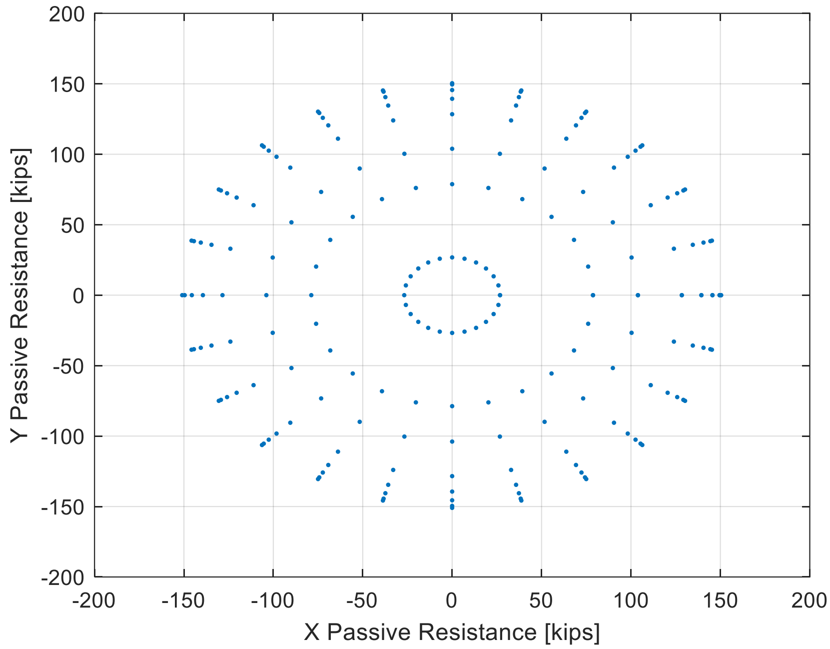

Figure 4-140 Passive resistance pattern per all prescribed displacements and orientations.

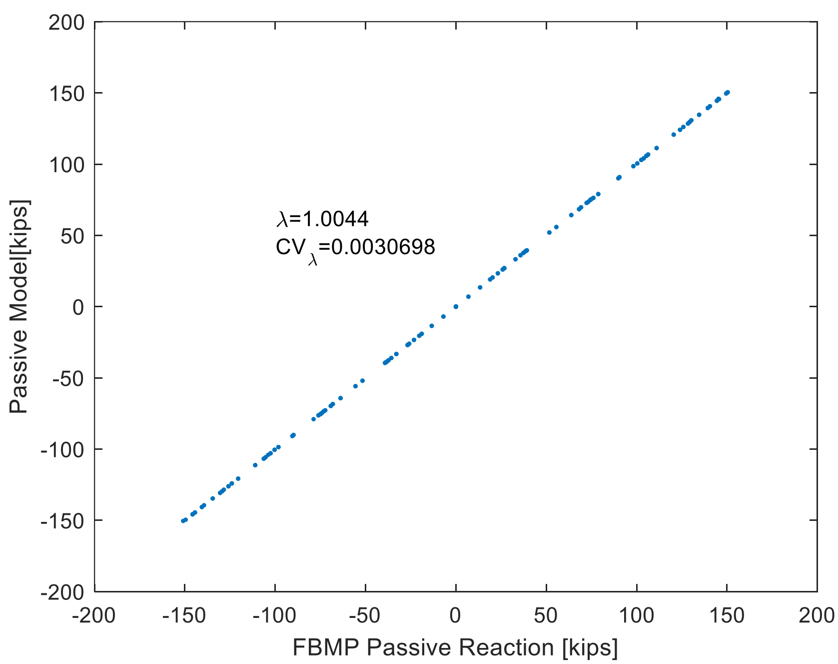

Figure 4-141 X direction FB-MultiPier (FBMP) passive reaction vs calculated passive reaction – prescribed displacement.

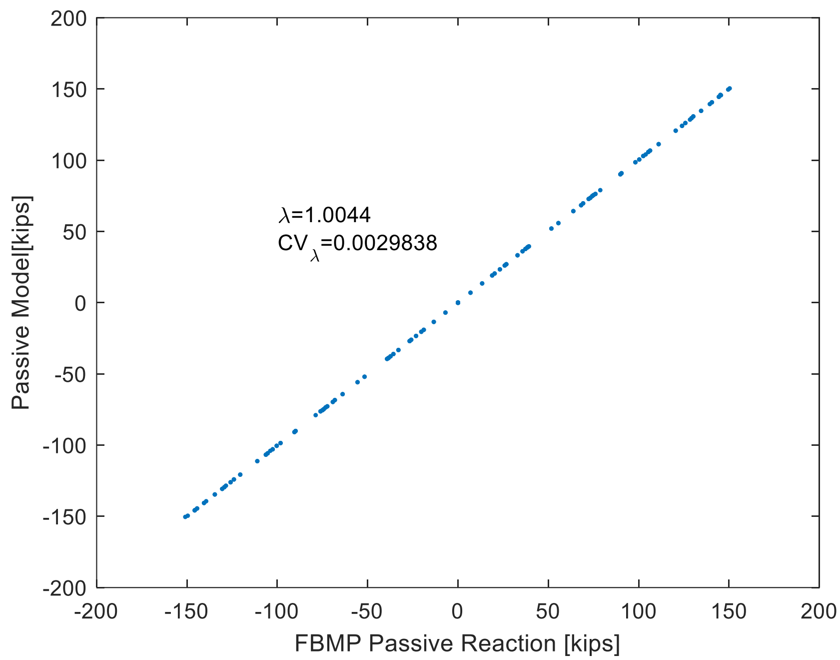

Figure 4-142 Y direction FB-MultiPier (FBMP) passive reaction vs calculated passive reaction – prescribed displacement.

The second validation method uses the same model with prescribed forces which are obliquely loaded, Figure *3-28*, with increments shown in Table *4-10* . After these models are run, displacements from the center of the footing, along with total passive resistance in both the X and Y direction are analyzed. In a similar manner for the prescribed displacement analysis, the first case presented in loading in 30 degree direction, Figure 4-144. These FB-MultiPier results are then plot along with calculated hyperbolic curve, which shows excellent agreement in both the X and Y directions.

That validation is then continued showing the displacement pattern, Figure 4-145, and passive resistance pattern, Figure 4-146. Both show a circular pattern as expected (i.e., the displacement vector and load vector are in the same direction). Additionally measured versus predicted results are presented in Figure 4-147 and Figure 4-148. Resulting in a $\lambda_R$value (FB-MultiPier /model) of approximately 1 (no significant over or under estimation) from the FB-MultiPier analysis. Additionally, the very low CV_λ confirm no scatter or inherent error in the FB-MultiPier analysis.

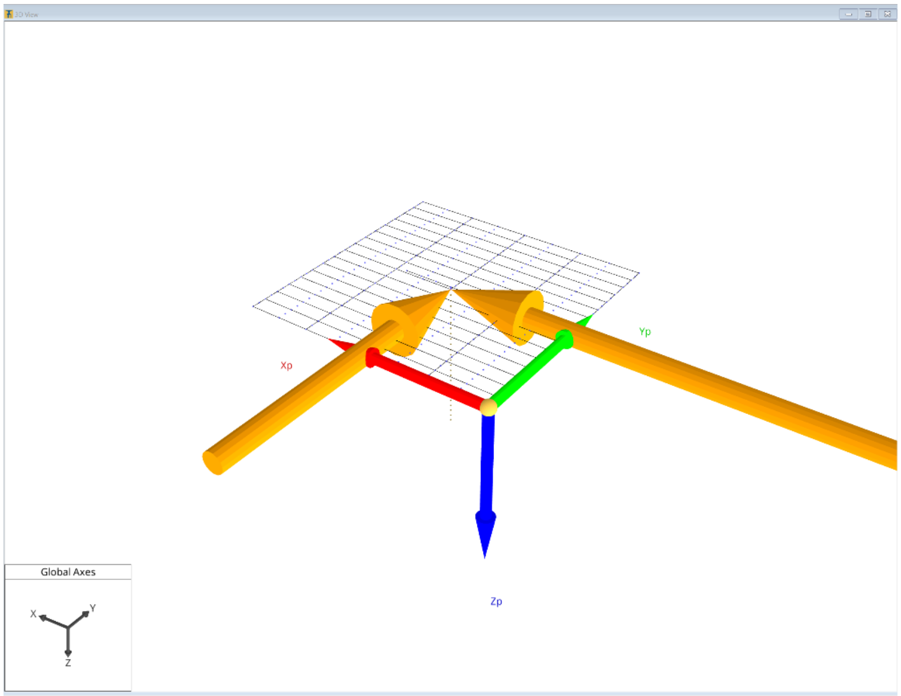

Figure 4-143 FB-MultiPier shallow foundation model prescribed force.

Table 4-26 Resultant loading increments.

Load Case	Load Percentage of P_{ult} [%]
1	1
2	5
3	10
4	25
5	50
6	75
7	95
8	99

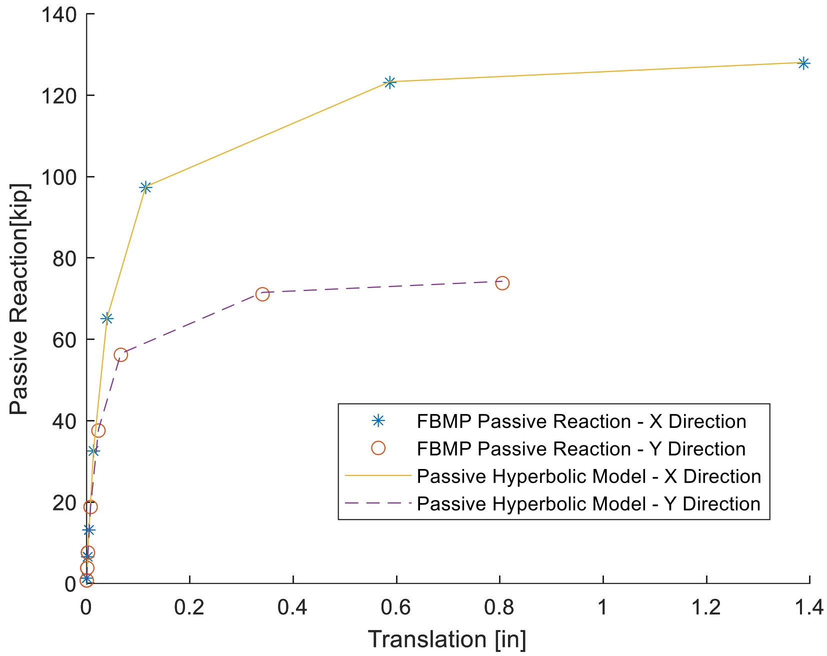

Figure 4-144 Passive resistance: FB-MultiPier (FBMP) and hyperbolic model – prescribed load – 30 degrees.

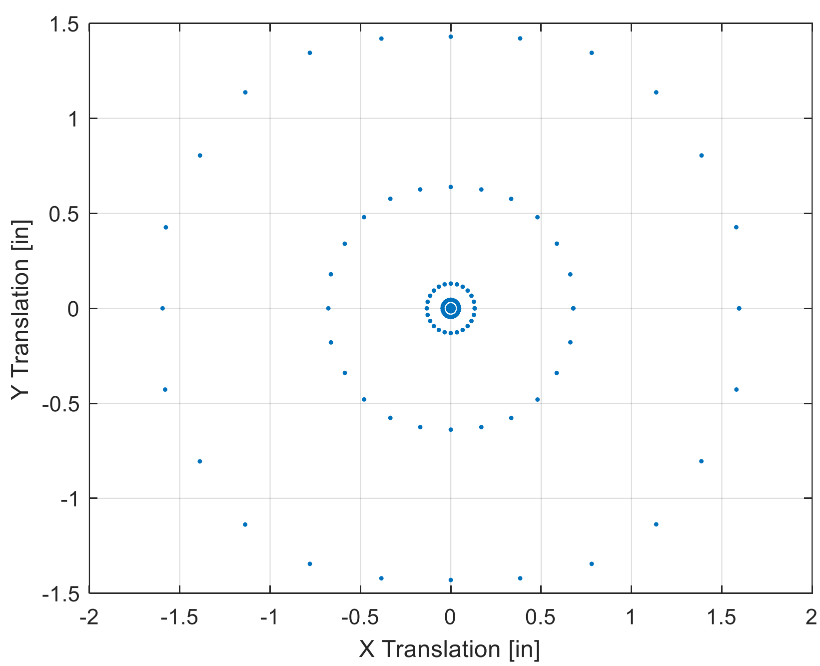

Figure 4-145 Displacement pattern per prescribed load and orientations.

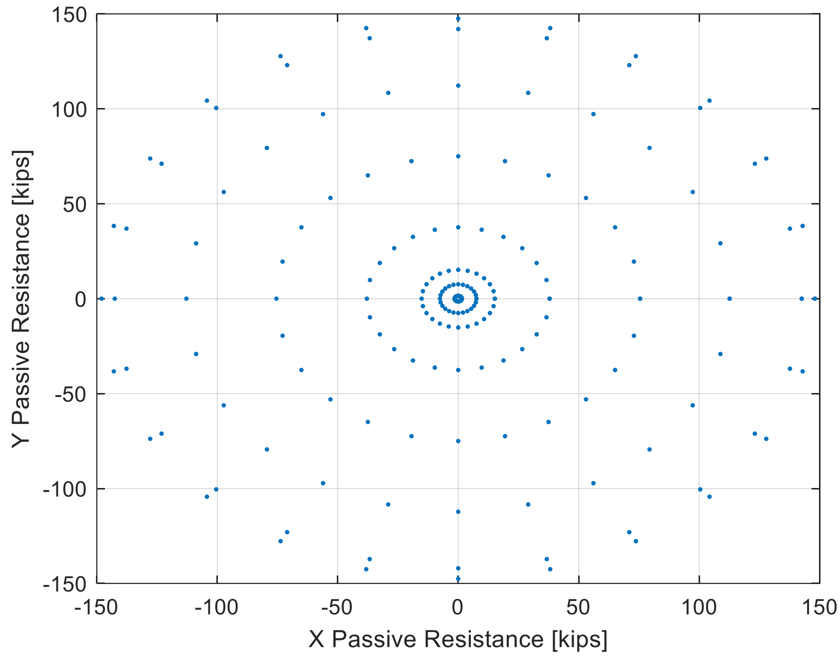

Figure 4-146 Passive resistance pattern per prescribed load and orientations.

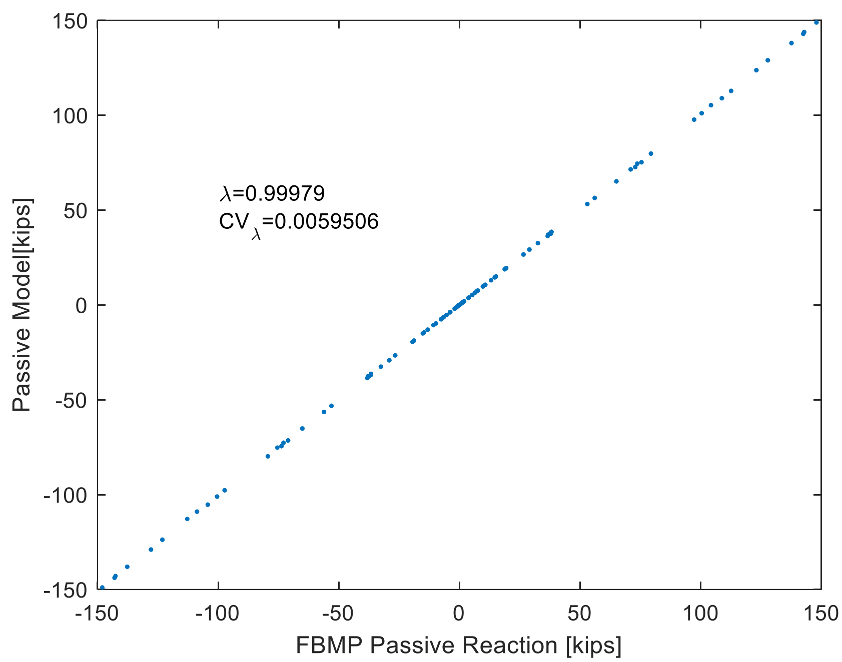

Figure 4-147 X direction FB-MultiPier (FBMP) passive reaction vs calculated passive reaction – prescribed load.

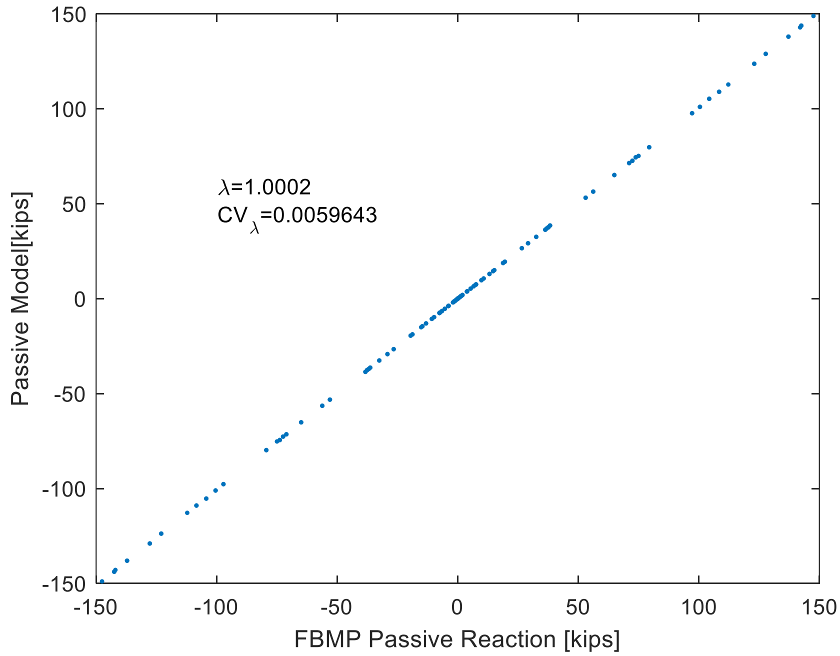

Figure 4-148 Y direction FB-MultiPier (FBMP) passive reaction vs calculated passive reaction – prescribed load.

To further validate the oblique loading a sensitivity study is conducted where multiple cases, Table 4-13 , confirming the algorithm works under various geometry and material properties. Results from these cases are compiled and presented in Figure 4-109 through Figure 4-152 for both prescribed displacement and prescribed force with their corresponding X and Y resistance. In these figures $\lambda_R$value (FB-MultiPier /model) of approximately 1 (no significant over or under estimation) from the FB-MultiPier analysis. Additionally, the very low CV_λ confirm no scatter or inherent error in the FB-MultiPier analysis.

Table 4-27 C-PHI model sensitivity study.

Cases	L [ft]	B [ft]	t [ft]	D_w [ft]	D_F [ft]	C [psf]	ϕ [°]	γ [pcf]	v	δ [°]	Ei [psi]	D_{max} [ft]	q [psf]
1	20	20	5	1000	5	0	30	100	0.25	20	10000	0.30	0
2	20	20	5	1000	5	0	25	100	0.25	16.67	10000	0.30	0
3	20	20	5	1000	5	500	30	100	0.25	20	10000	0.30	0
4	20	20	8	1000	8	0	30	100	0.25	20	10000	0.30	0
5	15	20	5	1000	5	0	30	100	0.25	20	10000	0.30	0
6	20	15	5	1000	5	0	30	100	0.25	20	10000	0.30	0
7	20	20	5	1000	5	0	30	115	0.25	20	10000	0.30	0
8	20	20	5	1000	5	0	30	100	0.15	20	10000	0.30	0
9	20	20	5	1000	5	0	30	100	0.25	10	10000	0.30	0
10	20	20	5	1000	5	0	30	100	0.25	20	10000	0.60	0
11	20	20	5	1000	5	0	30	115	0.25	20	5000	0.30	0
12	20	20	5	0	5	0	30	100	0.25	20	10000	0.30	0
13	20	20	5	3	5	0	30	100	0.25	20	10000	0.30	0
14	20	20	5	1000	3	0	30	100	0.25	20	10000	0.30	0
15	20	20	5	1000	10	0	30	100	0.25	20	10000	0.30	0
16	20	20	5	1000	5	0	30	100	0.25	20	10000	0.30	500
17	20	20	5	1000	10	0	30	100	0.25	20	10000	0.30	500
18	20	20	5	1000	5	250	0	100	0.25	0	10000	0.30	0
19	20	20	5	1000	11.25	250	0	100	0.25	0	10000	0.30	0
20	20	20	5	1000	5	250	0	100	0.25	0	10000	0.30	625

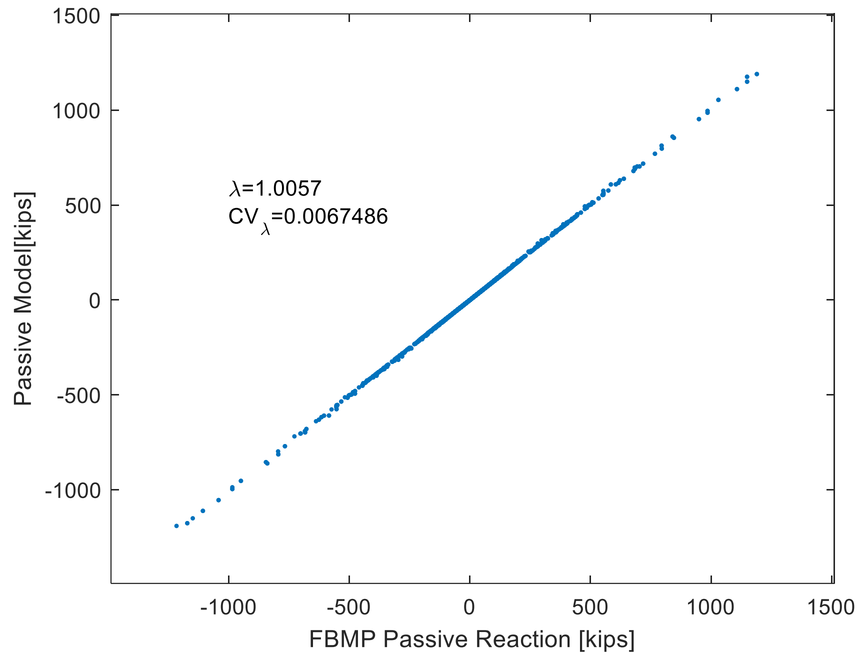

Figure 4-149 Sensitivity study x direction: FB-MultiPier (FBMP) passive reaction vs calculated passive reaction – prescribed displacement.

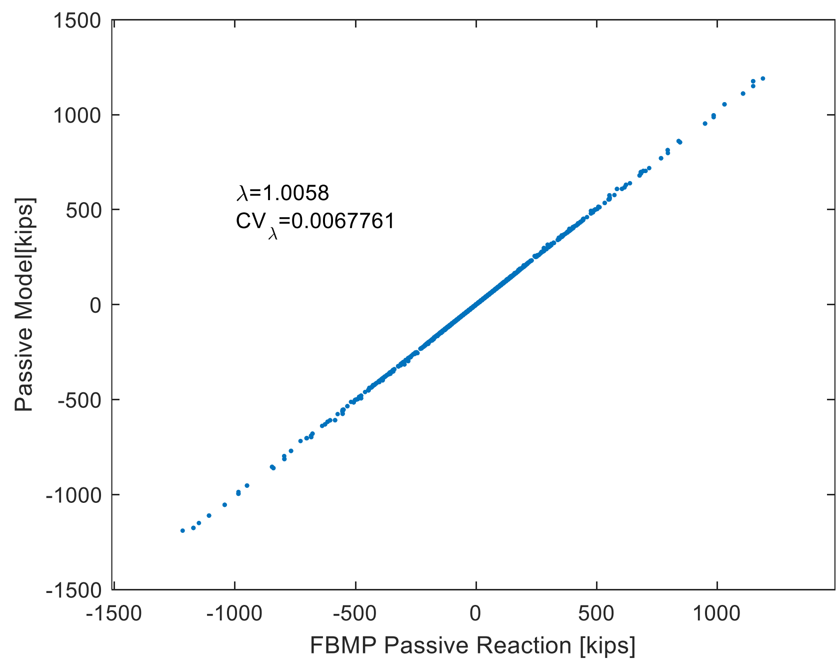

Figure 4-150 Sensitivity study y direction: FB-MultiPier (FBMP) passive reaction vs calculated passive reaction – prescribed displacement.

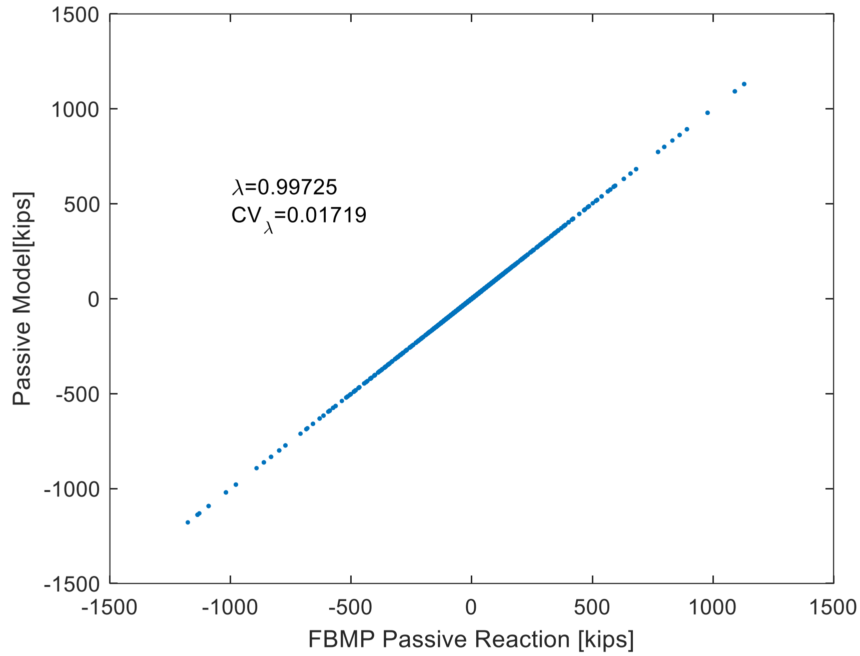

Figure 4-151 Sensitivity study x direction: FB-MultiPier (FBMP) passive reaction vs calculated passive reaction – prescribed load.

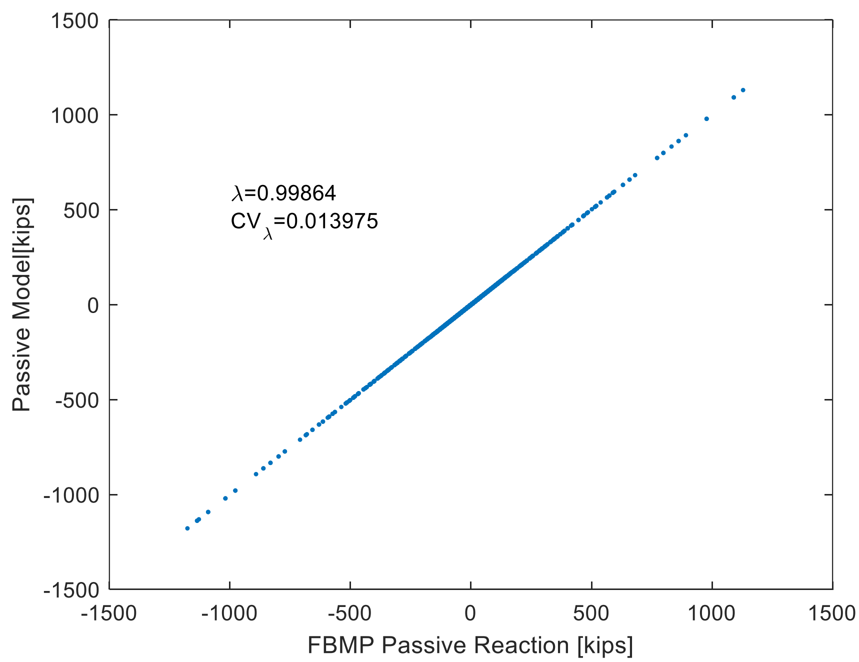

Figure 4-152 Sensitivity study y direction: FB-MultiPier (FBMP) passive reaction vs calculated passive reaction – prescribed load.

4.7.2 Plaxis Comparison

To validate implementation of the FL Limestone model. The validation consisted of confirming passive resistance from FB-MultiPier UI dialogs and engine output (i.e., .out file). Additionally, the load settlement response determined by FB-MultiPier was compared with Plaxis Results. The following cases were analyzed.

- Plaxis 30 Degree Analysis
- Plaxis Case Comparison

To confirm accuracy of oblique reduction, results from Plaxis analysis were used for comparison. Table 4-28 summarized material properties and footing geometries were used to create FB-MultiPier models, which used a prescribed displacement per the Plaxis models. In Table 4-28, cases 1 through 3 are soil models where the Plaxis used the Mohr Coulomb model. Cases 4 through 7 are Limestone models.

Table 4-28 Plaxis cases hyperbolic parameters.

Cases	L [ft]	B [ft]	t [ft]	D_w [ft]	D_F [ft]	C [psf]	ϕ [°]	γ [pcf]	v	δ (°)	Ei [psi]	D_{max} [ft]	q [psf]
1	5	5	5	100	5	208	39.0	121	0.27	26.1	13889	3.6	0
2	8	16	8	100	8	208	39.0	121	0.27	26.1	13889	3.6	0
3	5	5	5	100	5	69	27.0	102	0.27	18.0	4500	3.6	0
4	8	16	8	100	8	828	18.5	90	0.1	12.3	14280	3.6	0
5	8	16	8	100	8	2768	22.5	120	0.1	15.0	194040	3.6	0
6	5	5	5	100	5	828	18.5	90	0.1	12.3	14280	3.6	0
7	5	5	5	100	5	2768	22.5	120	0.1	15.0	194040	3.6	0

The first comparison was for prescribed displacement at an orientation of 30 degrees for Case 6, Figure 4-153. Agreement between FB-MultiPier and Plaxis is not where the initial displacement points are agreeable, however at further displacements the Plaxis resistances appear to converge. This behavior is expected, as it was previously presented the force vector deviates from the displacement at larger displacements.

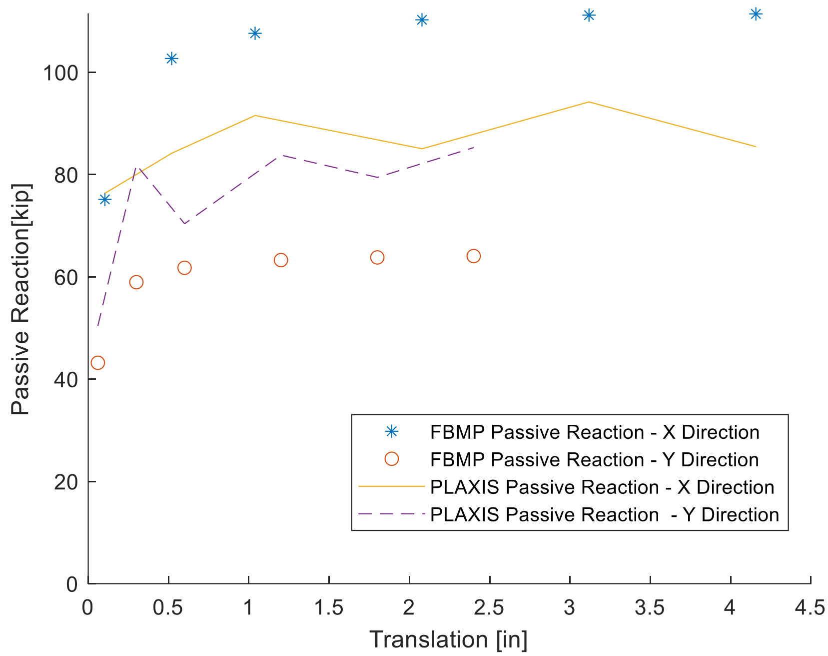

Figure 4-153 Case 6 – Passive resistance: FB-MultiPier (FBMP) and PLAXIS prescribed displacement – 30 degrees.

Passive resistance patterns are plotted for all cases in Figure 4-154 through Figure 4-160, where the blue dots are FB-MultiPier results and black stars are Plaxis results. Currently Plaxis results for oblique loading at 0, and 45 degrees is available. 90-degree Plaxis is available for Case 2. In cases 1 through 3, Figure 4-154 through Figure 4-156, all show radials patterns with an agreeable overlap between FB-MultiPier in Plaxis. Case 1 and Case 3 results show a circular pattern, where Case 2 has more of an elliptical shape. This difference in Case 2 is due to the geometry of the footing being a rectangle, resulting in the larger side (16 feet wide) having more passive resistance than its adjacent smaller side (8 feet wide). This is demonstrated for Case 2 where the X axis ultimate resistance is approximately 1,400 kips and the Y axis is 800 kips. It is also observed for Case 2, that FB-MultiPier also mimics this elliptical pattern.

For the limestone, Figure 4-157 through Figure 4-160, there is agreeable overlap between Plaxis and FB-MultiPier. However, the resistance values for Plaxis converge at force vector of 45 degrees near ultimate resistance. This is the same behavior that is illustrated in Figure 4-153 and Figure 4-42. At large displacements even though the x and y resistance components are not in agreement, qualitatively their resultant force is agreeable.

To quantify accuracy of this analysis where the λ_R and CV_λ are calculated (Plaxis/ FB-MultiPier) for all cases shown in Figure 4-154 through Figure 4-160 in Table 4-29. Presented are λ_R and CV_λ for the individual X and Y resistances, the resultant resistance and resistance directly along the X or Y axis (i.e., normal loading implementation from task 3 report). Table 4-30 presents the same information, however, summarizes cases by being either the Plaxis model being soil (Mohr Coulmb) or Limestone. For soil it can be seen that λ_R is approximately 1 suggesting good agreement between the Plaxis model and FB-MultiPier. When analyzed individually, Table 4-29, Case 2 have λ_R is less than 1, this is due to the large overprediction of FB-MultiPier resistance at small displacements. The CV_λ for the soil summary, Table 4-30, shows values of 0.2 magnitude.

For Limestone, Table 4-30, λ_R is 1.06 and 1.28 for X and Y resistance components respectively. The accuracy in the X direction is likely weight towards the initial loading condition being on the zero degree direction. The under predictions in the Y direction is the result of convergence of the force vector to 45 degrees, where the implemented model's force vector in in the same angle as the direction of motion. When comparing the resultant resistance this value is much more agreeable, 0.98, which confirms the previous observations from Figure 4-157 through Figure 4-160. The CV_λ for the X and Y resistances have values of 0.38 and 0.40 respectively. These values are higher than CV_λ for the resultant, 0.11, which is again due to Plaxis models force vector converging towards 45 degrees.

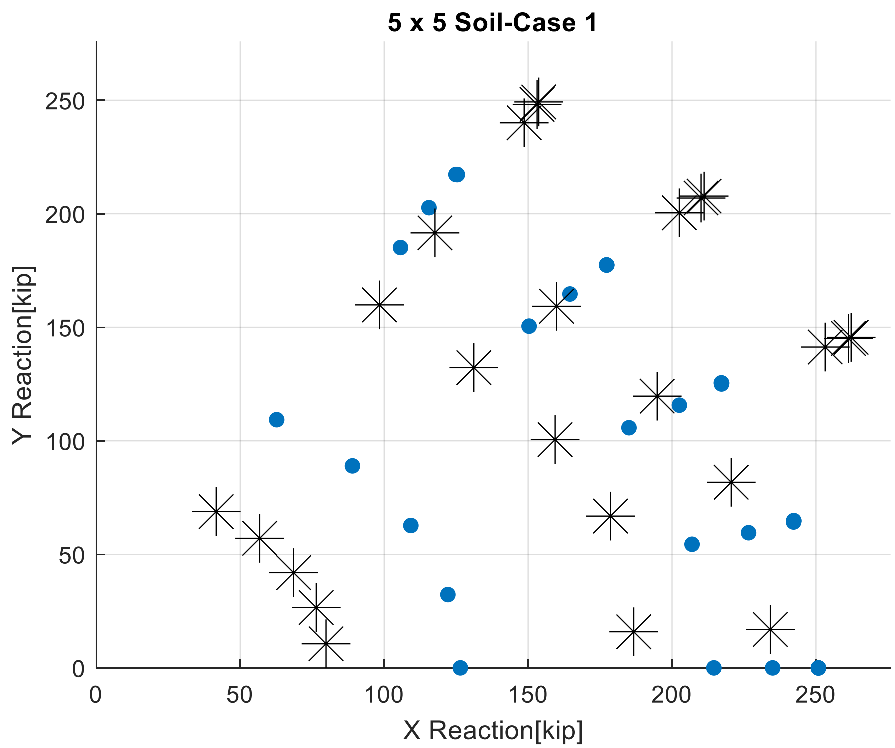

Figure 4-154 Case 1 passive resistance pattern per prescribed displacement and orientations.

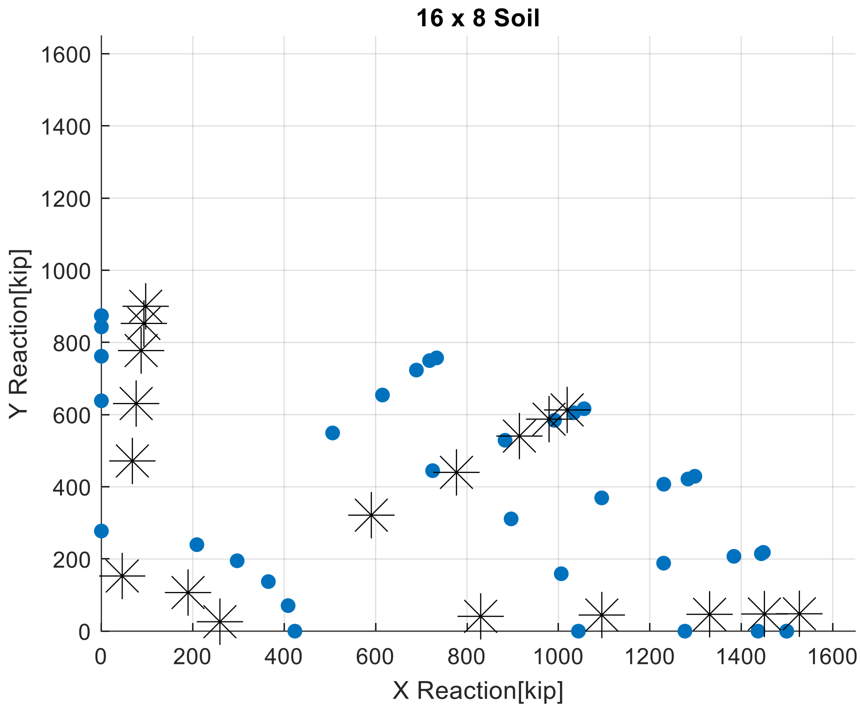

Figure 4-155 Case 2 passive resistance pattern per prescribed displacement and orientations.

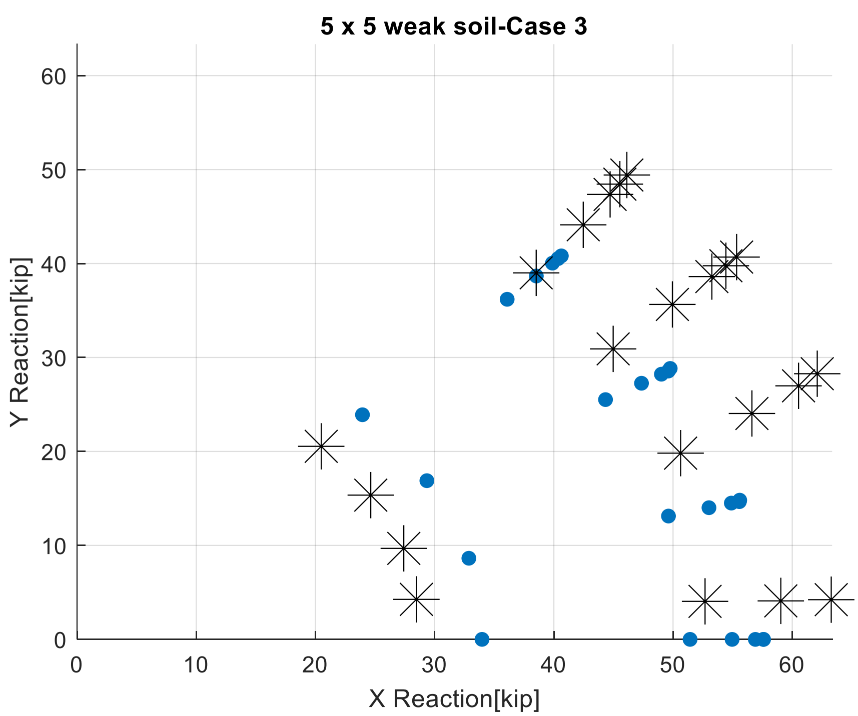

Figure 4-156 Case 3 passive resistance pattern per prescribed displacement and orientations.

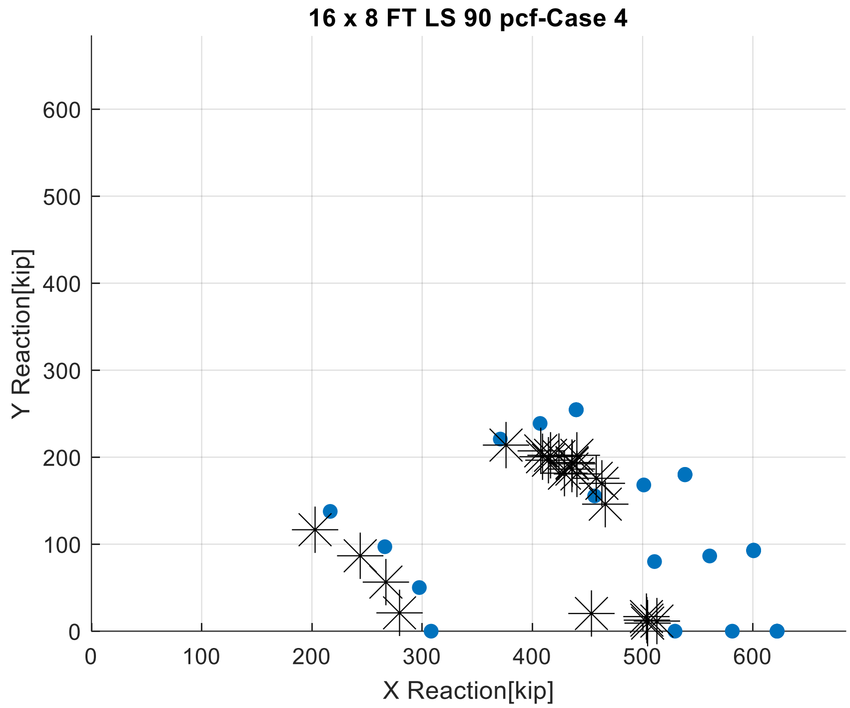

Figure 4-157 Case 4 passive resistance pattern per prescribed displacement and orientations.

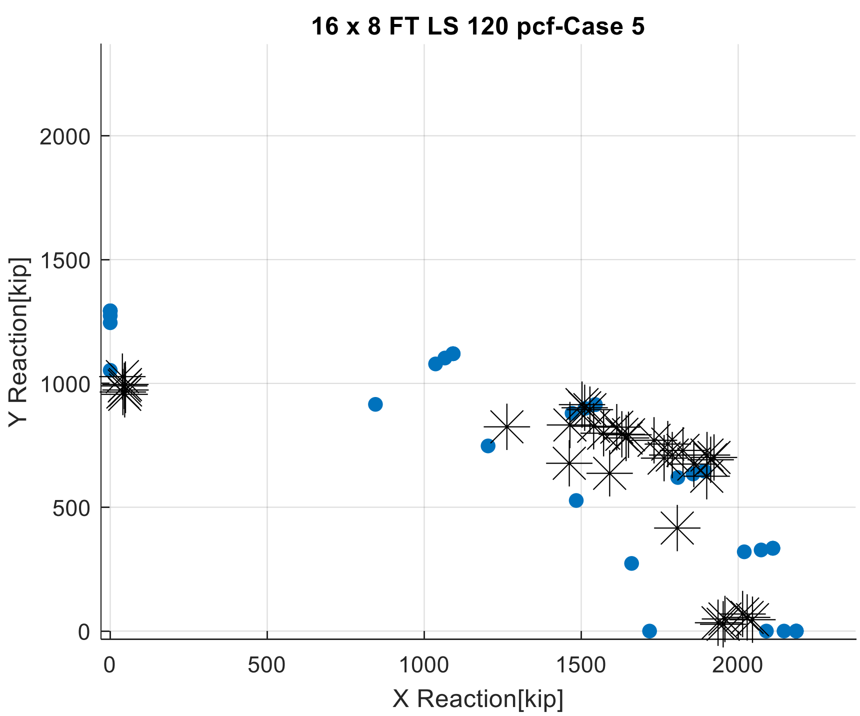

Figure 4-158 Case 5 passive resistance pattern per prescribed displacement and orientations.

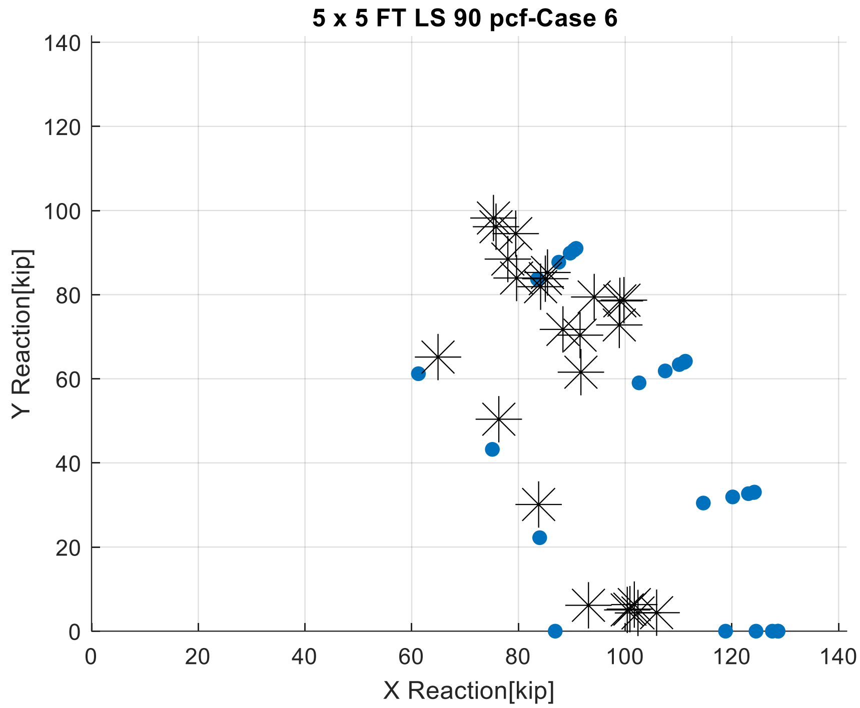

Figure 4-159 Case 6 passive resistance pattern per prescribed displacement and orientations.

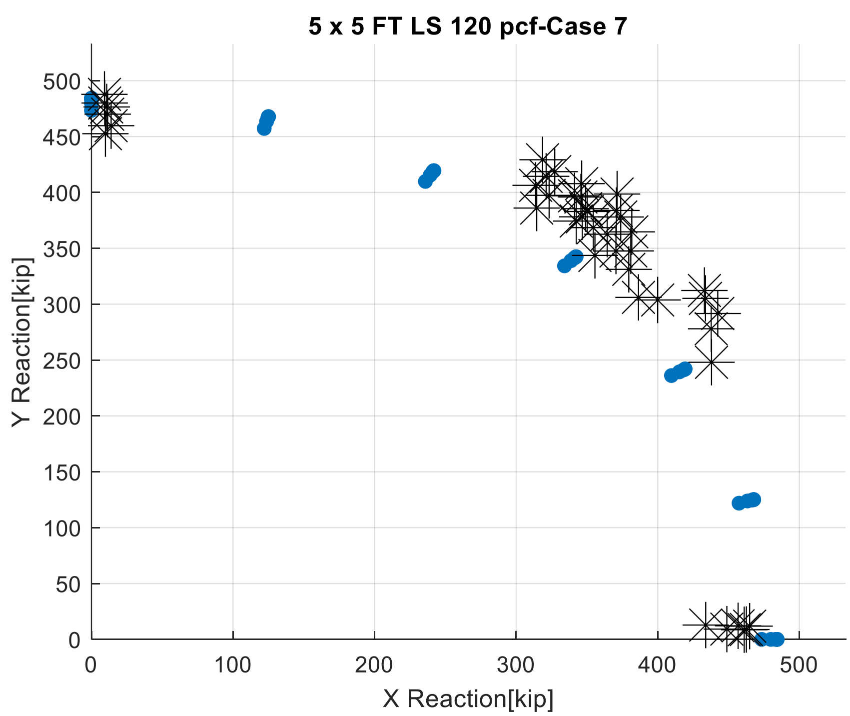

Figure 4-160 Case 7 passive resistance pattern per prescribed displacement and orientations.

Table 4-29 Plaxis passive comparison - case results.

	BIAS				CV			
CASE	X	Y	RESULTANT	0/90	X	Y	RESULTANT	0/90
1	1.02	1.07	1.02	1.05	0.22	0.23	0.21	0.25
2	0.88	0.91	0.86	0.85	0.15	0.24	0.16	0.18
3	1.05	1.35	1.09	1.06	0.10	0.24	0.11	0.11
4	0.87	1.24	0.88	0.85	0.10	0.37	0.07	0.04
5	1.08	1.12	0.99	0.88	0.18	0.41	0.12	0.13
6	0.86	1.47	0.94	0.86	0.11	0.35	0.09	0.12
7	1.02	1.07	1.02	1.05	0.46	0.41	0.06	0.03

Table 4-30 Plaxis passive comparison - soil and limestone results.

	BIAS				CV			
CASE	X	Y	RESULTANT	0/90	X	Y	RESULTANT	0/90
SOIL	0.98	1.07	0.97	0.95	0.18	0.29	0.19	0.21
LIMESTONE	1.06	1.26	0.98	0.90	0.38	0.40	0.11	0.10

4.7.3 Friction Hyperbolic (Coulomb) Model Validation

To validate implementation of the Hyperbolic (Coulomb) model. The validation consisted of confirming passive resistance from FB-MultiPier UI dialogs and engine output (i.e., .out file). Additionally, the load settlement response determined by FB-MultiPier was compared with the hyperbolic calculations. The following cases were analyzed.

- 30 Degree Orientation
- 360 Degree Prescribed Displacement
- 360 Degree Prescribed Displacement
- Sensitivity Analysis
- Plaxis Comparison

The first validation effort was conducted in same manner as previously discussed for the passive hyperbolic model. This consists of confirming the Engine calculation the correct frictional resistance curve but now is based on inputs required for Equation 4-11. Prescribed displacements and loads, Table 4-31 and Table 4-21 , were used in FB-MultiPier model using parameters specified in Table 4-34, Case 1. A smaller range of resultant displacements are specified as compared to the passive resistance analysis, since ultimate frictional resistance can be mobilized under smaller displacements. Note, loading for friction validation is based on a percentage of ultimate frictional resistance based Coulombic friction properties and footing.

The first analysis presented is prescribed displacement results oriented at 30 degrees, Figure 4-161. There is excellent agreement between FB-MultiPier (FBMP) and MATLAB calculation. Additionally, the reactions for the X and Y directions are of different magnitudes, due to oblique angle being oriented in the 30 degree direction. This results in more frictional reactions in the X direction as compared to the Y direction. This Case validation is expanded to analyze all orientations, as shown in Figure 4-162 and Figure 4-163. Both plots show a radial pattern that is circular which is expected. The accuracy of the 360 degree loading is presented in Table 4-33, which shown $\lambda_R$value (FB-MultiPier /model) of approximately 1 (no significant over or under estimation) from the FB-MultiPier analysis. Additionally, the very low CV_λ confirm no scatter or inherent error in the FB-MultiPier analysis.

Table 4-31 Prescribed Resultant Displacement.

Load Case	Prescribed Displacement [in]
1	0.001
2	0.005
3	0.010
4	0.025
5	0.050
6	0.100
7	0.250
8	0.500

Table 4-32 Resultant friction loading increments.

Load Case	Load Percentage of F_{ult} [%]
1	1
2	5
3	10
4	25
5	50
6	75
7	95
8	99

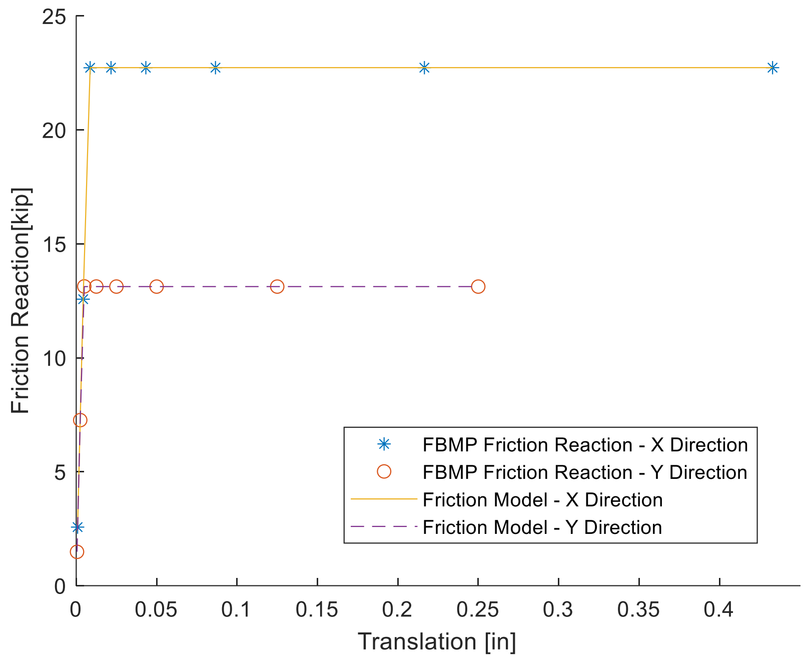

Figure 4-161 Passive resistance hyperbolic model – prescribed displacement – 30 degrees.

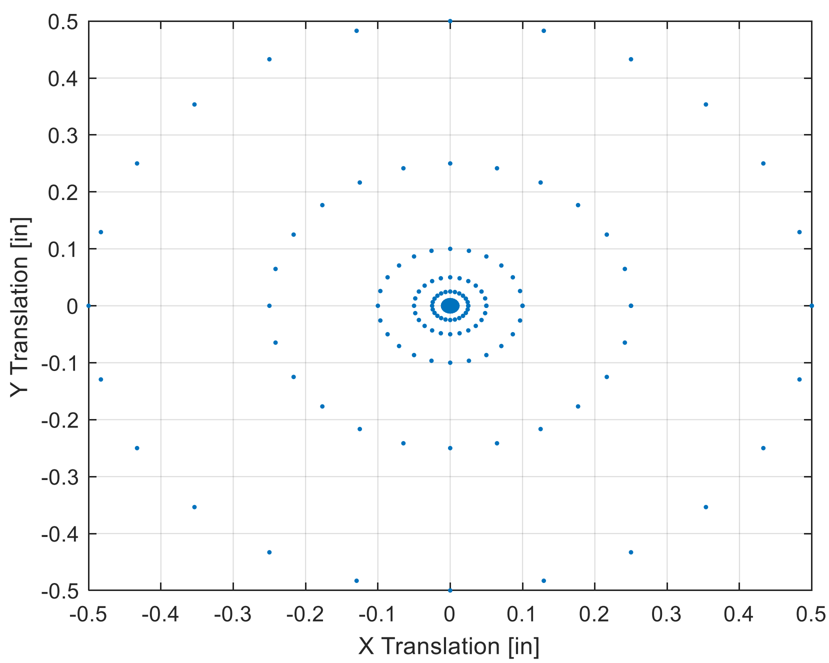

Figure 4-162 Displacement pattern per prescribed displacement and orientations.

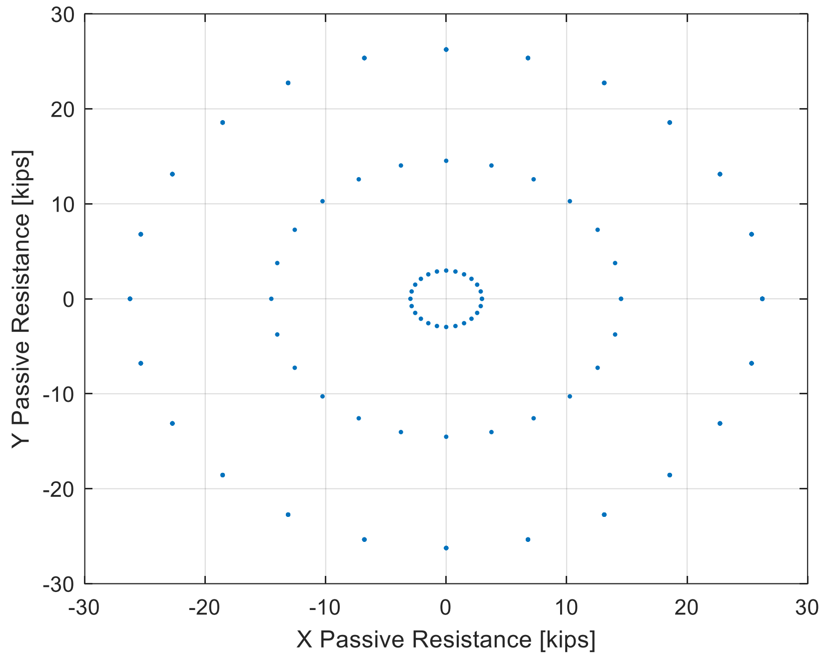

Figure 4-163 Passive resistance pattern per prescribed displacement and orientations.

The first analysis presented is prescribed load results oriented at 30 degrees, Figure 4-164. There is excellent agreement between FB-MultiPier (FBMP) and MATLAB calculation. Additionally, the reactions for the X and Y directions are of different magnitudes, due to oblique angle being oriented in the 30 degree direction. This results in more frictional reactions in the X direction as compared to the Y direction. This case validation is expanded to analyze all orientations, as shown in Figure 4-165 and Figure 4-166. Both plots show a radial pattern that is circular which is expected. It is observed in Figure 4-165 the resultant displacement at 45, 135, 225, and 315 is slightly larger than other angles. This a result loading at 99% of ultimate frictional resistance and FB-MultiPier convergence tolerance. This accuracy can be improved through smaller tolerance and additional iterations, however at such small displacements this result can be seen as acceptable.

The accuracy of the 360 degree loading is presented in Table 4-33, which shown $\lambda_R$value (FB-MultiPier /model) of approximately 1 (no significant over or under estimation) from the FB-MultiPier analysis. Additionally, the very low CV_λ confirm no scatter or inherent error in the FB-MultiPier analysis.

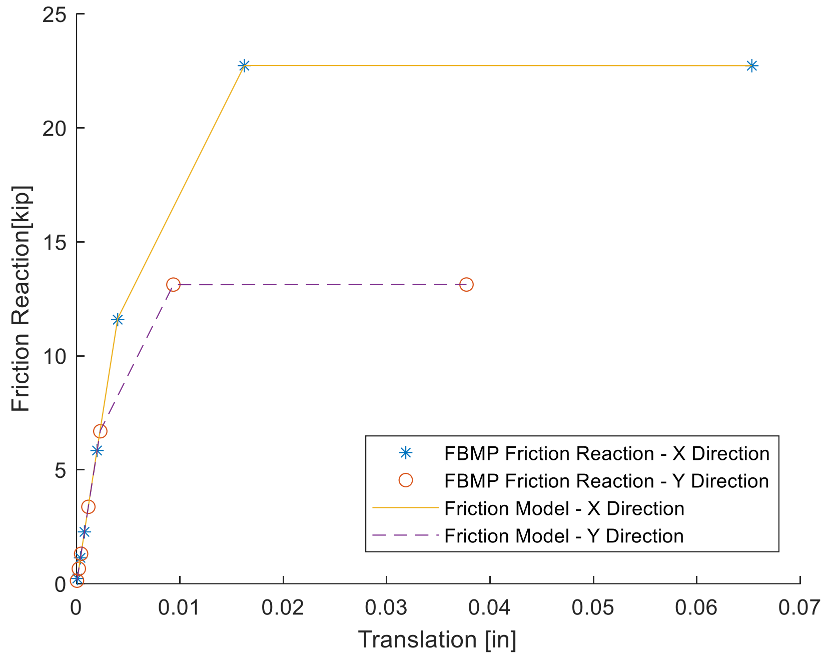

Figure 4-164 Passive resistance hyperbolic model – prescribed load – 30 degrees.

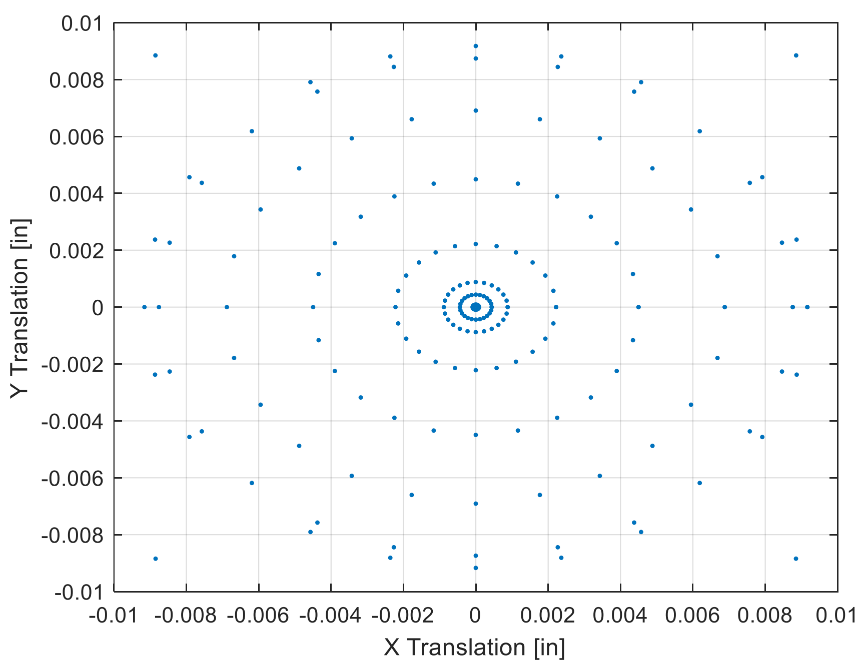

Figure 4-165 Displacement pattern per prescribed load and orientations.

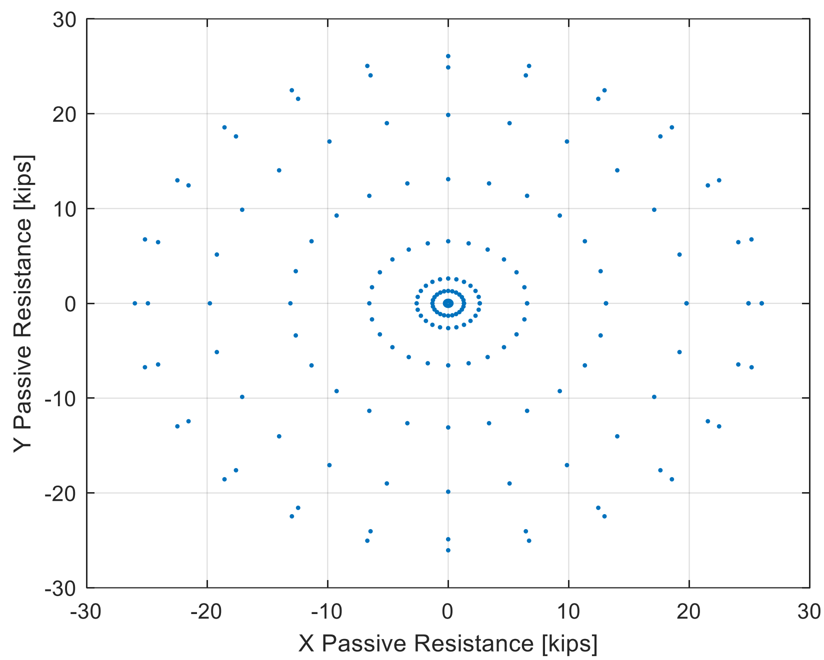

Figure 4-166 Passive resistance pattern per prescribed load and orientations.

Table 4-33 Friction hyperbolic (Coulomb) case 1 results.

Analysis Type	λ_R	CV_λ
Prescribed Displacement – X Direction	1.0013	0.0020
Prescribed Displacement – Y Direction	1.0009	0.0017
Prescribed Load – X Direction	1.0033	0.0022
Prescribed Load – Y Direction	1.0026	0.0018

The next validation effort was to conduct a sensitivity study where geometry and input parameters for the Hyperbolic (Coulomb) model are perturbated, to ensure FB-MultiPier is using each one appropriately. Input parameters for sensitivity study are shown in Table 4-34. These case are then analyzed in both prescribed displacement, Table 4-31, and prescribed load, Table 4-21 , in conjunction with multiple orientations, Table 4-25. The result of this analysis was shown in Table 4-23 , where for all loading conditions and unit types a $\lambda_R$value of approximately 1 (no significant over or under estimation) from the FB-MultiPier analysis. Additionally, the very low CV_λ confirm no scatter or inherent error in the FB-MultiPier analysis.

Table 4-34 Friction hyperbolic (Coulomb) sensitivity study.

Cases	L [ft]	B [ft]	t [ft]	k_{max}	R_f	P_{ult}	δ (°)	C [psf]	Adhesion	D_w [ft]
1	20	20	5	3000	0.95	500	5	0	0.00	1000
2	20	20	5	3000	0.95	500	10	0	0.00	1000
3	20	20	5	3000	0.95	500	15	0	0.00	1000
4	20	20	5	3000	0.95	500	20	0	0.00	1000
5	20	20	5	3000	0.95	500	0	100	0.10	1000
6	20	20	5	3000	0.95	500	0	500	0.10	1000
7	20	20	5	3000	0.95	500	0	1000	0.10	1000
8	20	20	5	3000	0.95	500	0	2000	0.10	1000
9	20	20	5	3000	0.95	500	0	500	0.25	1000
10	20	20	5	3000	0.95	500	0	500	0.50	1000
11	20	20	5	3000	0.95	500	0	500	0.75	1000
12	20	20	5	3000	0.95	500	0	500	1.00	1000
13	20	20	5	3000	0.95	500	5	100	0.25	1000
14	20	20	5	3000	0.95	500	10	500	0.50	1000
15	20	20	5	3000	0.95	500	15	1000	0.75	1000
16	20	20	5	3000	0.95	500	20	2000	1.00	1000
17	20	20	5	1500	0.95	500	15	1000	0.75	1000
18	20	20	5	3000	0.85	500	15	1000	0.75	1000
19	20	20	5	3000	0.95	2000	15	1000	0.75	1000
20	20	15	5	3000	0.95	500	15	1000	0.75	1000
21	20	20	8	3000	0.95	500	15	1000	0.75	1000
22	20	20	5	3000	0.95	500	15	1000	0.75	0.0

Table 4-35 Friction hyperbolic (Coulomb) sensitivity study results.

Analysis Type	λ_R	CV_λ
Prescribed Displacement – X Direction	1.0023	0.0020494
Prescribed Displacement – Y Direction	1.0017	0.0017311
Prescribed Load – X Direction	1.0031	0.0015545
Prescribed Load – Y Direction	1.0023	0.0013107

To confirm accuracy of oblique friction model, results from Plaxis analysis were used for comparison. Table 4-28 summarizes material properties and footing geometries were used to create FB-MultiPier models, which used a prescribed displacement per the Plaxis models. The adhesion factor was taken as 2/3. This same 30 degree analysis was conducted for case 6, Figure 4-167. Agreement between FB-MultiPier (FBMP) and Plaxis is good. It can be seen the reactions for the X and Y directions are of different magnitudes, due to oblique displacement being oriented in the 30 degree direction. This results in more frictional reactions in the X direction as compared to the Y direction.

Passive resistance patterns are plotted for all cases in Figure 4-168 through Figure 4-174. Figure 4-160, where the blue dots are FB-MultiPier results and black stars are Plaxis results. Currently Plaxis results for oblique loading at 0, and 45 degrees is available. 90-degree Plaxis is available for Case 2. In cases 1 through 3, Figure 4-168 through Figure 4-170, all show radials patterns with an agreeable overlap between FB-MultiPier in Plaxis. Case 1 and Case 3 results show a circular pattern. The FB-MultiPier points are all ultimate friction values (calculated as Coulombic shear force (Equation 8)), as it's fully mobilized based on the prescribed displacement. While the Plaxis model results include post-peak residual shear values (dilative material), the peak friction values are only included here for direct comparison to the FB-MultiPier results. Qualitatively the peak frictional resistance from Plaxis is agreeable with the ultimate frictional resistance from FB-MultiPier.

For the limestone, Figure 4-171 through Figure 4-174, there is agreeable overlap between Plaxis and FB-MultiPier Results from Plaxis and FB-MultiPier are agreeable and show a similar radial pattern. λ_R and CV_λ for the limestone comparison are shown in Table 4-36 and Table 4-37. λ_R ranges from 0.9-1.0 and CV_λ ranges from 0.01 to 0.13, which indicates the FB-MultiPier and Plaxis results are agreeable.

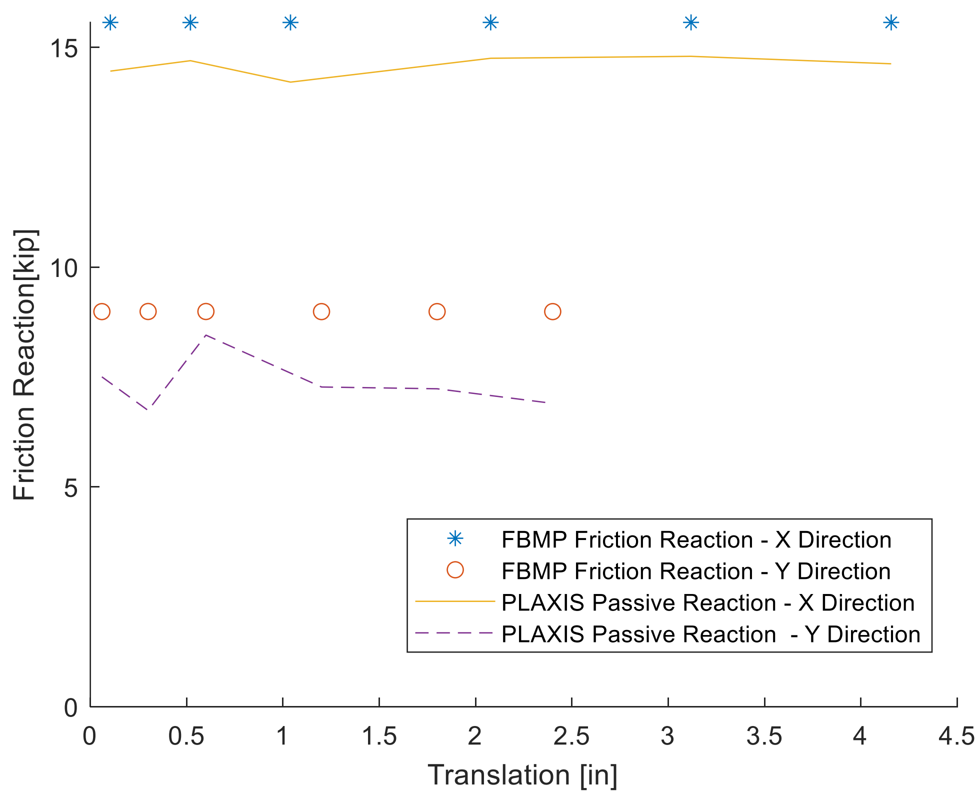

Figure 4-167 Case 6 – prescribed displacement – 30 degrees.

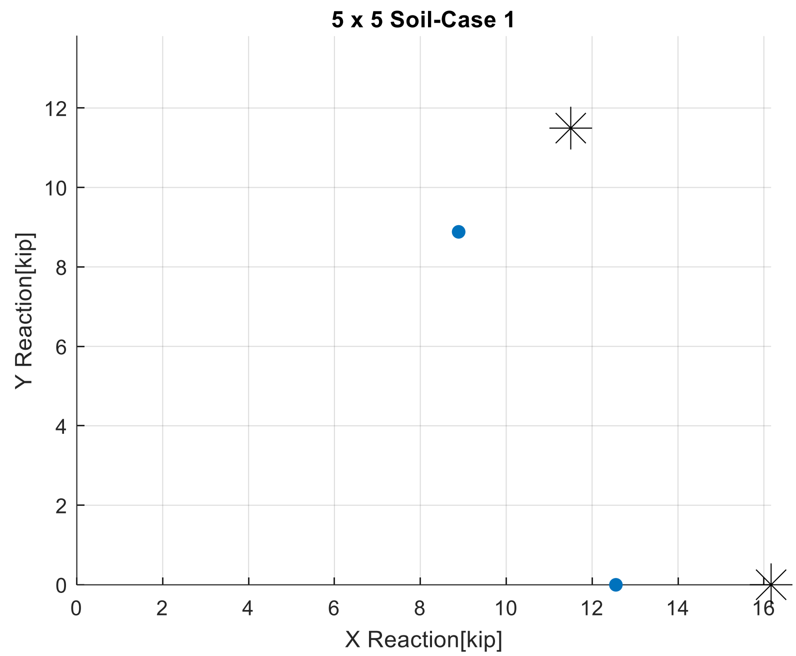

Figure 4-168 Case 1 friction resistance pattern per prescribed displacement and orientations.

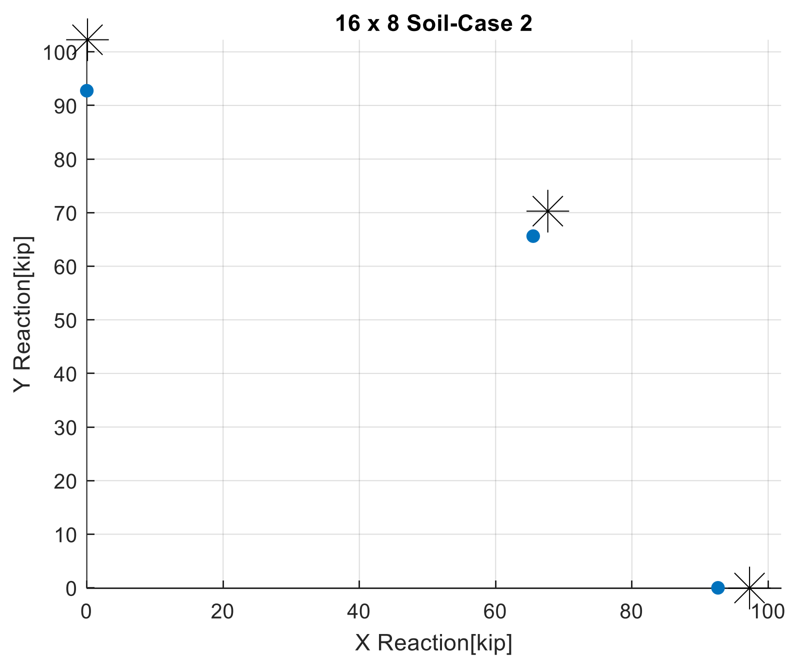

Figure 4-169 Case 2 friction resistance pattern per prescribed displacement and orientations.

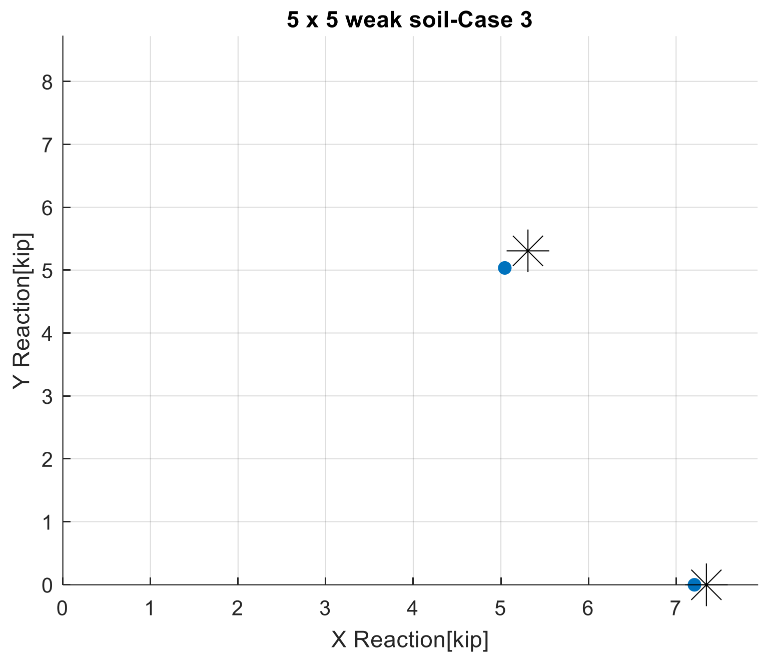

Figure 4-170 Case 3 friction resistance pattern per prescribed displacement and orientations.

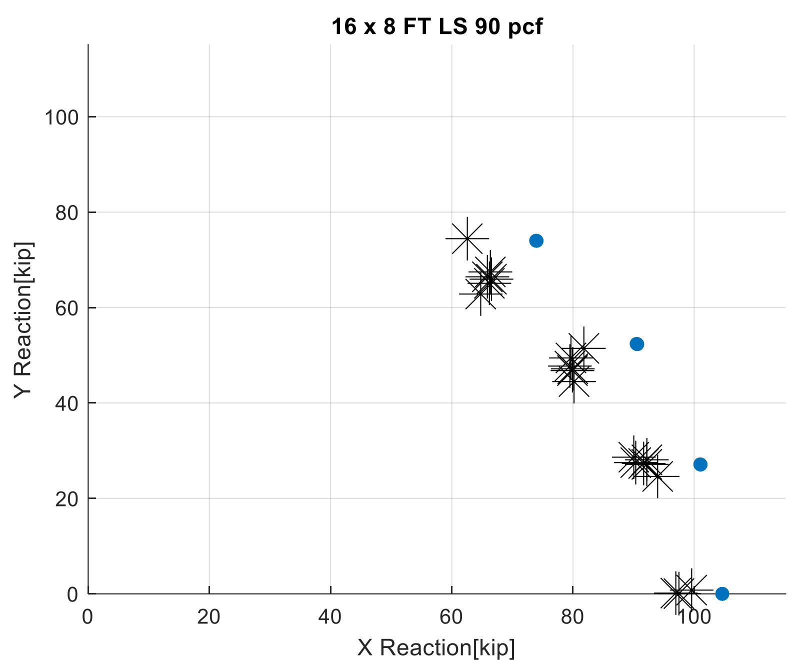

Figure 4-171 Case 4 friction resistance pattern per prescribed displacement and orientations.

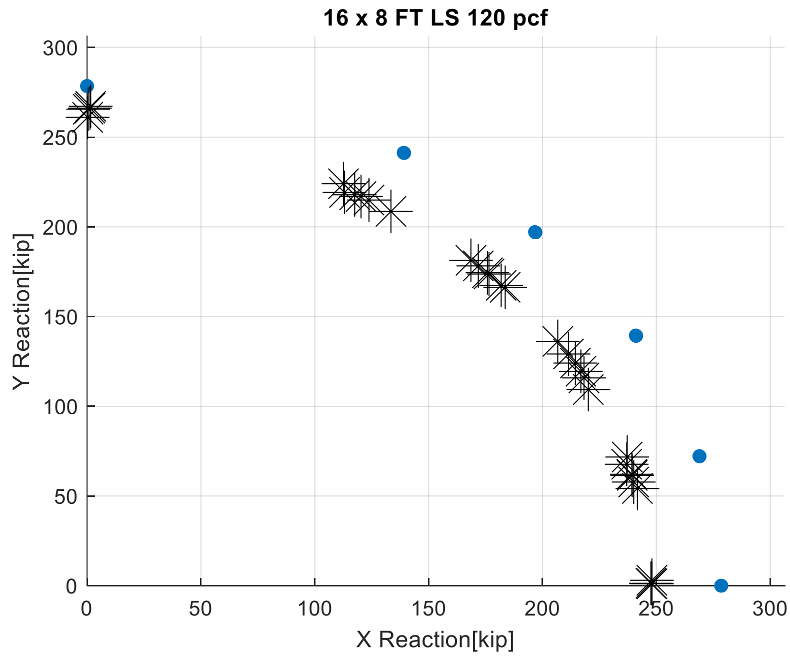

Figure 4-172 Case 5 friction resistance pattern per prescribed displacement and orientations.

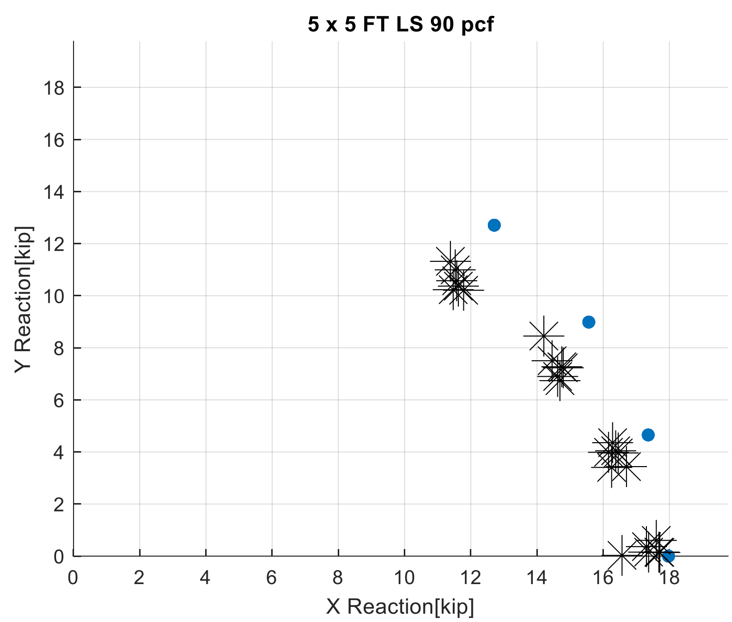

Figure 4-173 Case 6 friction resistance pattern per prescribed displacement and orientations.

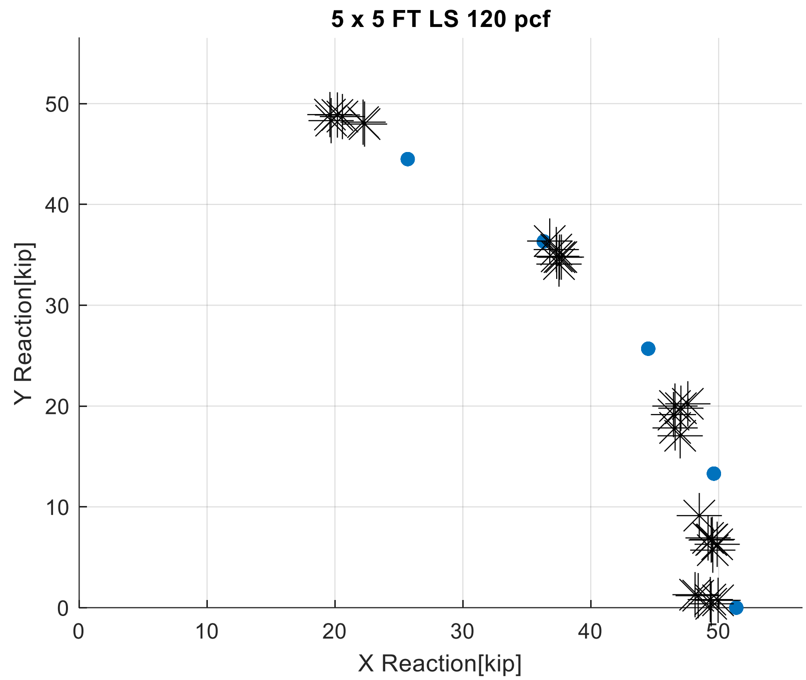

Figure 4-174 Case 7 friction resistance pattern per prescribed displacement and orientations.

Table 4-36 Plaxis friction comparison - case results.

	BIAS				CV			
CASE	X	Y	RESULTANT	0/90	X	Y	RESULTANT	0/90
4	0.91	0.94	0.91	0.94	0.03	0.07	0.03	0.02
5	0.89	0.90	0.90	0.92	0.03	0.06	0.03	0.03
6	0.94	0.83	0.92	0.97	0.03	0.07	0.04	0.02
7	0.97	0.83	0.99	0.95	0.09	0.27	0.03	0.01

Table 4-37 Plaxis friction comparison - soil and limestone results.

	BIAS				CV			
CASE	X	Y	RESULTANT	0/90	X	Y	RESULTANT	0/90
LIMESTONE	0.92	0.87	0.93	0.94	0.07	0.15	0.05	0.03

CHAPTER 5
INVESTIGATION OF INCLINED AND ECCENTRIC LOADS ON LIMESTONE BEARING CAPACITY

5.1 Introduction

Florida Limestone (calcium carbonate & dolomite) occurs in many different formations near the ground surface (e.g. Miami, Fort Thompson, Anastasia, Key Largo, etc.). Existing at many different bulk dry unit weights (85 pcf to 145 pcf), the majority exhibits ductile stress-strain response: a linear increasing stress vs strain response until yielding/failure (Mohr-Coulomb) and then a constant stress vs increasing strain. In general, Florida Limestone has a constant Young's Modulus that is 5 to 50 times (depending on bulk dry unit weight) the value of sand until yielding/failure; however, due to formation and age, Florida Limestone has a high median porosity (37%) which has a significant impact on volumetric and strength characteristics of the material. Specifically, under increasing hydrostatic or triaxial shear loading, the material will undergo significant compression volumetric straining as well as matrix crushing resulting in ductile response (bilinear stress-strain), as well as bilinear Mohr-Coulomb Strength Envelope (FDOT, Phase I report).

For footings embedded in Florida Limestone, the stress and strain behavior characteristic of the different formations influence the bearing capacity as shown in FDOT, Phase II report and incorporated into FB-MultiPier in Task 1. Of interest is the appropriate treatment of estimated bearing capacity when the footing is under inclined and eccentric loads. AASHTO Bridge Design Specifications recommend inclination factors to reduce the cohesion, overburden, and unit-weight contributions to bearing capacity of soil as a function of the angle of the inclined load or the ratio of the inclined load's horizontal and vertical components. Specifically, Vesić (1973) inclination factor equations (Equation 5-1 – Equation 5-2) for footings on soil, developed through small scale tests, are recommended. Also recommended for effects of eccentricity is Meyerhof's (1953) method which reduces the footing width, B, and length, L, to effective footing width, B´, and effective footing length, L´, as a function of the eccentricity as shown in Equation 5-5 and Equation 5-6.

$i_c = i_q - [(1 - i_q) / (N_q - 1)]$ for $\phi_f > 0$ Equation 5-1

$i_c = 1 - \frac{nH}{cBLN_c}$ for $\phi_f = 0$ Equation 5-2

$i_q = (1 - \frac{H}{(V + cBL\cot\phi_f)})^m$ Equation 5-3

$i_\gamma = (1 - \frac{H}{(V+cBLcot\phi_f)})^{m+1}$ Equation 5-4

where m = [(2+L/B)/(1+L/B)] $\cos^2\theta$ + [(2+B/L)/(1+B/L)] $\sin^2\theta$, B is foundation width, L is foundation length, H is unfactored horizontal load, V is unfactored vertical load, and θ is the projected direction of the resultant load, R, in

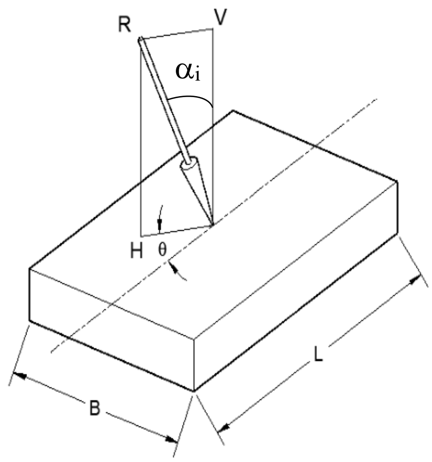

Figure 5-1 Footing with inclined load, r, in b and l directions.

$B' = B - 2e_B$ Equation 5-5

where $e_B = \frac{M_B}{V}$, M_B is the moment due to eccentric loads in the B direction and V is the total vertical load.

$L' = L - 2e_L$ Equation 5-6

where $e_L = \frac{M_L}{V}$, M_B is the moment due to eccentric loads in the L direction and V is the total vertical load.

Recent investigations of the bearing capacity of footings on rock masses under inclined and eccentric loading are limited to analytical and numerical studies of rock represented by Hoek-Brown failure criteria, not representative of Florida limestone stress-strain behavior. Chihi and Saada (2022) proposed analytical expressions based on the kinematic approach of limit analysis theory, which provides upper-bound solutions. Bearing capacity for strip footings on Hoek-Brown rock masses under eccentric and inclined loading were investigated using finite element limit analysis (Keawsawasvong, Thongchom, and Likitlersuang 2021). A bearing capacity factor, $P/\sigma_{ci}B^2$ was shown to be influenced by GSI, m_i, α_i (inclination angle), and e/B, with higher GSI, m_i, α_i, or smaller e/B, resulting in greater capacity. Larger GSI, m_i values create broader failure zones, while α_i and e/B significantly affect failure mechanics, causing lateral extensions in response to inclined loads. The authors compiled design charts for strip footings on Hoek-Brown rock masses under complex loading conditions.

5.2 Bearing Capacity of Footings Under Inclined and Eccentric Loads

This investigation focuses on the influence that inclined and eccentric loads have on the bearing capacity of Florida limestone though finite element simulations. PLAXIS 3D is used to model different footing sizes with and without embedment, where the limestone is modeled based on the custom calibrated models from Task 1. A displacement-controlled swipe analysis was conducted, applying specified displacements to the nodes of the footing in such a way that V and either M or H vary continuously and simultaneously, while the footing is kept in a collapse state the entire time. After footing reaches an initial failure (collapse) state, the value of the footing load V and either α_i (=$\tan^{-1}$(H/V)) or e (=M/V) change continuously so that the footing remains in an evolving state of failure.

5.2.1 Model Parameters

For this study square footing, rectangular footing and strip footing (Figure 5-2) model were created. For the square footing, the soil body of 50’x50’x50’and the footing size of length = width = 5 ft used. For the rectangular and strip footing, the soil body of 100’x50’x50’, 200’x50’x50’and the footing size of length = 50 ft, width = 5 ft & length = 110 ft, width = 5 ft were used respectively. Plates having the properties of footing have been used in all models (unit weight, γ_{dt} = 133.7 pcf, young modulus, E = 4.18E+09 lb/ft^2, poisson ratio, ν = 0.1 and plate is used as rigid body).

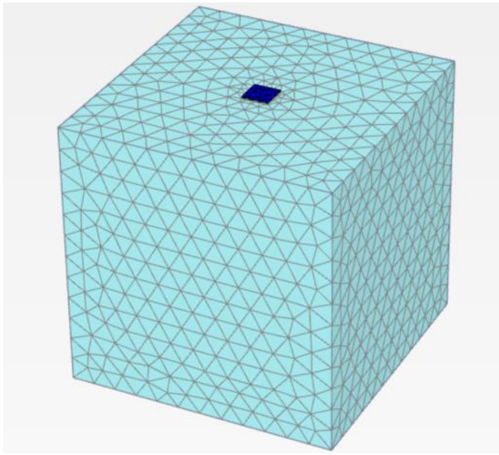

(a)

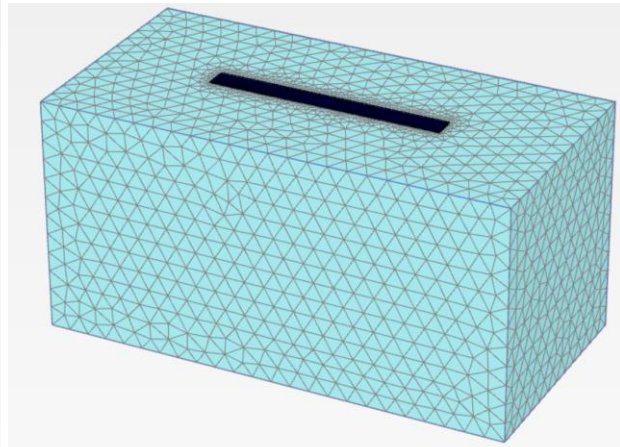

(b)

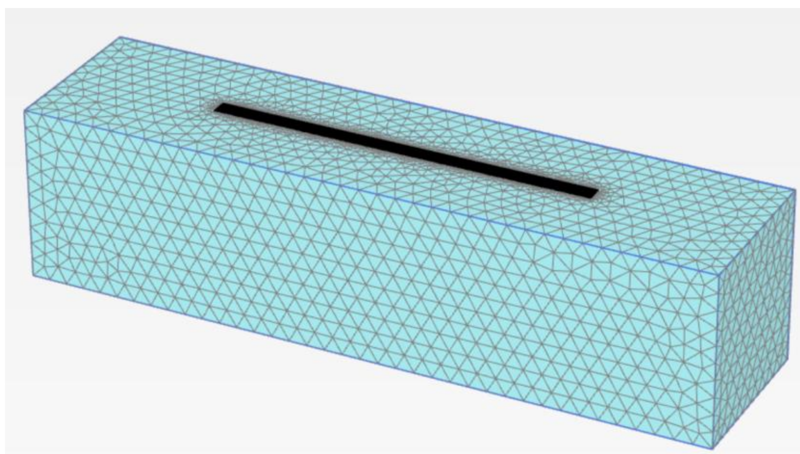

(c)

Figure 5-2 Plaxis meshed footing models (a) L/B = 1, (b) L/B = 10, (c) L/B = 20.

5.2.2 Florida Limestone Properties and Parametric Studies

Florida's limestone formations exhibit a wide range of geomechanical properties, reflecting their diverse geological origins and degrees of diagenesis. Based on the bilinear strength envelope and ductile stress–strain response of the Florida limestone, a perfectly elastic–plastic material model (modified MC) is used using four parameters (α, α, β and $p_{p\omega}$). The soil mechanical behavior is modelled using the user defined soil model. PLAXIS 3D allows users to implement and utilize User Defined Soil Models (UDSMs) to simulate complex soil behavior. This involves programming a constitutive model in Python and compiling it as a Dynamic Link Library (DLL), which is then integrated into PLAXIS. Table 5-1 summarizes the mass rock properties of prominent limestone formations used in this study: Miami Limestone, Anastasia Limestone, Shallow Fort Thompson Limestone.

Table 5-1 Limestone formation bi-linear failure envelope model mass properties.

Formation	γ_{dt}, pcf	c_m, psi	φ_m, °	$\sigma_{peak\ i}$, psi	ω_m, °	a_m, psi	α_m, °	Pp_m, psi	β_m, °
Miami Limestone	90	29.5	32.5	522.8	-2.4	24.88	28.3	247	-2.4
Anastasia Limestone	140	200.7	36.5	1985.3	18.8	161.44	30.7	977	17.8
Shallow Ft. Thompson Limestone	105	27.5	32.4	506.7	-0.1	23.2	28.2	239	-0.1

For the bearing capacity analysis, a footing with a width of 5 ft and a height of 5 ft was considered. The analysis incorporated varying footing ratios, with L/B values ranging from 1 to >20. Load eccentricities of 0, B/6, and B/12 were applied, along with load inclinations of 0°, 3°, 7°, 14° and 20°. Two embedment conditions were examined: surface footings (D_f=0), and fully embedded footings (D_f=B). This study included homogeneous rock profiles. A total of 3 distinct soil model variations were evaluated across all combinations of embedment depth, soil layering, aspect ratio, eccentricity, and inclination for the bearing capacity study.

5.2.3 Mesh Discretization and Boundary Conditions

The use of unstructured meshes composed of triangular elements provides flexibility in element arrangement and element size. For the study with a non-associated flow the meshes are composed of 6-noded triangular elements with three Gauss quadrature points. Optimized mesh is used for all the model cases in this study. Interface at the contact of soil and footing is used having properties same as that of the soil (limestone). For all the models, bottom surface was fixed in all directions, and a vertical roller was used on each side in the x-direction, and in the y-direction. Point displacement is applied at the center or eccentric (e=b/6=0.833 ft and e=b/12=0.4167) point of the plate using rigid body. For vertical displacement, 0.4ft is applied in z-direction and for 3-degree inclined displacement, 0.399 ft is applied at z-direction and 0.02093 ft applied in y-direction, for 7-degree inclined displacement, 0.397 ft is applied at z-direction and 0.04875 ft applied in y-direction. For vertical displacement, 0.4 ft is applied in z-direction and for 14-degree inclined displacement, 0.3881 ft is applied at z-direction and 0.0967 ft applied in y-direction and for 20-degree inclined displacement, 0.3758 ft is applied at z-direction and 0.1368 ft applied in y-direction. The translation condition of the rigid body is set as displacement, and rotation condition is set as moment=0.

5.2.4 PLAXIS Model Calibration

The PLAXIS models for each footing sizes (Figure 5-2) and formations (Table 5-1) were calibrated at first by comparing the different model results with the predicted bearing capacity for concentric loading using the bearing capacity equation developed for Florida limestone (Yang et al. 2023). The part of analysis in this study was to determine the correct constitutive model file based on the four parameters (α, α, β and $p_{p\omega}$) for each formation. For each formation, the concentric model is calibrated using the Florida Limerock equations were adopted (Yang et al. 2023), where the ultimate bearing capacity is the minimum (Equation 5-7) of Equation 5-8 and Equation 5-9.

$$Q_u = \min (Q_{u1}, Q_{u2})\ \xi \quad \text{Equation 5-7}$$

with

$$Q_{u1} = ncN_c\, i_c + qN_q i_q \quad \text{Equation 5-8}$$

$$Q_{u2} = n\ [cN'_c i_c + p_{pw}\ N_g i_\gamma] + qN_q i_q \quad \text{Equation 5-9}$$

where Q_{u1} and Q_{u2} represent the major principal stress (σ_1) associated with the points where the stress paths intercept the bilinear strength envelope to the left (Q_{u1}) or right (Q_{u2}) of $p_{p\omega}$ in the p-q space. c is the limestone cohesion, i_c, i_g, and i_q are the inclination factor for cohesion, unit weight, and surcharge (embedment), q (D_f x g). The equations of the factors N_c, N'_c, N_γ and N_q are developed for the Florida limestone:

$$N_c = \frac{1.8 cos\varphi}{0.8 - sin\varphi} \quad \text{Equation 5-10}$$

$$N'_c = \frac{1.8 cos\varphi}{0.8 - sin\omega} \quad \text{Equation 5-11}$$

$$N_\gamma = \frac{1.8\ [sin\varphi - sin\omega]}{0.8 - sin\omega} \quad \text{Equation 5-12}$$

$$N_q = (1.53 \text{ x } \frac{p_{pw}}{p_a} - 10) \text{ x } (3 \text{ x } \sin\varphi - 1) \quad \text{Equation 5-13}$$

n is the width factor and ξ is the shape factors respectively:

$$n = \frac{4}{B\ in\ meters}^{-0.055} \quad \text{Equation 5-14}$$

$$\xi = 1 + 0.245(\frac{B}{L})^{0.66} \quad \text{Equation 5-15}$$

where *B* and *L* denote the foundation width and length, respectively.

Miami Limestone

The comparative evaluation of bearing capacity values for shallow foundations placed on the Miami Limestone-1 (ML-1) formation, utilizing both PLAXIS 3D finite element simulations and Florida Limestone predictions is shown in Table 5-2. Figure 5-3 presents the PLAXIS pressure-displacement results showing mobilized bearing and the predicted bearing capacity as a solid line. The predictions were generated using a bearing capacity equation specifically developed for Florida Limestone, tailored to capture the unique geomechanical behavior of carbonate formations found in the region. Three footing configurations were investigated - square footing (L/B = 1), rectangular footing (L/B = 10), and strip footing (L/B > 20). Across all cases, the PLAXIS simulation results showed strong agreement with the bearing capacities predicted by the Florida Limestone equation, with percentage differences of 2.82%, 1.74%, and 1.09% for the square, rectangular, and strip footings, respectively. The decreasing trend in deviation with increasing L/B ratio underscores the equation's and model's improved accuracy under conditions approximating plane strain, where stress distributions are predominantly two-dimensional.

Table 5-2 Comparison of measured and predicted bearing capacities for footings on Miami limestone (ML-1).

ML-1					
Cases	**PLAXIS Bearing Capacity**	**Q_{u1}**	**Q_{u2}**	**Predicted Bearing Capacity, Q_u**	**% difference**
Square footing (L/B=1)	192.59	161.723	340.358	201.35	4.35
Rectangular footing (L/B=10)	173.35			170.39	1.74
Strip footing (L/B>20)	161.06			166.87	3.48

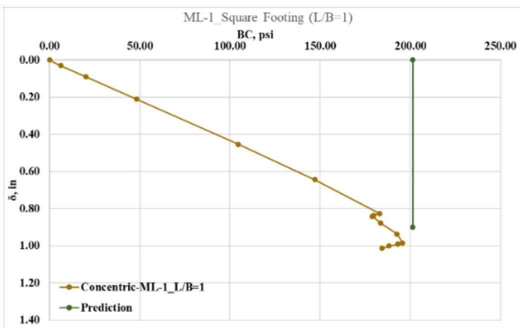

(a)

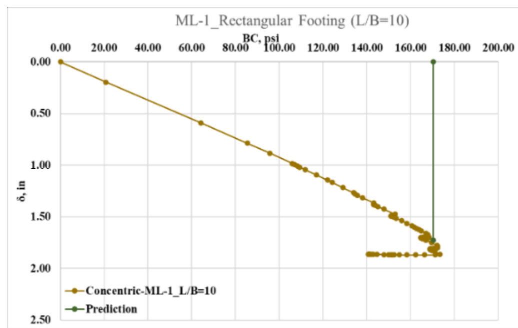

(b)

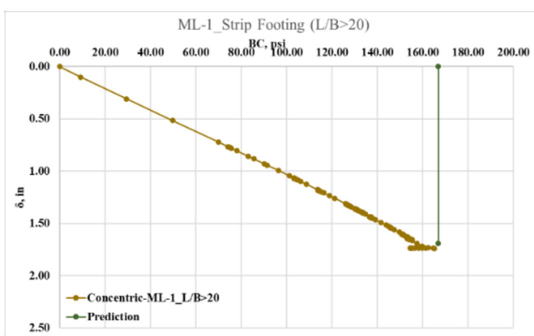

(c)

Figure 5-3 Load-settlement for footings on ML-1 formation: (a) square footing (L/B = 1), (b) rectangular footing (L/B = 10), and (c) strip footing (L/B = 20) from Plaxis models and Florida bearing capacity prediction.

Fort Thompson Limestone

Table 5-3 shows the results for the Fort Thompson Limestone (FTL-2) formation from the PLAXIS 3D numerical simulations and bearing capacity predictions for the footing configurations square footing (L/B = 1), rectangular footing (L/B = 10), and strip footing (L/B > 20). The square footing exhibits the largest percentage difference at 7.83%, with a predicted bearing capacity of 186.28 psi compared to 202.10 psi from PLAXIS model. Figure 5-4 presents the PLAXIS pressure-displacement results showing mobilized bearing and the predicted bearing capacity as a solid line. Rectangular and strip footings demonstrate considerably better agreement, with deviations of only 1.83% and 2.67%, respectively.

Table 5-3 Comparison of measured and predicted bearing capacities for footings on Fort Thompson limestone (FTL-2).

FTL-2					
Cases	**PLAXIS Bearing Capacity**	Q_{u1}	Q_{u2}	**Predicted Bearing Capacity**	**% difference**
Square footing (L/B=1)	164.57	149.622	322.477	186.28	11.65
Rectangular footing (L/B=10)	160.52			157.64	1.83
Strip footing (L/B>20)	158.51			154.39	2.67

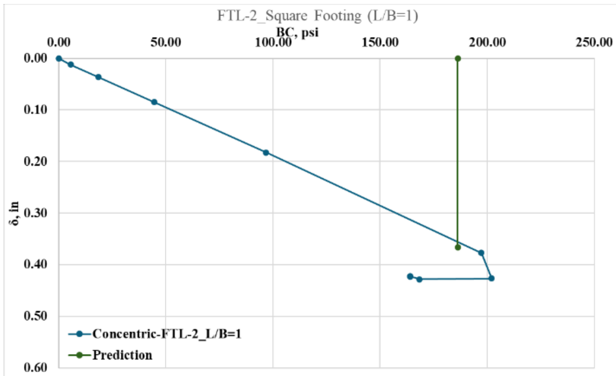

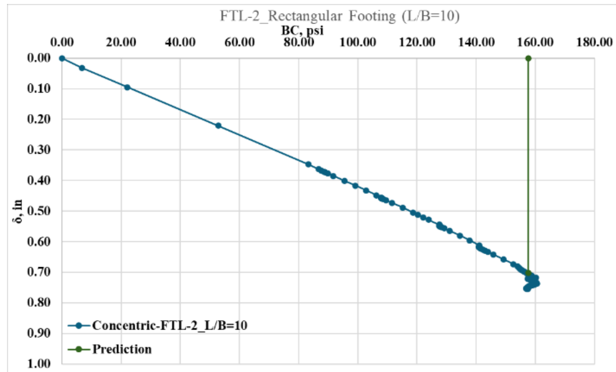

(a) (b)

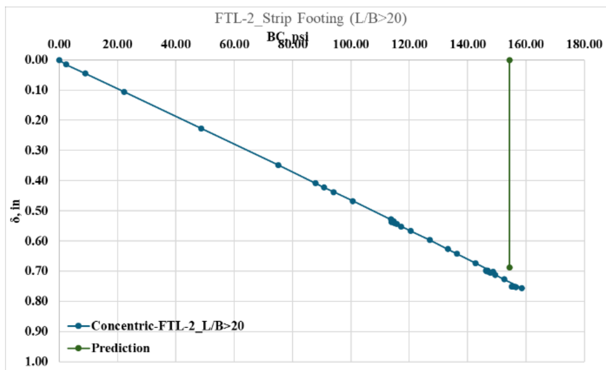

(c)

Figure 5-4 Load-settlement for footings on FTL-2 formation: (a) square footing (L/B = 1), (b) rectangular footing (L/B = 10), and (c) strip footing (L/B = 20) from Plaxis models and Florida bearing capacity prediction.

Anastasia Limestone

Table 5-4 shows the results for the Anastasia Limestone (AL-3) formation from the PLAXIS 3D numerical simulations and bearing capacity predictions for the footing configurations square footing (L/B = 1), rectangular footing (L/B = 10), and strip footing (L/B > 20). Figure 5-5 presents the PLAXIS pressure-displacement results showing mobilized bearing and the predicted bearing capacity as a solid line. The square footing yielded a PLAXIS capacity of 1600.43 psi, with the predicted model slightly overpredicting at 1665.09 psi, a deviation of 3.88%. For the rectangular and strip footings, the predicted capacities were 1409.10 psi and 1380.02 psi, compared to PLAXIS values of 1466.69 psi and 1426.46 psi, respectively. These differences, 4.09% and 3.37%, remain within an acceptable range, reaffirming the robustness of the prediction model when applied to stronger formations like AL-3.

Table 5-4 Comparison of measured and predicted bearing capacities for footings on Anastasia limestone (AL-3).

AL-3					
Cases	PLAXIS Bearing Capacity	Q_{u1}	Q_{u2}	Predicted Bearing Capacity	% difference
Square footing (L/B=1)	1600.43	1337.42	1524.74	1665.09	3.88
Rectangular footing (L/B=10)	1466.69			1409.10	4.09
Strip footing (L/B>20)	1426.46			1380.02	3.37

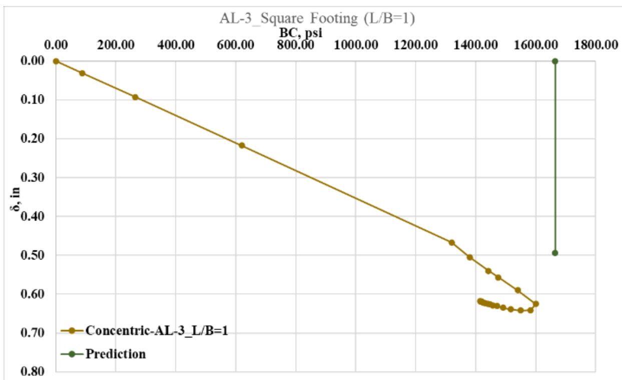

(a)

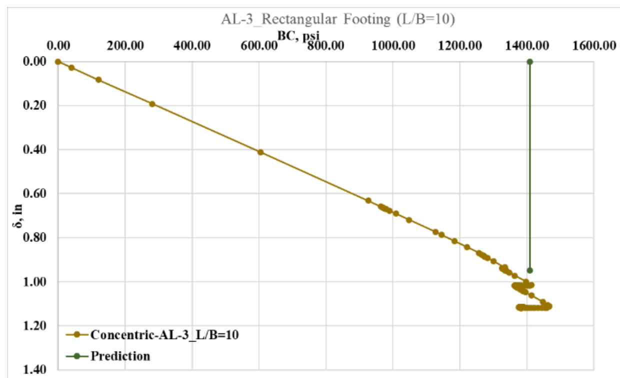

(b)

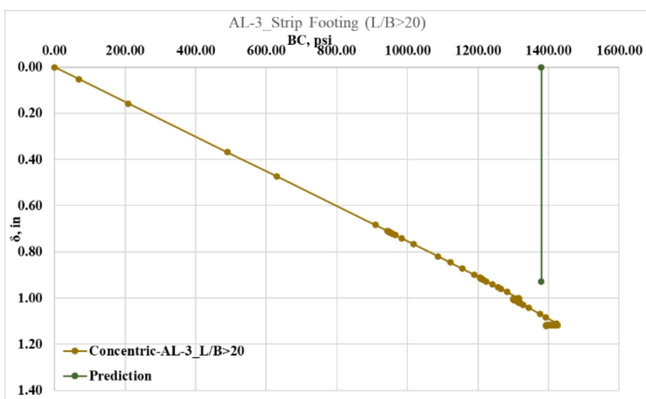

(c)

Figure 5-5 Load-settlement for footings on AL-3 formation: (a) square footing (L/B = 1), (b) rectangular footing (L/B = 10), and (c) strip footing (L/B = 20) from Plaxis models and Florida bearing capacity prediction.

The comparative evaluation of bearing capacities between the PLAXIS 3D simulations and the bearing capacity equation demonstrates suitable models for subsequent investigation of the influence of inclined and eccentric loads in the footing B direction. In the following sections, the PLAXIS simulations are referred to as “load tests” for brevity and their results as the “measured” as they are the only experiments conducted to date.

5.2.5 Inclination and Eccentricity Model Results

Square Footing (L/B = 1) PLAXIS Results and Observations

A total of 51 load tests were performed on the square footing: 17 with Miami Limestone properties, 17 with Fort Thompson Limestone properties and 17 with Anastasia Limestone properties. The square footing was loaded for inclined and eccentric loading with depths of embedment equal to zero and B, at inclination angle of 3 degrees, 7 degrees, 14 degrees and 20 degrees. All eccentric loads were applied B/6 and B/12 from the center of the footing. The model footing was tested using 5 feet long by 5 feet wide with the length-to width ratio of one.

Table 5-5, Table 5-6, and Table 5-7 shows the test parameters and results for square footing in the Miami, Fort Thompson, and Anastasia Limestone formations, respectively. Subsequent plots in Figure 5-6, Figure 5-7, and Figure 5-8 shows the bearing capacity curves obtained from each test in the tables for each formation. Inclined loading cases are plotted in combination with concentric loading cases, to reference any increase or decrease in bearing capacity associated with the change in embedment depth, eccentricity, inclined load conditions. Evident in each of the set of results, the bearing capacity decreases with an increase in inclination angle and eccentricity. The bearing capacity for each test was taken at the initial point of zero slope.

The load tests of L/B = 1 footings on Miami limestone, Fort Thompson limestone and Anastasia limestone were conducted to investigate the influence of inclined and eccentric loading on the bearing capacity when the depth of embedment is zero and B. For the tests on Miami limestone, the following observations of the bearing capacity were made.

- For the inclination of 3 degrees, when $D_f = 0$, the bearing capacity was 2.87% less than the concentrically loaded footing. When $D_f = B$, the bearing capacity was 2.95% less than the concentrically loaded footing with $D_f = B$ for the inclination angle of 3 degrees. When $\gamma=0$ for $D_f = 0$, the bearing capacity was 2.74% less than the concentrically loaded footing for the inclination angle of 3 degrees.
- For the inclination of 7 degrees, when $D_f = 0$, the bearing capacity was 4.20% less than the concentrically loaded footing. When $D_f = B$, the bearing capacity was 4.94% less than the concentrically loaded footing with $D_f = B$ for the inclination angle of 7 degrees. When $\gamma=0$ for $D_f = 0$, the bearing capacity was 3.60% less than the concentrically loaded footing for the inclination angle of 7 degrees.
- For the inclination of 14 degrees, when $D_f = 0$, the bearing capacity was 6.84% less than the concentrically loaded footing. When $D_f = B$, the bearing capacity was 7.44% less than the concentrically loaded footing with $D_f = B$ for the inclination angle of 14 degrees. When $\gamma=0$ for $D_f = 0$, the bearing capacity was 6.12% less than the concentrically loaded footing for the inclination angle of 14 degrees.

- For the inclination of 20 degrees, when $D_f = 0$, the bearing capacity was 7.76% less than the concentrically loaded footing. When $D_f = B$, the bearing capacity was 11.74% less than the concentrically loaded footing with $D_f = B$ for the inclination angle of 20 degrees. When $\gamma=0$ for $D_f = 0$, the bearing capacity was 6.59% less than the concentrically loaded footing for the inclination angle of 20 degrees.
- For the eccentricity of e=B/6, when $D_f = 0$, the bearing capacity was 14.12% less than the concentrically loaded footing. On the other hand, for the eccentricity of e=B/12, when $D_f = 0$, the bearing capacity was 1.95% less than the concentrically loaded footing.

For the tests on Fort Thompson limestone, the following observations of the bearing capacity were made.

- For the inclination of 3 degrees, when $D_f = 0$, the bearing capacity was 6.35% less than the concentrically loaded footing. When $D_f = B$, the bearing capacity was 7.31% less than the concentrically loaded footing with $D_f = B$ for the inclination angle of 3 degrees. When $\gamma=0$ for $D_f = 0$, the bearing capacity was 4.24% less than the concentrically loaded footing for the inclination angle of 3 degrees.
- For the inclination of 7 degrees, when $D_f = 0$, the bearing capacity was 8.92% less than the concentrically loaded footing. When $D_f = B$, the bearing capacity was 11.98% less than the concentrically loaded footing with $D_f = B$ for the inclination angle of 7 degrees. When $\gamma=0$ for $D_f = 0$, the bearing capacity was 6.32% less than the concentrically loaded footing for the inclination angle of 7 degrees.
- For the inclination of 14 degrees, when $D_f = 0$, the bearing capacity was 10.17% less than the concentrically loaded footing. When $D_f = B$, the bearing capacity was 13.76% less than the concentrically loaded footing with $D_f = B$ for the inclination angle of 14 degrees. When $\gamma=0$ for $D_f = 0$, the bearing capacity was 6.50% less than the concentrically loaded footing for the inclination angle of 14 degrees.
- For the inclination of 20 degrees, when $D_f = 0$, the bearing capacity was 12.47% less than the concentrically loaded footing. When $D_f = B$, the bearing capacity was 16.72% less than the concentrically loaded footing with $D_f = B$ for the inclination angle of 20 degrees. When $\gamma=0$ for $D_f = 0$, the bearing capacity was 8.61% less than the concentrically loaded footing for the inclination angle of 20 degrees.
- For the eccentricity of e=B/6, when $D_f = 0$, the bearing capacity was 29.91% less than the concentrically loaded footing. On the other hand, for the eccentricity of e=B/12, when $D_f = 0$, the bearing capacity was 18.97% less than the concentrically loaded footing.

For the tests on Anastasia limestone, the following observations of the bearing capacity were made.

- For the inclination of 3 degrees, when $D_f = 0$, the bearing capacity was 1.88% less than the concentrically loaded footing. When $D_f = B$, the bearing capacity was 2.11% less than the concentrically loaded footing with $D_f = B$ for the inclination angle of 3 degrees. When

γ=0 for D_f = 0, the bearing capacity was 1.31% less than the concentrically loaded footing for the inclination angle of 3 degrees.

- For the inclination of 7 degrees, when D_f = 0, the bearing capacity was 2.35% less than the concentrically loaded footing. When D_f = B, the bearing capacity was 2.64% less than the concentrically loaded footing with D_f =B for the inclination angle of 7 degrees. When γ=0 for D_f = 0, the bearing capacity was 1.64% less than the concentrically loaded footing for the inclination angle of 7 degrees.
- For the inclination of 14 degrees, when D_f = 0, the bearing capacity was 3.91% less than the concentrically loaded footing. When D_f = B, the bearing capacity was 4.25% less than the concentrically loaded footing with D_f =B for the inclination angle of 14 degrees. When γ=0 for D_f = 0, the bearing capacity was 3.01% less than the concentrically loaded footing for the inclination angle of 14 degrees.
- For the inclination of 20 degrees, when D_f = 0, the bearing capacity was 7.02% less than the concentrically loaded footing. When D_f = B, the bearing capacity was 7.62% less than the concentrically loaded footing with D_f =B for the inclination angle of 20 degrees. When γ=0 for D_f = 0, the bearing capacity was 5.90% less than the concentrically loaded footing for the inclination angle of 20 degrees.
- For the eccentricity of e=B/6, when D_f = 0, the bearing capacity was 35.70% less than the concentrically loaded footing. On the other hand, for the eccentricity of e=B/12, when D_f = 0, the bearing capacity was 19.85% less than the concentrically loaded footing.

Table 5-5 PLAXIS results for square footing (L/B = 1) with Miami limestone (ML-1).

Case	**Inclination angle**	**Eccentricity, e**	**Embedment, D_f**	**Unit Weight, γ (lb/ft3)**	**Φ_m (deg)**	**Bearing Capacity, psi**	**Displacement, in**
1	0	0	0	90	32.52	195.59	1.14
2	0	e/6	0	90	32.52	167.98	0.90
3	0	e/12	0	90	32.52	191.77	1.29
4	3	0	0	90	32.52	189.98	1.06
5	7	0	0	90	32.52	187.37	1.00
6	14	0	0	90	32.52	182.21	0.97
7	20	0	0	90	32.52	180.41	0.97
8	0	0	B	90	32.52	239.67	1.23
9	3	0	B	90	32.52	232.59	1.01
10	7	0	B	90	32.52	227.83	0.93
11	14	0	B	90	32.52	221.84	1.12
12	20	0	B	90	32.52	211.54	0.79
13	0	0	0	0	32.52	188.59	0.94
14	3	0	0	0	32.52	183.42	0.99
15	7	0	0	0	32.52	181.80	1.01
16	14	0	0	0	32.52	177.05	0.95
17	20	0	0	0	32.52	176.16	0.90

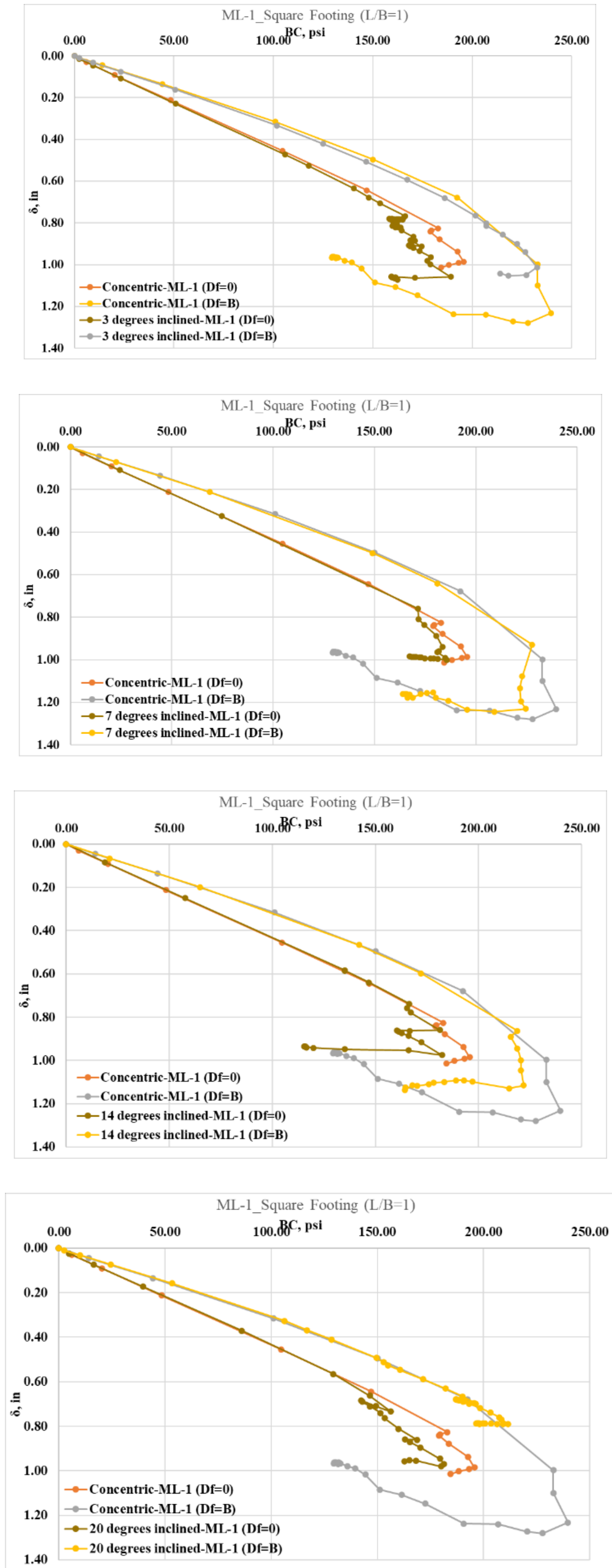

Figure 5-6 Load-settlement for square footings (L/B = 1) on ML-1 formation for load inclination angle of 3°, 7°, 14°, and 20°.

Table 5-6 PLAXIS results for square footing (L/B = 1) with Fort Thompson limestone (FTL-2).

Case	Inclination angle	Eccentricity, e	Embedment, D_f	Unit Weight, γ (lb/ft3)	Φ_m (deg)	Bearing Capacity, psi	Displacement, in
1	0	0	0	105	32.3814	202.10	0.56
2	0	e/6	0	105	32.3814	141.66	0.46
3	0	e/12	0	105	32.3814	163.77	0.41
4	3	0	0	105	32.3814	189.28	0.48
5	7	0	0	105	32.3814	184.08	0.43
6	14	0	0	105	32.3814	181.55	0.44
7	20	0	0	105	32.3814	176.90	0.46
8	0	0	B	105	32.3814	216.67	0.45
9	3	0	B	105	32.3814	200.84	0.44
10	7	0	B	105	32.3814	190.73	0.43
11	14	0	B	105	32.3814	186.87	0.32
12	20	0	B	105	32.3814	180.44	0.30
13	0	0	0	0	32.3814	185.97	0.41
14	3	0	0	0	32.3814	178.08	0.41
15	7	0	0	0	32.3814	174.22	0.42
16	14	0	0	0	32.3814	173.89	0.45
17	20	0	0	0	32.3814	169.95	0.41

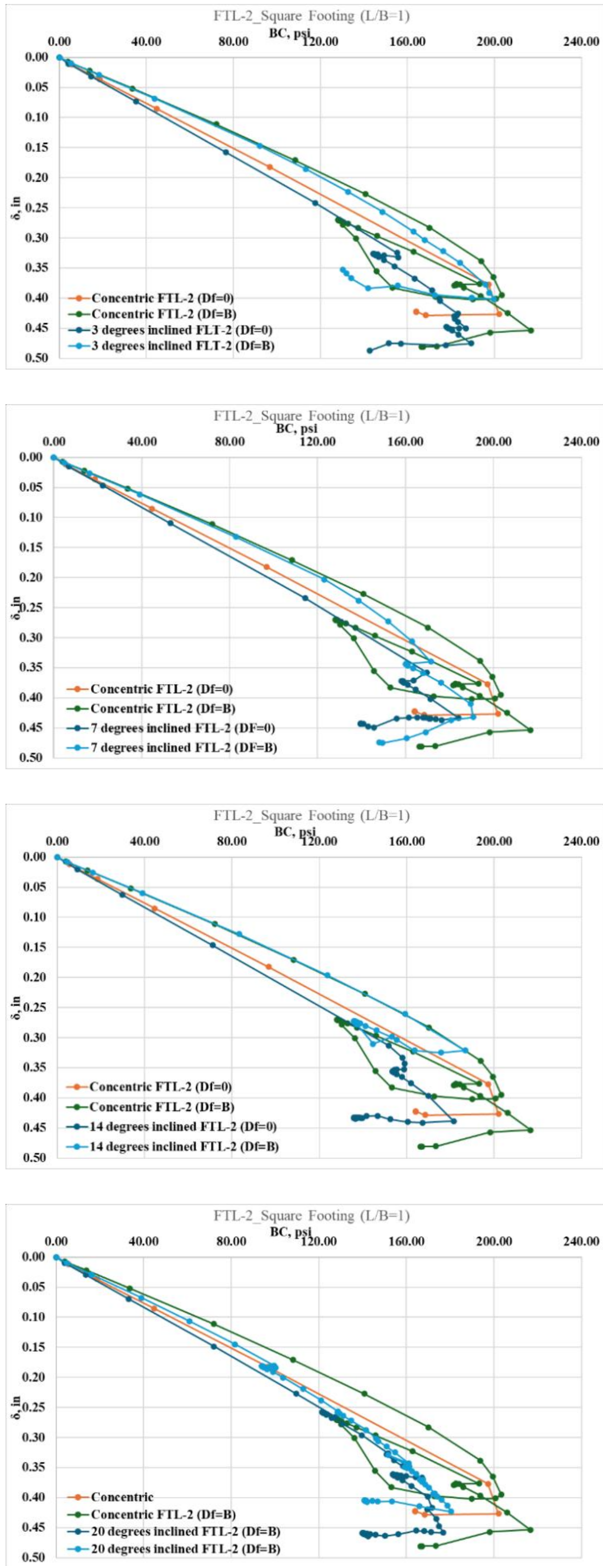

Figure 5-7 Load-settlement for square footings (L/B = 1) on FTL-2 formation for load inclination angle of 3°, 7°, 14°, and 20°.

Table 5-7 PLAXIS results for square footing (L/B = 1) with Anastasia limestone (AL-3).

Case	Inclination angle	Eccentricity, e	Embedment, D_f	Unit Weight, γ (lb/ft3)	Φ_m (deg)	Bearing Capacity, psi	Displacement, in
1	0	0	0	140	36.4508	1600.43	0.62
2	0	e/6	0	140	36.4508	1029.04	0.44
3	0	e/12	0	140	36.4508	1282.70	0.49
4	3	0	0	140	36.4508	1570.42	0.59
5	7	0	0	140	36.4508	1562.76	0.57
6	14	0	0	140	36.4508	1537.80	0.57
7	20	0	0	140	36.4508	1488.05	0.55
8	0	0	B	140	36.4508	1625.46	0.63
9	3	0	B	140	36.4508	1591.11	0.59
10	7	0	B	140	36.4508	1582.55	0.57
11	14	0	B	140	36.4508	1556.45	0.55
12	20	0	B	140	36.4508	1501.58	0.51
13	0	0	0	0	36.4508	1567.61	0.67
14	3	0	0	0	36.4508	1547.13	0.63
15	7	0	0	0	36.4508	1541.96	0.62
16	14	0	0	0	36.4508	1520.47	0.59
17	20	0	0	0	36.4508	1475.09	0.53

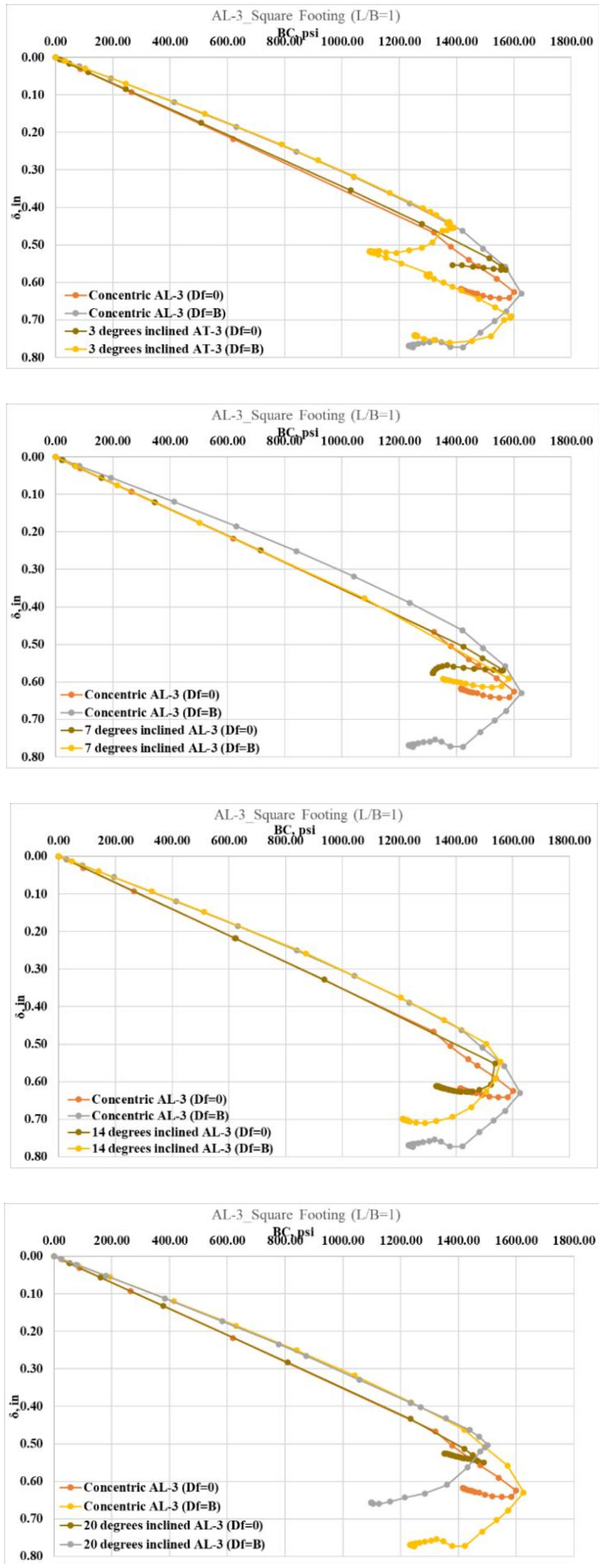

Figure 5-8 Load-settlement for square footings (L/B = 1) on AL-3 formation for load inclination angle of 3°, 7°, 14°, and 20°.

Rectangular Footing (L/B = 10) PLAXIS Results and Observations

A total of 51 load tests were performed on the rectangular footing: 17 with Miami Limestone properties, 17 with Fort Thompson Limestone properties and 17 with Anastasia Limestone properties. The square footing was loaded for inclined and eccentric loading with depths of embedment equal to zero and B, at inclination angle of 3 degrees, 7 degrees, 14 degrees and 20 degrees. All eccentric loads were applied B/6 and B/12 from the center of the footing. The model footing was tested using 50 feet long by 5 feet wide with the length-to width ratio of 10.

Table 5-8, Table 5-9, and Table 5-10 shows the test parameters and results for square footing in the Miami, Fort Thompson, and Anastasia Limestone formations, respectively. Subsequent plots in Figure 5-9, Figure 5-10, and Figure 5-11 shows the bearing capacity curves obtained from each test in the tables for each formation. Inclined loading cases are plotted in combination with concentric loading cases, to reference any increase or decrease in bearing capacity associated with the change in embedment depth, eccentricity, inclined load conditions. Evident in each of the set of results, the bearing capacity decreases with an increase in inclination angle and eccentricity. The bearing capacity for each test was taken at the initial point of zero slope.

The load tests of L/B = 10 footings on Miami limestone, Fort Thompson limestone and Anastasia limestone were conducted to investigate the influence of inclined and eccentric loading on the bearing capacity when the depth of embedment is zero and B. For the tests on Miami limestone, the following observations of the bearing capacity were made.

- For the inclination of 3 degrees, when $D_f = 0$, the bearing capacity was 1.07% less than the concentrically loaded footing. When $D_f = B$, the bearing capacity was 5.56% less than the concentrically loaded footing with $D_f = B$ for the inclination angle of 3 degrees. When $\gamma=0$ for $D_f = 0$, the bearing capacity was 0.65% less than the concentrically loaded footing for the inclination angle of 3 degrees.
- For the inclination of 7 degrees, when $D_f = 0$, the bearing capacity was 1.71% less than the concentrically loaded footing. When $D_f = B$, the bearing capacity was 10.86% less than the concentrically loaded footing with $D_f = B$ for the inclination angle of 7 degrees. When $\gamma=0$ for $D_f = 0$, the bearing capacity was 1.25% less than the concentrically loaded footing for the inclination angle of 7 degrees.
- For the inclination of 14 degrees, when $D_f = 0$, the bearing capacity was 3.32% less than the concentrically loaded footing. When $D_f = B$, the bearing capacity was 14.60% less than the concentrically loaded footing with $D_f = B$ for the inclination angle of 14 degrees. When $\gamma=0$ for $D_f = 0$, the bearing capacity was 2.70% less than the concentrically loaded footing for the inclination angle of 14 degrees.
- For the inclination of 20 degrees, when $D_f = 0$, the bearing capacity was 8.30% less than the concentrically loaded footing. When $D_f = B$, the bearing capacity was 19.69% less than the concentrically loaded footing with $D_f = B$ for the inclination angle of 20 degrees.

When γ=0 for D_f = 0, the bearing capacity was 7.53% less than the concentrically loaded footing for the inclination angle of 20 degrees.

- For the eccentricity of e=B/6, when D_f = 0, the bearing capacity was 33.18% less than the concentrically loaded footing. On the other hand, for the eccentricity of e=B/12, when D_f = 0, the bearing capacity was 22.15% less than the concentrically loaded footing.

For the tests on Fort Thompson limestone, the following observations of the bearing capacity were made.

- For the inclination of 3 degrees, when D_f = 0, the bearing capacity was 3.20% less than the concentrically loaded footing. When D_f = B, the bearing capacity was 7.01% less than the concentrically loaded footing with D_f =B for the inclination angle of 3 degrees. When γ=0 for D_f = 0, the bearing capacity was 2.09% less than the concentrically loaded footing for the inclination angle of 3 degrees.
- For the inclination of 7 degrees, when D_f = 0, the bearing capacity was 4.43% less than the concentrically loaded footing. When D_f = B, the bearing capacity was 11.17% less than the concentrically loaded footing with D_f =B for the inclination angle of 7 degrees. When γ=0 for D_f = 0, the bearing capacity was 2.87% less than the concentrically loaded footing for the inclination angle of 7 degrees.
- For the inclination of 14 degrees, when D_f = 0, the bearing capacity was 4.97% less than the concentrically loaded footing. When D_f = B, the bearing capacity was 13.83% less than the concentrically loaded footing with D_f =B for the inclination angle of 14 degrees. When γ=0 for D_f = 0, the bearing capacity was 3.06% less than the concentrically loaded footing for the inclination angle of 14 degrees.
- For the inclination of 20 degrees, when D_f = 0, the bearing capacity was 8.09% less than the concentrically loaded footing. When D_f = B, the bearing capacity was 17.05% less than the concentrically loaded footing with D_f =B for the inclination angle of 20 degrees. When γ=0 for D_f = 0, the bearing capacity was 5.45% less than the concentrically loaded footing for the inclination angle of 20 degrees.

  9.
- For the eccentricity of e=B/6, when D_f = 0, the bearing capacity was 38.82% less than the concentrically loaded footing. On the other hand, for the eccentricity of e=B/12, when D_f = 0, the bearing capacity was 17.87% less than the concentrically loaded footing.

For the tests on Anastasia limestone, the following observations of the bearing capacity were made.

- For the inclination of 3 degrees, when D_f = 0, the bearing capacity was 0.16% less than the concentrically loaded footing. When D_f = B, the bearing capacity was 1.28% less than the concentrically loaded footing with D_f =B for the inclination angle of 3 degrees. When γ=0 for D_f = 0, the bearing capacity was 0.12% less than the concentrically loaded footing for the inclination angle of 3 degrees.

- For the inclination of 7 degrees, when $D_f = 0$, the bearing capacity was 0.33% less than the concentrically loaded footing. When $D_f = B$, the bearing capacity was 4.25% less than the concentrically loaded footing with $D_f = B$ for the inclination angle of 7 degrees. When $\gamma=0$ for $D_f = 0$, the bearing capacity was 0.27% less than the concentrically loaded footing for the inclination angle of 7 degrees.
- For the inclination of 14 degrees, when $D_f = 0$, the bearing capacity was 1.29% less than the concentrically loaded footing. When $D_f = B$, the bearing capacity was 6.49% less than the concentrically loaded footing with $D_f = B$ for the inclination angle of 14 degrees. When $\gamma=0$ for $D_f = 0$, the bearing capacity was 0.92% less than the concentrically loaded footing for the inclination angle of 14 degrees.
- For the inclination of 20 degrees, when $D_f = 0$, the bearing capacity was 4.54% less than the concentrically loaded footing. When $D_f = B$, the bearing capacity was 10.22% less than the concentrically loaded footing with $D_f = B$ for the inclination angle of 20 degrees. When $\gamma=0$ for $D_f = 0$, the bearing capacity was 4.07% less than the concentrically loaded footing for the inclination angle of 20 degrees.
- For the eccentricity of e=B/6, when $D_f = 0$, the bearing capacity was 39.94% less than the concentrically loaded footing. On the other hand, for the eccentricity of e=B/12, when $D_f = 0$, the bearing capacity was 32.39% less than the concentrically loaded footing.

Table 5-8 PLAXIS results for rectangular footing (L/B = 10) with Miami limestone (ML-1).

Case	Inclination angle	Eccentricity, e	Embedment, D_f	Unit Weight, γ (lb/ft3)	Φ_m (deg)	Bearing Capacity, psi	Displacement, in
1	0	0	0	90	32.52	173.35	1.86
2	0	e/6	0	90	32.52	115.83	1.16
3	0	e/12	0	90	32.52	134.95	1,35
4	3	0	0	90	32.52	171.49	1.72
5	7	0	0	90	32.52	170.39	1.73
6	14	0	0	90	32.52	167.59	1.72
7	20	0	0	90	32.52	158.96	1.66
8	0	0	B	90	32.52	204.50	1.97
9	3	0	B	90	32.52	193.13	1.89
10	7	0	B	90	32.52	182.30	1.68
11	14	0	B	90	32.52	174.64	1.78
12	20	0	B	90	32.52	164.23	1.63
13	0	0	0	0	32.52	170.22	1.69
14	3	0	0	0	32.52	169.11	1.68
15	7	0	0	0	32.52	168.09	1.69
16	14	0	0	0	32.52	165.62	1.72
17	20	0	0	0	32.52	157.40	1.59

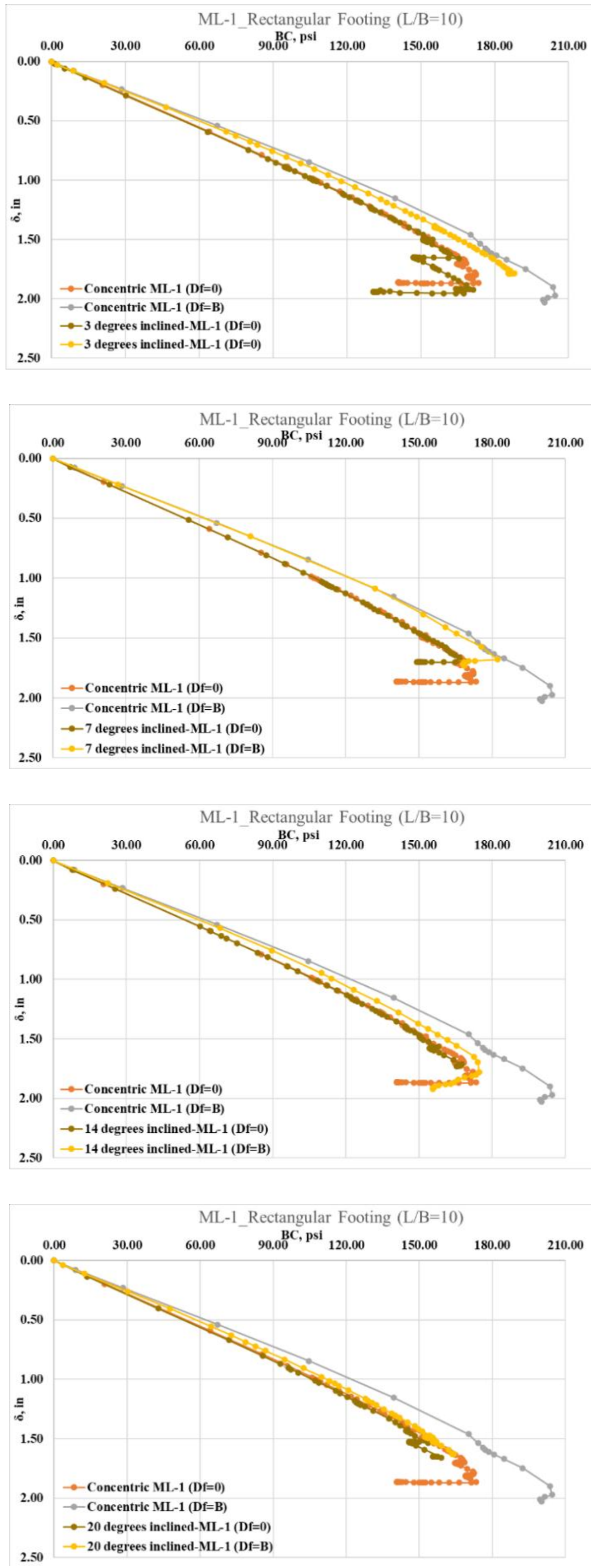

Figure 5-9 Load-settlement for rectangular footings (L/B = 10) on ML-1 formation for load inclination angle of 3°, 7°, 14°, and 20°.

Table 5-9 PLAXIS results for rectangular footing (L/B = 10) with Miami limestone (FTL-2).

Case	Inclination angle	Eccentricity, e	Embedment, D_f	Unit Weight, γ (lb/ft3)	Φ_m (deg)	Bearing Capacity, psi	Displacement, in
1	0	0	0	105	32.381	160.52	0.74
2	0	e/6	0	105	32.381	98.21	0.47
3	0	e/12	0	105	32.381	131.84	0.60
4	3	0	0	105	32.381	155.38	0.75
5	7	0	0	105	32.381	153.41	0.66
6	14	0	0	105	32.381	152.54	0.70
7	20	0	0	105	32.381	147.54	0.68
8	0	0	B	105	32.381	192.49	0.83
9	3	0	B	105	32.381	178.99	0.75
10	7	0	B	105	32.381	170.99	0.73
11	14	0	B	105	32.381	165.87	0.72
12	20	0	B	105	32.381	159.68	0.70
13	0	0	0	0	32.381	146.99	0.66
14	3	0	0	0	32.381	143.92	0.68
15	7	0	0	0	32.381	142.77	0.60
16	14	0	0	0	32.381	142.49	0.58
17	20	0	0	0	32.381	138.97	0.58

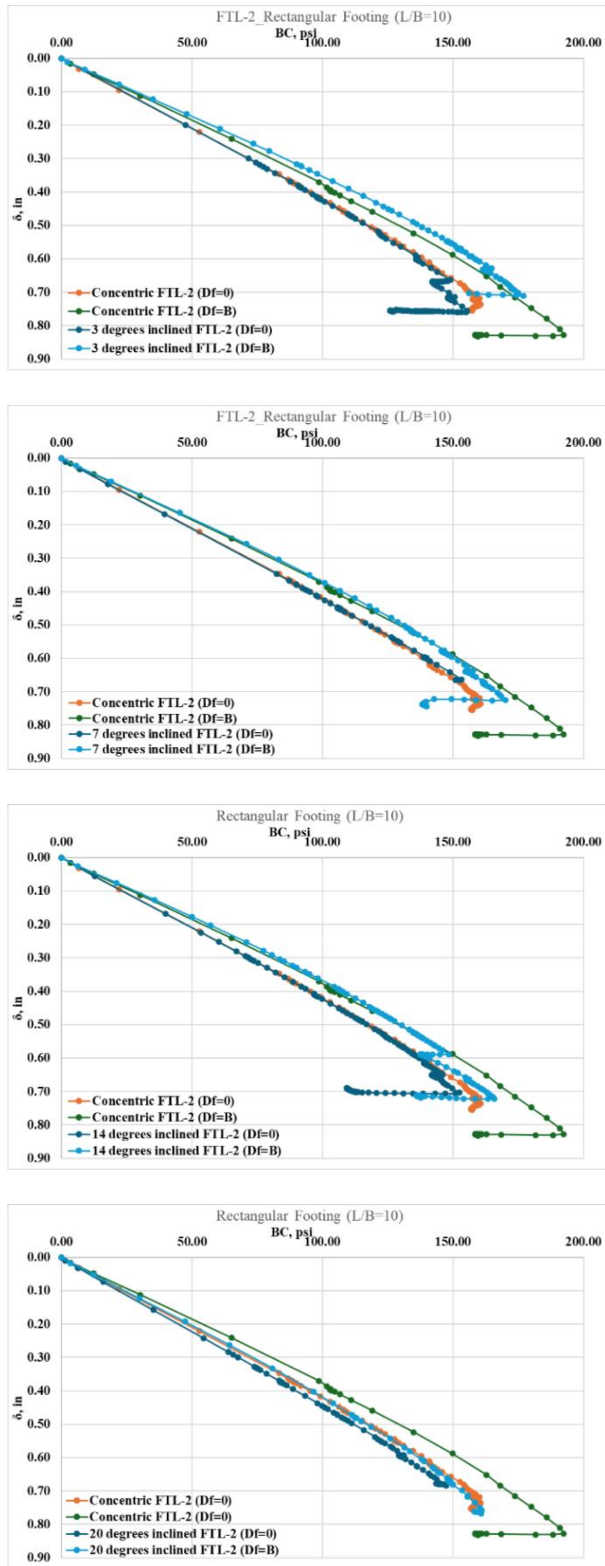

Figure 5-10 Load-settlement for rectangular footings (L/B = 10) on FTL-2 formation for load inclination angle of 3°, 7°, 14°, and 20°.

Table 5-10 PLAXIS results for rectangular footing (L/B = 10) with Anastasia limestone (AL-3).

Case	Inclination angle	Eccentricity, e	Embedment, D_f	Unit Weight, γ (lb/ft3)	Φ_m (deg)	Bearing Capacity, psi	Displacement, in
1	0	0	0	140	36.451	1466.69	1.11
2	0	e/6	0	140	36.451	880.86	0.67
3	0	e/12	0	140	36.451	991.60	0.73
4	3	0	0	140	36.451	1464.36	1.08
5	7	0	0	140	36.451	1461.90	1.07
6	14	0	0	140	36.451	1447.76	1.07
7	20	0	0	140	36.451	1400.16	0.98
8	0	0	B	140	36.451	1621.32	1.26
9	3	0	B	140	36.451	1600.57	1.23
10	7	0	B	140	36.451	1552.49	1.21
11	14	0	B	140	36.451	1516.14	1.15
12	20	0	B	140	36.451	1455.58	1.09
13	0	0	0	0	36.451	1361.95	0.98
14	3	0	0	0	36.451	1360.34	0.94
15	7	0	0	0	36.451	1358.30	0.97
16	14	0	0	0	36.451	1349.48	0.92
17	20	0	0	0	36.451	1306.45	0.91

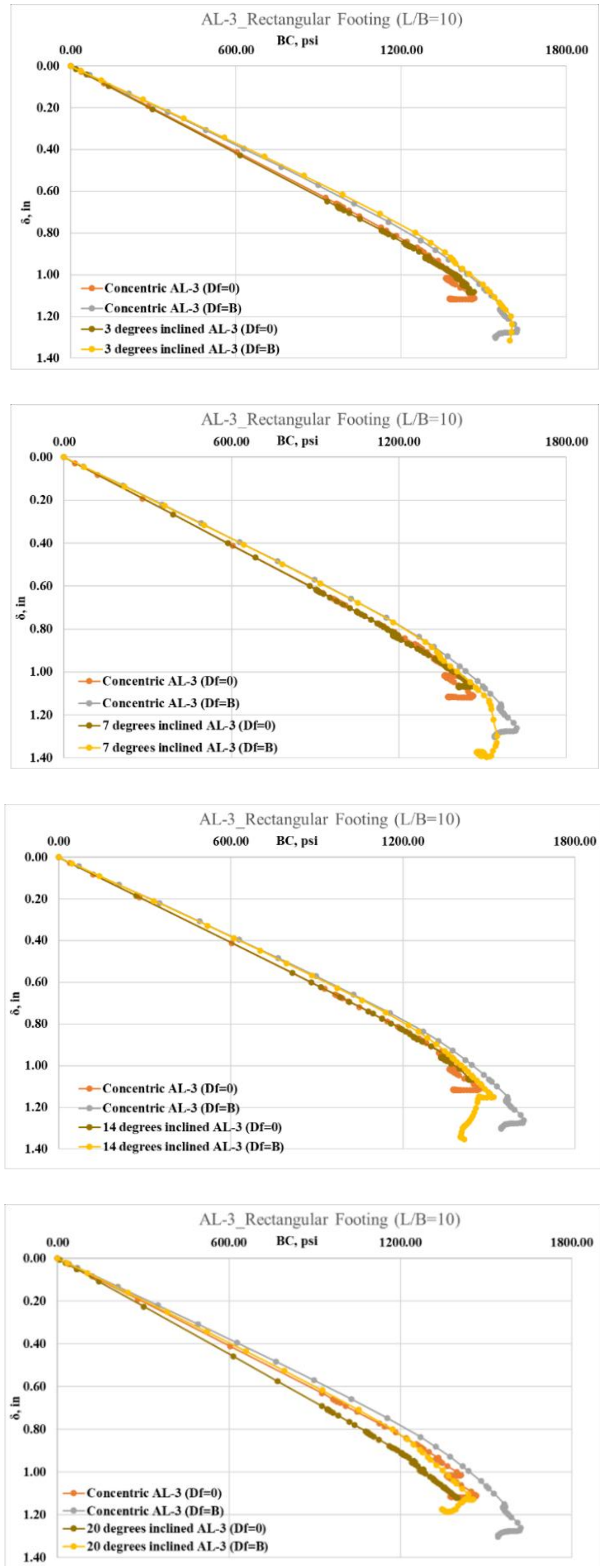

Figure 5-11 Load-settlement for rectangular footings (L/B = 10) on AL-3 formation for load inclination angle of 3°, 7°, 14°, and 20°.

Strip Footing (L/B = 20) PLAXIS Results and Observations

A total of 51 load tests were performed on the strip footing: 17 with Miami Limestone properties, 17 with Fort Thompson Limestone properties and 17 with Anastasia Limestone properties. The square footing was loaded for inclined and eccentric loading with depths of embedment equal to zero and B, at inclination angle of 3 degrees, 7 degrees, 14 degrees and 20 degrees. All eccentric loads were applied B/6 and B/12 from the center of the footing. Combined inclined-eccentric loads were applied in the same geometric loading conditions as the individual parts. The model footing was tested using 110 feet long by 5 feet wide with the length-to width ratio of 10.

Table 5-11, Table 5-12, and Table 5-13 show the test parameters and results for square footing in the Miami, Fort Thompson, and Anastasia Limestone formations, respectively. Subsequent plots in Figure 5-12, Figure 5-13, and Figure 5-14 show the bearing capacity curves obtained from each test in the tables for each formation. Inclined loading cases are plotted in combination with concentric loading cases, to reference any increase or decrease in bearing capacity associated with the change in embedment depth, eccentricity, inclined load conditions. Evident in each of the set of results, the bearing capacity decreases with an increase in inclination angle and eccentricity. The bearing capacity for each test was taken at the initial point of zero slope.

PLAXIS tests of L/B=20 footings on Miami limestone, Fort Thompson limestone and Anastasia limestone were conducted to investigate the influence of inclined and inclined-eccentric loading on the bearing capacity when the depth of embedment is zero and B. For the tests on Miami limestone, the following observations of the bearing capacity were made.

- For the inclination of 3 degrees, when $D_f = 0$, the bearing capacity was 1.08% less than the concentrically loaded footing. When $D_f = B$, the bearing capacity was 2.72% less than the concentrically loaded footing with $D_f = B$ for the inclination angle of 3 degrees. When $\gamma=0$ for $D_f = 0$, the bearing capacity was 0.56% less than the concentrically loaded footing for the inclination angle of 3 degrees.
- For the inclination of 7 degrees, when $D_f = 0$, the bearing capacity was 6.35% less than the concentrically loaded footing. When $D_f = B$, the bearing capacity was 7.87% less than the concentrically loaded footing with $D_f = B$ for the inclination angle of 7 degrees. When $\gamma=0$ for $D_f = 0$, the bearing capacity was 4.00% less than the concentrically loaded footing for the inclination angle of 7 degrees.
- For the inclination of 14 degrees, when $D_f = 0$, the bearing capacity was 11.52% less than the concentrically loaded footing. When $D_f = B$, the bearing capacity was 15.66% less than the concentrically loaded footing with $D_f = B$ for the inclination angle of 14 degrees. When $\gamma=0$ for $D_f = 0$, the bearing capacity was 9.27% less than the concentrically loaded footing for the inclination angle of 14 degrees.
- For the inclination of 20 degrees, when $D_f = 0$, the bearing capacity was 34.56% less than the concentrically loaded footing. When $D_f = B$, the bearing capacity was 39.05% less than the concentrically loaded footing with $D_f = B$ for the inclination angle of 20 degrees.

When $\gamma=0$ for $D_f = 0$, the bearing capacity was 33.40% less than the concentrically loaded footing for the inclination angle of 20 degrees.

- For the eccentricity of e=B/6, when $D_f = 0$, the bearing capacity was 35.42% less than the concentrically loaded footing. On the other hand, for the eccentricity of e=B/12, when $D_f = 0$, the bearing capacity was 21.19% less than the concentrically loaded footing.

For the tests on Fort Thompson limestone, the following observations of the bearing capacity were made.

- For the inclination of 3 degrees, when $D_f = 0$, the bearing capacity was 1.76% less than the concentrically loaded footing. When $D_f = B$, the bearing capacity was 2.72% less than the concentrically loaded footing with $D_f = B$ for the inclination angle of 3 degrees. When $\gamma=0$ for $D_f = 0$, the bearing capacity was 1.76% less than the concentrically loaded footing for the inclination angle of 3 degrees.
- For the inclination of 7 degrees, when $D_f = 0$, the bearing capacity was 2.97% less than the concentrically loaded footing. When $D_f = B$, the bearing capacity was 5.09% less than the concentrically loaded footing with $D_f = B$ for the inclination angle of 7 degrees. When $\gamma=0$ for $D_f = 0$, the bearing capacity was 2.27% less than the concentrically loaded footing for the inclination angle of 7 degrees.
- For the inclination of 14 degrees, when $D_f = 0$, the bearing capacity was 6.40% less than the concentrically loaded footing. When $D_f = B$, the bearing capacity was 8.94% less than the concentrically loaded footing with $D_f = B$ for the inclination angle of 14 degrees. When $\gamma=0$ for $D_f = 0$, the bearing capacity was 4.98% less than the concentrically loaded footing for the inclination angle of 14 degrees.
- For the inclination of 20 degrees, when $D_f = 0$, the bearing capacity was 10.85% less than the concentrically loaded footing. When $D_f = B$, the bearing capacity was 14.36% less than the concentrically loaded footing with $D_f = B$ for the inclination angle of 20 degrees. When $\gamma=0$ for $D_f = 0$, the bearing capacity was 9.34% less than the concentrically loaded footing for the inclination angle of 20 degrees.
- For the eccentricity of e=B/6, when $D_f = 0$, the bearing capacity was 30.40% less than the concentrically loaded footing. On the other hand, for the eccentricity of e=B/12, when $D_f = 0$, the bearing capacity was 14.93% less than the concentrically loaded footing.

For the tests on Anastasia limestone, the following observations of the bearing capacity were made.

- For the inclination of 3 degrees, when $D_f = 0$, the bearing capacity was 1.74% less than the concentrically loaded footing. When $D_f = B$, the bearing capacity was 3.01% less than the concentrically loaded footing with $D_f = B$ for the inclination angle of 3 degrees. When $\gamma=0$ for $D_f = 0$, the bearing capacity was 1.59% less than the concentrically loaded footing for the inclination angle of 3 degrees.
- For the inclination of 7 degrees, when $D_f = 0$, the bearing capacity was 2.57% less than the concentrically loaded footing. When $D_f = B$, the bearing capacity was 4.40% less than

the concentrically loaded footing with D_f =B for the inclination angle of 7 degrees. When γ=0 for D_f = 0, the bearing capacity was 2.39% less than the concentrically loaded footing for the inclination angle of 7 degrees.

- For the inclination of 14 degrees, when D_f = 0, the bearing capacity was 5.75% less than the concentrically loaded footing. When D_f = B, the bearing capacity was 8.62% less than the concentrically loaded footing with D_f =B for the inclination angle of 14 degrees. When γ=0 for D_f = 0, the bearing capacity was 4.82% less than the concentrically loaded footing for the inclination angle of 14 degrees.
- For the inclination of 20 degrees, when D_f = 0, the bearing capacity was 9.60% less than the concentrically loaded footing. When D_f = B, the bearing capacity was 12.91% less than the concentrically loaded footing with D_f =B for the inclination angle of 20 degrees. When γ=0 for D_f = 0, the bearing capacity was 7.04% less than the concentrically loaded footing for the inclination angle of 20 degrees.
- For the eccentricity of e=B/6, when D_f = 0, the bearing capacity was 33.58% less than the concentrically loaded footing. On the other hand, for the eccentricity of e=B/12, when D_f = 0, the bearing capacity was 27.80% less than the concentrically loaded footing.

Table 5-11 PLAXIS results for strip footing (L/B = 20) with Miami limestone (ML-1).

Case	Inclination angle	Eccentricity, e	Embedment, D_f	Unit Weight, γ (lb/ft3)	Φ_m (deg)	Bearing Capacity, psi	Displacement, in
1	0	0	0	90	32.52	165.06	1.74
2	0	e/6	0	90	32.52	106.60	1.42
3	0	e/12	0	90	32.52	130.08	1.54
4	3	0	0	90	32.52	163.27	1.85
5	7	0	0	90	32.52	154.58	1.67
6	14	0	0	90	32.52	146.05	1.55
7	20	0	0	90	32.52	108.02	1.13
8	0	0	B	90	32.52	195.98	2.14
9	3	0	B	90	32.52	190.65	2.13
10	7	0	B	90	32.52	180.55	2.12
11	14	0	B	90	32.52	165.29	2.03
12	20	0	B	90	32.52	119.45	1.34
13	0	0	0	0	32.52	156.85	1.72
14	3	0	0	0	32.52	155.98	1.74
15	7	0	0	0	32.52	150.58	1.74
16	14	0	0	0	32.52	142.31	1.58
17	20	0	0	0	32.52	104.46	1.03

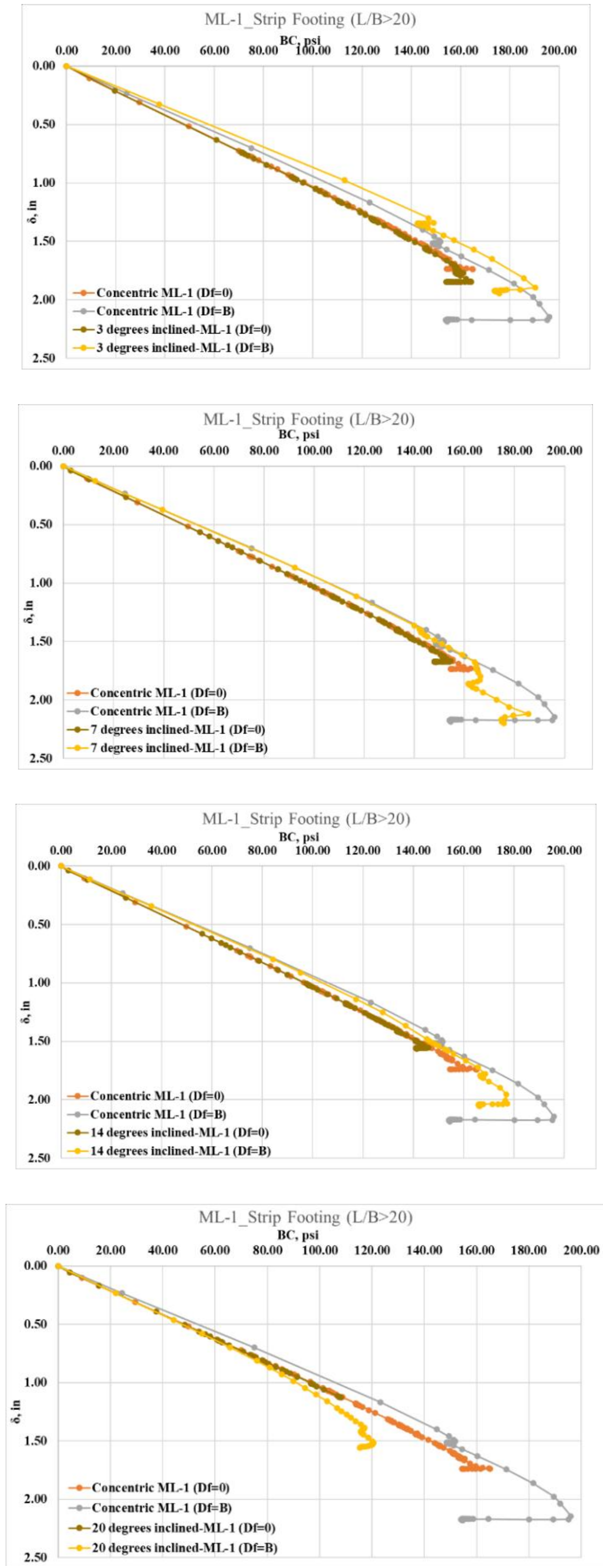

Figure 5-12 Load-settlement for strip footings (L/B = 20) on ML-1 formation for load inclination angle of 3°, 7°, 14°, and 20°.

Table 5-12 PLAXIS results for strip footing (L/B = 20) with Fort Thompson limestone (FTL-2).

Case	Inclination angle	Eccentricity, e	Embedment, D_f	Unit Weight, γ (lb/ft3)	Φ_m (deg)	Bearing Capacity, psi	Displacement, in
1	0	0	0	105	32.3814	158.51	0.76
2	0	e/6	0	105	32.3814	110.32	0.58
3	0	e/12	0	105	32.3814	134.84	0.67
4	3	0	0	105	32.3814	155.72	0.75
5	7	0	0	105	32.3814	153.79	0.75
6	14	0	0	105	32.3814	148.37	0.67
7	20	0	0	105	32.3814	141.31	0.66
8	0	0	B	105	32.3814	179.45	0.82
9	3	0	B	105	32.3814	174.57	0.81
10	7	0	B	105	32.3814	170.32	0.81
11	14	0	B	105	32.3814	163.40	0.80
12	20	0	B	105	32.3814	153.68	0.76
13	0	0	0	0	32.3814	149.75	0.71
14	3	0	0	0	32.3814	147.12	0.75
15	7	0	0	0	32.3814	146.35	0.69
16	14	0	0	0	32.3814	142.29	0.66
17	20	0	0	0	32.3814	135.77	0.64

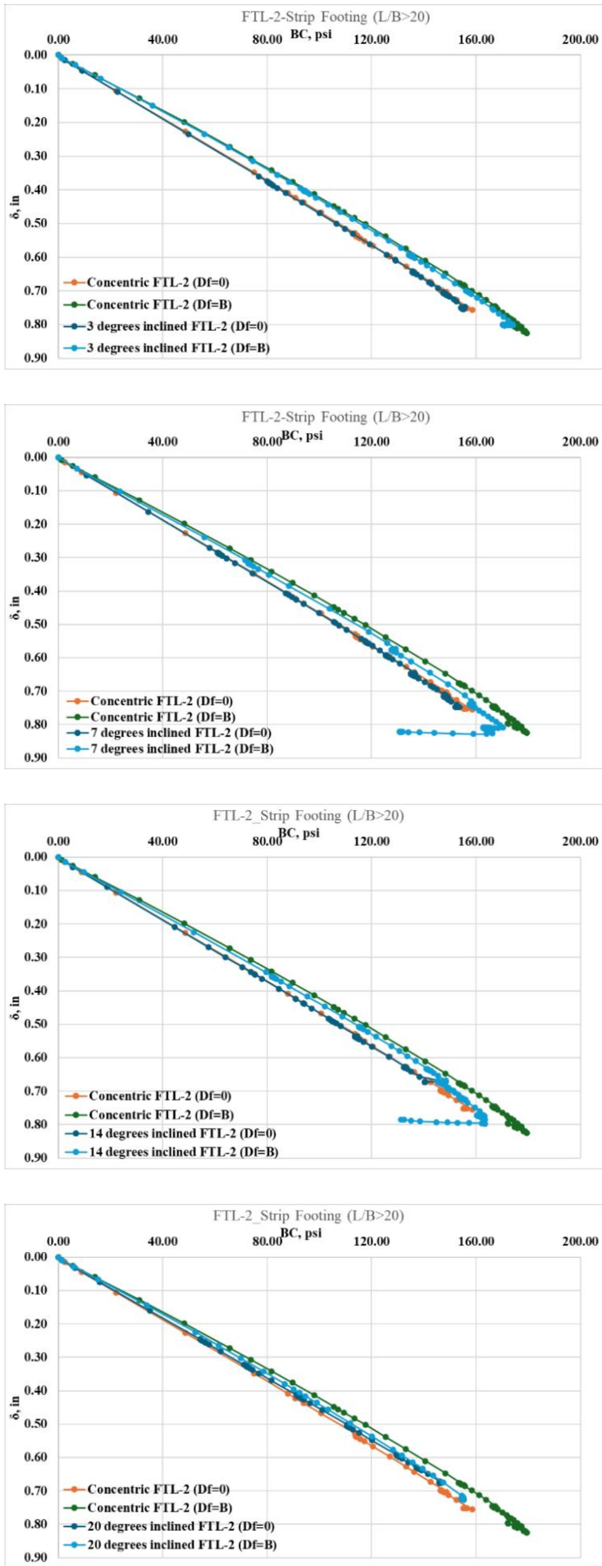

Figure 5-13 Load-settlement for strip footings (L/B = 20) on FTL-1 formation for load inclination angle of 3°, 7°, 14°, and 20°.

Table 5-13 PLAXIS results for strip footing (L/B = 20) with Anastasia limestone (AL-3).

Case	Inclination angle	Eccentricity, e	Embedment, D_f	Unit Weight, γ (lb/ft3)	Φ_m (deg)	Bearing Capacity, psi	Displacement, in
1	0	0	0	140	36.4508	1426.46	1.12
2	0	e/6	0	140	36.4508	947.41	0.78
3	0	e/12	0	140	36.4508	1029.86	0.80
4	3	0	0	140	36.4508	1401.66	1.11
5	7	0	0	140	36.4508	1389.76	1.10
6	14	0	0	140	36.4508	1344.45	1.03
7	20	0	0	140	36.4508	1289.48	1.02
8	0	0	B	140	36.4508	1571.68	1.23
9	3	0	B	140	36.4508	1524.37	1.22
10	7	0	B	140	36.4508	1502.52	1.20
11	14	0	B	140	36.4508	1436.15	1.18
12	20	0	B	140	36.4508	1368.77	1.15
13	0	0	0	0	36.4508	1307.87	0.99
14	3	0	0	0	36.4508	1286.98	0.89
15	7	0	0	0	36.4508	1276.54	0.83
16	14	0	0	0	36.4508	1244.87	0.79
17	20	0	0	0	36.4508	1215.79	0.72

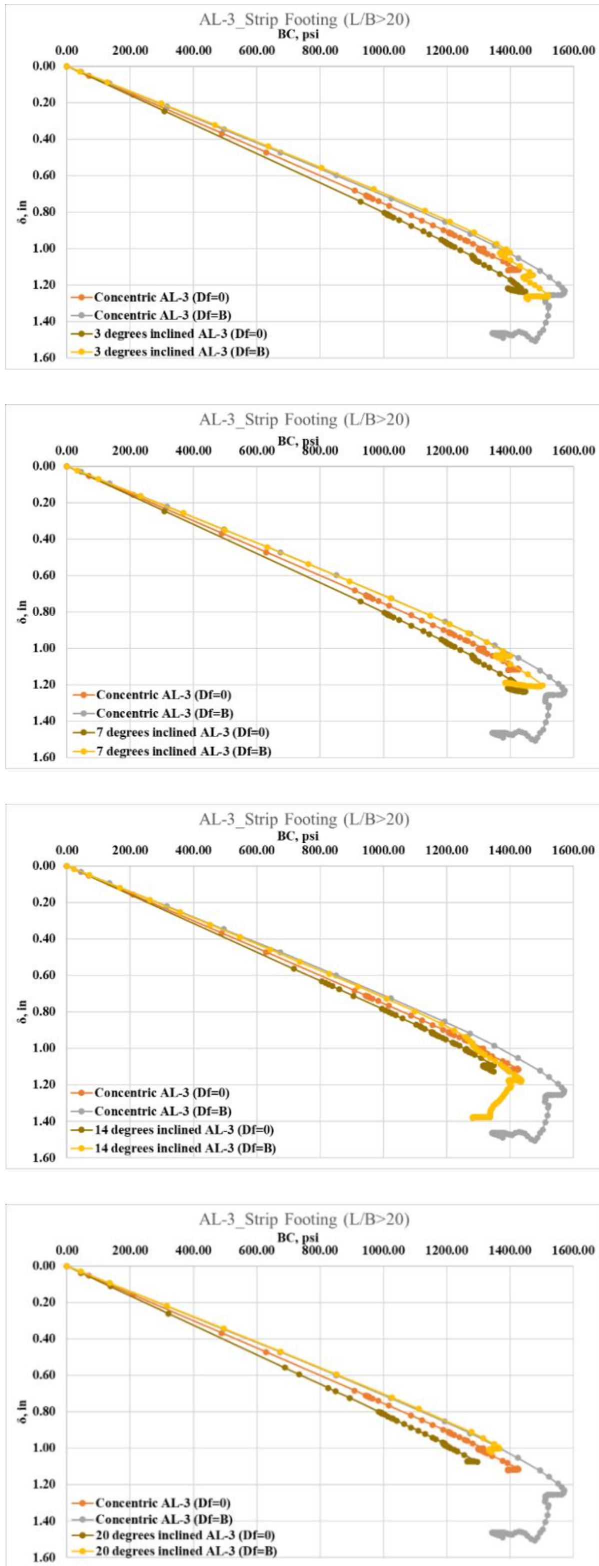

Figure 5-14 Load-settlement for strip footings (L/B = 20) on AL-3 formation for load inclination angle of 3°, 7°, 14°, and 20°.

5.2.6 Inclination Factor Analysis

The analysis of the inclination factors i_c, i_γ, and i_q focuses on isolating the influence of load inclination on the different components of bearing capacity - cohesion, unit weight, and surcharge, respectively.

For the cohesion inclination factor (i_c), the study considers surface footings while neglecting the effect of soil weight. The bearing capacities obtained for inclined loads (3°, 7°, 14° and 20°) are divided by the capacity of the concentric or vertical loading condition (where a_i = 0 and $i_c = 1$). The resulting i_c values are then plotted against the inclination angles, which are determined from the vertical and horizontal load components (V and H) obtained from PLAXIS results. For the unit weight inclination factor (i_γ), the analysis examines surface footings with and without cohesion (c). The bearing capacities obtained for inclined loads (3°, 7°, 14° and 20°) are divided by the capacity of the concentric or vertical loading condition (where a_i = 0 and $i_\gamma = 1$). This ratio isolates the iγ factor, which is then plotted against the inclination angle calculated from the V/H ratios in the PLAXIS simulations.

Finally, for the surcharge inclination factor (i_q), the comparison is made between embedded and surface footings to isolate the surcharge effect. The bearing capacities obtained for inclined loads (3°, 7°, 14° and 20°) are divided by the capacity of the concentric or vertical loading condition (where a_i = 0 and $i_q = 1$). These i_q values are also plotted against the inclination angles derived from the ratio of vertical to horizontal loads.

Measured inclination factors from the PLAXIS results for L/B = 1, 10, and 20 are shown in Figure 5-15 – Figure 5-23. The inclination factor using Vesić equations (AASHTO recommended method) are included in each figure for comparison.

For the L/B = 1 cases, Anastasia Limestone (AL-3) demonstrates the least influence from load inclination for cohesion, maintaining relatively higher i_c values across all inclination angles. This suggests that AL-3 has a more stable and less sensitive response to inclined loading, possibly due to its denser or more cemented structure. The Miami Limestone (ML-1) and Fort Thompson Limestone-2 (FTL-2) exhibit intermediate behavior, with FTL-2 generally having slightly lower i_c values than ML-1 at corresponding angles. Generally, among formations the factors begin to deviate beyond 10° inclination, where material differences strongly influence resistance.

Figure 5-16 shows the variation of the inclination factor for unit weight (i_γ) with respect to inclination angles for Miami Limestone (ML-1), Anastasia Limestone (AL-3), and Fort Thompson Limestone (FTL-2). The factor i_γ represents the reduction in the bearing capacity component contributed by the soil's unit weight when the load is inclined. All formations exhibit a sharp reduction in i_γ as the inclination angle increases, particularly within the initial range of 0° to 6°. Among them, Miami Limestone (ML-1) maintains the highest i_γ values throughout, indicating better resistance to inclined loading. In contrast, Fort Thompson formation (FTL-2) and Anastasia Limestone (AL-3) show steep declines, stabilizing at around 0.4 to 0.5 for angles beyond 14°.

The PLAXIS simulations show a consistent trend across all materials: as the inclination angle increases, all three reduction factors decrease, indicating reduced bearing capacity. However, the degree of reduction is highly dependent on the formation's strength. Anastasia Limestone, characterized by high cohesion (210.4 psi) and friction angle (49.4°), exhibits the least reduction in all three factors, maintaining high i_c, i_γ, and $i_q$values up to 20°. In contrast, the Fort Thompson and Miami limestones, with much lower cohesion (around 39–42 psi), show significantly sharper declines, especially in the surcharge factor i_q, where FTL-2 drops below 0.3 at 20°.

The PLAXIS results depict the variation of the inclination factor for cohesion (i_c) with inclination angles for Miami Limestone (ML-1), Anastasia Limestone (AL-3), and Fort Thompson Limestone (FTL-1 and FTL-2) formations under rectangular footing conditions (L/B=10). The inclination factor i_c quantifies the reduction in cohesive bearing capacity as the load applied to the footing becomes inclined. A general decreasing trend is evident across all formations as the inclination angle increases from 0° to 20°, indicating that the bearing capacity diminishes with higher load inclination due to reduced mobilization of cohesive strength.

For the L/B = 10 cases, the Anastasia Limestone (AL-3) consistently exhibits the highest i_c values across all inclination angles, also suggesting a greater resistance to the effects of load inclination. Miami Limestone (ML-1) and Fort Thompson Limestone-2 (FTL-2) display intermediate behaviors, with i_c values gradually decreasing at a moderate rate.

Figure 5-19 shows the variation of i_γ with inclination angle which exhibits a more gradual reduction compared to square footings. At smaller inclination angles (below 7°), Anastasia Limestone (AL-3) shows a notably high i_γ value, maintaining close to unity. Miami Limestone (ML-1), however, experiences a reduction in i_γ within the first few degrees. Fort Thompson Limestone-2 (FTL-2) display intermediate trends, with moderate reductions in i_γ and a gradual decline beyond 14°. Overall, the rectangular footing configuration shows reduced sensitivity to load inclination compared to square footings, reflecting the stabilizing effect of the larger footing length. Anastasia Limestone demonstrates the best stability, while ML-1 experiences the greatest decline in i_γ as inclination increases.

Figure 5-20 shows a more varied behavior in i_q across the different limestone formations. At low inclination angles (0°–3°), all formations begin at or near unity, but with increasing inclination, the rate of reduction differs significantly. Fort Thompson Limestone-2 (FTL-2) exhibits the highest i_q values throughout the range while Anastasia Limestone (AL-3) and Miami Limestone (ML-1) display declines, with ML-1 showing the steepest drop—reaching around 0.2 at 18°, indicating high sensitivity to load inclination.

In general, the PLAXIS results demonstrate that increasing the L/B ratio significantly reduces the sensitivity of the foundation to inclined loads. In the case of the cohesion reduction factor i_c, all formations show a gradual decrease with increasing inclination, but the reduction is far less steep compared to the L/B = 1 case. Anastasia Limestone, which possesses high cohesion (210.4 psi) and a high friction angle (49.4°), maintains the highest i_c values, showing strong resistance to inclination effects. FTL-2 and ML-1, which have lower cohesion values (around 40 psi), show slightly more reduction, but still perform better than in the shorter footing case. The unit weight reduction factor i_γ also declines with increasing inclination but again does so more gradually for $L/B = 10$. AL-3 remains the most stable due to its higher unit weight and strength. ML-1 and FTL-2 exhibit sharper reductions, though they still retain higher i_γ values than in the short footing case. The most pronounced reductions are observed in the surcharge reduction factor i_q, which drops rapidly with load inclination, especially in PLAXIS results for ML-1 and FTL-2. At 20°, the i_q values for these materials fall below 0.2, highlighting the significant influence of surcharge loss in weak formations under inclined loads.

For the L/B = 20 cases, the PLAXIS analysis illustrates the variation of the inclination factor for cohesion (i_c) with inclination angles for Miami Limestone (ML-1), Anastasia Limestone (AL-3), and Fort Thompson Limestone (FTL-2) formations. All formations exhibit a clear decreasing trend in i_c with increasing inclination angle. The Fort Thompson Limestone-2 (FTL-2) maintains the highest i_c values across all inclination angles, while Anastasia Limestone (AL-3) shows the most pronounced decrease in i_c, particularly beyond 14°. Miami Limestone (ML-1) exhibits an intermediate response, with i_c values decreasing moderately up to 10°, followed by a sharper decline at higher inclination angles.

Figure 5-22 shows the inclination factor i_γ decreases steadily with increasing inclination angles across all formations, with variability between the formations. Anastasia Limestone (AL-3) exhibits the highest i_γ values across the range, showing minimal reduction even at higher inclination angles, which indicates strong resistance to shear reduction under inclined loading. Conversely, Miami Limestone (ML-1) experiences the steepest decline, with i_γ dropping below 0.5 beyond 7°. Fort Thompson formation (FTL-2) demonstrate moderate decrease, stabilizing at values between 0.6 and 0.65 at higher inclination angles. Compared to square and rectangular footings, the strip footing configuration displays less abrupt variation, but the overall magnitude of reduction remains significant.

Figure 5-23 shows the behavior in i_q across the different limestone formations. At low inclination angles (0°–3°), all formations begin at or near unity, but with increasing inclination, the rate of reduction differs significantly. Fort Thompson Limestone-2 (FTL-2) exhibits the highest i_q values throughout the range, maintaining relatively strong resistance to inclination effects. Anastasia Limestone (AL-3) and Miami Limestone (ML-1) display more rapid declines, with ML-1 showing the steepest drop—reaching around 0.2 at 20°, indicating high sensitivity to load inclination. This suggests that Miami Limestone's surcharge component weakens as the footing length increases.

For comparison to AASHTO recommended method for reducing bearing capacity due to inclined loads, Vesić method (Equation 5-2 – Equation 5-4) was plotted for each case in Figure

5-15 – Figure 5-23. Vesić method was developed for soil and is not necessarily expected to predict reductions in bearing capacity of IGM or limestone. However, in general Vesić method predicts greater effects of inclination for cohesion and unit weight while for surcharge it gives similar or slightly greater. While inclination angle of 20° are not usually considered in design, the significant difference in inclination factors for cohesion and unit weight for 14° and less would lead to overly conservative designs and in some cases unconservative designs based on only the surcharge.

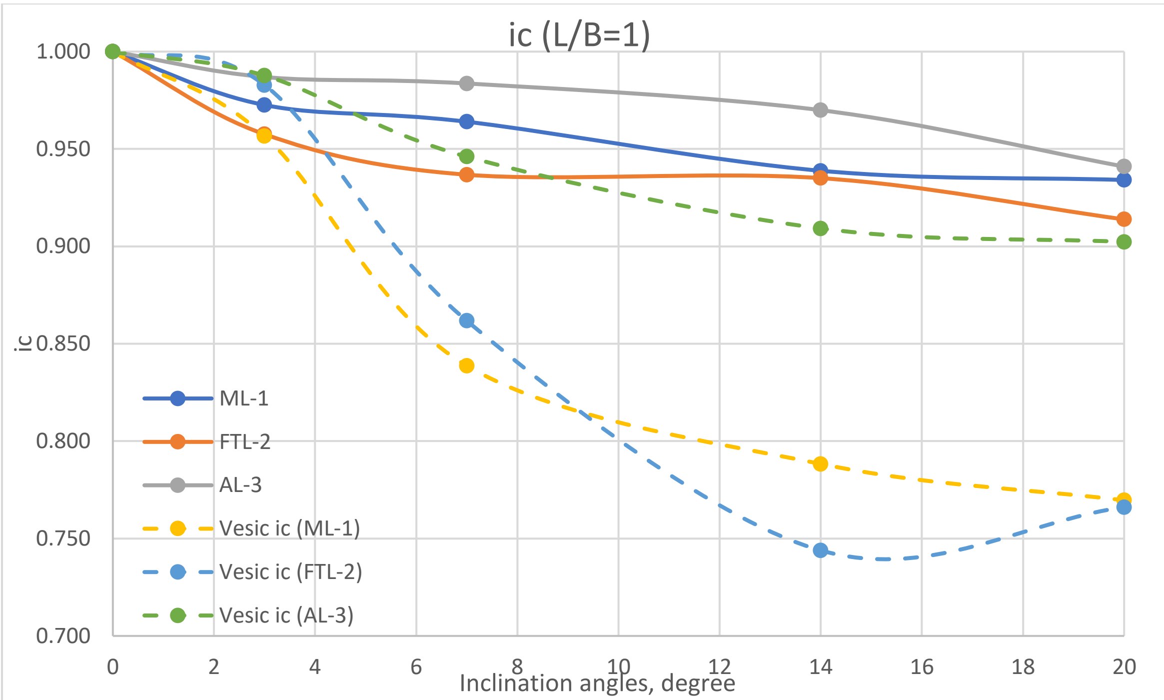

Figure 5-15 Measured and Vesić cohesion inclination factors for L/B = 1.

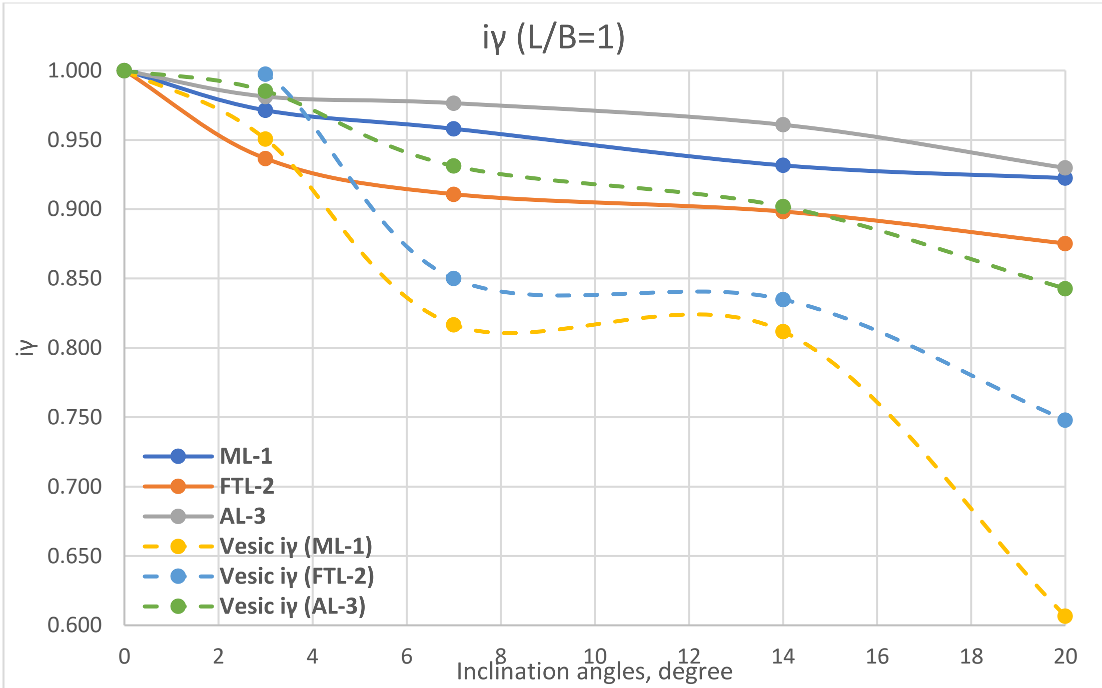

Figure 5-16 Measured and Vesić unit weight inclination factors for L/B = 1.

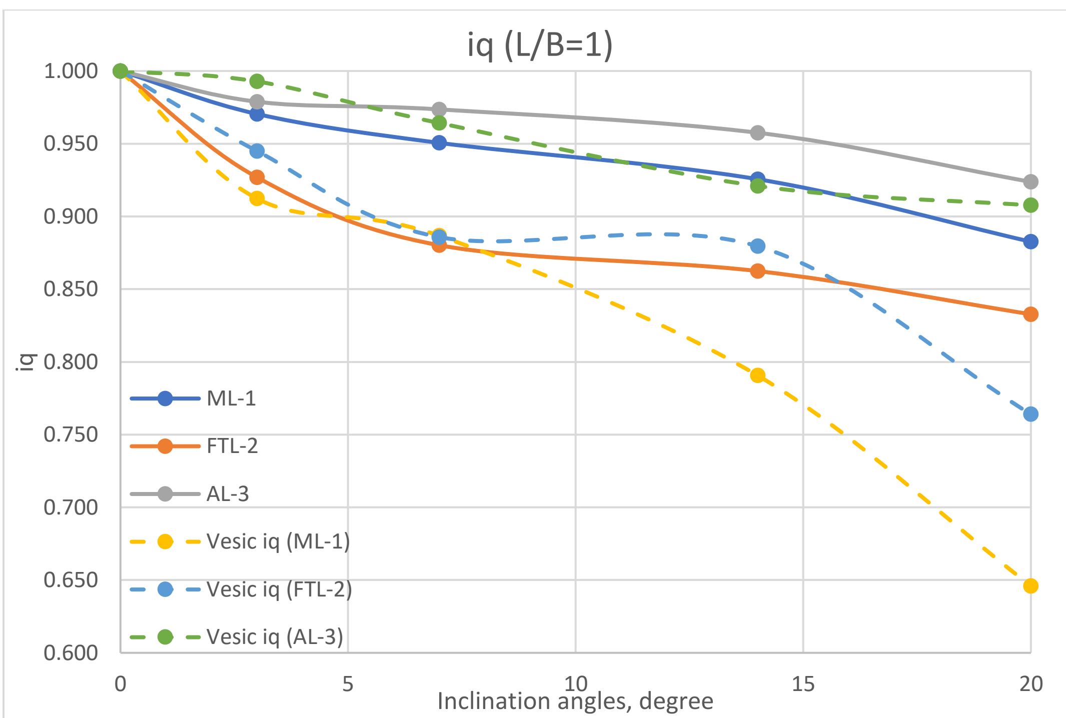

Figure 5-17 Measured and Vesić overburden inclination factors for L/B = 1.

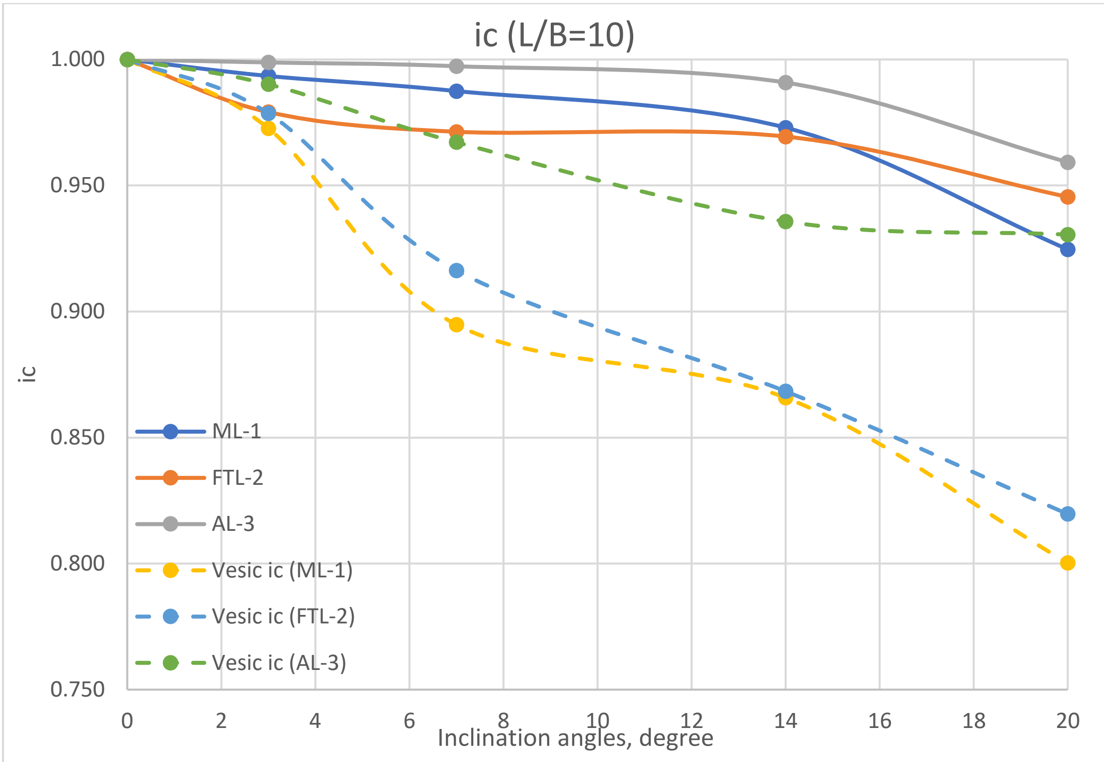

Figure 5-18 Measured and Vesić cohesion inclination factors for L/B = 10.

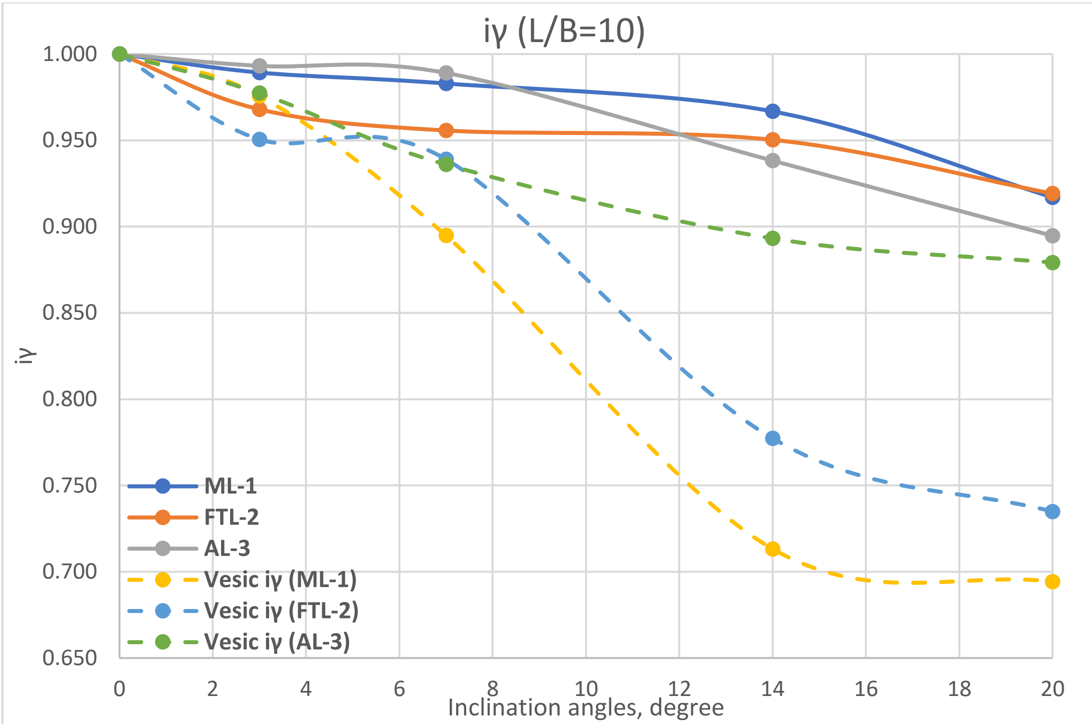

Figure 5-19 Measured and Vesić unit weight inclination factors for L/B = 10.

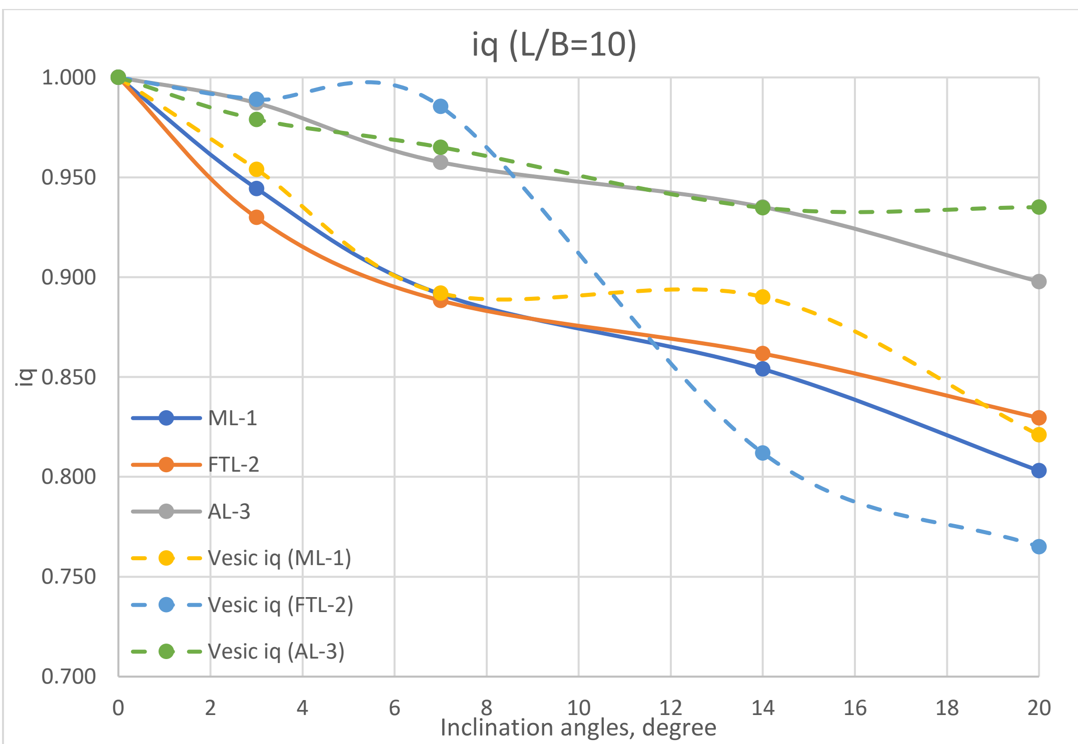

Figure 5-20 Measured and Vesić overburden inclination factors for L/B = 10.

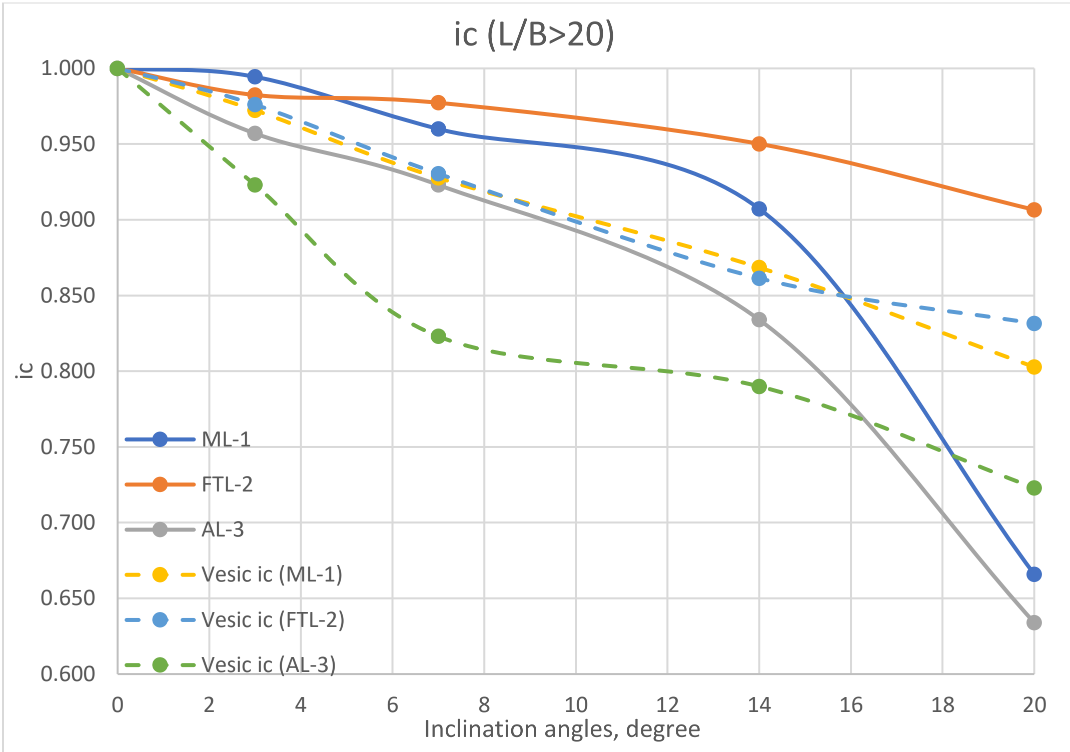

Figure 5-21 Measured and Vesić cohesion inclination factors for L/B = 20.

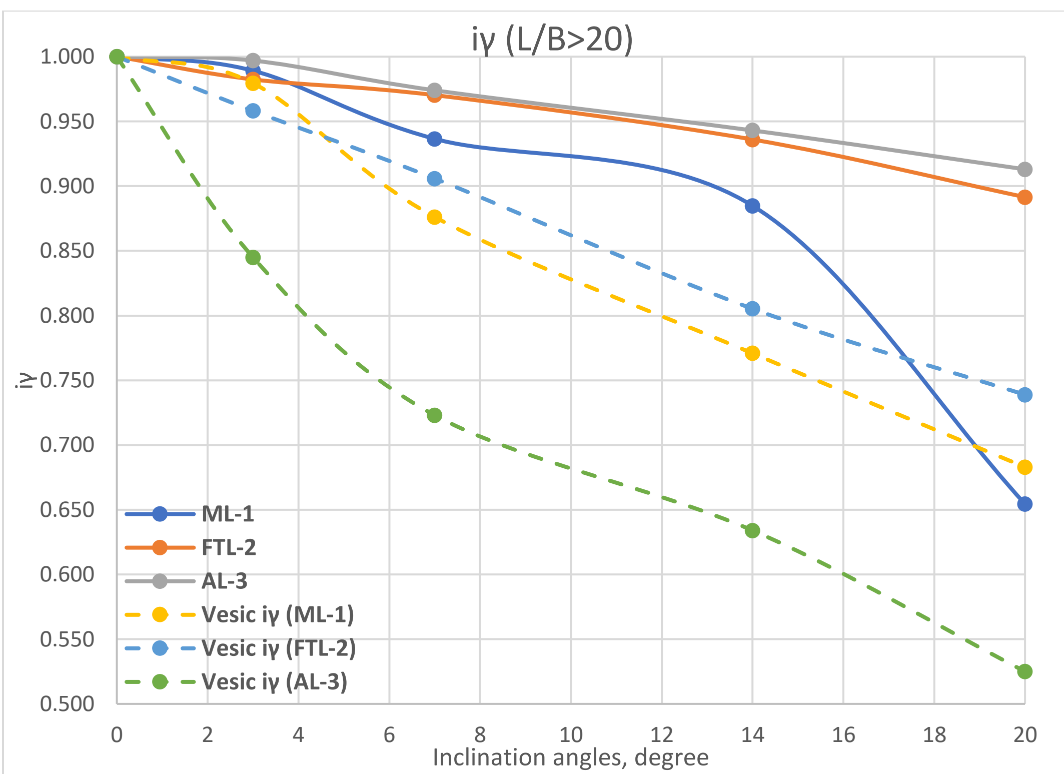

Figure 5-22 Measured and Vesić unit weight inclination factors for L/B = 20.

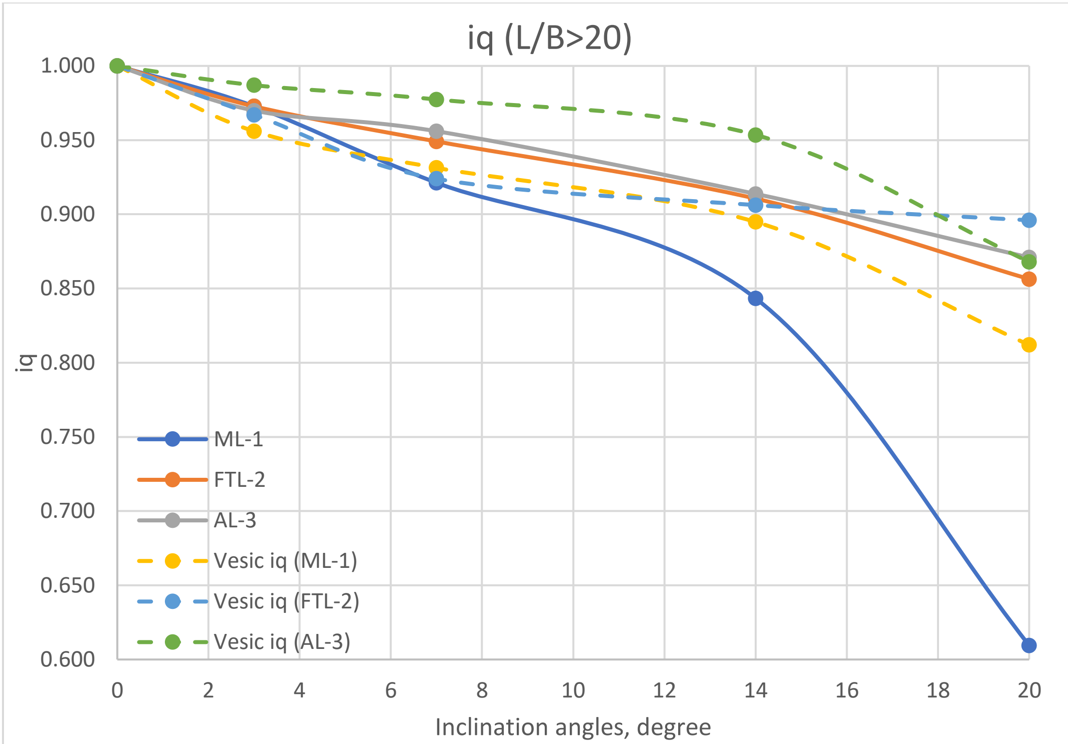

Figure 5-23 Measured and Vesić overburden inclination factors for L/B = 20.

Formation Specific and All Formation Inclination Factors

Initially, individual inclination factor equations were developed for each factor (i_c, i_q, i_γ) based on three footing sizes which have values of L/B ratios 1, 10, and greater than 20. This process was repeated for three distinct geological formations: Miami Limestone (ML-1), Fort Thompson Limestone (FTL-2), and Anastasia Limestone (AL-3). Subsequently, a generalized equation was formulated for the exponent p, applicable to all L/B ratios for each formation. This exponent p governs the sensitivity of the inclination factor with respect to the inclination angle a_i, following the Meyerhof formulation:

$$i_c = (1 - \frac{\alpha_i}{90^\circ})^{p_{ic}}$$ Equation 5-16

$$i_q = (1 - \frac{\alpha_i}{90^\circ})^{p_{iq}}$$ Equation 5-17

$$i_\gamma = (1 - \frac{\alpha_i}{\phi})^{p_{i\gamma}}$$ Equation 5-18

where ϕ is the internal friction angle of the limestone, and a_i is the angle of load inclination. Expressions for the exponents p_{ic}, p_{iq}, and p_{ig} in Equation 5-16, Equation 5-17, and Equation 5-18 were developed based on the analysis of each limestone formation tested and for all formations.

Miami Limestone

For the Miami Limestone formation, the inclination factors follow the classical Meyerhof form, with the corresponding exponent functions dependent on the L/B ratio:

p_{ic} = 0.0029(L/B)^2 - 0.0246(L/B) + 0.2879 Equation 5-19

p_{iq} = -8E-5(L/B)^2+0.0511(L/B)+0.4468 Equation 5-20

$p_{i\gamma}$ = 0.001(L/B)^2-0.0107(L/B)+0.1097 Equation 5-21

Table 5-15 shows the measured and predicted bearing capacities based on Equation 5-19, Equation 5-20, and Equation 5-21 for the Miami limestone (ML-1) case. The percent differences are generally less than 5% and not exceeding 10% overall.

Fort Thompson Limestone

For the Fort Thompson Limestone formation, the inclination factors follow the classical Meyerhof form, with the corresponding exponent functions dependent on the L/B ratio:

p_{ic} = 0.002(L/B)^2 - 0.04(L/B) + 0.4 Equation 5-22

p_{iq} = -0.0012(L/B)^2+0.0126(L/B)+0.853 Equation 5-23

$p_{i\gamma}$ = 0.0003(L/B)^2-0.0089(L/B)+0.158 Equation 5-24

An additional case of lower unit weight of the Fort Thompson limestone formation (Table 5-14) was modeled (FTL-1) and Table 5-16 and Table 5-17 shows the measured and predicted bearing capacities based on Equation 5-22, Equation 5-23, and Equation 5-24 for the cases of this formation, FTL-1 and FTL-2, respectively. For FTL-1, the percent differences are generally less than 10% and not exceeding 12% overall. For FTL-2 the percent differences are 10% or less.

Table 5-14 Properties of Anastasia limestone (AL-1) and Fort Thompson limestone (FTL-1).

Formation	γ_{dt}, pcf	c_m, psi	φ_m, °	$\sigma_{peak\ m}$, psi	ω_m, °	a_m, psi	α_m, °	Pp_m, psi	β_m, °
AL-1	90	37.8	29.1	379.4	-5.4	33.04	25.9	233	-5.4
FTL-1	90	16.5	30.0	287.3	-18.7	14.32	26.6	182	-17.7

Anastasia Limestone

For the Miami Limestone formation, the inclination factors follow the classical Meyerhof form, with the corresponding exponent functions dependent on the L/B ratio:

p_{ic} = 0.0066(L/B)^2 - 0.084(L/B) + 0.299 Equation 5-25

p_{iq} = -2E-4(L/B)^2+0.0154(L/B)+0.287 Equation 5-26

$p_{i\gamma}$ = 9E-6(L/B)^2-1E-4(L/B)+0.100 Equation 5-27

An additional case of lower unit weight of the Anastasia limestone formation (Table 5-14) was modeled (AL-1) and Table 5-18 and Table 5-19 show the measured and predicted bearing capacities based on Equation 5-25, Equation 5-26, and Equation 5-24 for the cases of this formation, AL-1 and AL-2, respectively. For AL-1, the percent differences are generally less than 10% and not exceeding 15% overall. For AL-2 the percent differences are generally less than 10%, with a few cases up to 25 % difference.

All Formation Limestone

For the Miami, Fort Thompson, and Anastasia Limestone formations tested the inclination factors follow the classical Meyerhof form, with the corresponding exponent functions dependent on the L/B ratio:

p_{ic} = 0.0044(L/B)^2 - 0.0614(L/B) + 0.373 Equation 5-28

p_{iq} = -3E-4(L/B)^2+0.0237(L/B)+0.523 Equation 5-29

$p_{i\gamma}$ = 9E-4(L/B)^2-0.152 (L/B)+0.152 Equation 5-30

The measured and predicted bearing capacities for the cases of the Miami, Fort Thompson, and Anastasia formations based on the Equation 5-28, Equation 5-29, and Equation 5-30 for all formations are shown in Table 5-20 – Table 5-24. Similarly, there is generally good agreement (less than 10% difference) except for a few cases of the Anastasia limestone at it's higher unit weight (AL-3).

Table 5-15 Summary of percent differences between measured and predicted for Miami limestone (ML-1).

ML-1															
Formation	**L/B ratio**	**Shape factor, ξ**	**p**				**Cases**	**i_c**	**i_q**	**i_γ**	**Q_{u1}**	**Q_{u2}**	**Predicted Bearing Capacity**	**PLAXIS Bearing Capacity**	**% difference**
			i_c	**i_q**	**i_γ**										
ML-1	1	1.245	0.3210	0.4978	0.1	Surface	0	1.00	1.00	1.00	161.72	340.36	201.35	195.59	2.9
							3	0.99	0.98	0.99	159.97	337.02	199.17	189.98	4.8
							7	0.97	0.96	0.98	157.57	332.12	196.18	187.37	4.7
							14	0.95	0.92	0.95	153.18	321.82	190.71	182.21	4.7
							20	0.92	0.88	0.91	149.19	310.05	185.74	180.41	3.0
						Embedded	0	1.00	1.00	1.00	190.84	369.47	237.59	239.67	0.9
							3	0.99	0.98	0.99	188.60	365.65	234.81	232.59	1.0
							7	0.97	0.96	0.98	185.54	360.09	231.00	227.83	1.4
							14	0.95	0.92	0.95	179.94	348.59	224.03	221.84	1.0
							20	0.92	0.88	0.91	174.88	335.75	217.73	211.54	2.9
	10	1.054	0.2543	0.9505	0.1	Surface	0	1.00	1.00	1.00	161.72	340.36	170.39	173.35	1.7
							3	0.99	0.97	0.99	160.33	337.13	168.93	171.49	1.5
							7	0.98	0.93	0.98	158.43	332.39	166.92	170.39	2.0
							14	0.96	0.85	0.95	154.92	322.36	163.22	167.59	2.6
							20	0.94	0.79	0.91	151.71	310.84	159.84	153.96	3.8
						Embedded	0	1.00	1.00	1.00	190.84	369.47	201.07	204.50	1.7
							3	0.99	0.97	0.99	188.53	365.32	198.63	193.13	2.8
							7	0.98	0.93	0.98	185.39	359.35	195.32	182.30	6.7
							14	0.96	0.85	0.95	179.71	347.16	189.34	174.64	7.8
							20	0.94	0.79	0.91	174.64	333.77	184.00	164.23	10.7
	>20	1.032	1.1391	1.519	0.3169	Surface	0	1.00	1.00	1.00	161.72	340.36	166.87	165.06	1.1
							3	0.96	0.95	0.97	155.60	329.69	160.55	163.27	1.7
							7	0.91	0.88	0.93	147.47	314.48	152.17	154.58	1.6
							14	0.82	0.77	0.84	133.39	284.15	137.64	146.05	5.8
							20	0.75	0.68	0.74	121.46	252.13	125.33	128.02	2.1
						Embedded	0	1.00	1.00	1.00	190.84	369.47	196.92	195.98	0.5
							3	0.96	0.95	0.97	183.25	357.34	189.09	190.65	0.8
							7	0.91	0.88	0.93	173.22	340.22	178.74	180.55	1.0
							14	0.82	0.77	0.84	155.91	306.67	160.88	165.29	2.7
							20	0.75	0.68	0.74	141.34	272.00	145.84	132.45	9.2

Table 5-16 Summary of percent differences between measured and predicted for Fort Thompson limestone (FTL-1).

FTL-1															
Formation	L/B ratio	Shape factor, ξ	p				Cases	i_c	i_q	i_γ	Q_{u1}	Q_{u2}	Predicted Bearing Capacity	PLAXIS Bearing Capacity	% difference
			i_c	i_q	i_γ										
FTL-2	1	1.245	0.4137	0.8642	0.1496	Surface	0	1.00	1.00	1.00	108.83	271.19	135.49	138.97	2.5
							3	0.99	0.97	0.98	107.31	266.95	133.60	130.67	2.2
							7	0.97	0.93	0.96	105.24	260.66	131.02	126.45	3.6
							14	0.93	0.86	0.91	101.47	247.13	126.33	119.31	5.9
							20	0.90	0.80	0.85	98.08	230.85	122.11	112.56	8.5
						Embedded	0	1.00	1.00	1.00	123.74	286.11	154.06	156.44	1.5
							3	0.99	0.97	0.98	121.80	281.43	151.64	145.68	4.1
							7	0.97	0.93	0.96	119.15	274.57	148.34	137.82	7.6
							14	0.93	0.86	0.91	114.36	260.02	142.38	130.19	9.4
							20	0.90	0.80	0.85	110.08	242.85	137.06	122.54	11.8
	10	1.0536	0.2283	0.8642	0.1	Surface	0	1.00	1.00	1.00	108.83	271.19	114.66	118.94	3.6
							3	0.99	0.97	0.99	107.99	268.39	113.77	115.46	1.5
							7	0.98	0.93	0.97	106.83	264.22	112.56	110.09	2.2
							14	0.96	0.86	0.94	104.70	255.09	110.32	105.43	4.6
							20	0.94	0.80	0.89	102.76	243.84	108.27	101.66	6.5
						Embedded	0	1.00	1.00	1.00	123.74	286.11	130.38	136.44	4.4
							3	0.99	0.97	0.99	122.47	282.88	129.04	130.65	1.2
							7	0.98	0.93	0.97	120.74	278.13	127.21	123.17	3.3
							14	0.96	0.86	0.94	117.59	267.98	123.90	118.26	4.8
							20	0.94	0.80	0.89	114.76	255.84	120.91	112.68	7.3
	>20	1.03185	0.3576	0.603	0.1054	Surface	0	1.00	1.00	1.00	108.83	271.19	112.29	114.18	1.7
							3	0.99	0.98	0.99	107.51	268.13	110.94	110.46	0.4
							7	0.97	0.95	0.97	105.72	263.57	109.09	108.72	0.3
							14	0.94	0.90	0.93	102.44	253.69	105.70	103.52	2.1
							20	0.91	0.86	0.89	99.47	241.63	102.64	96.67	6.2
						Embedded	0	1.00	1.00	1.00	123.74	286.11	127.68	135.34	5.7
							3	0.99	0.98	0.99	122.13	282.74	126.02	130.23	3.2
							7	0.97	0.95	0.97	119.93	277.78	123.75	128.38	3.6
							14	0.94	0.90	0.93	115.91	267.16	119.60	116.97	2.3
							20	0.91	0.86	0.89	112.29	254.45	115.87	108.32	7.0

Table 5-17 Summary of percent differences between measured and predicted for Fort Thompson limestone (FTL-2).

FTL-2																
Formation	**L/B ratio**	**Shape factor, ξ**	**p**				**Cases**	**i_c**	**i_q**	**i_γ**	**Q_{u1}**	**Q_{u2}**	**Predicted Bearing Capacity**	**PLAXIS Bearing Capacity**	**% difference**
			i_c	**i_q**	**i_γ**										
FTL-2	1	1.245	0.4137	0.8642	0.1496	Surface	0	1.00	1.00	1.00	149.62	322.48	186.28	202.10	7.8
							3	0.99	0.97	0.99	147.54	317.85	183.68	189.28	3.0
							7	0.97	0.93	0.96	144.69	311.08	180.14	184.08	2.1
							14	0.93	0.86	0.92	139.51	296.96	173.69	181.55	4.3
							20	0.90	0.80	0.87	134.85	281.02	167.88	176.90	5.1
						Embedded	0	1.00	1.00	1.00	176.90	349.75	220.24	216.67	1.6
							3	0.99	0.97	0.99	174.03	344.33	216.66	200.84	7.9
							7	0.97	0.93	0.96	170.13	336.51	211.81	190.73	10.0
							14	0.93	0.86	0.92	163.08	320.53	203.04	186.87	8.7
							20	0.90	0.80	0.87	156.80	302.97	195.21	180.44	8.2
	10	1.0536	0.2283	0.8642	0.1	Surface	0	1.00	1.00	1.00	149.62	322.48	157.64	160.52	1.8
							3	0.99	0.97	0.99	148.47	319.45	156.43	155.38	0.7
							7	0.98	0.93	0.98	146.88	315.00	154.75	153.41	0.9
							14	0.96	0.86	0.94	143.96	305.57	151.67	152.54	0.6
							20	0.94	0.80	0.91	141.28	294.69	148.85	147.54	0.9
						Embedded	0	1.00	1.00	1.00	176.90	349.75	186.38	192.49	3.2
							3	0.99	0.97	0.99	174.96	345.94	184.33	178.99	3.0
							7	0.98	0.93	0.98	172.31	340.43	181.55	170.99	6.2
							14	0.96	0.86	0.94	167.52	329.14	176.50	165.87	6.4
							20	0.94	0.80	0.91	163.23	316.64	171.98	159.68	7.7
	>20	1.03185	0.3576	0.603	0.1054	Surface	0	1.00	1.00	1.00	149.62	322.48	154.39	158.51	2.6
							3	0.99	0.98	0.99	147.82	319.10	152.53	155.72	2.1
							7	0.97	0.95	0.97	145.35	314.15	149.98	153.79	2.5
							14	0.94	0.90	0.94	140.84	303.76	145.33	148.37	2.0
							20	0.91	0.86	0.90	136.76	291.92	141.12	141.31	0.1
						Embedded	0	1.00	1.00	1.00	176.90	349.75	182.53	179.45	1.7
							3	0.99	0.98	0.99	174.54	345.82	180.10	174.57	3.2
							7	0.97	0.95	0.97	171.33	340.12	176.79	170.32	3.8
							14	0.94	0.90	0.94	165.48	328.39	170.75	163.40	4.5
							20	0.91	0.86	0.90	160.20	315.36	165.31	153.68	7.6

Table 5-18 Summary of percent differences between measured and predicted for Anastasia limestone (AL-1).

AL-1															
Formation	**L/B ratio**	**Shape factor, ξ**	**p**				**Cases**	**i_c**	**i_q**	**i_γ**	**Q_{u1}**	**Q_{u2}**	**Predicted Bearing Capacity**	**PLAXIS Bearing Capacity**	**% difference**
			i_c	**i_q**	**i_γ**										
FTL-2	1	1.245	0.2226	0.3031	0.100	Surface	0	1.00	1.00	1.000	179.69	321.01	223.71	215.02	4.0
							3	0.99	0.99	0.989	178.34	317.75	222.03	209.77	5.8
							7	0.98	0.98	0.973	176.48	312.89	219.72	204.79	7.3
							14	0.96	0.95	0.937	173.05	302.31	215.45	199.54	8.0
							20	0.95	0.93	0.890	169.91	289.28	211.54	193.46	9.3
						Embedded	0	1.00	1.00	1.000	199.46	340.78	248.32	241.65	2.8
							3	0.99	0.99	0.989	197.90	337.32	246.39	235.65	4.6
							7	0.98	0.98	0.973	195.77	332.18	243.73	228.90	6.5
							14	0.96	0.95	0.937	191.83	321.09	238.83	222.02	7.6
							20	0.95	0.93	0.890	188.23	307.60	234.35	218.71	7.1
	10	1.0536	0.1229	0.4259	0.100	Surface	0	1.00	1.00	1.000	179.69	321.01	189.32	188.86	0.2
							3	1.00	0.99	0.989	178.94	317.96	188.53	184.65	2.1
							7	0.99	0.97	0.973	177.91	313.39	187.44	180.54	3.8
							14	0.98	0.93	0.937	175.99	303.34	185.43	175.67	5.6
							20	0.97	0.90	0.890	174.22	290.79	183.56	167.93	9.3
						Embedded	0	1.00	1.00	1.000	199.46	340.78	210.15	207.23	1.4
							3	1.00	0.99	0.989	198.43	337.45	209.06	201.92	3.5
							7	0.99	0.97	0.973	197.01	332.49	207.57	197.81	4.9
							14	0.98	0.93	0.937	194.39	321.74	204.81	192.04	6.6
							20	0.97	0.90	0.890	191.98	308.56	202.28	183.51	10.2
	>20	1.03185	1.4715	0.5496	0.102	Surface	0	1.00	1.00	1.000	179.69	321.01	185.41	186.24	0.4
							3	0.95	0.98	0.989	170.94	315.10	176.39	181.32	2.7
							7	0.89	0.96	0.972	159.51	306.80	164.59	179.54	8.3
							14	0.78	0.91	0.935	140.11	290.44	144.57	165.45	12.6
							20	0.69	0.87	0.888	124.14	272.69	128.09	151.32	15.4
						Embedded	0	1.00	1.00	1.000	199.46	340.78	205.81	201.71	2.0
							3	0.95	0.98	0.989	190.35	334.50	196.41	195.38	0.5
							7	0.89	0.96	0.972	178.41	325.70	184.10	190.49	3.4
							14	0.78	0.91	0.935	158.12	308.45	163.16	180.33	9.5
							20	0.69	0.87	0.888	141.36	289.91	145.86	165.63	11.9

Table 5-19 Summary of percent differences between measured and predicted for Anastasia limestone (AL-3).

AL-3															
Formation	L/B ratio	Shape factor, ξ	p				Cases	i_c	i_q	i_γ	Q_{u1}	Q_{u2}	Predicted Bearing Capacity	PLAXIS Bearing Capacity	% difference
			i_c	i_q	i_γ										
FTL-2	1	1.245	0.2226	0.3031	0.100	Surface	0	1.00	1.00	1.000	1337.42	1524.74	1665.09	1600.73	4.0
							3	0.99	0.99	0.991	1327.36	1512.30	1652.57	1570.42	5.2
							7	0.98	0.98	0.979	1313.53	1494.44	1635.34	1562.76	4.6
							14	0.96	0.95	0.953	1288.02	1458.58	1603.58	1537.80	4.3
							20	0.95	0.93	0.924	1264.65	1420.84	1574.49	1488.05	5.8
						Embedded	0	1.00	1.00	1.000	1556.72	1744.04	1938.12	1625.46	16.1
							3	0.99	0.99	0.991	1544.42	1729.36	1922.81	1591.11	17.3
							7	0.98	0.98	0.979	1527.51	1708.42	1901.75	1582.55	16.8
							14	0.96	0.95	0.953	1496.36	1666.92	1862.97	1556.45	16.5
							20	0.95	0.93	0.924	1467.87	1624.05	1827.50	1501.58	17.8
	10	1.0536	0.1229	0.4259	0.100	Surface	0	1.00	1.00	1.000	1337.42	1524.74	1409.10	1466.69	3.9
							3	1.00	0.99	0.991	1331.86	1514.23	1403.25	1464.36	4.2
							7	0.99	0.97	0.979	1324.18	1499.02	1395.15	1461.90	4.6
							14	0.98	0.93	0.953	1309.91	1468.00	1380.13	1447.76	4.7
							20	0.97	0.90	0.924	1296.74	1434.65	1366.25	1400.16	2.4
						Embedded	0	1.00	1.00	1.000	1556.72	1744.04	1640.16	1621.32	1.2
							3	1.00	0.99	0.991	1548.02	1730.39	1630.99	1600.57	1.9
							7	0.99	0.97	0.979	1536.04	1710.88	1618.38	1552.49	4.2
							14	0.98	0.93	0.953	1513.98	1672.07	1595.13	1516.14	5.2
							20	0.97	0.90	0.924	1493.78	1631.69	1573.85	1455.58	8.1
	>20	1.03185	1.4715	0.5496	0.102	Surface	0	1.00	1.00	1.000	1337.42	1524.74	1380.02	1426.46	3.3
							3	0.95	0.98	0.991	1272.34	1488.46	1312.87	1401.66	6.3
							7	0.89	0.96	0.978	1187.20	1439.68	1225.01	1389.76	11.9
							14	0.78	0.91	0.952	1042.84	1352.20	1076.06	1344.45	24.9
							20	0.69	0.87	0.922	923.98	1272.84	953.41	1289.48	26.1
						Embedded	0	1.00	1.00	1.000	1556.72	1744.04	1606.31	1571.68	2.2
							3	0.95	0.98	0.991	1487.59	1703.71	1534.98	1524.37	0.7
							7	0.89	0.96	0.978	1396.95	1649.43	1441.45	1502.52	4.1
							14	0.78	0.91	0.952	1242.68	1552.04	1282.26	1436.15	10.7
							20	0.69	0.87	0.922	1114.99	1463.85	1150.50	1368.77	15.9

Table 5-20 Summary of percent differences between measured and predicted using all formation inclination factors for Miami limestone (ML-1).

ML-1														
L/B ratio	Shape factor, ξ	p				Cases	i_c	i_q	i_γ	Q_{u1}	Q_{u2}	Predicted Bearing Capacity	PLAXIS Bearing Capacity	% difference
		i_c	i_q	i_γ										
1	1.245	0.3170	0.547	0.13828	Surface	0	1.00	1.00	1.00	161.72	340.36	201.35	195.59	2.9
						3	0.99	0.98	0.99	159.99	335.96	199.19	189.98	4.8
						7	0.97	0.96	0.97	157.63	329.52	196.24	187.37	4.7
						14	0.95	0.91	0.93	153.28	316.01	190.84	182.21	4.7
						20	0.92	0.87	0.88	149.34	300.65	185.93	180.41	3.1
					Embedded	0	1.00	1.00	1.00	190.84	369.47	237.59	239.67	0.9
						3	0.99	0.98	0.99	188.57	364.54	234.78	232.59	0.9
						7	0.97	0.96	0.97	185.48	357.38	230.92	227.83	1.4
						14	0.95	0.91	0.93	179.83	342.55	223.88	221.84	0.9
						20	0.92	0.87	0.88	174.71	326.02	217.52	211.54	2.8
10	1.054	0.20274	0.736	0.09268	Surface	0	1.00	1.00	1.00	161.72	340.36	170.39	173.35	1.7
						3	0.99	0.98	0.99	160.62	337.42	169.22	171.49	1.3
						7	0.98	0.94	0.98	159.09	333.10	167.62	170.39	1.6
						14	0.97	0.88	0.95	156.27	323.92	164.65	167.59	1.8
						20	0.95	0.83	0.92	153.69	313.30	161.93	153.96	5.2
					Embedded	0	1.00	1.00	1.00	190.84	369.47	201.07	204.50	1.7
						3	0.99	0.98	0.99	189.01	365.82	199.14	193.13	3.1
						7	0.98	0.94	0.98	186.52	360.53	196.52	182.30	7.8
						14	0.97	0.88	0.95	181.98	349.63	191.74	174.64	9.8
						20	0.95	0.83	0.92	177.89	337.51	187.43	164.23	12.4
>20	1.032	1.0426	0.923	0.23887	Surface	0	1.00	1.00	1.00	161.72	340.36	166.87	165.06	1.1
						3	0.97	0.97	0.98	156.11	331.98	161.08	163.27	1.3
						7	0.92	0.93	0.94	148.63	319.97	153.37	154.58	0.8
						14	0.84	0.86	0.87	135.59	295.73	139.91	146.05	4.2
						20	0.77	0.79	0.80	124.45	269.62	128.41	128.02	0.3
					Embedded	0	1.00	1.00	1.00	190.84	369.47	196.92	195.98	0.5
						3	0.97	0.97	0.98	184.33	360.20	190.20	190.65	0.2
						7	0.92	0.93	0.94	175.65	346.99	181.25	180.55	0.4
						14	0.84	0.86	0.87	160.50	320.64	165.61	165.29	0.2
						20	0.77	0.79	0.80	147.53	292.71	152.23	132.45	13.0

Table 5-21 Summary of percent differences between measured and predicted using all formation inclination factors for Fort Thompson limestone (FTL-1).

FTL-1														
L/B ratio	**Shape factor, ξ**	**p**				**Cases**	**i_c**	**i_q**	**i_γ**	**Q_{u1}**	**Q_{u2}**	**Predicted Bearing Capacity**	**PLAXIS Bearing Capacity**	**% difference**
		i_c	**i_q**	**i_γ**										
1	1.245	0.3170	0.54731	0.13828	Surface	0	1.00	1.00	1.00	108.83	271.19	135.49	138.97	2.5
						3	0.99	0.98	0.99	107.66	267.33	134.04	130.67	2.6
						7	0.97	0.96	0.96	106.07	261.60	132.05	126.45	4.4
						14	0.95	0.91	0.92	103.15	249.18	128.42	119.31	7.6
						20	0.92	0.87	0.86	100.49	234.12	125.11	112.56	11.2
					Embedded	0	1.00	1.00	1.00	123.74	286.11	154.06	156.44	1.5
						3	0.99	0.98	0.99	122.31	281.97	152.27	145.68	4.5
						7	0.97	0.96	0.96	120.34	275.87	149.82	137.82	8.7
						14	0.95	0.91	0.92	116.75	262.78	145.35	130.19	11.6
						20	0.92	0.87	0.86	113.49	247.13	141.30	122.54	15.3
10	1.0536	0.20274	0.73555	0.09268	Surface	0	1.00	1.00	1.00	108.83	271.19	114.66	118.94	3.6
						3	0.99	0.98	0.99	108.08	268.61	113.87	115.46	1.4
						7	0.98	0.94	0.98	107.05	264.74	112.79	110.09	2.5
						14	0.97	0.88	0.94	105.16	256.28	110.79	105.43	5.1
						20	0.95	0.83	0.90	103.42	245.80	108.96	101.66	7.2
					Embedded	0	1.00	1.00	1.00	123.74	286.11	130.38	136.44	4.4
						3	0.99	0.98	0.99	122.63	283.16	129.20	130.65	1.1
						7	0.98	0.94	0.98	121.11	278.80	127.60	123.17	3.6
						14	0.97	0.88	0.94	118.33	269.45	124.67	118.26	5.4
						20	0.95	0.83	0.90	115.82	258.20	122.03	112.68	8.3
>20	1.03185	1.0426	0.92268	0.23887	Surface	0	1.00	1.00	1.00	108.83	271.19	112.29	114.18	1.7
						3	0.97	0.97	0.97	105.05	264.07	108.39	110.46	1.9
						7	0.92	0.93	0.94	100.02	253.71	103.20	108.72	5.1
						14	0.84	0.86	0.86	91.24	232.14	94.14	103.52	9.1
						20	0.77	0.79	0.76	83.74	207.42	86.41	96.67	10.6
					Embedded	0	1.00	1.00	1.00	123.74	286.11	127.68	135.34	5.7
						3	0.97	0.97	0.97	119.50	278.53	123.31	130.23	5.3
						7	0.92	0.93	0.94	113.86	267.56	117.49	128.38	8.5
						14	0.84	0.86	0.86	104.00	244.90	107.31	116.97	8.3
						20	0.77	0.79	0.76	95.57	219.25	98.61	108.32	9.0

Table 5-22 Summary of percent differences between measured and predicted using all formation inclination factors for Fort Thompson limestone (FTL-2).

FTL-2														
L/B ratio	**Shape factor, ξ**	**p**				**Cases**	**i_c**	**i_q**	**i_γ**	**Q_{u1}**	**Q_{u2}**	**Predicted Bearing Capacity**	**PLAXIS Bearing Capacity**	**% difference**
		i_c	**i_q**	**i_γ**										
1	1.245	0.3170	0.54731	0.13828	Surface	0	1.00	1.00	1.00	149.62	322.48	186.28	202.10	7.8
						3	0.99	0.98	0.99	148.02	318.30	184.29	189.28	2.6
						7	0.97	0.96	0.97	145.83	312.18	181.56	184.08	1.4
						14	0.95	0.91	0.92	141.81	299.33	176.56	181.55	2.7
						20	0.92	0.87	0.88	138.17	284.70	172.02	176.90	2.8
					Embedded	0	1.00	1.00	1.00	176.90	349.75	220.24	216.67	1.6
						3	0.99	0.98	0.99	174.80	345.08	217.62	200.84	7.7
						7	0.97	0.96	0.97	171.92	338.27	214.05	190.73	10.9
						14	0.95	0.91	0.92	166.68	324.20	207.52	186.87	9.9
						20	0.92	0.87	0.88	161.94	308.47	201.61	180.44	10.5
10	1.0536	0.20274	0.73555	0.09268	Surface	0	1.00	1.00	1.00	149.62	322.48	157.64	160.52	1.8
						3	0.99	0.98	0.99	148.60	319.69	156.56	155.38	0.8
						7	0.98	0.94	0.98	147.19	315.58	155.07	153.41	1.1
						14	0.97	0.88	0.95	144.58	306.85	152.33	152.54	0.1
						20	0.95	0.83	0.91	142.19	296.74	149.81	147.54	1.5
					Embedded	0	1.00	1.00	1.00	176.90	349.75	186.38	192.49	3.2
						3	0.99	0.98	0.99	175.20	346.29	184.59	178.99	3.0
						7	0.98	0.94	0.98	172.88	341.28	182.15	170.99	6.1
						14	0.97	0.88	0.95	168.67	330.94	177.71	165.87	6.7
						20	0.95	0.83	0.91	164.86	319.41	173.70	159.68	8.1
>20	1.03185	1.0426	0.92268	0.23887	Surface	0	1.00	1.00	1.00	149.62	322.48	154.39	158.51	2.6
						3	0.97	0.97	0.98	144.43	314.49	149.03	155.72	4.3
						7	0.92	0.93	0.94	137.51	303.04	141.89	153.79	7.7
						14	0.84	0.86	0.87	125.44	279.95	129.44	148.37	12.8
						20	0.77	0.79	0.79	115.13	255.06	118.80	141.31	15.9
					Embedded	0	1.00	1.00	1.00	176.90	349.75	182.53	179.45	1.7
						3	0.97	0.97	0.98	170.86	340.93	176.30	174.57	1.0
						7	0.92	0.93	0.94	162.82	328.36	168.01	170.32	1.4
						14	0.84	0.86	0.87	148.78	303.28	153.52	163.40	6.0
						20	0.77	0.79	0.79	136.76	276.69	141.12	153.68	8.2

Table 5-23 Summary of percent differences between measured and predicted using all formation inclination factors for Anastasia limestone (AL-1).

AL-1														
L/B ratio	**Shape factor, ξ**	**p**				**Cases**	**i_c**	**i_q**	**i_γ**	**Q_{u1}**	**Q_{u2}**	**Predicted Bearing Capacity**	**PLAXIS Bearing Capacity**	**% difference**
		i_c	**i_q**	**i_γ**										
1	1.245	0.3170	0.54731	0.13828	Surface	0	1.00	1.00	1.00	179.69	321.01	223.71	213.02	5.0
						3	0.99	0.98	0.99	177.77	316.49	221.32	207.77	6.5
						7	0.97	0.96	0.96	175.14	309.79	218.04	202.79	7.5
						14	0.95	0.91	0.91	170.31	295.36	212.04	195.54	8.4
						20	0.92	0.87	0.85	165.93	277.89	206.58	189.46	9.0
					Embedded	0	1.00	1.00	1.00	199.46	340.78	248.32	241.65	2.8
						3	0.99	0.98	0.99	197.17	335.89	245.48	230.65	6.4
						7	0.97	0.96	0.96	194.05	328.70	241.59	222.90	8.4
						14	0.95	0.91	0.91	188.33	313.38	234.48	218.02	7.5
						20	0.92	0.87	0.85	183.16	295.12	228.03	209.71	8.7
10	1.0536	0.20274	0.73555	0.09268	Surface	0	1.00	1.00	1.00	179.69	321.01	189.32	188.86	0.2
						3	0.99	0.98	0.99	178.46	317.99	188.02	184.65	1.8
						7	0.98	0.94	0.97	176.76	313.49	186.24	180.54	3.2
						14	0.97	0.88	0.94	173.63	303.67	182.94	175.67	4.1
						20	0.95	0.83	0.90	170.76	291.54	179.91	167.93	7.1
					Embedded	0	1.00	1.00	1.00	199.46	340.78	210.15	207.23	1.4
						3	0.99	0.98	0.99	197.74	337.28	208.34	201.92	3.2
						7	0.98	0.94	0.97	195.39	332.12	205.86	196.81	4.6
						14	0.97	0.88	0.94	191.09	321.13	201.33	191.04	5.4
						20	0.95	0.83	0.90	187.19	307.97	197.23	182.51	8.1
>20	1.03185	1.0426	0.92268	0.23887	Surface	0	1.00	1.00	1.00	179.69	321.01	185.41	186.24	0.4
						3	0.97	0.97	0.97	173.45	312.21	178.97	181.32	1.3
						7	0.92	0.93	0.94	165.14	299.50	170.40	179.54	5.1
						14	0.84	0.86	0.85	150.65	273.42	155.45	172.45	9.9
						20	0.77	0.79	0.76	138.27	243.95	142.67	161.32	11.6
					Embedded	0	1.00	1.00	1.00	199.46	340.78	205.81	201.71	2.0
						3	0.97	0.97	0.97	192.61	331.37	198.74	195.38	1.7
						7	0.92	0.93	0.94	183.49	317.85	189.33	190.49	0.6
						14	0.84	0.86	0.85	167.56	290.33	172.90	187.33	7.7
						20	0.77	0.79	0.76	153.95	259.63	158.85	177.63	10.6

Table 5-24 Summary of percent differences between measured and predicted using all formation inclination factors for Anastasia limestone (AL-3).

AL-3															
Formation	L/B ratio	Shape factor, ξ	p				Cases	i_c	i_q	i_γ	Q_{u1}	Q_{u2}	Predicted Bearing Capacity	PLAXIS Bearing Capacity	% difference
			i_c	i_q	i_γ										
FTL-2	1	1.245	0.2226	0.3031	0.100	Surface	0	1.00	1.00	1.000	1337.42	1524.74	1665.09	1600.73	4.0
							3	0.99	0.99	0.991	1327.36	1512.30	1652.57	1570.42	5.2
							7	0.98	0.98	0.979	1313.53	1494.44	1635.34	1562.76	4.6
							14	0.96	0.95	0.953	1288.02	1458.58	1603.58	1537.80	4.3
							20	0.95	0.93	0.924	1264.65	1420.84	1574.49	1488.05	5.8
						Embedded	0	1.00	1.00	1.000	1556.72	1744.04	1938.12	1625.46	16.1
							3	0.99	0.99	0.991	1544.42	1729.36	1922.81	1591.11	17.3
							7	0.98	0.98	0.979	1527.51	1708.42	1901.75	1582.55	16.8
							14	0.96	0.95	0.953	1496.36	1666.92	1862.97	1556.45	16.5
							20	0.95	0.93	0.924	1467.87	1624.05	1827.50	1501.58	17.8
	10	1.0536	0.1229	0.4259	0.100	Surface	0	1.00	1.00	1.000	1337.42	1524.74	1409.10	1466.69	3.9
							3	1.00	0.99	0.991	1331.86	1514.23	1403.25	1464.36	4.2
							7	0.99	0.97	0.979	1324.18	1499.02	1395.15	1461.90	4.6
							14	0.98	0.93	0.953	1309.91	1468.00	1380.13	1447.76	4.7
							20	0.97	0.90	0.924	1296.74	1434.65	1366.25	1400.16	2.4
						Embedded	0	1.00	1.00	1.000	1556.72	1744.04	1640.16	1621.32	1.2
							3	1.00	0.99	0.991	1548.02	1730.39	1630.99	1600.57	1.9
							7	0.99	0.97	0.979	1536.04	1710.88	1618.38	1552.49	4.2
							14	0.98	0.93	0.953	1513.98	1672.07	1595.13	1516.14	5.2
							20	0.97	0.90	0.924	1493.78	1631.69	1573.85	1455.58	8.1
	>20	1.03185	1.4715	0.5496	0.102	Surface	0	1.00	1.00	1.000	1337.42	1524.74	1380.02	1426.46	3.3
							3	0.95	0.98	0.991	1272.34	1488.46	1312.87	1401.66	6.3
							7	0.89	0.96	0.978	1187.20	1439.68	1225.01	1389.76	11.9
							14	0.78	0.91	0.952	1042.84	1352.20	1076.06	1344.45	24.9
							20	0.69	0.87	0.922	923.98	1272.84	953.41	1289.48	26.1
						Embedded	0	1.00	1.00	1.000	1556.72	1744.04	1606.31	1571.68	2.2
							3	0.95	0.98	0.991	1487.59	1703.71	1534.98	1524.37	0.7
							7	0.89	0.96	0.978	1396.95	1649.43	1441.45	1502.52	4.1
							14	0.78	0.91	0.952	1242.68	1552.04	1282.26	1436.15	10.7
							20	0.69	0.87	0.922	1114.99	1463.85	1150.50	1368.77	15.9

5.2.7 Eccentricity Analysis

In the case where eccentric loads act on the foundation, AASHTO recommends the effective dimension, B′ or L′, be used in place of the foundation dimension, B or L. The effective footing width, B′, is calculated according to Equation 31 while the eccentricity can be calculated with Equation 32, with the moment and resultant vertical force acting at the location of eccentricity. Eccentricity for design of shallow foundations on soil is conventionally limited to B/6 (FDOT practice) while ASHTO recommends limits of B/3 for soils and 0.45B for rock. The AASHTO recommendation for rock pertains to rigid very low porosity rock, unlike the limestone from shallow depths which have been studied in this work.

$$B' = B - 2e_B \qquad \text{Equation 5-31}$$

$$e_B = \frac{M_B}{V} \qquad \text{Equation 5-32}$$

where e_B is the load eccentricities is in the B directions, respectively, M_B is the moments due to eccentric loads in the B directions, respectively, and V is the total vertical load.

Bearing capacity of footings on Miami, Fort Thompson, and Anastatia limestone were modeled for eccentric loading of B/6 and B/12. This equates to an eccentricity of 10 inches and 5 inches respectively from the centerline of the footing. The eccentricity at the maximum bearing pressure (bearing capacity) of each PLAXIS simulation was calculated with Equation 5-32 using the moment and vertical force response at the location of the applied load. Table 25 – Table 27 are the measured and design eccentricity (e.g., B/6, B/12) for the cases of all footings L/B = 1, 10 , and 20 modeled.

For the square footings (Table 5-25), rectangular footings (Table 5-26), and strip footings (Table 5-27) the comparison between the measured and design eccentricities are generally the same. The measured eccentricities generally were between the design B/12 and B/6 for all formations (e.g., measured B/12 eccentricity > design B/12 and measured B/6 < design B/6).

A summary of the measured and predicted bearing capacities for the eccentric cases are shown in Table 5-28. The eccentricity for each case is accounted for in the prediction using B′ (Equation 5-31) for B in the Florida bearing capacity equations (Equation 5-8 – Equation 5-15). The PLAXIS bearing capacity is determined from the total load on the footing divided by the measured effective footing width (Table 25, Table 26, and Table 27) times the footing length. Figure 5-24 is the measured versus predicted (bias) bearing capacity for the eccentric cases that illustrates the generally good agreement with a mean bias of 1.07 and CV of 0.12 (Table 29). Note, PLAXIS bearing capacity was also calculated using the effective footing width based on the design eccentricity (i.e., B/12, B/6) and the mean bias is 1.04 and CV is 0.11, for a relative comparison on the measured and very good agreement between the bias statistics.

Table 5-25 Summary of eccentricity results for L/B =1.

Formation	**Load Cases**		**Square Footing, B=5ft, Df=0, L/B=1**			
			M (lbf-ft)	**V (lbf)**	**Measured, e=M/V (in)**	**Design Eccentricity, e (in)**
ML-1	2	e-b/6	1423	1603	10.7	10
	2	e-b/12	2104	2814	9.0	5
FTL-2	2	e-b/6	1585	2268	8.4	10
	2	e-b/12	1607	2622	7.4	5
AL-3	2	e-b/6	15261	20780	8.8	10
	2	e-b/12	12270	21003	7.0	5

Table 5-26 Summary of eccentricity results for L/B = 10.

Formation	Load Cases		Rectangular Footing, B=5ft, Df=0, L/B=10			
			M (lbf-ft)	V (lbf)	Measured, e=M/V (in)	Design Eccentricity, e (in)
ML-1	2	e-b/6	32956	40648	9.7	10
	2	e-b/12	13154	21610	7.3	5
FTL-2	2	e-b/6	12059	15727	9.2	10
	2	e-b/12	15672	23113	8.1	5
AL-3	2	e-b/6	14598	15318	11.4	10
	2	e-b/12	17482	25467	8.2	5

Table 5-27 Summary of eccentricity results for L/B = 20.

Formation	Load Cases		Strip Footing, B=5ft, Df=0, L/B>20			
			M (lbf-ft)	V (lbf)	Measured, e=M/V (in)	Design Eccentricity, e (in)
ML-1	2	e-b/6	27330	36344	9.0	10
	2	e-b/12	25471	44088	6.9	5
FTL-2	2	e-b/6	23230	35867	7.8	10
	2	e-b/12	29026	50366	6.9	5
AL-3	2	e-b/6	53875	92191	7.0	10
	2	e-b/12	27024	57298	5.7	5

Table 5-28 Summary of measured and predicted bearing capacity for eccentric PLAXIS models for ML-1, FTL-2, and AL-3.

Formation	L/B ratio	Shape factor, ξ	Eccentricity, e	Qu1 (psi)	Qu2 (psi)	Predicted Bearing (psi)	PLAXIS Bearing (psi)
ML-1	1	1.19	B/6	158.16	332.85	187.81	260.49
			B/12	160.11	336.96	194.89	273.59
	10	1.04	B/6	158.16	332.85	164.64	171.42
			B/12	160.11	336.96	167.72	178.38
	20	1.02	B/6	158.16	332.85	162.01	152.5
			B/12	160.11	336.96	164.63	169.18
FTL-2	1	1.19	B/6	146.32	315.36	173.75	196.60
			B/12	148.13	319.26	180.31	216.97
	10	1.04	B/6	146.32	315.36	152.32	141.66
			B/12	148.13	319.26	155.17	180.91
	20	1.02	B/6	146.32	315.36	149.89	148.89
			B/12	148.13	319.26	152.31	175.24
AL-3	1	1.19	B/6	1307.92	1491.12	1553.13	1457.08
			B/12	1324.07	1509.53	1611.69	1673.9
	10	1.04	B/6	1307.92	1491.12	1361.57	1420.74
			B/12	1324.07	1509.53	1387.00	1364.6
	20	1.02	B/6	1307.92	1491.12	1339.80	1301.54
			B/12	1324.07	1509.53	1361.47	1269.34

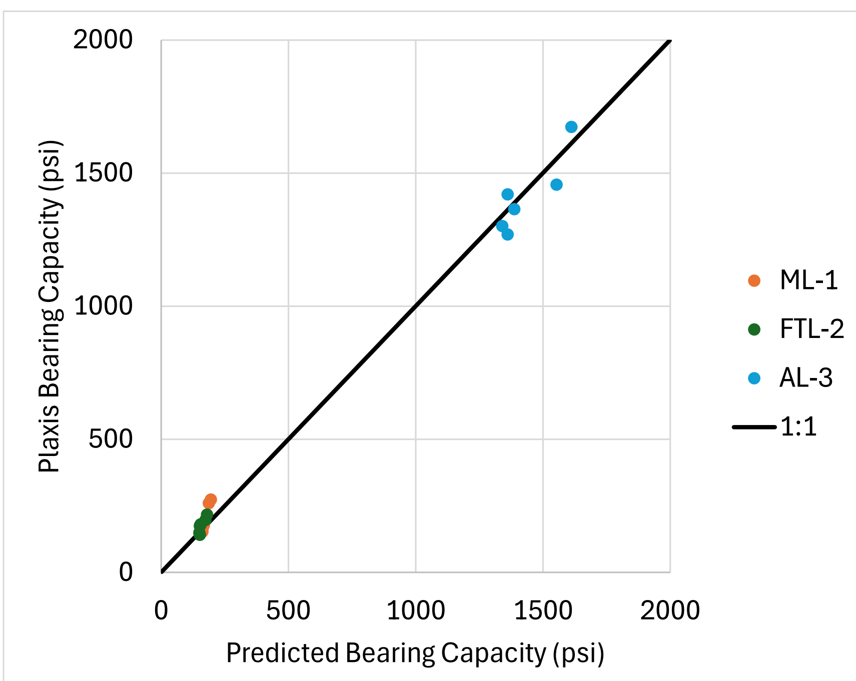

Figure 5-24 PLAXIS versus predicted bearing capacity for eccentric cases in Table 28.

Table 5-29 Summary statistics of bias for Florida bearing capacity with effective footing width, B′ (Meyerhof), for all data and for Miami (ML), Fort Thompson (FTL), and Anastasia (AL) limestone formations (Figure 5-24).

	All	ML-1	FTL-2	AL-3
μ =	1.07	1.14	1.10	0.98
σ =	0.13	0.17	0.10	0.05
cv =	0.12	0.15	0.09	0.05

Table 5-30 Summary statistics of bias for Florida bearing capacity with effective footing width, B′ (Meyerhof) in measured and predicted capacity, for all data and for Miami (ML), Fort Thompson (FTL), and Anastasia (AL) limestone formations.

	All	ML-1	FTL-2	AL-3
μ =	1.04	1.08	1.08	0.97
σ =	0.12	0.14	0.08	0.09
cv =	0.11	0.13	0.07	0.09

CHAPTER 6
DOCUMENTATION OF IMPLEMENTATION OUTCOMES AND FB-MULTIPIER FEATURE SETS

6.1 Introduction

Project tasks 1-4 (1) Implementation of bearing capacity equations for Florida Limestone; 2) Implementation of nonlinear axial load-settlement analysis; 3) Development and implementation of lateral resistance of shallow foundations under various loading scenarios to account for realistic designs of skewed loading; and 4) Investigation of inclined and eccentric load applied to shallow foundations in Florida Limestone) have been implemented in the FB-MultiPier software as a new shallow foundation feature. These tasks have resulted in multiple updates to FB-MultiPier in the form of:

1. New model category, shallow foundation, which has no pile or shaft elements present. The soil resistance only acts on the footing which is a shell element. This shell element was typically referred to the pile cap when modeled with pile/shaft elements.
2. New UI dialogs for each design model for both axial bearing and lateral passive and lateral frictional resistance.
3. Non-linear FEA engine analysis with newly implemented UI design models.
4. Output of engine results in the form 3D results and a text output file.

This chapter documents updates that have been made to UI, a walkthrough of the UI, new additions to the FB-MultiPier help manual, selection of worked examples for validation and recommendations for site investigation requirements to determine required Florida Limestone properties.

6.2 FB-MultiPier UI Updates

The following user-interface and analytical engine, FB-MultiPier program, is proposed for shallow foundation analyses incorporating the research efforts from Phase I (BDV31-977-51) and Phase II (BDV31-977-124) projects. The aim is to equip bridge design engineers with the capability to add and analyze a shallow foundation system on a Florida limestone layer beneath a bridge pier. Task #5 of the Phase III project is focused on 1) updating the UI for a shallow foundation only model 2) allowing user specified inclination angle for axial bearing capacity 3) updating 3D results window to show resultant eccentricity and inclination and 4) minor UI updates for consistent nomenclature.

6.2.1 Shallow Foundation Only Enhancement in FB-MultiPier UI

The update to the FB-MultiPier UI includes implementation of template models of Shallow Foundation, Figure 6-1, and Shallow Foundation with Pier, Figure 6-2 . These models provide users with a base from which they can modify footing dimensions, soil/rock layering, and properties to rapidly generate a shallow foundation model. More information for these models is provided in the UI walk through and help manual. Since FB-MultiPier was originally developed to analyze soil structure interaction of pile and shafts, both the UI and Engine required a pile or shaft element be present. The proposed FB-MultiPier UI and Engine have now been updated to allow the analysis for a shallow foundation without the required presence of a pile or shaft element.

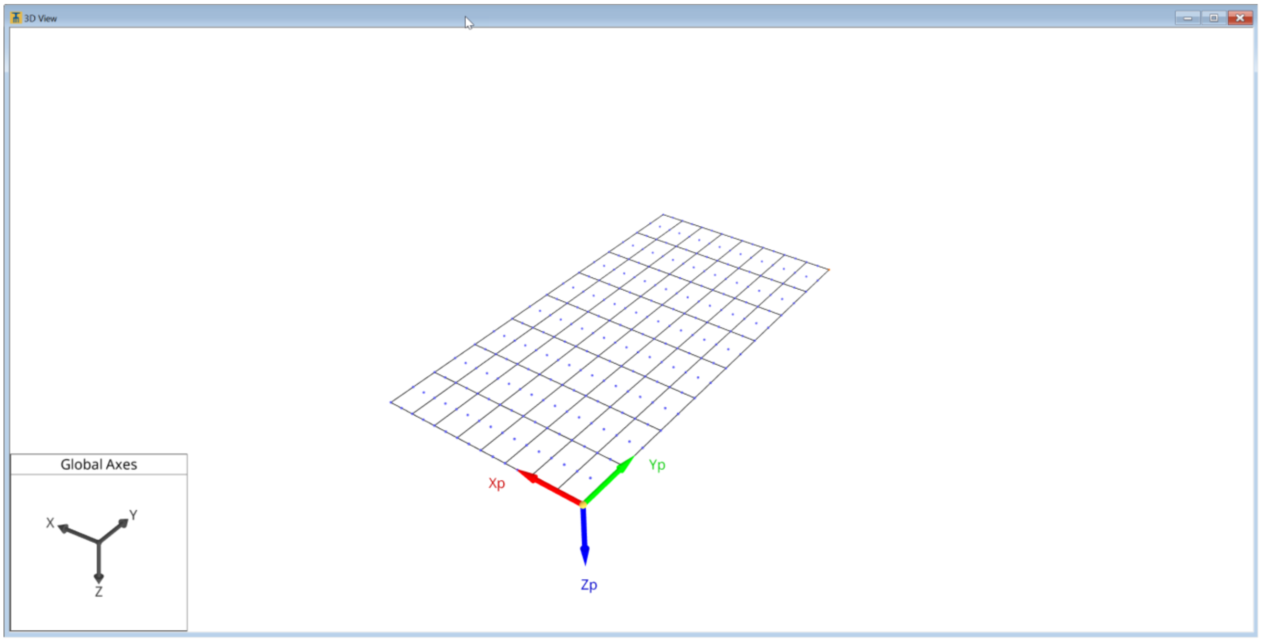

Figure 6-1 Shallow foundation model (no piles present).

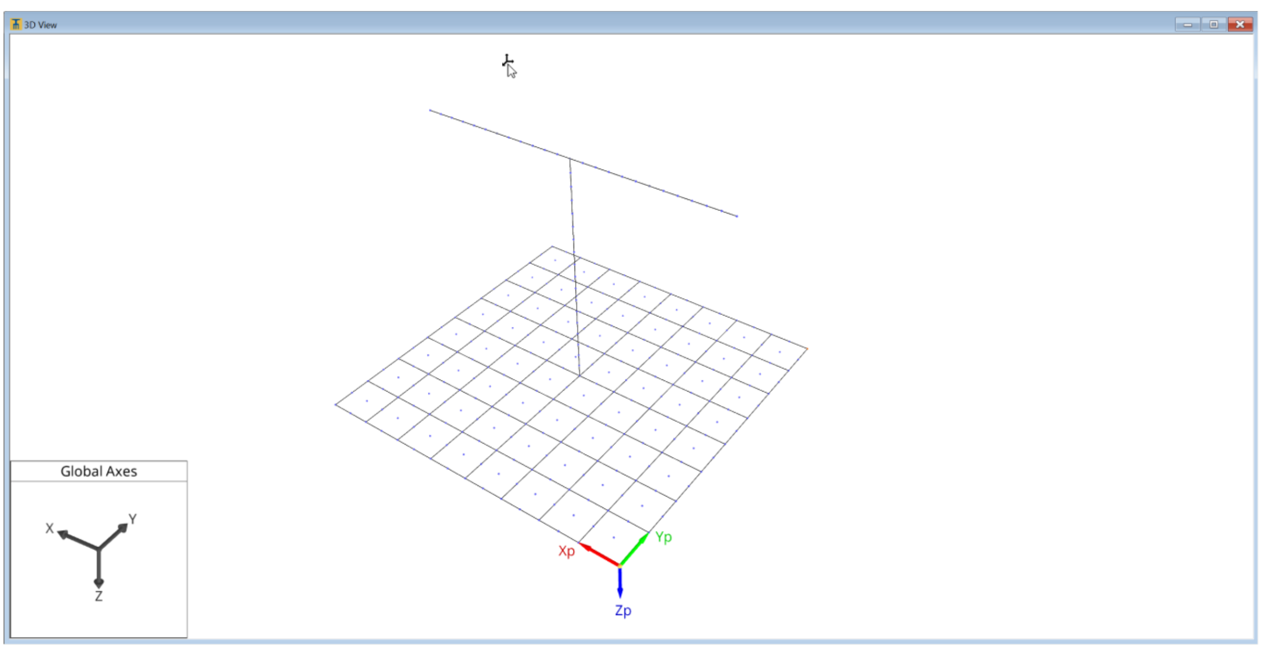

Figure 6-2 Shallow foundation model with pier (no piles present).

6.2.2 Shallow Foundation Inclination Enhancement in FB-MultiPier UI

The update to the FB-MultiPier UI includes implementation of Task 4 inclination factors. This implementation is provided as a user input “Inclination Angle” for Axial Bearing Florida Limestone models, Figure 6-3 This input allows the user to reduce the estimated bearing capacity, based on the “All Formation” factors specified in Task 4 report.

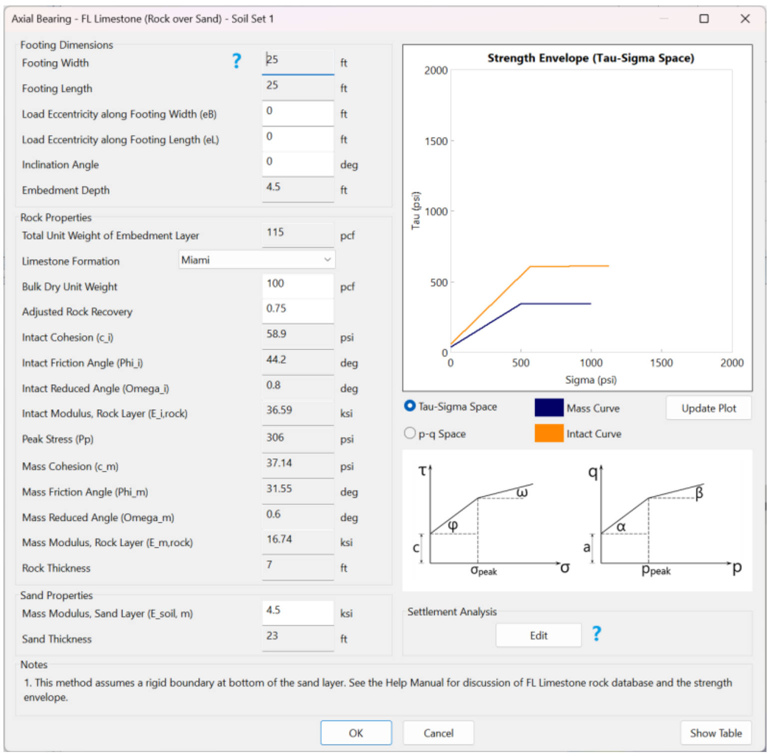

Figure 6-3 Axial bearing FL limestone dialog with inclination angle input.

An additional update to the FB-MultiPier UI includes implementation of following outputs: Eccentricity and Inclination in the 3D Results window, Figure 6-4. In this window, eccentricity is output in both the Xp and Yp directions. Also presented are the B/6 and L/6 limit values, to aid users to see if they exceed this design limit. Additionally, resultant eccentricities are output per each load case. Note the resultant eccentricity of the load case does not modify the calculated bearing capacity. The bearing capacity is only modified by the eccentricity specified in the Axial Bearing dialog and is used for each load case.

In the 3D results window, inclination angle is also shown with its corresponding resultant horizontal and vertical force used to calculate the angle. This resultant inclination angle is output per each load case. Note the resultant inclination angle of the load case does not modify the calculated bearing capacity. The bearing capacity is only modified by the inclination angle specified in the Axial Bearing dialog and is used for each load case.

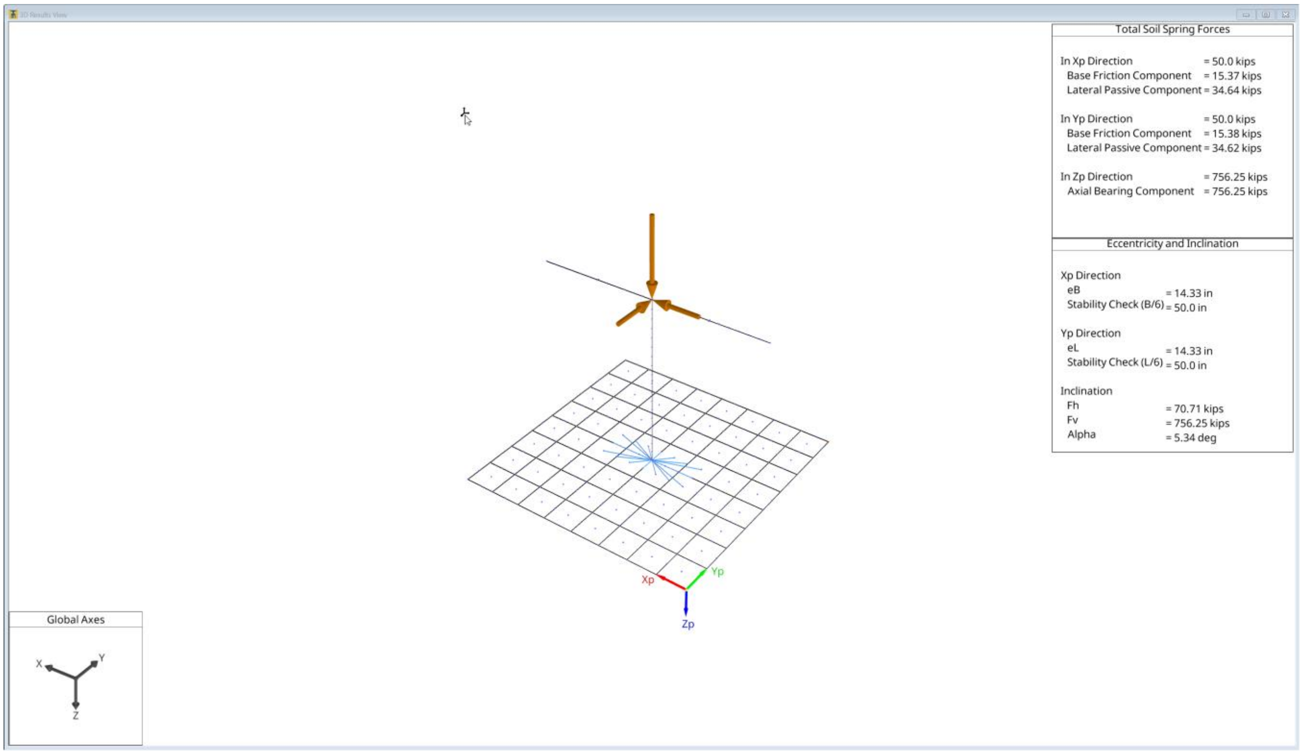

Figure 6-4 3D results window with outputs for eccentricity and inclination.

There have also been several minor updates to improve layout, nomenclature and labeling. These changes have not resulted in any major changes to the functionality or analysis as described in previous task reports. With the implementation of a shallow foundation only model, the UI now uses the labels of shallow foundation or footing instead of pile cap.

6.3 FB-MultiPier UI Walkthrough

For this walkthrough, we will be modeling a shallow foundation using the 'Pier with Shallow Foundation' model type in FB-MultiPier. The first step in utilizing the shallow foundation features is to open a default model type that has, as its footing, a shallow foundation. There are two types of such model types in FB-MultiPier, as follows:

- Pier with Shallow Foundation
- Shallow Foundation

For this walkthrough, the 'Pier with Shallow Foundation' model type will be used. Clicking the 'File' menu at the top left of the FB-MultiPier UI reveals a variety of options. Choose the 'New' option, which launches the 'Select New Model Type' dialog (Figure 6-5).

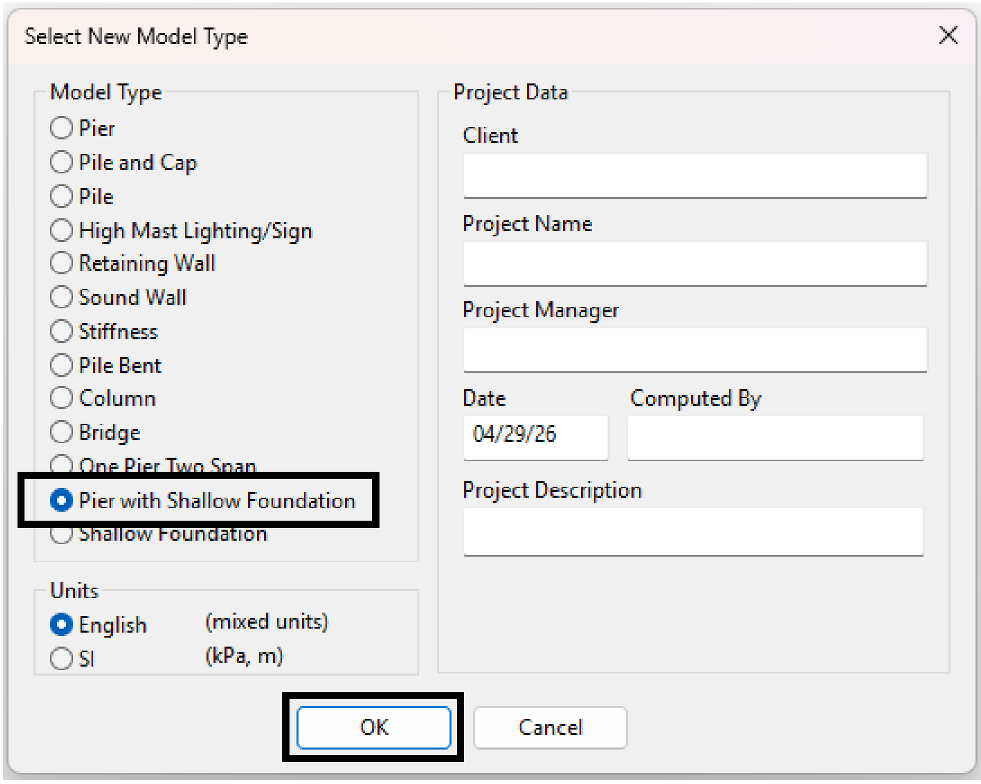

Figure 6-5 'Select New Model Type' dialog.

On the 'Select New Model Type' dialog, select the 'Pier with Shallow Foundation' model type. Leave the 'Units' selection as 'English'. Then click the 'OK' button. The UI views populate using the default 'Pier with Shallow Foundation' model. This includes the 'Model Data' window and graphical representations (Figure 6-6).

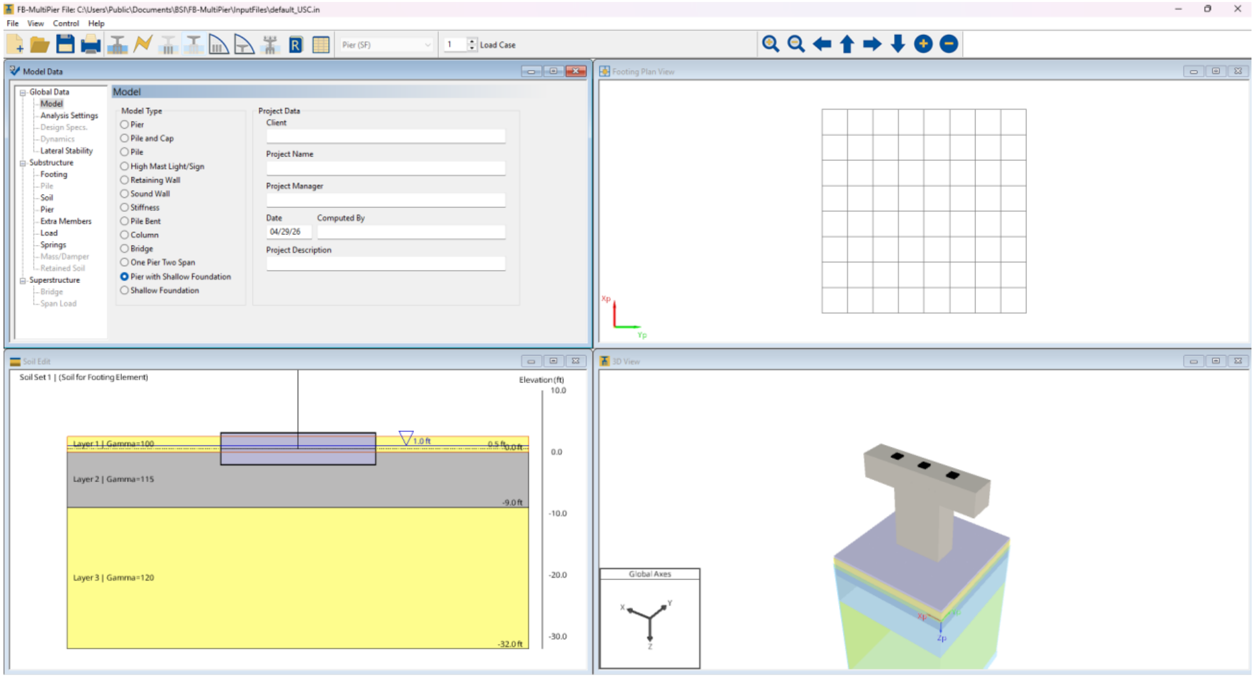

Figure 6-6 ‘Model Data’ window and graphics windows displaying pier with shallow foundations model.

Before proceeding, click the ‘File’ menu and select the ‘Save As’ option. Then assign a name to the input file and save the file to the desired location on your machine. This allows the user to exit the program and re-enter the program at a later time without losing any work.

Navigate to the ‘Footing’ page by selecting ‘Footing’ in the Model Data property page tree (Figure 6-7).

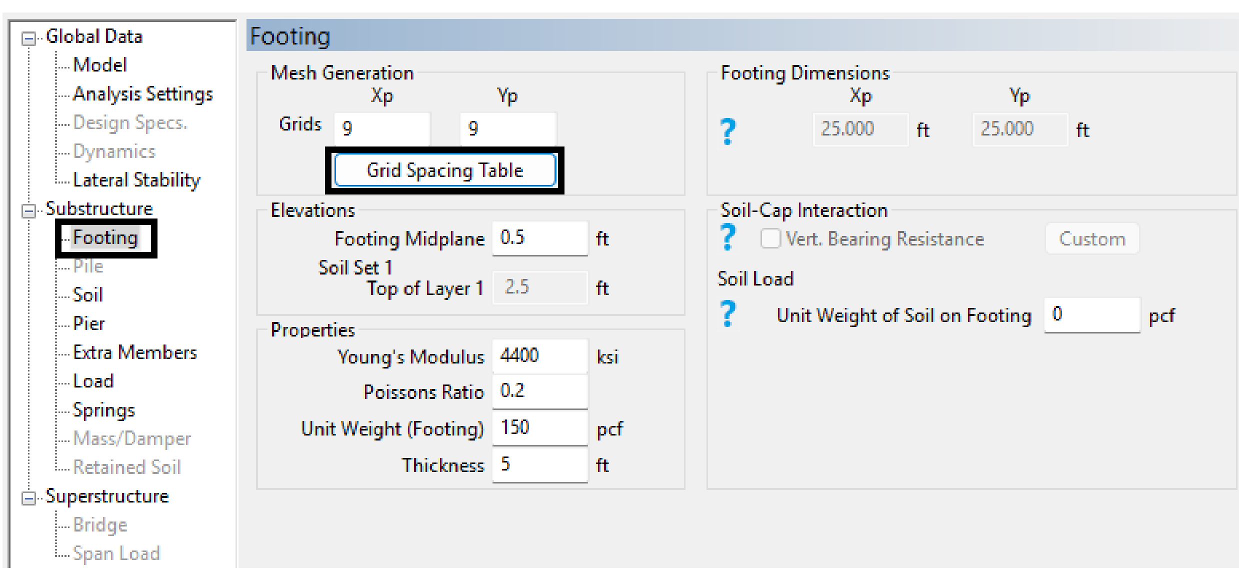

Figure 6-7 ‘Footing’ page.

The 'Footing' page is used to access the grid spacing options, namely the 'Grid Spacing Table' button. Clicking this button launches the 'Grid Spacing Table' dialog (Figure 6-8), on which the footing dimensions can be assigned.

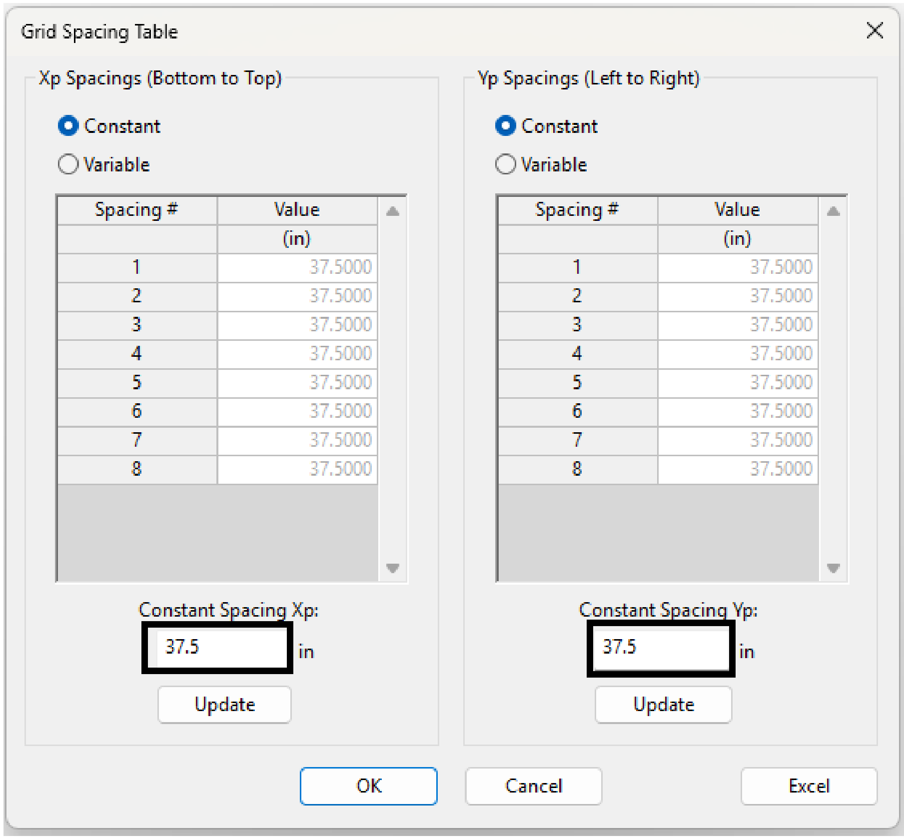

Figure 6-8 'Grid Spacing Table' dialog.

In the default model, the Xp and Yp grid spacing are set to 37.5 (inches). Modify the 'Constant Spacing Xp' edit box value to 30, and click the accompanying 'Update' button. This action updates the list of spacings displayed in the 'Xp Spacings' table (Figure 6-9). Modify the 'Constant Spacing Yp' edit box value to 22.5, and click the accompanying 'Update' button. This action updates the list of spacings displayed in the 'Yp Spacings' table (Figure 6-9).

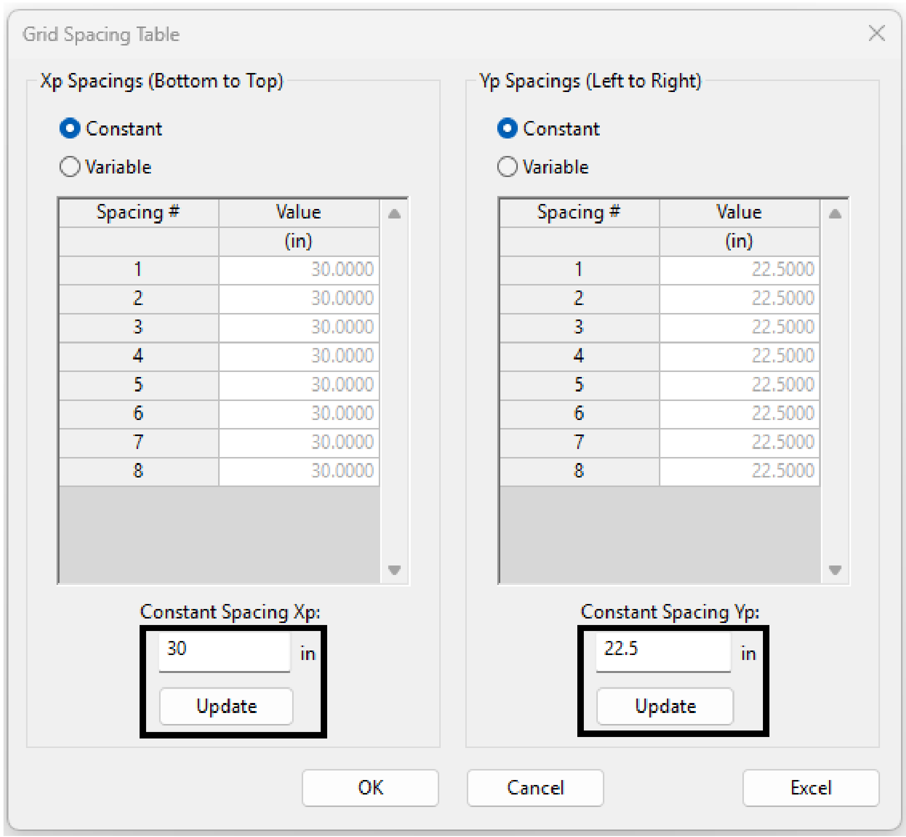

Figure 6-9 ‘Grid Spacing Table’ dialog with updated Xp and Yp spacings.

Click the ‘OK’ button on the ‘Grid Spacing Table’ dialog. The ‘Footing’ page is once again the active page. Observe that the ‘Footing Dimensions’ edit boxes have been automatically updated (Figure 6-10) to reflect the Xp and Yp spacings data that was just input in the most previous step. The footing now has an Xp dimension of 20’, and a Yp dimension of 15’. These edit boxes are read-only. Also, note that the Grid spacing is the only way to set the dimensions of the shallow foundation.

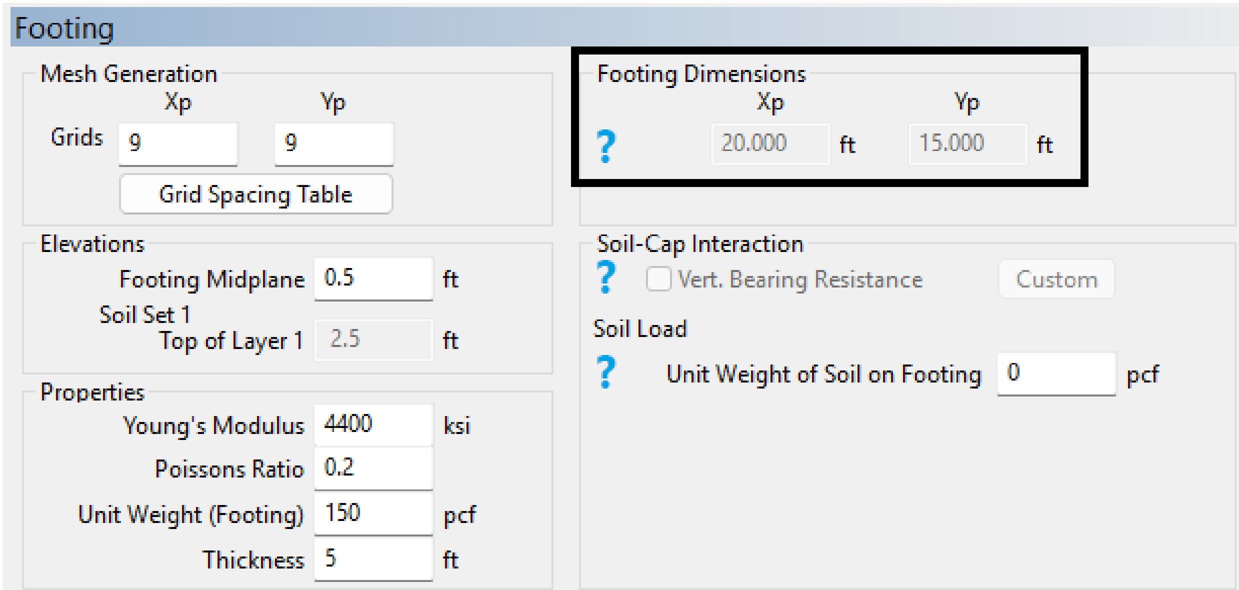

Figure 6-10 'Footing' page with footing dimensions.

Observe the graphical representation of the footing and its mesh discretization in the 'Footing Plan View' (Figure 6-11).

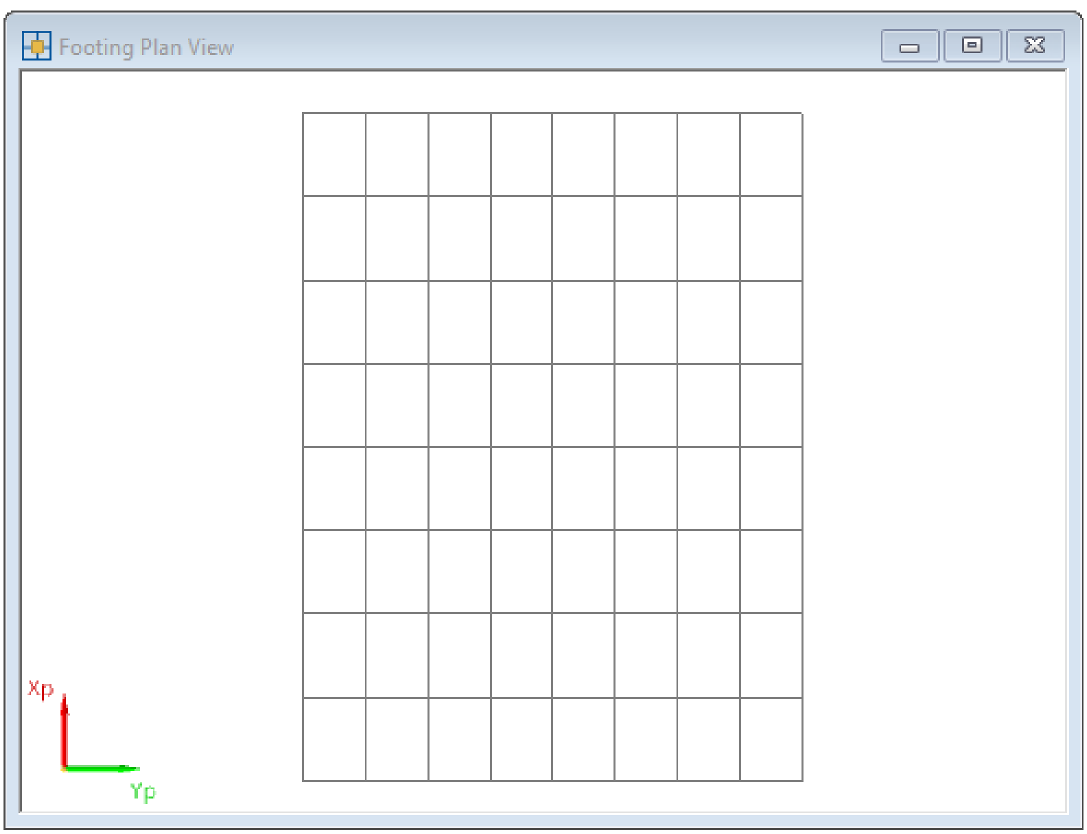

Figure 6-11 'Footing Plan View'.

On the ‘Footing’ page, modify the following data:

- ‘Footing Midplane’* = 3 (feet)
- ‘Thickness’ (of Footing) = 6 (feet)

*Note, Footing Midplane sets the depth location (centerline) of the footing in the soil or rock media.

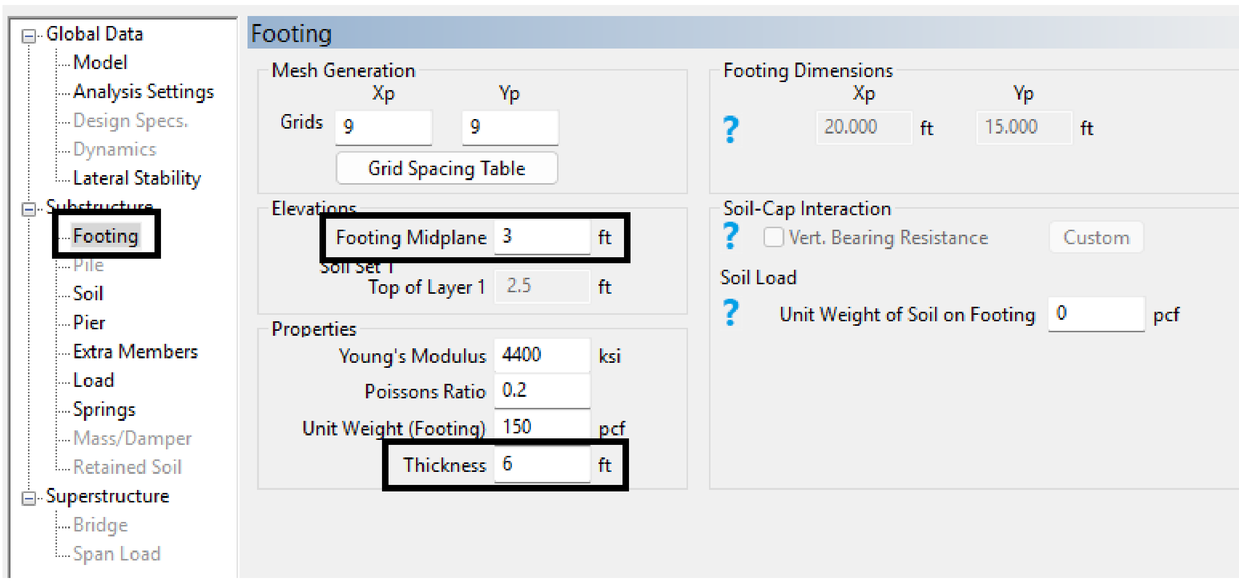

Figure 6-12 ‘Footing’ page with input updates.

Navigate to the ‘Pier’ page by selecting ‘Pier’ in the Model Data property page tree (Figure 6-13).

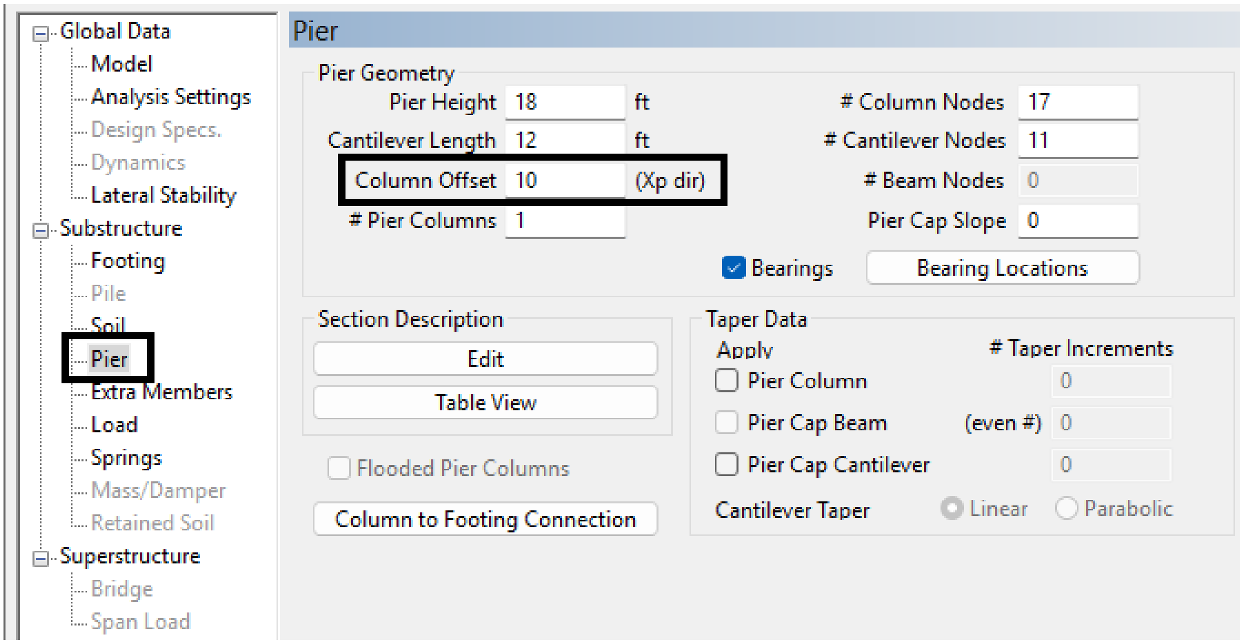

Figure 6-13 ‘Pier’ page with input updates.

On the ‘Pier’ page, modify the following data to center the column on the footing:

- ‘Column Offset’ = 10 (feet)
  10.

Now that significant changes to model geometry have been made, click the ‘Save’ toolbar button at the top of the program interface to save these changes.

Next, navigate to the ‘Load’ page by selecting ‘Load’ in the Model Data property page tree (Figure 6-14.).

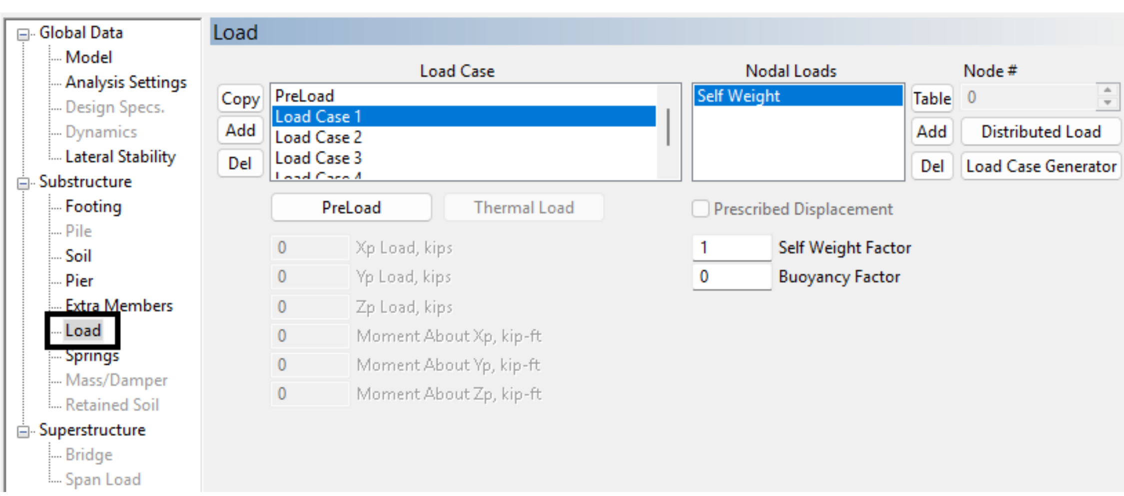

Figure 6-14 ‘Load’ page.

For this walkthrough, the existing load data from the default model will suffice. Doing an inspection of this data will make viewing the analysis results (later in this walkthrough) more intuitive.

The load data encompasses four (4) load cases. A brief inspection of each load case can be done by selecting each of the load cases (1-4) in the 'Load Case' list box (Figure 6-15 – Figure 6-19).

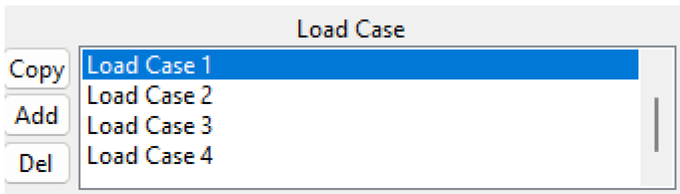

Figure 6-15 'Load Case' list box displaying load cases 1-4 on 'Load' page.

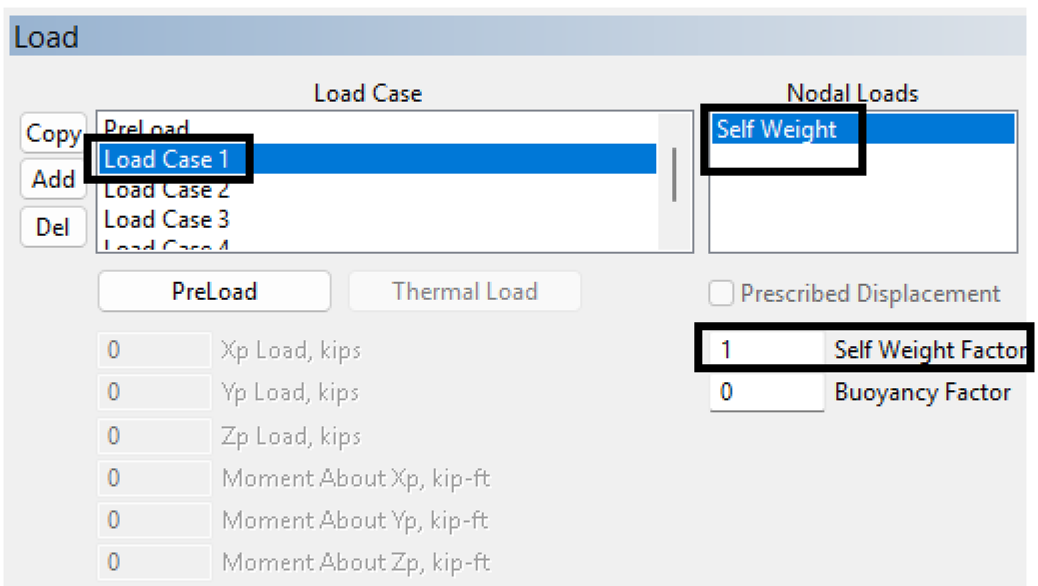

Figure 6-16 'Load Case' list box with load case 1 selected.

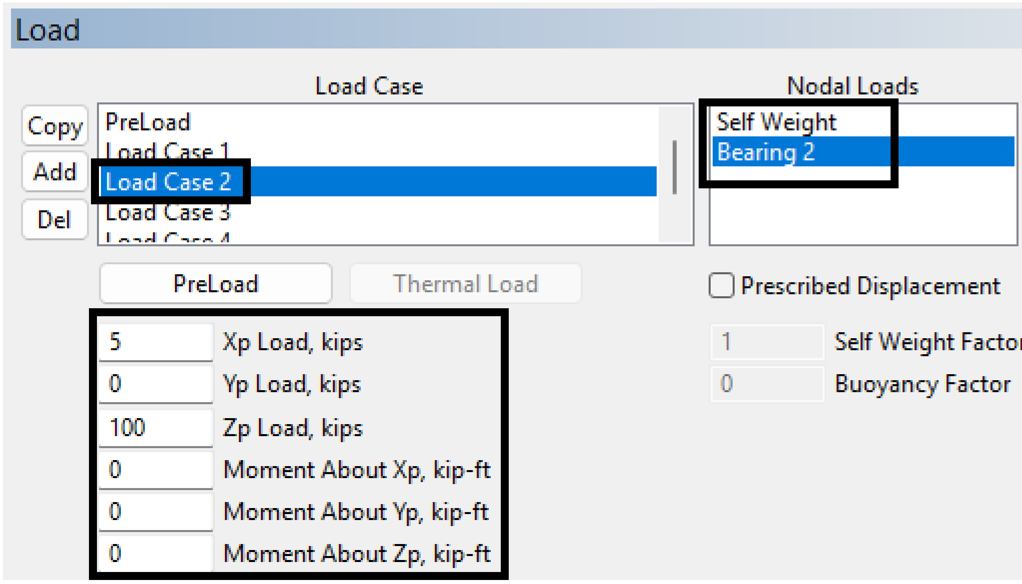

Figure 6-17 ‘Load Case’ list box with load case 2 selected.

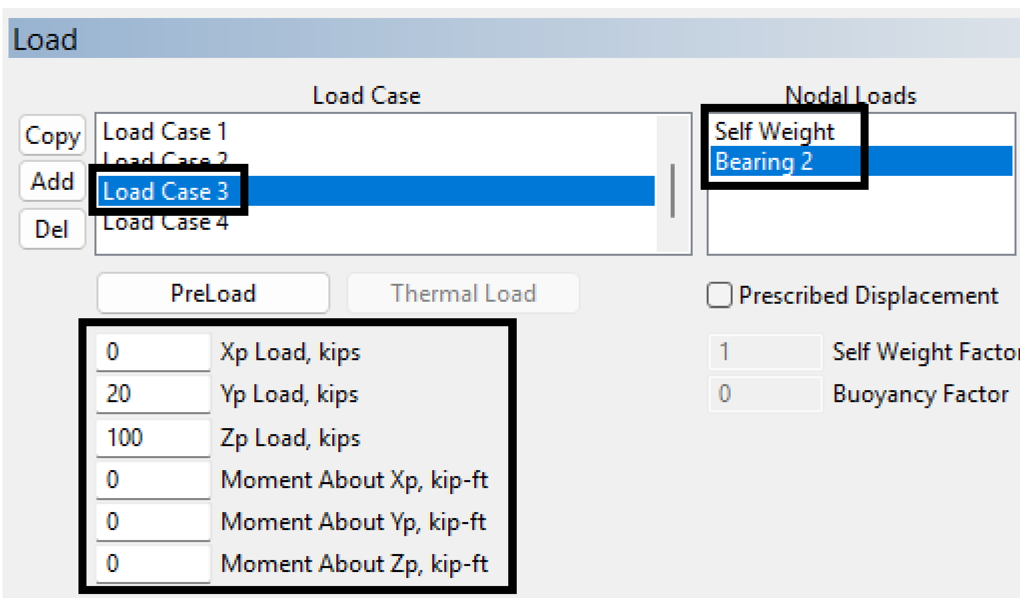

Figure 6-18 ‘Load Case’ list box with load case 3 selected.

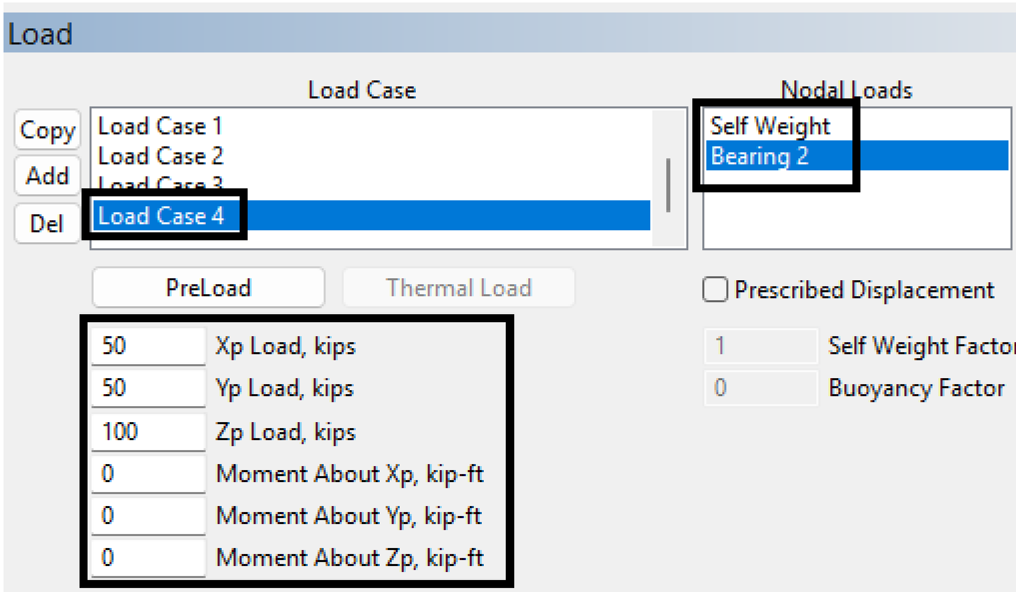

Figure 6-19 ‘Load Case’ list box with load case 4 selected.

Observe the model with loading for the currently selected load case in the 3D View (Figure 6-20).

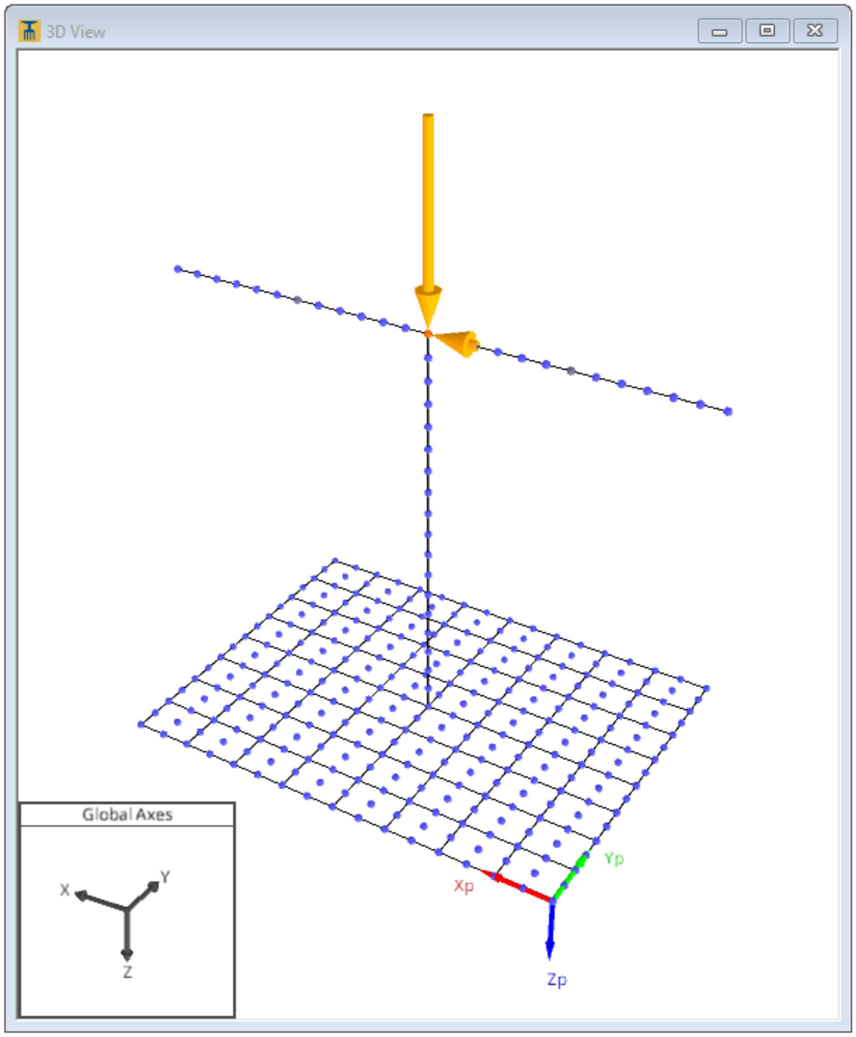

Figure 6-20 ‘3D View’ displaying nodal loads for a selected load case.

Navigate to the ‘Soil’ page by selecting ‘Soil’ in the Model Data property page tree (Figure 6-21).

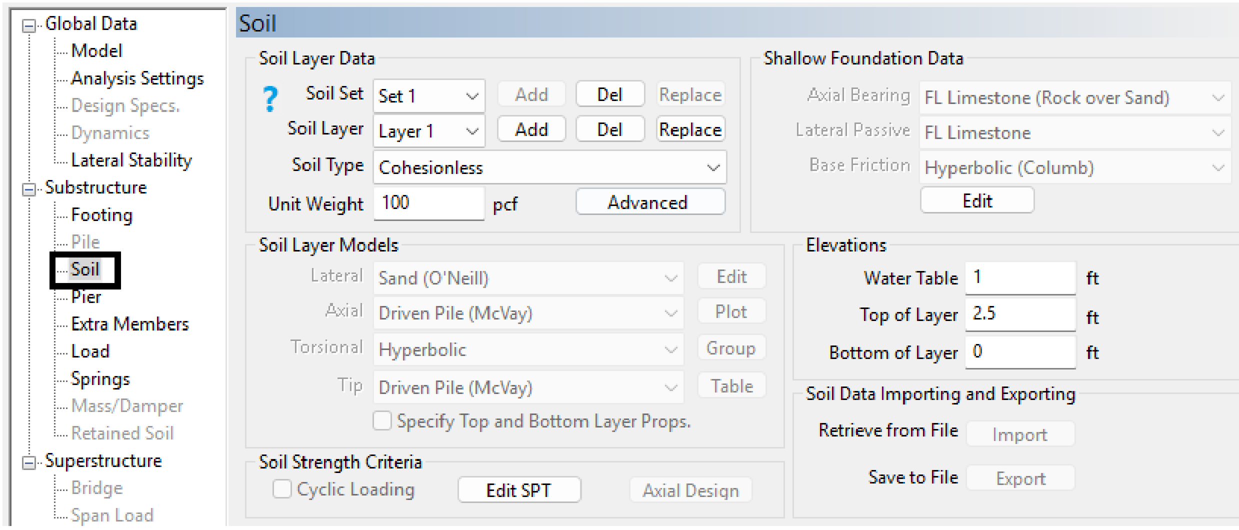

Figure 6-21 ‘Soil’ page.

On the ‘Soil’ page, firstly, the soil layering must be updated. The default model has three (3) soil layers. This can be seen by clicking the ‘Soil Layer’ combo box on the ‘Soil’ page (Figure 6-22).

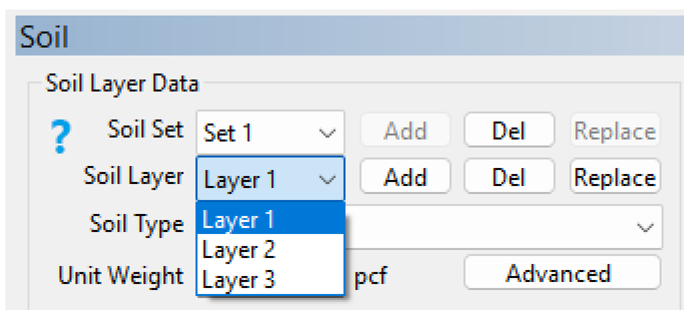

Figure 6-22 ‘Soil’ page’s ‘Soil Layer’ combo box showing 3 soil layers.

The default soil layering (3 layers) can also be seen in the ‘Soil Edit View’ (Figure 6-23). Observe that Layer 2 is the bearing layer (i.e., the bottom edge of the footing rests within Layer 2).

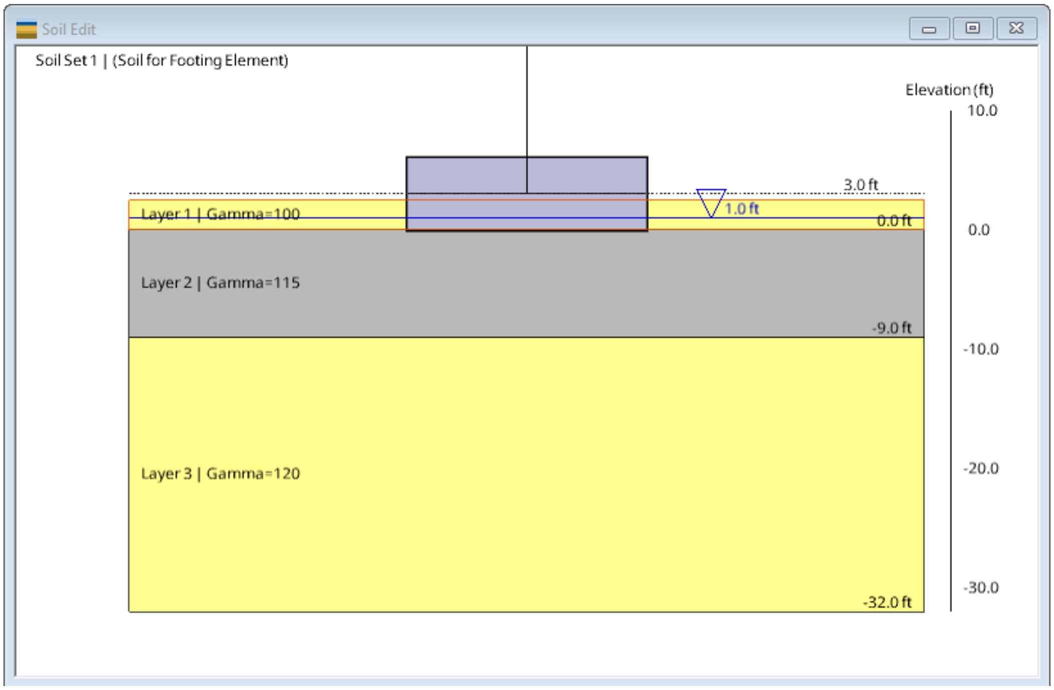

Figure 6-23 ‘Soil Edit View’ displaying original layering (3 soil layers).

To update the soil layering in the desired fashion, use the ‘Soil Layer’ combo box (dropdown) on the ‘Soil’ page to select Layer 1 (Figure 6-24). With Layer 1 selected, modify the ‘Water Table’ elevation to 0 (feet) (Figure 6-24).

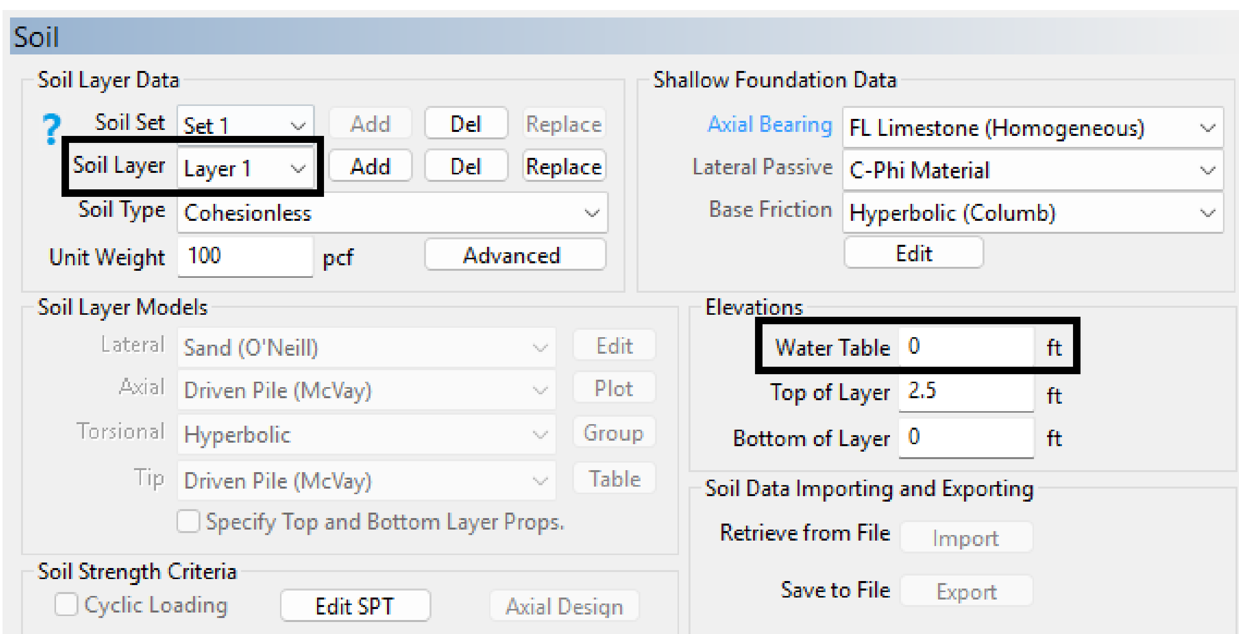

Figure 6-24 ‘Soil Layer’ combo box with layer 1 selected on ‘Soil’ page.

Next, use the ‘Soil Layer’ combo box (dropdown) on the ‘Soil’ page to select ‘Layer 2’ (Figure 6-25). With Layer 2 selected, modify the ‘Bottom of Layer’ elevation to -15 (feet) (Figure 6-25).

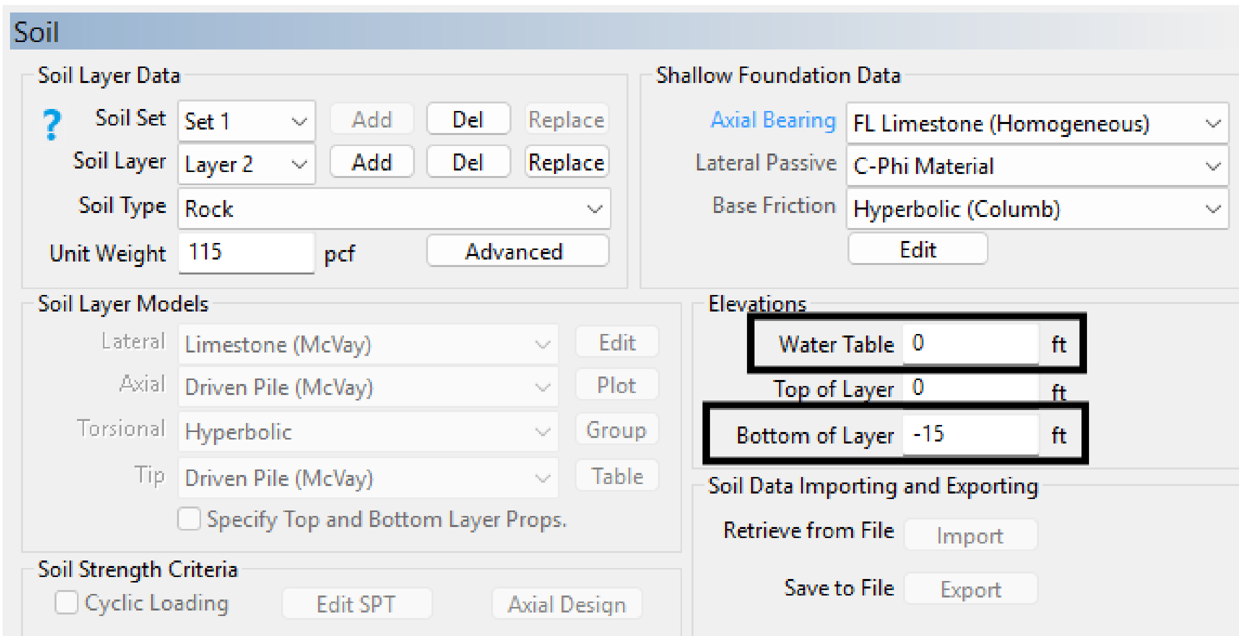

Figure 6-25 ‘Soil Layer’ combo box with layer 2 selected on ‘Soil’ page.

Next, use the ‘Soil Layer’ combo box (dropdown) on the ‘Soil’ page to select ‘Layer 3’ (Figure 6-26). With Layer 3 selected, click the ‘Del’ (delete) button to remove Layer 3 from the model.

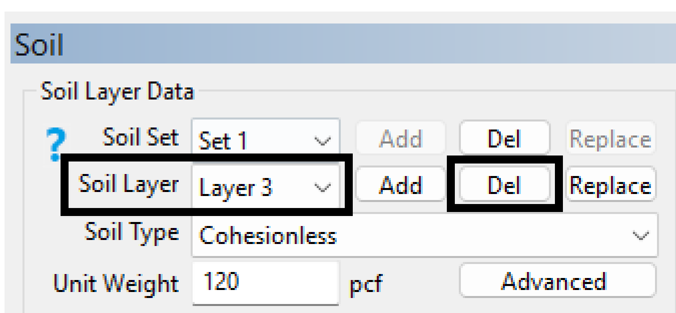

Figure 6-26 ‘Soil Layer’ combo box with layer 3 selected on ‘Soil’ page, and ‘Del’ button.

Use the ‘Soil Layer’ combo box (dropdown) on the ‘Soil’ page to inspect the list of remaining soil layers (Figure 6-27). There are now two (2) soil layers.

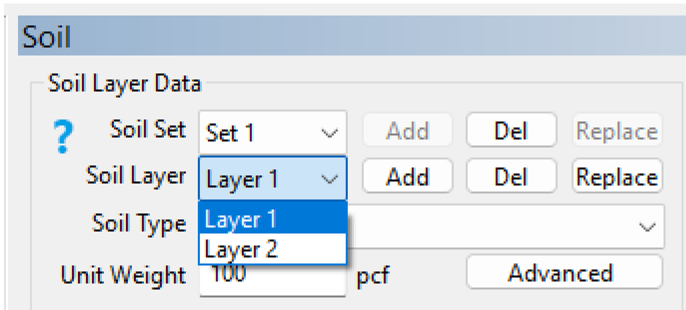

Figure 6-27 ‘Soil Layer’ combo box showing 2 soil layers.

The updated soil layering (2 layers) can also be seen in the ‘Soil Edit View’ (Figure 6-28. Observe that Layer 2 is the bearing layer (i.e., the bottom edge of the footing rests on the top of Layer 2.

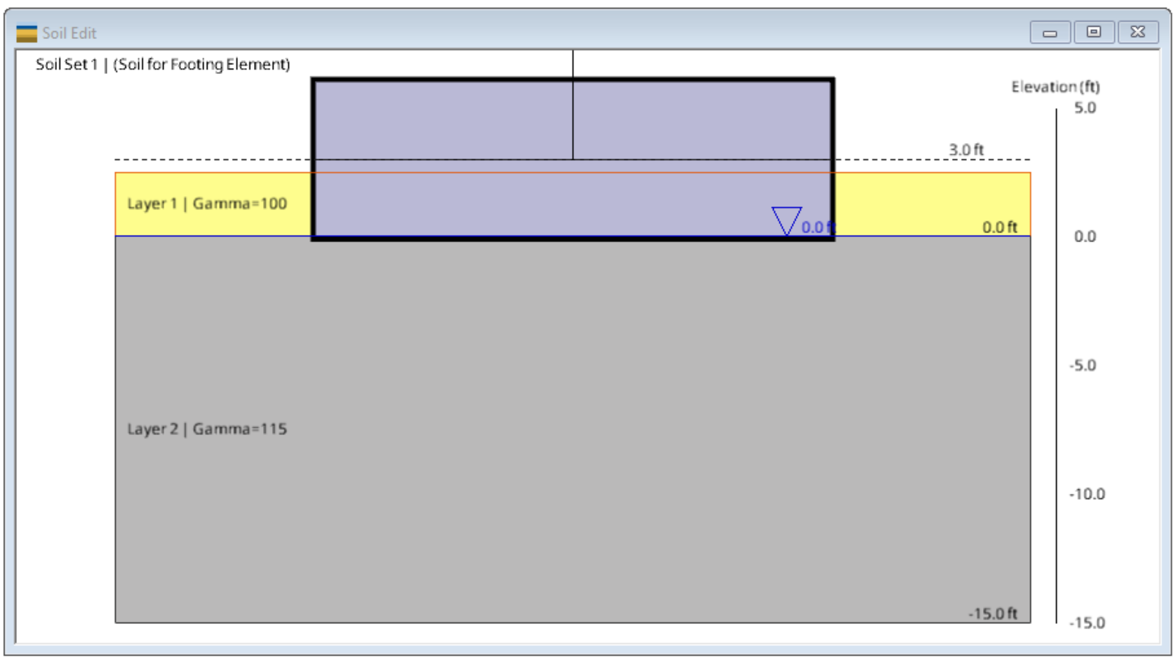

Figure 6-28 ‘Soil Edit View’ displaying updated soil layering (2 soil layers).

The updated model, including soil layering (2 layers), can also be seen in the ‘3D View’ (Figure 6-29).

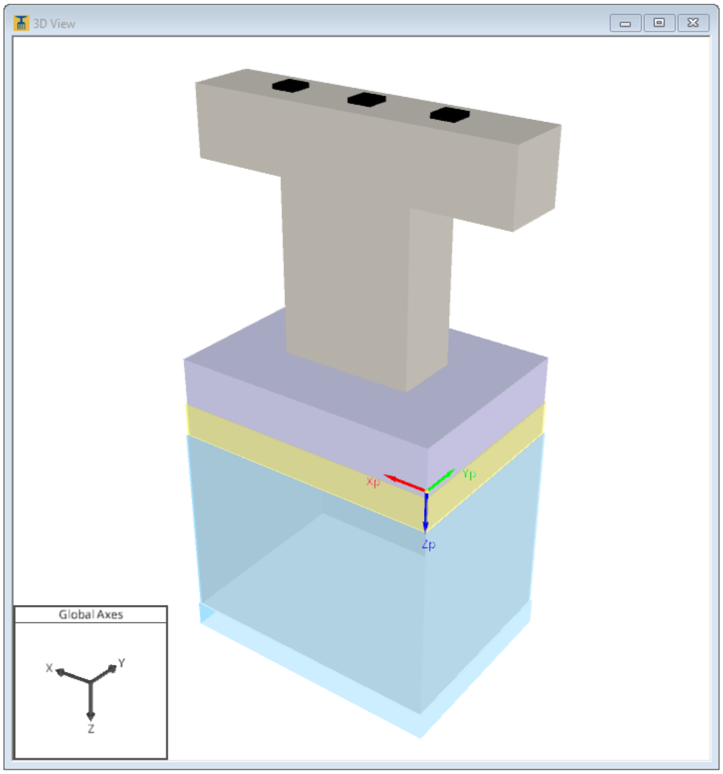

Figure 6-29 ‘3D View’ displaying updated model, including updated soil layering (2 soil layers).

Click the ‘Save’ toolbar button at the top of the program interface to ensure the model changes to this point are saved.

At this juncture of modeling, the soil layering data has been updated. Thus, the soil inputs specific to shallow foundation data can be applied to the model, using the controls on the ‘Soil’ page within the ‘Shallow Foundation Data’ frame (Figure 6-30).

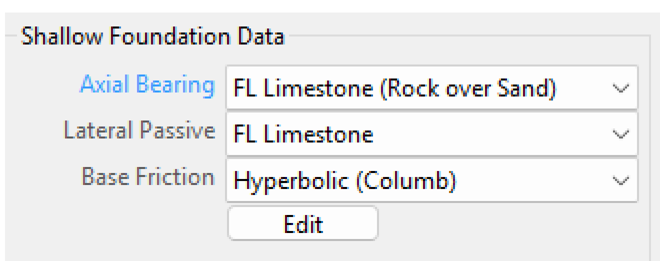

Figure 6-30 ‘Shallow Foundation Data’ controls on the ‘Soil’ page.

There are three (3) soil model categories, as follows:

- Axial Bearing
- Lateral Passive

- Base Friction

First, the Axial Bearing model selection will be made. The list of Axial Bearing models is as follows:

- FL Limestone (Homogeneous)
- FL Limestone (Rock over Sand)
- Hoek & Brown (Carter & Kulhawy)
- Linear (Subgrade)
- Custom

Using the ‘Axial Bearing’ combo box (dropdown), select ‘FL Limestone (Homogeneous)’ (Figure 6-31).

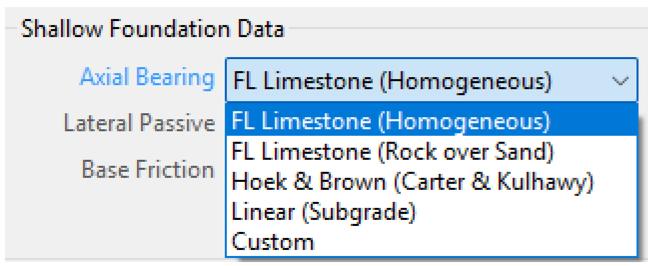

Figure 6-31 ‘Axial Bearing’ selection of ‘FL Limestone (Homogeneous)’.

Next, the Lateral Passive model selection will be made. The list of Lateral Passive models is as follows:

- FL Limestone
- C-Phi Material
- Hyperbolic
- Linear (Subgrade)
- Custom

Using the ‘Lateral Passive’ combo box (dropdown), select ‘C-Phi Material’ (Figure 6-32).

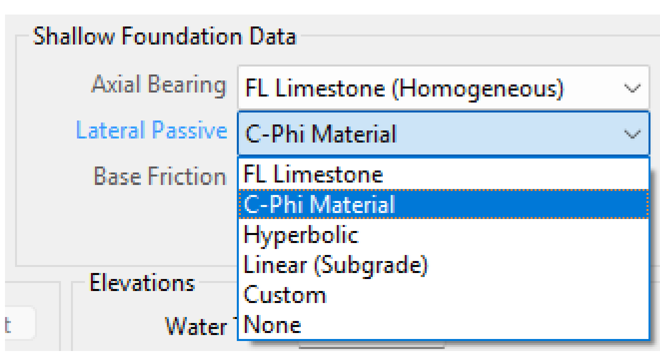

Figure 6-32 ‘Lateral Passive’ selection of ‘C-Phi Material’.

Thirdly, the Base Friction model selection will be made. The list of Base Friction models is as follows:

- Hyperbolic (Columb)
- Linear
- Custom

Using the ‘Base Friction’ combo box (dropdown), select ‘Hyperbolic (Columb)’ (Figure 6-33).

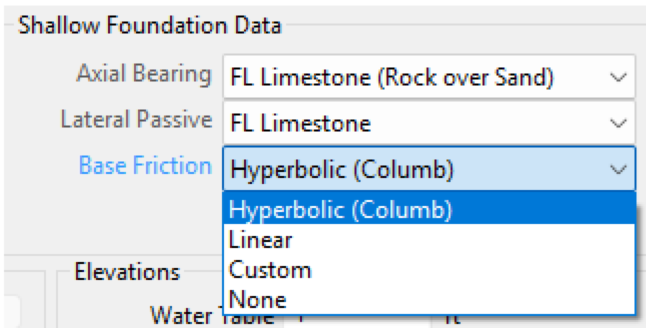

Figure 6-33 ‘Base Friction’ selection of ‘Hyperbolic (Columb)’.

With the shallow foundation model selections completed (Figure 6-34), the data pertaining to each model category must be input.

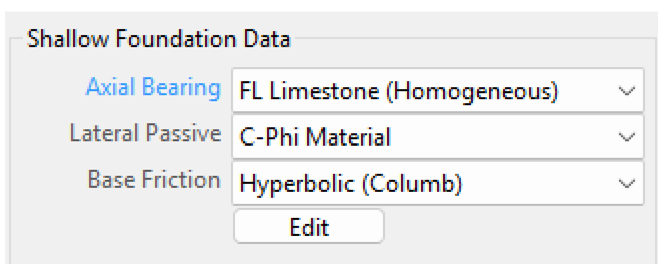

Figure 6-34 Model selections for shallow foundation data.

The data for the Axial Bearing model ‘FL-Limestone (Homogeneous)’ will now be input. To begin this step, left-click the mouse on the ‘Axial Bearing’ text within the ‘Shallow Foundation Data’ frame (Figure 6-35).

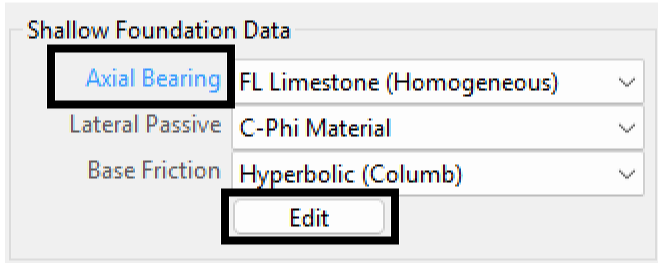

Figure 6-35 ‘Axial Bearing’ text selected, and ‘Edit’ button.

This will change the text color to blue, which means this is the currently selected model category, which means that when the ‘Edit’ button is clicked, the appropriate ‘Axial Bearing’ dialog will display.

Click the ‘Edit’ button to launch the ‘Axial Bearing – FL Limestone (Homogeneous)’ dialog (Figure 6-36).

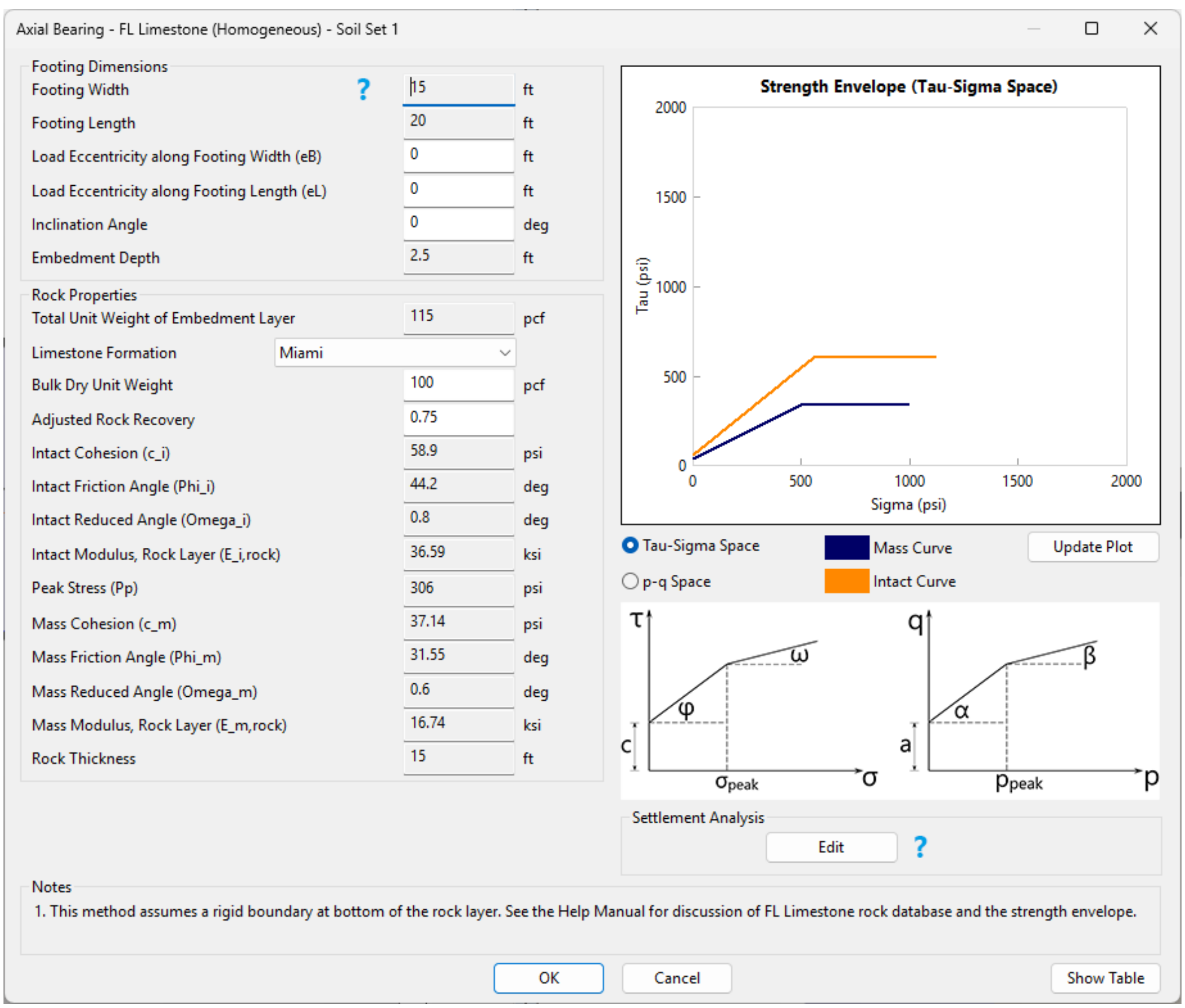

Figure 6-36 Axial bearing – FL limestone (homogeneous)’ dialog.

In ‘Footing Dimensions’ frames, various read-only data is automatically calculated and displayed. The default data in the ‘Footing Dimensions’ frame will be left as is for this walkthrough.

In the ‘Rock Properties’ frame, observe the ‘Limestone Formation’ combo box (dropdown). (Figure 6-37). The list of ‘Limestone Formation’ options is as follows:

- Miami
- Anastasia
- Hawthorn
- Key Largo
- Shallow Fort Thompson
- Ocala
- Custom Intact
- Custom Mass

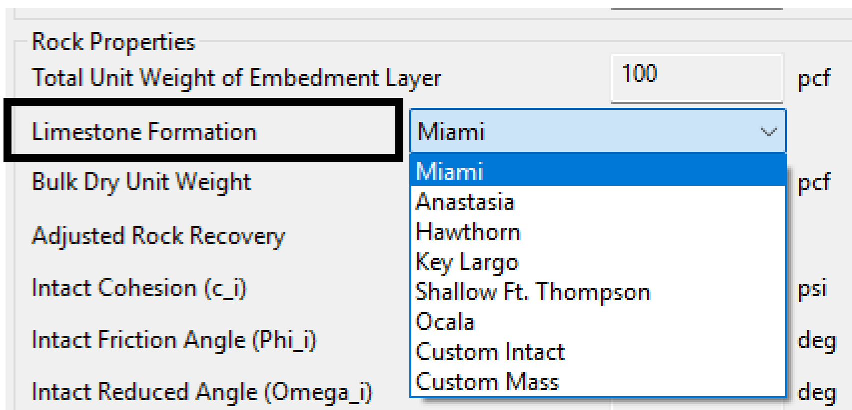

Figure 6-37 List of ‘Limestone Formation’ options.

In the ‘Limestone Formation’ combo box (dropdown), select ‘Key Largo’ (Figure 6-38).

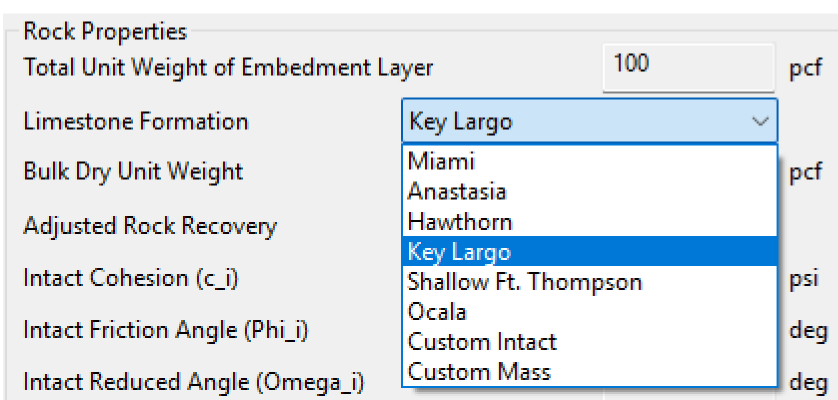

Figure 6-38 ‘Limestone Formation’ combo box (dropdown) with ‘Key Largo’ selected.

In the ‘Rock Properties’ frame, input the following data (Figure 6-39):

- ‘Bulk Dry Unit Weight’ = 115 (pcf)
- ‘Adjusted Rock Recovery’ = 0.65

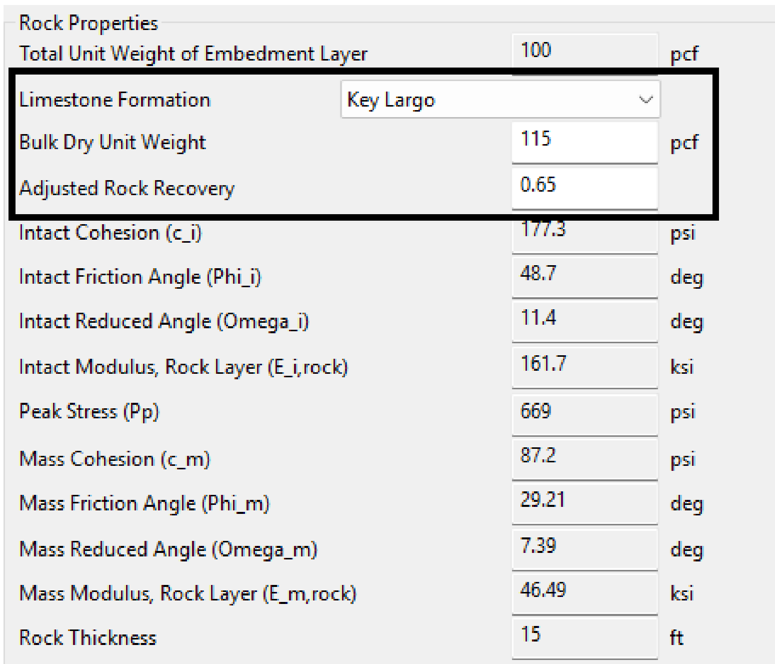

Figure 6-39 ‘Rock Properties’ frame with data input.

Based on the current data in the ‘Rock Properties’, various read-only intact and mass data are automatically calculated and displayed (Figure 6-39).

Based on the current data in the ‘Rock Properties’ and ‘Footing Dimensions’ frames, the Strength Envelope curves (Tau-Sigma or p-q Space) are generated and displayed in the plot window (Figure 6-40 and Figure 6-41).

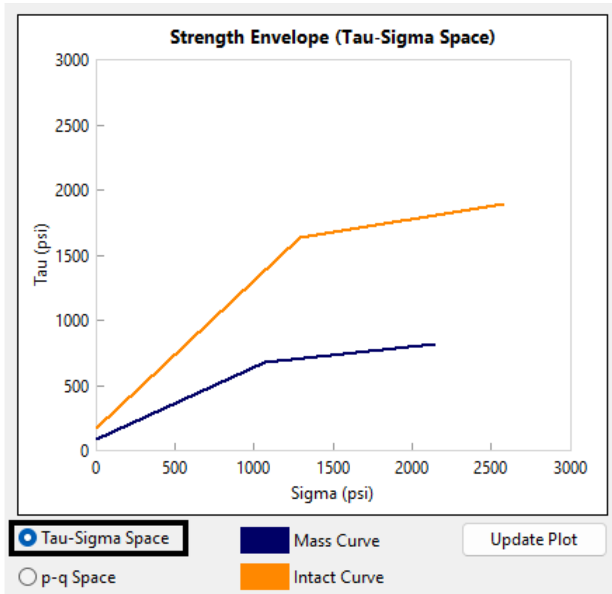

Figure 6-40 Strength envelope curve: tau-sigma space.

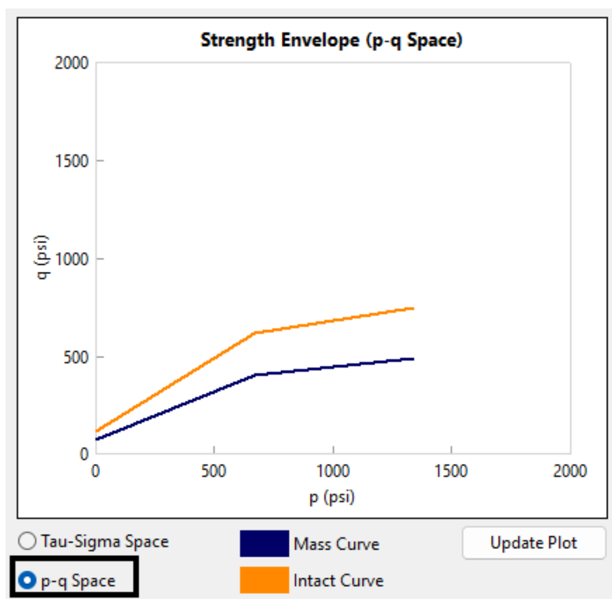

Figure 6-41 Strength envelope curve: p-q space.

To view the curve points numerically, click the ‘Show Table’ button (Figure 6-42). This action expands the dialog to include points tables for each curve. The points for the type of curve selection (Tau-Sigma or p-q Space) are displayed in the tables (Figure 6-43).

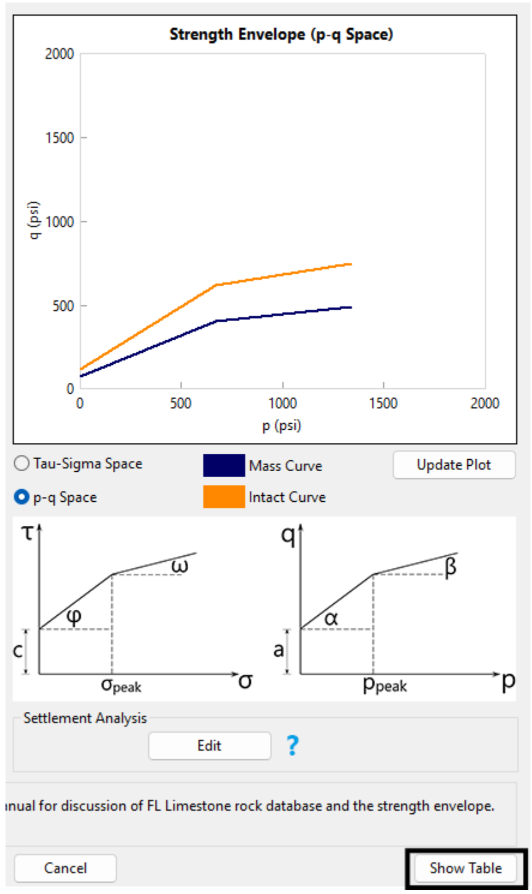

Figure 6-42 ‘Show Table’ button to view the points tables.

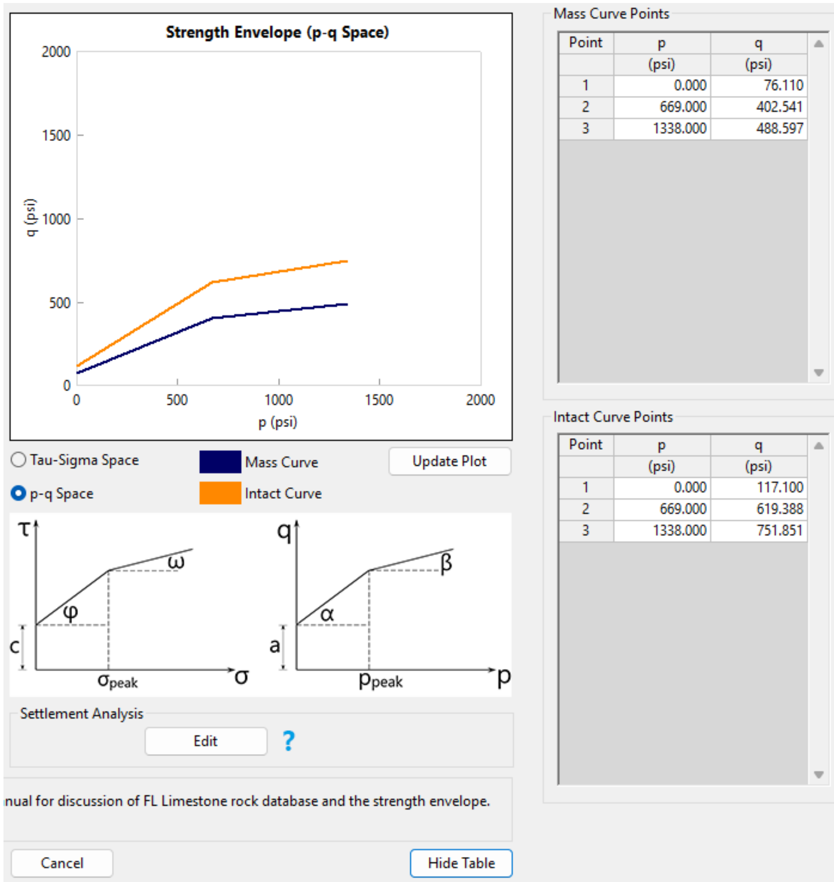

Figure 6-43 ‘Mass Curve Points’ and ‘Intact Curve Points’ tables for p-q space.

Now that the data has been fully inputted on the ‘Axial Bearing – FL Limestone (Homogeneous)’ dialog, click the ‘Edit’ button in the ‘Settlement Analysis’ frame (Figure 6-44). This launches the ‘Settlement Plot’ dialog (Figure 6-45).

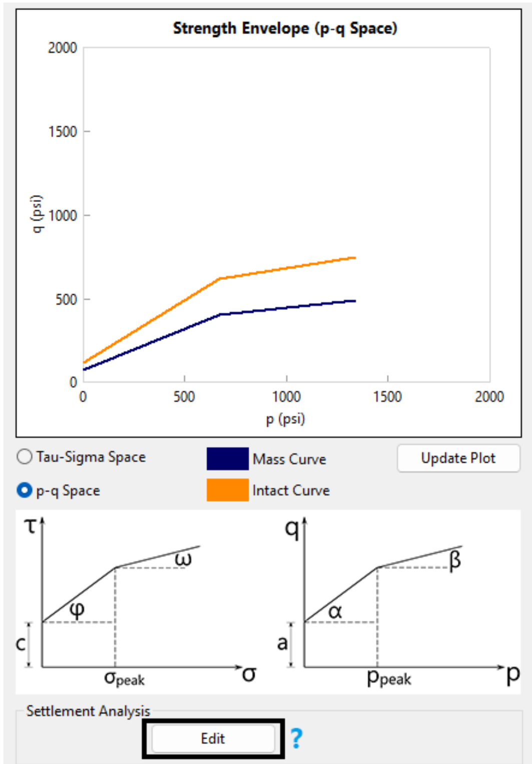

Figure 6-44 ‘Edit’ button on ‘Axial Bearing – FL Limestone (Homogeneous)’ dialog.

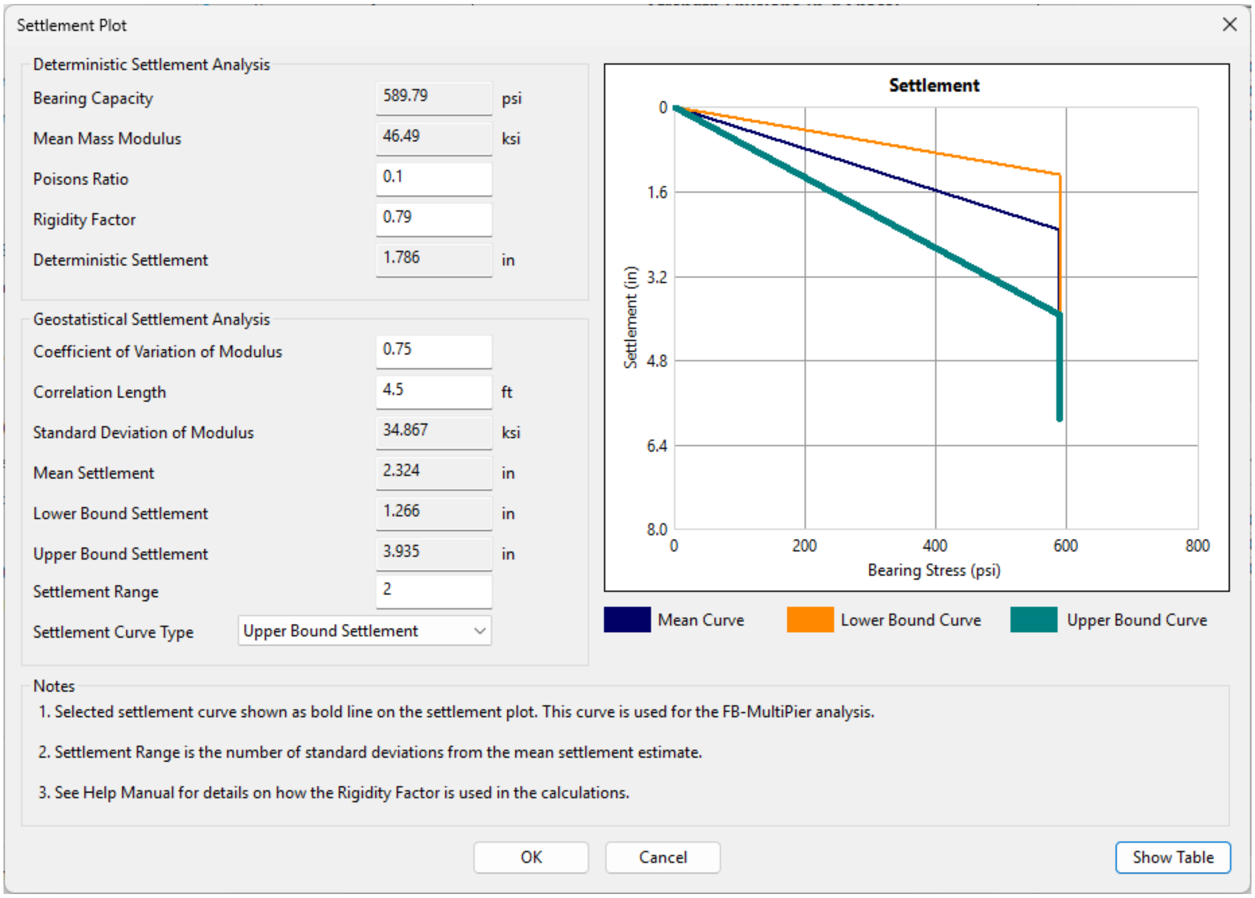

Figure 6-45 ‘Settlement Plot’ dialog.

On the ‘Settlement Plot’ dialog, the following inputs can be made in the ‘Deterministic Settlement Analysis’ frame:

- Poisson’s Ratio
- Rigidity Factor

For this walkthrough, the existing inputs from the default model will be left as is.

On the ‘Settlement Plot’ dialog, the following inputs can be made in the ‘Geostatistical Settlement Analysis’ frame:

- Coefficient of Variation of Modulus
- Correlation Length
- Settlement Range
- Settlement Curve Type (Mean, Lower Bound and Upper Bound Settlement)

For this walkthrough, the existing inputs from the default model will be left as is.

Figure 6-46 shows the three (3) curve types -- Mean, Lower Bound and Upper Bound Settlement.

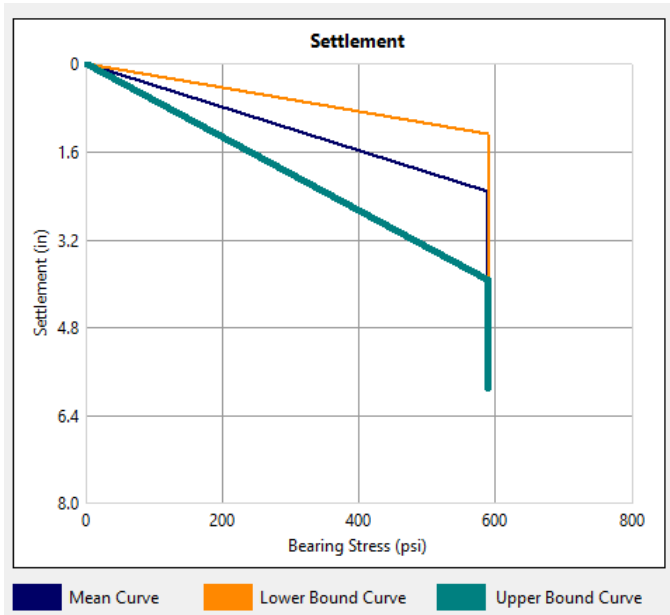

Figure 6-46 Settlement curves on 'Settlement Plot' dialog.

To view the points for each of the three (3) curves, click the 'Show Table' button (Figure 6-47). This action expands the dialog to include points tables for each curve (Figure).

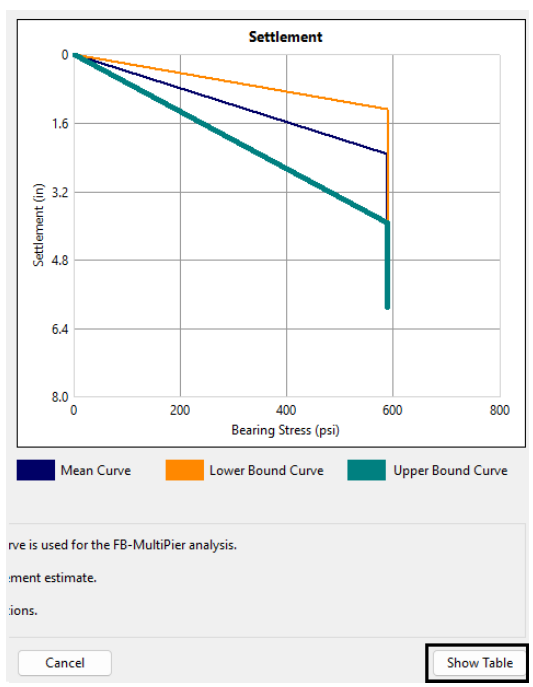

Figure 6-47 'Show Table' button on 'Settlement Plot' dialog.

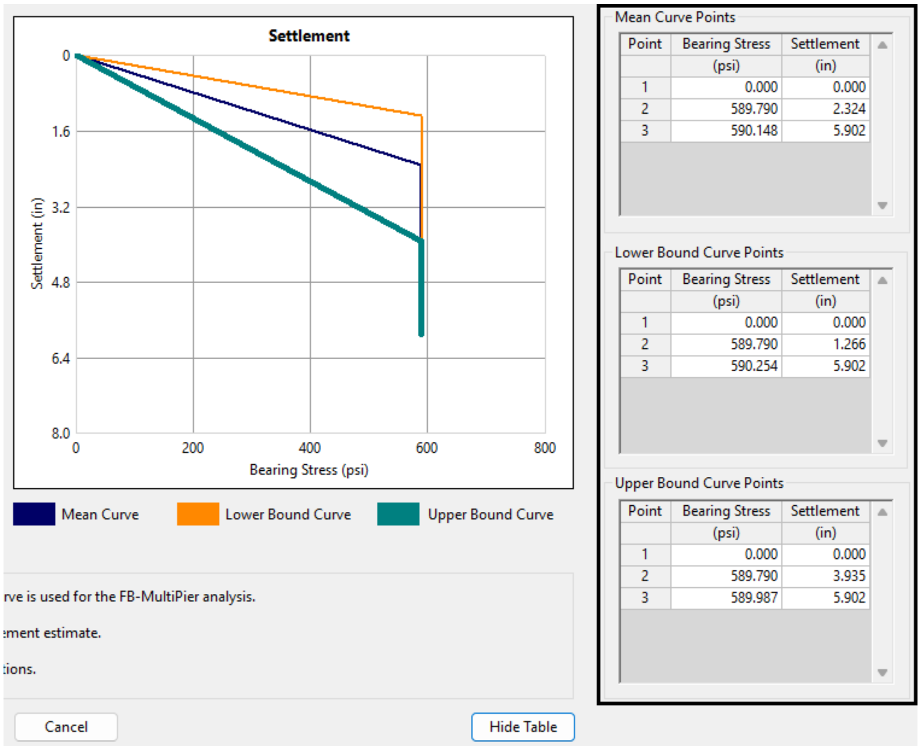

Figure 6-48 Points tables for mean, lower bound and upper bound curves on ‘Settlement Plot’ dialog.

Click the ‘OK’ button on the ‘Settlement Plot’ dialog.

Click the ‘OK’ button on the ‘Axial Bearing – FL Limestone (Homogeneous)’ dialog.

The ‘Soil’ page is once again the active page (Figure 6-49).

Click the ‘Save’ toolbar button at the top of the program interface to ensure the model changes to this point are saved.

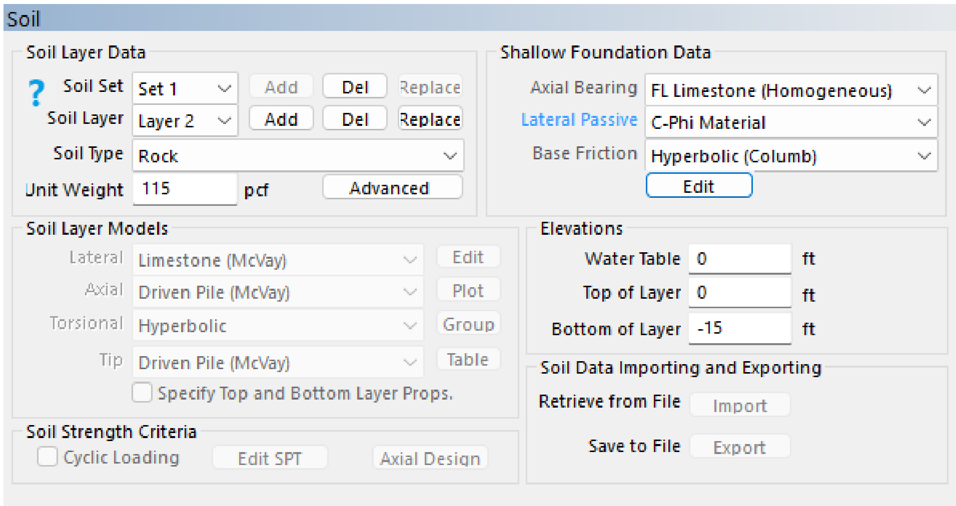

Figure 6-49 ‘Soil’ page.

Next, the data for the Lateral Passive C-Phi Material’ model will now be input. To begin this step, left-click the mouse on the ‘Lateral Passive’ text within the ‘Shallow Foundation Data’ frame (Figure 6-50). This will change the text color to blue and ensures the Lateral Passive dialog will display when the ‘Edit’ button is clicked.

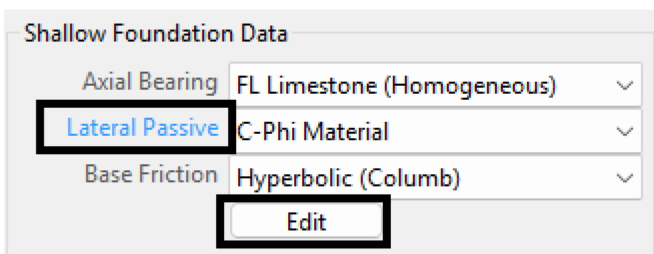

Figure 6-50 ‘Lateral Passive’ text selected, and ‘Edit’ button.

Click the ‘Edit’ button to launch the ‘Lateral Passive – C-Phi Material’ dialog (Figure 6-51).

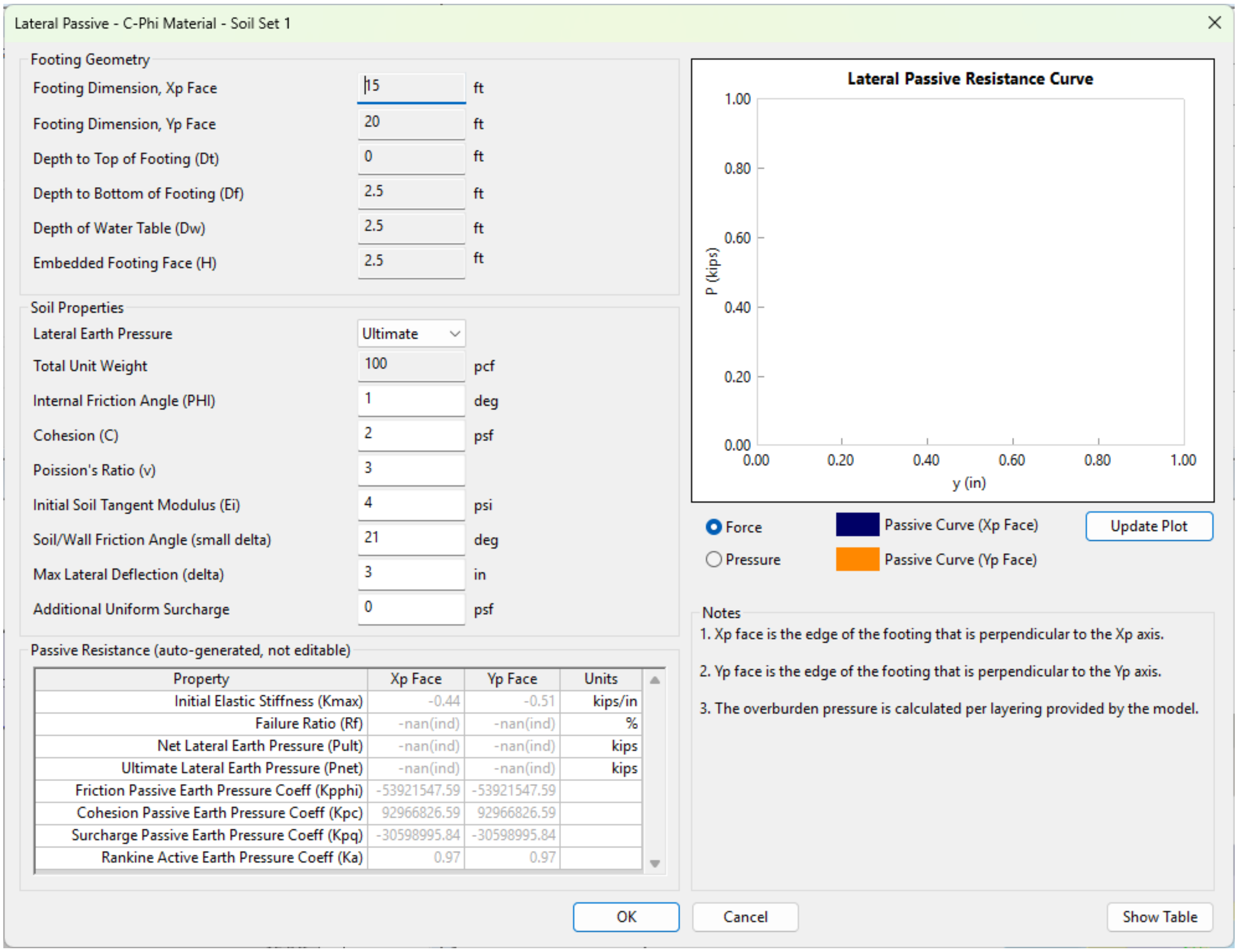

Figure 6-51 'Lateral Passive – C-Phi Material' dialog.

In the 'Soil Properties' frame, input the following data (Figure 6-52):

- Internal Friction Angle = 30 (deg)
- Cohesion = 0 (psf)
- Poisson's Ratio = 0.25
- Initial Soil Tangent Modulus = 500 (psi)
- Soil/Wall Friction Angle (small delta) = 20 (deg)

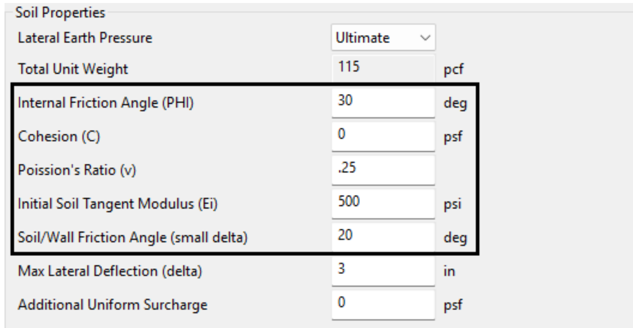

Figure 6-52 ‘Soil Properties’ frame with data input.

Based on the current data in the ‘Rock Properties’ and ‘Footing Geometry’ frames, various read-only data is automatically calculated and displayed (Figure 6-53) in the ‘Passive Resistance’ table. This table is read-only.

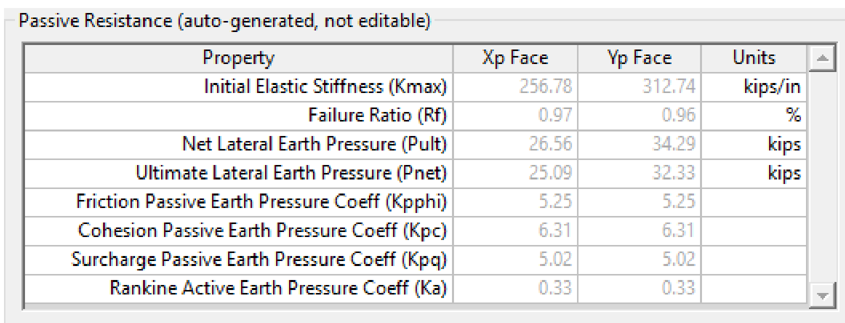
Passive Resistance (auto-generated, not editable)

Property	Xp Face	Yp Face	Units
Initial Elastic Stiffness (Kmax)	256.78	312.74	kips/in
Failure Ratio (Rf)	0.97	0.96	%
Net Lateral Earth Pressure (Pult)	26.56	34.29	kips
Ultimate Lateral Earth Pressure (Pnet)	25.09	32.33	kips
Friction Passive Earth Pressure Coeff (Kpphi)	5.25	5.25	
Cohesion Passive Earth Pressure Coeff (Kpc)	6.31	6.31	
Surcharge Passive Earth Pressure Coeff (Kpq)	5.02	5.02	
Rankine Active Earth Pressure Coeff (Ka)	0.33	0.33	

Figure 6-53 Passive resistance’ table on ‘Lateral Passive – C-Phi Material’ dialog.

Based on the current data in the ‘Rock Properties’ and ‘Footing Geometry’ frames, the Lateral Passive Resistance Curves are generated and displayed in the plot window (Figure 6-54).

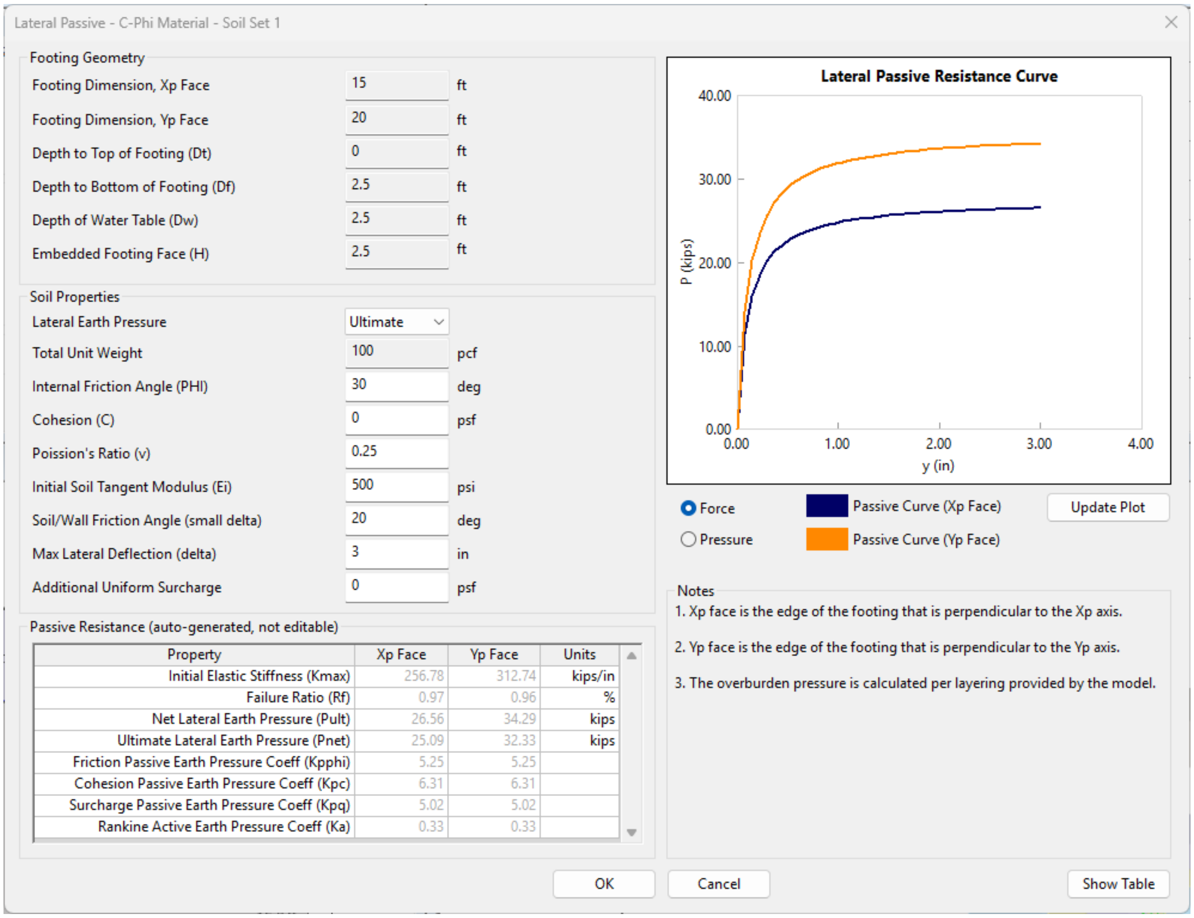

Figure 6-54 Lateral passive resistance curves on ‘Lateral Passive – C-Phi Material’ dialog.

Under the plot window, select the ‘Force’ resistance radio button to view the force resistance curves (Figure 6-55).

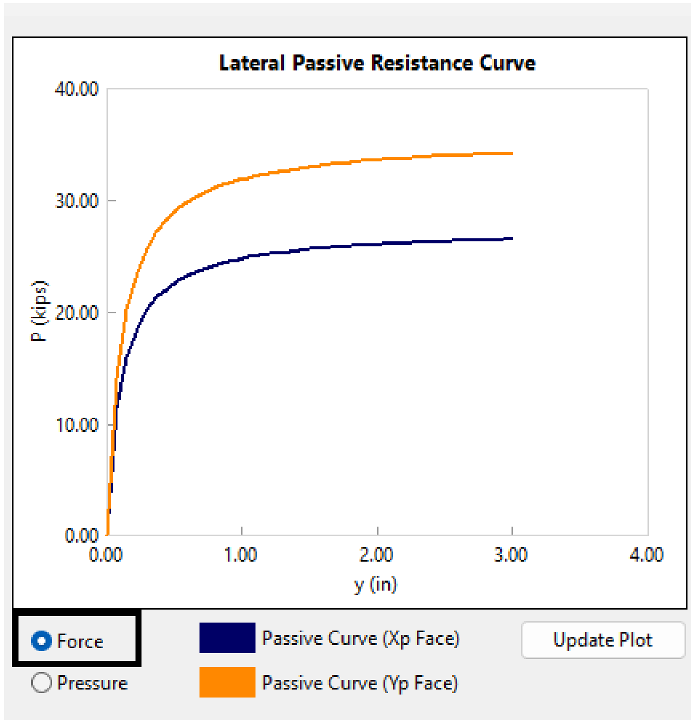

Figure 6-55 ‘Load’ curve selected on ‘Lateral Passive – C-Phi Material’ dialog.

Under the plot window, select the ‘Pressure’ radio button to view the pressure resistance curves (Figure 6-56).

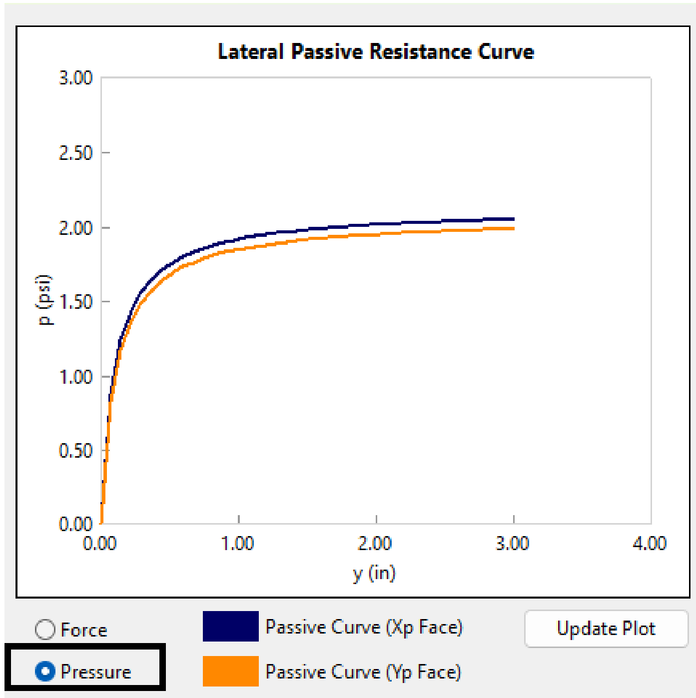

Figure 6-56 ‘Pressure’ curve selected on ‘Lateral Passive – C-Phi Material’ dialog.

To view the curve points numerically, click the ‘Show Table’ button (Figure 6-57). This action expands the dialog to include points tables for each curve. The points as per the type of curve selection (Force or Pressure) are displayed in the tables (Figure 6-58).

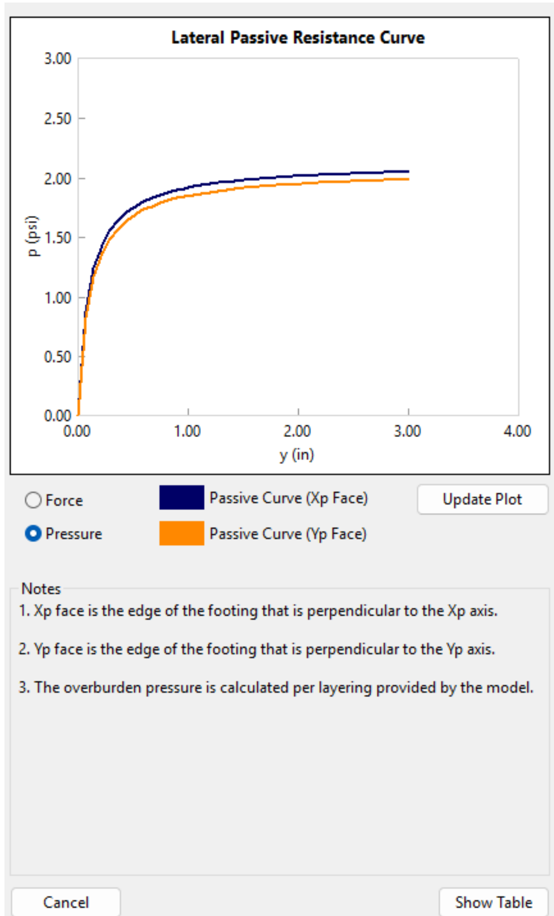

Figure 6-57 ‘Show Table’ button to view the points tables.

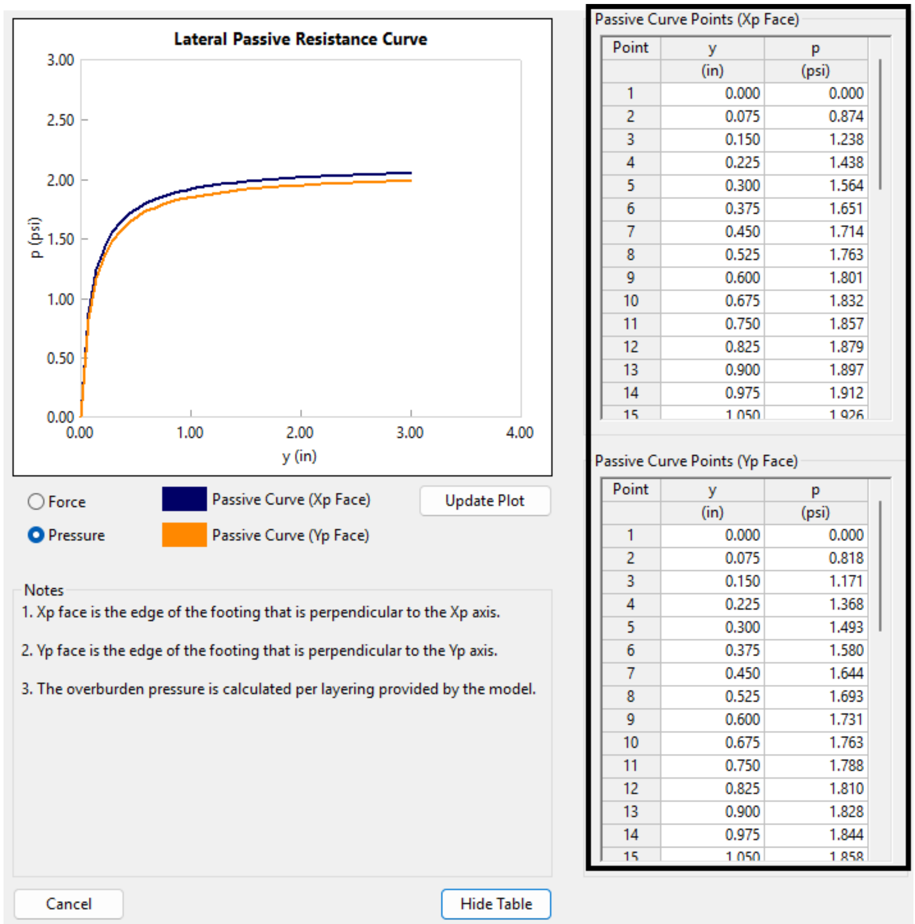

Passive Curve Points (Xp Face)

Point	y (in)	p (psi)
1	0.000	0.000
2	0.075	0.874
3	0.150	1.238
4	0.225	1.438
5	0.300	1.564
6	0.375	1.651
7	0.450	1.714
8	0.525	1.763
9	0.600	1.801
10	0.675	1.832
11	0.750	1.857
12	0.825	1.879
13	0.900	1.897
14	0.975	1.912
15	1.050	1.926

Passive Curve Points (Yp Face)

Point	y (in)	p (psi)
1	0.000	0.000
2	0.075	0.818
3	0.150	1.171
4	0.225	1.368
5	0.300	1.493
6	0.375	1.580
7	0.450	1.644
8	0.525	1.693
9	0.600	1.731
10	0.675	1.763
11	0.750	1.788
12	0.825	1.810
13	0.900	1.828
14	0.975	1.844
15	1.050	1.858

Figure 6-58 'Passive Curve Points' (Xp and Yp faces) for pressure.

Click the 'OK' button on the ''Lateral Passive – C-Phi Material' dialog.

The 'Soil' page is once again the active page (Figure 6-59).

Click the 'Save' toolbar button at the top of the program interface to save the model changes.

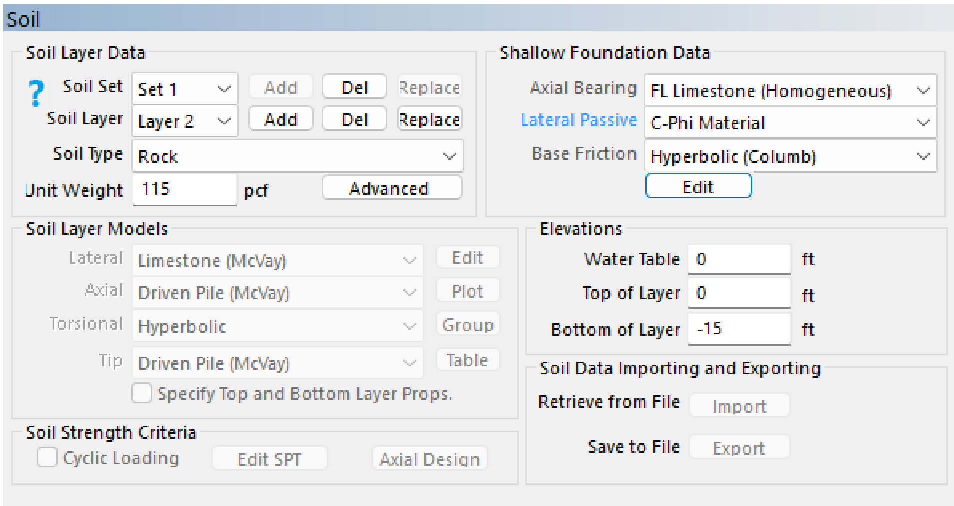

Figure 6-59 ‘Soil’ page.

Next, the ‘Base Friction’ data will be input. To begin this step, left-click the mouse on the ‘Base Friction’ text within the ‘Shallow Foundation Data’ frame (Figure 6-60). This will change the text color to blue and ensures the Base Friction dialog will display when the ‘Edit’ button is clicked.

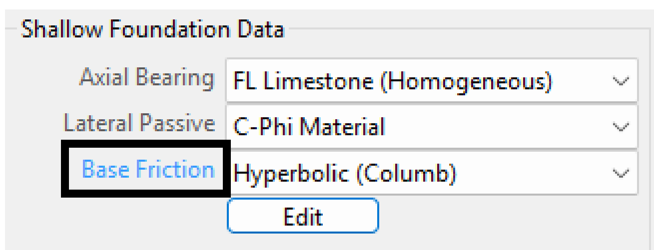

Figure 6-60 ‘Base Friction’ text selected, and ‘Edit’ button.

Click the ‘Edit’ button to launch the ‘Base Friction – Hyperbolic (Columb)’ dialog (Figure 6-61).

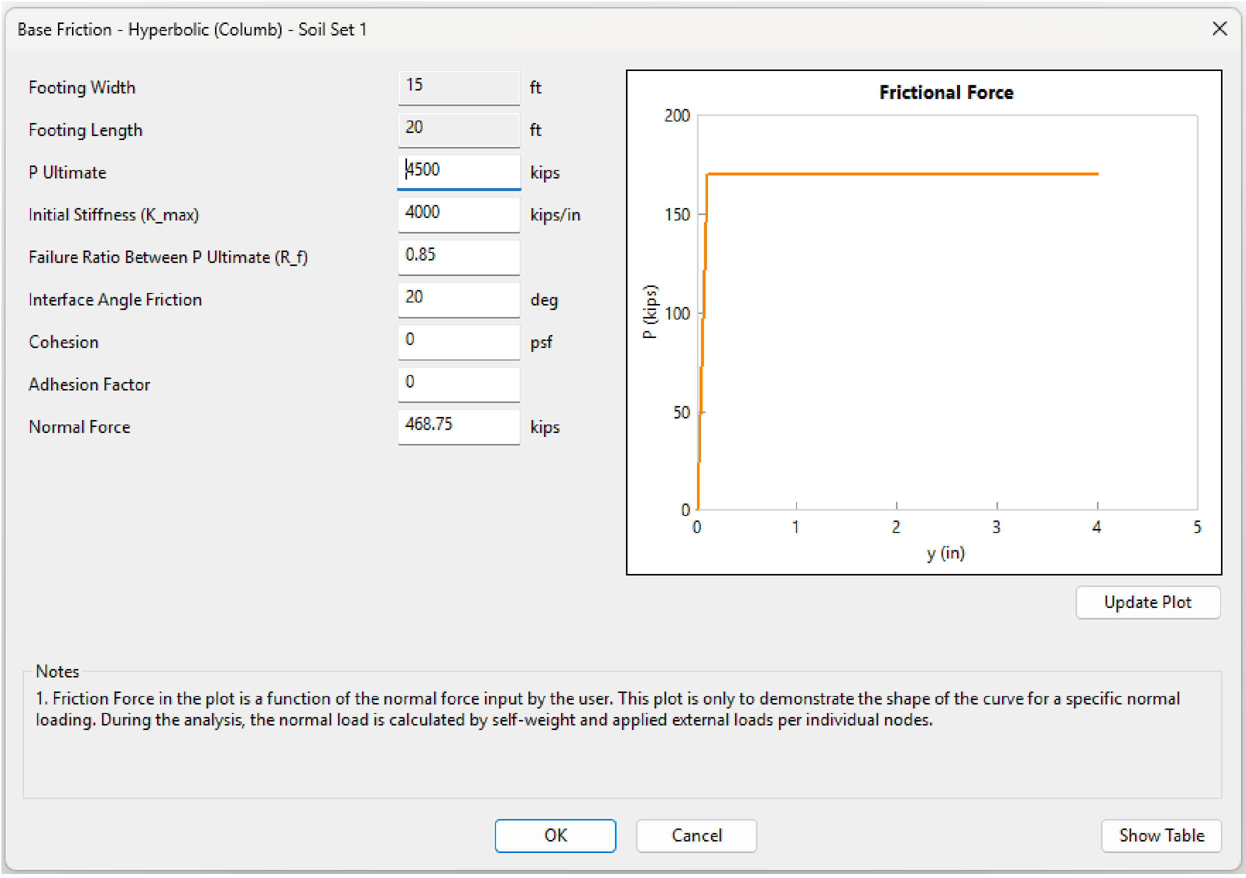

Figure 6-61 'Base Friction – Hyperbolic (Columb)' dialog.

As with the other shallow foundations dialogs visited during this walkthrough, the footing dimension edit boxes are read-only. Below them (Figure 6-62) are edit boxes for several pieces of data to be input, as follows:

- P Ultimate = 250 (kips)
- Initial Stiffness = 250 (kips/in)
- Failure Ratio Between P Ultimate = 0.85
- Internal Friction Angle = 20 (deg)
- Cohesion = 12528 (psf)
- Adhesion Factor = 0.5
- Normal Force = 135 (kips)

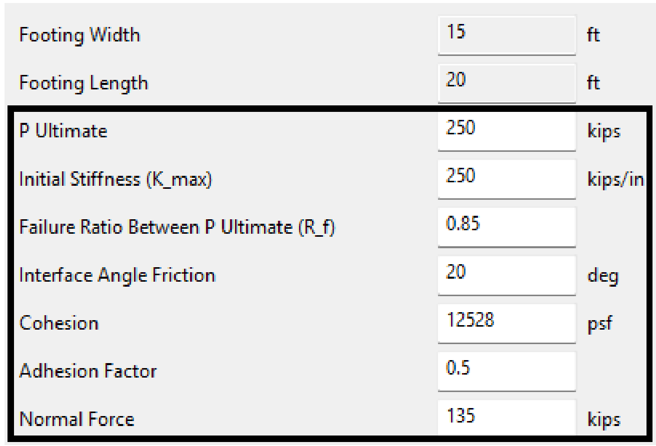

Figure 6-62 Inputs on ‘Base Friction – Hyperbolic (Columb)’ dialog.

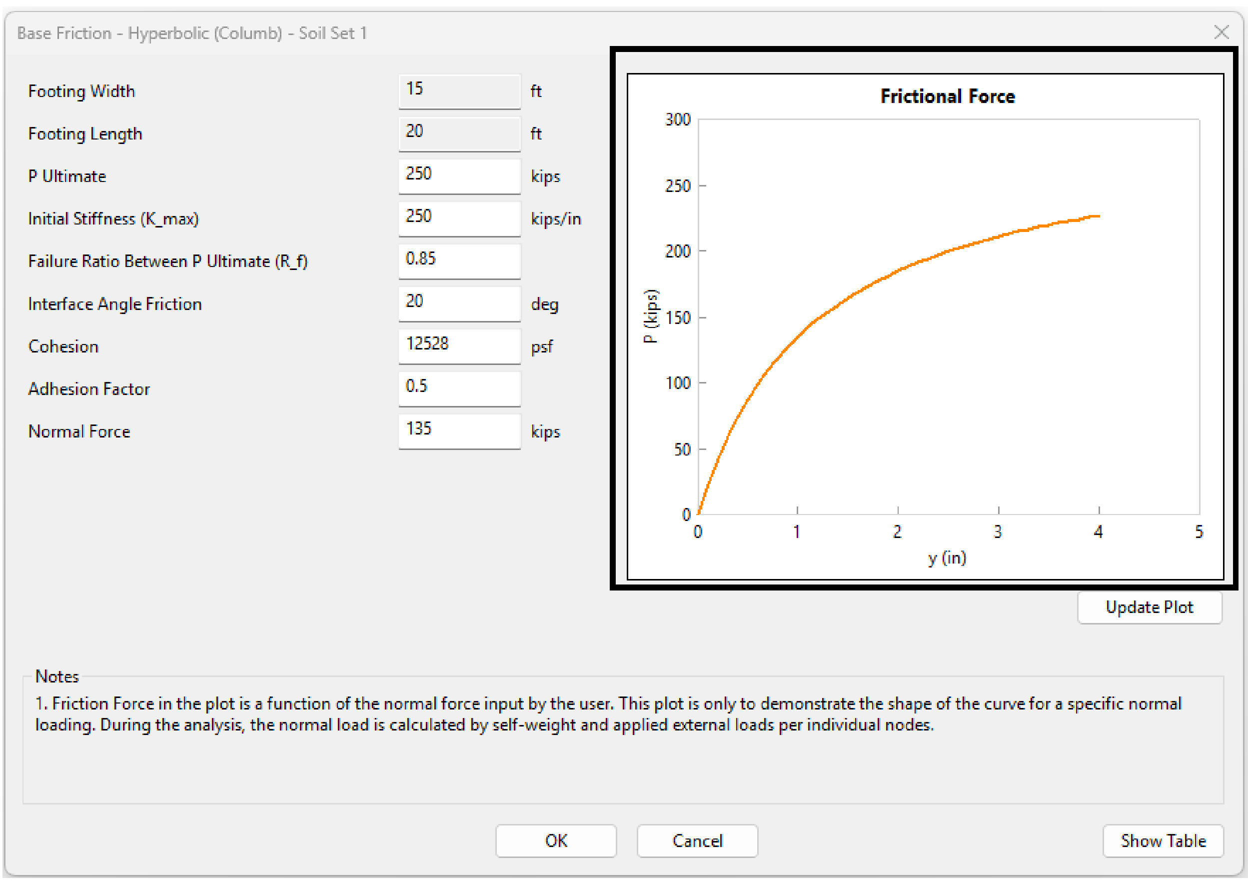

Figure 6-63 Frictional force curve on ‘Base Friction – Hyperbolic (Columb)’ dialog.

Based on the current data in the various edit boxes just mentioned, the Frictional Force curve is generated and displayed in the plot window (Figure 6-63).

To view the curve points numerically, click the ‘Show Table’ button (Figure 6-64). This action expands the dialog to include points tables for the Length and Width curves (Figure 6-65).

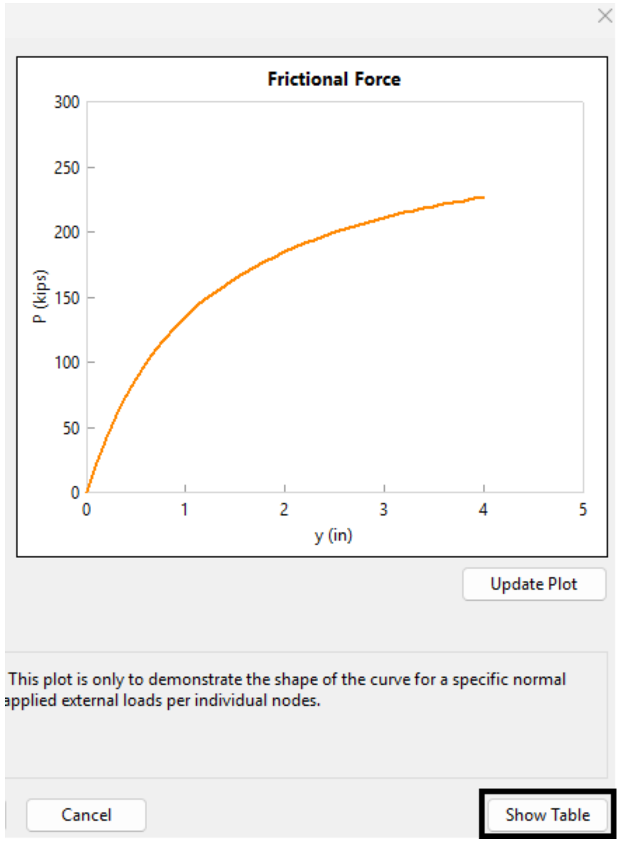

Figure 6-64 ‘Show Table’ button to view the points tables.

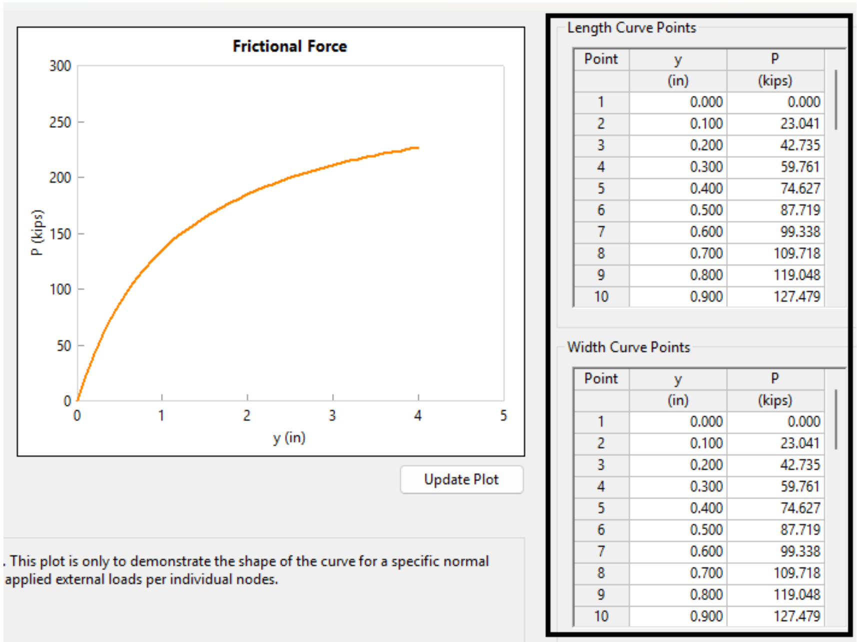

Figure 6-65 ‘Length Curve Points’ and ‘Width Curve Points’ tables.

Click the ‘OK’ button on the ‘‘Base Friction – Hyperbolic (Columb)’ dialog.

The ‘Soil’ page is once again the active page (Figure 6-66).

Click the ‘Save’ toolbar button at the top of the program interface to save the model changes.

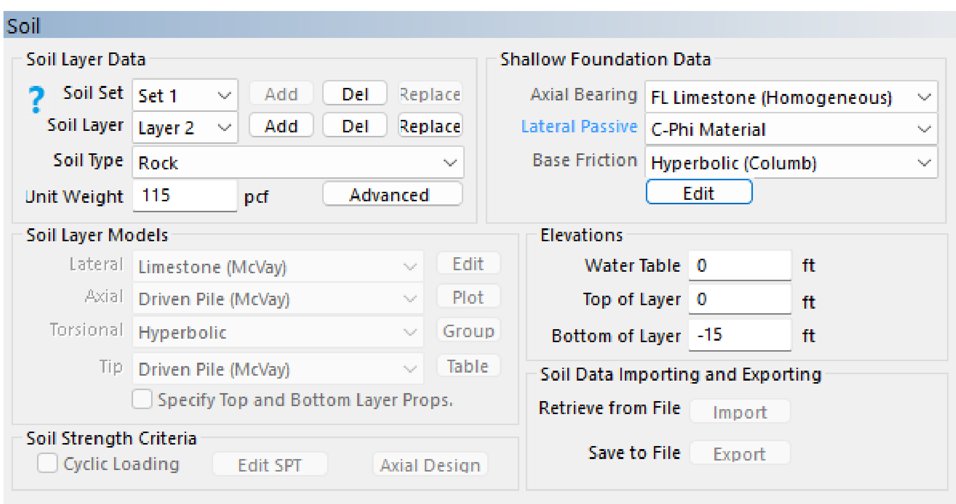

Figure 6-66 ‘Soil’ page.

The input phase of this walkthrough is now complete. Thus, it is time to run the analysis. Click the Analysis toolbar button (lightning bolt icon) at the top of the UI (Figure 6-67).

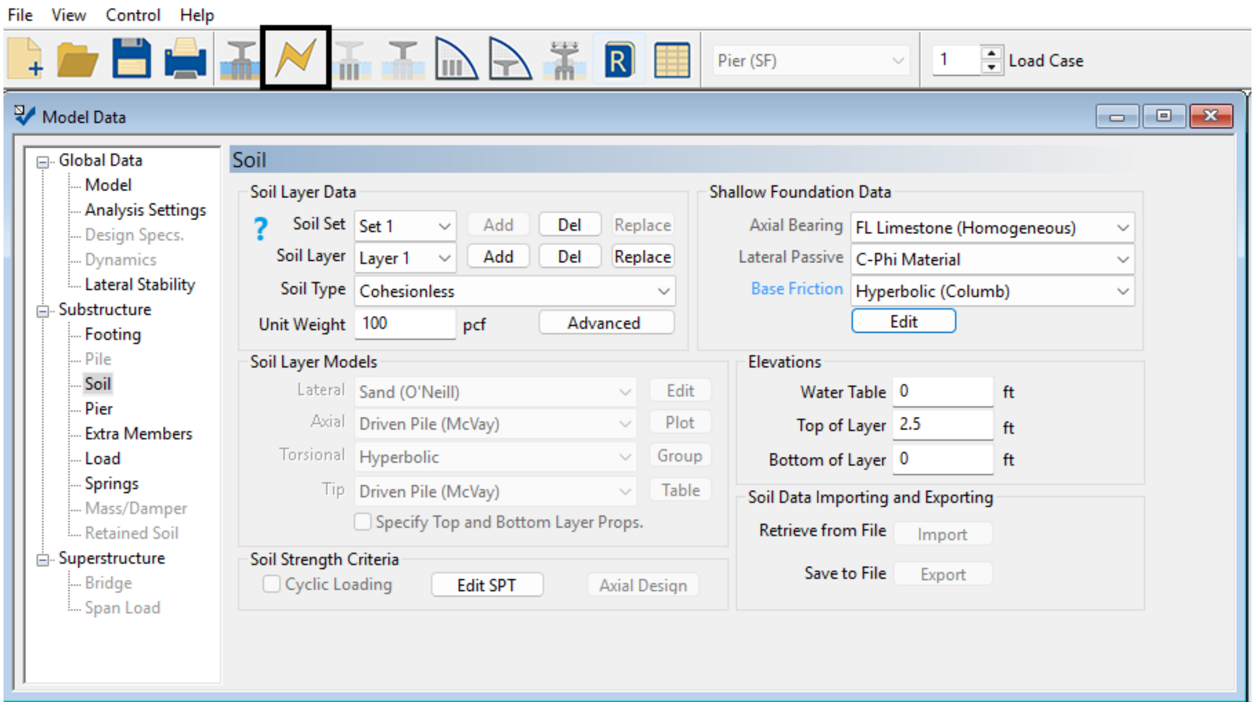

Figure 6-67 Analysis toolbar button used to run analysis.

During analysis, the 'Analysis' dialog will display (Figure 6-68). The analysis will take just a few seconds. When the analysis completes with convergence, the words 'ANALYSIS COMPLETE' will display in the 'Analysis' dialog.

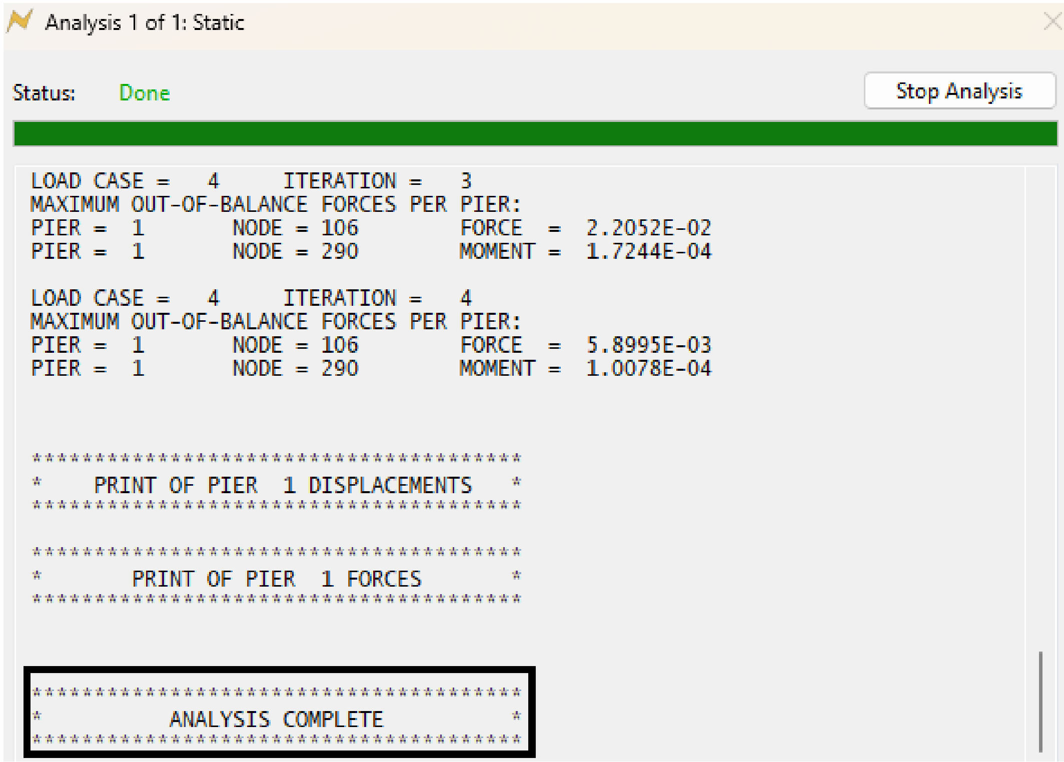

Figure 6-68 Analysis dialog.

To view analysis results, click the 3D Results toolbar button (Figure 6-69) at the top of the UI.

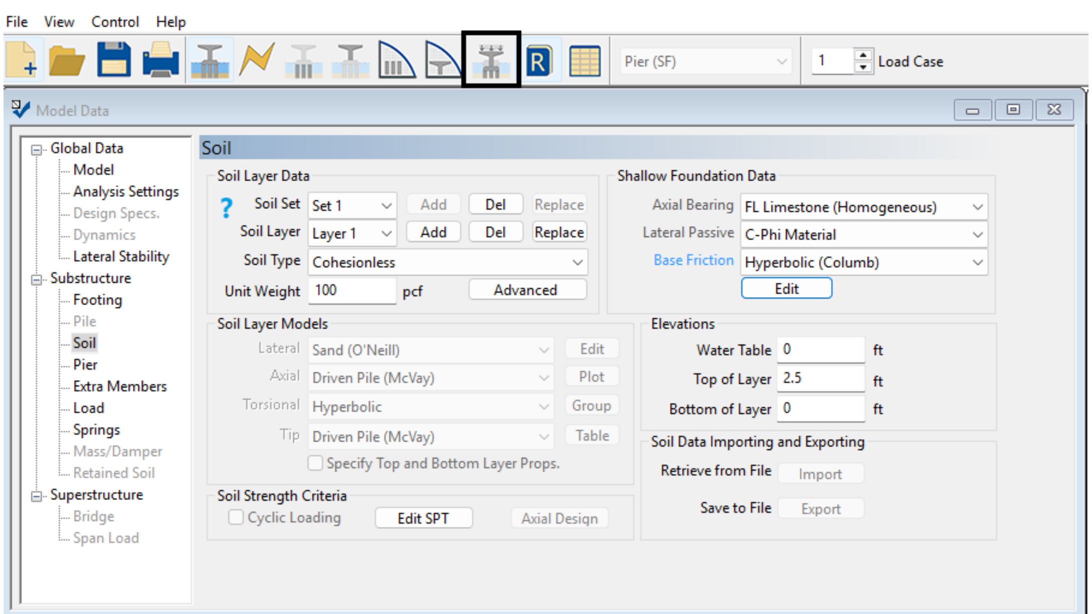

Figure 6-69 3D results toolbar button.

The 3D Result View displays, showing the displaced and undisplaced model by default (Figure 6-70). In the top right corner of the view, two data frames display results specific to the shallow foundation (Figure 6-70):

- Total Soil Spring Forces
- Eccentricity and Inclination

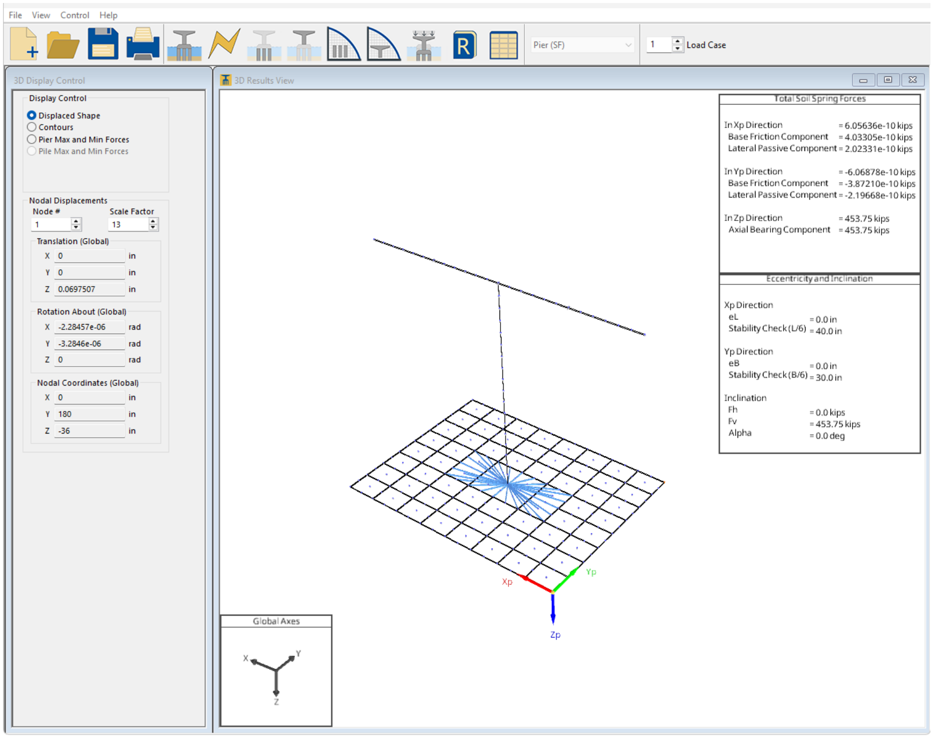

Figure 6-70 ‘Total Soil Spring Forces’ and ‘Eccentricity and Inclination’ data in 3d results view.

The ‘Total Soil Spring Forces’ data and ‘Eccentricity and Inclination’ data boxes can be hidden/show by toggling their respective context menu items. Select Load case 4.

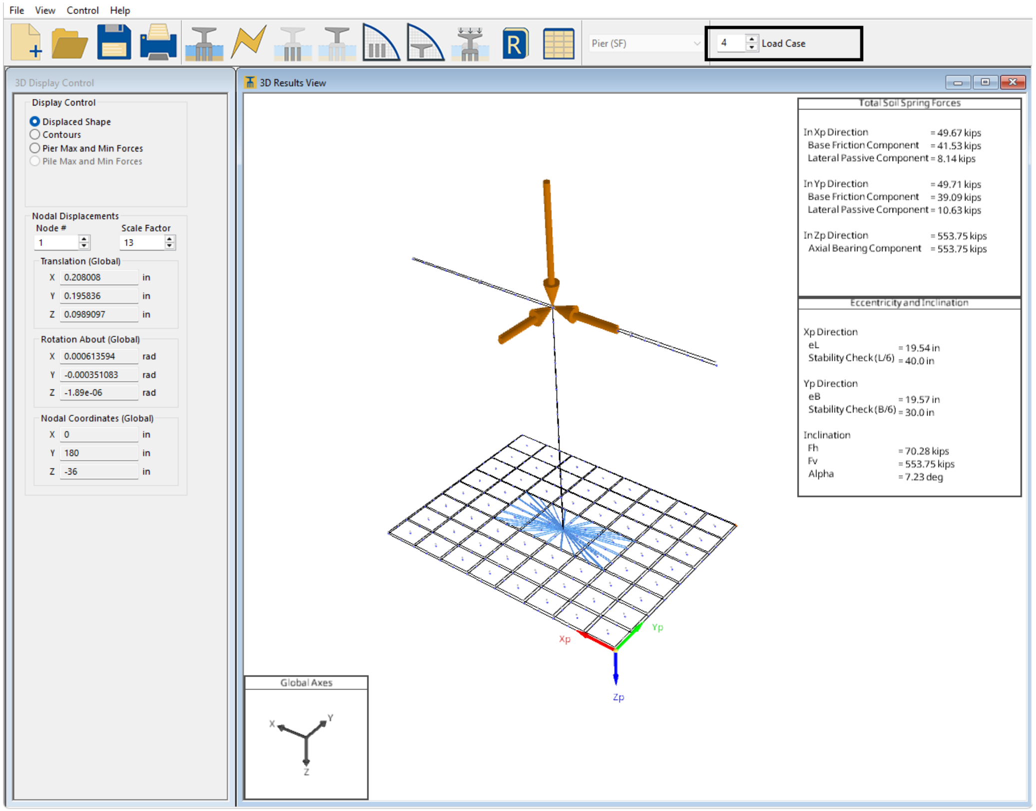

Figure 6-71 Load case 4 is selected in 3d results view.

Right-click in the 3D Result View to launch this context menu and access these toggles (Figure 6-72).

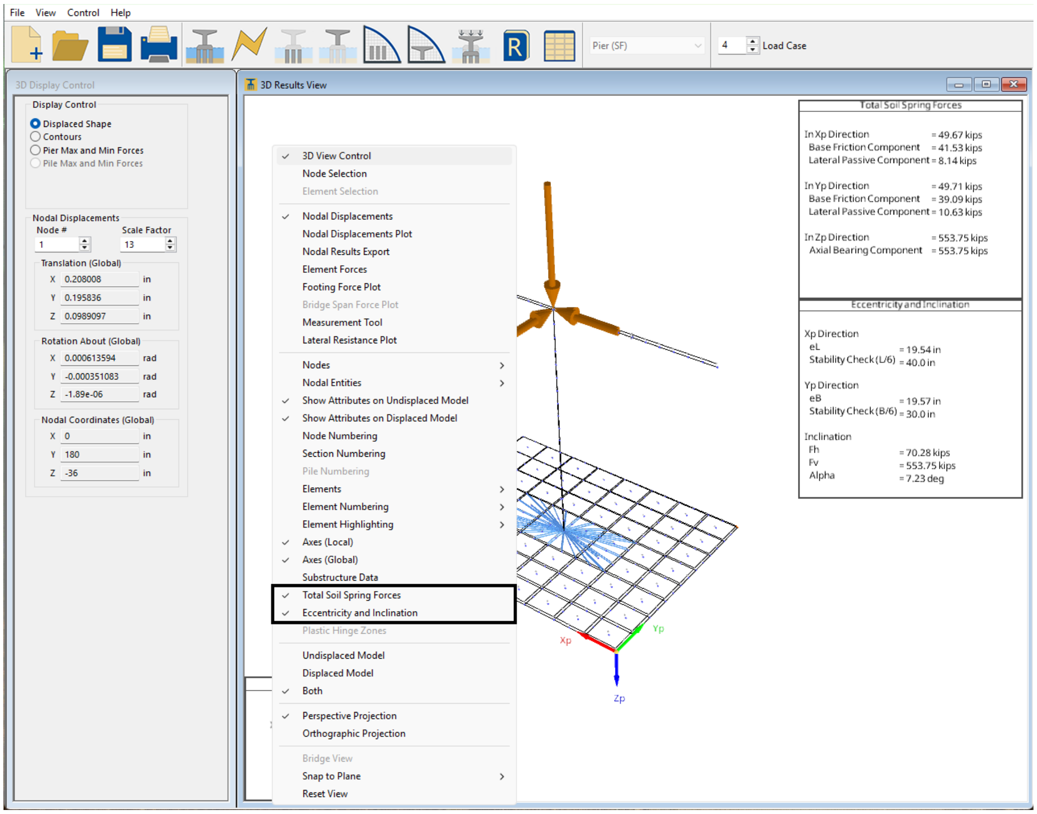

Figure 6-72 Context menu item to show/hide ‘Total Soil Spring Forces’ and ‘Eccentricity and Inclination’ data in 3d results view.

Right-click in the 3D Results View to launch the context menu and select ‘Lateral Resistance Plot’ (Figure 6-73).

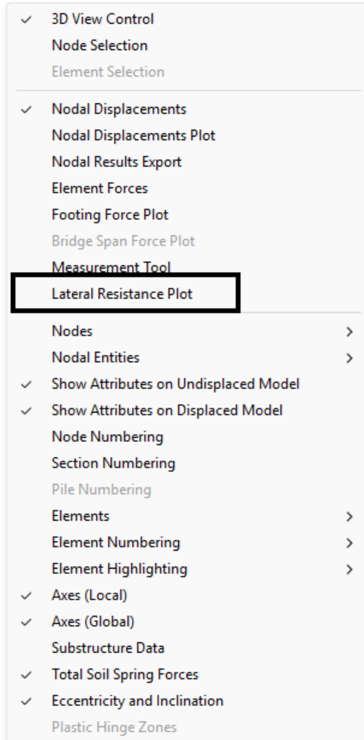

Figure 6-73 Context menu item to launch ‘Lateral Resistance Plot’ dialog.

The ‘Lateral Resistance Plot’ dialog launches (Figure 6-74) and the plots draw along the edge of the footing.

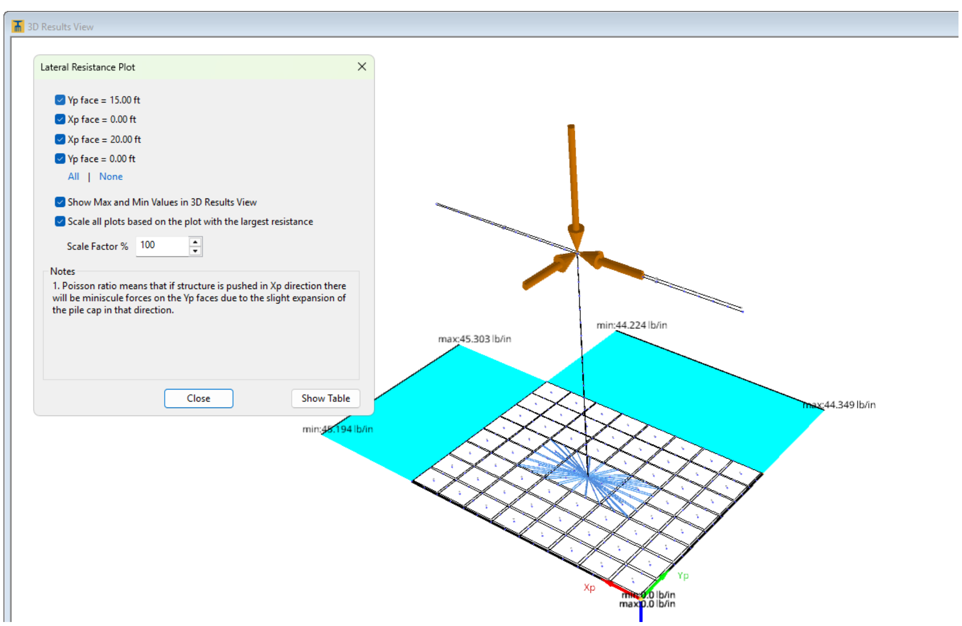

Figure 6-74 The ‘Lateral Resistance Plot’ dialog in the 3d results view.

By default, all four faces of the footing are selected on the ‘Lateral Resistance Plot’ dialog (Figure 6-75).

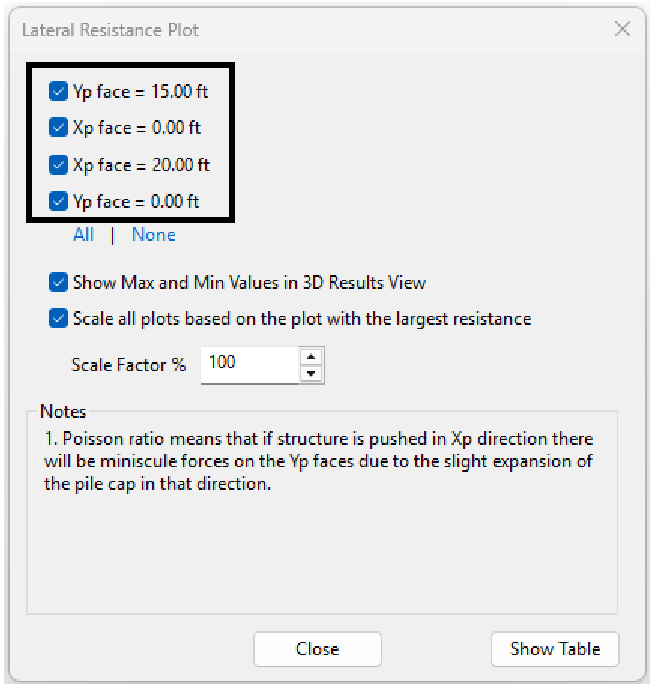

Figure 6-75 ‘Lateral Resistance Plot’ dialog with Xp and Yp faces selected.

Footing Faces can be selected and deselected as desired. For example, deselect all face checkboxes except the ‘Yp Face = 15.00 ft’ checkbox. This action clears all other lateral resistance plots from the 3D Results View except the plot for this particular (selected) face (Figure 6-76).

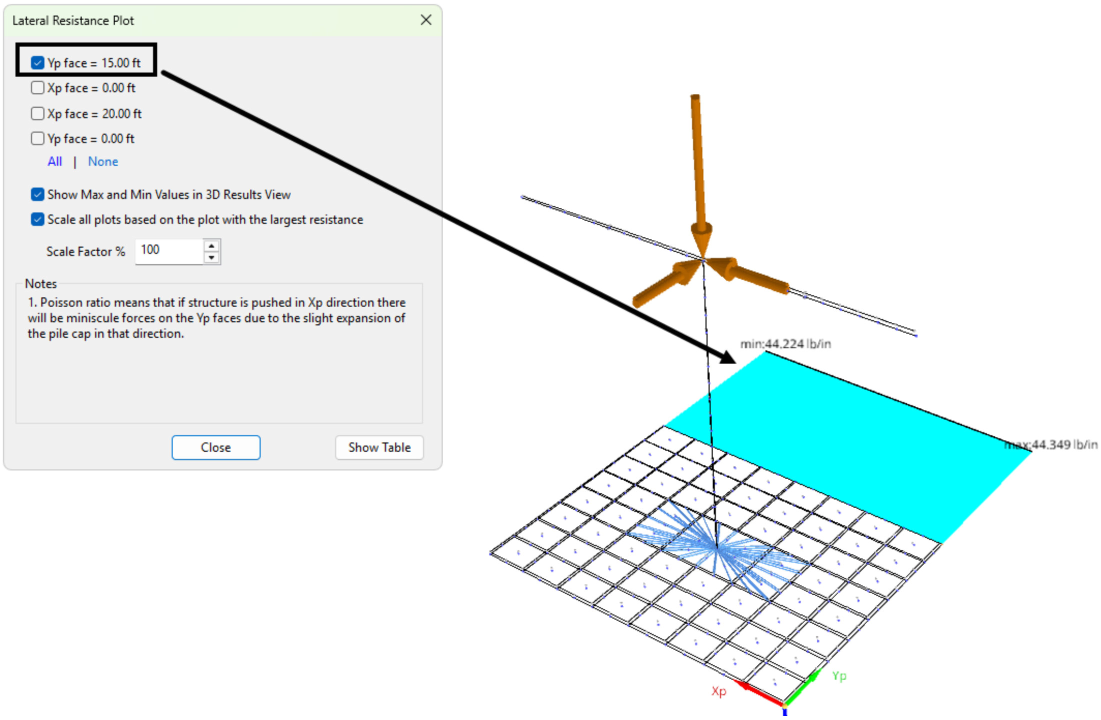

Figure 6-76 Lateral resistance plot dialog with one face selected.

To view the plot points numerically, click the ‘Show Table’ button (Figure 6-77). This action expands the dialog to include points tables for each selected curve. The points for the type of plot selection (‘Yp Face = 15.00 ft’) are displayed in the tables (Figure 6-78).

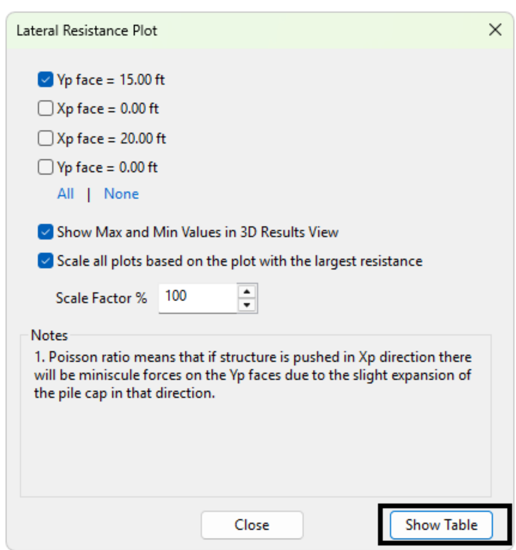

Figure 6-77 ‘Show Table’ button ‘Lateral Resistance Plot’ dialog.

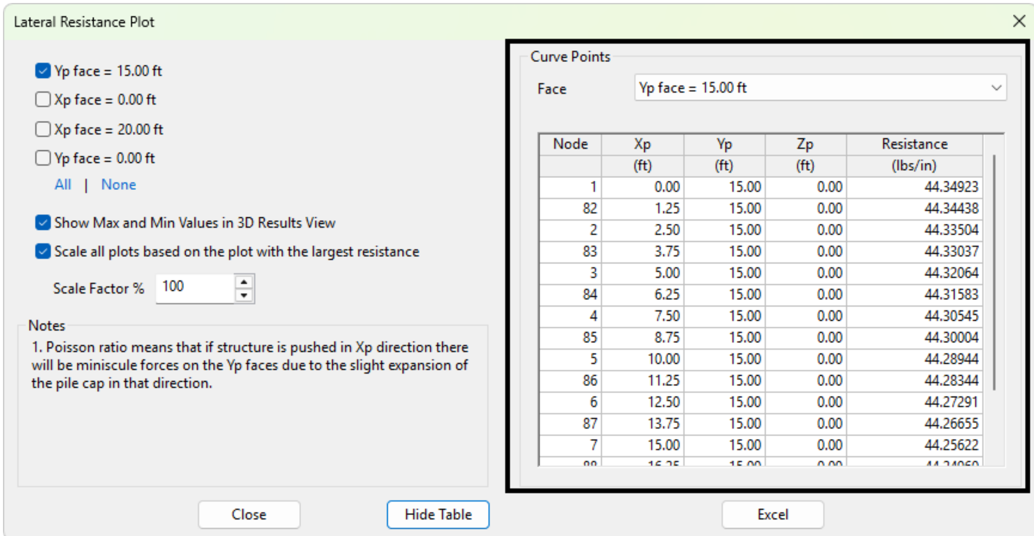

Figure 6-78 ‘Curve Points’ table for Yp face points.

This concludes the walkthrough for the ‘Pier with Shallow Foundation’ model.

6.4 FB-MultiPier Help Manual

Multiple updates have been made to the FB-MultiPier models and UI. To aid the user in understanding these new models and dialogs new sections have been added to the Help Manual as follows:

- 2. Model Data Pages
  - 2.1 New Project/Model Page
    - 2.1.12 Pier with Shallow Foundation Model
    - 2.1.12 Shallow Foundation Model
  - 2.8 Soil Page
    - 2.8.3 Shallow Foundation Data
      - 2.8.3.1 Axial Bearing — FL Limestone (Homogeneous) Dialog
      - 2.8.3.2 Axial Bearing — FL Limestone (Rock over Sand) Dialog
      - 2.8.3.3 Axial Bearing — Hoek & Brown (Carter & Kulhawy) Dialog
      - 2.8.3.4 Axial Bearing — Linear (Subgrade) Dialog
      - 2.8.3.5 Axial Bearing — Custom Curve Dialog
      - 2.8.3.6 Lateral Passive — FL Limestone Dialog
      - 2.8.3.7 Lateral Passive — C-Phi Material Dialog
      - 2.8.3.8 Lateral Passive — Hyperbolic Dialog
      - 2.8.3.9 Lateral Passive — Linear (Subgrade) Dialog
      - 2.8.3.10 Lateral Passive — Custom Curve Dialog
      - 2.8.3.11 Base Friction — Hyperbolic (Columb) Dialog
      - 2.8.3.12 Base Friction — Linear (Subgrade) Dialog

        - 2.8.3.13 Base Friction — Custom Curve Dialog

There have also been additions to the engine outputs for the user to analyze the results. These new additions are as follows:

- 4 Program Results
    - Shallow Foundation Results
        - 4.5.1.2 Contours Dialog
            - Base Friction and Axial Bearing
        - 4.5.2 3D Results Window
            - Update right-click context menu options
- 19. Engine Input Users Guide
    - 19.3 Substructure-Specific Headers
        - 19.3.24 Shallow Foundation Soil Data
- 20. Post Processing File Formats
    - 20.23 *.STR - Stresses of Pile Cap

The current commercial release version of FB-MultiPier Help Manual has 19 sections discussing the program. Section 13 of the help manual specifically discusses Soil-Structure Interaction. This section outlines soil properties, non-linear soil models and group interaction for deep foundation elements. To account for the updates for shallow foundation modeling, the help manual has been updated by first updating the title of section 13 to SSI – Deep Foundations and then adding a new section (now section 14) SSI-Shallow Foundations. Where SSI is an abbreviation for Soil Structure Interaction. An outline of this section is a follows:

- 14. SSI - Shallow Foundation
    - Shallow Foundation Model
    - Layering
    - Oblique Loading
    - Inclination
    - Eccentricity
    - Soil Properties
        - Florida Limestone Strength Envelope
        - Florida Limestone Rock Database
        - Mass Properties

        - Extension Space
    - Soil Sets
    - Axial
        - FL Limestone (Homogeneous)
        - FL Limestone (Rock over Sand)
        - Hoek & Brown (Carter and Kulhawy)
        - Linear (Subgrade)
        - Custom
    - Lateral
        - Passive
            - FL Limestone
            - C-PHI Material
            - Hyperbolic
            - Linear (Subgrade)
            - Custom
        - Friction
            - Hyperbolic (Columb)
            - Linear (Subgrade)
            - Custom

This section of the help is to provide the user 1) implementation on non-linear soil resistance springs on the footing 2) Allowable layer profiles that can be analyzed 3) discussion of FL Limestone intact and mass properties and 4) overview of axial and lateral resistance models. These discussion are an overview of critical information, but do not provide in depth presentation of theory. Reference are available in each subsection should the user want to further information. The updated FB-MultiPier manual will be made available for FDOT review.

6.5 Worked Examples

From the previous task reports, work examples were presented which detail hand calculations of the various shallow foundation models. These worked examples provided both a detailed walkthrough to aid in understanding the model, but also as method of validation of implementation of these models in FB-MultiPier. In the table below several worked examples have been selected to aid in the understanding and validation. The table provides the name of the example along with the model feature that is explained in the worked example. Additionally, there is a file name for the FB-MultiPier.in file which contains the inputs of the work example. These files will be provided to FDOT for comparison and training.

Table 6-1 Summary of worked examples.

Example Name	Model Feature	File Name
B.1.2 Cemex load test	Axial Bearing FL Limestone (Homogeneous)	CMEX.in
B.2.1 SR84 load test	Axial Bearing FL Limestone (Rock over Sand)	SR84.in
B.2.2 Bell load test	Axial Bearing FL Limestone (Rock over Sand)	BELL.in
B.3.1 Worked example 1	Axial Bearing Hoek & Brown (Carter Kulhawy)	HB.in
C.1.1 Passive C-PHI	Lateral Passive C-PHI Material	WE _PASSIVE_CPHI.in
C.2.1 Passive FL Limestone	Lateral Passive FL Limestone	WE_PASSIVE_FL_LIMESTONE.in
C.3.1 Friction Hyperbolic (Coulomb)	Lateral Hyperbolic (Columb)	WE _PASSIVE_HYPERBOLIC.in
D.1 Inclination	Axial Bearing FL Limestone (Homogeneous)	WE_INCLINATION.in
D.2 Eccentricity	Axial Bearing FL Limestone (Homogeneous)	WE_ECCENTRICITY.in
D.3 Eccentricity and Inclination	Axial Bearing FL Limestone (Homogeneous)	WE_ECCENTRICITY _INCLINATION.in
E.1 Axial Phase II Report Single Layer Example Section 9.2	Axial Custom Curve	WE_ P2_911_WHM.in & WE_P2_911_FLH

6.6 FL Limestone Site Characterization

6.6.1 Characterization of Rock Properties Beneath a Footing in Florida

Constructing a foundation within a Florida Limestone formation (e.g. Miami, Fort Thompson, etc), one must be concerned with the layering, strength and compressibility of all materials to a depth of 3B beneath the footing. In the case of layering, a formation may be a homogeneous single layer, a heterogeneous rock (multiple layers of rock) or a combined rock layer over a sand layer (e.g. Miami Formation). Impacting the strength (bearing capacity) and compressibility (modulus) of rock is its formation (Miami, Fort Thompson, Anastasia, etc – specific Gravity), and its dry unit weight (porosity, n) at any point. For example, FDOT BDV31-977-51 [Strength Envelopes for Florida Rock and Intermediate Geomaterials] developed bilinear strength envelopes and FDOT BDV31-977-124 [Phase II: Field Load Testing of Shallow Foundations in Florida Limestone], developed the elastic Young’s modulus of a formation’s rock sample based on its dry unit weight. Note, the dry unit weight of any sample in Florida Limestone may vary from a low of 85 pcf to a high of 140 pcf.

11. To assess layering, and properties (strength & compressibility), sufficient point values must be collected to evaluate the summary statistics (mean, geomean, CV) of a proposed layer. In the case of rock, coring with a drill rig is generally used to obtain 5ft core box samples. Generally, the intact cylindrical core samples are used to assess Young's Modulus, Ei, unconfined compression (qu), split tension (qt), and Mohr-Coulomb strength (triaxial) parameters. These properties are referred to intact values (e.g. E_i) and are strongly influenced by formation and porosity (i.e. dry unit weight) of each specimen. However, these properties will be larger than the full mass or larger volume values. This is evident by the volume/mass of rock collected in the core box vs. the total volume of box which is reported as Recovery (length of recovered pieces/ 60 in x 100) and RQD (length of pieces > 4"/ 60 in x 100) in the 60 inch core run. As discussed in FDOT BDV31-977-124, the adjusted Recovery [REC_{adjust} - testable cores (q_t, q_u and triaxial), i.e. cylindrical pieces], recommended by Hassan and O'Neil et al., (1997) and Carter and Kulhawy (1988) are used to assess the mass properties (strength, Young's Modulus) of the formation. The adjusted Recovery (REC_{adjust}) which is generally higher than RQD and less than REC represents the mass properties of the layer that are load bearing (have strength and stiffness).
12. Given the typical sizes of footings (8ft<B<20ft) borings from 30ft to 60ft are expected. In this depth range (0 – 3B) assessment of layering and associated strength and modulus are very important in the bearing and settlement analysis. For instance, the existence of a thin layer (e.g. 1ft – Bell test site, FDOT BDV31-977-124) both reduced bearing and increased settlement appreciably. Consequently, it is strongly recommended that data at 1ft scale be obtained. This may not be all strength testing (qu, qt, triax), but it is expected to include dry unit weight assessment measuring while drilling (MWD) and/ possibly seismic shear wave testing (2D assessment of dry unit weight, and Young's Modulus). In the case of a heterogeneous rock, assessment of the mean, CV and Geomean of Young's modulus of the rock in the footprint down to depth of 3B affects both the expected mean settlement as well as the differential settlement of the footing (i.e. Fenton & Griffith settlement estimate - FDOT BDV31-977-124). Note, since the variance (σ^2) is a 2nd order moment, the CV is strongly influenced by outliers, and the use of at least 20 to 25 E values is recommended. Again, the use of dry unit weight on rock pieces (e.g. from core box) with estimates of Modulus from plots (dry unit weight vs. modulus by formation – e.g. FDOT BDV31-977-124) is suggested. Note, some formations show an order of magnitude difference between modulus between low and high dry unit weights.
13. In the case of rock strength assessment (compression – bearing and extension – lateral), it is important to assess the bulk dry unit weight and associated strength parameters. In the core box all short cylindrical specimens should be tested for split tension (qt) and unconfined compression (qu) and compared with existing formation values based on bulk dry unit weight to validate existing reported strength envelopes. If different or if the formation strength (compression or

extension) doesn't exist, then triaxial compression and extension testing needs to performed at 50psi, 300 psi, and 600 psi initial cell confining pressures. Again, due to sample variability, multiple repetitive tests (same initial cell pressure), need to be performed to assess the average strength envelope for a representative bulk dry unit weight.

6.6.2 Development of a Rock Strength Envelope

The Florida limestone strength envelopes can be developed by formation and bulk dry unit weight (γ_{dt}) using results from the unconfined compression (q_u) , splitting tensile (BST) and triaxial compression and extension tests at multiple confining pressures for similar bulk dry unit weights. The research that developed the envelopes includes bulk dry unit weight to strength relationships for Key Largo, Anastasio, Miami, shallow Fort Thompson, Hoawthorne, and Ocala formations and can be found in these FDOT reports FDOT BDV31-977-51 (Strength Envelopes for Florida Rock and Intermediate Geomaterials) and FDOT BDV31-977-124 (Phase II: Field Load Testing of Shallow Foundations in Florida Limestone).

Four parameters were used to develop a simplified bi-linear strength envelope (a, α, β and p_p), as shown in Figure 6-79. The cohesion c, and the friction angle φ (slope of first segment) in τ-σ diagram can be evaluated through the q_u and q_{dt} ($q_{dt} = 0.7\times$BST) tests through Equation 35 and Equation 36 and converted to a, α in p-q space through Equation 109 and Equation 110. The location of slope change (p_p in Equation 113) can be considered as the onset of cementation breakage (micro-cracking) as a function of isotropic stress change (0.3 MPa, Figure 6-79) prior to shearing. The second slope on the strength envelope (β in p-q diagram, or ω in σ-τ diagram, Equation 110) is calculated between the stress state, p_p, and the higher confining stress test (e.g., 4.1 MPa) that spans the expected field load stress paths. In general, the second slope is a function of the porosity, mineral content and crystallization, which are controlled by bulk dry unit weight and formation.

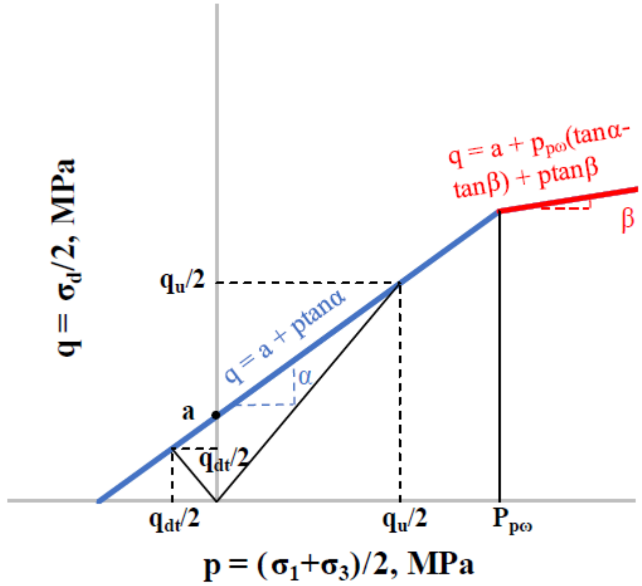

Figure 6-79 Simplified bilinear strength envelope.

$c = a / cos\varphi$ or $a = c\ cos\varphi$ Equation 33

$sin\varphi = tan\alpha$ and $sin\omega = tan\beta$ Equation 34

$c = 0.5\sqrt{q_u q_{dt}}$ Equation 35

$sin\varphi = \frac{q_u - q_{dt}}{q_u + q_{dt}}$ Equation 36

$p_{p\omega}\ (MPa) = \frac{0.35 + a}{1 - tan\,\alpha} = \frac{0.35 + c\ cos\,\varphi}{1 - sin\,\varphi}$ Equation 37

Florida limestone is porous with the possibility of encountering large porosities at depths of influence for shallow foundations. For this reason, it is recommended that the Florida strength envelope for the rock mass be reduced by an adjusted recovery (REC_{adjust}) as illustrated in Figure 6-80 and in Equation 114 below:

$q_m = q * REC_{adjust}$ Equation 38

which would result in the following parameters (Equation 116 – Equation 122), based on bulk dry unit weights of the maximum specimens (length, L) from the recovered core box and a weighted average unit weight is calculated as:

$\gamma_{dtw} = \Sigma(\gamma_{dti}\ L_i) / \Sigma L_i$ Equation 39

The three subscripts are: d for dry, t for total (or bulk, to differentiate with apparent dry unit weight, obtained from ASTM D6473 method), and w for weighted average.

$$a_m = REC_{adjust}*a=REC*0.5\sqrt{q_{uw}q_{tw}}\cos(\arcsin\frac{q_{uw}-q_{tw}}{q_{uw}+q_{tw}}) \qquad \text{Equation 40}$$

$$tan\alpha_m = REC_{adjust} *\tan\alpha = REC_{adjust}\frac{q_{uw}-q_{tw}}{q_{uw}+q_{tw}} \qquad \text{Equation 41}$$

$$tan\beta_m = REC_{adjust}*\tan\beta = REC_{adjust}*\sin\omega \qquad \text{Equation 42}$$

$$p_{pm} = p_p \qquad \text{Equation 43}$$

$$c_m = a_m / cos\varphi_m = REC_{adjust}* c * \cos\varphi / \cos\varphi_m \qquad \text{Equation 44}$$

$$c_m = REC_{adjust}* 0.5\sqrt{q_{uw} * q_{tw}} * \cos\varphi / \cos\varphi_m \leq REC_{adjust}* 0.5\sqrt{q_{uw} * q_{tw}}$$

where,

$$q_{tw} = q_t * e^{0.03(\gamma_{dtw}-\gamma_{dts})} \qquad \text{Equation 45}$$

$$q_{uw} = q_u * e^{0.04(\gamma_{dtw}-\gamma_{dts})} \qquad \text{Equation 46}$$

where q_t (based on 0.7*BST) and q_u are site specific test results for the evaluated rock layer (when many specimens are tested for BST and q_u, then the statistical procedure in Appendix A of FDOT Soil and Foundations Handbook can be followed to arrive at a single mean value of BST and q_u for the rock layer).

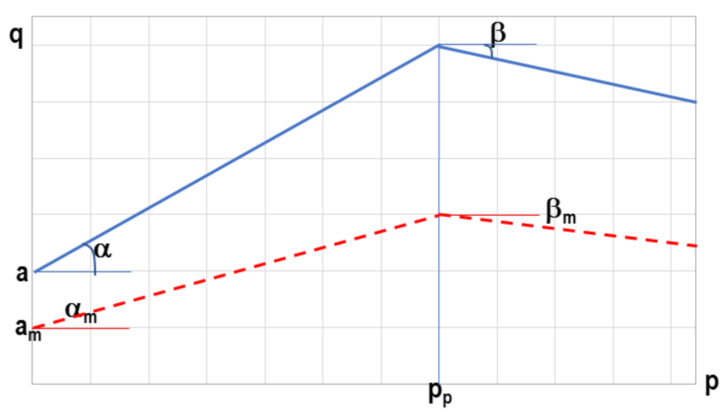

Figure 6-80 Bilinear strength envelope for rock mass from intact rock.

CHAPTER 7
CONCLUSIONS AND RECOMMENDATIONS

7.1 Conclusions

The Florida Department of Transportation (FDOT) has investigated the use of shallow foundations as alternatives to deep foundations (piles, drilled shafts, etc.) for support of bridge piers when limestone is near the ground surface (e.g., south Florida). Phase I (FDOT BDV31-977-51) investigated the engineering, physical, and geochemical properties of near-surface carbonate limestone in Florida (Anastasia, Miami, Fort Thompson, Key Largo, Hawthorn, and Ocala formations) and established bi-linear strength envelopes based on dry unit weight (porosity) and specific formation. Bearing capacity equations for surface and embedded square, rectangular, and strip footings were developed that capture the bi-linear nature of the limestone strength. Phase II (FDOT BDV31-977-124) conducted three full scale load tests for validation of the bearing capacity equations from Phase I and developed predictions of load-settlement response for cases of shallow foundations on a single layer and rock over sand based on the bi-linear stress-strain relationship (initial modulus and secant modulus at 2% strain). The findings identified the importance of assessing site spatial variability in the design of shallow foundations (e.g., differential settlement in spatially varying modulus). Significant recommendations included property assessment through lab (e.g. triaxial, moisture content, total and dry unit weight) and field invasive (e.g., MWD, coring) and non-invasive methods (e.g., Seismic FWI tomography), determining the mass properties of limestone based on the intact properties and the adjusted recovery of the core samples, accurately measuring natural moisture content for best determination of dry unit weight, and testing cores in their natural moisture content state (immediately testing or appropriately storing core boxes to retain natural moisture content).

The objectives of this project (Phase III) were to implement new shallow foundation analysis and design features and UI controls into the FB-MultiPier software package, and to develop corresponding software documentation. Those objectives have resulted in changes in the software in the following areas:

1. Implementation of the Florida limestone bearing capacity equations (Phase I) to facilitate predictions of shallow foundation capacities in design applications for Florida formations.

2. Implementation of nonlinear load-settlement analysis in the case of limestone or limestone over sand in order to assess forces, stresses and deformations within the structure.

3. Development and implementation of lateral resistance of shallow foundations under uni-directional and bi-directional loading, which is required for stability of the numerical model.

4. Investigation of the effects of inclined and eccentric loads applied to shallow foundations.

5. Documentation of outcomes and feature sets from the above four thrusts within the FEA software manual.

The study highlights the following key details: i) the analysis and design of shallow foundations on Florida limestone for bearing capacity, settlement, and passive resistance can be performed in FB-MultiPier; ii) Strength envelops specific to Florida limestone formations can be selected by the engineer or defined by entry of the intact properties and adjusted recovery or the mass properties; iii) Commonly encountered layering at shallow depths of single limestone layer and limestone over sand cases can be modeled for bearing capacity and settlement; iv) Strength envelopes for passive resistance can be defined with parameters defining limestone stress behavior where horizontal stress is greater than vertical stress (extension q-p space); v) Lateral resistance on a shallow foundation can be analyzed with base friction, side friction and passive resistance springs for oblique loading conditions; vi) Inclined loading on a shallow foundation on Florida limestone will result in a reduced bearing capacity as a function of the angle of the inclined load (ratio of horizontal to vertical loads); also the limestone friction angle and may be underpredicted using the inclination factor methods for soil in AASHTO LRFD Bridge Design Specifications; vii) Bearing capacity of eccentrically loaded shallow foundations on Florida limestone may be estimated using Meyerhof's effective footing width ($B' = B - 2e$); viii) Implementation outcomes and design example sets covering the full range of shallow foundation design features are available in FB-MultiPier manual.

To facilitate a rapid design in FB-MultiPier, two default models "Shallow Foundation" and "Shallow Foundation with Pier" are made available. These default models provide a user with a base configuration from which geometry and soil/rock profile can be changed. These default models provide a similar approach as the deep foundation models "Pile and Cap" and "Pier" models which have successfully been used by engineers.

For Task 1, estimates of bearing capacity based on Carter Kulhawy have also been implemented in FB-MultiPier. This method is recommended for strip footings with L/B > 10. However, the model does not account for the layering case of rock over sand. For the FL Limestone two variations are made available, FL Limestone (Homogeneous) and FL Limestone (Rock over Sand). Both models have dialogs from which a user can input rock strength properties. To help facilitate the selection of these properties, Phase 1 data from 6 Florida Limestone Formations is made available. The latter allows the user to select a formation of interest and input a bulk dry unit weight to automatically estimate intact rock strength properties. This feature would be useful for preliminary design only. In addition, to determine the mass strength properties, the user has to input` an Adjusted Rock Recovery, which will reduce the intact rock strength properties. With the mass strength envelope specified, the software will estimate the bearing capacity of the footing based on properties, geometry and layer profile.

For Task 2, estimation of axial load settlement behavior of the footing was implemented in FB-MultiPier. For FL Limestone (Homogeneous) and Carter Kulhawy models a geostatistical methodology was implemented. A new settlement dialog is accessible for each model where the user can input correlation length and coefficient of variation, CV, associated with the modulus of the rock. This analysis results in a range of settlement behavior based on the mean settlement and a lower and upper bound based on settlement range which is function of number of standard deviations inputted by the user. This allows the user to see the influence of the modulus CV on settlement in the design.

For the FL Limestone (Rock over Sand) model, a bilinear settlement estimate was implemented in the software. This method estimates a stress dependent harmonic mean, which is a function of both layer thickness of the rock and sand layers and their associated moduli. The load- settlement behavior of the system is bilinear, with the initial slope accounting for yielding of the rock layer, and the second slope controlled by the stiffness of underlying soil.

For the axial load vs settlement, FB-MultiPier uses a finite element model with Beam on Non-linear Winkler Foundation (BNWF) approach to analyze the embedded shallow foundation. A set of distributed 9-node thick shell elements are used to represent a shallow foundation (Footing in FB-MultiPier User Interface). The shell element nodes are discretized as per the grid spacing specified on the 'Footing' page and are positioned at the midplane of the foundation. Additionally, a set of non-linear soil springs are used to model the vertical soil resistance on the shallow foundation and are applied at each foundation node. These non-linear soil spring correspond to the bearing stresses developed due to foundation settlement. All soil springs are compression only and not active in tension.

All of axial non-linear soil spring develop axial resistance as a function of the foundation settlement per the model selected and footing bearing pressure qu-z curve. This pressure is converted to nodal force by multiplying by its corresponding nodal tributary area which results in a nodal bearing force response, Qui-z.

For Task 3, horizontal resistance due to passive pressure on the vertical face of the footing was also implemented. Three models are made available Hyperbolic, C-Phi Material, and FL Limestone. The C-Phi Material model allows Mohr Coulomb inputs, The FL Limestone model allows the user to utilize the rock database, however due to the horizontal loading resulting in horizontal stress being larger than vertical stress in the adjacent rock mass, extension properties are required to be used in conjunction with the hyperbolic model.

The shallow foundation uses the same BNWF approach for passive resistance by implementing horizontal non-linear soil springs on the nodes located on the edge of the footing element. These springs are only activated on the sides of the footing element and are active only for compression of soil/rock.

For horizontal resistance due to base friction on the bottom of the footing, a hyperbolic model using coulombic friction properties has been implemented. The shallow foundation model utilizes horizontal non-linear soil springs on the footing nodes. These non-linear springs account use normal forces (i.e., vertical resistance) to generate horizontal shear resistance (stress) and converted to corresponding horizontal frictional forces.

All horizontal resistance springs were implemented with their orientation in the X or Y axis of the model. Any oblique loading and associated motion will result in the overestimation of the horizontal resistance. Thus correction methods were implemented to ensure both passive and frictional non-linear soil spring resistance are reduced (tributary area) as function of oblique motion.

For Task 4, to account for eccentric or inclined load on the footing, inputs were added to the bearing capacity dialogs. These inputs allow the user to input resultant eccentricities in the length and width dimensions and an angle inclination. These inputs are then used to modify the estimated bearing capacity. Additionally, within the 3D results window and output file of the program, the resultant eccentricity and inclination is shown to aid users in design checks.

For Task 5, final modifications were made to FB-MultiPier to provide a standalone release. This included:

1. New model category, shallow foundation, which has no pile or shaft elements present. The soil resistance only acts on the footing which is a shell element. This shell element was typically referred to the pile cap when modeled with pile/shaft elements.

2. New UI dialogs for each design model for both axial bearing and lateral passive and lateral frictional resistance.

3. Non-linear FEA engine analysis with newly implemented UI design models.

4. Output of engine results in the form 3D results and a text output file.

5. Help Manual with overview of shallow foundation models (**6.4 FB-MultiPier Help Manual** shows the list of the help section that were updated). A web-based help manual is also available and can be accessed at: **https://bsi.ce.ufl.edu/documentation/fbmp/shallow_foundations_manual/default.htm?check=pass**

For all tasks, a rigorous validation process was conducted. This involved the use of hand calculations referred to as worked examples, field load tests, PLAXIS analysis, excel spread sheets, and MATLAB codes. For each model implemented validation of the UI and engine was implemented to ensure that the estimated resistance curves and resultant numerical analyses were correct. The result of this validation process were to ensure that FB-MultiPier produced both valid and reasonable results. Additionally, a group of worked examples have been selected/archived for validation cases when any subsequent updates to the program occur.

In this implementation of shallow foundation model there are several limitations:

1. The program does not calculate the bearing capacity and settlement of clay soils or bearing capacity of sand layers.

2. The program does not modify bearing capacity based on presence of an adjacent slope.

3. The program does not automatically adjust the bearing capacity based on the resultant eccentricity and inclination for an individual load case. A user can provide these values but is used for all load cases.

4. The program uses a linear elastic model for the footing shell element. This ensures model convergence. A separate structural analysis is required outside of the program.

5. The program is not recommended for cases where torsional loading about the vertical axis is the predominant load (e.g., wind load on mast arm).

7.2 Recommendations

- FB-MultiPier allows engineers to specify strength envelopes and modulus, based on Limestone formation and bulk dry unit weight from a database of rock data collected from the Phase 1 report. This feature is useful to rapidly specify a complex set of rock properties for preliminary analysis only. It's recommended that specifications be developed to guide engineers who want to take advantage of this rock database feature.

- **If an engineer wants to use the rock database feature for final design, researchers recommend that a site investigation and lab testing be conducted to confirm that the rock database properties is representative of the project site.**

- **The FL Limestone homogeneous settlement model uses a probabilistic approach to determine a range of settlements based on user inputs of modulus CV, correlation length, and number of standard deviations. It's recommended that the FDOT review this analysis type and determine what range is allowed for design along with corresponding number of samples collected.**

- For a field investigation it's recommended that one to two borings be located within the footprint. Collect rock samples at 1-foot intervals for determining bulk dry unit weight profile, 12 rock samples to estimate rock strength envelope for a given range of bulk dry unit weight. Modulus should also be evaluated during the strength assessment to characterize modulus variability of the site. If there is variability of the layering profile, then the boring investigation can be supplemented with MWD and/or seismic shear.

- To estimate passive resistance in FL Limestone it was determined that the extension strength envelope be used. This is due to the horizontal loading resulting in horizontal stress being larger than vertical stress in the adjacent rock mass. For this project extension test was performed on a limited number of samples to provide an indication that the extension strength envelope can be weaker than its corresponding compression strength envelope for a give bulk dry weight. Due to limited testing it's recommended that more samples from each FL Limestone formation be collected and tested to further define the extension envelope.

- The analysis for passive resistance in FL Limestone was based on numerical analysis from Plaxis. It is recommended that a field load test be conducted to confirm accuracy of the Plaxis analysis and hyperbolic model implemented in FB-MultiPier.

- In the literature review and numerical analysis conducted for the oblique loading of footings results in resistance from both passive resistance normal to the vertical footing face and shear resistance parallel to the vertical footing face. For this project it was elected to only model passive resistance with a reduction factor based on the angle of motion of the footing. Future work should determine a method to accurately predict the shear resistance of the vertical face of the footing.

- Investigation of the effects of inclined and eccentric loading was investigated only for the Miami, Fort Thompson and Anastasia formation. It is recommended that this investigation be extended to remaining Florida formations.

- It is recommended that inclination factors specified in AASHTO not be used with the FL Limestone bearing capacity method.

- AASHTO recommends the eccentricity limit of B/3 for soils and 0.45B for rock. It is recommended that B/6 be used for FL Limestone bearing capacity model until further investigation is conducted. This is due to the difference in compressibility of FL Limestone versus ridged rock.

- FB-MultiPier allows users to modify the estimated bearing capacity through inputs of eccentricity and inclination angle. These inputs modify the bearing capacity for all load cases. However, due to the numerous load cases that need to be analyzed, its recommended that FB-MultiPier evaluate the eccentricity and inclination for each individual load case and update accordingly.

- FB-MultiPier presents resultant resistance for bearing, passive and frictional resistances. Additionally, the program presents resultant eccentricity and inclination on the footing. It is recommended that the program prior to commercial release be updated with additional outputs to aid engineers in assessing required limit checks (i.e., maximum allowable bearing capacity, B/6, etc.) and capacity to demand ratios per load case.

LIST OF REFERENCES

American Association of State Highway and Transportation Officials (AASHTO). (2024). AASHTO-Chapter 10. In *AASHTO LRFD Bridge Design Specifications*. American Association of State Highway and Transportation Officials.

Bowles, J.E. (1996). *Foundation Analysis and Design*. McGraw-Hill.

Briaud, J.L. (2023). *Geotechnical engineering: unsaturated and saturated soils*. John Wiley & Sons.

Burmister, D.M. (1958). Evaluation of pavement systems of the WASHO road test by layered system methods. *Highway Research Board Bulletin*, (177).

Carter, J.P., & Kulhawy, F.H. (1988). *Analysis and Design of Foundations Socketed into Rock*. Report No. EL-5918. Empire State Electric Engineering Research Corporation and Electric Power Research Institute.

Chihi, O., & Saada, Z. (2022). Bearing capacity of strip footing on rock under inclined and eccentric load using the generalized Hoek-Brown criterion. *European Journal of Environmental and Civil Engineering*, *26*(6), 2258–2272. https://doi.org/10.1080/19648189.2020.1757513.

Coulomb, C.A. (1776). Essai sur une application des règles de maximis & minimis à quelques problèmes de statique, relatifs à l'architecture. De l'Imprimerie Royale (in French).

Duncan, J.M., & Mokwa, R.L. (2001). Passive earth pressures: theories and tests. *Journal of Geotechnical and Geoenvironmental Engineering*, *127*(3), 248–257.

Fang, H.Y. (Ed.). (2012). *Foundation engineering handbook*. Springer Science & Business Media.

Faraone, M.A. (2014). *Geostatistical analysis for reliability based design of foundations*. University of Florida.

Fenton, G.A., & Griffiths, D.V. (2002). Probabilistic foundation settlement on spatially random soil. *Journal of Geotechnical and Geoenvironmental Engineering*, *128*(5), 381–390.

Fox, L. (1948). Computation of traffic stresses in a simple road structure. *Proc. 2nd ICSMFE*, *1*, 236–246.

Guo, Z. (2015). *Numerical analysis of passive force on skewed bridge abutments*. Brigham Young University.

Hazzard, J.F., Yacoub, T.E., Vijayakumar, S., & Curran, J.H. (2007). Stresses under footings in multilayered soils: a comparative study. *Bearing Ground in the Nation's Capital*, Ottawa.

Hoek, E., Carranza-Torres, C., & Corkum, B. (2002). Hoek-Brown failure criterion-2002 edition. *Proceedings of NARMS-TAC*, *1*(1), 267–273.

Knappett, J., & Craig, R.F. (2012). *Craig's soil mechanics*. CRC Press.

Ko, J. (2010). *Evaluation of tip behavior of drilled shaft in Florida limestone* (Vol. 72, No. 05).

Lambe, T.W., & Whitman, R.V. (1991). *Soil mechanics* (Vol. 10). John Wiley & Sons.

Liu, S., Xia, Y., & Liang, L. (2018). A modified logarithmic spiral method for determining passive earth pressure. *Journal of Rock Mechanics and Geotechnical Engineering*, *10*(6), 1171–1182.

Lommler, J.C. (2012). *Geotechnical problem solving*. John Wiley & Sons.

Marinos, P., & Hoek, E. (2000). GSI: a geologically friendly tool for rock mass strength estimation. In *ISRM International Symposium* (pp. ISRM-IS). ISRM.

Mayne, P.W., & Poulos, H.G. (1999). Approximate displacement influence factors for elastic shallow foundations. *Journal of Geotechnical and Geoenvironmental Engineering*, *125*(6), 453–460.

McVay, M.C., Song, X., Wasman, S.J., Nguyen, T., & Wang, K. (2019). *Strength envelopes for Florida rock and intermediate geomaterials* (No. 00125485). Florida Department of Transportation.

O'Neil, M.W., & Reese, L.C. (1999). *Drilled shafts: construction procedures and design methods* (No. FHWA-IF-99-025). Federal Highway Administration, Office of Infrastructure.

Paikowsky, S.G., Canniff, M.C., Lesny, A., Amatya, S., Muganga, R., & Kisse, A. (2010). *LRFD Design and Construction of Shallow Foundations for Highway Bridge Structures*. NCHRP Report 651. Transportation Research Board, National Research Council. https://www.trb.org/Main/Blurbs/162110.aspx.

Patki, M.A., Mandal, J.N., & Dewaikar, D.M. (2015). Computation of passive earth pressure coefficients for a vertical retaining wall with inclined cohesionless backfill. *International Journal of Geo-Engineering*, *6*, 4. https://doi.org/10.1186/s40703-015-0004-5.

Poulos, H.G., & Davis, E.H. (1974). *Elastic solutions for soil and rock mechanics*.

Rodgers, M., McVay, M., Wasman, S., Tran, K., & Yang, K. (2022). *Phase II: Field load testing of shallow foundations in Florida limestone* (No. 00147823). Florida Department of Transportation.

Soubra, A.H., & Macuh, B. (2002). Active and passive earth pressure coefficients by a kinematical approach. *Proceedings of the Institution of Civil Engineers – Geotechnical Engineering*, *155*(2), 119–131.

Terzaghi, K. (1943). *Theoretical soil mechanics*. John Wiley & Sons.

Vesić, A.S. (1973). Analysis of ultimate loads of shallow foundations. *Journal of the Soil Mechanics and Foundations Division*, *99*(1), 45–73.

Yang, K., McVay, M., Nguyen, T., Wang, K., Song, X., Wasman, S., Rodgers, M., Horhota, D., & Herrera, R. (2023). Bearing capacity of shallow foundations on Florida limestone: a study of single layer and rock-over-sand subsurface. *Computers and Geotechnics*, *163*, Article 105742.

APPENDIX A
VALIDATION OF FB-MULTIPIER CODE FOR BEARING CAPACITY

To ensure the accuracy of the coding implemented in the FB-MultiPier engine, a comprehensive validation process was conducted using several distinct sources. The validation sets were selected to include detailed worked solutions, multiple examples with varying ranges of variable inputs, and a comparison between standard English and SI units. Three specific sources were employed to validate the implementation: a worked example set, an Excel spreadsheet utilized for in-depth sensitivity analysis, and selected problems from previous FDOT reports. Together, these methods form a robust assessment of the validations of the FB-MultiPier engine.

A.1 Worked Examples

For this project the first validation problems were a set of fully worked examples for the following cases implemented in FB-MultiPier.

A. Florida Limestone Homogeneous based on formation
B. Florida Limestone Homogeneous based on intact properties
C. Florida Limestone Homogeneous based on mass properties
D. Florida Limestone over Sand based on formation.
E. Florida Limestone over Sand based on intact properties.
F. Florida Limestone over Sand based on mass properties.
G. Carter-Kulhawy
H. Florida Limestone Homogeneous based on mass properties (SI Units).
I. Florida Limestone over Sand based on mass properties (SI Units).

The work examples not only provided solutions for a validation set but also served as guide for implementation of the method by listing required inputs and associated outputs required for the engineer. An example calculation for Case A is shown in Table A-1.

Table A-1 CASE a, Florida limestone homogeneous based on formation example.

Florida Bearing Capacity Equations	N_c	$\frac{1.8\ \cos\varphi_m}{0.8-\sin\varphi_m} = \frac{1.8\ \cos(33.9)}{0.8-\sin(33.9)} = 6.17$
	N'_c	$\frac{1.8\ \cos\varphi_m}{0.8-\sin\omega_m} = \frac{1.8\ \cos(33.9)}{0.8-\sin(0.6)} = 1.89$
	N_g	$\frac{1.8\ [\sin\varphi_m - \sin\omega_m]}{0.8-\sin\omega_m} = \frac{1.8\ [\sin(33.9) - \sin(0.6)]}{0.8-\sin(0.6)} = 1.25$
	q, psi	$1.5(D_w) \times 115/144 + 1.5(D_f - D_w) \times (115-62.4)/144 = 1.75$
	N_q	$(1.53 \times \frac{p_{pm}}{\sigma_a} - 10) \times (3 \times \sin\varphi_m - 1) = (1.53 \times \frac{306}{14.7} - 10) \times (3 \times \sin(33.9) - 1) = 14.71$
	n	$\left(\frac{4}{0.3B\ in\ ft}\right)^{-0.055} = \left(\frac{4}{0.3*10}\right)^{-0.055} = 0.99$
	ξ	$1 + 0.245 \left(\frac{B}{L}\right)^{0.66} = 1 + 0.245 \left(\frac{10}{15}\right)^{0.66} = 1.19$
	N_R	1 (Homogeneous Rock Case)
	Q_{u1}, psi	$n \times c_m \times N_c + q \times N_q = 0.99 \times 40.7 \times 6.17 + 1.75 \times 14.71 = 274.35$
	Q_{u2}, psi	$n \times [c_m \times N'_c + p_{pm} \times N_g] + q \times N_q = 0.99 \times [40.7 \times 1.89 + 306 \times 1.25] + 1.75 \times 14.71 = 480.57$
	Q_u, psi	$\min(Q_{u1}, Q_{u2}) \times \xi / N_R = \min(274.35, 480.57) \times 1.19/1 = 326.48$ psi = 23.5 tsf

FB-MultiPier input files were created for each case. The results for those analysis are presented in Table *A-2* for the English Units and Table A-3 for SI units. The percentage error was calculated for each case and was determined to be less than 0.7%. This percent error is acceptable and is likely due to the precision FB-MultiPier (FBMP) has versus a hand calculated worked solution.

Table A-2 Comparison of results between FBMP and worked examples.

CASE	-	A	B	C	D	E	F	G
Qu FBMP	ksf	46.7023	46.6872	46.6768	35.8195	35.8082	40.5374	70.8758
Qu Validation Problem	ksf	47.0000	47.0000	47.0000	36.0200	36.0200	40.7400	71.2300
% ERROR	%	-0.64%	-0.67%	-0.69%	-0.56%	-0.59%	-0.50%	-0.50%

Table A-3 Comparison of results between FBMP and SI Worked Examples.

CASE	-	H	I
Qu FBMP	kPa	2235.1116	1939.9941
Qu Validation Problem	kPa	2231.4285	1939.1100
% ERROR	%	0.16%	0.05%

A.2 Excel Calculation Comparison

To expand the validation to test multiple ranges for various inputs, an excel spreadsheet for the design methods was created. The sensitivity analysis would be used to validate the use of formation database, ensure interpolation of intact properties based on dry unit weight and test variation of all other input parameters. Results of this analysis are presented in Table A-4 through Table A-10.

Table A-4 Florida limestone homogeneous Miami formation.

Footing Geometry	B, ft	10	10	10	10	10	10	5
	L, ft	15	15	15	15	15	15	10
	D_f, ft	3	3	3	3	0	0	0
Depth of Water Table	D_w, ft	0	1.5	5	0	5	5	5
Total Unit Weight	g_{total}, pcf	115	115	115	115	115	115	115
REC	%	0.8	0.8	0.8	0.8	0.8	0.8	0.8
γ_{dt}	pcf	100	100	100	100	100	102.5	102.5
FORMATION	-	MIAMI	MIAMI	MIAMI	MIAMI	MIAMI	MIAMI	MIAMI
Qu Excel	ksf	45.0772	46.7147	48.3521	45.0772	42.3167	47.1928	44.1873
Qu FBMP	ksf	45.0646	46.7023	48.34	45.0646	42.3037	47.177	44.1724
% ERROR	%	0.03%	0.03%	0.03%	0.03%	0.03%	0.03%	0.03%

Table A-5 Florida limestone homogeneous Key Largo formation.

Footing Geometry	B, ft	5	5	5	5
	L, ft	10	10	10	5
	D_f, ft	0	0	0	0
Depth of Water Table	D_w, ft	5	5	5	5
Total Unit Weight	g_{total}, pcf	115	115	125	125
REC	%	0.8	0.25	0.75	0.75
γ_{dt}	pcf	67	67	67	67
FORMATION	-	KEY LARGO	KEY LARGO	KEY LARGO	KEY LARGO
Qu Excel	ksf	19.6622	2.8738	16.7049	18.0058
Qu FBMP	ksf	19.6563	2.8737	16.7029	18.0036
% ERROR	%	0.03%	0.00%	0.01%	0.01%

Table A-6 Florida limestone homogeneous SI units.

Footing Geometry	B, m	3	3	3	3
	L, m	9	3	3	3
	D_f, m	1	0	1	1
Depth of Water Table	D_w, m	0	0	10	0
Total Unit Weight	g_{total}, kN/m^3	17.5	17.5	17.5	17.5
REC	%	0.8	0.8	0.8	0.8
γ_{dt}	kN/m^3	17	17	17	17
FORMATION	-	MIAMI	MIAMI	MIAMI	MIAMI
Qu Excel	kPa	2862.4942	2984.6981	3442.3658	3185.8103
Qu FBMP	kPa	2862.4957	2984.6998	3442.3674	3185.8120
% ERROR	%	0.00%	0.00%	0.00%	0.00%

Table A-7 Florida limestone over sand.

Footing Geometry	B, ft	10	10	10	10	10
	L, ft	15	15	15	15	20
	D_f, ft	3	3	3	3	0
Depth of Water Table	D_w, ft	1	1	1	1	25
Total Unit Weight	g_{total}, pcf	115	115	115	115	135
REC	%	0.8	0.8	0.8	0.8	1
γ_{dt}	pcf	100	100	100	100	135
Rock Thickness	T, ft	4	8	4	4	5
E_{rock} (mass modulus)	psi	36000	36000	36000	36000	1
E_{soil} (mass modulus)	psi	5000	1200	1200	5000	0.03
FORMATION	-	MIAMI	MIAMI	MIAMI	MIAMI	MIAMI
Qu Excel	ksf	36.1966	35.8291	25.335	36.1966	228.11
Qu FBMP	ksf	36.1869	35.8195	25.3282	36.1869	228.107
% ERROR	%	0.03%	0.03%	0.03%	0.03%	0.00%

Table A-8 Florida limestone over sand SI units.

Footing Geometry	B, m	3	3	3	3
	L, m	3	9	3	3
	D_f, m	1	1	1	1
Depth of Water Table	D_w, m	10	0	0	10
Total Unit Weight	g_{total}, kN/m^3	17.5	17.5	17.5	17.5
REC	%	0.8	0.8	0.8	0.8
γ_{dt}	kN/m^3	17	17	17	17
Rock Thickness	T, m	2	3	3	3
E_{rock} (mass modulus)	kPa	36000	36000	36000	36000
E_{soil} (mass modulus)	kPa	5000	5000	5000	5000
FORMATION	-	MIAMI	MIAMI	MIAMI	MIAMI
Qu Excel	kPa	3007.8924	2662.7853	2963.5445	3202.2007
Qu FBMP	kPa	3007.5104	2662.4456	2963.1664	3201.7940
% ERROR	%	0.01%	0.01%	0.01%	0.01%

Table A-9 Carter Kulhawy.

m_i	-	10	20	20	20
GSI	-	80	80	50	50
q_u, psi	psi	300	300	300	150
s	-	0.11	0.11	0.00	0.00
m	-	4.90	9.79	3.35	3.35
Q_u, Excel	ksf	70.8758	93.0708	22.5945	11.2973
Qu, FBMP	ksf	70.8758	93.0708	22.5945	11.2973
% ERROR	%	0.000%	0.000%	0.000%	0.000%

Table A-10 Carter Kulhawy SI.

m_i	-	20	10	20	20
GSI	-	40	80	40	40
q_u	kPa	1034.214	2068.43	2068.43	1034.214
s	-	0.00	0.11	0.00	0.00
m	-	2.35	4.90	2.35	2.35
Q_u, Excel	kPa	338.38	3393.55	676.75	338.38
Qu, FBMP	kPa	338.38	3393.56	676.76	338.38
% ERROR	%	0.000%	0.000%	0.000%	0.000%

Reviewing the results in Table A-4 through Table A-10, shows that the percent error is less than 0.03%. This result is acceptable is shown a high precision of accuracy due to full calculation of significant digits used by excel spread sheet versus the worked examples.

A.3 Previous Worked Examples

The final validation was to compare FB-MultiPier results to the case studies presented in the FDOT reports BDV31-977-51, Phase I, and BDV31-977-124, Phase II. The first case study analyzed is from the phase I report which presents 3 design examples for shallow foundation on Miami Limestone overlaying a sand layer. Geometry of the design examples are shown in Figure A-1. through Figure A-3.

For implementation in FB-MultiPier it is assumed that total unit weight is equal to the dry unit weight, the recovery is 1 and no water table is present in the embedment depth. Summary of input parameters for each case is shown in Table A-11 through Table A-13 . It is presented in these tables the percentage error between FB-MultiPier and the Excel Spread Sheet and FB-MultiPier and the FDOT Report. Between the excel sheet and the FB-MultiPier the percent error is less the 0.01% and between FB-MultiPier and the FDOT Report the percent error is less than 2.6%. The larger percent error difference between FB-MultiPier and the FDOT report can be attributed to 1) precision the FB-MultiPier engine carries through all its calculations, 2) the precision of the width metric conversion in equation 2-4 and 3) equation 2-12 the coefficient 1.53 was originally 1.5 in the FDOT repot. The percent error calculated is found to be acceptable.

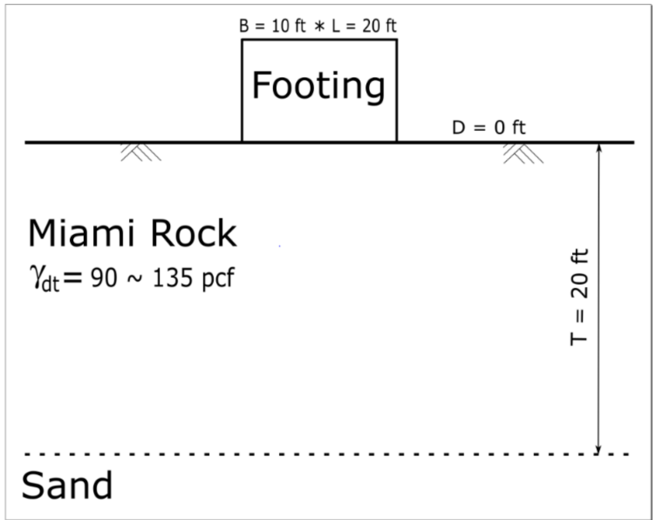

Figure A-1 Design case 1, BDV31-977-51.

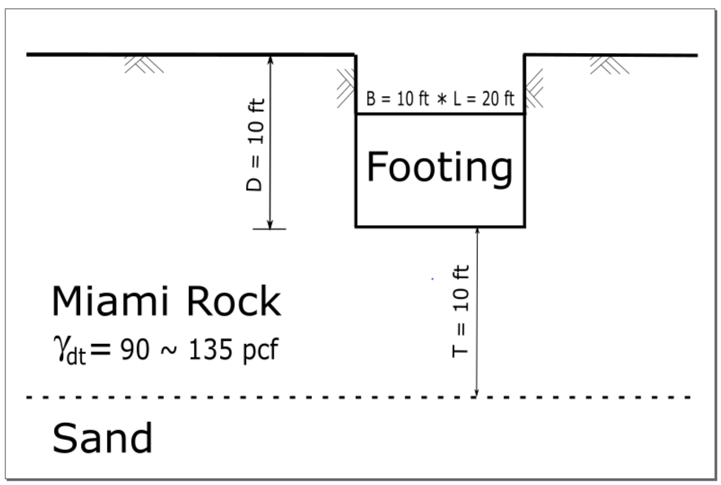

Figure A-2 Design case 2, BDV31-977-51.

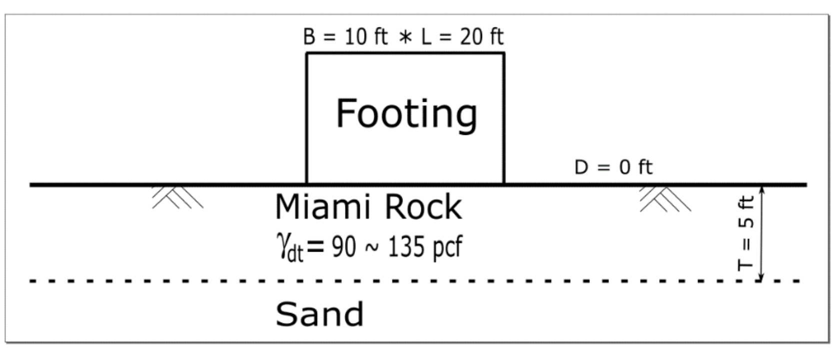

Figure A-3 Design case 3, BDV31-977-51.

Table A-11 FB-MultiPier (FBMP) vs design case 1, BDV31-977-51.

Problem		CASE 1		
Footing Geometry	B, ft	10	10	10
	L, ft	20	20	20
	D_f, ft	0	0	0
Depth of Water Table	D_w, ft	25	25	25
Total Unit Weight	g_{total}, pcf	90	110	135
REC	%	1	1	1
γ_{dt}	pcf	90	110	135
Rock Thickness	T, ft	20	20	20
E_{rock} (mass modulus)	psi	1	1	1
E_{soil} (mass modulus)	psi	0.03	0.03	0.03
FORMATION	-	MIAMI	MIAMI	MIAMI
Qu Excel	ksf	65.8283	117.076	350.726
Qu FBMP	ksf	65.8246	117.067	350.721
% ERROR	%	0.01%	0.01%	0.00%
FDOT REPORT	ksf	66.48	118.3	354.06
% ERROR	%	-1.00%	-1.05%	-0.95%

Table A-12 FB-MultiPier (FBMP) vs design case 2, BDV31-977-51.

Problem		CASE 2		
Footing Geometry	B, ft	10	10	10
	L, ft	20	20	20
	D_f, ft	10	10	10
Depth of Water Table	D_w, ft	25	25	25
Total Unit Weight	g_{total}, pcf	90	110	135
REC	%	1	1	1
γ_{dt}	pcf	90	110	135
Rock Thickness	T, ft	10	10	10
E_{rock} (mass modulus)	psi	1	1	1
E_{soil} (mass modulus)	psi	0.03	0.03	0.03
FORMATION	-	MIAMI	MIAMI	MIAMI
Qu Excel	ksf	74.568	146.172	450.613
Qu FBMP	ksf	74.5711	146.17	450.643
% ERROR	%	0.00%	0.00%	-0.01%
FDOT REPORT	ksf	75.2	147.46	454.18
% ERROR	%	-0.84%	-0.88%	-0.78%

Table A-13 FB-MultiPier (FBMP) vs Design Case 3, BDV31-977-51.

Problem		CASE 3		
Footing Geometry	B, ft	10	10	10
	L, ft	20	20	20
	D_f, ft	0	0	0
Depth of Water Table	D_w, ft	25	25	25
Total Unit Weight	$g_{total,}$ pcf	90	110	135
REC	%	1	1	1
γ_{dt}	pcf	90	110	135
Rock Thickness	T, ft	5	5	5
E_{rock} (mass modulus)	psi	1	1	1
E_{soil} (mass modulus)	psi	0.03	0.03	0.03
FORMATION	-	MIAMI	MIAMI	MIAMI
Qu Excel	ksf	42.8143	76.1456	228.11
Qu FBMP	ksf	42.8119	76.1394	228.107
% ERROR	%	0.01%	0.01%	0.00%
FDOT REPORT	ksf	43.88	78.08	233.7
% ERROR	%	-2.49%	-2.55%	-2.45%

From report BDV31-977-124 the following case studies were analyzed. The worked examples from this report are presented in Table A-14 through Table A-20 . Summary of input parameters for each case is shown in Table A-21 and Table *A-22* . It is presented in these tables the percent error between FB-MultiPier (FBMP) and the Excel Spread Sheet and FB-MultiPier and the FDOT report. Between the excel sheet and the FB-MultiPier the percent error is less the 0.01% and between FB-MultiPier and the FDOT Report the percent error is less than 0.67%. The percent error calculated is found to be acceptable.

Table A-14 CEMEX bearing capacity, BDV31-977-124.

Footing Geometry	B, ft	3.5
	L, ft	3.5
	D_f, ft	5
Mass Properties	c, psi	31.9
	φ, °	32.4
	P_p, psi	341.8
	ω, °	4.35
Florida Bearing Capacity Equations	N_c	$\frac{1.8\ \cos\varphi}{0.8-\sin\varphi} = \frac{1.8\ \cos(32.4)}{0.8-\sin(32.4)} = 5.75$
	N'_c	$\frac{1.8\ \cos\varphi}{0.8-\sin\omega} = \frac{1.8\ \cos(32.4)}{0.8-\sin(4.35)} = 2.10$
	N_g	$\frac{1.8\ [\sin\varphi - \sin\omega]}{0.8-\sin\omega} = \frac{1.8\ [\sin(32.4) - \sin(4.35)]}{0.8-\sin(4.35)} = 1.14$
	q, psi	$(D_f) \times 100/144 = 3.47$ (overburden stress)
	N_q	$(1.5 \times \frac{p_p}{\sigma_a} - 10) \times (3 \times \sin\varphi\ -\ 1) = (1.5 \times \frac{341.8}{14.7} - 10) \times (3 \times \sin(32.4)\ -\ 1)\ = 15.1$
	n	$\left(\frac{4}{0.3B\text{ in ft}}\right)^{-0.055} = \left(\frac{4}{0.3*3.5}\right)^{-0.055} = 0.93$
	ξ	$1\ +\ 0.245\ \left(\frac{B}{L}\right)^{0.66} = 1\ +\ 0.245\ \left(\frac{3.5}{3.5}\right)^{0.66} = 1.245$
	N_R	1
	Q_{u1}, psi	$n \times c \times N_c + q \times N_q = 0.93 \times 31.9 \times 5.75 + 3.47 \times 15.1 = 223.1$
	Q_{u2}, psi	$n \times [c \times N'_c + p_p \times N_g] + q \times N_q = 0.93 \times [31.9 \times 2.1 + 341.8 \times 1.14] + 3.47 \times 15.1 = 477.7$
	Q_u	$\min(Q_{u1}, Q_{u2}) \times \xi/N_R = \min(223.1, 477.7) \times 1.245/1 = 277.8$ psi $= 20$ tsf

Table A-15 SR-84 bearing capacity, BDV31-977-124.

Footing Geometry	B, ft	5
	L, ft	6
	D_f, ft	3
	T, ft	10
Mass Properties	c, psi	44.08
	φ, °	35.4
	P_p, psi	392
	ω, °	6.01
	E_{sand}/E_{mass}	E_{sand}/E_{mass} = 1100/35261.8 (median) = 0.031
Florida Bearing Capacity Equations	N_c	$\frac{1.8\ \cos\varphi}{0.8-\sin\varphi} = \frac{1.8\ \cos(35.4)}{0.8-\sin(35.4)} = 6.64$
	N'_c	$\frac{1.8\ \cos\varphi}{0.8-\sin\omega} = \frac{1.8\ \cos(35.4)}{0.8-\sin(6.01)} = 2.11$
	N_γ	$\frac{1.8\ [\sin\varphi - \sin\omega]}{0.8-\sin\omega} = \frac{1.8\ [\sin(35.4) - \sin(6.01)]}{0.8-\sin(6.01)} = 1.23$
	q, psi	$(D_f) \times 110/144 = 2.29$ (overburden stress)
	N_q	$(1.5 \times \frac{p_p}{\sigma_a} - 10) \times (3 \times \sin\varphi\ -\ 1) = (1.5 \times \frac{392}{14.7} - 10) \times (3 \times \sin(35.4)\ -\ 1)\ = 22.11$
	R	$0.093T^2\ E_{soil} / E_{rock} = 0.093T^2\ E_{sand} / E_{mass} = 0.093 \times 10^2\times (0.031) = 0.29$
	N_R	$0.86 \times R^{-0.25} = 0.86 \times 0.29^{-0.25} = 1.17$
	n	$\left(\frac{4}{0.3B\text{ in ft}}\right)^{-0.055} = \left(\frac{4}{0.3\times5}\right)^{-0.055} = 0.95$
	ξ	$1\ +\ 0.245\ \left(\frac{B}{L}\right)^{0.66} = 1\ +\ 0.245\ \left(\frac{5}{6}\right)^{0.66} = 1.22$
	Qu1, psi	$ncN_c + qN_q = 0.95\times 44.08 \times 6.64 + 2.29\times 22.11 = 327.6$
	Qu2, psi	$n[cN'_c + p_pN_g] + qN_q = 0.95\times [44.08 \times 2.11 + 392\times 1.23] + 2.29\times22.11 = 594.8$
	Qu	min $(Q_{u1}, Q_{u2}) \times \xi/N_R$ = min(327.6, 594.8) ×1.22/1.17= 340.8 psi = 24.54 tsf

Table A-16 Bell bearing capacity, BDV31-977-124.

Footing Geometry	B, ft	5
	L, ft	5
	D_f, ft	5
	T, ft	5
Mass Properties	c, psi	48
	φ, °	30
	P_p, psi	251.5
	ω, °	19.7
	E_{sand}/E_{mass}	E_{sand}/E_{mass} = 1950/36000 (median) = 0.054
Florida Bearing Capacity Equations	N_c	$\frac{1.8\ \cos\varphi}{0.8-\sin\varphi} = \frac{1.8\ \cos(30)}{0.8-\sin(30)} = 5.19$
	N'_c	$\frac{1.8\ \cos\varphi}{0.8-\sin\omega} = \frac{1.8\ \cos(30)}{0.8-\sin(19.7)} = 3.37$
	N_γ	$\frac{1.8\ [\sin\varphi - \sin\omega]}{0.8-\sin\omega} = \frac{1.8\ [\sin(30) - \sin(19.7)]}{0.8-\sin(19.7)} = 0.632$
	q, psi	$(D_f) \times 80/144 = 2.78$ (overburden stress)
	N_q	$(1.5 \times \frac{p_p}{\sigma_a} - 10) \times (3 \times \sin\varphi\ -\ 1) = (1.5 \times \frac{251.5}{14.7} - 10) \times (3 \times \sin(30)\ -\ 1)\ = 8.03$
	R	$0.093T^2\ E_{soil}\ /\ E_{rock} = 0.093T^2\ E_{sand}\ /\ E_{mass} = 0.093\times5\text{^}2\times\ (0.054) = 0.13$
	N_R	$0.86 * R^{-0.25} = 0.86 \times 0.13^{-0.25} = 1.44$
	n	$\left(\frac{4}{0.3\text{B in ft}}\right)^{-0.055} = \left(\frac{4}{0.3\times5}\right)^{-0.055} = 0.95$
	ξ	$1\ +\ 0.245\ \left(\frac{B}{L}\right)^{0.66} = 1\ +\ 0.245\ \left(\frac{5}{5}\right)^{0.66} = 1.245$
	Qu1, psi	$ncN_c + qN_q = 0.95\times\ 48 \times 5.19 + 2.78\times\ 8.03 = 258.4$
	Qu2, psi	$n[cN'_c + p_pN_g\ ] + q*N_q = 0.95\times\ [48 \times 3.37 + 251.5\times\ 0.632] + 2.78\times\ 8.03 = 326.1$
	Qu	min (Q_{u1}, Q_{u2}) × ξ/N_R =min(258.4, 326.1) ×1.245/1.44= 222.8 psi = 16.04 tsf

Table A-17 Case a bearing capacity, BDV31-977-124.

Footing Geometry	B, ft	6
	L, ft	6
	D_f, ft	0
	T, ft	3
Mass Properties	c, psi	45.7
	φ, °	36.4
	P_p, psi	392
	ω, °	6.1
	E_{sand}/E_{mass}	E_{sand}/E_{mass} = 800/35655 = 0.0224
Florida Bearing Capacity Equations	N_c	$\frac{1.8\ \cos\varphi}{0.8-\sin\varphi} = \frac{1.8\ \cos(36.4)}{0.8-\sin(36.4)} = 7.03$
	N'_c	$\frac{1.8\ \cos\varphi}{0.8-\sin\omega} = \frac{1.8\ \cos(36.4)}{0.8-\sin(6.1)} = 2.09$
	N_g	$\frac{1.8\ [\sin\varphi - \sin\omega]}{0.8-\sin\omega} = \frac{1.8\ [\sin(36.4) - \sin(6.1)]}{0.8-\sin(6.1)} = 1.26$
	q, psi	0 (overburden stress)
	N_q	$(1.5\frac{p_p}{\sigma_a} - 10)(3\sin\varphi\ -\ 1) = (1.5 \times \frac{392}{14.7} - 10) \times (3 \times \sin(36.4)\ -\ 1)\ = 23.5$
	R	$0.093T^2\ E_{soil} / E_{rock} = 0.093T^2\ E_{sand} / E_{mass} = 0.093 \times 3^2\times (0.0224) = 0.019$
	N_R	$0.86 \times R^{-0.25} = 0.86 \times 0.019^{-0.25} = 2.32$
	n	$\left(\frac{4}{0.3\text{B in ft}}\right)^{-0.055} = \left(\frac{4}{0.3\times6}\right)^{-0.055} = 0.96$
	ξ	$1\ +\ 0.245\ \left(\frac{B}{L}\right)^{0.66} = 1\ +\ 0.245\ \left(\frac{6}{6}\right)^{0.66} = 1.245$
	Qu1, psi	$ncN_c + qN_q = 0.96\times 45.7 \times 7.03 + 0 = 307.6$
	Qu2, psi	$n[cN'_c + p_pN_g] + q*N_q = 0.96\times [45.7 \times 2.09 + 392\times 1.26] + 0 = 565.8$
	Qu	min (Q_{u1}, Q_{u2}) × ξ/N_R =min(307.6, 565.8) ×1.245/2.32= 164.8 psi = 11.9 tsf

Table A-18 Case c bearing capacity, BDV31-977-124.

Footing Geometry	B, ft	6
	L, ft	12
	D_f, ft	3
	T, ft	3
Mass Properties	c, psi	31.8
	φ, °	36.3
	P_p, psi	308
	ω, °	0.43
	E_{sand}/E_{mass}	E_{sand}/E_{mass} = 800/20124 = 0.04
Florida Bearing Capacity Equations	N_c	$\frac{1.8\ \cos\varphi}{0.8-\sin\varphi} = \frac{1.8\ \cos(36.3)}{0.8-\sin(36.3)} = 6.98$
	N'_c	$\frac{1.8\ \cos\varphi}{0.8-\sin\omega} = \frac{1.8\ \cos(36.3)}{0.8-\sin(0.43)} = 1.83$
	N_g	$\frac{1.8\ [\sin\varphi - \sin\omega]}{0.8-\sin\omega} = \frac{1.8\ [\sin(36.3) - \sin(0.43)]}{0.8-\sin(0.43)} = 1.33$
	q, psi	$(D_f) \times 100/144 = 2.08$ (overburden stress)
	N_q	$(1.5\frac{p_p}{\sigma_a} - 10)(3\sin\varphi j\ -\ 1) = (1.5 \times \frac{308}{14.7} - 10) \times (3 \times \sin(36.3)\ -\ 1)\ = 16.6$
	R	$0.093T^2\ E_{soil}\ /\ E_{rock} = 0.093T^2\ E_{sand}\ /\ E_{mass} = 0.093\times3$^$2\times(0.04) = 0.033$
	N_R	$0.86 \times R^{-0.25} = 0.86 \times 0.033^{-0.25} = 2.01$
	n	$\left(\frac{4}{0.3\text{B in ft}}\right)^{-0.055} = \left(\frac{4}{0.3\times6}\right)^{-0.055} = 0.96$
	ξ	$1\ +\ 0.245\ \left(\frac{B}{L}\right)^{0.66} = 1\ +\ 0.245\ \left(\frac{6}{12}\right)^{0.66} = 1.16$
	Qu1, psi	$ncN_c + qN_q = 0.96\times 31.8 \times 6.98 + 2.08\times16.6 = 246.9$
	Qu2, psi	$n[cN'_c + p_pN_g] + qN_q = 0.96\times [31.8 \times 1.83 + 308\times 1.33] + 2.08\times16.6 = 481.8$
	Qu	$\min(Q_{u1}, Q_{u2})\ \xi/N_R = \min(246.9, 481.8) \times1.16/2.01 = 141.63$ psi = 10.2 tsf

Table A-19 Case 9-11 bearing capacity, BDV31-977-124.

Footing Geometry	B, ft	10
	L, ft	15
	D_f, ft	3
Mass Properties	c, psi	31.77
	φ, °	36.31
	P_p, psi	308
	ω, °	0.43
Florida Bearing Capacity Equations	N_c	$\frac{1.8\ \cos\varphi}{0.8-\sin\varphi} = \frac{1.8\ \cos(36.31)}{0.8-\sin(36.31)} = 6.98$
	N'_c	$\frac{1.8\ \cos\varphi}{0.8-\sin\omega} = \frac{1.8\ \cos(36.31)}{0.8-\sin(0.43)} = 1.83$
	N_g	$\frac{1.8\ [\sin\varphi - \sin\omega]}{0.8-\sin\omega} = \frac{1.8\ [\sin(36.31) - \sin(0.43)]}{0.8-\sin(0.43)} = 1.33$
	q, psi	(3) × 100/144 = 2.08 (overburden stress)
	N_q	$(1.5 \times \frac{p_p}{\sigma_a} - 10) \times (3 \times \sin\varphi\ -\ 1) = (1.5 \times \frac{308}{14.7} - 10) \times (3 \times \sin(36.31)\ -\ 1)\ = 16.64$
	n	$\left(\frac{4}{0.3B\text{ in ft}}\right)^{-0.055} = \left(\frac{4}{0.3*10}\right)^{-0.055} = 0.98$
	ξ	$1\ +\ 0.245\ \left(\frac{B}{L}\right)^{0.66} = 1\ +\ 0.245\ \left(\frac{10}{15}\right)^{0.66} = 1.19$
	N_R	1
	Qu1, psi	$n \times c \times N_c + q \times N_q = 0.98 \times 31.77 \times 6.98 + 2.08 \times 16.64 = 252.95$
	Qu2, psi	$n \times [c \times N'_c + p_p \times N_g] + q \times N_q = 0.98 \times [31.77 \times 1.83 + 308 \times 1.33] + 2.08 \times 16.64 = 494.51$
	Qu	min (Q_{u1}, Q_{u2}) × ξ/N_R = min (252.95, 494.51) ×1.19/1= 300.4 psi = 21.63 tsf

Table A-20 Case 9-18 bearing capacity, BDV31-977-124.

Footing Geometry	B, ft	15
	L, ft	15
	D_f, ft	3
	T, ft	10
Mass Properties	c, psi	33.77
	φ, °	34.75
	P_p, psi	344
	ω, °	2.61
	E_{sand}/E_{mass}	E_{sand}/E_{mass} = 1100/25668 (median) = 0.04285
Florida Bearing Capacity Equations	N_c	$\frac{1.8\ \cos\varphi}{0.8-\sin\varphi} = \frac{1.8\ \cos(34.75)}{0.8-\sin(34.75)} = 6.43$
	N'_c	$\frac{1.8\ \cos\varphi}{0.8-\sin\omega} = \frac{1.8\ \cos(34.75)}{0.8-\sin(2.61)} = 1.96$
	N_g	$\frac{1.8\ [\sin\varphi - \sin\omega]}{0.8-\sin\omega} = \frac{1.8\ [\sin(34.75) - \sin(2.61)]}{0.8-\sin(2.61)} = 1.25$
	q, psi	(D_f) × 100/144 = 2.08 (overburden stress)
	N_q	$(1.5\frac{p_p}{\sigma_a} - 10)(3\sin\varphi\ -\ 1) = (1.5 \times \frac{344}{14.7} - 10) \times (3 \times \sin(34.75)\ -\ 1) = 17.82$
	R	$0.093T^2\ E_{soil}\ /\ E_{rock} = 0.093T^2\ E_{sand}\ /\ E_{mass} = 0.093\times10^\wedge2\times (0.04285) = 0.4$
	N_R	$1.2\ -\ 0.1 \times R = 1.2-0.1\times0.4 = 1.16$
	n	$\left(\frac{4}{0.3B\ \text{in ft}}\right)^{-0.055} = \left(\frac{4}{0.3\times15}\right)^{-0.055} = 1$
	ξ	$1\ +\ 0.245\ \left(\frac{B}{L}\right)^{0.66} = 1\ +\ 0.245\ \left(\frac{15}{15}\right)^{0.66} = 1.245$
	Qu1, psi	$ncN_c + qN_q$ = 1× 33.77 × 6.43 + 2.08× 17.82= 255.72
	Qu2, psi	$n[cN'_c + p_pN_g] + qN_q$= 1× [33.77 × 1.96 + 344× 1.25] + 2.08× 17.82 = 537
	Qu	min (Q_{u1}, Q_{u2}) × ξ/N_R =min(255.72, 537) ×1.245/1.16= 274.4 psi = 19.8 tsf

Table A-21 Florida limestone comparison to BDV31-977-124.

CASE	-	CMEX	9-11
Mass Properties	c, psi	31.90	31.77
	φ, °	32.40	36.31
	ω, °	4.35	0.43
	P_p, psi	341.80	308.00
Footing Geometry	B, ft	3.5	10
	L, ft	3.5	15
	D_f, ft	5	3
Depth of Water Table	D_w, ft	25	25
Total Unit Weight	g_{total}, pcf	100	100
REC	%	1	1
Qu Excel	ksf	40.2663	43.4506
Qu FBMP	ksf	40.2699	43.4530
% ERROR	%	-0.01%	-0.01%
FDOT REPORT	ksf	40	43.26
% ERROR	%	0.67%	0.44%

Table A-22 Florida limestone over sand comparison to BDV31-977-124.

CASE	-	SR84	BELL	CASE A	CASE C	9-18
Mass Properties	c, psi	44.08	48.00	45.70	31.80	33.77
	φ, ˚	35.40	30.00	36.40	36.30	34.75
	ω, ˚	6.01	19.70	6.10	0.43	2.61
	P_p, psi	392.00	251.50	392.00	308.00	344.00
Footing Geometry	B, ft	5	5	6	6	15
	L, ft	6	5	6	12	15
	D_f, ft	3	5	0	3	3
Depth of Water Table	D_w, ft	25	25	25	25	25
Total Unit Weight	$g_{total,}$ pcf	110	80	100	100	100
REC	%	1	1	1	1	1
Rock Thickness	T, ft	10	5	3	3	10
E_{rock} (mass modulus)	psi	1	36000	35655	20124	25668
E_{soil} (mass modulus)	psi	0.031	1950	800	800	1100
Qu Excel	ksf	49.2778	32.1630	23.6919	20.4949	39.7021
Qu FBMP	ksf	49.2806	32.1642	23.6919	20.4961	39.7043
% ERROR	%	-0.01%	0.00%	0.00%	-0.01%	-0.01%
FDOT REPORT	ksf	49.08	32.08	23.8	20.4	39.6
% ERROR	%	0.41%	0.26%	-0.46%	0.47%	0.26%

APPENDIX B
VALIDATION OF FB-MULTIPIER CODE FOR NON-LINEAR LOAD SETTLEMENT

B.1 Worked Example and Cemex Load Test (Homogeneous)

B.1.1 Worked Example

The worked example is for a 10 ft by 15 ft rectangular rigid footing embedded 3 ft on a homogeneous Miami limestone subsurface. The thickness of rock bearing layer is 20 ft with a bulk dry unit weight of 100 pcf and an adjusted Recovery of 80%. Rock mass properties and footing geometry are summarized in Table B-1, using a mass cohesion (c_m) of 40.7 psi, a mass friction angle (φ_m) of 33.9°, a peak stress (P_p) of 306 psi and a mass reduced angle (ω_m) of 0.6°, the bearing capacity calculation is shown in Table B-1 . For the settlement prediction, Fenton and Griffiths method is used with the mean mass modulus, CV of mass modulus and vertical correlation length. The deterministic settlement (CV_E = 0) is required to implement the probabilistic settlement prediction, the analytical solution to account for different footing geometry and rigidity is provided. The settlement calculation is shown in Table B-2 and the load-settlement response is plotted in Figure B-1.

Table B-1 Bearing capacity calculation of worked example for Florida homogeneous case.

Florida Bearing Capacity Equations	N_c	$\frac{1.8\ \cos\varphi_m}{0.8-\sin\varphi_m} = \frac{1.8\ \cos(33.9)}{0.8-\sin(33.9)} = 6.17$
	N'_c	$\frac{1.8\ \cos\varphi_m}{0.8-\sin\omega_m} = \frac{1.8\ \cos(33.9)}{0.8-\sin(0.6)} = 1.89$
	N_g	$\frac{1.8\ [\sin\varphi_m - \sin\omega_m]}{0.8-\sin\omega_m} = \frac{1.8\ [\sin(33.9) - \sin(0.6)]}{0.8-\sin(0.6)} = 1.25$
	q, psi	$1.5(D_w) \times 115/144 + 1.5(D_f - D_w) \times (115-62.4)/144 = 1.75$
	N_q	$(1.53 \times \frac{p_{pm}}{\sigma_a} - 10) \times (3 \times \sin\varphi_m - 1) = (1.53 \times \frac{306}{14.7} - 10) \times (3 \times \sin(33.9) - 1) = 14.71$
	n	$\left(\frac{4}{0.3048B'\text{ in ft}}\right)^{-0.055} = \left(\frac{4}{0.3048*10}\right)^{-0.055} = 0.99$
	ξ	$1 + 0.245\left(\frac{B'}{L'}\right)^{0.66} = 1 + 0.245\left(\frac{10}{15}\right)^{0.66} = 1.19$
	N_R	1 (Homogeneous Rock Case)
	Q_{u1}, psi	$n \times c_m \times N_c + q \times N_q = 0.99 \times 40.7 \times 6.17 + 1.75 \times 14.71 = 274.35$
	Q_{u2}, psi	$n \times [c_m \times N'_c + p_{pm} \times N_g] + q \times N_q = 0.99 \times [40.7 \times 1.89 + 306 \times 1.25] + 1.75 \times 14.71 = 480.57$
	Q_u, psi	$\min(Q_{u1}, Q_{u2}) \times \xi/N_R = \min(274.35, 480.57) \times 1.19/1 = 326.48$ psi = 23.5 tsf

Table B-2 Probabilistic settlement calculation of worked example for Florida homogeneous case.

Mass properties	E_m, ksi	20.7
	CV_{Em}	0.75
	σ_E, ksi	$CV_{Em} \times E_m$, = 0.75× 20.7 = 15.5
	ν	0.1 (Poisson's ratio)
	a_v, ft	4.5 (Correlation length)
	n	2
Geometry	B, ft	10 (Footing width)
	L, ft	15
	T_r, ft	20
	t, in	72
	$E_{foundation}$, ksi	4400
	K_F	$\frac{E_{foundation}}{E_m}\left(\frac{t}{a}\right)^3 = \frac{4400}{20.7}\left(\frac{72}{\sqrt{BL/\pi}}\right)^3 = \frac{4400}{20.7}\left(\frac{72}{\sqrt{144\times10\times15/3.14}}\right)^3 =$ 139.16 (perfectly rigid)
	I_F	$\frac{\pi}{4} + \frac{1}{(4.6+10K_F)} = \frac{\pi}{4} + \frac{1}{(4.6+10\times139.16)} = 0.79$
	C	C_s*I_F = 1.36*0.79 = 1.07 (L/B = 15/10 = 1.5, C_s = 1.36 from Table 3)
Bearing value	Q_u, psi	326.48
Fenton and Griffiths' method	δ_{det}, in	$Qu\frac{B}{\mu_E}C(1-\nu^2) = \frac{326.48\times10\times12\times1.07\times(1-0.1\hat{}2)}{20700} = 2$
	$\sigma_{\ln E}$	$\sqrt{ln(1+\sigma_E^2(above)/\mu_E^2(above))} = \sqrt{ln(1+15525^2/20700^2)} = 0.668$
	$\gamma(T_r)$	$\frac{2a_v^2}{9{T_r}^2}\left[\frac{3\lvert T_r\rvert}{a_v} + e^{\left(-\frac{3\lvert T_r\rvert}{a_v}\right)} - 1\right] = \frac{2\times4.5^2}{9\times20^2}\left[\frac{3\lvert 20\rvert}{4.5} + e^{\left(-\frac{3\lvert 20\rvert}{4.5}\right)} - 1\right] = 0.14$
	$\sigma_{\ln\delta}$	$\sqrt{\gamma(T)}\sigma_{\ln E}$(above) $=\sqrt{0.14}\times 0.668 = 0.24884$
	$\mu_{\ln\delta}$	$\ln(\delta_{det}(above)) + \frac{1}{2}\sigma_{\ln E}^2$(above)=ln(2)+ $\frac{1}{2}0.668^2 = 0.917$
	μ_δ, in	$exp\left\{\mu_{\ln\delta}(above) + \frac{1}{2}\sigma_{\ln\delta}^2(above)\right\}$= exp(0.917+ $\frac{1}{2}0.24884^2$)= 2.580
	σ_δ, in	$\mu_\delta(above)\sqrt{e^{\sigma_{\ln\delta}^2(above)} - 1} = 2.580\sqrt{e^{0.24884^2} - 1} = 0.652$
	δ_{LB}, in	$\exp(\mu_{\ln\delta} - n\,\sigma_{\ln\delta})$ = exp(0.917-2*0.24884) = 1.520
	δ_{UB}, in	$\exp(\mu_{\ln\delta} + n\,\sigma_{\ln\delta})$ = exp(0.917+2*0.24884) = 4.114

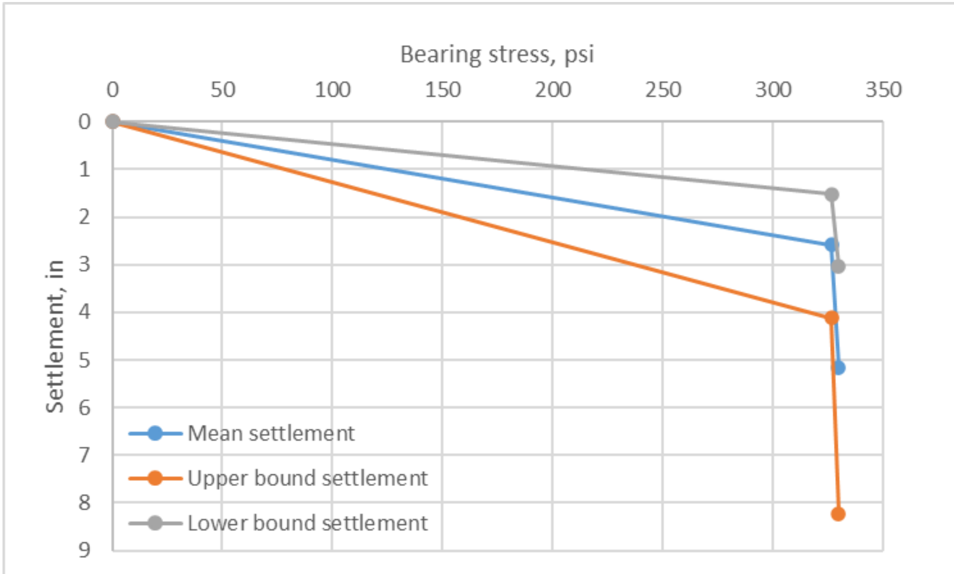

Figure B-1 Load-settlement response of worked example for Florida homogeneous case.

B.1.2 Cemex Load Test

For the Cemex load test, a 3.5 ft by 3.5 ft square footing embedded 5 ft is found on a 5.3-ft-thick medium strength rock (a geomean of 93 pcf) underlain by a much stronger layer (120 pcf) beneath. Using a closest mass strength envelope of 97.2 pcf, the bearing capacity calculation is shown in Table B-3 . For the probabilistic settlement prediction, a vertical correlation length (a_v) of 4.5 ft is used to provide a better quantification of spatial correlation structure instead of 3 ft used in Phase 2. Detailed settlement calculations are shown in Table B-4 using mass properties and footing geometry provided in Table B-3. The measured and predicted load-settlement response is shown in Figure B-3. ,great agreement is achieved.

Table B-3 Bearing capacity calculation of Cemex load test.

<table>
<tr><td rowspan="4">Footing Geometry</td><td>B, ft</td><td>3.5</td></tr>
<tr><td>L, ft</td><td>3.5</td></tr>
<tr><td>D_f, ft</td><td>5</td></tr>
<tr><td>D_w, ft</td><td>0</td></tr>
<tr><td>Total unit weight</td><td>γ_{total}, pcf</td><td>115</td></tr>
<tr><td rowspan="4">Mass Properties</td><td>c_m, psi</td><td>31.9</td></tr>
<tr><td>φ_m, °</td><td>32.4</td></tr>
<tr><td>P_p, psi</td><td>341.8</td></tr>
<tr><td>ω_m, °</td><td>4.35</td></tr>
<tr><td rowspan="11">Florida Bearing Capacity Equations</td><td>N_c</td><td>$\frac{1.8\ \cos\varphi}{0.8-\sin\varphi} = \frac{1.8\ \cos(32.4)}{0.8-\sin(32.4)} = 5.75$</td></tr>
<tr><td>N'_c</td><td>$\frac{1.8\ \cos\varphi}{0.8-\sin\omega} = \frac{1.8\ \cos(32.4)}{0.8-\sin(4.35)} = 2.10$</td></tr>
<tr><td>N_g</td><td>$\frac{1.8\ [\sin\varphi - \sin\omega]}{0.8-\sin\omega} = \frac{1.8\ [\sin(32.4) - \sin(4.35)]}{0.8-\sin(4.35)} = 1.14$</td></tr>
<tr><td>q, psi</td><td>5 × (115-62.4)/144 = 1.83 (overburden stress)</td></tr>
<tr><td>N_q</td><td>$(1.5 \times \frac{p_p}{\sigma_a} - 10) \times (3 \times \sin\varphi\ -\ 1) = (1.5 \times \frac{341.8}{14.7} - 10) \times (3 \times \sin(32.4)\ -\ 1)\ = 15.1$</td></tr>
<tr><td>n</td><td>$\left(\frac{4}{0.3\text{B in ft}}\right)^{-0.055} = \left(\frac{4}{0.3*3.5}\right)^{-0.055} = 0.93$</td></tr>
<tr><td>ξ</td><td>$1\ +\ 0.245\ \left(\frac{B}{L}\right)^{0.66} = 1\ +\ 0.245\ \left(\frac{3.5}{3.5}\right)^{0.66} = 1.245$</td></tr>
<tr><td>N_R</td><td>1</td></tr>
<tr><td>Q_{u1}, psi</td><td>$n \times c \times N_c + q \times N_q = 0.93 \times 31.9 \times 5.75 + 1.83 \times 15.1 = 198.22$</td></tr>
<tr><td>Q_{u2}, psi</td><td>$n \times [c \times N'_c + p_p \times N_g] + q \times N_q = 0.93 \times [31.9 \times 2.1 + 341.8 \times 1.14] + 1.83 \times 15.1 = 452.31$</td></tr>
<tr><td>Q_u</td><td>$\min(Q_{u1}, Q_{u2}) \times \xi / N_R = \min(198.22, 452.31) \times 1.245/1 = 246.78$ psi = 17.77 tsf</td></tr>
</table>

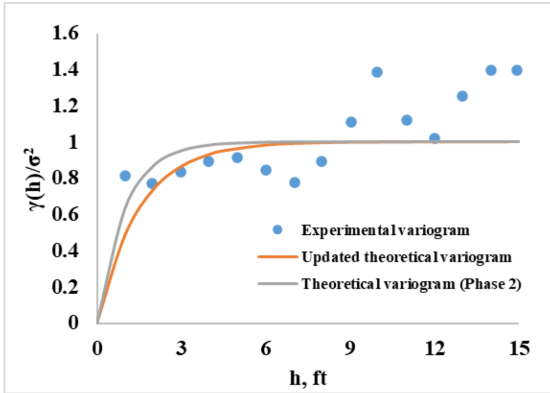

Figure B-2 Updated variogram analysis for Cemex load test.

Table B-4 Probabilistic settlement calculation of worked example for Cemex load test.

Mass properties	E_m, ksi	13.324
	CV_{Em}	1.37
	σ_E, ksi	$CV_{Em} \times E_m$, = 1.37 × 13.324 = 18.25
	ν	0.1 (Poisson's ratio)
	a_v, ft	4.5 (Correlation length)
	n	0.75
Geometry	B, ft	3.5 (Footing width)
	L, ft	3.5
	T_r, ft	5.3
	t, in	2
	$E_{foundation}$, ksi	29000
	K_F	$\frac{E_{foundation}}{E_m}(\frac{t}{a})^3 = \frac{29000}{13.324}(\frac{2}{\sqrt{BL/\pi}})^3 = \frac{29000}{13.324}(\frac{2}{\sqrt{144\times3.5\times3.5/3.14}})^3 = 1.31$
	I_F	$\frac{\pi}{4}+\frac{1}{(4.6+10K_F)} = \frac{\pi}{4}+\frac{1}{(4.6+10\times1.31)} = 0.84$
	C	C_s*I_F = 0.84*1.12 = 0.94 (L/B = 3.5/3.5 = 1, C_s = 1.12 from Table 3)
Bearing value	Q_u, psi	246.78
Fenton and Griffiths' method	δ_{det}, in	$Qu\frac{B}{\mu_E}C(1-\nu^2) = \frac{246.78\times3.5\times12\times0.94\times(1-0.1^{\wedge}2)}{13324} = 0.73$
	σ_{lnE}	$\sqrt{ln(1+\sigma_E^2(above)/\mu_E^2(above))} = \sqrt{ln(1+18250^2/13324^2)} = 1.03$
	$\gamma(T_r)$	$\frac{2a_v^2}{9{T_r}^2}\left[\frac{3\|T_r\|}{a_v}+e^{(-\frac{3\|T_r\|}{a_v})}-1\right] = \frac{2\times4.5^2}{9\times5.3^2}\left[\frac{3\|5.3\|}{4.5}+e^{(-\frac{3\|5.3\|}{4.5})}-1\right] = 0.41$
	$\sigma_{ln\delta}$	$\sqrt{\gamma(T)}\sigma_{\ln E}$(above) $=\sqrt{0.41}\times 1.03 = 0.66$
	$\mu_{ln\delta}$	$\ln(\delta_{det}(above))+\frac{1}{2}\sigma^2_{\ln E}$(above)=ln(0.73)+$\frac{1}{2}1.03^2$= 0.21
	μ_δ, in	$exp\left\{\mu_{\ln\delta}(above)+\frac{1}{2}\sigma^2_{\ln\delta}(above)\right\}$= exp(0.21+$\frac{1}{2}66^2$)= 1.54
	σ_δ, in	$\mu_\delta(above)\sqrt{e^{\sigma^2_{\ln\delta}(above)}-1} = 1.54\sqrt{e^{0.66^2}-1} = 1.13$
	δ_{LB}, in	exp($\mu_{ln\delta}$ - n $\sigma_{ln\delta}$) = exp(0.21-0.75*0.66) = 0.76
	δ_{UB}, in	exp($\mu_{ln\delta}$ + n $\sigma_{ln\delta}$) = exp(0.21+0.75*0.66) = 2.03

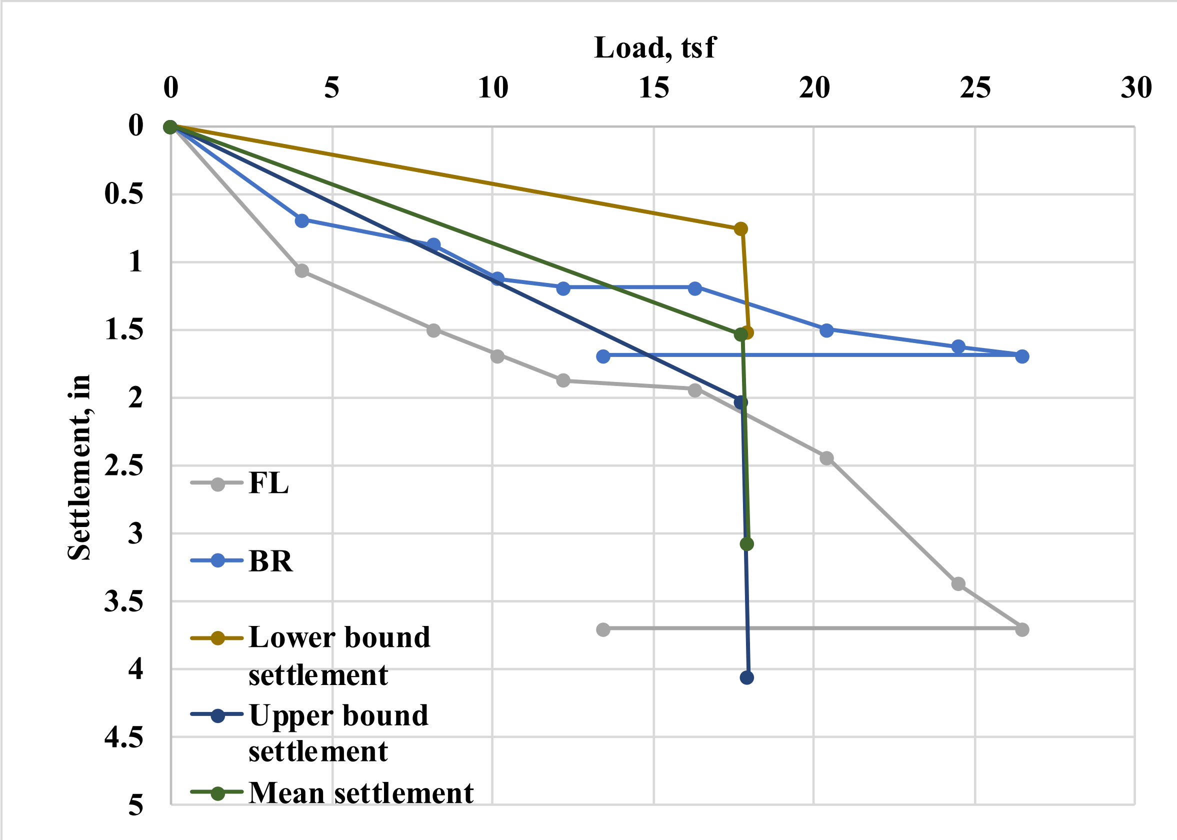

Figure B-3 Measured and predicted load-settlement response for Cemex load test (BR: back right, FL: front left, representing corners of footing).

B.2 SR84 and Bell Load Tests (Rock-Over-Sand)

B.2.1 SR84 Load Test

Figure B-4. presents the bulk dry unit weight versus depth at the load test location (B-03) and a SPT profile (B-04) 40 ft away from footing location. Competent Miami limestone starts around 3 ft below ground surface down to 13 ft and a 20-ft-thick medium-dense sand layer beneath it overlying a Fort Thompson rock layer down to a depth of 60 ft.

The median bulk dry unit weight of Miami limestone layer is 109.8 pcf, it is recommended to use the median or geomean value (lower one) to characterize the strength and stiffness of rock layer. A site-specific strength envelope of 108.85 pcf is used here with an adjusted recovery of 78% is used. A set of mass strength parameters are obtained: c_m = 44 psi, φ_m = 35.4°, P_{pm} = 392 psi and ω_m = 6° and a mass modulus of 33710.52 psi is assessed for the Miami limestone layer (E_{mass}/E_{intact} = 0.52). Using Bowles' method (Bowles, 1996) for saturated sand, a sand modulus of 2031 psi (SPT-N_{ES} = 41) is obtained. Please note that $N_{ES} = 1.24N_{AUTO}$ as recommended by Soils and Foundations Handbook (FDOT, 2022). The bearing capacity calculation using Florida bearing capacity equation for a footing with a width (B) of 5 ft, a length (L) of 6 ft and an embedment depth (D_f) of 3 ft, shown in Table B-5 .

For the settlement prediction, mass modulus is obtained based on the bulk dry unit weight and adjusted REC using Figure 3-5 and Figure 3-12a. Using modulus ratio (E_m/E_s) of rock and sand layer as well as the ratio of rock thickness (Tr) and equivalent footing radius ($a = \sqrt{BL/\pi}$), stress-dependent weighted harmonic mean modulus (E_{eq}) is assessed at the rock failure and post-failure with Figure 3-7 & Figure 3-8. The post bearing capacity is assumed to be 1.175Qu and the secant modulus used for post-settlement is reduced to half of the initial modulus. The predicted versus measured load-settlement response is shown in Figure B-5. , great agreement is achieved.

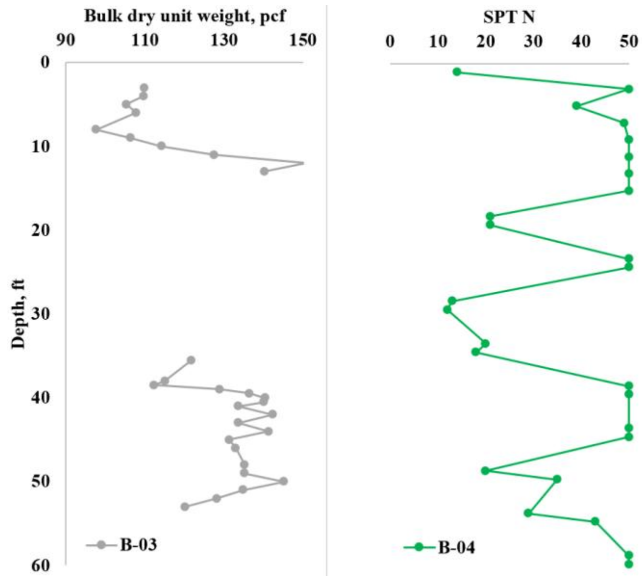

Figure B-4 Rock coring and SPT profile at SR84 site.

Table B-5 Bearing capacity calculation at SR84 site.

Footing Geometry	B, ft	5
	L, ft	6
	e_B, ft	0
	e_L, m	0
	D_f, ft	3
	D_w, ft	3
	T_r, ft	10
	T_s, ft	20
Total Unit Weight	g_{total}, pcf	110
Mass Properties	c_m, psi	44
	φ_m, °	35.4
	P_{pm}, psi	392
	ω_m, °	6
	E_m, psi	33710.52
Sand Modulus	E_s, psi	2031 (250×(41+15) = 14000 kPa to 2031 psi)
Florida Bearing Capacity Equations	N_c	$\frac{1.8\ \cos\varphi_m}{0.8-\sin\varphi_m} = \frac{1.8\ \cos(35.4)}{0.8-\sin(35.4)} = 6.65$
	N'_c	$\frac{1.8\ \cos\varphi_m}{0.8-\sin\omega_m} = \frac{1.8\ \cos(35.4)}{0.8-\sin(6)} = 2.11$
	N_g	$\frac{1.8\ [\sin\varphi_m - \sin\omega_m]}{0.8-\sin\omega_m} = \frac{1.8\ [\sin(35.4) - \sin(6)]}{0.8-\sin(6)} = 1.23$
	q, psi	$3(D_f) \times 110/144 = 2.30$
	N_q	$(1.53 \times \frac{p_{pm}}{\sigma_a} - 10) \times (3 \times \sin\varphi_m - 1) = (1.53 \times \frac{392}{14.7} - 10) \times (3 \times \sin(35.4) - 1) = 22.73$
	n	$\left(\frac{4}{0.3048\text{B in ft}}\right)^{-0.055} = \left(\frac{4}{0.3048*5}\right)^{-0.055} = 0.95$
	ξ	$1 + 0.245 \left(\frac{B}{L}\right)^{0.66} = 1 + 0.245 \left(\frac{5}{6}\right)^{0.66} = 1.22$
	R	$0.093 T_r^2 \left(\frac{E_s}{E_m}\right) = 0.093 \times 10^2 \frac{2031}{33710.52} = 0.56$
	N_R	$1.2-0.1R = 1.2-0.1\times0.56 = 1.14$
	Q_{u1}, psi	$n\times c_m\times N_c + q\times N_q = 0.95\times 44 \times 6.65 + 2.3\times22.73 = 329.64$
	Q_{u2}, psi	$n\times [c_m\times N'_c + p_{pm}\times N_g] + q\times N_q = 0.95\times [44 \times 2.11 + 392\times 1.23] + 2.3\times22.73 = 597.07$
	Q_u, psi	$\min(Q_{u1}, Q_{u2}) \times \xi/N_R = \min(329.64, 597.07) \times1.22/1.14 = 352.77$ psi = 25.4 tsf

Table B-6 Settlement calculation for SR84 case.

Problem Geometry	B, ft	5
	L, ft	6
	T_r, ft	10
	T_s, ft	20
Settlement Parameters	a, ft	$\sqrt{(BL/\pi)} = 3.09$
	T_r/a	10/3.09 = 3.23
	E_m/E_s	33710.52/2031 = 16.60
	Q_u, psi	352.77 (25.4 tsf)
	σ_{sand}, psi	0.054×352.77= 19.05 (Figure 3-7)
Settlement @ rock bearing stress	Stress in rock: σ_i, psi	(352.77+19.05)/2 = 185.91
	Rock thickness T_i, ft	10
	Stress in sand: σ_i, psi	(19.05+0)/2=9.525
	Sand thickness T_i, ft	14.56 (T_{sz}, Figure 3-8)
	E_{eq}, psi	$\frac{10\times12\times185.91+14.56\times12\times9.525}{10\times12\times\frac{185.91}{33710.52}+14.56\times12\times\frac{9.525}{2031}} = 16185.4$ (Equation Equation 3-16)
	$E_{foundation}$, psi	29,000,000
	t (foundation thickness), in	8
	K_F	$\frac{E_{foundation}}{E_{eq}}\left(\frac{t}{a}\right)^3 = \frac{29000000}{16185.4}\left(\frac{8}{3.09\times12}\right)^3 = 17.99$
	C	$K_F > 10$, C = 0.79
	δ_{Qu}	$\frac{352.77\times12\times2\times3.09\times0.79\times(1-0.1^2)}{16185.4} = 1.26$ (Equation Equation 3-14)
Post settlement parameters	Qp_u, psi	352.77×1.175 = 414.50
	Post E_m, psi	16855.26 (E_m/2)
	Post E_m/E_s	16855.26/2031 = 8.3
	Post σ_{sand}, psi	0.0809×414.5 = 33.54 (Figure 3-7)
Post settlement	Stress in rock: σ_i, psi	(414.5+33.54)/2 = 224.02
	Rock thickness T_i, ft	10
	Stress in sand: σ_i, psi	(33.54+0)/2 = 16.77
	Sand thickness T_i, ft	11.47 (T_{sz}, Figure 3-8)

Problem Geometry	B, ft	5
	L, ft	6
	T_r, ft	10
	T_s, ft	20
	E_{eq}, psi	$\frac{10\times12\times224.02+11.47\times12\times16.77}{10\times12\times\frac{224.02}{16855.26}+11.47\times12\times\frac{16.77}{2031}} = 10687.32$ (Equation Equation 3-16)
	$E_{foundation}$, psi	29,000,000
	t (foundation thickness), in	8
	K_F	$\frac{E_{foundation}}{E_{eq}}(\frac{t}{a})^3 = \frac{29000000}{10687.32}(\frac{8}{3.09\times12})^3 = 27.25$
	C	$K_F > 10$, $C = 0.79$
	δ_{Qpu}	$\frac{(414.5)\times12\times2\times3.09\times0.79\times(1-0.1^2)}{10687.32} = 2.25$ (Equation Equation 3-15)

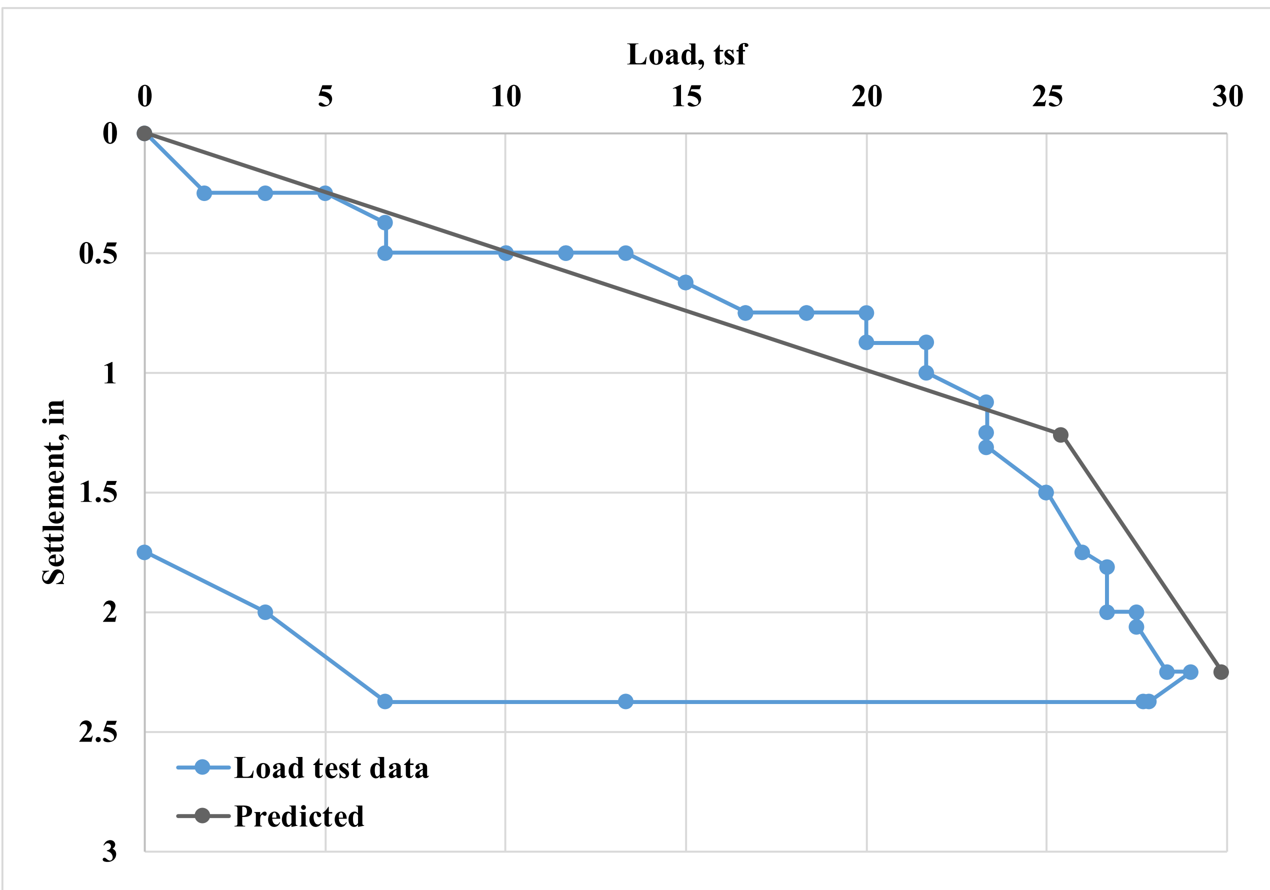

Figure B-5 Measured versus predicted load-settlement response at SR84 site.

B.2.2 Bell Load Test

The median bulk dry unit weight of Ocala limestone layer is 105 pcf, it is recommended to use the median or geomean value to characterize the strength and stiffness of rock layer. A site-specific strength envelope of 105 pcf is used here with an updated adjusted recovery of 78% compared to 83% used in Phase 2 due to lack of direct measurements at footing location. The nearest boring (20 ft from footing location) shows a geomean of 102 pcf and a median 100 pcf with an adjusted recovery of 58%, the seismic shear tests show a bulk dry unit weight of 106 pcf at the footing location and a bulk dry unit weight of 100 pcf at the nearest boring location.

A set of mass strength parameters are obtained: cm = 44.2 psi, φm = 28.07°, Ppm = 251.5 psi and ωm = 18.46° and a mass modulus of 31710.4 psi is assessed for the Miami limestone layer (Emass/Eintact = 0.52). Using Bowles' method, a sand modulus of 2067 psi (SPT-NES = 42) is obtained. The bearing capacity calculation using Florida bearing capacity equation for a footing with a width (B) of 5 ft, a length (L) of 5 ft and an embedment depth (Df) of 5 ft, shown in Table 47.

For the case of Ts smaller than Tsz, i.e., actual sand layer thickness smaller than the sand layer thickness from Figure 3-8, it is assumed that the stress at the bottom of the sand layer is σs×(1-Ts/Tsz) and use the half of σs and σs×(1-Ts/Tsz) as the induced stress in the sand layer in the calculation of stress-dependent weighted harmonic mean modulus, Eeq. The predicted settlement is evaluated in Table B-8 and plotted in Figure B-6. , great agreement is achieved compared to the measured response.

Table B-7 Bearing capacity calculation at Bell site.

Footing Geometry	B, ft	5
	L, ft	5
	e_B, ft	0
	e_L, m	0
	D_f, ft	5
	D_w, ft	12
	T_r, ft	5
	T_s, ft	2
Total Unit Weight	g_{total}, pcf	80
Mass Properties	c_m, psi	44.2
	φ_m, °	28.07
	P_{pm}, psi	251.5
	ω_m, °	18.46
	E_m, psi	31710.4
Sand Modulus	E_s, psi	2067 (250×(42+15) = 14250 kPa to 2067 psi)
Florida Bearing Capacity Equations	N_c	$\frac{1.8\ \cos\varphi}{0.8-\sin\varphi} = \frac{1.8\ \cos(28.07)}{0.8-\sin(28.07)} = 4.82$
	N'_c	$\frac{1.8\ \cos\varphi}{0.8-\sin\omega} = \frac{1.8\ \cos(28.07)}{0.8-\sin(18.46)} = 3.29$
	N_g	$\frac{1.8\ [\sin\varphi - \sin\omega]}{0.8-\sin\omega} = \frac{1.8\ [\sin(28.07) - \sin(18.46)]}{0.8-\sin(18.46)} = 0.57$
	q, psi	5 (D_f) × 80/144 = 2.78
	N_q	$(1.53 \times \frac{p_p}{\sigma_a} - 10) \times (3 \times \sin\varphi\ -\ 1) = (1.53 \times \frac{251.5}{14.7} - 10) \times (3 \times \sin(28.07)\ -\ 1) = 6.66$
	R	$0.093T^2\ E_{soil} / E_{rock} = 0.093T^2\ E_{sand} / E_{mass} = 0.093 \times 5\text{^}2 \times (2067/31710.4) = 0.15$
	N_R	$0.86 * R^{-0.25} = 0.86 \times 0.15^{-0.25} = 1.38$
	n	$\left(\frac{4}{0.3\text{B in ft}}\right)^{-0.055} = \left(\frac{4}{0.3\times5}\right)^{-0.055} = 0.95$
	ξ	$1\ +\ 0.245\ \left(\frac{B}{L}\right)^{0.66} = 1\ +\ 0.245\ \left(\frac{5}{5}\right)^{0.66} = 1.245$
	Q_{u1}, psi	$ncN_c + qN_q = 0.95 \times 44.2 \times 4.82 + 2.78 \times 6.66 = 220.59$
	Q_{u2}, psi	$n[cN'_c + p_pN_g] + q*N_q = 0.95 \times [44.2 \times 3.29 + 251.5 \times 0.57] + 2.78 \times 6.66 = 292.94$
	Q_u, psi	min (Q_{u1}, Q_{u2}) × ξ/N_R =min(220.59, 292.94) ×1.245/1.38= 199.25 psi = 14.34 tsf

Table B-8 Settlement calculation at Bell site.

Problem Geometry	B, ft	5
	L, ft	5
	T_r, ft	5
	T_s, ft	2
Settlement Parameters	a, ft	$\sqrt{(BL/\pi)} = 2.82$
	T_r/a	5/2.82 = 1.77
	E_m/E_s	31710.4/2067 = 15.34
	Q_u, psi	199.25 (14.34 tsf)
	σ_{sand}, psi	0.1152×199.25 = 22.95 (Figure 3-7)
Settlement @ rock bearing stress	Stress in rock: σ_i, psi	(199.25+22.95)/2 = 111.10
	Rock thickness T_i, ft	5
	Stress in sand: σ_i, psi	$(22.95+22.95\times(1-\frac{2\ (Ts)}{10.73\ (Tsz,\ \text{Figure 3-7})}))/2 =$ 20.81
	Sand thickness T_i, ft	2 (Ts < Tsz)
	E_{eq}, psi	$\frac{60\times111.1+24\times20.81}{60\times\frac{111.1}{31710.4}+24\times\frac{20.81}{2067}} = 15856.89$ (Equation Equation 3-16)
	$E_{foundation}$, psi	29,000,000
	t (foundation thickness), in	6.7
	K_F	$\frac{E_{foundation}}{E_{eq}}(\frac{t}{a})^3 = \frac{29000000}{15856.89}(\frac{6.7}{2.82\times12})^3 = 14.18$
	C	$K_F > 10$, C = 0.79
	δ_{Qu}	$\frac{199.25\times12\times2\times2.82\times0.79\times(1-0.1^2)}{15856.89} = 0.67$ (Equation Equation 3-14)
Post settlement parameters	Qp_u, psi	199.25×1.175 = 234.12
	Post E_m, psi	15855.19 ($E_m/2$)
	Post E_m/E_s	15855.19/2067 = 7.67
	Post σ_{sand}, psi	0.1742×238.91 = 41.62 (Figure 3-7)
Post settlement	Stress in rock: σ_i, psi	(238.91+41.62)/2 = 140.26
	Rock thickness T_i, ft	5
	Stress in sand: σ_i, psi	$(41.62+41.62\times(1-\frac{2\ (Ts)}{8.66\ (Tsz,\ \text{Figure 3-7})}))/2 = 36.07$
	Sand thickness T_i, ft	2 (Ts < Tsz)
	E_{eq}, psi	$\frac{5\times12\times140.26+2\times12\times36.07}{5\times12\times\frac{140.26}{15855.19}+2\times12\times\frac{36.07}{2067}} = 9704.77$ (Equation Equation 3-16)
	$E_{foundation}$, psi	29,000,000
	t (foundation thickness), in	6.7

Problem Geometry	B, ft	5
	L, ft	5
	T_r, ft	5
	T_s, ft	2
	K_F	$\frac{E_{foundation}}{E_{eq}}(\frac{t}{a})^3 = \frac{29000000}{9704.77}(\frac{6.7}{2.82\times12})^3 = 23.17$
	C	$K_F > 10$, C = 0.79
	δ_{Qpu}	$\frac{(234.12)\times12\times2\times2.82\times0.79\times(1-0.1^2)}{9704.77} = 1.28$ (Equation Equation 3-15)

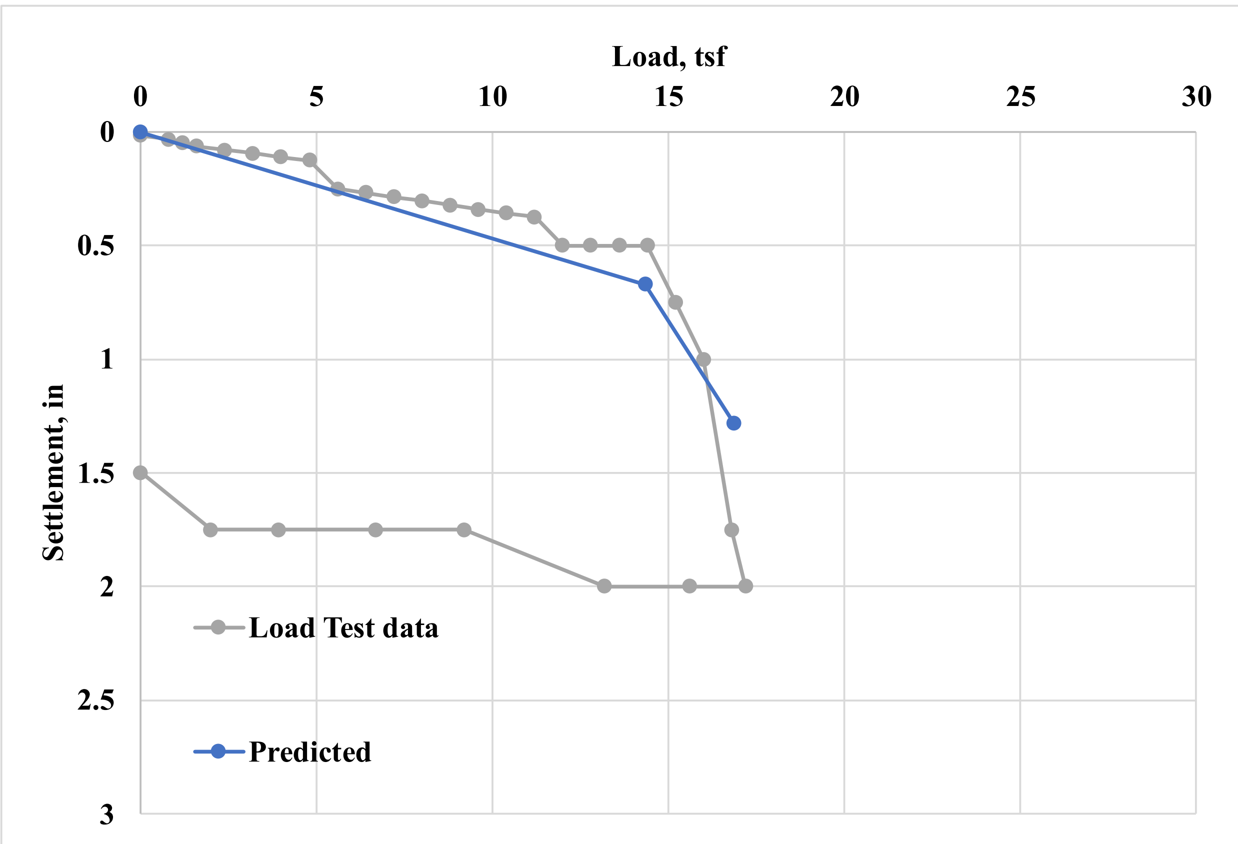

Figure B-6 Measured versus predicted load-settlement response at Bell site.

B.3 Worked Examples of Carter and Kulhawy Strip Footing (Homogeneous)

B.3.1 Worked Example 1

Table B-9 Bearing capacity calculations for Carter-Kulhawy bearing analysis.

<table>
<tr><td rowspan="5">Input Properties</td><td>B, ft</td><td>10</td></tr>
<tr><td colspan="2">This method is only for the case of plane-strain condition at the ground surface of an infinite rock subsurface</td></tr>
<tr><td>q_u, psi</td><td>281.2</td></tr>
<tr><td>m_i</td><td>10</td></tr>
<tr><td>GSI</td><td>61</td></tr>
<tr><td rowspan="2">Mass strength</td><td>s</td><td>s = $e^{(GSI-100)/9}$ = $e^{(61-100)/9}$= 0.01</td></tr>
<tr><td>m</td><td>m = $m_i e^{(GSI-100)/28}$ = $10e^{(61-100)/28}$= 2.48</td></tr>
<tr><td>Carter-Kulhawy Bearing</td><td>Q_u, psi</td><td>$[\sqrt{s} + \sqrt{m\sqrt{s} + s}]q_u = [\sqrt{0.01} + \sqrt{2.48\sqrt{0.01} + 0.01}]281.2 =$ 185.63 psi = 13.36 tsf</td></tr>
</table>

Table B-10 Settlement calculation of flexible footing using Carter and Kulhawy bearing.

Input parameters	E_m, psi	11342.46
	CV_{Em}	1 (σ_E = CV ×E_m = 1×11342.46 = 11342.46)
	ν	0.1 (Poisson's ratio)
	a_v, ft	5 (Correlation length)
	B, ft	10 (Footing width)
	T, ft	40
	Settlement Range (n)	0.5
	Rigidity	flexible
Bearing value	Q_u, psi	185.63
Fenton and Griffiths' method	δ_{det}, in	$Qu\frac{B}{\mu_E}\,C(1-\nu^2) = \frac{185.63\times10\times12\times2.54\times(1-0.01)}{11342.46}$= 4.94 (C=2.54 for flexible footing)
	σ_{lnE}	$\sqrt{ln(1+\sigma_E^2(above)/\mu_E^2(above))}$ = $\sqrt{ln(1+11342.46^2/11342.46^2)}$ = 0.83
	$\gamma(T)$	$\frac{2a_v^2}{9T^2}\left[\frac{3\lvert T\rvert}{a_v}+e^{(-\frac{3\lvert T\rvert}{a_v})}-1\right]$=$\frac{2\times5^2}{9\times40^2}\left[\frac{3\lvert 40\rvert}{5}+e^{(-\frac{3\lvert 40\rvert}{5})}-1\right]$ = 0.08
	$\sigma_{ln\delta}$	$\sqrt{\gamma(T)}\sigma_{\ln E}$(above) =0.28 × 0.83 = 0.23
	$\mu_{ln\delta}$	$\ln(\delta_{det}(above))+\frac{1}{2}\sigma_{\ln E}^2$(above)=ln(4.94)+ $\frac{1}{2}0.83^2$= 1.94
	μ_δ, in	$exp\left\{\mu_{\ln\delta}(above)+\frac{1}{2}\sigma_{\ln\delta}^2(above)\right\}$= exp(1.94+ $\frac{1}{2}0.23^2$)= 7.15
	σ_δ, in	$\mu_\delta(above)\sqrt{e^{\sigma_{\ln\delta}^2(above)}-1}$ = $7.15\sqrt{e^{0.23^2}-1}$ = 1.67
	δ_{LB}, in	exp($\mu_{ln\delta}$ - n $\sigma_{ln\delta}$) = exp(1.94-0.5*0.23) = 6.20
	δ_{UB}, in	exp($\mu_{ln\delta}$ + n $\sigma_{ln\delta}$) = exp(1.94+0.5*0.23) = 7.81

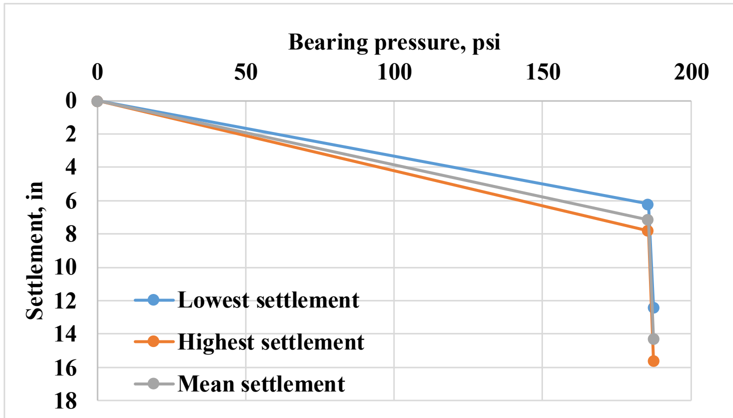

Figure B-7 Load-settlement response of flexible footing.

B.3.2 Worked Example 2

Table B-11 Settlement calculation of rigid footing using Carter and Kulhawy bearing.

Input parameters	E_m, psi	11342.46
	CV_{Em}	1 (σ_E = CV $\times E_m$ = 1×11342.46 = 11342.46)
	ν	0.1 (Poisson's ratio)
	a_v, ft	5 (Correlation length)
	B, ft	10 (Footing width)
	T, ft	40
	Settlement Range (n)	0.5
	Rigidity	rigid
Bearing value	Q_u, psi	185.63
Fenton and Griffiths' method	δ_{det}, in	$Qu\frac{B}{\mu_E}\,C(1-\nu^2) = \frac{185.63\times10\times12\times2.10\times(1-0.01)}{11342.46} = 4.08$ (C = 2.10 for rigid footing)
	$\sigma_{\ln E}$	$\sqrt{ln(1+\sigma_E^2(above)/\mu_E^2(above))} = \sqrt{ln(1+11342.46^2/11342.46^2)} = 0.83$
	$\gamma(T)$	$\frac{2a_v^2}{9T^2}\left[\frac{3\lvert T\rvert}{a_v}+e^{(-\frac{3\lvert T\rvert}{a_v})}-1\right]=\frac{2\times5^2}{9\times40^2}\left[\frac{3\lvert 40\rvert}{5}+e^{(-\frac{3\lvert 40\rvert}{5})}-1\right] = 0.08$
	$\sigma_{\ln\delta}$	$\sqrt{\gamma(T)}\sigma_{\ln E}$(above) $=0.28\times0.83=0.23$
	$\mu_{\ln\delta}$	$\ln(\delta_{det}(above))+\frac{1}{2}\sigma^2_{\ln E}$(above)=ln(4.08)+ $\frac{1}{2}0.83^2$= 1.75
	μ_δ, in	$exp\left\{\mu_{\ln\delta}(above)+\frac{1}{2}\sigma^2_{\ln\delta}(above)\right\}$= exp(1.75+ $\frac{1}{2}0.23^2$)= 5.91
	σ_δ, in	$\mu_\delta(above)\sqrt{e^{\sigma^2_{\ln\delta}(above)}-1} = 5.91\sqrt{e^{0.23^2}-1} = 1.38$
	δ_{LB}, in	exp($\mu_{\ln\delta}$ - n $\sigma_{\ln\delta}$) = exp(1.75-0.5*0.23) = 5.13
	δ_{UB}, in	exp($\mu_{\ln\delta}$ + n $\sigma_{\ln\delta}$) = exp(1.75+0.5*0.23) = 6.46

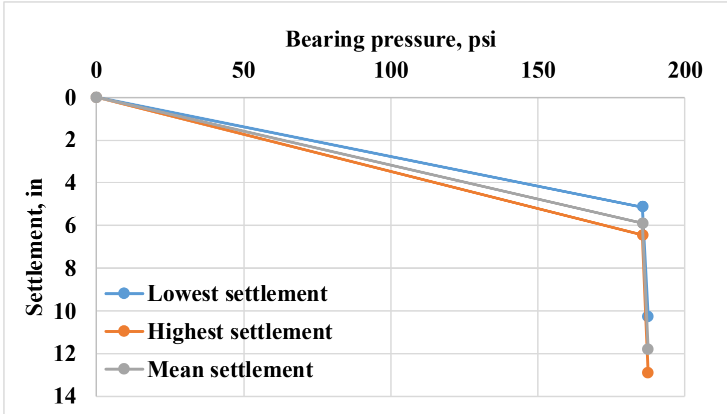

Figure B-8 Load-settlement response of rigid footing.

APPENDIX C
VALIDATION OF FB-MULTIPIER CODE FOR PASSIVE RESISTANCE

C.1 Worked Example Passive C-PHI Material Model

C.1.1 Passive C-PHI

The worked example is for a 5 ft by 5 ft rectangular rigid footing embedded 5 ft in a granular material. This worked example determines the passive hyperbolic curve Soil properties, footing geometry and calculations are provided in Table B-1 . Passive footing load vs displacement is plotted in Figure B-1.

Table C-1 Bearing capacity calculation of worked example for Florida homogeneous case.

Footing Geometry	B, ft	5
	L, ft	5
	t,ft	5
	D_f, ft	5
	D_t, ft	0
	H, ft	$H = D_f - D_t = 5 - 0 = 5$ $H \leq t$
	D_w, ft	100
Soil Properties	$g_{total,}$ pcf	121
	f, °	39
	c, psf	208
	ν	0.27
	E_i, psi	13888
	d, °	26
	Δ_{max}, in	3
	q_{FBMP}, psf	(Vertical Effective stress calculated at top of footing) 0
	q_{user}, psf	0
Initial Stiffness	K_1	$K_1 = \frac{2D_f}{B} = \frac{2*5}{5} = 2$
	K_2	$K_2 = \frac{2D_t}{B} = \frac{2*0}{5} = 0.0000001$ If Dt=0, than K2 = 0.0000001
	F_1	

Footing Geometry	B, ft	5
	L, ft	5
	t,ft	5
	D_f, ft	5
	D_t, ft	0
	H, ft	$H = D_f - D_t = 5 - 0 = 5$ $H \leq t$
	D_w, ft	100
		$F_1 = -(K_1 - K_2)\ln\left(\frac{K_1 - K_2}{2 + \sqrt{4 + (K_1 - K_2)^2}}\right) - 2\ln\left(\frac{2}{(K_1 - K_2) + \sqrt{4 + (K_1 - K_2)^2}}\right) = 3.5255$
Initial Stiffness (cont.)	F_2	$F_2 = 2\ln\left(\frac{2\left(K_1 + \sqrt{1 + K_1^2}\right)}{(K_1 + K_2) + \sqrt{4 + (K_1 + K_2)^2}}\right) + (K_1 - K_2)\ln\left(2 + \frac{\sqrt{4 + (K_1 + K_2)^2}}{(K_1 + K_2)}\right) - K_1^2\left(\frac{\sqrt{4 + (K_1 + K_2)^2}}{(K_1 + K_2)} - \frac{\sqrt{1 + K_1^2}}{K_1}\right) = 2.3957$
	F_3	$F_3 = -2K_1\ln\left(\frac{K_1}{1 + \sqrt{1 + K_1^2}}\right) + (K_1 + K_2)\ln\left(\frac{(K_1 + K_2)}{2 + \sqrt{4 + (K_1 + K_2)^2}}\right) - \ln\left(\frac{(K_1 + K_2) + \sqrt{4 + (K_1 + K_2)^2}}{2\left(K_1 + \sqrt{1 + K_1^2}\right)}\right) + \frac{(K_1 + K_2)}{4}\left[\sqrt{4 + (K_1 + K_2)^2} - (K_1 + K_2)\right] - K_1\left(\sqrt{1 + K_1^2} - K_1\right) = 0.6664$
	F_4	$F_4 = -2\ln\left(\frac{2\left(K_2 + \sqrt{1 + K_2^2}\right)}{(K_1 + K_2) + \sqrt{4 + (K_1 + K_2)^2}}\right) + (K_1 - K_2)\ln\left(\frac{2 + \sqrt{4 + (K_1 + K_2)^2}}{(K_1 + K_2)}\right) + K_2^2\left(\frac{\sqrt{4 + (K_1 + K_2)^2}}{(K_1 + K_2)} - \frac{\sqrt{1 + K_2^2}}{K_2}\right) = 3.5255$

Footing Geometry	B, ft	5
	L, ft	5
	t,ft	5
	D_f, ft	5
	D_t, ft	0
	H, ft	$H = D_f - D_t = 5 - 0 = 5$ $H \leq t$
	D_w, ft	100
	F_5	$F_5 = 2K_2 \ln\left(\frac{K_2}{1+\sqrt{1+K_2^2}}\right) - (K_1+K_2)\ln\left(\frac{(K_1+K_2)}{2+\sqrt{4+(K_1+K_2)^2}}\right) + \ln\left(\frac{(K_1+K_2)+\sqrt{4+(K_1+K_2)^2}}{2\left(K_2+\sqrt{1+K_2^2}\right)}\right) - \frac{(K_1+K_2)}{4}\left[\sqrt{4+(K_1+K_2)^2}-(K_1+K_2)\right] - K_2\left(K_2-\sqrt{1+K_2^2}\right) = 2.2299$
	p ksi	1 ksi Arbitrary value
	y_1	$y_1 = \frac{pB(1+\nu)}{16\pi E_i(1-\nu)}\{(3-4\nu)F_1 + F_4 + 4(1-2\nu)(1-\nu)F_5\} = 1.987\ in$
Initial Stiffness (cont.)	y_2	$y_2 = \frac{pB(1+\nu)}{16\pi E_i(1-\nu)}\{(3-4\nu)F_1 + F_2 + 4(1-2\nu)(1-\nu)F_3\} = 1.504\ in$
	y_c	$y_c = \frac{y_1+y_2}{2} = 1.746\ in$
	P	$P = pBt = 3600\ kips$
	k_{max}	$k_{max} = \frac{P}{y_c} = \frac{360000\ lbs}{0.09735\ in} = 2062\ kip/in$
Ultimate Earth Pressure Force	$K_{p\phi}$	$K_{p\phi} = 11.08$ Kphi equation
	K_{pc}	$K_{pc} = 10.64$ Kc equation
	K_{pq}	$K_{pq} = 10.18$ Kq equation
	K_a	Ka Rankine $K_a = tan^2\left(45^{\circ} - \frac{\phi}{2}\right) = 0.228$

Footing Geometry	B, ft	5
	L, ft	5
	t,ft	5
	D_f, ft	5
	D_t, ft	0
	H, ft	$H = D_f - D_t = 5 - 0 = 5$ $H \leq t$
	D_w, ft	100
	S	$S = 1 - \frac{H}{D_t + H} = 0$
	R	$R = 1 + (K_{p\phi} - K_a)^{\frac{2}{3}} \left[1.1S^4 + \frac{1.6x}{1 + 5\frac{B}{H}} + \frac{0.4(K_{p\phi} - K_a)S^3x^2}{1 + 0.05\frac{B}{H}} \right] \leq 2 = 2.202 \rightarrow 2$ x=1 for single face.
	P_{ult}	$P_{ult} = R(0.5\gamma' H^2 K_{p\phi} + c'HK_{pc} + q_{FBMP}HK_{pq} + q_{user}HK_{pq})Bcos(\delta) = 250\ kip$
	R_f	$R_f = 1 - \frac{P_{ult}}{D_{max}\, k_{max}}$ =0.96
	P_{net}	$P_{net} = P_{ult} - P_{active} = R(0.5\gamma' H^2 K_{p\phi} + c'HK_{pc} + q_{FBMP}HK_{pq} + q_{user}HK_{pq})Bcos(\delta) - (0.5\gamma' H^2 K_a - 2c'H\sqrt{K_a} + q_{FBMP}HK_a + q_{user}HK_a)Bcos(\delta) = 253\ kip$ $P_{net} \geq P_{ult} \rightarrow P_{net} = P_{ult}$ Pnet results in being larger than Pult due to the negative cohesion term in the active portion of the equation. Thus the Pult value should be used.

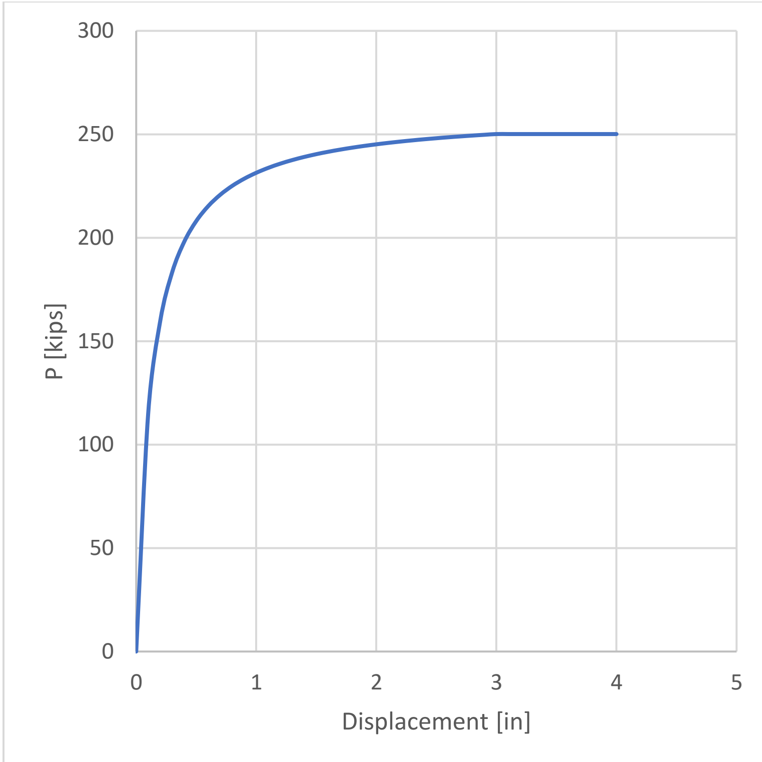

Figure C-1 Passive resistance vs displacement of worked example for granular material.

C.2 Worked Example Passive FL Limestone Model

C.2.1 Passive FL Limestone

The worked example is for a 5 ft by 5 ft rectangular rigid footing embedded 5 ft in a granular material. This worked example determines the passive hyperbolic curve Soil properties, footing geometry and calculations are provided in Table *C-2* . Passive footing load vs displacement is plotted in Figure C-1.

Table C-2 Worked example passive FL limestone model.

Formation	-	Miami Limestone
REC	%	80
γ_{dt}	pcf	100
ν		0.27
Extension Reduction Parameters	R_a	0.95
	R_α	0.75
	R_β	0.75
	R_{Pp}	0.8
	R_E	0.9
Compression Intact Properties (Output)	c_{ic}, psi	58.9 (Interpolated from Miami Limestone Database based on γ_{dt})
	φ_{ic}, °	44.2 (Interpolated from Miami Limestone Database based on γ_{dt})
	$\sigma_{peak\ ic}$, psi	562 (Interpolated from Miami Limestone Database based on γ_{dt})
	ω_{ic}, °	0.8 (Interpolated from Miami Limestone Database based on γ_{dt})
	a_{ic}, psi	42.2 (Interpolated from Miami Limestone Database based on γ_{dt})
	α_{ic}, °	34.9 (Interpolated from Miami Limestone Database based on γ_{dt})
	P_{pc}, psi	306 (Interpolated from Miami Limestone Database based on γ_{dt})
	β_{ic}, °	0.8 (Interpolated from Miami Limestone Database based on γ_{dt})
	E_{ic}, ksi	36.6
Compression Mass Properties (Output)	a_{mc}, psi	a_{mc} = REC*a_{ic} = 33.8
	α_{mc}, °	α_{mc} = atan(REC*tanα_{ic}) = 29.2
	P_{pc}, psi	$P_{pc} = P_{pc}$ = 306
	β_{mc}, °	β_{mc} = atan(REC*tanβ_{ic}) = 0.6
	c_{mc}, psi	$c_{mc} = \frac{a_{mc}}{cos\varphi_{mc}}$ = 40.7
	φ_{mc}, °	φ_{mc} = asin($tan\alpha_{mc}$) = 33.9

Formation	-	Miami Limestone
	$\sigma_{peak\ mc}$, psi	$\sigma_{peak\ mc} = P_{pc} + tan\alpha_{mc} * P_{pc} + a_{mc} = 511$
	ω_{mc}, °	$\omega_{mc} = asin(tan\beta_{mc}) = 0.6$
	E_{mc}, ksi	Emc/Eic =2.17 × REC_{adj} -1.17 = 0.566, Emc = 20.7
Extension Intact Properties (Output)	a_{ie}, psi	$a_{ie} = R_a * a_{ic} = 40.1$
	α_{ie}, °	$\alpha_{ie} = R_\alpha\ \alpha_{ic} = 26.2$
	P_{pe}, psi	$P_{pe} = R_{Pp}\ P_{pc} = 244.8$
	β_{ie}, °	$B_{ie} = R_\beta\ \beta_{ic} = 0.6$
	φ_{ie}, °	$\varphi_{ie} = asin(tan\alpha_{ie}) = 29.4$
	c_{ie}, psi	$c_{ie} = \frac{a_{ie}}{cos\varphi_{ie}} = 46.0$
	$\sigma_{peak\ ie}$, psi	$\sigma_{peak\ ie} = P_{pe} + tan\alpha_{ie} * P_{pe} + a_{ie} = 405.28$
	ω_{ie}, °	$\omega_{ie} = asin(tan\beta_{ie}) = 0.6$
	E_{ie}, ksi	$E_{ie} = R_E * E_{ic} = 32.9$
Extension Mass Properties (Output)	a_{me}, psi	$a_{me} = REC * a_{ie} = 32.1$
	α_{me}, °	$\alpha_{me} = atan(REC * tan\alpha_{ie}) = 21.5$
	P_{pe}, psi	$P_{pe} = P_{pe} = 244.8$
	β_{me}, °	$\beta_{me} = atan(REC * tan\beta_{ie}) = 0.5$
	c_{me}, psi	$c_{me} = \frac{a_{me}}{cos\varphi_{me}} = 34.9$
	φ_{me}, °	$\varphi_{me} = asin(tan\alpha_{me}) = 23.2$
	$\sigma_{peak\ me}$, psi	$\sigma_{peak\ me} = P_{pe} + tan\alpha_{me} * P_{pe} + a_{me} = 373.1$
	ω_{me}, °	$\omega_{me} = asin(tan\beta_{me}) = 0.5$
	E_{me}, ksi	Eme/Eie =2.17 × REC_{adj} -1.17 = 0.566, Eme = 18.6
Footing Geometry and Interface Properties	B, ft	5
	L, ft	5
	t,ft	5
	D_f, ft	5
	D_t, ft	0
	H, ft	$H = D_f - D_t = 5 - 0 = 5$ $H \leq t$
	D_w, ft	100
	d, °	26
	Δ_{max}, in	1.5
Rock Properties for Passive Dialog	g_{total}, pcf	121
	f, °	$\varphi_{me} = 23.2$
	c, psf	$c_{me} = 5023$
	ν	0.27
	E_i, psi	Eme = 18644
	d, °	15.5

Formation	-	Miami Limestone
	Δ_{max}, in	3
	q_{FBMP}, psf	(Vertical Effective stress calculated at top of footing) 0
	q_{user}, psf	0

Initial Stiffness	K_1	$K_1 = \frac{2D_f}{B} = \frac{2*5}{5} = 2$
	K_2	$K_2 = \frac{2D_t}{B} = \frac{2*0}{5} = 0.0000001$ If Dt=0, than K2 = 0.0000001
	F_1	$F_1 = -(K_1 - K_2)\ln\left(\frac{K_1 - K_2}{2 + \sqrt{4 + (K_1 - K_2)^2}}\right) - 2\ln\left(\frac{2}{(K_1 - K_2) + \sqrt{4 + (K_1 - K_2)^2}}\right) = 3.5255$
	F_2	$F_2 = 2\ln\left(\frac{2\left(K_1 + \sqrt{1 + K_1^2}\right)}{(K_1 + K_2) + \sqrt{4 + (K_1 + K_2)^2}}\right) + (K_1 - K_2)\ln\left(2 + \frac{\sqrt{4 + (K_1 + K_2)^2}}{(K_1 + K_2)}\right) - K_1^2\left(\frac{\sqrt{4 + (K_1 + K_2)^2}}{(K_1 + K_2)} - \frac{\sqrt{1 + K_1^2}}{K_1}\right) = 2.3957$
	F_3	$F_3 = -2K_1\ln\left(\frac{K_1}{1 + \sqrt{1 + K_1^2}}\right) + (K_1 + K_2)\ln\left(\frac{(K_1 + K_2)}{2 + \sqrt{4 + (K_1 + K_2)^2}}\right) - \ln\left(\frac{(K_1 + K_2) + \sqrt{4 + (K_1 + K_2)^2}}{2\left(K_1 + \sqrt{1 + K_1^2}\right)}\right) + \frac{(K_1 + K_2)}{4}\left[\sqrt{4 + (K_1 + K_2)^2} - (K_1 + K_2)\right] - K_1\left(\sqrt{1 + K_1^2} - K_1\right) = 0.6664$
	F_4	$F_4 = -2\ln\left(\frac{2\left(K_2 + \sqrt{1 + K_2^2}\right)}{(K_1 + K_2) + \sqrt{4 + (K_1 + K_2)^2}}\right) + (K_1 - K_2)\ln\left(\frac{2 + \sqrt{4 + (K_1 + K_2)^2}}{(K_1 + K_2)}\right) + K_2^2\left(\frac{\sqrt{4 + (K_1 + K_2)^2}}{(K_1 + K_2)} - \frac{\sqrt{1 + K_2^2}}{K_2}\right) = 3.5255$

	F_5	$F_5 = 2K_2 \ln\left(\frac{K_2}{1+\sqrt{1+K_2^2}}\right) - (K_1+K_2)\ln\left(\frac{(K_1+K_2)}{2+\sqrt{4+(K_1+K_2)^2}}\right) + \ln\left(\frac{(K_1+K_2)+\sqrt{4+(K_1+K_2)^2}}{2\left(K_2+\sqrt{1+K_2^2}\right)}\right) - \frac{(K_1+K_2)}{4}\left[\sqrt{4+(K_1+K_2)^2}-(K_1+K_2)\right] - K_2\left(K_2-\sqrt{1+K_2^2}\right) = 2.2299$
Initial Stiffness (cont)	P, ksi	1 Arbitrary value
	y_1	$y_1 = \frac{pB(1+\nu)}{16\pi E_i(1-\nu)}\{(3-4\nu)F_1 + F_4 + 4(1-2\nu)(1-\nu)F_5\} = 1.4803$
	y_2	$y_2 = \frac{pB(1+\nu)}{16\pi E_i(1-\nu)}\{(3-4\nu)F_1 + F_2 + 4(1-2\nu)(1-\nu)F_3\} = 1.1205\ in$
	y_c	$y_c = \frac{y_1+y_2}{2} = 1.3004\ in$
	P	$P = pBt = 3600\ lbs$
	k_{max}	$k_{max} = \frac{P}{y_c} = \frac{250000\ lbs}{0.046725\ \ in} = 2768.4\ kip/in$
Ultimate Earth Pressure Force	$K_{p\phi}$	$K_{p\phi} = 3.3016$ K_{phi} equation
	K_{pc}	$K_{pc} = 4.5742$ K_c equation
	K_{pq}	$K_{pq} = 3.2226$ K_q equation
	K_a	Ka Rankine $K_a = tan^2\left(45^\circ - \frac{\phi}{2}\right) = 0.4348$
	S	$S = 1 - \frac{t}{D_t + t} = 0$
	R	$R = 1 + \left(K_{p\phi} - K_a\right)^{\frac{2}{3}}\left[1.1S^4 + \frac{1.6x}{1+5\frac{B}{t}} + \frac{0.4\left(K_{p\phi}-K_a\right)S^3x^2}{1+0.05\frac{B}{t}}\right] = 1.5381$ x=1 for single face.
	P_{ult}	$P_{ult} = R\left(0.5\gamma' H^2 K_{p\phi} + c'HK_{pc} + q_{FBMP}HK_{pq} + q_{user}HK_{pq}\right)Bcos(\delta) = 889\ kip$
	R_f	$R_f = 1 - \frac{P_{ult}}{D_{max}\,k_{max}}$ =0.8896

	P_{net}	$P_{net} = R\big(0.5\gamma' H^2 K_{p\phi} + c' H K_{pc} + q_{FBMP} H K_{pq} + q_{user} H K_{pq}\big) B cos(\delta) - \big(0.5\gamma' H^2 K_a - 2c' H\sqrt{K_a} + q_{FBMP} H K_a + q_{user} H K_a\big) B cos(\delta) = 1045\ kip$ $P_{net} \geq P_{ult} \rightarrow P_{net} = P_{ult}$ Pnet results in being larger than Pult due to the negative cohesion term in the active portion of the equation. Thus the Pult value should be used.

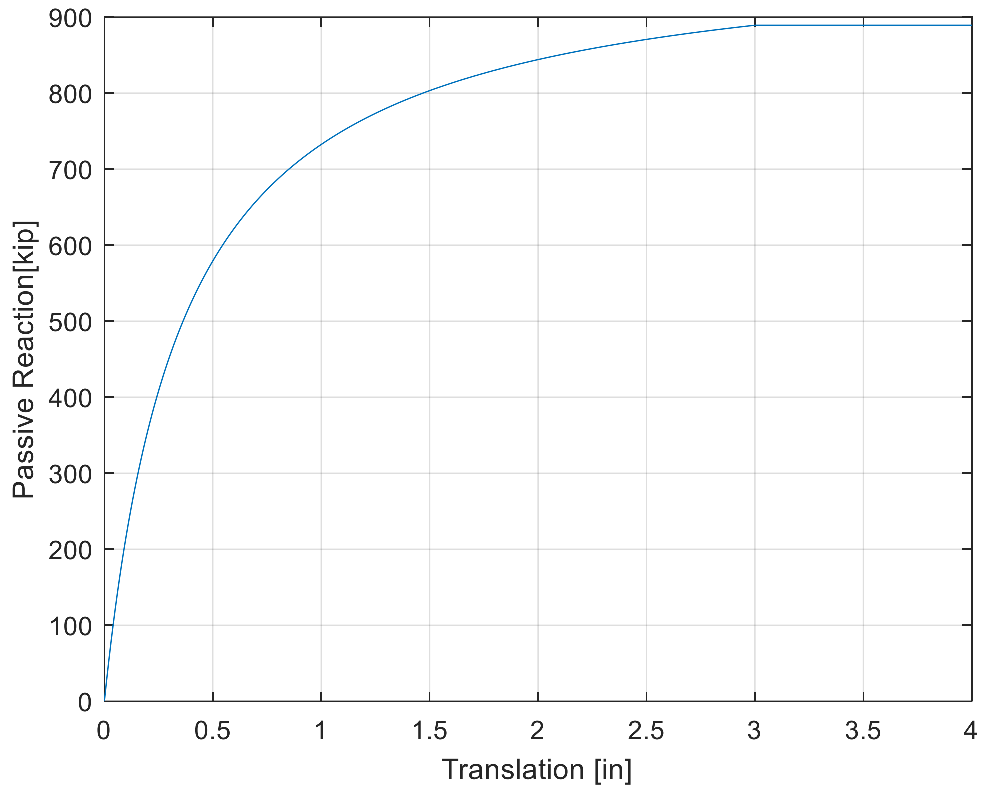

Figure C-2 Passive load displacement of worked example for FL limestone

C.3 Worked Example Friction Hyperbolic (Coulomb) Model

C.3.1 Friction Hyperbolic (Coulomb)

The worked example is for a 5 ft by 5 ft rectangular rigid footing embedded 5 ft in FL Limestone. This example determines the hyperbolic friction curve based on interface friction properties, and footing geometry provided in Table C-3 . Friction resistance vs displacement is plotted in Figure C-3. , based on the Normal load and footing dimensions specified in Table C-3.

Table C-3 Coulomb friction calculation of worked example.

Footing Geometry	B, ft	5
	L, ft	5
	t,ft	5
Footing Interface Properties	c, psf	5023
	α	0.5
	d, °	15
Hyperbolic Curve Parameters	P_{ult}, kips	1217
	R_f	0.85
	k_{max}, kip/in	2768
Footing Weight	N, kips	$N = 5 * 5 * 5 * 150 = 1875\ lbs = 18.75\ kips$
Ultimate Friction	F_{ult}, kips	$F_{ult} = BL\alpha c + Ntan(\delta) = 5 * 5 * 0.5 * \frac{5023}{1000} + 18.75 \tan(15) = 67.8\ kips$

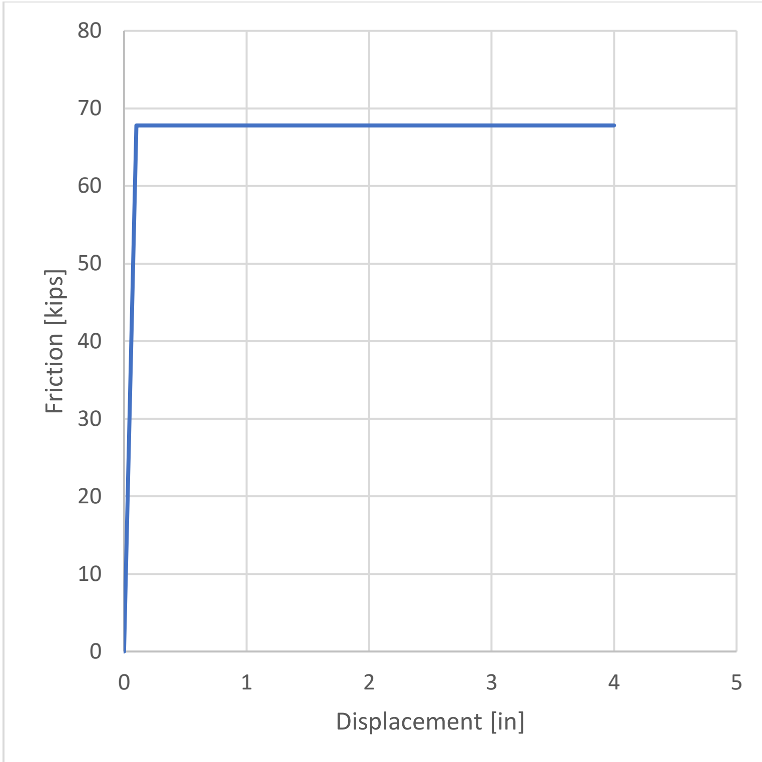

Figure C-3 Friction load displacement of worked example.

C.4 Equations for Kpf, Kpc, and Kpq

C.4.1 Kpϕ

Table C-4 Kpϕ from Liu et al. (2018).

Given Table from paper, K_{pphi}					
ϕ	δ/ϕ				
	0	***0.33333***	***0.50***	***0.67***	***1.00***
20	2.04	2.38	2.56	2.73	3.07
25	2.46	3.06	3.39	3.72	4.42
30	3.00	4.02	4.61	5.26	6.68
35	3.69	5.42	6.52	7.78	10.76
40	4.60	7.58	9.67	12.24	18.86

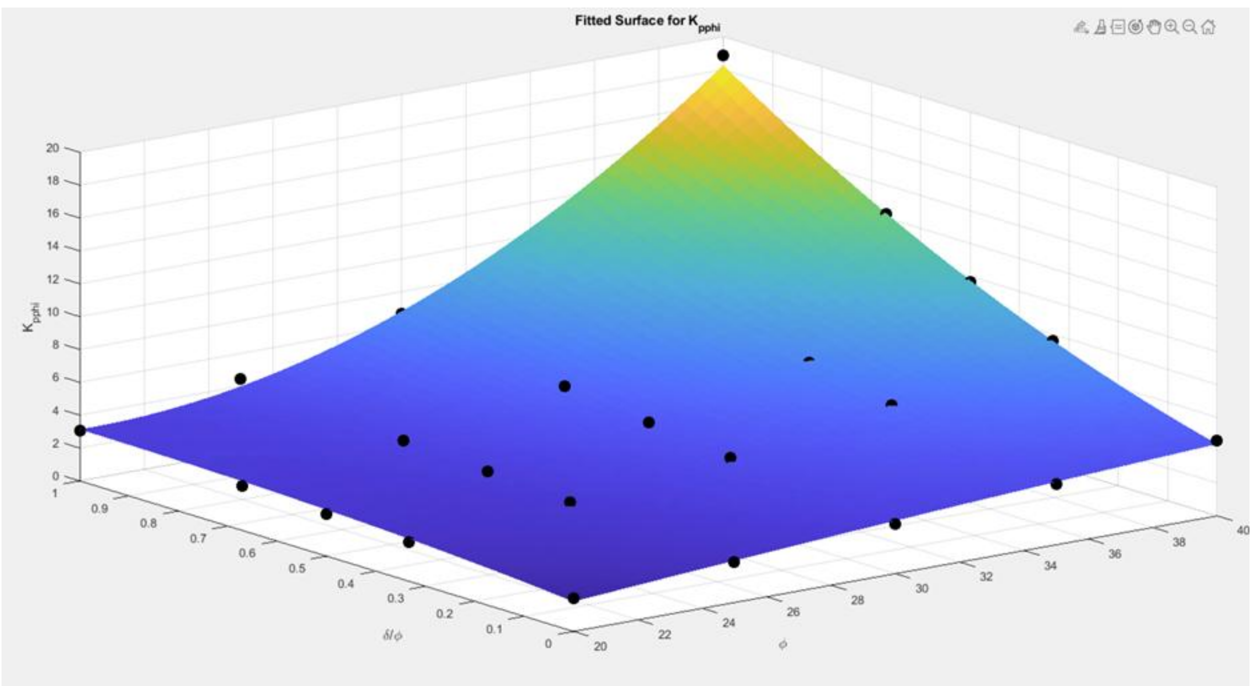

Figure C-4 Surface plot and fitted function for Kpϕ.

Fitted Function from Matlab for K_{pphi}:

Polynomial Coefficients (c_ij for phi^i * delta_phi^j):

c(0,0) = 2.3600000000

c(0,1) = 80.2361624599

c(0,2) = -420.9684289190

c(0,3) = 726.3721495375

c(0,4) = -354.2798830784

c(1,0) = -0.1626666667

c(1,1) = -11.5535100154

c(1,2) = 60.0271502396

c(1,3) = -103.9907139442

c(1,4) = 50.5169070534

c(2,0) = 0.0113333333

c(2,1) = 0.6107495371

c(2,2) = -3.1179450284

c(2,3) = 5.4346716587

c(2,4) = -2.6267595008

c(3,0) = -0.0002533333

c(3,1) = -0.0139688950

c(3,2) = 0.0700767589

c(3,3) = -0.1233346786

c(3,4) = 0.0592334813

c(4,0) = 0.0000026667

c(4,1) = 0.0001191685

c(4,2) = -0.0005733436

c(4,3) = 0.0010265177

c(4,4) = -0.0004890093

Fitted Polynomial Equation:

Kpphi(phi, delta_phi) =

(2.3600000000 * phi^0 * delta_phi^0) + (80.2361624599 * phi^0 * delta_phi^1) + (-420.9684289190 * phi^0 * delta_phi^2) + (726.3721495375 * phi^0 * delta_phi^3) + (-354.2798830784 * phi^0 * delta_phi^4) + (-0.1626666667 * phi^1 * delta_phi^0) + (-11.5535100154 * phi^1 * delta_phi^1) + (60.0271502396 * phi^1 * delta_phi^2) + (-103.9907139442 * phi^1 * delta_phi^3) + (50.5169070534 * phi^1 * delta_phi^4) + (0.0113333333 * phi^2 * delta_phi^0) + (0.6107495371 * phi^2 * delta_phi^1) + -(3.1179450284 * phi^2 * delta_phi^2) + (5.4346716587 * phi^2 * delta_phi^3) + (-2.6267595008 * phi^2 * delta_phi^4) + (-0.0002533333 * phi^3 * delta_phi^0) + (-0.0139688950 * phi^3 * delta_phi^1) + (0.0700767589 * phi^3 * delta_phi^2) + (-0.1233346786 * phi^3 * delta_phi^3) + (0.0592334813 * phi^3 * delta_phi^4) + (0.0000026667 * phi^4 * delta_phi^0) + (0.0001191685 * phi^4 * delta_phi^1) + (-0.0005733436 * phi^4 * delta_phi^2) + (0.0010265177 * phi^4 * delta_phi^3) + (-0.0004890093 * phi^4 * delta_phi^4)

Table C-5 Kpϕ values using fit function.

Using Fit Function, K_{pphi}					
ϕ	**δ/ϕ**				
	0	***0.33333***	***0.50***	***0.67***	***1.00***
20	2.04	2.38	2.56	2.73	3.07
25	2.46	3.06	3.39	3.71	4.42
30	3.00	4.02	4.61	5.25	6.68
35	3.69	5.42	6.52	7.75	10.76
40	4.60	7.58	9.67	12.18	18.86
45	5.84	10.98	14.86	20.01	34.47
50	7.56	16.26	23.14	33.23	62.37
55	9.95	24.22	35.81	54.37	108.63

Table C-6 Differences between fit and Liu et al. (2018) Kpϕ values.

% Difference, K_{pphi}					
ϕ	**δ/ϕ**				
	0	***0.33333***	***0.5***	***0.67***	***1.00***
20	0.00	0.00	0.00	0.12	0.00
25	0.00	0.00	0.00	0.17	0.00
30	0.00	0.00	0.00	0.25	0.00
35	0.00	0.00	0.00	0.34	0.00
40	0.00	0.00	0.00	0.45	0.00

Table C-7 Kpϕ values using fit function.

Using Fit Function, K_{pphi}										
δ	ϕ									
	15	***20***	***25***	***30***	***35***	***39***	***40***	***45***	***50***	***55***
0	1.75	2.04	2.46	3.00	3.69	4.40	4.60	5.84	7.56	9.95
5	1.98	2.29	2.80	3.48	4.34	5.25	5.52	7.31	10.10	14.37
10	2.38	2.56	3.19	4.02	5.13	6.33	6.68	8.98	12.48	17.81
15	3.01	2.81	3.58	4.61	6.03	7.60	8.07	10.98	15.20	21.36
20		3.07	3.98	5.25	7.03	9.06	9.67	13.44	18.67	25.88
25			4.42	5.93	8.13	10.72	11.51	16.43	23.14	32.01
26				6.08	8.37	11.08	11.91	17.10	24.17	33.47
30				6.68	9.36	12.61	13.62	20.01	28.79	40.14
35					10.76	14.79	16.05	24.22	35.66	50.45
40							18.86	29.05	43.68	62.87
45								34.47	52.69	77.09
50									62.37	92.60
55										108.6

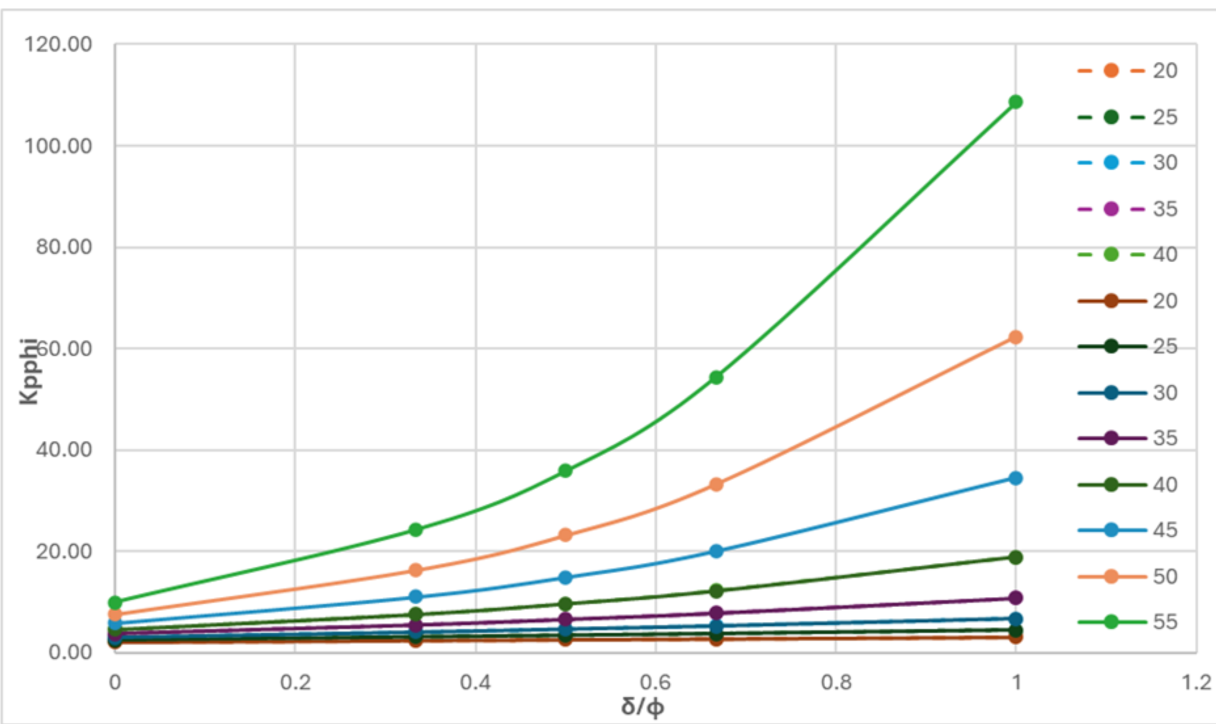

Figure C-5 Kpϕ versus δ/ϕ for ϕ = 20° – 55°.

C.4.2 Kpc

Table C-8 Kpc from Liu et al. (2018).

Given Table, K_{pc}					
ϕ	δ/ϕ				
	0	***0.33333***	***0.50***	***0.67***	***1.00***
20	2.86	3.38	3.68	4	4.64
25	3.14	4	4.46	4.97	5.98
30	3.46	4.73	5.51	6.33	7.89
35	3.84	5.76	7	8.33	10.79
40	4.29	7.2	9.22	11.41	15.53

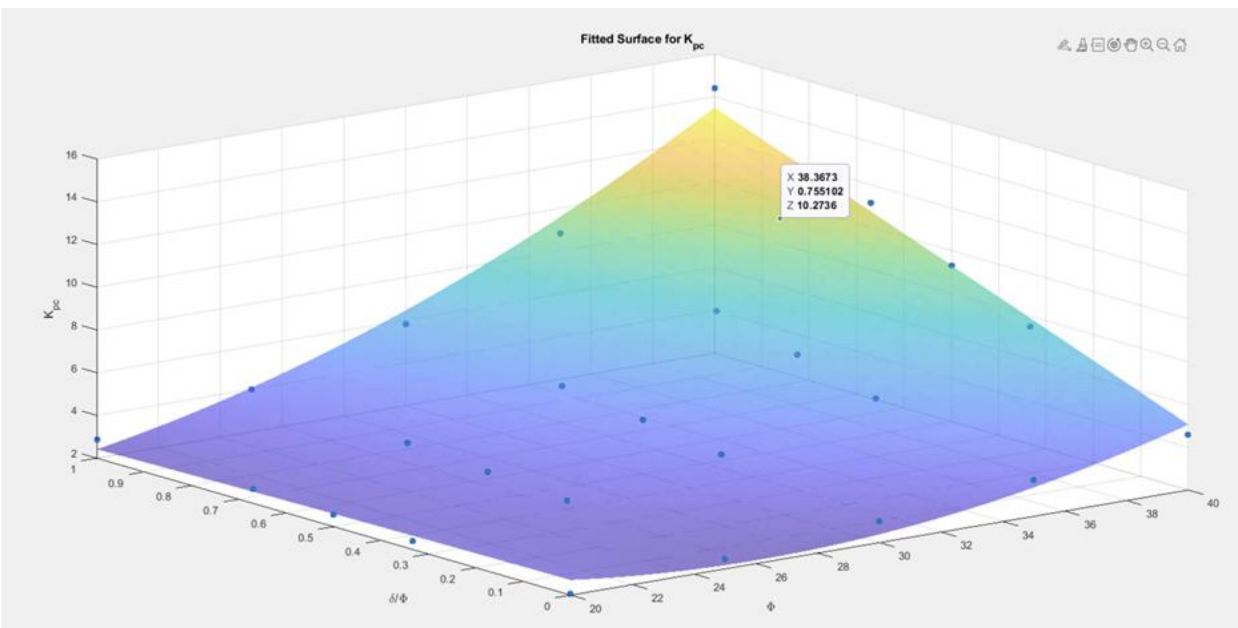

Figure C-6 Surface plot and fitted function for Kpc.

Fitted Function from Matlab for K_{pc}:

Polynomial Coefficients (c_ij for phi^i * delta_phi^j):

c(0,0) = 1.3900000000

c(0,1) = -199.1316008566

c(0,2) = 914.6029968195

c(0,3) = -1317.4077844622

c(0,4) = 612.1763884993

c(1,0) = 0.1225000000

c(1,1) = 27.6763468241

c(1,2) = -127.7591825741

c(1,3) = 184.3101199540

c(1,4) = -85.8449508706

c(2,0) = -0.0041833333

c(2,1) = -1.4033287010

c(2,2) = 6.5392595536

c(2,3) = -9.4422110869

c(2,4) = 4.4081469010

c(3,0) = 0.0001000000

c(3,1) = 0.0310883566

c(3,2) = -0.1458548970

c(3,3) = 0.2105861946

c(3,4) = -0.0985129876

c(4,0) = -0.0000006667

c(4,1) = -0.0002527905

c(4,2) = 0.0012037552

c(4,3) = -0.0017323991

c(4,4) = 0.0008107677

Fitted Polynomial Equation:

Kpc(phi, delta_phi) =

1.3900000000 * phi^0 * delta_phi^0 + -199.1316008566 * phi^0 * delta_phi^1 + 914.6029968195 * phi^0 * delta_phi^2 + -1317.4077844622 * phi^0 * delta_phi^3 +

612.1763884993 * phi^0 * delta_phi^4 + 0.1225000000 * phi^1 * delta_phi^0 + 27.6763468241 * phi^1 * delta_phi^1 + -127.7591825741 * phi^1 * delta_phi^2 + 184.3101199540 * phi^1 * delta_phi^3 + -85.8449508706 * phi^1 * delta_phi^4 + -0.0041833333 * phi^2 * delta_phi^0 + -1.4033287010 * phi^2 * delta_phi^1 + 6.5392595536 * phi^2 * delta_phi^2 + -9.4422110869 * phi^2 * delta_phi^3 + 4.4081469010 * phi^2 * delta_phi^4 + 0.0001000000 * phi^3 * delta_phi^0 + 0.0310883566 * phi^3 * delta_phi^1 + -0.1458548970 * phi^3 * delta_phi^2 + 0.2105861946 * phi^3 * delta_phi^3 + -0.0985129876 * phi^3 * delta_phi^4 + -0.0000006667 * phi^4 * delta_phi^0 + -0.0002527905 * phi^4 * delta_phi^1 + 0.0012037552 * phi^4 * delta_phi^2 + -0.0017323991 * phi^4 * delta_phi^3 + 0.0008107677 * phi^4 * delta_phi^4

Table C-9 Kpc values using fit function.

Using Fit Function, K_{pc}					
ϕ	**δ/ϕ**				
	0	***0.33333***	***0.50***	***0.67***	***1.00***
20	2.86	3.38	3.68	3.99	4.64
25	3.14	4.00	4.46	4.96	5.98
30	3.46	4.73	5.51	6.31	7.89
35	3.84	5.76	7.00	8.30	10.79
40	4.29	7.20	9.22	11.37	15.53
45	4.81	9.08	12.58	16.13	23.39
50	5.39	11.35	17.61	23.41	36.08
55	6.01	13.88	24.96	34.21	55.74

Table C-10 Differences between fit and Liu et al. (2018) Kpc values.

% Difference, K_{pc}					
ϕ	**δ/ϕ**				
	0	***0.33333***	***0.5***	***0.67***	***1.00***
20	0.00	0.00	0.00	0.16	0.00
25	0.00	0.00	0.00	0.21	0.00
30	0.00	0.00	0.00	0.25	0.00
35	0.00	0.00	0.00	0.32	0.00
40	0.00	0.00	0.00	0.38	0.00

Table C-11 Kpc values using fit function.

Using Fit Function, K_{pc}										
δ	ϕ									
	15	***20***	***25***	***30***	***35***	***39***	***40***	***45***	***50***	***55***
0	2.59	2.86	3.14	3.46	3.84	4.19	4.29	4.81	5.39	6.01
5	2.60	3.24	3.66	4.02	4.54	5.02	5.13	5.48	5.10	3.34
10	3.36	3.68	4.18	4.73	5.43	6.12	6.29	7.02	7.00	5.30
15	3.88	4.15	4.76	5.51	6.46	7.42	7.68	9.08	10.15	9.99
20		4.64	5.38	6.31	7.56	8.85	9.22	11.39	13.85	15.92
25			5.98	7.11	8.68	10.34	10.83	13.77	17.61	22.05
26				7.27	8.90	10.64	11.15	14.25	18.34	23.23
30				7.89	9.77	11.84	12.44	16.13	21.17	27.71
35					10.79	13.29	14.02	18.45	24.50	32.69
40							15.53	20.82	27.78	37.17
45								23.39	31.43	41.75
50									36.08	47.46
55										55.74

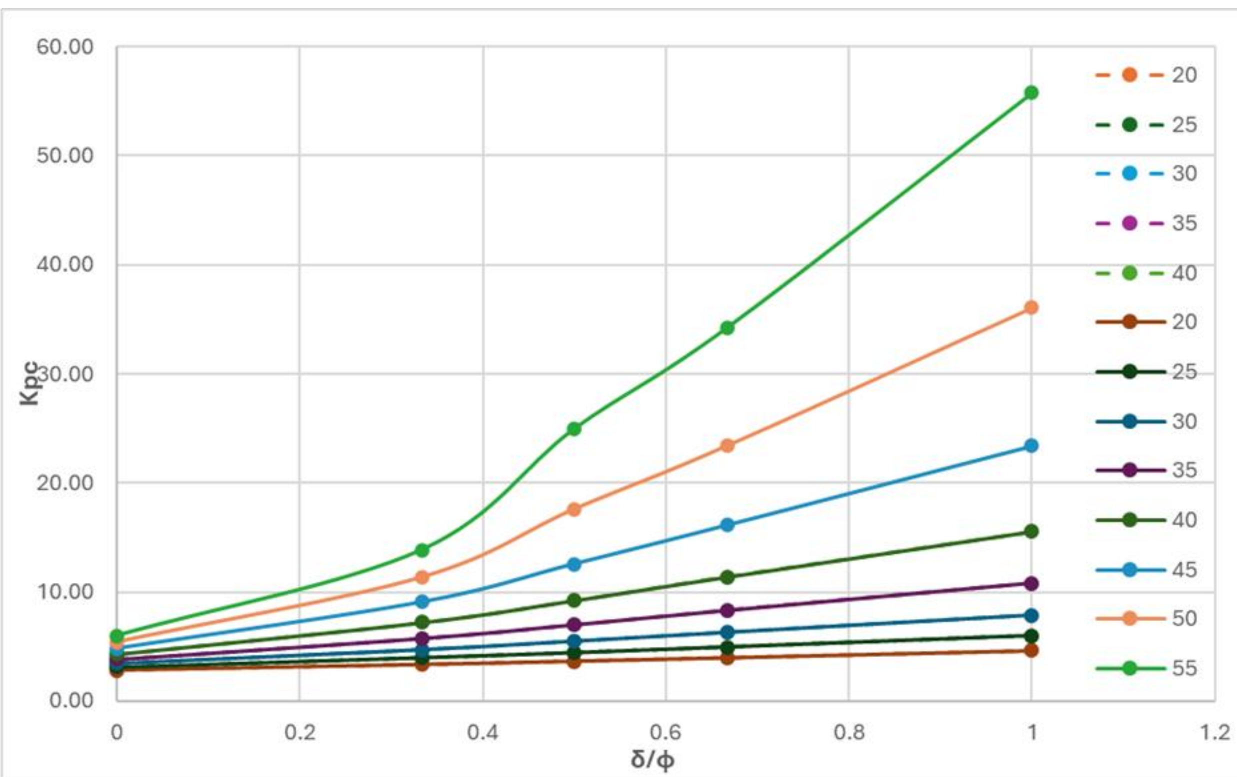

Figure C-7 Kpc versus δ/ϕ for ϕ = 20° – 55°.

C.4.3 Kpq

Table C-12 Kpq from Liu et al. (2018).

Given table, K_{pq}					
ϕ	δ/ϕ				
	0	*0.33333*	*0.50*	*0.67*	*1.00*
20	2.04	2.38	2.54	2.68	2.87
25	2.46	3.05	3.35	3.61	4
30	3	4	4.53	5.03	5.8
35	3.69	5.38	6.35	7.3	8.85
40	4.6	7.5	9.31	11.15	14.39

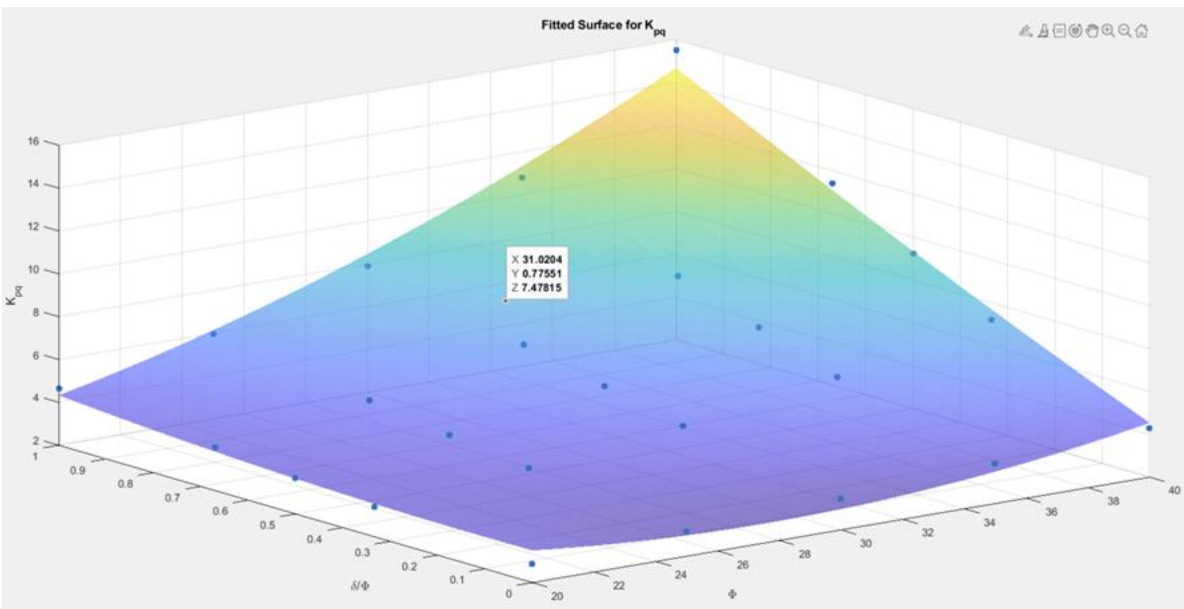

Figure C-8 Surface plot and fitted function for Kpq.

Fitted Function from Matlab for K_{pq}:

Polynomial Coefficients (c_ij for phi^i * delta_phi^j):

c(0,0) = 2.3600000000

c(0,1) = 50.9646310445

c(0,2) = -240.3633972912

c(0,3) = 402.7877745623

c(0,4) = -199.1990083156

c(1,0) = -0.1626666667

c(1,1) = -6.9964669066

c(1,2) = 32.2171788736

c(1,3) = -54.4262682747

c(1,4) = 26.9128896410

c(2,0) = 0.0113333333

c(2,1) = 0.3536460177

c(2,2) = -1.5608251523

c(2,3) = 2.6689199998

c(2,4) = -1.3207741985

c(3,0) = -0.0002533333

c(3,1) = -0.0077092679

c(3,2) = 0.0323621647

c(3,3) = -0.0564816187

c(3,4) = 0.0280153885

c(4,0) = 0.0000026667

c(4,1) = 0.0000633568

c(4,2) = -0.0002381388

c(4,3) = 0.0004322519

c(4,4) = -0.0002161366

Fitted Polynomial Equation:

Kpq(phi, delta_phi) =

2.3600000000 * phi^0 * delta_phi^0 + 50.9646310445 * phi^0 * delta_phi^1 + -240.3633972912 * phi^0 * delta_phi^2 + 402.7877745623 * phi^0 * delta_phi^3 + -

199.1990083156 * phi^0 * delta_phi^4 + -0.1626666667 * phi^1 * delta_phi^0 + -6.9964669066 * phi^1 * delta_phi^1 + 32.2171788736 * phi^1 * delta_phi^2 + -54.4262682747 * phi^1 * delta_phi^3 + 26.9128896410 * phi^1 * delta_phi^4 + 0.0113333333 * phi^2 * delta_phi^0 + 0.3536460177 * phi^2 * delta_phi^1 + -1.5608251523 * phi^2 * delta_phi^2 + 2.6689199998 * phi^2 * delta_phi^3 + -1.3207741985 * phi^2 * delta_phi^4 + -0.0002533333 * phi^3 * delta_phi^0 + -0.0077092679 * phi^3 * delta_phi^1 + 0.0323621647 * phi^3 * delta_phi^2 + -0.0564816187 * phi^3 * delta_phi^3 + 0.0280153885 * phi^3 * delta_phi^4 + 0.0000026667 * phi^4 * delta_phi^0 + 0.0000633568 * phi^4 * delta_phi^1 + -0.0002381388 * phi^4 * delta_phi^2 + 0.0004322519 * phi^4 * delta_phi^3 + -0.0002161366 * phi^4 * delta_phi^4

Table C-13 Kpq values using fit function.

Using Fit Function, K_{pq}					
ϕ	**δ/ϕ**				
	0	***0.33333***	***0.50***	***0.67***	***1.00***
20	2.04	2.38	2.54	2.68	2.87
25	2.46	3.05	3.35	3.61	4.00
30	3.00	4.00	4.53	5.02	5.80
35	3.69	5.38	6.35	7.28	8.85
40	4.60	7.50	9.31	11.11	14.39
45	5.84	10.83	14.14	17.61	24.32
50	7.56	16.00	21.80	28.23	41.20
55	9.95	23.80	33.48	44.79	68.25

Table C-14 Differences between fit and Liu et al. (2018) Kpq values.

% Difference, K_{pq}					
ϕ	**δ/ϕ**				
	0	***0.33333***	***0.5***	***0.67***	***1.00***
20	0.00	0.00	0.00	0.09	0.00
25	0.00	0.00	0.00	0.13	0.00
30	0.00	0.00	0.00	0.18	0.00
35	0.00	0.00	0.00	0.24	0.00
40	0.00	0.00	0.00	0.32	0.00

Table C-15 Kpq values using fit function.

Using Fit Function, K_{pq}										
δ	**ϕ**									
	15	***20***	***25***	***30***	***35***	***39***	***40***	***45***	***50***	***55***
0	1.75	2.04	2.46	3.00	3.69	4.40	4.60	5.84	7.56	9.95
5	2.00	2.29	2.80	3.47	4.33	5.23	5.49	7.14	9.57	13.11
10	2.25	2.54	3.17	4.00	5.11	6.29	6.64	8.84	12.04	16.68
15	2.49	2.74	3.51	4.53	5.93	7.48	7.95	10.83	14.95	20.76
20		2.87	3.78	5.02	6.76	8.72	9.31	13.01	18.22	25.42
25			4.00	5.45	7.53	9.94	10.67	15.29	21.80	30.66
26				5.52	7.68	10.18	10.94	15.75	22.55	31.77
30				5.80	8.23	11.10	11.98	17.61	25.61	36.43
35					8.85	12.19	13.22	19.91	29.55	42.65
40							14.39	22.16	33.54	49.16
45								24.32	37.46	55.77
50									41.20	62.23
55										68.25

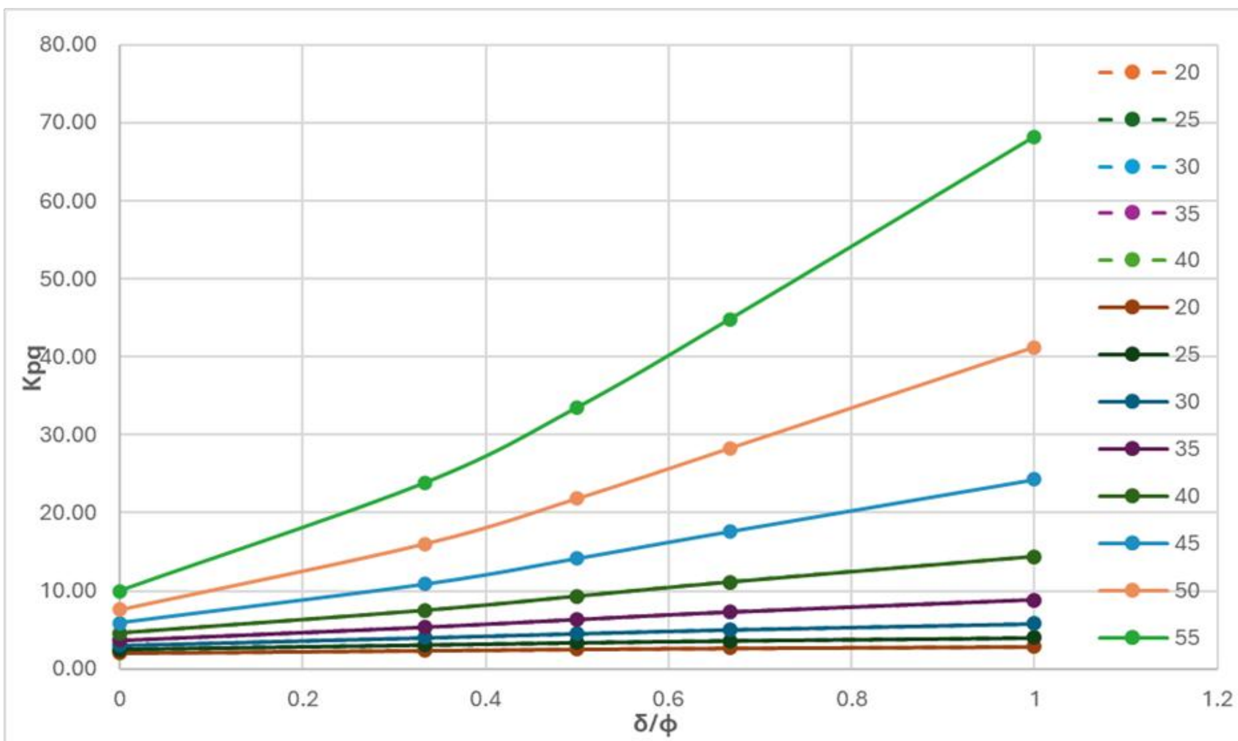

Figure C-9 Kpq versus δ/ϕ for ϕ = 20° – 55°.

C.5 Cases of Footing On and In Florida Limestone

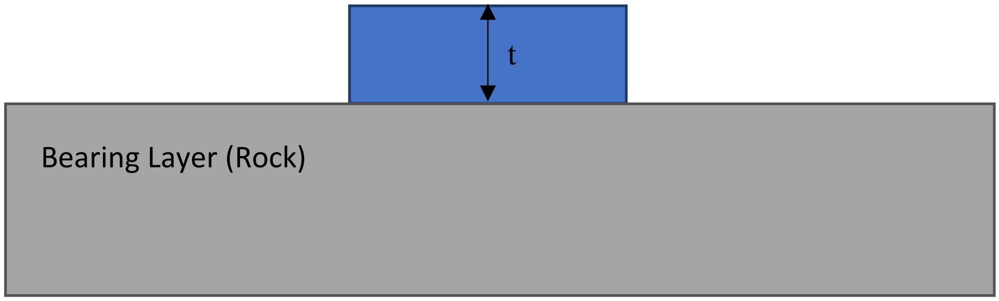

Case 1a. No Embedment, Bearing on Florida Limestone

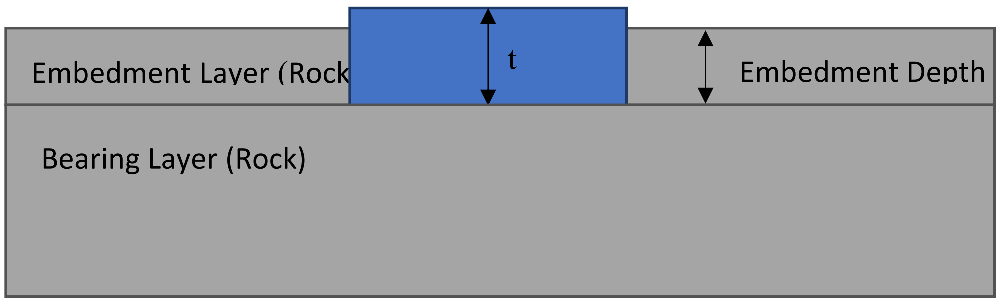

Case 1b. Embedment in Florida Limestone, Bearing on Florida Limestone.

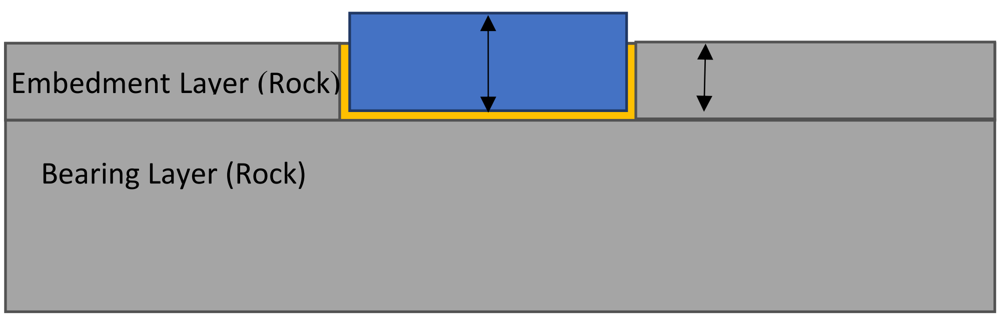

Case 1c. Embedment in Florida Limestone with aggregate backfill around foundation perimeter and base while Bearing on Florida Limestone.

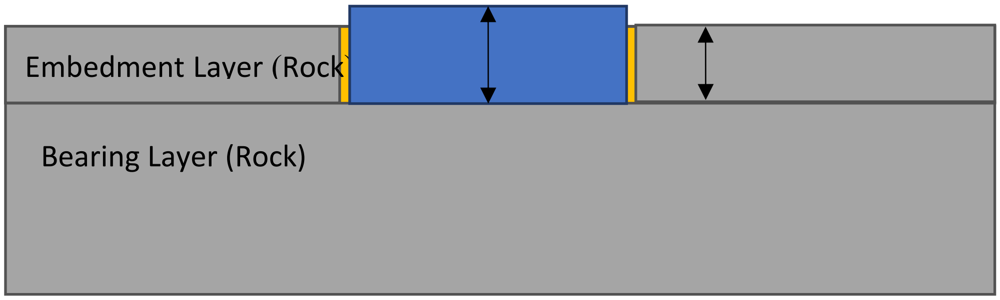

Case 1d. Embedment in Florida Limestone with aggregate backfill around foundation perimeter and Bearing on Florida Limestone.

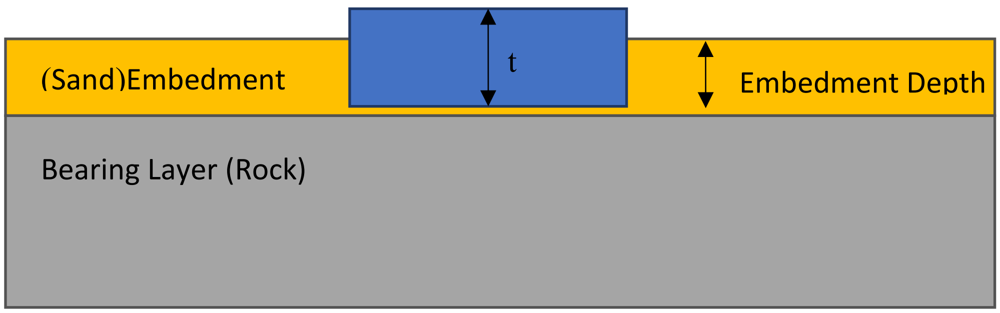

Case 1e. Embedment in Sand underlain by Florida Limestone.

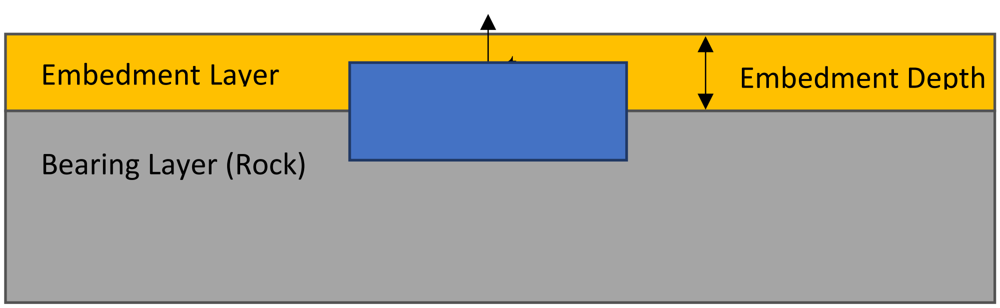

Case 1f. Embedment in Sand, Bearing on Florida Limestone.

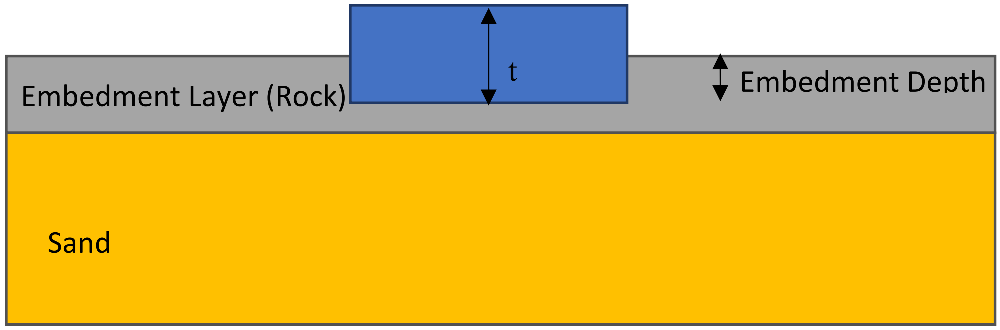

Case 2a. Partial Embedment in Florida Limestone underlain by Sand.

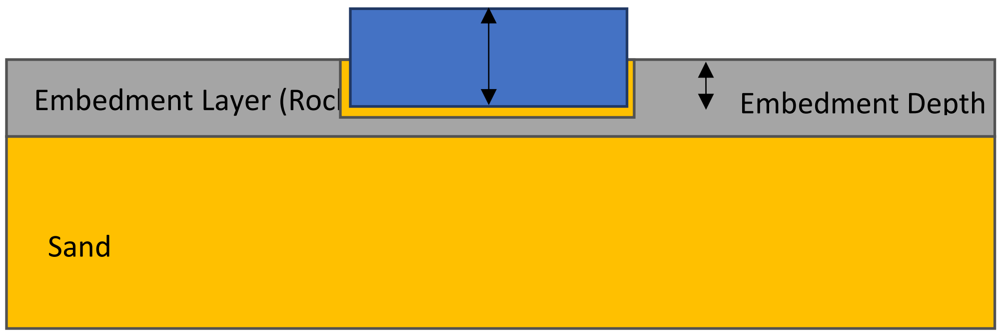

Case 2b. Partial Embedment in Florida Limestone underlain by Sand with sand or aggregate backfill around foundation perimeter and base while Bearing on Florida Limestone.

Case	Description	Bearing Model	Passive Model	Friction Model
1a	No embedment, Bearing of FL Limestone	FL Limestone (Homogeneous)	None	Hyperbolic (Coulomb)
1b	Embedment in FL Limestone, Bearing on FL Limestone	FL Limestone (Homogeneous)	FL Limestone	Hyperbolic (Coulomb)
1c	Embedment in FL Limestone with aggregate backfill around perimeter and base, Bearing on FL Limestone	FL Limestone (Homogeneous)	None	Hyperbolic (Coulomb)
1d	Embedment in FL Limestone with aggregate backfill around base, Bearing on FL Limestone	FL Limestone (Homogeneous)	None	Hyperbolic (Coulomb)
1e	Embedment in sand with sand under base, bearing on FL limestone	FL Limestone (Homogeneous)	C-Phi Material	Hyperbolic (Coulomb)
1f	Embedment in sand, bearing on FL limestone	FL Limestone (Homogeneous)	C-Phi Material	Hyperbolic (Coulomb)
2a	Partial Embedment in Florida Limestone underlain by Sand.	FL Limestone (Rock over Sand)	FL Limestone	Hyperbolic (Coulomb)
2b	Embedment in FL Limestone underlain by Sand with aggregate backfill around perimeter and base, Bearing on FL Limestone	FL Limestone (Rock over Sand)	None	Hyperbolic (Coulomb)

C.6 In-built strength envelope parameters for all the FL limestone formation

Table C-16 Intact properties of Florida limestone in tau-sigma space and p-q space.

Formation	γ_{dt}, pcf	c_i, psi	φ_i, °	$\sigma_{peak\ i}$, psi	ω_i, °	a_i, psi	α_i, °	Pp, psi	β_i, °
Miami Limestone	90	42.0	42.2	444	-3.0	31.1	33.9	247	-3
	95	49.9	43.2	498	-1.4	36.4	34.4	274	-1.4
	100	58.9	44.2	562	0.8	42.2	34.9	306	0.8
	105	70.9	45.3	640	3.7	49.9	35.4	345	3.7
	110	84.1	46.4	730	7.3	58	35.9	390	7.2
	115	99.9	47.3	840	11.6	67.8	36.3	445	11.4
	120	118.8	48.2	969	16.6	79.2	36.7	510	15.9
	125	141.8	49.1	1126	22.2	92.8	37.1	588	20.7
	130	169.0	50.1	1314	28.5	108.4	37.5	682	25.5
	135	202.5	51.1	1541	35.4	127.1	37.9	795	30.1
Anastasia Limestone	90	52.0	37.4	416	-6.7	41.3	31.3	233	-6.7
	95	62.1	38.7	474	-6.7	48.5	32	262	-6.7
	100	74.0	39.8	542	-6.7	56.9	32.6	296	-6.7
	105	88.1	40.9	624	-6.7	66.6	33.2	337	-6.7
	110	104.9	41.8	722	-6.7	78.2	33.7	386	-6.7
	115	124.9	42.8	839	-6.7	91.6	34.2	445	-6.7
	120	149.1	44.0	980	-6.7	107.2	34.8	515	-6.7
	125	178.3	45.1	1151	-4.3	125.9	35.3	600	-4.3
	130	211.8	45.9	1354	1.6	147.3	35.7	702	1.6
	135	253.1	47.0	1603	10.9	172.5	36.2	826	10.7
	140	301.3	48.0	1904	23.7	201.8	36.6	977	21.9
Hawthorn Limestone	85	26.0	41.8	368	1.4	19.4	33.7	209	1.4
	90	31.0	43.0	408	2.4	22.7	34.3	229	2.4
	95	37.0	44.0	452	4.1	26.6	34.8	251	4.1
	100	44.0	45.1	506	6.2	31.1	35.3	278	6.2
	105	52.9	45.9	568	9.0	36.8	35.7	309	8.9
	110	63.1	47.0	642	12.3	43	36.2	346	12
	115	75.0	48.0	728	16.1	50.2	36.6	389	15.5
	120	88.8	48.9	832	20.5	58.4	37	441	19.3
	125	106.0	49.9	956	25.5	68.3	37.4	503	23.3
	130	126.1	50.9	1104	31.1	79.6	37.8	577	27.3
	135	149.8	51.6	1279	37.1	93	38.1	665	31.1
	65	31.0	38.1	340	-23.2	24.4	31.7	195	-21.5

Formation	γ_{dt}, pcf	c_i, psi	φ_i, °	$\sigma_{peak\ i}$, psi	ω_i, °	a_i, psi	α_i, °	Pp, psi	β_i, °
Key Largo Limestone	70	36.9	39.2	378	-19.7	28.6	32.3	214	-18.6
	75	43.9	40.3	424	-16.3	33.5	32.9	237	-15.7
	80	51.9	41.4	478	-12.8	38.9	33.5	264	-12.5
	85	62.0	42.6	542	-9.4	45.6	34.1	296	-9.3
	90	74.0	43.6	618	-5.9	53.6	34.6	334	-5.9
	95	88.1	44.7	708	-2.5	62.7	35.1	379	-2.5
	100	104.9	45.5	815	1.0	73.5	35.5	433	1
	105	125.0	46.6	946	4.4	85.9	36	498	4.4
	110	148.8	47.5	1099	7.9	100.5	36.4	575	7.8
	115	177.3	48.7	1288	11.4	117.1	36.9	669	11.2
	120	210.4	49.4	1513	14.8	137	37.2	782	14.3
Shallow Fort Thompson Limestone	90	22.9	38.7	314	-23.6	17.9	32	182	-21.8
	95	28.0	39.9	347	-15.8	21.5	32.7	198	-15.2
	100	32.9	40.9	384	-7.9	24.9	33.2	217	-7.8
	105	39.0	42.0	428	-0.1	29	33.8	239	-0.1
	110	46.9	43.0	480	7.8	34.3	34.3	265	7.7
	115	55.9	44.0	542	15.7	40.2	34.8	296	15.1
	120	66.0	45.1	614	23.4	46.6	35.3	332	21.7
Ocala Limestone	85	9.1	30.8	188	13.5	7.8	27.1	119	13.1
	90	17.1	35.4	254	16.6	13.9	30.1	152	15.9
	95	28.2	37.6	320	19.3	22.3	31.4	185	18.3
	100	43.0	38.0	386	21.8	33.9	31.6	218	20.4
	105	62.7	37.1	454	24.0	50	31.1	252	22.1

Intact Strength and Recovery (rock core)

For a design project, it is recommended to establish site-specific strength envelopes (Appendix F of Phase I final report (McVay et al., 2019)), a minimum of 10 unconfined compression strength test samples, 10 split tensile test samples, 8 to 16 triaxial test samples to estimate p_p and the second slope, w. With the site-specific intact strength parameters and REC, the mass strength parameters can be obtained by using Table C-5.

Table C-17 Intact and mass strength parameters conversion from intact strength parameters.

REC (Input)	%	80
Intact properties (Input)	c_i, psi	58.9
	φ_i, °	44.2
	P_p, psi	306
	ω_i, °	0.8
Intact properties (Output)	a_i, psi	$a_i = c*\cos(\varphi_i) = 42.2$
	α_i, °	$\alpha_i = \text{atan}(\sin(\varphi_i)) = 34.9$
	$\sigma_{peak\ i}$, psi	$\sigma_{peak\ i} = a_i + \tan(\alpha_i)*P_p + P_p = 562$
	β_i, °	$\beta_i = \text{atan}(\sin(\omega_i)) = 0.8$
Mass Properties (Output)	a_m, psi	$a_m = REC*a_i = 33.8$
	α_m, °	$\alpha_m = \text{atan}(REC*\tan\alpha_i) = 29.2$
	P_p, psi	$P_p = P_p = 306$
	β_m, °	$\beta_m = \text{atan}(REC*\tan\beta_i) = 0.6$
	c_m, psi	$c_m = \frac{a_m}{cos\varphi_m} = 40.7$
	φ_m, °	$\varphi_m = \text{asin}(tan\alpha_m) = 33.9$
	$\sigma_{peak\ m}$, psi	$\sigma_{peak\ m} = P_p + tan\alpha_m * P_p + a_m = 511$
	ω_m, °	$\omega_m = \text{asin}(tan\beta_m) = 0.6$

Mass Strength (rock mass)

Users can directly input the mass strength parameters (c_m, φ_m, P_p, ω_m),

The rock mass mean modulus ($E_m = \mu_E$ in probabilistic settlement) is obtained from the intact modulus (E_i) and the ratio of mass modulus to intact modulus (E_{mass}/E_{intact}, Figure C-4. Adjusted REC versus Emass/Eintact.). Green trend line (Ko, 2010) in Figure C-4. Adjusted REC versus Emass/Eintact. is recommended to obtain the mass modulus based on the REC_{adj}:

a. When $REC_{adj} \leq 50\%$, $E_m/E_i = 0.2 \times REC_{adj}$
b. When $50\% < REC_{adj} \leq 70\%$, $E_m/E_i = 1.25 \times REC_{adj} - 0.525$
c. When $70\% < REC_{adj}$, $E_m/E_i = 2.17 \times REC_{adj} - 1.17$

Figure C-5. Intact initial modulus versus bulk dry unit weight for (a) Miami limestone (b) Ocala limestone (c) Key Largo limestone (d) Anastasia limestone (e) Hawthorn limestone (f) Fort Thompson limestone from Phase I & II. provides the intact initial modulus versus bulk dry unit weights for 6 formations from Phase I & II. However, the intact moduli are recommended to be measured for a specific site due to the inherent variability of Florida limestone (CV of modulus around 1~3) and uncertainty of the site investigation (method errors).

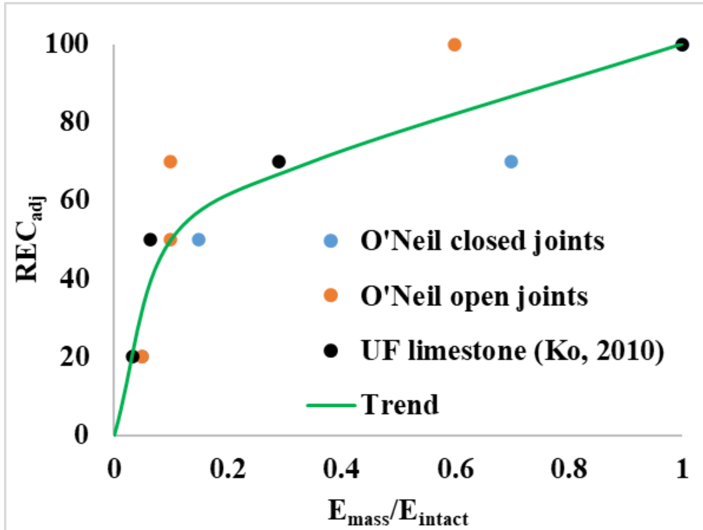

Figure C-10 Adjusted REC versus E_{mass}/E_{intact}.

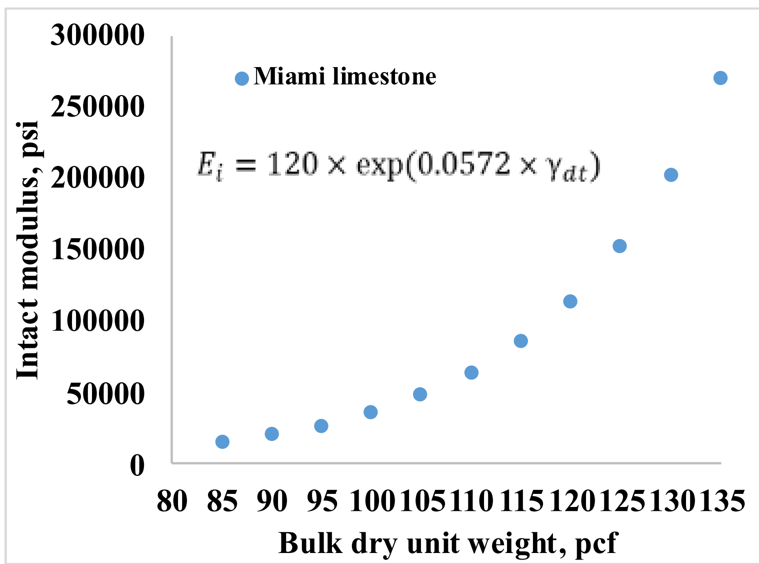

(g)

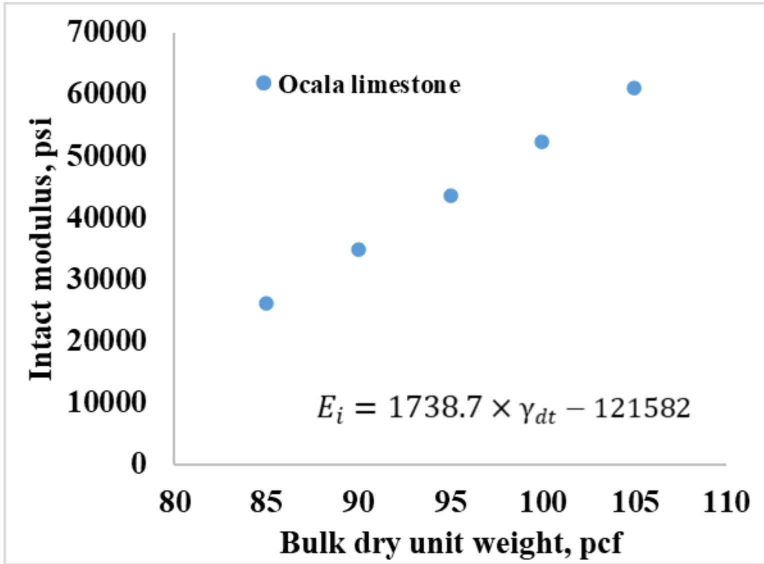

70000
60000
50000
40000
30000
20000
10000
0
Intact modulus, psi
Ocala limestone
$E_i = 1738.7 \times \gamma_{dt} - 121582$
80
85
90
95
100
105
110
Bulk dry unit weight, pcf

(h)

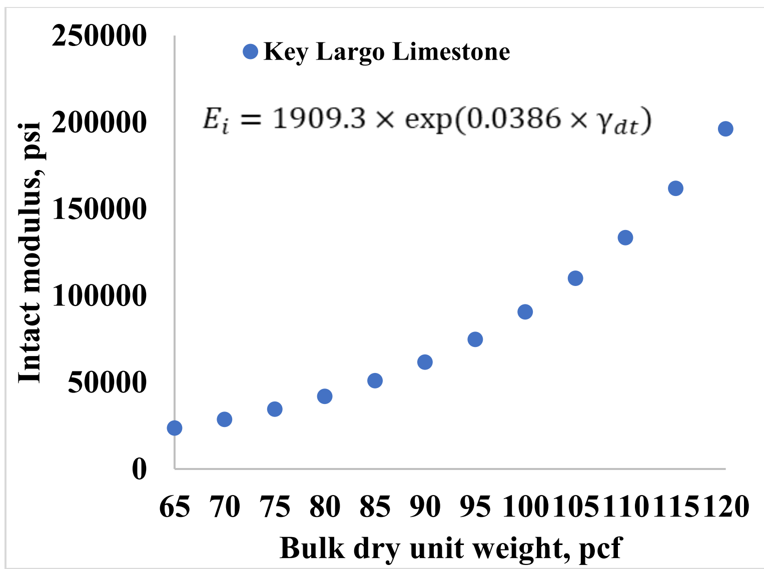

250000
200000
150000
100000
50000
0
Intact modulus, psi
Key Largo Limestone
$E_i = 1909.3 \times \exp(0.0386 \times \gamma_{dt})$
65 70 75 80 85 90 95 100 105 110 115 120
Bulk dry unit weight, pcf

(i)

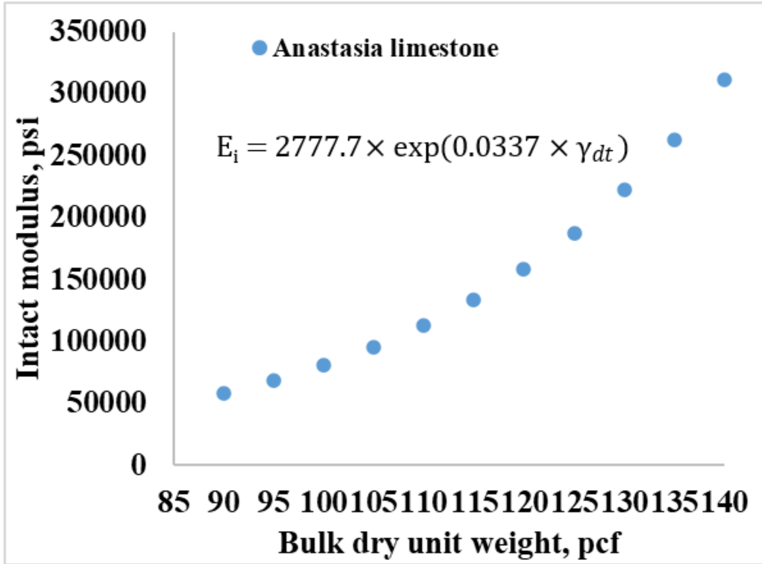
Anastasia limestone
$E_i = 2777.7 \times \exp(0.0337 \times \gamma_{dt})$
Intact modulus, psi
350000
300000
250000
200000
150000
100000
50000
0
85 90 95 100 105 110 115 120 125 130 135 140
Bulk dry unit weight, pcf

(j)

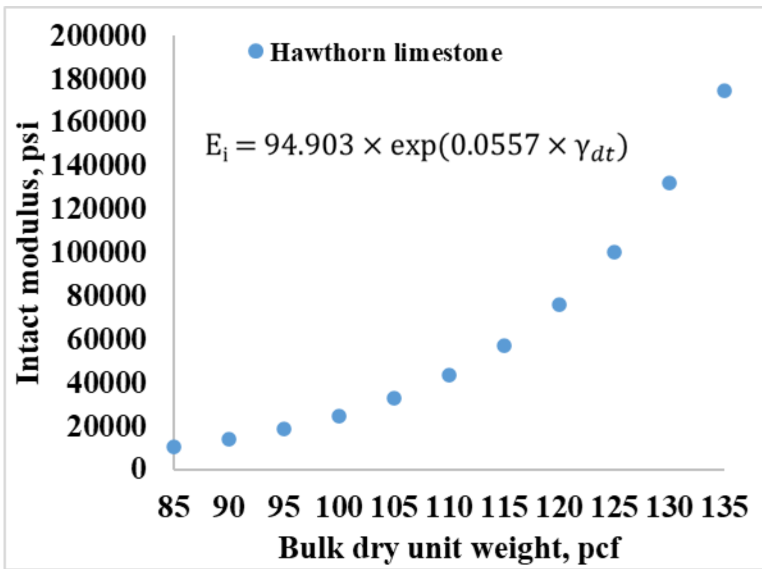
Hawthorn limestone
$E_i = 94.903 \times \exp(0.0557 \times \gamma_{dt})$
Intact modulus, psi
200000
180000
160000
140000
120000
100000
80000
60000
40000
20000
0
85 90 95 100 105 110 115 120 125 130 135
Bulk dry unit weight, pcf

(k)

(l)

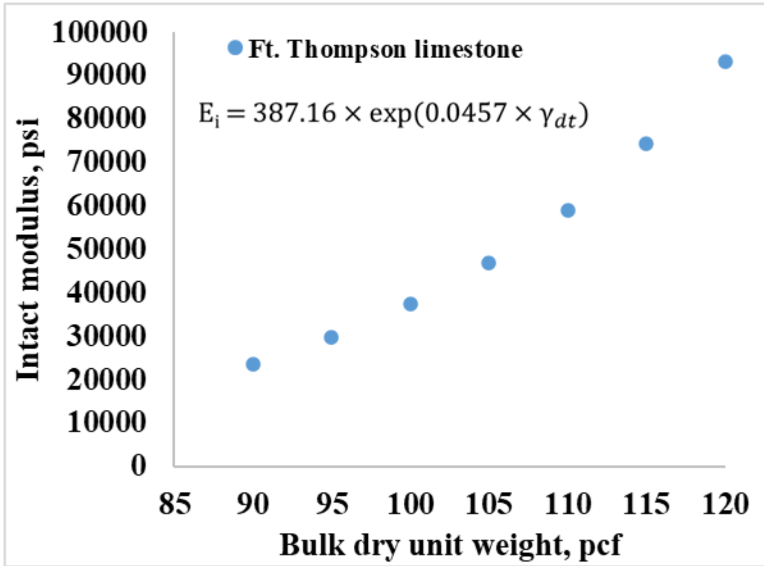

Figure C-11 Intact initial modulus versus bulk dry unit weight for (a) Miami limestone (b) Ocala limestone (c) Key Largo limestone (d) Anastasia limestone (e) Hawthorn limestone (f) Fort Thompson limestone from phase I & II.

C.7 Plaxis Results

C.7.1 Results

5 ft x 5 ft Soil

	Face 1	
Ux(in)	0-deg-Pp (kips)	0-deg-PT (kips)
0	0	0.0
0.12	-80	0.0
0.6	-187	-0.1
1.2	-234	-0.5
6	-309	-0.7
10.8	-322	0.3
12	-324	0.5

	Face 2	
Uy(in)	0-deg-Pp (kips)	0-deg-PT (kips)
0.00	0.0	0.0
0.00	-10.6	-10.3
0.00	-15.9	-13.5
0.00	-16.9	-14.1
0.00	-18.1	-14.8
0.00	-18.4	-14.9
0.00	-18.3	-14.9

*Pp = passive force, PT = shear force on passive face

	Face 1	
Ux(in)	45-deg-Pp (kips)	45-deg-PT (kips)
0	0	0.0
0.08	-57	-19.2
0.42	-131	-51.4
0.85	-160	-63.1
4.24	-203	-75.7
7.64	-210	-77.3
8.49	-211	-77.5

	Face 2	
Uy(in)	45-deg-Pp (kips)	45-deg-PT (kips)
0.00	0.0	0.0
0.08	-57.1	-19.3
0.42	-132.2	-51.5
0.85	-159.3	-63.6
4.24	-200.4	-77.4
7.64	-206.9	-78.8
8.49	-207.8	-79.0

*Ux = displacement in x-direction, Uy = displacement in y-direction, Pp = passive force, PT = shear force on passive face

16 ft x 8 ft Soil

	Face 1	
Ux(in)	0-deg-Pp (kips)	0-deg-PT (kips)
0	0	0.0
0.12	-259	0.5
0.6	-830	-1.6
1.2	-1095	-2.7
2.4	-1331	-2.7
3.6	-1451	-4.3
4.8	-1527	-5.6

	Face 2	
Uy(in)	0-deg-Pp (kips)	0-deg-PT (kips)
0.00	0.0	0.0
0.00	-26.2	-25.8
0.00	-41.1	-34.9
0.00	-44.7	-37.1
0.00	-46.7	-38.2
0.00	-47.6	-38.8
0.00	-48.2	-39.2

*Ux = displacement in x-direction, Uy = displacement in y-direction, Pp = passive force, PT = shear force on passive face

	Face 1	
Ux(in)	45-deg-Pp (kips)	45-deg-PT (kips)
0	0	0.0
0.08	-190	-70.2
0.42	-591	-245.7
0.85	-777	-324.3
1.70	-915	-384.1
2.55	-980	-410.5
3.39	-1019	-424.3

	Face 2	
Uy(in)	45-deg-Pp (kips)	45-deg-PT (kips)
0.00	0.0	0.0
0.08	-107.0	-37.3
0.42	-321.4	-125.7
0.85	-440.0	-173.6
1.70	-540.7	-219.0
2.55	-587.5	-241.1
3.39	-613.0	-252.2

*Ux = displacement in x-direction, Uy = displacement in y-direction, Pp = passive force, PT = shear force on passive face

5 ft x 5 ft Weak Soil

	Face 1	
Ux(in)	0-deg-Pp (kips)	0-deg-PT (kips)
0	0	0.0
0.12	-28	0.0
0.6	-53	0.3
1.2	-59	0.5
2.4	-63	0.8
3.6	-65	1.0
6	-67	1.1

	Face 2	
Uy(in)	0-deg-Pp (kips)	0-deg-PT (kips)
0.00	0.0	0.0
0.00	-4.3	-3.5
0.00	-4.0	-3.4
0.00	-4.1	-3.4
0.00	-4.2	-3.5
0.00	-4.3	-3.5
0.00	-4.4	-3.6

*Ux = displacement in x-direction, Uy = displacement in y-direction, Pp = passive force, PT = shear force on passive face

	Face 1	
Ux(in)	45-deg-Pp (kips)	45-deg-PT (kips)
0.00	0	0.0
0.08	-20	-6.7
0.42	-39	-13.5
0.85	-42	-14.8
1.70	-45	-15.3
2.55	-46	-15.4
4.24	-46	-15.5

	Face 2	
Uy(in)	45-deg-Pp (kips)	45-deg-PT (kips)
0.00	0.0	0.0
0.08	-20.5	-6.8
0.42	-39.0	-13.6
0.85	-44.1	-14.9
1.70	-47.4	-15.5
2.55	-48.4	-15.7
4.24	-49.4	-15.9

*Ux = displacement in x-direction, Uy = displacement in y-direction, Pp = passive force, PT = shear force on passive face

5 ft x 5 ft 90 pcf Limestone

	Face 1	
Ux(in)	0-deg-Pp (kips)	0-deg-PT (kips)
0	0	0.0
0.12	-93	-0.1
0.6	-100	-3.0
1.2	-102	1.6
2.4	-102	-3.4
3.6	-106	-3.4
4.8	-101	0.0

	Face 2	
Uy(in)	0-deg-Pp (kips)	0-deg-PT (kips)
0.00	0.0	0.0
0.00	-6.2	-15.1
0.00	-5.1	-14.8
0.00	-6.3	-15.2
0.00	-4.3	-14.7
0.00	-4.4	-14.7
0.00	-5.2	-14.7

*Ux = displacement in x-direction, Uy = displacement in y-direction, Pp = passive force, PT = shear force on passive face

	Face 1	
Ux(in)	15-deg-Pp (kips)	15-deg-PT (kips)
0.00	0	0.0
0.12	-84	-11.6
0.58	-92	-21.0
1.16	-88	-22.2
2.32	-99	-20.7
3.48	-100	-21.3
4.64	-99	-22.7

	Face 2	
Uy(in)	15-deg-Pp (kips)	15-deg-PT (kips)
0.00	0.0	0.0
0.03	-30.1	-20.3
0.16	-61.6	-26.4
0.31	-71.7	-28.3
0.62	-72.8	-29.0
0.93	-78.7	-30.4
1.24	-78.5	-29.9

*Ux = displacement in x-direction, Uy = displacement in y-direction, Pp = passive force, PT = shear force on passive face

	Face 1	
Ux(in)	30-deg-Pp (kips)	30-deg-PT (kips)
0.00	0	0.0
0.10	-76	-20.3
0.52	-84	-25.2
1.04	-92	-25.7
2.08	-85	-24.6
3.12	-94	-27.7
4.16	-85	-26.8

	Face 2	
Uy(in)	30-deg-Pp (kips)	30-deg-PT (kips)
0.00	0.0	0.0
0.06	-50.4	-24.4
0.30	-81.9	-29.1
0.60	-70.4	-26.8
1.20	-83.8	-29.8
1.80	-79.4	-28.5
2.40	-85.3	-28.7

*Ux = displacement in x-direction, Uy = displacement in y-direction, Pp = passive force, PT = shear force on passive face

	Face 1	
Ux(in)	45-deg-Pp (kips)	45-deg-PT (kips)
0.00	0	0.0
0.08	-65	-25.2
0.42	-78	-28.5
0.85	-79	-29.0
1.70	-75	-27.8
2.55	-80	-26.9
3.39	-76	-27.3

	Face 2	
Uy(in)	45-deg-Pp (kips)	45-deg-PT (kips)
0.00	0.0	0.0
0.08	-65.2	-25.6
0.42	-88.5	-24.8
0.85	-94.5	-24.8
1.70	-98.2	-23.6
2.55	-84.0	-25.1
3.39	-96.1	-23.9

*Ux = displacement in x-direction, Uy = displacement in y-direction, Pp = passive force, PT = shear force on passive face

16 ft x 8 ft 90 pcf Limestone

	Face 1	
Ux(in)	0-deg-Pp (kips)	0-deg-PT (kips)
0	0	0.0
0.12	-279	-1.5
0.6	-454	13.8
1.2	-503	1.7
6	-513	-11.8
10.8	-504	-14.3
12	-505	-17.0

	Face 2	
Uy(in)	0-deg-Pp (kips)	0-deg-PT (kips)
0.00	0.0	0.0
0.00	-21.0	-39.7
0.00	-20.3	-39.8
0.00	-16.8	-39.0
0.00	-11.6	-37.9
0.00	-12.7	-38.1
0.00	-9.2	-37.3

*Ux = displacement in x-direction, Uy = displacement in y-direction, Pp = passive force, PT = shear force on passive face

	Face 1	
Ux(in)	15-deg-Pp (kips)	15-deg-PT (kips)
0.00	0	0.0
0.12	-267	-38.5
0.58	-466	-100.8
1.16	-463	-112.7
5.80	-429	-110.8
10.43	-436	-112.8
11.59	-458	-114.6

	Face 2	
Uy(in)	15-deg-Pp (kips)	15-deg-PT (kips)
0.00	0.0	0.0
0.03	-56.4	-47.2
0.16	-146.0	-66.8
0.31	-169.9	-71.2
1.55	-181.6	-70.2
2.80	-186.3	-71.3
3.11	-175.7	-71.6

*Ux = displacement in x-direction, Uy = displacement in y-direction, Pp = passive force, PT = shear force on passive face

	Face 1	
Ux(in)	30-deg-Pp (kips)	30-deg-PT (kips)
0.00	0	0.0
0.10	-244	-71.9
0.52	-440	-127.7
1.04	-415	-123.5
5.20	-436	-127.7
9.35	-440	-126.0
10.39	-436	-127.6

	Face 2	
Uy(in)	30-deg-Pp (kips)	30-deg-PT (kips)
0.00	0.0	0.0
0.06	-86.7	-53.0
0.30	-180.7	-72.7
0.60	-196.5	-65.0
3.00	-192.4	-71.0
5.40	-202.1	-74.7
6.00	-193.8	-70.0

*Ux = displacement in x-direction, Uy = displacement in y-direction, Pp = passive force, PT = shear force on passive face

	Face 1	
Ux(in)	45-deg-Pp (kips)	45-deg-PT (kips)
0.00	0	0.0
0.08	-203	-95.2
0.42	-376	-134.5
0.85	-416	-142.9
4.24	-408	-138.5
7.64	-424	-142.6
8.49	-409	-140.2

	Face 2	
Uy(in)	45-deg-Pp (kips)	45-deg-PT (kips)
0.00	0.0	0.0
0.08	-116.6	-51.2
0.42	-213.9	-55.5
0.85	-202.1	-63.6
4.24	-207.2	-59.5
7.64	-200.7	-64.4
8.49	-200.5	-66.0

*Ux = displacement in x-direction, Uy = displacement in y-direction, Pp = passive force, PT = shear force on passive face

5 ft x 5 ft 120 pcf Limestone

	Face 1	
Ux(in)	0-deg-Pp (kips)	0-deg-PT (kips)
0	0	0.0
0.6	-457	-0.4
1.2	-461	-5.2
2.4	-434	6.0
3.6	-465	-0.9
4.8	-449	-6.3
6	-463	-4.8

	Face 2	
Uy(in)	0-deg-Pp (kips)	0-deg-PT (kips)
0.00	0.0	0.0
0.00	-12.2	-47.6
0.00	-8.6	-47.6
0.00	-12.8	-49.3
0.00	-11.8	-47.9
0.00	-9.2	-46.8
0.00	-8.8	-47.5

*Ux = displacement in x-direction, Uy = displacement in y-direction, Pp = passive force, PT = shear force on passive face

	Face 1	
Ux(in)	15-deg-Pp (kips)	15-deg-PT (kips)
0	0	0.0
0.58	-400	-69.9
1.16	-438	-73.8
2.32	-434	-71.2
3.48	-438	-73.7
4.64	-433	-72.6
5.80	-442	-75.2

	Face 2	
Uy(in)	15-deg-Pp (kips)	15-deg-PT (kips)
0.00	0.0	0.0
0.16	-303.7	-121.1
0.31	-248.0	-107.2
0.62	-305.2	-120.4
0.93	-278.0	-111.9
1.24	-312.2	-123.6
1.55	-291.6	-118.5

*Ux = displacement in x-direction, Uy = displacement in y-direction, Pp = passive force, PT = shear force on passive face

	Face 1	
Ux(in)	30-deg-Pp (kips)	30-deg-PT (kips)
0.00	0	0.0
0.52	-386	-106.1
1.04	-380	-102.6
2.08	-356	-106.8
3.12	-381	-110.7
4.16	-382	-104.7
5.20	-370	-104.5

	Face 2	
Uy(in)	30-deg-Pp (kips)	30-deg-PT (kips)
0.00	0.0	0.0
0.30	-306.1	-112.2
0.60	-331.2	-123.0
1.20	-343.6	-122.1
1.80	-347.7	-125.8
2.40	-364.7	-130.8
3.00	-347.6	-126.2

*Ux = displacement in x-direction, Uy = displacement in y-direction, Pp = passive force, PT = shear force on passive face

	Face 1	
Ux(in)	45-deg-Pp (kips)	45-deg-PT (kips)
0.00	0	0.0
0.42	-364	-123.5
0.85	-354	-120.2
1.70	-374	-123.6
2.55	-371	-121.2
3.39	-350	-118.1
4.24	-371	-120.8

	Face 2	
Uy(in)	45-deg-Pp (kips)	45-deg-PT (kips)
0.00	0.0	0.0
0.42	-362.6	-108.6
0.85	-368.5	-109.8
1.70	-378.0	-116.3
2.55	-383.9	-118.7
3.39	-382.9	-114.1
4.24	-398.6	-119.1

*Ux = displacement in x-direction, Uy = displacement in y-direction, Pp = passive force, PT = shear force on passive face

	Face 1	
Ux(in)	60-deg-Pp (kips)	60-deg-PT (kips)
0	0	0.0
0.3	-349	-128.7
0.6	-341	-127.7
1.2	-346	-128.4
1.8	-342	-126.7
2.4	-346	-128.5
3	-347	-128.9

	Face 2	
Uy(in)	60-deg-Pp (kips)	60-deg-PT (kips)
0.00	0.0	0.0
0.52	-385.4	-89.1
1.04	-397.0	-84.5
2.08	-395.9	-84.6
3.12	-374.4	-80.6
4.16	-407.9	-86.0
5.20	-378.2	-89.0

*Ux = displacement in x-direction, Uy = displacement in y-direction, Pp = passive force, PT = shear force on passive face

	Face 1	
Ux(in)	75-deg-Pp (kips)	75-deg-PT (kips)
0	0	0.0
0.2	-314	-124.9
0.3	-314	-124.9
0.6	-319	-125.8
0.9	-323	-127.6
1.2	-321	-126.2
1.6	-327	-128.8

	Face 2	
Uy(in)	75-deg-Pp (kips)	75-deg-PT (kips)
0.00	0.0	0.0
0.58	-406.3	-70.5
1.16	-386.0	-73.1
2.32	-429.2	-68.8
3.48	-397.4	-71.6
4.64	-414.4	-68.3
5.80	-418.6	-76.4

*Ux = displacement in x-direction, Uy = displacement in y-direction, Pp = passive force, PT = shear force on passive face

	Face 1	
Ux(in)	90-deg-Pp (kips)	90-deg-PT (kips)
0	0	0.0
0	-11	-46.7
0	-9	-47.9
0	-9	-44.9
0	-14	-48.1
0	-11	-44.9
0	-10	-46.7

	Face 2	
Uy(in)	90-deg-Pp (kips)	90-deg-PT (kips)
0.00	0.0	0.0
0.60	-470.0	0.0
1.20	-480.0	0.0
2.40	-487.8	-9.3
3.60	-459.7	-3.5
4.80	-476.5	-2.5
6.00	-452.6	-2.3

*Ux = displacement in x-direction, Uy = displacement in y-direction, Pp = passive force, PT = shear force on passive face

16 ft x 8 ft 120 pcf Limestone

	Face 1	
Ux(in)	0-deg-Pp (kips)	0-deg-PT (kips)
0	0	0.0
0.12	-1952	-2.3
0.6	-1936	45.9
1.2	-1958	-6.1
6	-2029	8.5
10.8	-2014	9.3
12	-2046	-5.7

	Face 2	
Uy(in)	0-deg-Pp (kips)	0-deg-PT (kips)
0.00	0.0	0.0
0.00	-27.5	-124.6
0.00	-33.7	-126.5
0.00	-48.9	-129.9
0.00	-55.2	-132.0
0.00	-68.9	-135.7
0.00	-46.0	-129.0

*Ux = displacement in x-direction, Uy = displacement in y-direction, Pp = passive force, PT = shear force on passive face

	Face 1	
Ux(in)	15-deg-Pp (kips)	15-deg-PT (kips)
0	0	0.0
0.12	-1806	-363.0
0.58	-1900	-395.4
1.16	-1912	-428.8
5.80	-1901	-434.7
10.43	-1859	-445.3
11.59	-1923	-430.9

	Face 2	
Uy(in)	15-deg-Pp (kips)	15-deg-PT (kips)
0.00	0.0	0.0
0.03	-416.0	-229.2
0.16	-625.2	-280.9
0.31	-691.7	-297.6
1.55	-710.7	-301.9
2.80	-674.3	-286.1
3.11	-701.0	-299.6

*Ux = displacement in x-direction, Uy = displacement in y-direction, Pp = passive force, PT = shear force on passive face

	Face 1	
Ux(in)	30-deg-Pp (kips)	30-deg-PT (kips)
0.00	0	0.0
0.10	-1591	-498.3
0.52	-1776	-497.3
1.04	-1732	-505.6
5.20	-1764	-497.4
9.35	-1824	-496.0
10.39	-1790	-490.6

	Face 2	
Uy(in)	30-deg-Pp (kips)	30-deg-PT (kips)
0.00	0.0	0.0
0.06	-637.0	-276.1
0.30	-755.1	-307.4
0.60	-770.3	-303.8
3.00	-698.3	-290.2
5.40	-729.5	-301.4
6.00	-710.7	-289.5

*Ux = displacement in x-direction, Uy = displacement in y-direction, Pp = passive force, PT = shear force on passive face

	Face 1	
Ux(in)	45-deg-Pp (kips)	45-deg-PT (kips)
0.00	0	0.0
0.08	-1462	-600.0
0.42	-1571	-573.8
0.85	-1629	-598.0
4.24	-1651	-598.4
7.64	-1613	-585.0
8.49	-1643	-590.6

	Face 2	
Uy(in)	45-deg-Pp (kips)	45-deg-PT (kips)
0.00	0.0	0.0
0.08	-677.5	-271.4
0.42	-798.9	-281.3
0.85	-794.5	-283.2
4.24	-792.7	-289.6
7.64	-823.3	-293.6
8.49	-779.8	-291.6

*Ux = displacement in x-direction, Uy = displacement in y-direction, Pp = passive force, PT = shear force on passive face

	Face 1	
Ux(in)	60-deg-Pp (kips)	60-deg-PT (kips)
0	0	0.0
0.06	-1263	-573.9
0.3	-1511	-623.1
0.6	-1540	-628.1
3	-1503	-622.3
5.4	-1528	-627.5
6	-1464	-608.2

	Face 2	
Uy(in)	60-deg-Pp (kips)	60-deg-PT (kips)
0.00	0.0	0.0
0.10	-824.7	-231.4
0.52	-901.7	-241.0
1.04	-826.9	-235.6
5.20	-914.3	-251.7
9.35	-894.0	-248.5
10.39	-832.2	-244.7

*Ux = displacement in x-direction, Uy = displacement in y-direction, Pp = passive force, PT = shear force on passive face

	Face 1	
Ux(in)	90-deg-Pp (kips)	90-deg-PT (kips)
0	0	0.0
0	-49	-261.7
0	-46	-261.0
0	-48	-261.6
0	-40	-259.4
0	-45	-260.7
0	-39	-259.1

	Face 2	
Uy(in)	90-deg-Pp (kips)	90-deg-PT (kips)
0.00	0.0	0.0
0.12	-973.4	4.4
0.60	-955.9	-15.4
1.20	-995.5	-3.2
6.00	-965.3	2.7
10.80	-989.9	0.9
12.00	-1027.5	9.3

*Ux = displacement in x-direction, Uy = displacement in y-direction, Pp = passive force, PT = shear force on passive face

C.8 Oblique Passive Reduction Derivation

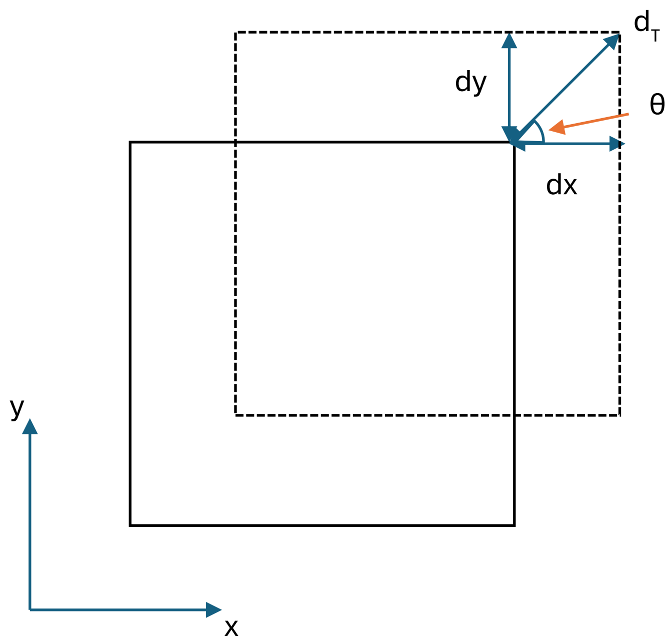

Figure C-12 Oblique displacement of footing and displacement vectors.

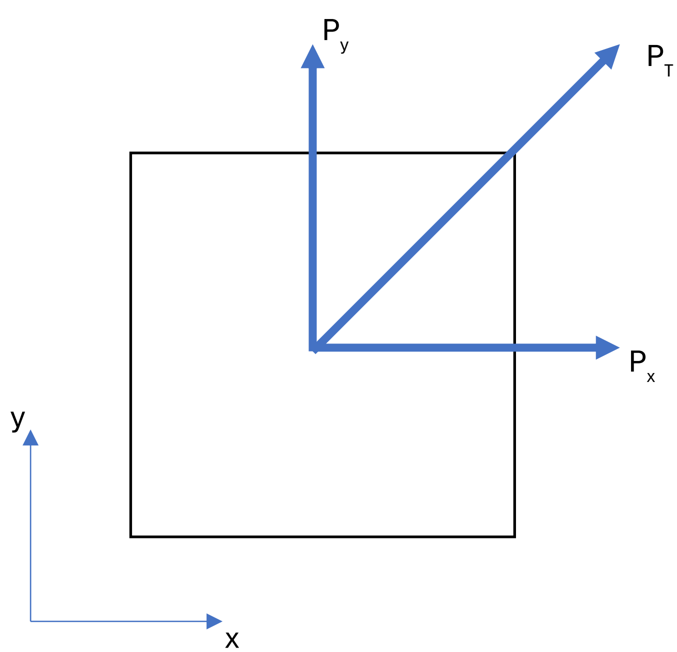

Figure C-13 Oblique loading of footing and loading vectors.

Trigonometric Assumptions based on Figure C-12 and assuming the force vector is oriented in the same direction as the displacement vector.

$$\frac{\mathrm{d}y}{\mathrm{d}x} = \tan\theta \qquad \frac{\mathrm{d}y}{\mathrm{d}T} = \sin\theta \qquad \frac{\mathrm{d}x}{\mathrm{d}T} = \cos\theta$$

$$\frac{\mathrm{P}y}{\mathrm{P}x} = \tan\theta \qquad \frac{\mathrm{P}y}{\mathrm{P}T} = \sin\theta \qquad \frac{\mathrm{P}x}{\mathrm{P}T} = \cos\theta$$

Need to determine a reduction value Rx and Ry that reduces the ultimate passive resistance based on the specified oblique angle.

$$Px = \frac{dx}{\frac{1}{k_{max}} + \frac{R_f}{P_{ult}Rx}dx} \qquad Py = \frac{dy}{\frac{1}{k_{max}} + \frac{R_f}{P_{ult}Ry}dy} \qquad Pt = \frac{dT}{\frac{1}{k_{max}} + \frac{R_f}{P_{ult}}dT}$$

To determine Rx,

$$\frac{\mathrm{P}x}{\mathrm{P}t} = \cos\theta = \frac{\dfrac{dx}{\frac{1}{k_{max}} + \frac{R_f}{P_{ult}Rx}dx}}{\dfrac{dT}{\frac{1}{k_{max}} + \frac{R_f}{P_{ult}}dT}}$$

$$= \cos\theta = \frac{dx}{dT}\frac{\frac{1}{k_{max}} + \frac{R_f}{P_{ult}}dT}{\frac{1}{k_{max}} + \frac{R_f}{P_{ult}Rx}dx} = \cos\theta\,\frac{\frac{1}{k_{max}} + \frac{R_f}{P_{ult}}dT}{\frac{1}{k_{max}} + \frac{R_f}{P_{ult}Rx}dx}$$

$$\rightarrow 1 = \frac{\frac{1}{k_{max}} + \frac{R_f}{P_{ult}}dT}{\frac{1}{k_{max}} + \frac{R_f}{P_{ult}Rx}dx}$$

$$\rightarrow \frac{1}{k_{max}} + \frac{R_f}{P_{ult}Rx}dx = \frac{1}{k_{max}} + \frac{R_f}{P_{ult}}dT$$

$$\rightarrow \frac{R_f}{P_{ult}Rx}dx = \frac{R_f}{P_{ult}}dT$$

$$\rightarrow \frac{dx}{dT} = Rx = \cos\theta$$

By inspection,

$$Ry = \sin\theta$$

APPENDIX D
WORKED EXAMPLES OF INCLINED AND ECCENTRIC BEARING CAPACITY

D.1 Inclination

Table D-1 Case 9-11 bearing capacity, BDV31-977-124 with 7° inclined load and all formation inclination factor method.

Footing Geometry	B, ft	10
	L, ft	15
	D_f, ft	3
Load Inclination	α_i, °	7
Mass Properties	c, psi	31.77
	φ, °	36.31
	P_p, psi	308
	ω, °	0.43
Florida Bearing Capacity Equations	N_c	$\frac{1.8\ \cos\varphi}{0.8-\sin\varphi} = \frac{1.8\ \cos(36.31)}{0.8-\sin(36.31)} = 6.98$
	N'_c	$\frac{1.8\ \cos\varphi}{0.8-\sin\omega} = \frac{1.8\ \cos(36.31)}{0.8-\sin(0.43)} = 1.83$
	N_γ	$\frac{1.8\ [\sin\varphi - \sin\omega]}{0.8-\sin\omega} = \frac{1.8\ [\sin(36.31) - \sin(0.43)]}{0.8-\sin(0.43)} = 1.33$
	q, psi	(3) × 100/144 = 2.08 (overburden stress)
	N_q	$(1.53 \times \frac{p_p}{\sigma_a} - 10) \times (3 \times \sin\varphi\ -\ 1) = (1.53 \times \frac{308}{14.7} - 10) \times (3 \times \sin(36.31)\ -\ 1) = 17.11$
	n	$\left(\frac{4}{0.3B \text{ in ft}}\right)^{-0.055} = \left(\frac{4}{0.3*10}\right)^{-0.055} = 0.98$
	ξ	$1\ +\ 0.245\ \left(\frac{B}{L}\right)^{0.66} = 1\ +\ 0.245\ \left(\frac{10}{15}\right)^{0.66} = 1.19$
	N_R	1
	i_c	$i_c = (1-\frac{\alpha_i}{90^\circ})^{0.0044(L/B)^2\ -\ 0.0614(L/B)\ +\ 0.373}$=0.976 (all formation)
	i_q	$i_q = (1-\frac{\alpha_i}{90^\circ})^{-3E-4(L/B)^2+0.0237(L/B)+0.523}$=0.955 (all formation)
	i_γ	$i_\gamma = (1-\frac{\alpha_i}{\phi^\circ})^{9E-4(L/B)^2-0.0152\ (L/B)+0.152}$=0.972 (all formation)
	Qu1, psi	$n \times c \times N_c \times i_c + q \times N_q \times i_q = 0.98 \times 31.77 \times 6.98 \times 0.976 + 2.08 \times 17.11 \times 0.955 = 246.09$
	Qu2, psi	$n \times [c \times N'_c \times i_c + p_p \times N_\gamma \times i_\gamma] + q \times N_q \times i_q = 0.98 \times [31.77 \times 1.83 \times 0.976 + 308 \times 1.33 \times 0.972] + 2.08 \times 17.11 \times 0.955 = 479.80$
	Qu	$\min(Q_{u1}, Q_{u2}) \times \xi/N_R = \min(246.09, 479.80) \times 1.19/1 = 292.8$ psi = 21.0 tsf

Table D-2 Inclination worked example comparison to FBMP.

Parameter	Worked Example	FBMP UI	FBMP OUTPUT
Q_u, psi	292.8	293.85	293.8469

D.2 Eccentricity

Table D-3 Case 9-11 bearing capacity, BDV31-977-124 with eccentricity b/6.

Footing Geometry	B, ft	10
	L, ft	15
	D_f, ft	3
Eccentricity	e, ft	1.67
Mass Properties	c, psi	31.77
	φ, °	36.31
	P_p, psi	308
	ω, °	0.43
Florida Bearing Capacity Equations	N_c	$\frac{1.8\ \cos\varphi}{0.8-\sin\varphi} = \frac{1.8\ \cos(36.31)}{0.8-\sin(36.31)} = 6.98$
	N'_c	$\frac{1.8\ \cos\varphi}{0.8-\sin\omega} = \frac{1.8\ \cos(36.31)}{0.8-\sin(0.43)} = 1.83$
	N_γ	$\frac{1.8\ [\sin\varphi-\sin\omega]}{0.8-\sin\omega} = \frac{1.8\ [\sin(36.31)-\sin(0.43)]}{0.8-\sin(0.43)} = 1.33$
	q, psi	(3) × 100/144 = 2.08 (overburden stress)
	N_q	$(1.53 \times \frac{p_p}{\sigma_a} - 10) \times (3 \times \sin\varphi - 1) = (1.53 \times \frac{308}{14.7} - 10) \times (3 \times \sin(36.31) - 1) = 17.11$
	B′, ft	B-2e = 6.67
	n	$\left(\frac{4}{0.3B'\ \text{in ft}}\right)^{-0.055} = \left(\frac{4}{0.3*6.67}\right)^{-0.055} = 0.96$
	ξ	$1 + 0.245\left(\frac{B'}{L}\right)^{0.66} = 1 + 0.245\left(\frac{6.67}{15}\right)^{0.66} = 1.14$
	N_R	1
	Qu1, psi	$n \times c \times N_c + q \times N_q = 0.96 \times 31.77 \times 6.98 + 2.08 \times 17.11 = 248.47$
	Qu2, psi	$n \times [c \times N'_c + p_p \times N_\gamma] + q \times N_q = 0.96 \times [31.77 \times 1.83 + 308 \times 1.33] + 2.08 \times 17.11 = 484.65$
	Qu	$\min(Q_{u1}, Q_{u2}) \times \xi/N_R = \min(248.47, 484.65) \times 1.14/1 = 283.2$ psi = 20.3 tsf

Table D-4 Eccentricity worked example comparison to FB-MultiPier (FBMP).

Parameter	Worked Example	FBMP UI	FBMP OUTPUT
Q_u, psi	283.2	285.03	285.0261

D.3 Eccentricity and Inclination

Table D-5 Task 1: case 9-11 bearing capacity, BDV31-977-124 with an eccentric and 7° inclined load and all formation inclination factor method.

Footing Geometry	B, ft	10
	L, ft	15
	D_f, ft	3
Eccentricity	e, ft	1.67
Load Inclination	α_i, °	7
Mass Properties	c, psi	31.77
	φ, °	36.31
	P_p, psi	308
	ω, °	0.43
Florida Bearing Capacity Equations	N_c	$\frac{1.8\ \cos\varphi}{0.8-\sin\varphi}=\frac{1.8\ \cos(36.31)}{0.8-\sin(36.31)}$ = 6.98
	N'_c	$\frac{1.8\ \cos\varphi}{0.8-\sin\omega}=\frac{1.8\ \cos(36.31)}{0.8-\sin(0.43)}$ = 1.83
	N_γ	$\frac{1.8\ [\sin\varphi-\sin\omega]}{0.8-\sin\omega}=\frac{1.8\ [\sin(36.31)-\sin(0.43)]}{0.8-\sin(0.43)}$= 1.33
	q, psi	(3) × 100/144 = 2.08 (overburden stress)
	N_q	$(1.53\times\frac{p_p}{\sigma_a}-10)\times(3\times\sin\varphi\ -\ 1)$= $(1.53\times\frac{308}{14.7}-10)\times(3\times\sin(36.31)\ -\ 1)$ = 17.11
	B′, ft	B-2e = 6.67
	n	$\left(\frac{4}{0.3B'\text{ in ft}}\right)^{-0.055}$=$\left(\frac{4}{0.3*6.67}\right)^{-0.055}$ = 0.96
	ξ	$1\ +\ 0.245\ \left(\frac{B'}{L}\right)^{0.66}$=$1\ +\ 0.245\ \left(\frac{6.67}{15}\right)^{0.66}$ = 1.14
	N_R	1
	i_c	$i_c=(1-\frac{\alpha_i}{90^\circ})^{0.0044(L/B')^2-0.0614(L/B')+0.373}$=0.979 (all formation)
	i_q	$i_q=(1-\frac{\alpha_i}{90^\circ})^{-3E-4(L/B')^2+0.0237(L/B')+0.523}$=0.954 (all formation)
	i_γ	$i_\gamma=(1-\frac{\alpha_i}{\phi^\circ})^{9E-4(L/B')^2-0.0152\ (L/B')+0.152}$=0.974 (all formation)
	Qu1, psi	$n\times c\times N_c\times i_c+q\times N_q\times i_q$ = 0.96× 31.77 × 6.98 × 0.976 + 2.08×17.11× 0.955 = 243.07
	Qu2, psi	$n\times[c\times N'_c\times i_c+p_p\times N_\gamma\times i_\gamma]+q\times N_q\times i_q$ = 0.96× [31.77 ×1.83× 0.976 + 308×1.33× 0.972] + 2.08× 17.11 × 0.955 = 472.45
	Qu	min (Q_{u1}, Q_{u2}) × ξ/N_R = min (246.09,479.80) ×1.14/1= 277.8 psi = 20.0 tsf

Table D-6 Eccentricity and inclination worked example comparison to FB-MultiPier (FBMP).

Parameter	Worked Example	FBMP UI	FBMP OUTPUT
Q_u, psi	277.8	278.14	278.1353

APPENDIX E
WORKED EXAMPLE OF SINGLE LAYER

E.1 Axial Phase II Report Single Layer Example Section 9.2

This worked example is from Phase II report. In this example, a 10 ft by 15 ft footing (embedded 3ft) is planned for a bridge pier located in downtown Miami. Given its location, Borings RC-1 and RC-2 from Cemex site are used as well as rock data from borings B-1 to B-3 from the SR-84 site which showed similar trends (dry unit weight versus depth) as depicted in Figure E-1. (Note: core runs not from same initial depth). Next, using the dry unit weights (Table E-1), the Young's Modulus as a function of dry unit weight is estimated from modulus correlation. Presented in Table E-2 are the summary statistics of Table E-1 . The CV of dry unit weight (strength) is 0.11 but the CV of modulus is 1.43.

For estimation of bearing capacity of the footing, a representative set of strength parameters is required based on dry unit weight. A 10 ft wide footing generally has a bearing failure 1.5B to 2B below the bottom of footing. However, if a much stronger layer exists deeper, its' penetration may be limited from B to 1.5B (Button, 1953). Therefore, for this example, the rupture surface or bearing zone is limited to 1.5B (depths 3 to 18 ft). Using the dry unit weights within this zone (3-18 ft), a geomean of 97.5 pcf was estimated. Using the closest dry unit specimen strength envelope correlation available (100 pcf), an adjusted mass strength envelope, was developed based on the rock adjusted-recovery (80 %) as discussed.

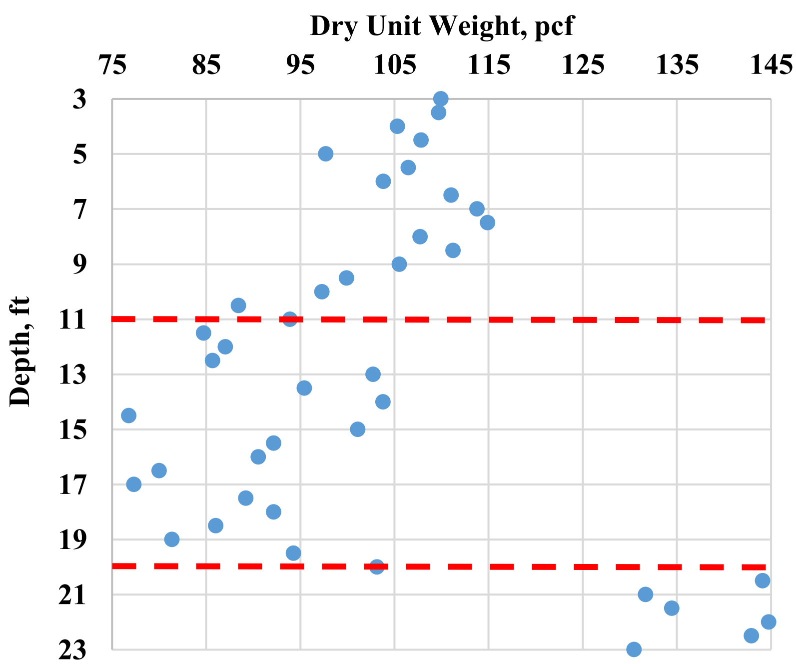

Figure E-1 Dry unit weight versus depth: single layer case.

Table E-1 Dry unit weight and Modulus profile.

Depth, ft	γ_{dt}, pcf	E_i, psi (Figure 2-5a, trendline)	Depth, ft (Continued)	γ_{dt}, pcf	E_i, psi (Figure 2-5a, trendline)
3	109.9	64526.7	13.5	95.4	28132.5
3.5	109.7	63698.1	14	103.8	45430.4
4	105.3	49513.1	14.5	76.8	9681.6
4.5	107.8	57158.5	15	101.1	38922.4
5	97.7	32064.1	15.5	92.2	23369.1
5.5	106.4	52911.9	16	90.5	21298.8
6	103.8	45497.0	16.5	80.0	11655.0
6.5	111.0	68679.2	17	77.3	9985.6
7	113.8	80455.5	17.5	89.2	19714.6
7.5	114.9	85690.2	18 (End of Bearing Layer)	92.2	23369.1
8	107.7	56922.2	18.5	86.0	16427.2
8.5	111.2	69468.0	19	81.4	12591.7
9	105.5	50115.8	19.5	94.3	26365.4
9.5	99.9	36389.5	20	103.1	43743.4
10	97.3	31352.6	20.5	144.1	455892.2
10.5	88.4	18869.8	21	131.7	223959.6
11	93.9	25782.5	21.5	134.5	262681.7
11.5	84.7	15248.0	22	144.8	473204.1
12	87.0	17421.1	22.5	142.9	425740.3
12.5	85.7	16125.3	23	130.4	208682.9
13	102.7	42706.4			

Table E-2 Summary statistics.

	γ_{dt}, pcf	E_i, psi
Count	31	41
Mean	98.2	81986.4
Geomean	97.5	44221.4
Harmonic Mean $\left(E_h = \frac{n}{\Sigma \frac{1}{E_i}}\right)$	96.9	29978.6
Median	99.9	42706.4
Standard Deviation	10.8	117358.8
CV	0.11	1.43

Next, knowing the mass strength properties of the 100 pcf rock from a depth of 3 ft to 18 ft, the bearing capacity of a 10 ft by 15 ft footing may be estimated, as shown in Table E-3 . First, the bearing capacity factors Nc, Nc', N_q, and Ng (see Table E-3) are determined based on the mass angles of friction (f, w), along with overburden bearing stress, q (g D_f see Table E-3). Next, the minimum bearing capacity (smaller of Q_{u1} and Q_{u2}) is found (depends on strength angles f, w), and shape factor ξ is found and combined ($Q_{u1} \times \xi$) to give the final bearing capacity of 300.4 psi (21.63 tsf) of the 10 ft by 15 ft footing.

Table E-3 Bearing capacity calculations.

Footing Geometry	B, ft	10
	L, ft	15
	D_f, ft	3
Mass Properties	c, psi	31.77 (Table E-2)
	φ, °	36.31(Table E-2)
	P_p, psi	308 (Table E-2)
	ω, °	0.43 (Table E-2)
Florida Bearing Capacity Equations	N_c	$\frac{1.8\ \cos\varphi}{0.8-\sin\varphi} = \frac{1.8\ \cos(36.31)}{0.8-\sin(36.31)}$ = 6.98 (Equation 2-14)
	N'_c	$\frac{1.8\ \cos\varphi}{0.8-\sin\omega} = \frac{1.8\ \cos(36.31)}{0.8-\sin(0.43)}$ = 1.83 (Equation 2-15)
	N_γ	$\frac{1.8\ [\sin\varphi - \sin\omega]}{0.8-\sin\omega} = \frac{1.8\ [\sin(36.31) - \sin(0.43)]}{0.8-\sin(0.43)}$ = 1.33 (Equation 2-16)
	q, psi	3 (D_f) × 100/144 = 2.08 (Equation 2-17, overburden stress)
	N_q	$(1.5 \times \frac{p_p}{\sigma_a} - 10) \times (3 \times \sin\varphi\ -\ 1)$= $(1.5 \times \frac{308}{14.7} - 10) \times (3 \times \sin(36.31)\ -\ 1)$ = 16.64 (Equation 2-18)
	n	$\left(\frac{4}{0.3B\ \text{in ft}}\right)^{-0.055}$=$\left(\frac{4}{0.3*10}\right)^{-0.055}$ = 0.98 (Equation 2-10)
	ξ	$1\ +\ 0.245\ \left(\frac{B}{L}\right)^{0.66}$=$1\ +\ 0.245\ \left(\frac{10}{15}\right)^{0.66}$ = 1.19 (Equation 2-11)
	N_R	1 (Equation 2-12)
	Qu1, psi	$n \times c \times N_c + q \times N_q$ = 0.98× 31.77 × 6.98 + 2.08×16.64 = 252.95 (Equation 2-8)
	Qu2, psi	$n \times [c \times N'_c + p_p \times N_\gamma] + q \times N_q$= 0.98× [31.77 ×1.83 + 308×1.33] + 2.08× 16.64 = 494.51 (Equation 2-9)
	Qu	min (Q_{u1}, Q_{u2}) × ξ/N_R = min (252.95, 494.51) ×1.19/1= 300.4 psi = 21.63 tsf (Equation 2-7)

In the case of settlements two approaches maybe considered. One approach is to further subdivide the rock into 3 layers (3 ft to 8 ft, 8 ft to 11 ft and 11 ft to 22 ft), due to the difference in dry unit weights. Then using the weighted (based on stress) harmonic mean modulus (each layer), 2, the load-settlement response may be predicted. Note, in the harmonic stress weighted modulus (Table E-4), the ratio of stress/modulus of each sub-layer in the E_h calculation represents the settlement of each sublayer. For the stress in each sublayer, one must interpolate between square and strip, Figure E-2. Finally, the weighted specimen harmonic modulus of 35,124 psi is computed (Table E-4), and the mass weighted harmonic modulus, E_{mass} is found by multiplying specimen modulus, E_h, by mass/specimen ratio (0.55),

$$E_{mass} = 0.55\ \times\ 35{,}124\ psi = 19{,}318\ psi$$

Subsequently, the settlement of footing may be obtained from elastic theory as

$$d = \Delta q_s \frac{B\,S_f}{E_{mass}}\,1.12(1-\nu^2) = \frac{300.4\times10\times12\times1.12\times1.25\times(1-0.01)}{19318.3} = 2.6 \text{ inches}$$

Where Dq_s = bearing stress 300.4 psi

B = footing width 10 ft

n = Poisson's ratio = 0.1

S_f = shape factor = 1.25 for L/B =2

Even though the above approach does account for layering, it does not account for the variability within any layer (see Figure E-1.). Implemented in FB-MultiPier for FL Limestone homogeneous model accounts for variability using a probabilistic settlement approach. In this example using the geomean of moduli of all rock data, as well as the CV of the moduli (assumed lognormal) to calculate the mean settlement as shown in Table E-5. Comparison of this estimated settlement with the previous weighted harmonic mean show good agreement as seen in Figure E-2.

Table E-4 Layering, modulus, and additional stress.

Depth, ft	γ_{dt}, pcf (average)	h_i, ft	E_i, psi (Figure 2-5a, trendline, based on γ_{dt})	σ_i, psi (Figure E-2, interpolated between strip and square footings)
3~11	105	8	48580.9	225.3
11~20	90.2	9	20863.3	108.9
20~23	138.1	3	322619.3	63.8
$E_h = \frac{\sum h_i\sigma_i}{\sum\frac{h_i\sigma_i}{E_i}} = \frac{(8\times225.3+9\times108.9+3\times63.8)}{(8\times225.3/48580.9+9\times108.9/20863.3+3\times63.8/322619.9)}$ =35124.3 psi				

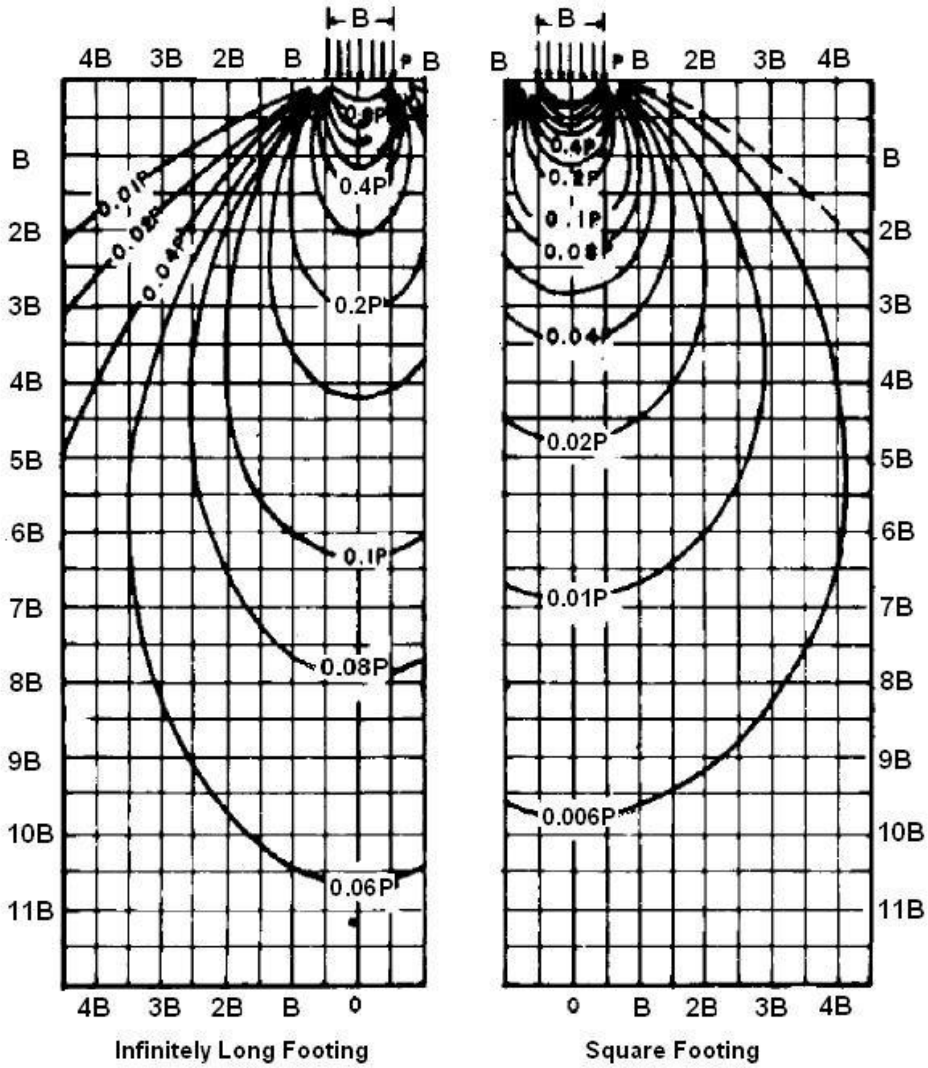

Figure E-2 Boussinesq stress chart, interpolated between the strip and square footings (Lambe and Whitman, 1969).

Table E-5 FB-MultiPier FL Limestone (Homogeneous) Probabilistic Settlement.

Mass properties	E_m, ksi	24.321
	CV_{Em}	1.43
	ν	0.1 (Poisson's ratio)
	a_v, ft	3 (Correlation length)
Geometry	B, ft	10 (Footing width)
	L, ft	15
	T_r, ft	15
	t, in	3
	$E_{foundation}$, ksi	29000
Bearing value	Q_u, psi	301.76
Fenton and Griffiths' method	δ_{det}, in	1.582
	μ_δ, in	2.959

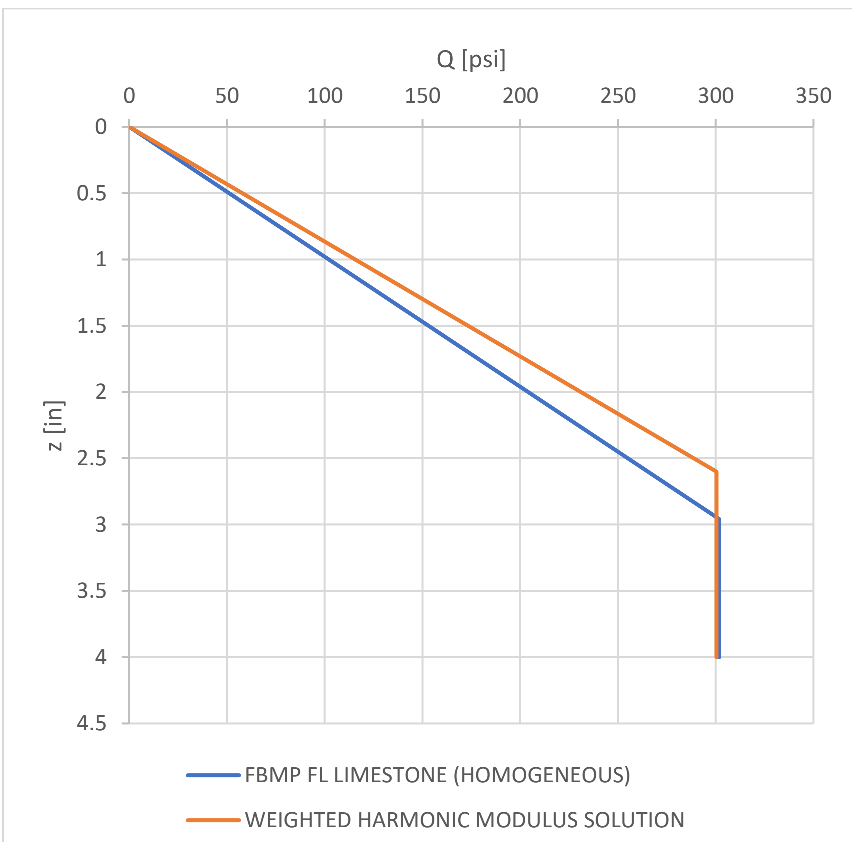

Figure E-3 Load-settlement prediction of single layer case.

APPENDIX F
FB-MULTIPIER INPUT FILE UPDATE

The input parameters associated with soil resistance models for the shallow foundation are entered using the FB-MultiPier UI. These shallow foundation data are then saved in the input (.in) file. The input for the shallow foundation geometric and soil properties are written under header SHALLOWFOUND in the input file as mentioned below.

F.1 User-Guide for Input File Update

SHALLOWFOUND

N= NSET // LINE 2

S= SSET A= AM P= PM F= FM C= PS X=FORM L=PF E=OF V= SF R=PR K=RPF // LINE 3

W= WD D= DPT E= LEFW F= LEFL H= GD R= RT U=TUW A= ABD T= BBD B= DB M= ED // LINE 4

V= SIGPEAK C= MC T= MC2 F= MF R= MR W= IPPEAK X= IC Y= IF Z= IR M= IM // LINE 5

Q= QU G= GSI M= IMC R= REC D= DS Y= BC A= MMR B= MMS T= ST F= TBF S= ASM // LINE 6

M= PFO U=PDB R=PRR P= PULP S= ISLP F= FRLP B= FWLP L=FLLP H= FTLP D= DTFLP X= DBFLP T= DWTLP E= EFFLP I=DTBL Z= LSM C= SGF G= SRF // LINE 7

W= ULP A= PLP C= CLP V= VLP I= EILP R= FALP M= LDLP U= AUSLP H=ALP G= ALLP J= BLP K= PPLP N= EMLP E= EPLP B= PGF D= PRF // LINE 8

X= ICC Y= IFAC Z= IRAC M= IMC V=IPSC S= MPSC C= MCC T= MFAC F= MRAC R= MMRC P= PRC // LINE 9

X= ICE Y= IFAE Z= IRAE M= IME V=IPSE S= MPSE C= MCE T= MFAE F= MRAE R= MMRE P= PRE //LINE 10

P= PULF S= ISLF F= FRLF A= AFLF C= CLF L= FLLF W= FWLF N= NFLF I= IFLF M= IMLF ~~T= TNFLF~~ // LINE 11

V= CVM D= SDM P= PRS C= CL E= SR R= RF B= MS L= LBS U= UBS S= SCT // LINE 12

A= DABC01 PABC01 DABC02 PABC02 … DABC20 PABC20 // LINE 13

P= DLPC01 PLPC01 DLPC02 PLPC02 … DLPC20 PLPC20 // LINE 14

F= DBFC01 PBFC01 DBFC02 PBFC02 … DBFC20 PBFC20 // LINE 15

:

//Header close

Where,

NSET is the number of soil sets, each of the lines repeated per soilset for which data will be written (integer)

LINE 3: General Information

SSET is the soil set number (integer)

AM is the axial bearing model for shallow foundation (integer).

= 0 - FL Limestone (Homogeneous)

= 2 - Hoek and Brown (Carter & Kulhawy)

= 3 – FL Limestone (Rock over sand)

= 5 - Linear (Subgrade)

= 6 - Custom

PM is the lateral passive model for shallow foundation (integer),

= 0 - FL Limestone

= 1 - C-Phi Material

= 2 - Hyperbolic

= 3 – Linear (Subgrade)

= 4 - Custom

= 5 - None

FM is the base friction model for shallow foundation (integer)

= 1 - Hyperbolic (Columb)

= 2 - Linear

= 3 - Custom

= 4 - None

PS is the Plot Space for strength envelop (UI use Only) (integer)

= 0 - Tau-sigma space

= 1 - p-q Space

FORM is the Rock Formation used in Axial Bearing Model (UI use Only) (integer)

PF is the passive model availability flag (UI use Only) (integer)

OF is the flag to account for Oblique effect (integer)

= 0 for Oblique effect is not included.

= 1 for Oblique effect is included.

SF is the flag to account for Shear Effect (integer)

= 0 for Shear effect is not included.

= 1 for Shear effect is included.

PR is the flag to account for Pultimate Reduction (integer)

= 0 for Pultimate Reduction is not considered.

= 1 for Pultimate Reduction is considered. The reduction/gain factors are not used.

RPF is the flag to account for rock layer as a passive model (integer)

= 0 for rock does not present as a bearing layer for passive model.

= 1 for rock present as a bearing layer for passive model.

LINE 4: Axial model data

WD is the footing width (double)

DPT is the footing length (double)

LEFW is the load eccentricity along the footing width (double)

LEFL is the load eccentricity along the footing length (double)

GD is the Groundwater Depth (double)

RT is the Rock Thickness (double)

TUW is the Total Unit Weight of Embedment Layer (double)

ABD is the Total Unit Weight of Soil Above Bearing Layer (double)

BBD is the Total Unit Weight of Soil Below Depth of the Footing (double)

DB is the Bulk Dry Unit Weight (UI use Only) (double)

ED is the Embedment Depth (double)

LINE 5: Axial model data (Contd.)

SIGPEAK is the Mass Ppeak Stress (double)

MC is the Mass Cohesion (double)

MC2 is the Mass Cohesion for Layer 2 (double)

MF is the Mass Friction Angle (double)

MR is the Mass Reduced Angle (double)

IPPEAK is the Intact Ppeak stress (double)

IC is the Intact Cohesion (UI use Only) (double)

IF is the Intact Friction Angle (UI use Only) (double)

IR is the Intact Reduced Angle (UI use Only) (double)

IM is the Intact Modulus (UI use Only) (double)

LINE 6: Axial model data (Contd.)

QU is the Unconfined Compressive Strength (qu) (double)

GSI is the Geological Strength Index (double)

IMC is the Intact Material Constant (double)

REC is the Rock Recovery (UI use only) (double)

DS is the Deterministic Settlement (UI use only) (double)

BC is the Bearing Capacity (UI use only) (double)

MMR is the Mass Modulus Rock (double)

MMS is the Mass Modulus Sand/Soil (double)

ST is the Sand Layer Thickness (double)

TBF is the Layer Thickness Below Footing (Hs2) (double)

ASM is the Subgrade Modulus (double)

LINE 7: Lateral Passive Data

PFO is the Lateral Passive Model Formation data (UI use only) (integer)

PDB is the Dry Bulk Unit Weight (UI use only) (double)

PRR is the Rock Recovery (UI use only) (double)

PULP is p ultimate (Pu) (double)

ISLP is initial stiffness (Kmax) (double)

FRLP is the failure ratio (Rf) (double)

FWLP is footing width (B) (double)

FLLP is footing length (L) (double)

FTLP is footing thickness (T) (double)

DTFLP is soil depth to top of footing (Dt) (double)

DBFLP is soil depth to bottom of footing (Df) (double)

DWTLP is depth of water table from groundsurface (Dw) (double)

EFFLP is embedded footing face (H) (double)

DTBL is depth to the top elevation of rock bearing layer of passive model (Dbl) (double)

LSM is the Subgrade Modulus (double)

SGF is the Shear Gain Factor (double)

SRF is the Shear Reduction Factor (double)

LINE 8: Lateral Passive Data (Contd.)

ULP is total unit weight (double)

PLP is the friction angle (phi) (double)

CLP is cohesion (double)

VLP is poissons ratio (v) (double)

EILP is initial soil tangent modulus (Ei) (double)

FALP is soil wall friction angle (double)

LDLP is max lateral deflection (double)

AUSLP is an additional uniform surcharge (double)

ALP is Ra, extension reduction factor (double)

ALLP is Ralpha, extension reduction factor (double)

BLP is Rbeta, extension reduction factor (double)

PPLP is Rpp, extension reduction factor (double)

EMLP is Rem, extension reduction factor (double)

EPLP is the type of lateral earth pressure (integer)

= 0 - use Ultimate lateral earth pressure

= 1 - use Net lateral earth pressure

PGF is the Passive Gain Factor (double)

PRF is the Passive Reduction Factor (double)

LINE 9: Lateral Passive Data (Contd.)

ICC is intact cohesion for compression (double)

IFAC is intact friction angle for compression (double)

IRAC is intact reduced angle for compression (double)

IMC is intact modulus for compression (double)

IPSC is intact peak stress for compression (double)

MPSC is mass peak stress for compression (double)

MCC is mass cohesion for compression (double)

MFAC is mass friction angle compression (double)

MRAC is mass reduced angle for compression (double)

MMRC is mass modulus for compression (double)

PRC is poissons ratio for compression (double)

LINE 10: Lateral Passive Data (Contd.)

ICE is intact cohesion for extension (double)

IFAE is intact friction angle for extension (double)

IRAE is intact reduced angle for extension (double)

IME is intact modulus for extension (double)

IPSE is intact peak stress for extension (double)

MPSE is mass peak stress for extension (double)

MCE is mass cohesion for extension (double)

MFAE is mass friction angle extension (double)

MRAE is mass reduced angle for extension (double)

MMRE is mass modulus for extension (double)

PRE is poisson’s ratio for extension (double)

LINE 11: Base Friction Data

PULF is p ultimate (Pu) (double)

ISLF is initial stiffness (Kmax) (double)

FRLF is failure ratio between p ultimate (Rf) (double)

AFLF is adhesion factor (double)

CLF is cohesion (double)

FLLF is footing length (double)

FWLF is footing width (double)

NFLF is normal force (double) (UI use Only)

IFLF is interface friction (double)

IMLF initial modulus (double)

LINE 12: Settlement Data

CVM is the coefficient of variation modulus (double)

SDM is the standard deviation of modulus (double)

PRS is the poison's ratio (v) (double)

CL is the correlation length (av) (double)

SR is the settlement range (n) (double)

RF is the rigidity factor (C) (double)

MS is the mean settlement (double)

LBS is the lower bound settlement (double)

UBS is the upper bound settlement (double)

SCT is the settlement curve type (integer)

= 0 – Mean settlement

= 1 – Upperbound settlement

= 2 – Lowerbound settlement

LINE 13: Custom Axial Bearing Resistance Curve

DABC01, DABC02, … DABC20 is the vertical displacement terms (double)

PABC01, PABC02, … PABC20 is the bearing pressure terms (double)

LINE 14: Custom Lateral Passive Resistance Curve

DLPC01, DLPC02, … DLPC20 is the lateral displacement terms (double)

PLPC01, PLPC02 … PLPC20 is the lateral passive pressure terms (double)

LINE 15: Custom Base Friction Resistance Curve

DBFC01, DBFC02, … DBFC20 is the lateral displacement terms (double)

PBFC01, PBFC02, … PBFC20 is the base friction force terms (double)